भौतिक अनुसंधान प्रयोगशाला, अहमदाबाद

Physical Research Laboratory, Ahmedabad

प्लैटिनम जयंती 1947 2022 PLATINUM JUBILEE

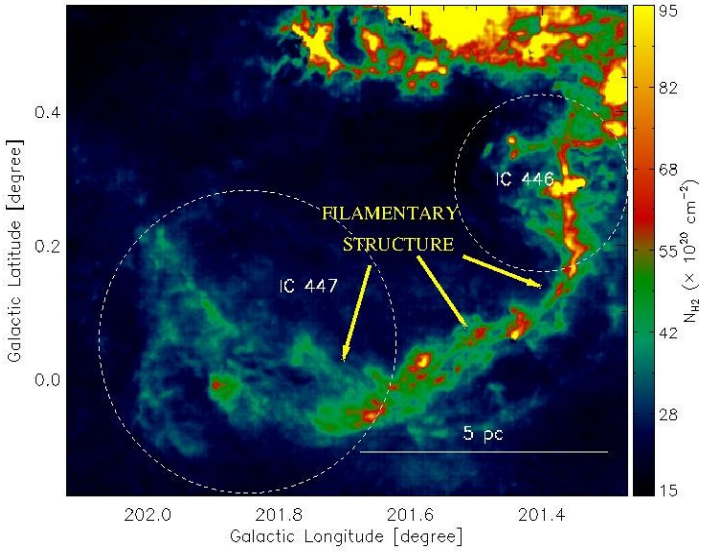

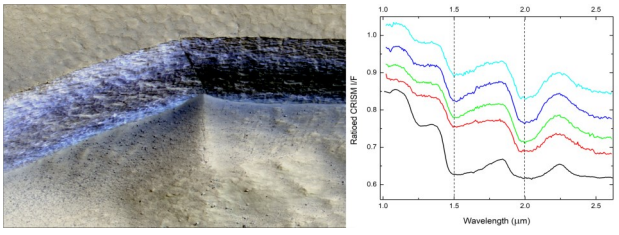

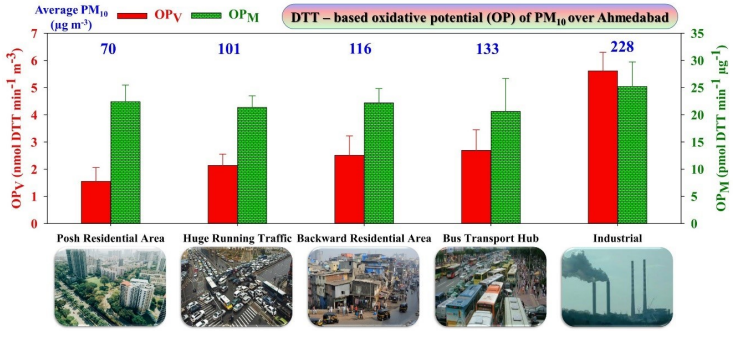

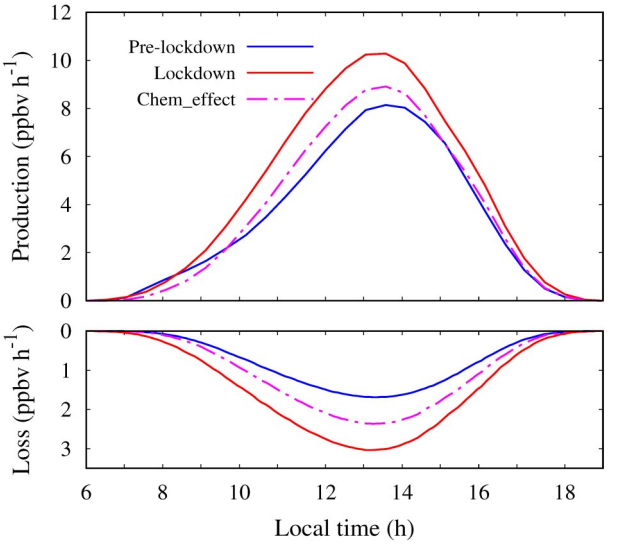

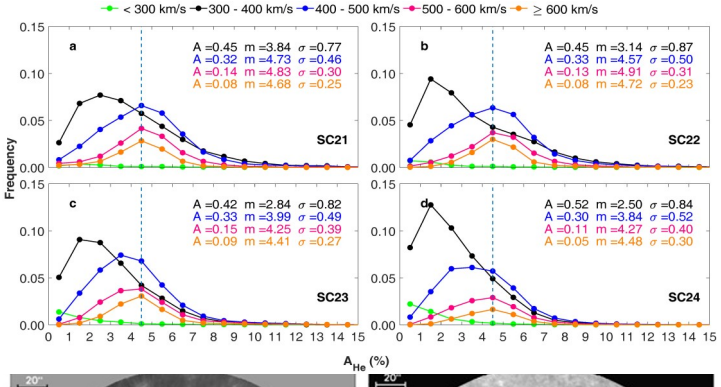

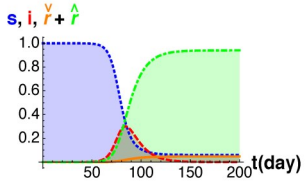

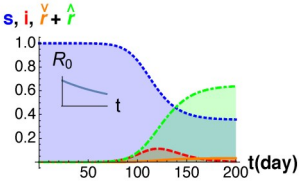

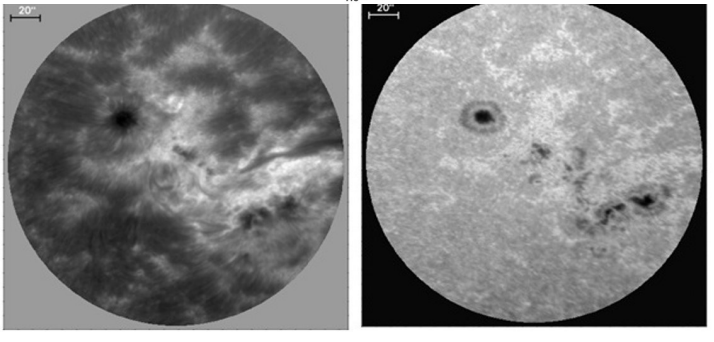

वार्षिक प्रतिवेदन

Annual Report

2020-2021

Front cover page:

Top left Panel: Star-forming sites IC 446 and IC 447: an outcome of end-dominated collapse of Monoceros R1 filament.

Top right Panel: Water-Ice exposing scarps within the northern midlatitude craters on the Mars.

Top Center left Panel: Volume normalized oxidative potential (OP_V) and mass-normalized OP (OP_M) over five different sites of Ahmedabad.

Top Center right Panel: N-Graphene Synthesized in Astrochemical Ices (Pencil lead in Space).

Center Left Panel: Evidence for distinctive changes in the solar wind helium abundance in solar cycle 24.

Center Right Panel: Model derived production and loss rates of ozone for pre-lockdown and lockdown conditions over Ahmedabad during COVID-19.

Bottom left Panel: Observations of the active region 12781 obtained with narrow-band spectral imager on MAST while adaptive optics system in operation.

Bottom right Panel: Modelling the influence of progressive social awareness, lockdown and anthropogenic migration on the dynamics of an epidemic.

Inside back cover pages: Events at PRL

Back cover page:

PRL Campuses

Compilation and Layout by:
Office of the Dean, PRL.

Published by:
Physical Research Laboratory, Ahmedabad.

Contact:
Physical Research Laboratory
Navrangpura
Ahmedabad - 380 009, India
Phone: +91-79-2631 4000 / 4855
Fax: +91-79-2631 4900
Email: info@prl.res.in
Website: `https://www.prl.res.in/`

Contact

Website

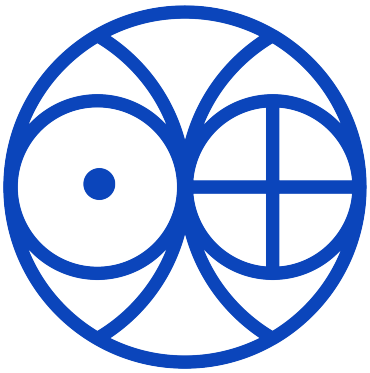

Annual Report

2020 – 2021

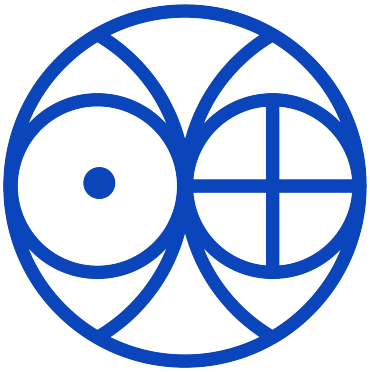

PRL research

encompasses

the Earth, the Sun

Immersed in the fields

and radiations

reaching from and to infinity,

all that man’s curiosity

and intellect can reveal

PRL Council of Management

Three nominees of the Government of India

Shri A. S. Kiran Kumar Prof. Vikram Sarabhai Professor, Department of Space/ISRO Former Secretary Department of Space Antariksh Bhavan, New BEL Road Bengaluru-560231	Chairman
Dr. K. Sivan, Chairman, ISRO Secretary, Department of Space, Government of India Antariksh Bhavan, New BEL Road Bengaluru-560231	Member
Shri Anoop Srivastava, IDAS Joint Secretary & Financial Advisor, Department of Space Antariksh Bhavan, New BEL Road Bengaluru-560231	Member (Upto 09.12.2020)
Shri M. Maheshwar Rao, IAS Joint Secretary & Financial Advisor, Department of Space Antariksh Bhavan, New BEL Road Bengaluru-560231	Member (From 10.12.2020)

A nominee of the Karmakshetra Education Foundation

Shri Kartikeya V. Sarabhai Director, Centre for Environment Education Ahmedabad-380054	Member

A nominee of Ahmedabad Education Society

Shri Sanjay S. Lalbhai Chancellor & Chairman, Board of Governors, Ahmedabad University Chairman & Managing Director, Arvind Limited Ahmedabad-380009	Member

A nominee of the Govt. of Gujarat, Gandhinagar

Smt. Anju Sharma, IAS The Principal Secretary, Higher and Technical Education Government of Gujarat, Gandhinagar-382 010	Member

Director, Physical Research Laboratory

Dr. Anil Bhardwaj	Member (Ex-Officio)

Registrar, Physical Research Laboratory

Mr. C. V. R. G. Deekshitulu	Member (Ex-Officio)

Areas of Scientific Research and Activities

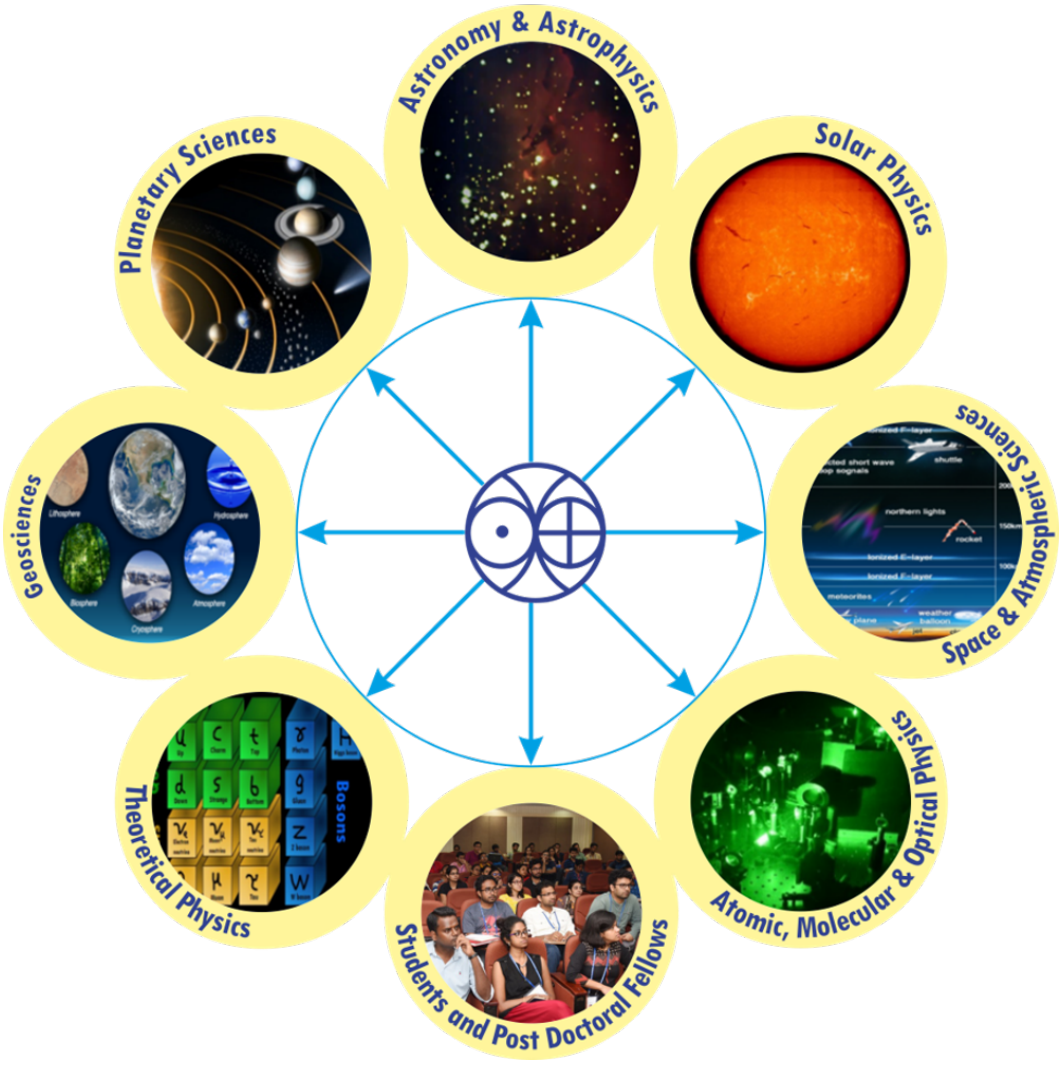

Contents

From The Director's Desk

In keeping up with the spirit of the founding fathers of PRL to boldly face adverse conditions head-on, PRL quickly raised to the occasion this year (2020-21) to the unprecedented challenges imposed by the COVID-19 pandemic. In spite of the difficulties with regard to official working, health concerns, and well-being of colleagues and family, limitations and accessibility to resources, PRL practiced several austerity measures and strived hard to arrive at ways to keep the spirit of research by prioritizing the activities. I commend my colleagues for their understanding and standing tall in maintaining high morale and self-confidence in this year of uncertainty and anxiety. This resulted in continuity of high-quality research contributions, as evidenced through the insightful results obtained in various domains of fundamental sciences, and excellent participation in collaborative activities at national and international level.

This year PRL's research resulted in 257 peer-reviewed scientific publications. Excellence in science continues to be the hallmark of research at PRL that includes robust training of young scientists through the vibrant Post-Doctoral and Research Fellowship programs. Fourteen research fellows were awarded Ph.D. degrees and several researchers have won best paper prizes for the work they pursued during their doctoral career. This year the list of coveted awards and recognitions span from national and international Academy Fellowships to the international Young Scientist and Early Career awards. Several colleagues received invitations to serve as the member of editorial board of national and international peer-reviewed journals, board of studies in universities, science advisory committees, and governing council of research and academic institutes. Several colleagues were elected to leadership positions in committees of international bodies. Five PRL faculty members are listed in the list of Top 2% of Scientists in the world in their respective fields published by Stanford University. Over 150 invitations were received by PRL faculty to deliver plenary or invited talks in conferences or symposia, universities, and institutes, which befits well with the leadership role played by PRL in different fields of research, both internationally and nationally. A few sample of the results from the diverse fields are given below to provide a flavour of the research at PRL.

The Solar X-ray Monitor (XSM) onboard Chandrayaan-2 mission is functioning exceedingly well since September 2019 and has conducted 1-15 keV X-ray observations of the deepest solar minimum in the past century with unprecedented sensitivity. Detailed spectroscopic analysis of these observations has, for the first time, revealed that in the absence of any active regions, the bulk of X-ray emission above 1 keV arises in the X-ray Bright Points (XBP) and that the abundances of the low FIP (First Ionization Potential) elements in the XBPs are at an intermediate level compared to their photospheric and coronal abundances. The quiet Sun observations by XSM detected a large number of microflares occurring outside the active regions. These observations have significant impact in understanding the coronal heating mechanism.

The massive star-forming regions G18.88-0.49 and Monoceros R1 have been examined using a multi-scale and multi-wavelength approach. An elongated filament (length 14pc, mass 1465 $M_\odot$) in Monoceros R1 is identified as a promising sample of the "end-dominated collapse" scenario. Results of the investigation of a hub-filament system and the molecular gas flow toward the central hub along the filaments together can explain the observed morphology and star formation in and around G18.88-0.49.

For the first time, the UV spectroscopy capability of Ultra-Violet Imaging Telescope (UVIT) onboard India's space observatory AstroSat is used to resolve the nature of a peculiar cool red giant star named SU Lyn. The PRL team recorded the Far-UV (1300-1800 angstroms) spectrum of SU Lyn, obtained with the UVIT instrument, which showed emission lines of Si IV, C IV, OIII, and N III. These observations confirmed the symbiotic nature of SU Lyn. The results are significant scientifically as, for the first time, they firmly establish the existence of SU Lyn type symbiotic systems, which are not identifiable from traditional ground-based optical spectroscopy.

A detailed X-ray timing and spectral analysis of the Seyfert 2 galaxy NGC 6300 using observations from the Suzaku, Chandra, and the NuSTAR X-ray Observatories during 2007 and 2016 have revealed significant variability in various energy bands. The nature of the circumnuclear 'torus' was investigated and found that the torus was clumpy and not uniform and that the torus and the nucleus independently evolve over the years.

A detailed analysis of the evolution of photospheric magnetic fields in the solar active regions accompanying major flares has shown that impulsive changes in the Lorentz force associated with abrupt changes in these magnetic fields can drive seismic emission in the sunspots. These magnetically driven acoustic waves are important as they can propagate upward in the solar atmosphere and thereby can heat the active region atmospheres.

A comprehensive study of the evolutionary phases of a major M6.6 long duration flare shows that it had an active pre-flare phase lasting for about an hour during which a hot EUV coronal channel developed which displayed co-spatial hard X-ray (HXR) emission up to energies of 25 keV indicative of first evidence of the HXR coronal channel.

Set of magnetohydrodynamic simulations with analytical boundary, relevant to solar atmosphere were carried out to investigate the role of magnetic reconnection in the presence of multiple preferable sites of reconnection, like magnetic null points (where $|B|$=0) and quasi-separatrix layers (QSLs) (where there is a sharp change in field line connectivity). It is found that nature and magnitude of the plasma flow is as crucial as the presence of nulls and/or QSLs.

The Grimaldi Basin on the Moon experienced mare volcanism $\sim$700 Ma, which is $\sim$500 Ma younger than the earlier reported youngest late phase mare volcanism on the Moon. The basin also experienced very recent tectonism $\sim$50 Ma, thus suggesting that the Moon is geologically active.

The Mukundpura CM2 (precisely 2.1) preserves a unique combination of relict chondrules and highly aqueous altered variegated matrix. Different extent of alteration also proposed mainly in the asteroidal parent body. Furthermore, the surface mineralogy of Mukundpura resembles the C-type asteroids recently probed by OSIRIS-REx and Hayabusa-2.

The ion density distribution in the inner coma of comet C/2016R2 (Pan-STARRS) is analysed with a model developed at PRL and it is found that photon and electron impact ionization and excitation of corresponding neutrals significantly contribute to the observed ionic emissions for distances less than 300 km. At larger distances, solar resonance fluorescence is the major excitation source.

A new approach, using radio measurements in Digisonde, is developed at PRL, using which daytime thermospheric wave characteristics have been obtained as a function of annual, seasonal, and solar flux during both geomagnetic quiet and disturbed times. It is found that the gravity wave activity (both in propagation speeds and numbers) is greater during periods of higher solar flux and equinoxes. Empirical relations have been obtained for all these interactions which can potentially form inputs to the global scale dynamical models.

Using high quality, two-decade long time series of ground-based and satellite observations and model simulations, the trends in the existing dipole pattern of aerosol loading are diverging with a rapidly decreasing trend since 2010 over the North China Plain (NCP) in East Asia and an increasing trend over the Indo-Gangetic Plain (IGP) in South Asia, two major global aerosol emission hotspots are documented for the first time.

The aerosol composition is also changing over both regions, making aerosols more light-scattering, which has resulted in reduction in aerosol-induced atmospheric heating rate over both regions, a more rapid decrease over the NCP than over the IGP, indicating a clear climate benefit of air pollution reduction in Asia.

The COVID-19 lockdown created a rare opportunity to quantify effect of human activities on urban ozone pollution. Interestingly, in contrast with precursors, ozone over Ahmedabad showed build up (39%) during lockdown. Model, incorporating measurements of chemical species and environmental conditions, revealed that ozone is enhanced by changes in chemistry ($\sim$25%) as well as meteorological effects ($\sim$16%). The findings of this unprecedented lockdown would serve as a reference in planning future policies to curb ozone pollution over this region.

Using a recently developed paleo-thermometer based on doubly substituted isotopologues (clumped isotopes) in carbonate eggshells, a new insight into the thermoregulations of dinosaurs have been revealed. Dinosaurs, being reptiles, are considered to be cold blooded. PRL scientists applied the clumped isotope thermometer on well preserved fossil eggshells of Late Cretaceous dinosaurs, recovered from western and central India, and estimated that the body temperatures of dinosaurs varied between 29°C and 46°C. The findings suggest that dinosaurs were well evolved and endowed with a capacity of variable thermoregulation.

The evaporative loss of water from falling raindrops is an important factor in hydrological budget since it affects the total rainfall received on land. This has been a major knowledge gap since it is difficult to estimate the evaporation from falling raindrops. Using stable isotope composition of daily rain fall samples at four stations of Jammu, Jorhat, Hyderabad and Ahmedabad, the evaporation from falling raindrop has been estimated. The maximum evaporation of 52% is estimated for Jammu, and minimum evaporation of 4% is estimated for Jorhat.

Nitrogen (N) and phosphorus (P) determine the strength of the ocean's biological carbon (C) pump and variation in N:P ratio is key to phytoplankton growth. A fixed C:N:P ratio (106:16:1) in organic matter and deep-water nutrients has been a tenet in ocean biogeochemistry. However, recent studies have challenged this tenet. Our observations from the Bay Bengal suggest that C:N:P ratio deviate greatly from the Redfield Ratio. The C:N:P ratio in particulate organic matter varied from 232:25:1 in the top layer to 966:72:1 in the deep water. In dissolved organic matter, the ratio varied from 357:30:1 in the top layer to 245:66:1 in the deep water. The N:P ratio in nutrients varied from 3 in the top layer to 12 in the deep water. Our C:N:P ratios support the nutrient supply hypothesis for low latitude ecosystems.

An equation of state for neutron star matter in the presence of magnetic field is derived within the ambit of sigma model. It was shown that the maximum mass, radius and tidal deformability of the neutron star estimated in the model is consistent with constrained from gravitational wave data GW170817.

Obtained comprehensive constraints on parameter spaces in minimal left-right symmetric models from mass variables –namely the mass probed in beta decay, the effective neutrino mass governing neutrino-less double beta decay and sum of the masses from cosmology. The work includes the constraints from neutrino less double beta decay, cosmological mass bound and lepton flavour violation and obtains the allowed range for the mass variables as well as the constraints on the masses of the heavy neutrinos and triplet scalars in the model. Constraints on heavy particle masses, complementary to collider searches were obtained.

The Higgs invisible branching ratio is still very poorly constrained, with best available analysis from the vector boson fusion (VBF) channel. Improvement of same can rule out many of the dark matter motivated BSM models. However, such signatures are experimentally challenging. Moreover, many background processes, many folds more extensive, mimic the same signature. With the unique capability of machine-learning, especially deep-learning algorithms with an incredibly powerful Convolutional Neural Network (CNN), used commonly in image-based techniques like classification and segmentation. They have shown exceptional capabilities, overtaking humans in numerous circumstances. To use CNNs, we address the problem of finding the signal as a classification of images. We do this by using the analogy of the detectors to a camera. The energy's spatial distribution essentially forms a picture with the energy deposits as the pixels' values. Using these so-called 'Tower Images,' we trained CNNs to identify signal type events from background ones. We improved the existing upper bounds on the invisible-branching ratio of the Higgs by a factor of three using the same amount of data. Such a tight constraint is even more impressive, given that we used the unprocessed low-level information directly from the detector, which is typically processed by our knowledge of physics first to derive these bounds.

A state-of-the-art technique of an active atomic clock to provide a continuous super-radiant lasing signal and a fractional uncertainty about 10^{-15} level using an ensemble of trapped Cs atoms in the optical lattice has been demonstrated. An appropriate magic wavelength of the clock transition, and pertinent optical lines for carrying out pumping and repumping of atoms are identified to carry out the clock frequency measurement. Further, a technique was demonstrated to tune the higher dimensional entanglement using orbital angular momentum states of light, which can potentially find applications in quantum information processing.

A study has been performed on the LIBS signal enhancement using colloidal silver nanoparticles (10 nm) on the brass sample. A Q-switched Nd: YAG laser operating at a wavelength of 1064 nm, pulse duration of 7 ns with 90 mJ/pulse energy, was used as an irradiation source. A clear enhancement of spectral intensities up to 4-times has been observed in the case of silver nanoparticles LIBS compared to conventional LIBS. The temporal evolution of the NELIBS plasma has also been investigated.

PRL continues to strive towards building new systems, instruments and models. A full working concept model of the neutral & ion mass spectrometer for the measurement of neutral and ion densities was demonstrated. Flight model of the ASPEX onboard Aditya-L1 mission is being developed and will be delivered to the project soon. Design of an antenna and matching network for a lightning detector was carried out. A laboratory model of a microwave receiver and multiplier-based transmitter for radio occultation experiment was designed, developed and tested in the laboratory at PRL. Detailed testing of impact ionization dust detector and front-end electronics is being carried out in the laboratory.

PRL continued with zeal its activities towards outreach and popularization of science at various levels and fora. PRL is committed towards spreading the scientific temper and spirit, not only at the highest level in terms of organizing the weekly colloquiua for advancement of research in various fields of specialization in PRL, but also, very importantly, of education and outreach at the level of schools and colleges, and to the common public at large. Through various events from time to time, particular attention is given to students from rural backgrounds by encouraging them to visit PRL, and get a chance to gain hands on experience. During the last year, in view of pandemic, PRL has been using the online platform for its outreach activities to the best extent possible. To take our efforts further in this direction, PRL has instituted a scholarship scheme exclusively for the students of economically weaker sections living in rural areas of the state of Gujarat: Vikram Sarabhai Protsahan Yojana "VIKAS".

The year 2019-2020 was the Birth Centenary of Dr. Vikram Sarabhai, the founder of PRL, and 12th August 2020 was his 101st Birth Anniversary. In the normal circumstances, PRL would have celebrated this momentous occasion with a great fervour, but due to the COVID-19 pandemic situation, an online webinar was organized with the theme "Dr. Vikram Sarabhai and Physical Research Laboratory (PRL)".

In-spite of the challenges posed by COVID-19 pandemic, the National Science Day celebrations saw a significant participation of close to 700 students from the state of Gujarat of which 110 were selected for participation in the online program by PRL on the 28th February 2021. Five brilliant students were awarded the Aruna Lal Fellowship. Additionally, special efforts were made to popularize science among girl children by inviting more than 80 girl students to participate in online science day celebrations.

Our unfettered and relentless efforts towards capacity building continued this year with enhanced vigour. Nearly 40 students did their four-months final project training with PRL faculty during December 2020 - April 2021. The major online meetings and programs organized include, Students Conference in Optics and Photonics (SCOP), 3rd PRL-IAPT Dr. Vikram Sarabhai Lecture, and 2nd Indian Planetary Science Conference (IPSC-2021). A four-day online summit on Fundamental Sciences & Quantum Technologies (FSQT 2020) was held during 28 September – 01 October 2020. PRL organized a webinar series of 13 astrobiology lectures from international and national academics who are engaged in research and teaching of astrobiology. PRL has instituted Dr. Bibha Chowdhuri Memorial Lecture in honour of Dr. Bibha Chowdhuri - the first Indian woman particle physicist who spent most of her work life at PRL. This memorial lecture will be an occasion to celebrate eminent women researchers in the field of science, technology, or social science.

A short online course on "Space and Atmospheric Sciences" was conducted during 7-14 December 2020 under the auspices of Center for Space Science and Technology Education in Asia and the Pacific (CSSTEAP), affiliated to the United Nations. 61 delegates from 11 countries (Bangladesh, Ethiopia, India, Lao PDR, Mongolia, Myanmar, Nepal, Sri Lanka, Thailand, Uzbekistan, and Yemen) participated in this course. PRL continues its strong academic and capacity building by association with many universities and institutes all over the country, and by participating in organizing national and international meetings.

Use of Hindi in all areas of administration and official communications is ensured in PRL. Bilingual communication is encouraged in all administrative orders. The website of PRL is bilingual. The participation in Hindi Pakhwada celebrations continues to rise. PRL received the year's 2019-2020 Third Prize for best work in Hindi from Town Official language Implementation Committee, Ahmedabad.

Established in the year 1947, PRL has entered its Platinum Jubilee year along with 75-years of young India. In the year of PRL's platinum

jubilee we recount the legacy of PRL's contributions, and remind ourselves to remain committed to the very spirit of PRL's ethos of research in fundamental science and space exploration leading to a better understanding of the nature.

In this endeavour we are constantly encouraged and whole-heartedly supported by Shri. A. S. Kiran Kumar, Chairman, PRL Council of Management, Dr. K. Sivan, Secretary, Department of Space, and all the members of the PRL Council of Management. I gratefully thank them for their astute advices and guidance, and their unflinching faith laid on PRL.

Anil Bhardwaj

Director

PRL in News

1. “Mystery of a peculiar star SU Lyn resolved by PRL scientists using AstroSat” published as ISRO Story of the Week. http://t.ly/hhNS
2. “Blast from the Past — Observations led by the PRL scientist enables breakthrough in centuries-old effort to unravel astronomical mystery” published as ISRO story of the week. http://t.ly/eCfL
3. “Cosmic stone Mahadeva that hit Bihar village decoded at Physical Research Laboratory” published in the Times of India. http://t.ly/RBlI
4. “Photoelectron distribution on sunlit surface of the Moon: A formalism” published in AIP Scilight. http://t.ly/l1yY
5. “Gauging the Sun’s Mood” published in Current Science Reports. http://t.ly/SxHC
6. “Goutam K. Samanta on Mentoring” published in Optics and Photonics News. http://t.ly/8e5X
7. “Puzzling signal on Saturn’s moon Rhea may finally be explained” was covered as news in New Scientist. http://t.ly/ac5b
8. “Pencil Lead in Space” covered in astrobites. http://t.ly/Uxgn

Science Highlights

Astronomy and Astrophysics

- The Solar X-ray Monitor (XSM), designed and developed at PRL, is successfully operational onboard Chandrayaan-2 since September 2019. The XSM has carried out X-ray observations of the deepest solar minimum in the past century with unprecedented sensitivity. Detailed spectroscopic analysis of these observations has, for the first time, revealed that in the absence of any active regions, the bulk of X-ray emission above 1 keV arises in the X-ray Bright Points (XBP). Further, the abundances of the low FIP elements in the XBPs are at an intermediate level compared to their photospheric and coronal abundances. During the same period of the quiet Sun observations XSM has detected the largest sample of 98 microflares occurring outside active regions. These observations have significant impact in understanding the coronal heating mechanisms.
- Filamentary structures have been commonly traced in star-forming regions, and are often associated with star formation activities. Furthermore, massive OB stars (M $>$ 8 M$\odot$) and clusters of young stellar objects (YSOs) are also seen at a junction of multiple filaments (i.e., hub-filament system). In the hub-filament system, the gas flow through the filaments is expected to the central hub (i.e., accretion through filaments). Interestingly, the fragmentation and collapse can also occur at the ends of the filaments (i.e., end-dominated collapse), where the gas has an enhanced acceleration. These processes can explain the birth of massive stars and cluster of YSOs. However, observational assessment of such numerical simulations is very limited in the literature. In this context, massive star-forming regions G18.88-0.49 and Monoceros R1 have been observationally examined using a multi-scale and multi-wavelength approach. An elongated filament (length $\sim$14 pc, mass $\sim$1465 M$\odot$) in Monoceros R1 is identified as a promising sample of the "end-dominated collapse" scenario. In the site G18.88-0.49, a hub-filament system and the molecular gas flow toward the central hub along the filaments are observationally investigated, and these results together explain the observed morphology and star formation in and around G18.88-0.49.
- Using upgraded Giant Metrewave Radio Telescope (uGMRT) we detected HI 21-cm absorption associated with a radio source 8C 0604+728 located at the distance of 84.5 Giga light-year with corresponding redshift z = 3.53. The source is at the highest redshift in which associated HI 21-cm absorption has been discovered till date, surpassing earlier known absorber at z = 3.39. This AGN also shows UV variability on year time-scale and we find that the luminosity and photon rate at the later epoch are higher than the thresholds suggested in the literature above which all the neutral hydrogen in an active galactic nucleus (AGN) host galaxy is expected to be ionized. The detection demonstrates that the neutral hydrogen can survive in the host galaxies of AGNs with high ultraviolet luminosities.
- The first Galactic ultraluminous X-ray pulsar Swift J0243.6+6124 was observed during its 2017-2018 outburst with AstroSat at both sub- and super-Eddington levels of accretion with X-ray luminosities of 7 $\times$ 10^{37} and 6 $\times$ 10^{38} erg/s, respectively. X-ray pulsations at 9.85s are detected in the light curves up to 150 keV when the source was accreting at the super-Eddington level. The pulse profiles are a strong function of both energy and source luminosity, and show a double-peaked profile with increasing pulse fraction with energy. The continuum X-ray spectra are well modelled with a high-energy cut-off power law and one or two blackbody components with temperatures of $\sim$0.35 keV and 1.2 keV, depending on the accretion level. No iron line emission is observed at sub-Eddington level, while a broad emission feature at around 6.9 keV is observed at the super-Eddington level, along with a blackbody radius (121$-$142 km) that indicates the presence of optically thick outflows.
- The Galactic black hole candidate MAXI$\sim$J1348-630 was observed with MAXI and Swift satellites during its first outburst

in 2019 January, which continued for 4 months. The combined 1-150 keV Swift/XRT, Swift/BAT, and MAXI/GSC spectra are investigated with the two-component advective flow (TCAF) solution. Physical flow parameters of TCAF, such as the Keplerian disk accretion rate, the sub-Keplerian halo accretion rate, the shock location, and the shock compression ratio are estimated from our spectral fits. Based on the variation of flux in soft and hard X-ray ranges, the hardness ratio, TCAF model fitted accretion rates, and the accretion rate ratio, we show the evolution of the source through four spectral states, viz., hard, hard-intermediate, soft-intermediate, and soft, in rising and declining phases of the outburst. Low-frequency quasi-periodic oscillations are observed in two observations during the rising phase of the outburst. From the spectral analysis, we estimate the mass of the BH to be $9.1^{+1.6}_{-1.2}$ $M_{\odot}$. The distance of the source is also estimated as 5-10 kpc from state transition luminosity.

- A detailed X-ray timing and spectral analysis of the Seyfert 2 galaxy NGC 6300 was carried out by using observations from the Suzaku observatory, the Chandra X-ray Observatory and the Nuclear Spectroscopic Telescope Array (NuSTAR) mission between 2007 and 2016. The variance and the rms fractional variability of the source in different energy bands was calculated and variabilities in various energy bands were found. Spectral properties of the source are studied by using several phenomenological and physical models. The properties of the Compton clouds, reflection, Fe Kα line emission and soft X-ray excess are studied in detail. Several physical parameters of the source have been extracted and investigated to establish the presence/absence of any correlation between them. The nature of the circumnuclear 'torus' was investigated and it was found that the torus is not uniform, but clumpy. The observed changes in the line-of-sight column density can be explained in terms of transiting clouds. The iron line-emitting region is found to be different in the different epochs of observations. It was also observed that the torus and the nucleus evolve independently over the years.

Solar Physics

- A detailed analysis of the evolution of photospheric magnetic fields in the solar active regions accompanying major flares has shown that impulsive changes in the Lorentz force associated with abrupt changes in these magnetic fields can drive seismic emission in the sunspots. These magnetically driven acoustic waves are important as they can propagate upward in the solar atmosphere and thereby can heat the active region atmospheres.
- The study of relation between North-South asymmetry in solar coronal rotation and solar activity cycle for solar cycle 24 has shown that this rotational hemispheric asymmetry leads the sunspot cycle by nearly 1.56 years. This gives a clear indication that hemispheric asymmetry triggers the formation of sunspots working together with the differential rotation of the Sun.
- A study of the topological properties of sub-photospheric flows and photospheric solar magnetic fields shows a similar hemispheric pattern in kinetic helicity of flows and current helicity of magnetic fields, which supports the mean-field dynamo mode.
- A comprehensive study of the evolutionary phases of a major M6.6 long duration flare showed that it had an active pre-flare phase lasting for about an hour during which a hot EUV coronal channel developed which displayed co-spatial hard X-ray (HXR) emission up to energies of 25 keV indicative of first evidence of the HXR coronal channel.
- Light bridges are bright, extended structures within the umbrae of sunspots/pores, the formation of which is generally regarded to stem from vigorous overturning convection within a sunspot. A recent observational study indicates that the light bridge formation is part of a flux emergence event with its envelope reaching a height of about 29 Mm before dissolving after about 13 hr. The results also show that existence of persistent, large-scale photospheric blueshifts in light bridges is the most likely criterion for distinguishing between flux emergence events and overturning convection in field-free umbral intrusions.
- A comprehensive analysis of the formation and the evolution of a fan-spine-like configuration that developed over a unique photospheric configuration, analogous to the geological 'atoll' shape, which hosted four homologous quasi-circular ribbon flares within its boundary. The coronal magnetic configuration associated with the atoll region was characterized by the presence of a hyperbolic flux tube, which differed from the usual configurations associated with circular ribbon flares, which involve the presence of coronal null point.
- Study of a highly compact sigmoidal flaring region which was associated with a intertwined double−decker flux rope configuration suggested that high storage of non-potential magnetic energy in the mini-sigmoidal region was able to power two M−class flares within an interval of an hour. These impulsive homologous flares were associated with 'anomalous' jet-like plasma eruption, which not only drastically changed their direction but also underwent a large angular expansion, due to the deflection of erupting material by the large-scale open field lines originating near the mini-sigmoidal region.
- A magnetohydrodynamic simulation is performed to explore the onset of an X-class flare in the concurrent presence of complex magnetic topologies involving a three-dimensional magnetic null point (where $|B|$=0), flux ropes and sheared arcades. The dynamics found in the simulation, matches with the observational features remarkably and hence proves the efficacy of the models employed in the simulation.
- Set of magnetohydrodynamic simulations with analytical boundary, relevant to solar atmosphere were carried out to investigate the role of magnetic reconnection in the presence of multiple preferable sites of reconnection like magnetic null points (where $|B|$ =0) and quasi-separatrix layers (QSLs) (where there is a sharp change in field line connectivity). It was found that nature and magnitude of the plasma flow was as crucial as the presence of nulls and/or QSLs.

Planetary Sciences

- Temperature dependent thermal properties of certain lunar analogous samples under simulated lunar environment have been experimentally determined using a custom-developed setup and compared with limited Apollo measurements. Results show a significant temperature dependence of thermal conductivity particularly under vacuum conditions. Such a

behaviour is not understood due to lack of measurements. This data would be useful in proper understanding of lunar thermophysical behaviour and help in interpretation of data that may become available in the future missions.

- The Mukundpura CM2 (precisely 2.1) preserves a unique combination of relict chondrules and highly aqueous altered variegated matrix. Different extent of alteration also proposed mainly in the asteroidal parent body. Furthermore, the surface mineralogy of Mukundpura resembles the C-type asteroids recently probed by OSIRIS-REx and Hayabusa-2 missions.
- The morphology, texture, geochemistry and spectroscopic investigations of Jhuran iron concretions suggest its formation of sedimentary diagenesis in fluvio-deltaic condition with role of limited eolian activity in the terminal phase. This study has the relevance for understanding the formation processes of Martian "blueberries" and can be considered for possible Martian terrestrial analog locality.
- The Grimaldi Basin on the Moon experienced mare volcanism at $\sim$ 700 Ma, which is $\sim$ 500 Ma younger than the earlier reported youngest late phase mare volcanism on the Moon. The basin also experienced very recent tectonism at $\sim$ 50 Ma. Thus, it can be inferred that the Moon is geologically active.
- Mars 2020 Perseverance rover landed in the Jezero crater on February 18, 2021. For the first time, we found tracks left by falling boulders in the landing site of the Mars 2020 Perseverance rover. The boulder tracks are observed on the slopes of the delta deposits that the rover will explore. Boulders of a few meters in size have fallen down moderately steep slopes, moving distances from a few tens of meters to nearly a kilometer. The simple existence of the boulder tracks suggests that the boulder falls are recent and could be ongoing. Our results reveal a new location on Mars where boulder fall activity is observed and indicate a new hazard to be taken into account by the rover team. These recently fallen boulders may also have surfaces less exposed to radiation and could be ideal candidates for obtaining samples that could be analyzed for signs of ancient life.
- The electrostatic equilibrium in the dark region of polar craters on Moon is established by fine particle overlying on the surface.
- Electrostatic charge fluctuation is the key for lifting dust from the Moon surface.
- The surface charging characterizes the non-Maxwellian nature of photoelectrons on Moon.
- One third of the planet Mars is rich in water ice which is mostly preserved a few meters below the surface. Identification of new water-ice-rich regions is indeed required to understand their spatial spread across Mars, vital role in identifying future landing/robotic missions and for the $in-situ$ resource utilization. New report of water-ice exposure within two craters located in the northern hemisphere of Mars. Within a crater, the exposed ice is stable after one week of interval, this gives a direct proof for the stable exposed ice. These ice deposits within crater got exposed within a million year ago. Our new locations to the existing list of identified water-ice deposits ensure their widespread nature and at higher latitudes the water ice are few meters below the surface of Mars.
- We examined the 3-μm absorption band of six bright swirls associated with magnetic anomalies of variable strength using Chandrayaan-1 Moon Mineralogy Mapper (M3) hyperspectral image data. The spectral trends in the near-infrared wavelength range at on-swirl and off-swirl locations suggest that the reduced space-weathering alone cannot be the only explanation. Our study suggests that an external mechanism of interaction between a comet and the uppermost regolith layer might play a significant role in lunar swirl formation. Further, we focused on the Reiner Gamma swirl that can be observed using the ground based telescopic facilities. We obtained polarimetric observations of Reiner Gamma using the Mount Abu IR Observatory facility. The telescopic analysis suggests differences in grain sizes and roughness within the Reiner Gamma swirl, indicating the presence of surface alteration processes that might have disrupted the regolith microstructure.
- A large dust storm was detected beginning InSight 40 Sol and ending round 90 Sol. The examination of 20 Hz magnetometer data during the storm period does not reveal clearly identifiable Schumann Resonance on Mars. The search for electrical activity on Mars is continued.
- The Poynting flux obtained from the VEX magnetometer during solar maximum shows a decrease with increasing altitude, providing an evidence that the waves were generated below the ionosphere. This conclusion is less clear during solar minimum, even though the detection rates are about twice as high compared to solar maximum.
- The excitation processes of CO^+ first-negative band emission in upper atmosphere of Mars was studied. For this, a photochemical model was developed at PRL and results were compared with MAVEN observations. The emission is found to be dominated by the ionization of CO by solar photons and photoelectrons, and the role of dissociative ionization of CO_2 is negligible.
- The ion density distribution in the inner coma of comet C/2016 R2 (Pan-STARRS) was analysed with a model developed at PRL. It was found that photon and electron impact ionization and excitation of corresponding neutrals significantly contribute to the observed ionic emissions for distances less than 300 km. At larger distances, solar resonance fluorescence is the major excitation source.

Space and Atmospheric Sciences

- An analysis using new and high quality $in-situ$ observations, performed for the first time, revealed that black carbon (BC) aerosols dominate ($\geq$75%) the aerosol absorption over the Indo-Gangetic Plain (IGP) and the Himalayas throughout the year. This quantification will be valuable as observational constraints to help improve regional simulations of climate change, impacts on the glaciers and the hydrological cycle, and will help to direct the focus toward study of BC as the main contributor to aerosol-induced warming in the region.
- Using high quality, two-decade long time series of ground-based and satellite observations and model simulations, the trends in the existing dipole pattern of aerosol loading are found to be diverging. A rapidly decreasing trend since 2010 is seen over the North China Plain (NCP) in East Asia and an increasing trend over the Indo-Gangetic Plain (IGP) in South Asia, the two major global aerosol emission hotspots. These trends are documented for the first time. The aerosol composition is also changing over both regions,

making aerosols more light-scattering, which has resulted in reduction in aerosol-induced atmospheric heating rate over both regions, a more rapid decrease over the NCP than over the IGP, indicating a clear climate benefit of air pollution reduction in Asia.

- The Indo-Gangetic Plain (IGP), home to about one seventh of world's total population, experiences elevated loadings of fine particulate matter ($PM_{2.5}$), typically during post-monsoon and winter. High-resolution modelling has been performed to unravel the roles of emissions and atmospheric dynamics over this region. Simulations revealed remarkable impact of crop-residue burning on regional air quality, e.g. by up to 55% in $PM_{2.5}$ over Delhi, during post-monsoon. Whereas, in contrast, the stagnant atmospheric conditions confine the anthropogenic effects near the surface leading to the widespread enhancement during winter. The study highlights that the role of unfavourable atmospheric dynamics should be considered in the mitigation policies, besides emissions.
- A comprehensive analysis of seasonal and inter-annual variations of aerosol properties (optical, physical, and chemical) and radiative effects over Pokhara Valley in the foothills of central Himalayas utilizing the high-quality multi-year columnar aerosol data observed recently from January 2010 to December 2017 showed that carbonaceous aerosols (CA) dominate ($\geq$60%) aerosol absorption during whole year. Black carbon (BC) alone contributes $>$60% to aerosol optical depth $(AOD)_{CA}$ while brown carbon (BrC) contributes the rest. The absorbing aerosol types are determined to be BC, and mixed (BC and dust) only. Dust as absorbing aerosol type is absent over the Himalayan foothills. These quantitative results can be used as inputs in global/regional climate models to assess the climate impact of aerosols, including on regional temperature, hydrological cycle and melting of glaciers and snowfields in the region.
- Analysis of aerosol characteristics and radiative effects using recently available high-quality columnar aerosol data collected at several sites in South Asia, with a focus on pollution outflow from continental South Asia observed over Hanimaadhoo in Maldives, a small island in northern Indian Ocean, revealed that aerosol loading and atmospheric warming have increased over this background site over the last decade. A regional-scale analysis of aerosol properties and radiative effects across and surrounding the Indo-Gangetic Plain aerosols reduce seasonally 30-50 Wm^{-2} of solar radiation reaching the surface, contributing significantly to solar dimming effect over the region.
- The COVID-19 lock-down created in 2020 a rare opportunity to quantify effect of human activities on urban ozone pollution. Interestingly, in contrast with precursors, ozone over Ahmedabad showed more build up during lock-down (by 39%). Model, incorporating measurements of chemical species and environmental conditions, revealed that ozone was enhanced by changes in chemistry ($\sim$25%) as well as meteorological effects ($\sim$16%). The findings of this unprecedented lock-down would serve as a reference in planning future policies to curb ozone pollution over this region.
- Air-sea exchange of volatile organic compounds (VOCs) and transformation in the atmosphere lead to the production of ozone (O_3) and secondary organic aerosols (SOA) in the remote marine air. Ocean microbes and dissolved organic compounds are important natural sources of many non-methane hydrocarbons (NMHCs) to the atmosphere. In our recent studies, for the first time, the measurements of the concentrations of light alkenes in marine air and the physical and biological parameters of surface seawater of the Arabian Sea during the inter-monsoon period were analyzed to investigate oceanic sources of light alkenes in the marine air. In this interdisciplinary approach, seawater parameters were used to explain the distributions of NMHCs in the atmosphere over the highly productive and oxygen-deficient region of the Arabian Sea. In addition to the photo-degradation processes of dissolved organic carbon (DOC), marine microorganisms can lead to the generation of many reactive species including C_2-C_4 NMHCs. In particular, the high levels of alkenes were associated with the higher abundances of *Trichodesmium* and *Thalassiosira* species.
- Land-atmosphere exchange of biogenic-VOC (BVOCs) and transformation in the atmosphere lead to the production O_3 and SOA in the remote continental (vegetated) regions. However, lack of representative parameterization of BVOC emissions particularly from tropical biosphere is one of the largest sources of uncertainty in the chemistry-climate model. We measured the ambient concentration of monoterpenes (mainly α-pinene) using PTR-TOF-MS at a semi-arid site in western India during winter-to-summer transition period. The dependencies of monoterpenes on meteorological parameters such as temperature, sunlight, relative humidity, etc. were analyzed in details. From mid-January to March, the estimated increase of $\sim$53% in the biogenic contributions of monoterpenes were associated with the change in meteorological conditions. We emphasized the critical needs to address the existing lack of knowledge of BVOC emission focused on atmospheric chemistry leading to the environmental and climatic change in tropical South Asia.
- A study of the impact of mesoscale gravity waves on the microphysical characteristics of cirrus clouds over the subtropical Indian region using Raman Lidar, satellite measurements, model simulations, and reanalysis data revealed that the cirrus clouds are modulated by the upward propagating gravity waves with time periods $\sim$40 and $\sim$20 min. The ice crystals size in the cirrus clouds increases and transforms to irregular shapes in the presence of wave activity. The present work is unique and will have implications toward the uncertainties associated with cirrus clouds in both regional and global climate models.
- Effect of solar flux versus compositional variations on the variability of daytime oxygen optical emission rates over low- and mid-latitudes was brought out wherein it is shown using long term optical data that the compositional changes affect the mid-latitude dayglow emissions significantly and that it governs the seasonal pattern in the emissions.
- From the analysis of PRL's digisonde data for over two years, thermospheric wave dynamics has been obtained as a function of annual, seasonal, and solar flux during both geomagnetic quiet and disturbed times, all of which are quantified with empirical relations. Greater wave activity, both in terms of propagation speeds and number of independent waves, is seen during the times of higher solar flux and equinoxes.
- Evident signature of the 27-day variability is found in the tidal amplitudes in the mesosphere and lower thermosphere (MLT) at low and mid latitudes. Observed strong correlation between the solar UV radiation and the tides indicates predominate

solar influence on the MLT tidal dynamics. Additionally, a conspicuous imprint of a rare 120-day oscillation is observed in the MLT with a plausible linkage with the third annual harmonic. The intermittent behavior of the 120-day oscillation implies it to be a feature of the MLT wind circulation.

- The relative abundance of alpha particles with respect to protons, usually expressed as A_{He} = (n_α/n_p)∗100, is known to respond to solar activity, although changes in its behaviour in the last four solar cycles are not known. By systematically analysing inter-calibrated A_{He} data obtained, onboard Advanced Composition Explorer satellite mission, from the first Lagrangian point of the Sun-Earth system, it is shown that the A_{He} variations are distinctively different in solar cycle 24 as compared to the last three cycles. The investigation suggests that the coronal magnetic field configuration started undergoing systematic changes starting from cycle 23 and this altered magnetic field configuration affected the way helium got processed and depleted in the solar atmosphere.
- A plasmaspheric hiss event, observed by the Van Allen probes in response to two successive interplanetary (IP) shocks occurring within an interval of ∼2 h on December 19, 2015, are presented for the first time. The first shock arrived at 16:16 UT and caused disappearance of hiss for ∼30 min. The recovery of hiss began at ∼16:45 UT. Subsequently, the second shock arrived at 18:02 UT and generated patchy hiss persisting up to ∼19:00 UT. Based on calculation of electron phase space density and linear wave growth rate analyses, the investigation brings out the important roles of IP shocks, substorms, ULF waves, and background plasma density in the variability of plasmaspheric hiss.
- Based on 10 years' (2010–2019) of vertical total electron content (VTEC) variations from Ahmedabad (23.0°N, 72.6°E, dip angle 35.2°), campaign-based OI 630.0 nm airglow intensity variations from Mt. Abu (24.6°N, 72.7°E, dip angle 38.0°), regional TEC variations captured by the Indian Satellite-based Augmentation, GAGAN (GPS Aided Geo Augmented navigation) and global empirical model drifts, it is shown that the post-sunset enhancements in VTEC occurs ∼1.7 h after the PRE and are significant only during December solstice and equinoctial months in high solar activity years similar to seasonal variations in PRE amplitudes. This time delay (response time of EIA crest) is almost half compared to the average response time (3-4 h) associated with the daytime fountain. This result brings out the important role of the PRE in conditioning the EIA crest region.

Geosciences

- The evaporative loss of water from falling raindrops is an important factor in hydrological budget since it affects the total rainfall received on land. This has been a major knowledge gap since it is difficult to estimate the evaporation from falling raindrops. Using stable isotope composition of daily rainfall samples at four stations of Jammu, Jorhat, Hyderabad and Ahmedabad, the evaporation from falling raindrop has been estimated. The maximum evaporation of 52% is estimated for Jammu, and minimum evaporation of 4% is estimated for Jorhat.
- Nitrogen (N) and phosphorus (P) determine the strength of the ocean's biological carbon (C) pump and variation in N:P ratio is key to phytoplankton growth. A fixed C:N:P ratio (106:16:1) in organic matter and deep-water nutrients has been a tenet in ocean biogeochemistry. However, recent studies have challenged this tenet. Our observations from the Bay Bengal suggest that C:N:P ratio deviate greatly from the Redfield Ratio. The C:N:P ratio in particulate organic matter varied from 232:25:1 in the top layer to 966:72:1 in the deep water. In dissolved organic matter, the ratio varied from 357:30:1 in the top layer to 245:66:1 in the deep water. The N:P ratio in nutrients varied from 3 in the top layer to 12 in the deep water. Our C:N:P ratios support the nutrient supply hypothesis for low latitude ecosystems.
- Using a recently developed paleo-thermometer based on doubly substituted isotopologues (clumped isotopes) in carbonate eggshells, a new insight into the thermoregulations of dinosaurs have been revealed. Modern animals can be broadly categorized into warm blooded (e.g., mammals and birds) and cold blooded (e.g., reptiles) animals. The former maintains a stable body temperature irrespective of the environmental temperature while the latter fails to do so and their body temperatures fluctuate depending on the ambient temperatures. Dinosaurs being reptiles are considered to be cold blooded. Scientists from Geosciences Division applied the clumped isotope thermometer on well preserved fossil eggshells of Late Cretaceous dinosaurs recovered from western and central India and estimated that the body temperatures of dinosaurs varied between 29°C and 46°C. The findings suggested that dinosaurs were well evolved and endowed with a capacity of variable thermoregulation.
- Vehicular catalytic converters are used to regulate, reduce, and convert toxic and harmful compounds in exhaust gases into less harmful/inert species. The efficiency of the converters, however, is largely affected by their operating temperatures, set by the hot exhaust gas released from the combustion chamber. The role of catalytic converter temperature (estimated using clumped isotope thermometry in exhaust CO_2) in reducing the toxic compounds such as oxides of nitrogen (NO_x) has been investigated through isotopic analysis of the exhaust nitrous oxide (N_2O). The catalytic converters were found to act as sinks and sources of N_2O to the atmosphere in gasoline and diesel operated vehicles, respectively. The degree of N_2O reduction to N_2 in gasoline powered vehicle is high when the temperature is above 200°C, whereas diesel powered vehicles produce N_2O in abundance, a consequence of selective catalytic reduction of NO_x. The emission of N_2O or the extent of reduction of NO_x in diesel vehicle increase with increasing converter temperature.
- A new perspective of quantifying the pollutants from different anthropogenic sources such as fossil combustion and biomass burning was made using a non-traditional stable isotope proxy namely, ^{17}O excess along with conventional carbon and oxygen isotopes in CO_2. Isotopic ratios were measured in atmospheric CO_2 at a site in Delhi and two nearby remote places and near some crop burning point sources. The authors showed that the CO_2 contribution from anthropogenic sources varied between 4 and 40% in Delhi. Out of the total anthropogenic CO_2, biomass burning from the upstream region was much higher (∼70%) compared to the local fossil fuel emission (∼30%) during the peak pollution time of October, 2017. The proportion of CO_2 from biomass burning indirectly gives estimates of contribution of pollutants from

those two sources in Delhi.

- One of the pre-requisite for paleoclimatic studies using marine archives is assigning chronology of sediment cores by radiocarbon dating. Marine reservoir age is important for radiocarbon dating of marine and coastal samples. Reservoir age correction for the first time was assigned to the Andaman Basin as applicable for the radiocarbon ages. A study based on the AMS radiocarbon dating of planktonic and benthic formaminifera demonstrated that the ventilation age estimates from the Central Indian Ocean Basin were much higher than other oceanic regions implying poor ventilation throughout the last glaciation.
- The coastal ecosystems remain largely affected by direct discharge of pollutants and sediments from rivers. Based on ^{210}Pb and ^{137}Cs dating of sediments from the coastal Arabian Sea, it was shown that the sedimentation in the continental shelf region of the coastal Arabian Sea is primarily controlled by discharge of sediments from rivers during Indian summer monsoon. Another study on a sediment core chronologically constrained using ^{210}Pb dating technique from the northwest Bay of Bengal demonstrated the role of estuarine environment and/or high riverine flux of sediments causing either removal or dilution of trace elements during its transport from the river to the sea.

Theoretical Physics

- An equation of state for neutron star matter in the presence of magnetic field is derived within the ambit of sigma model. It was shown that the maximum mass, radius and tidal deformabilty of the neutron star estimated in the model is consistent with constrained from gravitational wave data GW170817.
- Obtained comprehensive constraints on parameter spaces in minimal left-right symmetric models from mass variables – namely the mass probed in beta decay, the effective neutrino mass governing neutrino-less double beta decay and sum of the masses from cosmology. The work includes the constraints from neutrino less double beta decay, cosmological mass bound and lepton flavour violation and obtains the allowed range for the mass variables as well as the constraints on the masses of the heavy neutrinos and triplet scalars in the model. Constraints on heavy particle masses, complementary to collider searches were obtained.
- A predictive model for light sterile neutrinos was constructed within the extended sessaw mechanism using flavour symmetry groups. The appeal of the model lies in minimal number of free parameters and also ability to explain both active and sterile neutrino parameters.
- Implications of the dark-LMA solution to the solar neutrino problem was studied for neutrino-less double beta decay in presence of a sterile neutrino and compared with the standard LMA parameter space.
- The modes, $\mathrm{B} \to \mathrm{K}\ell^+\ell^-$, with $\ell = e, \mu$, have attracted a lot of theoretical and experimental attention as the ratio of the muon to electron final states presents a very clean observable in the quest for physics beyond the Standad Model (SM). Experimentally, this ratio deviates from unity as expected from SM (universality between electrons and muons) by about 15%. However, the theoretical calculations don't include the corrections due to Quantum Electrodynamics (QED). Proper inclusion of these turns out to be notorious due to the fact that unless the measurements are made photon inclusive, there are large logarithmic factors, dependent on the lepton mass, that affect the modes significantly, and worsen the ratio to some degree. Detailed theoretical expressions are presented to enable a comparison with the experimental results once the energy and angular cuts adopted in the experiments are provided, making the theoretical predictions more robust.
- Gravitational lensing of neutrinos has been investigated and the probability amplitude of their flavour transitions has been computed. It is found that the neutrino oscillation in the presence of lensing is qualitatively very different from the standard oscillations in the flat space-time.
- In-house epidemiology model to include progressive social awareness and effects of lockdown. The governing equations are based on the classical SIR (Susceptible-Infected-Recovered) model. The choice of the SIR as a base model is motivated by its simpler construction, leading to an easier physical interpretation of appropriate mathematical modification made. The focus of the advanced SIR model is to check efficacy of various social interventions and progressive social awareness to decelerate the infection spreading. For the purpose, the model treats the basic reproduction parameter R0 as a continuous and discrete functions of time, separately. The progressive social awareness is infused into the model phenomenologically by assuming an exponentially decaying form of R_0. The analyses show a society already adapting to an ongoing epidemic will be immensely benefited by an aggressive campaign to further raise the awareness. Based on the findings, an inclusion of basic epidemiology course at the school curriculum is proposed since for epidemics like COVID19, where the only deterrents are the social interventions like proper cough/respiratory hygiene, frequent hand washing and social distancing. Effects of lockdowns, including a single and a staggered exit are also studied and is found that a lockdown with progressive social awareness can flatten the infection curve dramatically and attributes the relatively lower infection spread in India to the proactive efforts by the Government.
- The Higgs invisible branching ratio is still very poorly constrained, with best available analysis from the vector boson fusion (VBF) channel. Improvement of same can rule out many of the dark matter motivated BSM models. However, such signatures are experimentally challenging. Moreover, many background processes, many folds more extensive, mimic the same signature. With the unique capability of machine-learning, especially deep-learning algorithms with an incredibly powerful Convolutional Neural Network (CNN), used commonly in image-based techniques like classification and segmentation. They have shown exceptional capabilities, overtaking humans in numerous circumstances. To use CNNs, we address the problem of finding the signal as a classification of images. We do this by using the analogy of the detectors to a camera. The energy's spatial distribution essentially forms a picture with the energy deposits as the pixels' values. Using these so-called 'Tower Images,' we trained CNNs to identify signal type events from background ones. We improved the existing upper bounds on the invisible-branching ratio of the Higgs by a factor of three using the same amount of data. Such a tight constraint is even more impressive, given that we used the unprocessed low-level information directly from

the detector, which is typically processed by our knowledge of physics first to derive these bounds.

- For the first time, compact analytic expressions for Higgs+4-partons one-loop helicity amplitudes are achieved when a massive colour triplet fermion or scalar is circulating in the loop.
- A critical analysis of the leading theoretical approaches in the field of cuprate high temperature superconductivity was undertaken. We start out by defining the problem and ask the question: whether an overarching theory possible? If it is possible, what should we expect from the overarching theory? We list various experimental facts, and point out what can we learn from them and where do current theories stand in addressing them? Next, we present a critique of the current leading approaches. It is concluded that although progress in the field has been unprecedented, we still lack a coherent understanding.

Atomic, Molecular and Optical Physics

- Strong-field ionization of CH_3OH has been investigated to understand the ultrafast H atom migration and bond formation. Using the combined approach of experiments and theory, we have successfully explained the mechanism of intramolecular hydrogen migration and predicted the dissociative channels of singly-ionized CH_3OH.
- A study has been performed on the LIBS signal enhancement using colloidal silver nanoparticles (10 nm) on the brass sample. A Q-switched Nd: YAG laser operating at a wavelength of 1064 nm, pulse duration of 7 ns with 90 mJ/pulse energy, was used as an irradiation source. A clear enhancement of spectral intensities up to 4-times has been observed in the case of silver nanoparticles LIBS compared to conventional LIBS. The temporal evolution of the NELIBS plasma has also been investigated.
- Photoionization of carbon dioxide (CO_2) molecules by linearly and circularly polarized pulses has been performed. The results from the measurement with linear and circular polarization are consistent with the adiabatic ionization approximation.
- Photoionization of CH_3OH and CO_2 with a stretched femtosecond laser pulses has been investigated and found that the double ionization yield is more in the case of stretch pulses (295 fs) compared to 29 fs pulses. The pulse stretching of femtosecond (29 fs) pulses is performed using SF11 crystal and characterized by Spectral Phase Interferometry for Direct Electric-field Reconstruction (SPIDER) technique.
- By combining ingenious atomic calculations, performed using an in-house developed relativistic all-order many-body method, along with isotope shift measurements in the radioactive potassium isotopes, possible magic behaviour of nuclei around neutron number 32 has been probed. It shed light to the limited understanding of sizes of neutron-rich nuclei, and exposed problems that are manifested in some of the popular models of nuclear theory.
- A state-of-the-art technique of an active atomic clock to provide a continuous superradiant lasing signal and a fractional uncertainty about 10^{-15} level using an ensemble of trapped Cs atoms in the optical lattice has been demonstrated. An appropriate magic wavelength of the clock transition, and pertinent optical lines for carrying out pumping and repumping of atoms are identified to carry out the clock frequency measurement.
- Our understanding on the fate of complex biomolecules in extreme events, such as impacts, are limited. When we subjected a set of amino acids to the extreme conditions experienced in a collision, the random amino acid particles were observed to form complex three-dimensional architecture made of polypeptides.
- The absorption feature centered at 184 nm just beyond the water edge ($\sim$ 165 nm) observed in the UVIS spectra of Rhea recorded by the Cassini Spacecraft, during Rhea flyby, is now known to be from the hydrazine monohydrate molecular absorption. The occurrence of this molecule on the surface of Rhea may be due to irradiation leading to $in-situ$ synthesis and the other possibility would be from the molecular transfer from largest Saturnian moon Titan, which is next to Rhea.
- It has been shown that moonlight can bleach up to 70% of the fast component of bluelight stimulated luminescence signal, which may hamper the accuracy of ages of sediments which are only transported during nighttime.
- A technique was demonstrated to tune the higher dimensional entanglement using orbital angular momentum states of light, which might find applications in quantum information processing.
- Ultraslow light propagation to $\sim$2.8 m/s was demonstrated experimentally in ruby rod of length 7.6 cm suggesting its applications in developing the tuneable optical delay-based devices. The slowing down of light forms the basis for a quantum memory.

Awards and Honors

Faculty

A. Bhardwaj

1. 6^{th} A. P. Mitra Memorial Lecture, NPL, Delhi, September, 2020.
2. DAE – C. V. Raman Lecture of the Indian Physics Association, March 2021.

Duggirala Pallamraju

3. Elected as Vice-Chair Scientific Commission C: on "Space Studies of the Upper Atmospheres of the Earth and Planets Including Reference Atmospheres" in COSPAR for the year 2021-2024.

A.K. Singhvi

4. SK Mitra Memorial Lecture Medal by Indian National Science Academy.

S. A. Haider

5. Elected Core-member of "Programme Advisory Committee (PAC) on Earth and Atmospheric Sciences & Engineering Research Board (SERB) under DST'' for the period 2019-2022.
6. Main Scientific Organizer (MSO) of C3.2 event held in 43^{rd} COSPAR Scientific Assembly 2021, Sydney, Australia between 28 Jan-03 Feb 2021.

Shyam Lal

7. INSA KR Ramanathan Medal for the year 2020.

Srubabati Goswami

8. Received the J.C. Bose National Fellowship
9. Elected as Fellow of The World Academy of Sciences

S. Ramachandran

10. Top 2% of Scientists in the world in their respective fields (Atmospheric and Climate Science) published by Stanford University.
11. Affiliate Scholar, Institute for Advanced Sustainability Studies, Potsdam, Germany.

Nandita Srivastava

12. Nominated as Science Discipline Representative, of SCOSTEP in 2020 for 8 years

V. Sheel

13. Elected as Vice-Chair of "Sub-Commission B4: Terrestrial Planets" of COSPAR (2021-2024).

D. Banerjee

14. Member, Technical Advisory Committee for Science, Technology and Innovation (STI) Policy Funds, GUJCOST.

B.K. Sahoo

15. Listed among Top 2% of Scientists in the world in the respective research fields published in 2020 by Stanford University.
16. Invited as a panelist under "Computational Natural Sciences" to the VAIBHAV summit organized by PMO, India on 3 and 14 October, 2020.

Neeraj Rastogi

17. Nodal Faculty for Gujarat, the National Clean Air Programme (NCAP), Ministry of Environment, Forest & Climate Change, 2019 to Present.
18. Panelist of Vaishwik Bharatiya Vaigyanik (VAIBHAV) Summit; Vertical: Environmental Sciences; Horizontal: Clean Air; Session Topic: Air Pollution Management through Monitoring and Modelling, 2020.(Mode: Online)

G.K.Samanta

19. Served as the technical committee of the IEEE Photonics Conference (IPC) 2020 for last three years.
20. Served as the session chair IEEE Photonics Conference (IPC) 2020 held online during 28th September – 1st October 2020
21. Featured by Optics and Photonics News (OPN) as Optical Society of America (OSA) Senior member insight
22. Selected as the member of the Advisory panel of the Journal of Optics (JOPT), IOP, UK.

Arvind Singh

23. Young Researcher Award, Ministry of Earth Sciences, India, 2020.
24. M.S. Krishnan Medal, Indian Geophysical Union, 2020.
25. Topical Editor: Ocean Science (an EGU Journal), June 2020 – present.

A. Basu Sarbadhikari

26. Section Editor (Mineralogy, Petrology and Geochemistry of the surface of the Moon) for "Encyclopedia of Lunar Science", Springer Publishing.

Neeraj Srivastava

27. An Expert Member for ISRO- Korean Aerospace Research Institute (KARI) Space cooperation for Lunar Surface Exploration.

M. Bhatt

28. Elected as a "Vice-Chair of Sub-commission B3: The Moon" of COSPAR for the duration 2021-2024.

Vineet Goswami

29. Appointed member of the Scientific Steering Committee (SSC) of the international GEOTRACES program, 2020.

Research Fellow

Surendra Vikram Singh

30. Shock processed mixture of amino acids is selected for the consolation prize in the International Sci-Art Image Competition 2021, which was organized by INYAS in association with the National Young Academy of Bangladesh (NYAB) and Thai Young Scientists Academy (TYSA). Title of the contribution: Nature's play - Complex route from molecules to life.

Recognition, Best paper & Thesis awards

Faculty

Anil Bhardwaj

1. Member, Governing Council, Indian Institute Astrophysics, Bangalore.
2. Member, Sunanda & Satimay Basu International Early Career Award Committee of American Geophysical Union, 2021.
3. Member, Governing Council, Indian Institute of Geomagnetism, Mumbai.
4. Member, AOGS Publication Committee, 2020-2022.
5. Chairman, INSA-International Science Council Joint Committee for COSPAR, URSI and SCOSTEP.
6. Member, National Advisory Committee for the IAGA-IASPEI Joint Scientific Assembly, 21-27 August, 2021, Hyderabad.
7. Chief Guest, International Day of Light Celebration, Lucknow University, Lucknow, May 16, 2020.
8. Distinguished Speaker, Engineer's Day celebration at Ganpat University, 5 Sept. 2020.
9. Special Invited Guest, Alumni Meet on Centenary Celebration of Lucknow University, Nov. 24, 2020.
10. Chief Guest at Inaugural Program of CHASCON-2020, Punjab University, Dec. 17, 2020.
11. Chief Guest, at Science Day Celebration – 2021, Ramaiah University of Applied Sciences (RUAS), 27 Feb, 2021.
12. Book Chapter on Anil Bhardwaj: "**A Rocket to Poke Martians**", A chapter on Life and work of Anil Bhardwaj in Book "**They Made What?, They Found What?**" – Stories of Ingenious Inventions by Indian Scientists, by Shweta Taneja, Published by Hachette India, 2021.

Duggirala Pallamraju

13. Member, Local Organizing Committee for the IAGA-IASPEI, Joint Scientific Assembly, 21-27 August 2021.
14. Lead of the sub-group "Atmospheric Dynamics" Aditya-L1 Space Weather Monitoring and Prediction (ASWMP) committee, ISRO, 2020.

Srubabati Goswami

15. Member, Editorial Board, Pramana
16. Chair Person, Gender in Physics Working Group of Indian Physics Association (2021-2022)
17. Member of Executive Council, Indian Physics Association (2021-2022)
18. Member, Inter academy panel of women in science

Nandita Srivastava

19. Member, SOC of COSPAR-2020-E2.3 session: Driving solar eruptions, 29 Jan-Feb 3, 2021
20. Member, SOC of COSPAR-2020-D2.4 session on "Sun-Heliosphere connection events: Origin, Propagation, Impact and Prediction", 29 Jan-Feb 3, 2021.
21. Co-Chair, SOC, short course on "Space and atmospheric Science" organized by UN-CSSTEAP, PRL, 7-14 December, 2020.
22. Co-chair, SOC, 39^{th} annual meeting of Astronomical Society of India, 18 - 23 February, 2021
23. PI of Indo-Uzbekistan collaborative proposal on "Space Weather consequences of Coronal Mass Ejections", jointly with Dr. ZavkiddinMirtoshev, Samarkand University, Uzbekistan, sanctioned in March 2021.
24. Session Chair, session on "Physics of the Solar Dynamo & Sub-photospheric Flows in Active Regions", a one-day workshop on "Insights into Solar Active Region Dynamics" during the 39^{th} annual meeting of the Astronomical Society of India, 18 February 2021.
25. Member, Aditya-L1 Space Weather Monitoring and Prediction (ASWMP) committee by ISRO

Shibu K. Mathew

26. Session Chair, session on "Numerical simulations & Machine learning in Solar physics", a one-day workshop on "Insights into Solar Active Region Dynamics" during the 39^{th} annual meeting of the Astronomical Society of India, 18 February 2021

Bijaya.K.Sahoo

27. Convener of an International Webinar on "Fundamental Sciences & Quantum Technologies (FSQT 2020)" held at PRL, Ahmedabad, India during 28 September - 1 October, 2020.

Kuljeet. K. Marhas

28. Awarded CEFIPRA Indo-french project for 3 years on "High precision Chronology of refractory Inclusions from primitive chondrites" March 2021.

Sachindra Naik

29. Member, National Organizing Committee, DAE-BRNS High Energy Physics Symposium, NISER Bhubaneswar India, December 14-18, 2020.

30. Member, Scientific Organizing Committee, Conference on 5 years of AstroSat, ISRO Bangalore, 19-21 January, 2021.
31. External examiner for Ph.D. thesis submitted to Indian Institute of Science, Bangalore and Pondicherry University, Puducherry.

Dibyendu Chakrabarty

32. Reviewer for proposal evaluation as part of the Satellite Technology Day Celebration of URSC, 2021.
33. Member, Technical Evaluation Committees constituted by the Indian Institute of Geomagnetism, 2021.
34. Member, Peer Review Committee for science payloads in the Venus Orbiter Mission, ISRO, 2021.
35. Member, Local Organizing Committee (LOC), 2nd Indian Planetary Science Conference, February, PRL, 2021.
36. Reviewer, Payload proposal for the PS4-Orbital Platform of ISRO, 2020.
37. Reviewer, IIG's Science Programme (Space Weather-Observations and Modelling, SWOM), 2020.
38. Member, Aditya-L1 Science Working Group (ASWG), ISRO, 2020
39. Member, Aditya-L1 Space Weather Monitoring and Prediction (ASWMP) committee, and the lead author in the chapter "Ionospheric and Magnetospheric impacts", ISRO, 2020.
40. Reviewer, Gandhian Young Technological Innovation (GYTI-2019) Award, 2020.
41. Member, Working Group, Pillar 2 (Space weather and Earth's atmosphere) of the international program PRESTO (Predictability of the Variable Solar-Terrestrial Coupling), 2020.
42. Chaired a session entitled "Solar wind and heliospheric studies" in the 39^{th} ASI workshop (Workshop 6) on "Mult-payload and Multi-observatory science with Aditya-L1" on 16 February, 2021.

Ramit Bhattacharyya

43. The article entitled, "Magnetohydrodynamics model of an X-class flare in NOAA active region 12017 initiated with non-force-free extrapolation" has been featured on the cover page in Physics of Plasmas.

Lokesh Kumar Sahu

44. A review Article [Sahu, L. K., Tripathi, N., & Yadav, R. (2020). Observations of trace gases in the earth's lower atmosphere: instrumentation and platform. Current Science, 118(12), 1893. doi:10.18520/cs/v118/i12/1893-1902] was selected as a highlight ("The Air We Breathe") in the 25 June 2020 issue of Current Science.
45. Vigyan Samachar News 16.11.2020 — Environment (VS/MoES/MFA/16/11/2020) featured an article based on our paper [Dave, P. N., Sahu, L. K., & Tripathi, N. (2020). Emissions of non-methane volatile organic compounds from a landfill site in a major city of India: Impact on local air quality. Heliyon, 6(7), e04537. https://doi.org/10.1016/j.heliyon.2020.e04537.]

Som Kumar Sharma

46. Invited as a panelist for Vaishwik BharatiyaVaigyanik (VAIBHAV) Summit - 2020, Govt. of India.
47. Expert member for the review of the proposals under NASA's National PDF program (NPP) November 2020 and March 2021 review cycles.
48. Member, organizing committee for Short Course on "Space and Atmospheric Sciences" under the CSSTEAP program, during 7-14 December 2020 at PRL, Ahmedabad.
49. Member, panel of Judges for the best paper award during Symposium on Tropical Meteorology (TROPMET-2020), 14-17 December 2020, at NESAC, Shillong.
50. Member, Technical Program committee, Indian Society of Remote Sensing (ISRS)-National Symposium-2020, 18-19 December 2020 at SAC (ISRO), Ahmedabad.
51. Member, panel of Judges for the best paper award during Indian Society of Remote Sensing (ISRS) National Symposium-2020, 18-19 December 2020 at SAC (ISRO), Ahmedabad.

Shashikiran Ganesh

52. Session Chair, in the International Conference on Dust in Astrophysics (ICDA-2020), Dept. of Physics, Assam University, Silchar, India, 31 Aug - 01 Sep 2020 [ONLINE].
53. Session Chair, in "UVIT: 5 years of operation", meeting organized by IIA during 1-3 December, 2020.
54. Session coordinator for ASI Workshop on "Ultraviolet space astronomy: UVIT and beyond", 18 Feb 2021.
55. External examiner for PhD thesis submitted to Pondicherry University, March 2021.

Bhuwan Joshi

56. Session Chair, session on "Active Sun Physics", a one-day workshop on "Multi-payload and Multi-Observatory Science with Aditya-L1" during the 39^{th} annual meeting of the Astronomical Society of India, 19 February 2021

Neeraj Rastogi

57. Member of Scientific Organizing Committee of the international conference "Aerosol Air Quality, Climate Change and Impact on Water Resources and Livelihoods in the Greater Himalayas", organized by ARIES, Nainital, and HNB Garhwal University, September 14 –16, 2020.

Goutam. K.Samanta

58. The experiment on "Watt-level, ultrafast, tunable yellow source based on single-pass, fourth-harmonic generation of Cr^{2+}:ZnS laser at 2360 nm", has received great attention from the scientific community through the NEW RELEASE by OSA-Optical Society of America and the Optics and Photonics News (OPN) by OSA.

Brajesh Kumar

59. Co-chair, session on “Solar Interior: Convection, Large scale flows and Magnetism” during the IIA-50 international conference on ”Advances in Observations and Modelling of Solar Magnetism and Variability” held in online mode at the Indian Institute of Astrophysics, Bangalore, during 1-4 March 2021.
60. Appointed as an external expert by the Vice chancellor of MLS University, Udaipur, in the JRF selection committee of the Post Graduate Dept. of Physics, MLS University

Arvind Singh

61. Member, Indian National Young Academy of Sciences (INYAS), 2021-2025.
62. Member, Board of Studies, Pandit Deendayal Petroleum University, India, 2020 - present.
63. Board of Studies in the Geology Department, Gujarat University, Ahmedabad, 2019 - present.
64. Member, International Science Planning Committee of IIOSC–2020, Goa (postponed to 2021).

Manash R. Samal

65. Chair for the session “Stars, ISM and the Galaxy I”, 39th Astronomical Society of India (ASI) meeting, 18 - 23 February, 2021.

Veeresh Singh

66. Served as a subject expert panelist for PDF review at ARIES Nainital, 13th Oct 2020.

Amitava Guharay

67. Examiner for thesis submitted to Department of Astronomy, Osmania University, February 2020.

Jayesh. P. Pabari

68. Member, Local Organizing Committee, for the “2nd Indian Planetary Science Conference (IPSC-2020)”, held at PRL, 25-26, February, 2021.
69. Expert for Doctoral Admission and Dissertation Examination, GTU, Ahmedabad.

K. Durga Prasad

70. Session Chair, Geosciences session (TH4.R1), IEEE International India Geoscience and Remote Sensing Symposium (InGARSS) 2020, Ahmedabad, 1-4 Dec., 2020.
71. Executive Member, Planetary Rock Sampling Technology Project, “My Vision 2030”, DTDI, ISRO HQ.
72. Member-Secretary, “2nd Indian Planetary Science Conference (IPSC-2021”, held at PRL, 25-26, February 2021.

S. Vijayan

73. Member, Peer review committee, for the Chandrayaan-2 TMC and OHRC images.

Neeraj Srivastava

74. Science Principal Investigator, Planetary Rock Sampling Technology Project, “My Vision 2030”, DTDI, ISRO HQ.
75. Session Chair, Terrestrial planets – Geology and Surface Processes, Indian Planetary Science Conference 2021, PRL, Ahmedabad.

Megha Bhatt

76. Member, Peer review committee for the Chandrayaan-2 Imaging Infrared Spectrometer (IIRS) dataset.

Bhushit Vaishnav

77. Member, Board of Studies (BOS), Faculty of Sciences (Physics), Kadi Sarva Vishwavidyalay, Gandhinagar, from July 2020.

Rishitosh. K. Sinha

78. Member, Peer Review Committee, the Chandrayaan-2 TMC-2 and OHRC datasets.

Research Fellows

Prabir K. Mitra

79. First prize for the (online) talk entitled “Multi-wavelength Analysis and Modeling of the Largest Solar Flare in the Solar Cycle 24” during “International Workshop on Space Science”, jointly organized by Space Education and Research Foundation, Ahmedabad, and Department of Physics, School of Science, 18-21 May 2020.

K. Aravind

80. Our research article on the interstellar comet observed using two Indian observatories has been discussed as a research highlight in Nature Astronomy journal with the title ”An Interstellar Carbon Copy” doi: https://doi.org/10.1038/s41550-021-01316-0.

Sushant Dutta

81. Best poster award in the category of extragalactic astronomy for the poster titled “Population of remnant radio galaxies in deep radio surveys” 39th Annual Meeting of the Astronomical Society of India (ASI), February 18 - 23, 2021.

P. Halder

82. Best poster award for the poster “A comet dust model based on the findings from the Rosetta mission,” 39th meeting of the Astronomical Society of India, February 18-23, 2021.

Human Resource Development

Human Resource Development at PRL PRL has a strong Human Resource Development (HRD) component with Doctoral, Post-Doctoral and Visiting Scientist programs. In addition, we have an Associate program for university teachers and project training for graduate and post graduate students in both science and engineering. PRL organizes project training as a part of the curriculum for students of undergraduate and post graduate levels from Science and Engineering disciplines. The purpose is to provide the students with an insight into current research activities being pursued at PRL which they can continue even after returning to their colleges. It is also aimed at motivating them to take up research in basic sciences in their higher studies and career. Brief details of scientific output and staff in numbers during the reporting year are provided here.

This year due to pandemic the training programmes were conducted only via virtual mode in view of the safety of students and in complete adherence with various advisories issued from time to time by the State and Central Governments.

Research Programmes

One of the important aims of the laboratory is to serve as a post-graduate and post-doctoral study centre in physics, earth & planetary sciences and chemistry to train research students in various aspects of experimental and theoretical physics. With this in view, PRL offers a graduate programme through Research Fellowship leading to Ph. D. degree. PRL provides opportunities for carrying out post-doctoral research. The strength of fellows under these programmes are presented in figure 1.

Research Programmes through Externally funded schemes

PRL encourages candidates with external funding from Government agencies such as DST, CSIR, NBHM, UGC, ISRO RESPOND, etc., to carry out their research in all campuses of PRL.

Such candidates will be governed by fellowship rules of the concerned funding agencies as applicable from time to time. Such candidates will have an option to register for a Ph.D. degree in any of the institutes/universities with which PRL has an MoU with, subject to their fulfilling the required eligibility criteria and course work requirement of the concerned university/Institute. Following table summarize the ongoing externally funded projects in PRL and figure 1 give statistics of the Research Scholars/PDFs/RAs in PRL including the ones employed through the externally funded projects.

Sr. No.	Funding agency	PI	Status	Duration
1.	DST Quantum I.T Photonic Devices	R P Singh	Active	2019-2022
2.	INDO ISRAEL	R P Singh	Active	2019-2022
3.	ISRO GBP AT-CTM	S Ramachandran	Active	2007-Ongoing
4.	Indo Uzbek SWC	Nandita Srivastava	Active	2021-2024
5.	DST CEFIPRA	Kuljeet Kaur Marhas	Active	2021-2024
6.	DST CEFIPRA	Neeraj Rastogi	Active	2021-2024
7.	DST CEFIPRA	Arvind Singh	Active	2015-2021
8.	ISRO GBP I.N.M.N.	Arvind Singh	Active	2019-2022
9.	ISRO GBP I.N.M.N.	Som Kumar Sharma	Active	2019-2022
10.	ISRO GBP I.N.M.N.	Sanjeev Kumar	Active	2019-2022
11.	CARS	Goutam K Samanta	Active	2021-2023

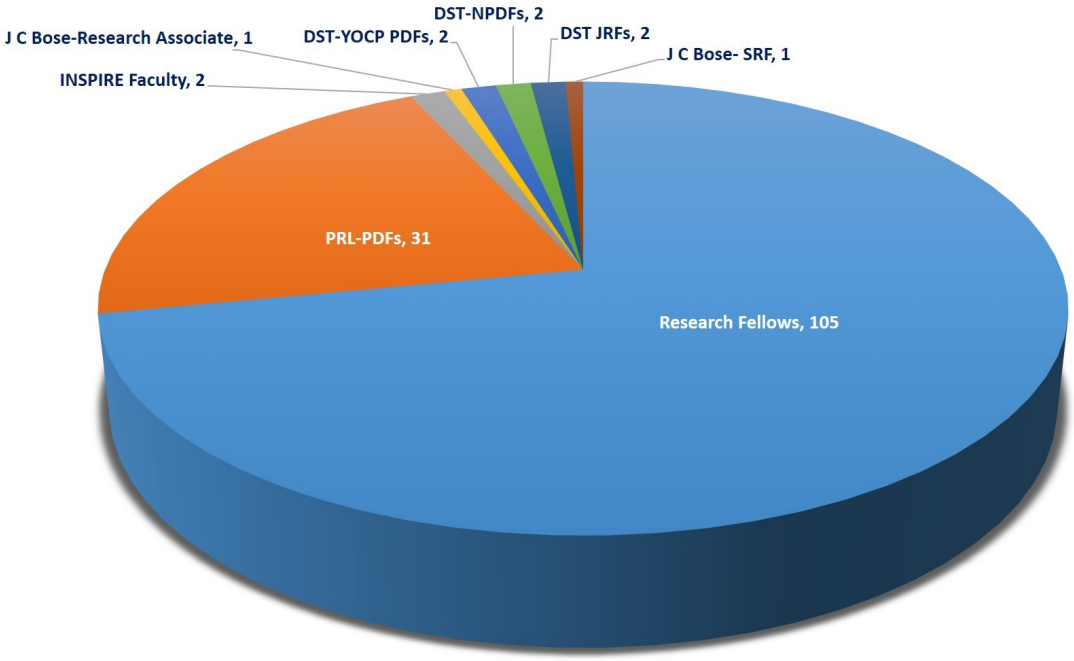

Figure 1: Research Programmes.

Training Opportunities

PRL provides project training in engineering disciplines like computer engineering, electronics & communication, instrumentation & control, information technology to graduate/post-graduate students. Details of the same are presented in figure 2.

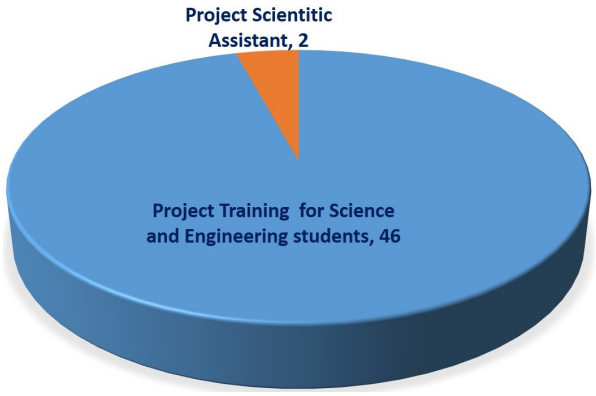

Figure 2: Internship Training Programmes.

PRL also offers training programmes in computers, electronics, library science, engineering and administrative services (Fig. 3).

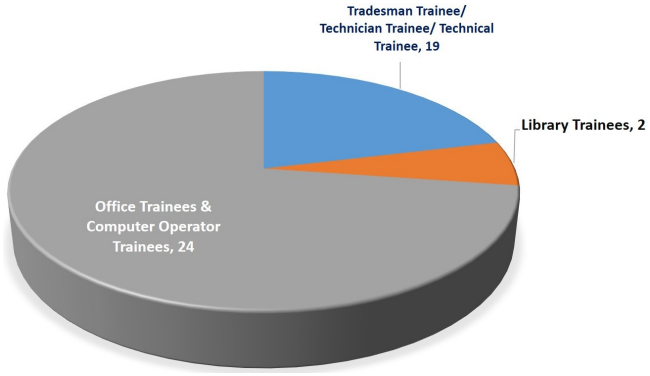

Figure 3: Training Programmes in technical and administrative areas.

Research Contributions

The research work carried out by PRL scientists are published in reputed and peer reviewed national and international journals. Few of our scientists are also invited to write review articles in the field of their specialization. Some of our scientists have also edited books.

Many of our scientists attend conferences and symposia at home and abroad where they present the results of their research investigations. Some of them are invited to present review talks. Few of them serve as chairpersons and Members of scientific committees for organizing national and International conferences and symposia. They are also invited to Convene and Chair sessions during symposia and meetings. The research output during the AY 2020-21 is shown in figure 4. All these activities were held in ONLINE mode only due to the prevailing COVID-19 situation.

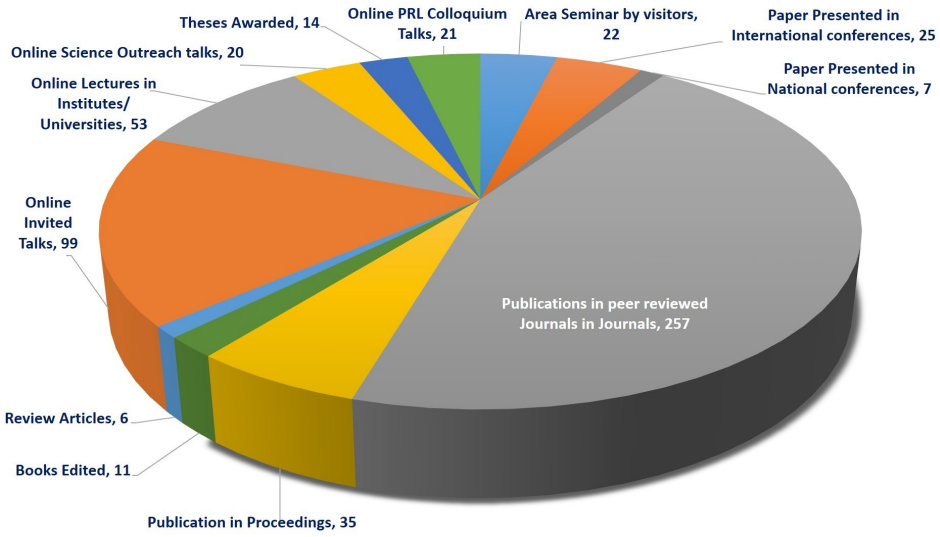

Figure 4: Research Contributions.

Administrative Support

Behind the scientific achievements of PRL is the able and efficient support given by the administrative and the technical staff. The administrative section of our laboratory continues to play an important role in providing an excellent management support to carry out our scientific activities. In addition, it also provides management support to the Solar Observatory at Udaipur and the Infrared Observatory al Mt. Abu. The staff structure of PRL is shown in figure 5.

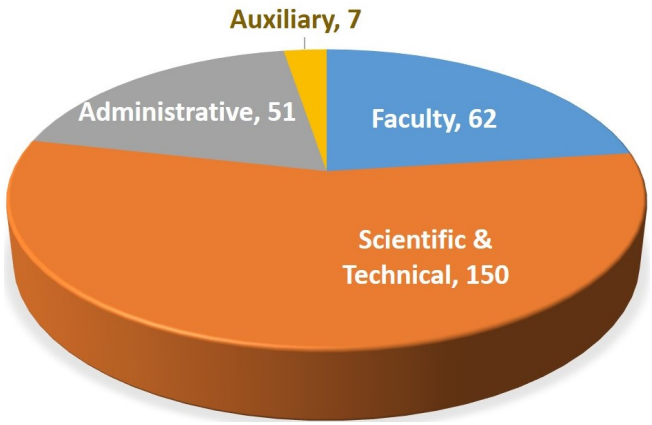

Figure 5: The distribution of PRL staff.

Research Fellowship Programme and Pre-PhD courses

PRL offers Junior Research Fellowships (JRFs) leading to a Ph.D. degree in the broad areas of ongoing research activities in PRL. Since inception of PRL around 460 research scholars have obtained their Ph.D. degree. PRL alumni have played a key role in the development of institutions and programmes in India and abroad. The Indian Space Research Organization (ISRO) was nucleated in PRL in the early seventies and two of the past ISRO Chairmen, Prof. U.R. Rao and Prof. K. Kasturirangan - are distinguished alumni of PRL. After admission to PRL, each JRF needs to undergo a prescribed pre-Ph.D. course work prior to joining the research. In consideration of the requirements of (a) various Universities / IIT, where PRL research scholars register for their Ph.D. degree, and (b) University Grants Commission guidelines, two semesters of rigorous course work is offered to JRFs. In addition, JRFs are also required to do four projects as a part of their course work. In the year 2020-21, 16 new JRFs have joined PRL and 14 SRFs have been awarded Ph.D. degree. Following

is the list of courses that were offered to the Junior Research Fellows of 2020 batch. Each course is of four credits and 40 hours of teaching.

Semester 1 courses

1. AA 601 - Fundamentals of Astronomy & Astrophysics-[Instructors: Dr. Mudit Srivastava and Dr. Vishal Joshi]
2. AMO 602 - Light-matter interaction-[Instructors: Prof. RP Singh and Dr. Rajesh Kushwaha]
3. ES 601 - Stable Isotopes in Nature-[Instructors: Dr. Amzad Laskar]
4. ES 602 - Isotope Geochemistry-[Instructors: Dr. Vineet Goswami]
5. PS 601 - Basic Cosmochemistry-[Instructors: Prof. D. Banerjee and Prof. K. K. Marhas]
6. PS 602 - Planetary Atmospheres and Environment-[Instructors: Dr. Jayesh Pabari, Dr. Durga Prasad & Prof. Varun Sheel]
7. PS 603 - Planetary Geology-[Instructors: Dr. S. Vijayan and Dr. Neeraj Srivastava]
8. SA 601 - Physics of the Earth's Lower and Middle Atmosphere-[Instructors: Prof. S. Ramachandran, Dr. Som Kumar Sharma]
9. SA 602 - Physics and Diagnostics of Near Earth Space-[Instructors: Dr. Ravindra Pratap Singh, Dr. Dibyendu Chakrabarty]
10. SP 601 - Basics of Solar Physics-[Instructors: Dr. Brajesh Kumar]
11. TH 601 - Advanced Electrodynamics-[Instructors: Prof. Srubabati Goswami]
12. TH 602 - Introduction to Quantum Field Theory-[Instructors: Dr. Satyajit Seth]
13. TH 603 - Statistical Mechanics-[Instructors: Dr. Navinder Singh]
14. FP 602 - Writing-[Instructors: Sharmita Lahiri (I+T), Jooyoung Kim (T), Dyotana Banerjee (T), Sudipta Basu (T)]

Semester 2 courses

15. RS 701 - Research Methodology-[Instructors: Prof. Varun Sheel & Dr. Naveen Chauhan]
16. AA 701 - Stellar Astrophysics and Radiative transfer-[Instructors: Dr. Lokesh Dewangan & Dr. Aveek Sarkar]
17. AA 702 - Galactic and Extragalactic Astronomy-[Instructors: Prof. Sachindra Naik and Dr. Veeresh Singh]
18. AA 703 - Instrumentation & Techniques Part A-[Instructors: Prof. Santosh Vadawale (Instrumentation : X-ray Astronomy) & Dr. Mudit Srivastava (Optical & Infrared instrumentation)]
19. AMO 701 - Experimental techniques in AMOPH-[Instructors: Dr. G K Samanta]
20. AMO 702 - Physics and Chemistry of the ISM-[Instructors: Dr. B Sivaraman]
21. AMO 703 - Theoretical methods for atomic spectroscopy-[Instructors:Prof. B. K. Sahoo]
22. ES 701 - Geochemical Methods and Applications-[Instructors: Dr. A K Sudheer and Dr. A D Shukla]
23. ES 702 - Paleoclimate studies-[Instructors: Prof. Ravi Bhushan and Prof. M G Yadava]
24. ES 703 - Aerosol Characterization & Aquatic and Terrestrial Biogeochemistry-[Instructors: Dr. Neeraj Rastogi and Dr. Arvind Singh]
25. PS 701 - Physical and Chemical Processes in Planetary Atmospheres-[Instructors: Prof. Varun Sheel & Dr. Sanjay Kumar Mishra]
26. ES 702 - Paleoclimate studies-[Instructors: Prof. Kuljeet Kaur Marhas & Dr. Amit Basu Sarbadhikari]
27. PS 703 - Planetary Geology and Geophysics-[Instructors: Dr. Megha Bhatt & Dr. Karanam Durga Prasad]
28. SA 701 - Aerosols, trace gases, and radiative effects-[Instructors: Prof. S. Ramachandran and Dr. Narendra Ojha]
29. SP 702 - Coronal and heliospheric processes-[Instructors: Dr. Som Kumar Sharma and Dr. Amitava Guharay]
30. SA 703 - Ionospheric and thermospheric dynamics, processes and space weather-[Instructors: Prof. Dibyendu Chakrabarty]
31. SP 701 - Solar magnetohydrodynamics-[Instructors: Dr. Ramit Bhattacharyya]
32. SP 702 - Coronal and heliospheric processes-[Instructors: Dr. Bhuwan Joshi and Dr. Girjesh Gupta]
33. SP 703 - Instrumentation and diagnostic techniques-[Instructors: Dr. Rohan Eugene Louis]
34. TH 701 - GTR + Cosmology-[Instructors: Dr. Ketan M. Patel]
35. TH 702 - Particle physics-[Instructors: Dr. Partha Konar]
36. TH 703 - Advanced Quantum Field Theory-[Instructors: Prof. Namit Mahajan]

List of projects done by JRF of 2020 batch are as follows:

Ayush Joshi

1. "Applications of Microwave Remote Sensing in Planetary Sciences: Case study on SHAllow RADar (SHARAD) onboard Mars Reconnaissance Orbiter", Semester 2 project, from January, 2021 to May, 2021, [Supervisior: Dr. Neeraj Srivastava & Mr. Rajiv Ranjan Bharti, Division: Planetary Sciences].

Ananya Rawat

2. "Photometry using IRAF", Semester 2 project, from January, 2021 to May, 2021, [Supervisior: Dr Shashikiran Ganesh, Division: Astronomy and Astrophysics].

Trinesh Sana

3. "Parametric Study of Schumann Resonance on Mars", Semester 2 project, from January, 2021 to May, 2021, [Supervisior: Dr. Jayesh P. Pabari, Division: Planetary Sciences].

Sandeep Kumar

4. “Ionospheric Storms”, Semester 2 project, from January, 2021 to May, 2021, [Supervisior: Prof. Dibyendu Chakrabarty, Division: Space and Atmospheric Sciences Division].

Shikhar Dubey

5. “Estimation of the fossil fuel component in atmospheric CO_2 in Ahmedabad based on radiocarbon measurements”, Semester 2 project, from January, 2021 to May, 2021, [Supervisior: Dr. Amzad Hussain Laskar, Division: Geosciences].

Debashis Pachhar

6. “Event Generation and Physics at the LHC using MADGRAPH5”, Semester 2 project, from January, 2021 to May, 2021, [Supervisior: Dr. Partha Konar, Division: Theoretical Physics].

Sudhanshu

7. “Estimating the contributions of CO_2 from different sources in air in Ahmedabad using stable carbon and oxygen isotope ratios”, Semester 2 project, from January, 2021 to May, 2021, [Supervisior: Dr. Amzad Hussain Laskar, Division: Geosciences].

Arup Kumar Maity

8. “Study of gas kinematics toward massive star-forming sites IRAS 17008-4040 and IRAS 17009-4042”, Semester 2 project, from January, 2021 to May, 2021, [Supervisior: Dr. Lokesh Kumar Dewangan, Division: Astronomy and Astrophysics].

Chandrima Shaw

9. “Sr isotopic composition of the Girna river waters: implication to weathering in the catchment”, Semester 2 project, from January, 2021 to May, 2021, [Supervisior: Dr. Vineet Goswami, Division: Geosciences].

Kamran Ansari

10. “Validation and inter-comparison of reanalysis datasets over Indian region”, Semester 2 project, from January, 2021 to May, 2021, [Supervisior: Dr. Narendra Ojha, Division: Space and Atmospheric Sciences Division].

Gurucharan Mohanta

11. “Dark Matter”, Semester 2 project, from January, 2021 to May, 2021, [Supervisior: Prof. Srubabati Goswami, Division: Theoretical Physics].

Mansi Gupta

12. “Concept of air-sea exchange of trace constituents”, Semester 2 project, from January, 2021 to May, 2021, [Supervisior: Dr. Lokesh Kumar Sahu, Division: Space and Atmospheric Sciences Division].

Dharmendra Kumar Kamat

13. “Spectroscopic Measurement of Mesosphere Temperatures using Hydroxyl (OH) Airglow Emission”, Semester 2 project, from January, 2021 to May, 2021, [Supervisior: Dr. R. P. Singh, Division: Space and Atmospheric Sciences Division].

Aditya Das

14. “Jezero Western Delta lithostratigraphy & Evolution”, Semester 2 project, from January, 2021 to May, 2021, [Supervisior: Dr. Vijayan S., Division: Planetary Sciences].

Sanjay Baliwal

15. “Ultra-violet Excess in Asymptotic Giant Branch (AGB) Stars”, Semester 2 project, from January, 2021 to May, 2021, [Supervisior: Dr. Mudit K. Srivastava, Division: Astronomy and Astrophysics].

Akanksha

16. “Evaluation of atmospheric boundary layer over Ahmedabad region”, Semester 2 project, from January, 2021 to May, 2021, [Supervisior: Dr. Som Kumar Sharma, Division:Space and Atmospheric Sciences Division].

Arup Chakraborty

17. “Spectroscopic Technique and Data Collection”, Semester 2 project, from January, 2021 to May, 2021, [Supervisior: Dr. Bhalamurugan Sivaraman, Division: Atomic, Molecular and Optical Physics].

Wafikul Khan

18. “Different Quantum Cryptography Protocols and Their Advantages”, Semester 2 project, from January, 2021 to May, 2021, [Supervisior: Prof.R.P Singh, Division: Atomic, Molecular and Optical Physics].

Malika Singhal

19. “Rotation sensitive measurements in a free space resonant Sagnac interferometer”, Semester 2 project, from January, 2021 to May, 2021, [Supervisior: Dr. G. K. Samanta, Division: Atomic, Molecular and Optical Physics].

Ph.D. Awarded

[**PRL students/project associates/employees**]

1. **Siddhi Y. Shah**

   "Chemistry and modeling of lower atmosphere of Mars", Pacific University, Udaipur, 03-07-2020, . [Supervisor: S. A. Haider]

2. **Anil A. Patel**

   "Oxidative Potential of Ambient Aerosols over Different Regions in India", Mohanlal Sukhadia University, Udaipur, 16-09-2020, . [Supervisor: Neeraj Rastogi]

3. **Pullabhatla Kiran Kumar**

   "Paleomonsoon Reconstruction using Marine Proxies of the Indian Ocean", Mohanlal Sukhadia University, Udaipur, 13-10-2020, . [Supervisor: M.G. Yadava]

4. **Akanksha Bhardwaj**

   "Probing New Physics with hadronic final states at the Large Hadron Collider", Indian Institute of Technology, Gandhinagar, 27-11-2020, . [Supervisor: Partha Konar]

5. **Ranadeep Sarkar**

   "On the Solar Origin of Space Weather", IIT Gandhinagar, 01-12-2020, . [Supervisor: Nandita Srivastava]

6. **Balbeer Sigh**

   "Dynamics of heavy quarks in a medium", Indian Institute of Technology, Gandhinagar, 04-12-2020, . [Supervisor: Hiranmaya Mishra]

7. **Prashant Kumar**

   "Laser Induced Breakdown Spectroscopy Utilising Synthetic Spectrum Method for Optically Thick Plasmas", IIT Gandhinagar, 22-12-2020, . [Supervisor: R.P.Singh]

8. **Harsh Oza**

   "Understanding Hydrometeorological Processes Concerning Indian Precipitation: Insights from Oxygen and Hydrogen Stable Isotopes in Conjunction with Meteorological Parameters", Indian Institute of Technology, Gandhinagar, 23-12-2020, . [Supervisor: R.D. Deshpande]

9. **Shefali Uttam**

   "An Investigation of Martian Dust Devil Characteristics", IIT Gandhinagar, 22-01-2021, . [Supervisor: V. Sheel]

10. **Masoom P. Jethwa**

    "Investigation of thermal emission from lower atmosphere of Mars", Pacific University, Udaipur, 27-01-2021, . [Supervisor: S. A. Haider]

11. **Shivangi Gupta**

    "Understanding the properties of accretion powered Be/X-ray binary pulsars", Indian Institute of Technology Gandhinagar, Gandhinagar, 10-02-2021, . [Supervisor: Sachindra Naik]

12. **Harsh Raj**

    "High resolution paeloclimatic studies using corals", Indian Institute of Technology, Gandhinagar, 17-02-2021, . [Supervisor: R. Bhushan]

13. **Kaustav Chakraborty**

    "Phenomenology of Neutrino Oscillations and Masses", Indian Institute of Technology, Gandhinagar, 24-02-2021, . [Supervisor: Srubabati Goswami]

14. **Nidhi Tripathi**

    "Emission and atmospheric variability of volatile organic compounds over the Indian subcontinent and surrounding oceanic regions", IIT, Gandhinagar, 09-03-2021, . [Supervisor: Lokesh Kumar Sahu]

Colloquia/Public Lectures by Visitors

1. **Prof. Andrew Forbes**
   University of the Witwatersrand, South Africa
   Shaping Waves, 23 September 2020, PRL Student Chapter Public Lecture

2. **Prof. Bobby K Antony**
   Department of Physics, Indian Institute of Technology (Indian School of Mines), Dhanbad, India
   Electron and positron scattering from molecules 28 October 2020

3. **Dr. Mudit Srivastava**
   Physical Research Laboratory, Ahmedabad
   Search for Symbiotic Systems: The ASTROSAT Revelation 21 October 2020

4. **Dr. Neeraj Srivastava**
   Physical Research Laboratory, Ahmedabad
   Discovery of Recent Volcanism on the Moon 07 October 2020

5. **Dr. Girjesh R. Gupta**
   Physical Research Laboratory, Ahmedabad
   Role of waves and small-scale transients in the coronal heating 25 November 2020

6. **Dr. Lokesh Kumar Dewangan**
   Physical Research Laboratory, Ahmedabad
   New insights into the formation of massive stars 18 November 2020

7. **Dr. Satyajit Seth**
   Physical Research Laboratory, Ahmedabad
   Precision @ LHC 11 November 2020

8. **Dr. Dibyendu Chakrabarty**
   Physical Research Laboratory, Ahmedabad
   Space weather: From anomaly to insights 04 November 2020

9. **Prof. S. Gurubaran**
   Indian Institute of Geomagnetism, Navi Mumbai
   Internal Bores in the Mesosphere: A manifestation of Atmospheric Gravity Waves 23 December 2020

10. **Prof. Dipankar Banerjee**
    Aryabhatta Research Institute of Observational Sciences (ARIES), Nainital, Uttarakhand
    Long term study of the Sun using the Kodaikanal Digitised archive 16 December 2020

11. **Prof. Pankaj Joshi**
    International Center for Cosmology (ICC), CHARUSAT University, Anand
    Beyond Penrose - Blackholes and Spacetime Singularities 09 December 2020

12. **Prof. Praveen Nahar**
    National Institute of Design (NID), Ahmedabad
    Design Thinking and Innovation 27 January 2021

13. **Dr. Mrutyunjay Mohapatra**
    India Meteorological Department (IMD), Govt. of India, New Delhi
    Weather Forecasting in India : Current status and future plan 20 January 2021

14. **Prof. Ravi Shankar Nanjundiah**
    Indian Institute of Tropical Meteorology, Pune
    Variability of Monsoons at Different Scales 06 January 2021

15. **Prof. Srubabati Goswami**
    Physical Research Laboratory, Ahmedabad
    Neutrinos: the invisible messengers 11 February 2021, 3rd PRL-IAPT Dr. Vikram Sarabhai Lecture

16. **Dr. Bhaskar Mukherjee**
    School of Physics, The University of Sydney, Australia and Institute of Radiation Medicine of Helmholtz Institution, Munich, Germany
    Radiation Dosimetry and Radiation Protection in Space Missions 03 February 2021

17. **Prof. Devesh K Sinha**
    Department of Geology, Centre of Advanced Study, Delhi University
    Paleobiogeographic and biostratigraphic evidences for role of Ocean gateways in changing ocean circulation and global climate during Cenozoic 24 March 2021

18. **Prof. Tanusri Saha-Dasgupta**
    Department of Condensed Matter Physics and Materials Science S.N. Bose National Centre for Basic Sciences, Salt Lake, Kolkata

Electrons in Complex Materials: from Theory to Practice 17 March 2021

19. **Prof. Bimla Buti**
    Centre for Science and Society, Buti Foundation, New Delhi
    Coherence, Chaos and Turbulence in Plasmas 03 March 2021

20. **Prof. Alexander Tielens**
    Astronomy Department, Leiden University and University of Maryland
    The Molecular Universe 02 December 2020

21. **Prof. Mohit Randeria**
    The Ohio State University, Columbus, United States
    Are there Upper Bounds on the Superconducting Transition Temperature? 13 January 2021

22. **Dr. Archana Sharma**
    The CERN Laboratory in Geneva, Switzerland
    Unlocking secrets of the Universe at CERN 31 March 2021, 1^{st} Dr. Bibha Chowdhuri Memorial Lecture

Conference/Symposium/Workshop organized by PRL

Solar Physics

1. "Insights into Solar Active Region Dynamics", A one-day workshop organized jointly with IIA, Bengaluru and IIT-BHU, during the 39^{th} annual meeting of the Astronomical Society of India jointly organized by ICTS-TIFR Bengaluru, IISER Mohali, IIT Indore and IUCAA Pune, India, in online mode ASI, 18 February, 2021.

Planetary Sciences

2. "2^{nd} Indian Planetary Science Conference (IPSC-2021)", Physical Research Laboratory, 25-26, February, 2021 (via online).

Space and Atmospheric Sciences

3. "UN-CSSTEAP course on Space and Atmospheric Sciences", 7-14 December 2020 [held online].

Atomic, Molecular and Optical Physics

4. "Astrobiology Webinar", PRL, Ahmedabad, 2 June - 1 September,2020.
5. "SCOP-the Students' conference in optics and photonics", PRL Ahmedabad, 23-25 September, 2020 (Online).
6. "Fundamental Sciences and Quantum Technologies (FSQT 2020)", PRL, Ahmedabad, 28 September - 1 October, 2020 (Online).

Invited Talks at Conference / Symposia / Workshops

Keeping with the COVID-19 guidelines almost all the Conference / Symposia / Workshops were held in Online mode. All the invited talks listed below have been delivered online.

Astronomy and Astrophysics

Shashikiran Ganesh

1. "Recent observations of astrophysical dust", International Conference on Dust in Astrophysics (ICDA-2020), Assam, Silchar, Mode: ONLINE, 1 September 2020.
2. "Spectroscopy of comets from the HCT", 20 Years of Himalayan Chandra Telescope, Bangalore, Mode: ONLINE, 30th Sep 2020.
3. "Minor bodies and their composition", 39th meeting of the Astronomical Society of India, Mode: ONLINE, 18 — 23 February 2021.

Vishal Joshi

4. "Exploration of the cataclysmic variables and symbiotic stars through ILMT", science with International Liquid Mirror Telescope (ILMT), ARIES Nainital, India, Mode: ONLINE, 28 June 2020.
5. "Exploration of the cataclysmic variables and symbiotic stars through ILMT", Virtual International Conference on PHYSICAL SCIENCES (ICPS-2021), Sardar Vallabhbhai National Institute of Technology, India, Mode: ONLINE, 6 February 2021.

Sachindra Naik

6. "X-ray pulsations at the lowest luminosity of Be/X-ray binary pulsar EXO 2030+375 with AstroSat", 5 years of AstroSat, ISRO, Mode: ONLINE, 19 — 21 January 2021.

Manash R. Samal

7. "Unveiling properties and evolutionary status of five Galactic open star clusters with GAIA", Gaia Symposium: DR2 and Beyond, Mode: ONLINE., 4th Nov 2021.
8. "Star Formation, Exoplanets and Solar System Bodies: An INSIST Perspective", Ultraviolet Space Astronomy : UVIT and Beyond, Mode: ONLINE., 18th Feb 2021.

Santosh Vadawale

9. "X-ray Astronomy: Techniques and Telescopes", MPCST Winter School in Observational Astronomy, IIT Indore. Mode: ONLINE, 1 — 12 Feb 2021.

Mithun N. P. S.

10. "Coronal studies with X-ray payloads on-board Aditya-L1", IIA Golden Jubilee Conference on Advances in Observations and Modeling of Solar Magnetism and Variability, Bangalore. Mode: ONLINE, 1 — 4 March 2021.
11. "Prospects of microflare studies with Aditya-L1 a Multi-payload and Multi-Observatory", 39th meeting of Astronomical Society of India, Mode: ONLINE, 18 — 23 Feb 2021.
12. "Soft X-ray Spectroscopy of the Sun with Chandrayaan-2 XSM", Aditya Science Working Group Meet, Mode: ONLINE, 12 August 2020.

Sushant Dutta

13. "Search and Characterization of Remnant Radio Galaxies with SKA Pathfinders", International conference on a new window on the radio emission from galaxies, clusters and cosmic web : Current status and new perspectives, Mode: ONLINE, 8 — 11 March 2021.

Arghajit Jana

14. "Accretion Properties of Black Hole Candidate MAXI J1348-630", 43rd COSPAR Assembly, Mode : ONLINE, 31 January 2021.

Abhijit Kayal

15. "AstroSat/LAXPC hard X-ray observations of Compton-thick AGN Circinus galaxy", 5 year of AstroSat conference, ISRO. Mode: ONLINE, 19 — 21 January 2021.
16. "AstroSat/LAXPC hard X-ray observations of Compton-thick AGN Circinus galaxy", 39th annual meeting of Astronomical Society of India, Mode: ONLINE., 8 — 23 February, 2021.

Vipin Kumar

17. "The symbiotic nature of SU Lyn :Confirmation from UVIT spectroscopy", UVIT: 5 Years Of Operation, Bengaluru. Mode: ONLINE, December 2020.
18. "Optical and Near-Infrared spectroscopy studies of a very slow nova V2891 Cyg", 39th Annual Meeting of Astronomical Society of India, Mode: ONLINE, 18-23 February 2021.

Neeraj Kumari

19. "Correlation between UV/optical and X-rays in Mrk 509", 39th Astronomical Society of India Meeting, Mode: ONLINE, 18 — 23 Feb 2021.

Solar Physics

B. Joshi

20. "Signatures of 3D magnetic reconnection in circular ribbon flares", IIA-50 international conference on Advances in Observations and Modelling of Solar Magnetism and Variability (online mode), Indian Institute of Astrophysics, Bangalore, 1 - 4 Mar, 2021.
21. "Outstanding Problems in Solar Flares and Particle Acceleration – Observational perspective", The Second Aditya-L1 Science Meet, SSPO, 17 Dec, 2020.
22. "Solar flares and associated phenomena: Multi-wavelength investigations", Aditya-L1 Science Working Group (SWG) meeting, online, 13 May, 2020.

B. Kumar

23. "USO's contribution to GONG Program", Celebrating 25 years of GONG @ USO-PRL" held in online mode on the occasion of Udaipur Solar Observatory Foundation Day, PRL/USO, Udaipur, 20 Sept, 2020.

Nandita Srivastava

24. "Space Weather Prediction: Solar Perspective", short course on "Space and atmospheric Science" organized by UN-CSSTEAP, PRL Ahmedabad, 7 — 14 Dec, 2020.
25. "Research Areas in Space Sciences", ISRO Academia Day, online, 7 Jan, 2021.

R. Bhattacharyya

26. "Exploring coronal magnetic structures related to solar eruptive events: Aditya-L1 perspective", a one-day workshop "Multi-payload and Multi-Observatory Science with Aditya-L1" during the 39^{th} annual meeting of the Astronomical Society of India jointly organized by ICTS-TIFR Bengaluru, IISER Mohali, IIT Indore and IUCAA Pune, India, online, 19 Feb, 2021.
27. "On modeling and simulation of coronal magnetic structures: coronal transients", IIA-50 international conference on Advances in Observations and Modelling of Solar Magnetism and Variability (online mode), Indian Institute of Astrophysics, Bangalore, 1 — 4 Mar, 2021.
28. "The solar coronal field extrapolation: Background and Applications", Aditya Science Meet Discussion,, online, 20 Apr, 2020.
29. "Outstanding Problems in Solar Flares and Particle Acceleration – Theory & modeling perspective", The Second Aditya-L1 Science Meet, 17 December, 2020., SSPO, 17 Dec, 2020.

R. E. Louis

30. "Structure of the Sun and Inferring Physical Conditions in the Solar Atmosphere", two lectures during short course on "Space and atmospheric Science" organized by UN-CSSTEAP, PRL Ahmedabad, 7 — 14 Dec, 2020.

S. K. Mathew

31. "Ground and Space based solar observatories and Instrumentation", at High-End workshop on "Solar Activities and their Influences in the Heliosphere and Planetary Atmospheres", NIT, Calicut, 9 Mar, 2021.

G. R. Gupta

32. "Heating of small-scale loops by solar UV bursts", 39^{th} meeting of the Astronomical Society of India jointly organized by ICTS-TIFR Bengaluru, IISER Mohali, IIT Indore and IUCAA Pune, India, Online, 18 — 23 February, 2021.
33. "Study of sunspot waves and oscillations with SUIT/Aditya-L1", 2^{nd} SUIT science meeting, IUCAA, Pune, 11 — 13 Jan, 2021.

A. Ambastha

34. "An overview of Solar physics", High-End workshop on "Solar Activities and their Influences in the Heliosphere and Planetary Atmospheres", NIT, Calicut, 8 — 14 March, 2021.

Planetary Sciences

A. Basu Sarbadhikari

35. "Character of the lunar mantle", "Lunar Composition", a web event, organized by Dr. Deepak Dhingra, Assistant Professor, IIT Kanpur, IIT Kanpur, 16 May 2020.

D. Banerjee

36. "Discovery of water in inner solar system", National Workshop on Solar activities and their influences in the Heliosphere and Planetary Atmosphere, National Institute of Technology, Calicut, 8 — 14 March 2021.

K. Durga Prasad

37. "Monitoring Solar spectral irradiance at Mars and Venus by using an EUV instrument onboard future missions", 43^{rd} COSPAR Scientific Assembly 2021, Sydney, Australia, 28 Jan — 03 Feb 2021.

S. A. Haider

38. "Analysis of high altitude ionopause like boundaries observed from LPW onboard MAVEN", 43^{rd} COSPAR Scientific Assembly 2021, Sydney, Australia, 28 Jan − 03 Feb 2021.

K. Acharyya

39. "Formation Of Water In The Star-Forming Regions Of Low Metallicity Galaxies", 43^{rd} COSPAR Scientific Assembly 2021, Sydney, Australia, 28 Jan − 03 Feb 2021.
40. "A New Route For The Formation Of Molecules In The Astronomical Environment", 43^{rd} COSPAR Scientific Assembly 2021, Sydney, Australia, 28 Jan − 03 Feb 2021.
41. "The Universe as a Giant Laboratory : The Making of Complex Molecules from Atoms", 'Astronomical Soceity of India Meeting 2021' in Workshop 1 titled "Computational Astrophysics: An emerging Avenue for Indian Astronomy Community", Ahmedabad, 18 Feb 2021.

N. Srivastava

42. "Lunar Volcanism and its flavors", Lunar Science meet (Web Event), IIT Kanpur & Space Science Programme Office (SSPO), ISRO HQ, 15 May 2020.

R. R. Mahajan

43. "Indian sample curation and processing facility", 2^{nd} Indian Planetary Science Conference, PRL, Ahmedabad, 25−26 Feb 2021.

Sanjay K. Mishra

44. "A Brief Discussion on the Electrostatics of the Moon", 5^{th} Mini Moon Seminar Series, Taiwan Space Union., Taiwan Space Union, NCU, Taiwan, 19 Feb 2021.

S. Vijayan

45. "Planetary remote sensing study of Mars/Moon through Impact craters", CSIR-SUMMER RESEARCH TRAINING PROGRAMME-2020, CSIR-NEIST, 09, 16 & 23 July 2020.

V. Sheel

46. "Recent developments in Planetary Sciences", Lead talk in technical session on Planetary and Astronomical remote sensing, ISRS-ISG National Symposium (ISRSNS2020), Space Application Center, Ahmedabad, 19 Dec 2020.
47. "Odd Oxygen Photochemistry of Martian Atmosphere and the Role of Dust", Subsession C3.2, 43^{rd} COSPAR Scientific Assembly 2021, Sydney, Australia, 28 Jan − 03 Feb 2021.

M. Bhatt

48. "Determining Composition - Challenges with Vis-NIR Data", 5^{th} Lunar science meeting, IIT Kanpur, 16 May 2020.

J. P. Pabari

49. "Lunar Escape Process due to Micrometeorite Bombardment", Venus Science Working Group, ISRO Forum, SSPO, ISRO HQ, 24 April 2020.

A. Bhardwaj

50. "Indian Mars Orbiter Mission", Virtual Mini-Symposium on "Mars: 2020 and Beyond", Center for Space Science at NYU Abu Dhabi and the UAE Space Agency, 21 July 2020.
51. "Indian Planetary Missions and Science", 43^{rd} COSPAR Scientific Assembly 2021, Sydney, Australia, 28 Jan − 03 Feb 2021.

Space and Atmospheric Sciences

Shyam Lal

52. Webinar on "Developments in Atmospheric Chemistry in India and Future Directions", organised by Indian National Science Academy (INSA) (Ahmedabad Local Chapter) and Gujarat Science Academy (GSA), 24 Dec, 2020.

Dibyendu Chakrabarty

53. "Aditya Solar wind Particle Experiment", in the session "Aditya-L1 Mission: Instruments and Science" in the IIA-50 conference on the "Advances in Observation and Modelling of Solar Magnetism and Variability", IIA, Bengaluru (online), 1-4 Mar, 2021.
54. "Plenary talk on "Why are in-situ measurements from Aditya-L1 important?", 34^{th} annual meeting of the Astronomical Society of India (ASI), ASI, 18 - 23 Feb, 2021.
55. "Space instrumentation", to the participants of A short course on Space and Atmospheric Science organized by The Center for Space Science and Technology Education in Asia and Pacific (CSSTEAP, affiliated to the United Nations), PRL, Ahmedabad, 07-14 Dec, 2020.

Duggirala Pallamraju

56. "Small satellite constellation for ionospheric/thermospheric magnetospheric studies for space weather investigations", in Online meeting on space weather research using small satellite constellations, organized by the Space Science Programme Office, ISRO HQ, 22 Sept, 2020.
57. "The Earth's ionosphere, thermosphere, magnetosphere, and their response to solar influences", delivered on 9 Dec, 2020 during UN-CSSTEAP course on Space and Atmospheric Sciences, PRL, Ahmedabad (held online), 7-14 Dec, 2020.
58. "New directions in Space Research", delivered on 22 Jan, 2021 in Brainstorming webinar on Threshold Areas in Atmospheric, Space, and Planetary Sciences, Space Physics Laboratory, VSSC, 21, 22 and 25 Jan, 2021.

Lokesh Kumar Sahu

59. "Emission and photochemical processes of VOCs in urban and suburban regions of in winter", Northern India Air Pollution Meeting, Webinar, hosted by JAMSTEC, Japan and IIT Kanpur, 23-24 Aug, 2020.
60. "Air-sea exchange of volatile organic compounds (VOCs) over the Arabian Sea", SOLAS Indian Ocean online meeting, IITM, Pune, 30 Sept, 2020.

Narendra Ojha

61. "Gaseous pollutants and photochemical box modelling", to the participants of the Training Program on Modelling Air quality and Hydro-meteorological Extremes over Indian Megacities (approved by AICTE), IIT Madras (online), 23 Mar, 2021.
62. "Modelling of atmospheric chemistry and dynamics over South Asia: Challenges and opportunities", to the participants of the International Workshop on ICTP Regional climate Model: Applications over South Asia CORDEX domain, Dibrugarh University, Assam (online), 27 Feb, 2021.

S. Ramachandran

63. "Ozone: Past, Present and Future", International Ozone Day, Gujarat Science City, Ahmedabad, 16 Sept, 2020.
64. "Aerosols and Climate Change", 1^{st} Virtual Winter School on Climate Change: Past-Present-Future, Madurai Kamaraj University, Madurai, 18-27 Nov, 2020.
65. "Trends in Atmospheric Parameters", 1^{st} Virtual Winter School on Climate Change: Past-Present-Future, Madurai Kamaraj University, Madurai, 18-27 Nov, 2020.
66. "Ozone: Past, Present & Future", 1^{st} Virtual Winter School on Climate Change: Past-Present-Future, Madurai Kamaraj University, Madurai, 18-27 Nov, 2020.
67. "Aerosols and Monsoon Rainfall", TROPMET 2020 – National Symposium on "Weather and Climate Services over Mountainous Regions", NESAC, Shillong, 14-17 Dec, 2020.
68. "Atmospheric Composition and Chemistry", UN-CSSTEAP Online Short Course on "Space and Atmospheric Science", PRL, Ahmedabad (online), 7-14 Dec, 2020.
69. "Aerosols and Climate Impacts", UN-CSSTEAP Online Short Course on "Space and Atmospheric Science", PRL, Ahmedabad (online), 7-14 Dec, 2020.
70. "Global Warming and Climate Change", National Science Day, PRL, Ahmedabad, 29 Feb, 2020.

Som Kumar Sharma

71. "Lidar and Satellite-based Observations of the Earth's Atmosphere", UN-CSSTEAP Online Short Course on "Space and Atmospheric Science", PRL, Ahmedabad (online), 10 Dec, 2020.
72. "Investigation of Atmospheric Clouds and Boundary Layer over India using Ground-based Lidar", TROPMET-2020, NESAC (ISRO), Shillong, 14-17 Dec, 2020.
73. "Earth's Atmospheric Climate Change: Science and Society", National Symposium on "Remote Sensing for Environment Monitoring & Climate Change Assessment: Opportunities and Challenges", conducted by ISRS at SAC, Ahmedabad, 18-19 Dec, 2020.

Amitava Guharay

74. "Intraseasonal oscillations in the middle atmosphere from an equatorial station", International Symposium on Physics, Federal University of Campina Grande, Campina Grande, Brazil. (online), 15-18 Dec, 2020.
75. "Upper, Middle, Lower atmospheric dynamics and coupling", for short course on Space and Atmospheric Science, conducted by PRL under the auspices of Center for Space Science and Technology Education in Asia and the Pacific (CSSTEAP), affiliated to the United Nations, Mode: Online, PRL, Ahmedabad, 07-14 Dec, 2020.

Geosciences

N. Rastogi

76. "Brown Carbon Aerosols Characteristics over the Indo-Gangetic Plain", International conference on 'Aerosol Air Quality, Climate Change and Impact on Water Resources and Livelihoods in the Greater Himalayas' organized by ARIES, Nainital, and HNB Garhwal University, Mode: Online, 14 - 16 Sept, 2020.
77. "Oxidative Potential of Ambient Aerosols over North India: Linking Particulate Pollution and Human Health", International meeting 'Northern India Air Pollution Meeting (NIAPM)' organized by JAMSTEC, Yokohama, Japan, Mode: ONLINE, 23 - 24 August, 2021.

A. Singh

78. "Nitrogen Cycling in the northern Indian Ocean", MoES Webinar Series, Mode: ONLINE, 15 Sept., 2020.
79. "Bioavailable Nitrogen Inputs in the Northern Indian Ocean", SOLAS Indian Ocean Meeting, Mode: ONLINE, 30 Sept., 2020.
80. "Estimating the loss of Himalayan glaciers under global warming using the δ^{18}O-salinity relation in ocean", 57^{th} Annual Convention of Indian Geophysical Union, Mode: ONLINE, 3 February, 2021.

A.H. Laskar

81. "Paleoclimate reconstruction using stable isotopes in natural archives", Webinar series 'Emerging Areas of Research in Quaternary Science' organized by Association of Quaternary Research India, Mode: ONLINE, 7 Sept., 2020.

Theoretical Physics

Hiranmaya Mishra

82. "Color superconductivity in dense matter: an NJL model approach", Nambu Centennial Symposium at Univ of Hyderabad, Univ of Hyderabad, 20 Jan 2021.
83. "Matter under extreme conditions", Workshop on Astroparticle Physics and cosmology, Department of Physics, National Institute of Technology, Meghalay, NIT, Meghalay, 12 - 16 March 2021.

Srubabati Goswami

84. "Beyond Standard Model Physics at ICAL", Outlook for INO, IICHEP and beyond, ONLINE, 19 - 20 Feb 2021.

Satyajit Seth

85. "Compact Analytic Results for Higgs+4-partons One-Loop Amplitudes", High Energy Physics group of Michigan State University, Michigan, USA, 29 Oct 2020.

S. Mohanty

86. "Ultra light dark matter", Less Travelled Path of Dark Matter: Axions and Primordial Black Holes, ICTS, Bengaluru, 13 Nov 2020.

Navinder Singh

87. "An introduction to unconventional superconductivity", Current Trends in Condensed Matter Physics (CTCMP), NIT, Jalandhar, 25 Sept 2020.

Atomic, Molecular and Optical Physics

B.K.Sahoo

88. "Implications of Particle Physics from Atomic Parity Violation in ^{133}Cs atom", Discussion session at the MITP Virtual Workshop on Parity Violation and Related Topics, Mainz Institute for Theoretical Physics, Mainz, Germany, 27 July — 30 July, 2020.
89. "Atomic probes of nuclear properties", 29th DAE-BRNS National Laser Symposium (NLS 29) organized in association with Indian Laser Association (ILA), RRCAT, Indore, 12 Feb — 15 Feb, 2021.

R.P.Singh

90. "Hong-Ou-Mandel Interferometer and Orbital Angular Momentum of Photons", Quantum Foundations, Technologies and Applications (QFTA-2020), IISER, Mohali, 4 Dec — 9 Dec, 2020.
91. "Satellite based quantum communication: Extension of free space quantum communication", Fundamental Sciences and Quantum Technologies using Atomic Systems (FSQT 2020), PRL, Ahmedabad, 28 September — 1 October, 2020.
92. "Quantum Key Distribution: Using Multi-photon Pulses to the Advantage", Quantum Workshop(2020), RRI, Bangalore, 17 Aug — 18 Aug, 2020.
93. "Road to satellite quantum communication: Indian effort", Student Conference on Photonics and Quantum Technology (CPQT), School of Physical Sciences, NISER,Bhubaneswar, 24 Feb — 26 Feb, 2021.

G.K.Samanta

94. "Structured beam optical parametric oscillator based mid-IR sources", OSA High-brightness Sources and Light-driven Interactions Congress, OSA Virtual Event, 16 Nov — 20 Nov, 2020.
95. "Spatial structured optical beams", SRM Institute of Science and Technology, SRM Institute of Science and Technology, Chennai, 16 May, 2020.

A.K.Singhvi

96. "Science and Technology of the future and the Challenges for Academies and Academicians", Inaugural talk at Annual meeting of Early Career Researchers in Geosciences June 23, 2020, Wadia Institute,Dehradun, 23 June, 2020.
97. "Some thoughts on future Paleo-sciences", Invited Expert talk, Society of Earth Scientists, Lucknow, 13 Oct, 2020.
98. "Luminescence Dating: Some possibilities", Inaugural Talk at Annual national meeting of Luminescence Dating and Applications, Wadia Institute of Himalayan Geology,Dehradun, 25 Nov, 2020.
99. "Making proposals for scientific grants effective through clarity of ideas, economy of words, frugality of resources and assurance of science delivery", Ministry of Education, STARS Program, IISc, Bangaluru, 16 Dec, 2020.
100. "Science Diplomacy: Indian Initiatives and A vision for the Future", Workshop on Science Diplomacy and Future,, National Academy of Science, Engineering and Mathematics,Washington, 12 Mar — 16 Mar, 2021.

Lectures at Universities / Institutions

Astronomy and Astrophysics

Lokesh Dewangan

1. "New insights into the formation of massive stars", Colloquium delivered at Physical Research Laboratory, Ahmedabad, November 18, 2020

Vishal Joshi

2. "Black Hole: a master choreographer", Webinar delivered at the Dept. of Physics, National Institute of Technology Calicut, India. Mode : ONLINE, October 20, 2020
3. "Excitement of research in astrophysics", A webinar delivered at the Department of Physics, Marwadi University, Rajkot, Gujarat. Mode: ONLINE, January 22, 2021
4. "Current affairs in Astrophysics", A webinar delivered at the Dept. of Physics, VIT, Bhopal. Mode: ONLINE, February 3, 2021
5. "Anant Brahmand ni Safare", A lecture delivered at the Dept. of Physics, Govt. Science College, Gandhinagar. Mode: ONLINE, February 27, 2021
6. "Universal Secrets", A webinar delivered at the Dept. of Physics, Saurashtra University, Rajkot, Gujarat. Mode: ONLINE, May 22, 2020

Sachindra Naik

7. "Astronomy and Astrophysics", A lecture delivered at the Department of Physics, Christ College, Rajkot. Mode: ONLINE., June 4, 2020.

Prachi Prajapati

8. "Particle Acceleration in Wolf-Rayet stars", A lecture delivered to the members of the Horizon Physics and Astronomy club IIT-Madras. Mode: ONLINE, Sept 5, 2020

Mudit K. Srivastava

9. "Search for Symbiotic Systems: The ASTROSAT Revelation", A colloquium delivered at Physical Research Laboratory Ahmedabad. Mode : ONLINE., October 21, 2020

Solar Physics

B. Joshi

10. "Solar flares and associated phenomena: Multi-wavelength investigations", webinar organized by JECRC University, Jaipur, October 01, 2020

G. R. Gupta

11. "Observations of small-scale short-lived hot and cool loops heated by UV bursts", A&A Group, University of Glasgow, UK, December 03, 2020

R. Bhattacharyya

12. "The solar coronal transients: an enigma", Astronomy club of the Physics and Electronics department of St. Xavier's college, Ahmedabad, March 08, 2021

R. E. Louis

13. "Application of Fluid Dynamics to Astrophysical Systems", Post Graduate Students of Mathematics at Nirmala College for Women, Coimbatore, September 18, 2020

Planetary Sciences

Rishitosh K. Sinha

14. "Ice related flow processes on the Earth and Mars", Lecture webinar, Dayananda Sagar College of Engineering, Bangalore, August 05, 2020
15. "Ice related flow processes on Mars", Lecture webinar, Government College Kasargod, Vidya Nagar, Kerala, August 05, 2020

M. Bhatt

16. "Earth-Moon system: formation, surface, and motions", Lecture webinar, Mathematical and Physical Sciences Division, Ahmedabad University, September 09, 2020

J. P. Pabari

17. "Wireless Sensor Network - Research Possibilities", Lecture webinar, VGEC, GTU, May 29, 2020

A. Bhardwaj

18. "Indian Planetary Mission", Engineer's Day Talk, Ganpat University, September 14, 2020
19. "Planetary Science and Exploration", Chief Guest Lecture at National Science Day Celebration, Ramaiah University of Applied Sciences, Bangalore, December 27, 2021
20. "Indian Planetary Missions", Chief Guest Lecture at International Day of Light Celebration, Lucknow University, May 16, 2020
21. "Indian Planetary Missions", Chief Guest Lecture at 14^{th} Chandigarh Science Congress (CHASCON-2020), Punjab University, December 17, 2020

K. K. Marhas

22. "Sample preparation for nanoSIMS", Lecture webinar, IUAC, Delhi, February 24, 2021

Space and Atmospheric Sciences

Harish Gadhavi

23. "Atmospheric Radiative Transfer", Online lecture series of 12 lectures for M.Sc. (Physics) students of St. Xavier's College, Ahmedabad, 6 Jan - 21 Mar, 2021.
24. "Role of aerosol and trace gases in Earth's climate", Lecture at UGC Sponsored Online Refresher Course at Human Resource Development Centre of Gujarat University in Physics at Gujarat University, 09 Sept, 2020.

Narendra Ojha

25. "Distribution of ozone and fine particulate matter over India: Integrating measurements with modelling", Department of Civil and Infrastructure Engineering, IIT Jodhpur, as part of the Webinar series on Energy and Environment, 20 Feb, 2021.
26. "Atmospheric ozone: distribution and trend", Department of Environmental Sciences, School of Basic Sciences and Research, Sharda University, as part of the webinar on the eve of world ozone day, 15 Sept, 2020.

Som Kumar Sharma

27. "Uniqueness of the Earth's Atmosphere: Scientific Perspectives", DAV Mahavidyalaya, University of Lucknow, Lucknow, 20 Dec, 2020.
28. "Raman Scattering: Its usefulness in Science and Society", an Invited talk during National Science Day (NSD-2021) celebrations, jointly organized by Ahmedabad chapters of Indian Society of Remote Sensing (ISRS), Indian Society of Geomatics (ISG), Indian Meteorological Society (IMS), along with Gujarat Council on Science and Technology, and Space Applications Centre (SAC), Ahmedabad, 28 Feb, 2021.

S. Ramachandran

29. "Atmospheric Aerosols", Colloquium delivered at IIST, Thiruvananthapuram, 25 Nov, 2020.

Geosciences

M.G. Yadava

30. "Paleoclimate from cave deposits (speleothems)", National Webinar in, "Proxies in climate reconstruction", delivered at Mohanlal Sukhadia University, Udaipur (mode: ONLINE), November 27, 2020

A.D. Shukla

31. "Natural Disasters (Extreme hydrological events) in Indian Himalaya: lessons to be learnt", Webinar on 'Resilient Infrastructure in Hilly Areas: Avalanche, GLOF & Debris Flow' organized by National Institute of Disasters & Mitigation (NIDM) and Federation of Indian Chambers of Commerce & Industry (FICCI), February 18 - 20, 2021. (Mode: Online)

Arvind Singh

32. "Sustainable forest management", Course Lectures to III semester M.Sc. students at Gujarat University, Ahmedabad. (8 Lectures), June- August, 2020
33. "Palaeoclimate", Course lectures to to the I semester M.Sc. students at Gujarat University, Ahmedabad. (8 Lectures), Jan - March, 2021

Theoretical Physics

Srubabati Goswami

34. "Neutrinos: The invisible messenger", Assam University, Shilchar Assam, December 7, 2020
35. "Neutrinos : The Nobel connection", Dr. B.R. Ambedkar National Institute of Technology, Jalandhar, June 19, 2020

Namit Mahajan

36. "B-physics at hadron colliders", to the participants of India CMS School, September 16, 2020

Partha Konar

37. "Status report on Solar flair prediction using Machine learning", DTDI AI/ML training - phase III, Oct 13, 2020
38. "Status report on Solar flair prediction using Machine learning", DTDI AI/ML training - phase IV, December 8, 2020

Navinder Singh

39. "The cuprate and Nickelate superconductivity: a comparison", IIT Ropar, Feb 2, 2020

Atomic, Molecular and Optical Physics

B. Sivaraman

40. “Laboratory astrochemistry – Ices to dust”, IGCAR, Kalpakkam, Chennai, March 15, 2021
41. “Complex molecules in impact induced astrochemical shock conditions”, NYUAD Center for Space Science and UAE Space Agency, UAE, September 29. 2020
42. “On the physical nature of astrochemical dust”, Astrochemistry Webinar Series – University of Central Florida, USA, June 4, 2020

A. K. Singhvi

43. “On Being a Responsible Teacher”, Valedictory lecture delivered at Faculty Induction Program, Guru Dakshta, Pondicherry University, January 1, 2021
44. “Future Geosciences and Opportunities”, DST Golden Jubilee Lecture by MHRD-IIC-DDUC Chapter. Science Academies workshop on Frontiers of Science, September 19, 2020
45. “Quaternary in the Indian Context: Past Glories and Future Challenges ”, Annual meeting of the Association of Quaternary Researchers at Birbal Sahni Insitute of Paleosciences, December 12, 2020
46. “Musings on an Academia with a Social Responsibility”, INYAS Webinar and INSA-S K Mitra Memorial Medal Lecture, January 30,2021
47. “Preparing for a Career in an Increasingly Competitive World: Some Suggestions”, National Science Day lecture, Ganpat University, February 28, 2021
48. “On being a responsible teacher”, Inaugural talk at Faculty Improvement Program,Christ Church College, November 3, 2020
49. “Responsibilities of Institutions, Teachers and Students for a competent, rational and ethical society”, Foundation day Lecture at Charusat university, January 28, 2021
50. “Musings on an Academia with a Social Responsibility, Reliance R and D”, National Science Day Lecture, February 26, 2021

R.P.Singh

51. “Free space quantum communication: The way forward to satellite-based quantum communication”, Webinar on Quantum Communication at Society for Electronic Transactions and Security (SETS), MGR Knowledge City, CIT Campus, Taramani, Chennai, September 19, 2020

N. Chauhan

52. “Luminescence Dating Basics”, Invited lecture in Down the Asian Trails lecture series organized by Sharma center of Archaeology Chennai, May 7, 2020.
53. “Luminescence Dating Technique and New Applications”, Invited lecture in E-workshop organized by Wadia Institute of Himalayan Geology, November 25 - November 27, 2020.

Science Outreach Talks by PRL Scientists

Astronomy and Astrophysics

Vishal Joshi

1. "Twinkle Twinkle ohh big stars", A webinar delivered at the Astronomy Club, Xaviers College, Ahmeabad, Gujarat, on 12-04-2020
2. "Discovering Black hole in our Galaxy", A webinar delivered at the Faculty Development Program in the Christ college, IrinJalakuda, Kerala. Mode: ONLINE, on 20-11-2020
3. "Chandrashekhar limit and death of stars", A webinar delivered at Science City, Ahmedabad, Gujarat. Mode: ONLINE, on 19-10-2020
4. "Dancing with the black holes", A webinar delivered at Science City, Ahmedabad, Gujarat. Mode: ONLINE, on 10-12-2020

Solar Physics

Nandita Srivastava

5. "Observing Facilities at USO", National Science Day, 2021, PRL, Ahmedabad, on 28-02-2021

Planetary Sciences

M. Bhatt

6. "Moon Remote Sensing", Guest lecture on the occasion of Science Week, Delhi Public School, Nacharam, on 27-07-2020

K. K. Marhas

7. "First Million Years", Weekly Seminar, University College of London, on 30-10-2020
8. "Women in Science during Corona times", University IIT Hyderabad, on 04-11-2020
9. "Formation of Solar system", Lecture on Physics, Physical Sciences Consultorium, Lucknow, on 24-09-2020

A. Bhardwaj

10. "Future of Science, Technology & Innovation (STI): Impact on Education, Skills and Work", Workshop on "Solar Activities and their Influences in the Heliosphere and Planetary Atmospheres (SAIHPA", National Institute of Technology, Calicut, on 08-03-2021
11. "Indian Mars Orbiter Mission", National Science Day Celebration-2021, GUJCOST, Gujarat Council of Science and Technology, on 28-02-2021

Geosciences

Anil D. Shukla

12. "Natural Disasters (Extreme hydrological events) in Indian Himalaya: lessons to be learnt", webinar on "Resilient Infrastructure in Hilly Areas: Avalanche, GLOF & Debris Flow" organized by National Institute of Disasters & Mitigation (NIDM) and Federation of Indian Chambers of Commerce & Industry (FICCI) [Mode: ONLINE], on 18-02-2021

Theoretical Physics

Srubabati Goswami

13. "Neutrinos: the Nobel Connection", as part of the INO online interactive Lecture Series, on 08-05-2020
14. "The Stars From Another Sky" as part of the Nari Vigyan Utsav, 2020", WOW: Celebrating Women Of Wonders, on 01-07-2020
15. "Neutrino: the Nobel Connection", as a part of the National Webinar organized by Bhawanipur Education Society College, on 28-08-2020
16. "Neutrinos: The Invisible messenger from space", as a part of the National Webinar, BKC College, Calcutta, on 29-08-2020
17. "Neutrinos: from Impossible Dreams to Unreachable Stars", as a part of the National Webinar "Living in the world of Neutrinos", on 30-09-2020
18. "Neutrinos: The Invisible messenger from space", 3rd PRL-IAPT Vikrama Sarabhai Lecture, on 11-02-2021

Dean's office

Bhushit Vaishnav

19. "Training Opportunities for Students at PRL", Invited talk in World Space Week 2020 celebrations jointly done by Gujarat Council on Science & Technology, Gujarat Council of Science City and Space Applications center, Ahmedabad, 10-10-2020.

Area Seminar by visitors

Dr. Viral Parekh

1. “The beginning of the SKA era : Exciting initial results from the South African SKA pathfinder MeerKAT”, Rhodes University South Africa, on 24-12-2020

Dr. Vineet Ojha

2. “Understanding the nature of Narrow-line Seyfert 1 galaxies”, ARIES, Nainital, on 25-03-2021

Ms. Sherry Chhabra

3. “Radio diagnostics of impulsive events on the Sun”, New Jersey Institute of Technology & NASA Goddard Space Flight Center, USA, on 22-12-2020

Dr. Sriram Saran Bhiravarasu

4. “Radar exploration of the Moon: Scientific potentials of Chandrayaan-2 DFSAR”, Space Applications Centre, Ahmedabad, on 01-01-2021

Dr. Prabir Patra

5. “Global budgets of 3 major greenhouse gases (CO_2, CH_4 and N_2O)”, Japan Agency for Marine-Earth Science and Technology, Japan, on 07-12-2020

Dr. Liji M. David

6. “Air pollution in India: Is it confined to urban regions only?”, Colorado State University, USA, on 21-12-2020

Dr. Sushant Das

7. “Response of Indian summer monsoon dynamics to aerosol direct radiative and snow darkening effects”, International Centre for Theoretical Physics, Italy, on 11-01-2021

Dr. Alaa Mhawish

8. “Estimating the daily $PM_{2.5}$ concentrations over the Indo-Gangetic Plain in South Asia using an Ensemble Model”, Banaras Hindu University, India, on 01-02-2021

Dr. Sonal Kumari

9. “Variation of tropospheric ozone during episodic events: Dust, crop-residue burning and haze”, Dayalbagh Educational Institute, India, on 01-03-2021

Dr. Anoop Mahajan

10. “Oceanic emissions of reactive trace gases, and their impact on the atmosphere”, Indian Institute of Tropical Meteorology, India, on 15-03-2021

Dr. Soumendra Bhanja

11. “Groundwater storage quantification and biogeochemical model development for water quality applications”, Indian Institute of Science, Bangalore, on 25-08-2020

Dr. Sabyasachi Chatopadyaya

12. “Cratons to supracrustal belts: growth and unification of the Indian landmass”, Jamboree Education Pvt. Ltd, on 15-09-2020

Dr. Anupam Banerjee

13. “Applications of radiogenic and non-traditional stable isotopes to investigate silicate weathering, crustal recycling and mantle geodynamics”, Niigata University, Japan, on 22-09-2020

Dr. Shubra Sharma

14. “Late Quaternary glacier fluctuations in the Himalaya: Evolving perspectives”, Banaras Hindu University, Varanasi, on 29-09-2020

Dr. Nikita Susan Saji

15. “Primordial differentiation to modern continents: Isotopic record of Earth’s chemical evolution through time”, University of Copenhagen, Denmark, on 06-10-2020

Dr. Subha Anand S.

16. “Understanding and Quantifying the Biological Carbon Pump in the Indian Ocean using naturally occurring radionuclides in seawater as tracers”, CSIR-National Institute of Oceanography, Goa, on 13-10-2020

Dr. Yama Dixit

17. “Abrupt climate anomalies recorded in lacustrine and marine sediments during the Quaternary Earth Observatory of Singapore”, Nanyang Technological University (NTU), Singapore, on 20-10-2020

Dr. Surya Prakash Tiwari

18. “Optical properties and remote sensing of coastal and open ocean environments”, King Fahd University of Petroleum and Minerals (KFUPM), Saudi Arabia, on 03-11-2020

Dr. Sahadev Sharma

19. “Role of coastal ecosystems as nature-based climate solutions”, Institute of Ocean and Earth Sciences, University of Malaya, Malaysia, on 17-11-2020

Shubham Maheshwari

20. “Stable, ghost-free solutions in UV non-local gravity”, University of Groningen, on 18-11-2020

Padmanath Madanagopalan

21. “Understanding sub-nuclear physics using Lattice Quantum ChromoDynamics”, University of Mainz, on 25-11-2020

Sabyasachi Chakraborty

22. “Physics at fundamental frontiers”, University of Florida, on 03-12-2020

Student Training

Astronomy and Astrophysics

1. Harshal Gudaghe, Delhi Technological University, New Delhi, “Understanding the Evolution of Star Clusters with the GAIA Space Observatory”, from Feb 2021 to May 2021, [Supervisor: Manash R. Samal].
2. Abhijeet Patil, St. Xavier’s college, Mumbai, “Understanding the Evolution of Star Clusters with the GAIA Space Observatory”, from Feb 2021 to May 2021, [Supervisor: Manash R. Samal].

Solar Physics

3. Ashutosh Pattnaik, College of Engineering and Technology, Bhubaneswar, “Coronal Cavity Evolution”, from June 2020 to March 2021, [Supervisor: Nandita Srivastava].
4. Urmi Doshi, M.P. Birla Institute of Fundamental Research, Bangalore, “Comparative study of ICMEs in SC23 and SC24”, from August 2020 to March 2021, [Supervisor: Nandita Srivastava].
5. Babu Ram Sharma, Tribhuvan University, Pokhara, Nepal and CSSTEAP, Dehradun, “Study of Solar Radio bursts at low frequencies by e-CALLOSTO network”, from February 2020 to October 2020, [Supervisor: Bhuwan Joshi].

Planetary Sciences

6. Souti Das, Department of Human Physiology, University of Calcutta, “Life in Earth and Mars: An Astrobiological study”, from August 2020 to October 2020, [Supervisor: D. Ray].
7. Shubham Banik, Department of Human Physiology, University of Calcutta, “Life in Earth and Mars: An Astrobiological study”, from August 2020 to October 2020, [Supervisor: D. Ray].
8. Nabanita Ghosh, Department of Human Physiology, University of Calcutta, “Life in Earth and Mars: An Astrobiological study”, from August 2020 to October 2020, [Supervisor: D. Ray].
9. Rimpa Kar, Department of Human Physiology, University of Calcutta, “Life in Earth and Mars: An Astrobiological study”, from August 2020 to October 2020, [Supervisor: D. Ray].
10. Eisikha Das, Department of Human Physiology, University of Calcutta, “Life in Earth and Mars: An Astrobiological study”, from August 2020 to October 2020, [Supervisor: D. Ray].
11. Sreeranjana Mitra Chowdhury, Department of Human Physiology, University of Calcutta, “Life in Earth and Mars: An Astrobiological study”, from August 2020 to October 2020, [Supervisor: D. Ray].
12. Diksha Dhakde, Department of Physics & Electronics, Institute for Excellence in Higher Education, Bhopal, “Reflectance spectroscopy - a powerful tool for studying planetary surface composition”, from Jan 2020 to May 2020, [Supervisor: N. Srivastava].
13. Nitika Sachdeva, Bhagwan Parshuram Institute of Technology, Guru Gobind Singh Indraprastha University, New Delhi, “Study of aeolian dominated landscapes in Jezero crater, Mars”, from Feb 2021 to May 2021, [Supervisor: R. K. Sinha].
14. Hephzibah Catherine, B.E, College of Engineering, Anna Univ, Chennai, “Impact craters and its role in Lunar evolution”, from April 2020 to March 2021, [Supervisor: S. Vijayan].
15. Tuhi Saumya, B.E, College of Engineering, Anna Univ, Chennai, “Impact craters and its role in Mars evolution”, from April 2020 to March 2021, [Supervisor: S. Vijayan].
16. Rashmi Kumari, Banaras Hindu University, “Impact Craters On The Mars And Its Role In Fluvial Activities”, from Jan 2021 to March 2021, [Supervisor: S. Vijayan].
17. Karan Bhuva, Gujarat University, “SIR-2 global data spectral classification using machine learning methods”, from Feb 2021 to June 2021, [Supervisor: M. Bhatt].
18. Parth Patadiya, Gujarat University, “SIR-2 global data spectral classification using machine learning methods”, from Feb 2021 to June 2021, [Supervisor: M. Bhatt].
19. Hetvi Julasana, Gujarat University, “SIR-2 global data spectral classification using machine learning methods”, from Feb 2021 to March 2021, [Supervisor: M. Bhatt].
20. Gagan Dhote, Department of Physics, Barkatullah University, Bhopal, “Lightning data analysis”, from Jan 2020 to June 2020, [Supervisor: J. P. Pabari].
21. Rashmika D. Chaudhari, Department of Physics, H. N. G. U., Patan, “Development and testing of analog electronics for lightning detector”, from Nov 2019 to May 2020, [Supervisor: J. P. Pabari].
22. Niki J. Panchal, Department of Physics, H. N. G. U., Patan, “Development and testing of analog electronics for lightning detector”, from Nov 2019 to May 2020, [Supervisor: J. P. Pabari].
23. Suchika Yadav, Department of Remote Sensing, Banasthali Vidyapith, Jaipur, Rajasthan, “Revisiting Venusian Lightning Phenomenon”, from August 2019 to May 2020, [Supervisor: J. P. Pabari].
24. Jay M. Jakhariya, GTU, Ahmedabad, “Comparative Analysis of Dust Detector Configuration and FE Electronics”, from Oct 2019 to June 2020, [Supervisor: J. P. Pabari].

25. Harsh V. Parmar, GTU, Ahmedabad, “Investigation of Hypervelocity Dust and Processing Electronic For It’s Detection”, from August 2019 to June 2020, [Supervisor: J. P. Pabari].
26. Avantika V. Gupta, Charotar University of Science and Technology, Changa, Nadiad, “Venus Lightning: Design and Testing of Processing Electronics for Hypervelocity Dust Detection”, from Jan 2020 to April 2020, [Supervisor: J. P. Pabari].
27. Aditi Sharma, Banasthali Vidyapith, “Modelling and analysis of Schumann Resonance due to lightning”, from Jan 2021 to May 2021, [Supervisor: J. P. Pabari].
28. Tanu Garg, Banasthali Vidyapith, “Modelling and analysis of Schumann Resonance due to lightning”, from Jan 2021 to May 2021, [Supervisor: J. P. Pabari].
29. Srishti Iyer, M. S. University, Vadodara, “Study of interplanetary dust around planets”, from Feb 2021 to May 2021, [Supervisor: J. P. Pabari].
30. Sonal Mashram, IEHE, Bhopal, “Study of group velocity in the planetary ionosphere”, from Feb 2021 to June 2021, [Supervisor: J. P. Pabari].
31. Prerak Majumdar, Charotar University of Science and Technology, Changa, Nadiad, “Prototype design of thermal conductivity sensor for Heat Flow Studies on the Moon”, from Jan 2020 to June 2020, [Supervisor: K. Durga Prasad].
32. Rohit Dutta, Amity University, “Mechanical design and analysis of deployment mechanism of boom for future planetary missions”, from Jan 2020 to June 2020, [Supervisor: K. Durga Prasad].

Space and Atmospheric Sciences

33. Mr. Kshitiz Upadhyay, PRL, “Photometry for measurement of Daytime optical airglow emissions”, from Jan 2020 to May 2020, [Supervisor: Duggirala Pallamraju].
34. Mr. Kashyap Patel, Gujarat University, “Climate Change Impacts Management”, from Mar 2019 to May 2020, [Supervisor: Lokesh Kumar Sahu].
35. Mr. Hrishikesh Dubey, Institute for Excellence in Higher Education, Bhopal, “Study of AOT, TCO, and WV of the Lower and Middle Atmosphere using Microtops II Sunphotometer”, from Feb 2020 to Sept 2020, [Supervisor: Som Kumar Sharma].
36. Ms. Nancy Abraham, Pandit Deendayal Petroleum University, Gandhinagar, “Mesospheric temperatures using spectroscopic techniques”, from Feb 2021 to May 2021, [Supervisor: Ravindra Pratap Singh].
37. Ms. Gitanjali Palai, Sambhalpur University, Burla, “Study of Earth’s Upper Atmosphere”, from Feb 2021 to June 2021, [Supervisor: Ravindra Pratap Singh].
38. Mr. Dharmendra Kumar Kamat, PRL, “Spectroscopic measurement of hydroxyl rotational temperatures”, from Jan 2021 to May 2021, [Supervisor: Ravindra Pratap Singh].

Geosciences

39. Mr. Ninaad Desai, St. Xavier’s College, Ahmedabad, “Assessing Feasibility of Wind-Solar PV Hybrid Power Plants in Gujarat”, from Feb, 2021 to April, 2021, [Supervisor: R. D. Deshpande].
40. Deeksha Gautam, Dayalbagh Educational Institute, Agra, “Characteristics of light absorbing organics in ambient aerosols”, from Feb, 2021 to March, 2021, [Supervisor: Neeraj Rastogi].
41. Jay Dave, Gujarat University, “Characteristics of brown carbon aerosol, and Organic aerosol Characterization”, from Sept, 2018 to Sept, 2019, [Supervisor: Neeraj Rastogi].
42. Saurabh Shukla, Physical Research Laboratory, “Understanding climate change and its consequences”, from May 2020 to July 2020, [Supervisor: Vineet Goswami].

Theoretical Physics

43. Pratik B Domadiya, Dharmsinh Desai University , Nadiad, “Deep Learning Based Solar-Flare Forecasting Model”, from Jan 2020 to April 2020, [Supervisor: Partha Konar].
44. Parth Patel, Dharmsinh Desai University , Nadiad, “High Energy Physics (HEP) Data Analysis with jet images using GANs Networks”, from Jan 2020 to April 2020, [Supervisor: Partha Konar].
45. Rithvik Sreekantham, PRL, Ahmedabad, “Understanding the AI Physicist Learning Agent”, from May 2020 to July 2020, [Supervisor: Partha Konar].
46. Debashis Pachhar, PRL, Ahmedabad, “Understanding HEP events at collider experiment”, from Jan 2021 to April 2021, [Supervisor: Partha Konar].

Astronomy and Astrophysics

Observations of the Quiet Sun During the Deepest Solar Minimum of the Past Century with Chandrayaan-2 XSM: Sub-A Class Microflares Outside Active Regions

Solar flares, with energies ranging over several orders of magnitude, result from impulsive release of energy due to magnetic reconnection in the corona. It is now well known that these strong but in-frequent flares cannot provide the required energy to maintain the coronal temperature. However, it is theorized that much weaker magnetic reconnection events termed as 'nanoflares' with typical energies of 10^{24} erg, if happening at sufficiently high frequency all over the solar corona, may keep the temperature high. Since observations of individual nanoflares have not been possible so far due to technological limitations, one possible way to infer their frequency is by extrapolating the power law of the observable microflare distribution to lower energies. However, barring a handful, almost all microflares observed in X-rays are associated with the solar active regions.

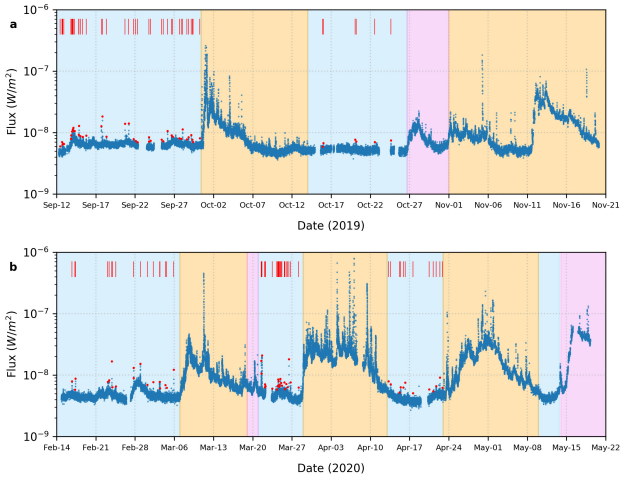

Figure no 1: Solar X-ray flux in the 1 – 15 keV energy range as measured by XSM. Different background shades represent activity levels on the Sun, with orange representing periods when NOAA active regions are present; pink representing periods of enhanced activity visible in both the XSM light curve as well as EUV/X-ray images but not classified as AR; and blue representing periods selected for the present study when no major activity was observed on the Sun. The microflares detected during the quiet periods are marked with red points, representing their peaks; and red vertical bars, representing their time.

The *Solar X-ray Monitor* (XSM) on board the Chandrayaan-2 mission carried out observations of the Sun during 2019-20 solar minimum, which was the deepest in the past 100 years when there were extended periods without any active regions present on the solar disk. Figure no. 1 shows the XSM light curve during this period where 98 microflares identified during the periods of quiet Sun are also marked. We find that most of the microflares are impulsive in nature and in all cases where the microflare location could be identified from the EUV images, they are associated with magnetic bipolar regions. By fitting the observed X-ray spectra of microflares with a two-temperature isothermal emission model, we obtained the temperature and emission measure associated with the flaring plasma, which are shown in Figure no. 2a.

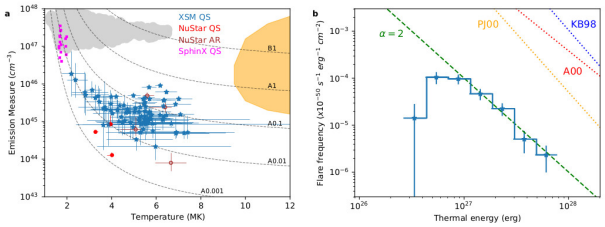

Figure no. 2: Solar X-ray flux in the 1 – 15 keV energy range as measured by XSM. Different background shades represent activity levels on the Sun, with orange representing periods when NOAA active regions are present; pink representing periods of enhanced activity visible in both the XSM light curve as well as EUV/X-ray images but not classified as AR; and blue representing periods selected for the present study when no major activity was observed on the Sun. The microflares detected during the quiet periods are marked with red points, representing their peaks; and red vertical bars, representing their time.

Further, by using these spectroscopic results with the volume estimates from analysis of EUV images from SOD/AIA, we estimated that the thermal energies of these microflares range from $\sim 3 \times 10^{26}$ – 6×10^{27} erg and the flare frequency distribution follows a power law as shown in Figure no 2b. These observations provide the first comprehensive analysis of a large sample of quiet Sun microflares, demonstrating that microflares are not confined only to the active regions and supports the hypothesis on presence of small scale impulsive events everywhere on the solar corona.

doi : https://doi.org/10.3847/2041-8213/abf0b0

(S. Vadawale, N. P. S. Mithun, B. Mondal, A. Sarkar, P. Janardhan, B. Joshi, A. Bhardwaj, M. Shanmugam, A. R. Patel, H. L. Adalja, S. K. Goyal, T. Ladiya, N. K. Tiwari, N. Singh, S. Kumar)

Observations of the Quiet Sun During the Deepest Solar Minimum of the Past Century with Chandrayaan-2 XSM: Elemental Abundances in the Quiescent Corona

Elements with low First Ionization Potential (FIP) are known to be three to four times more abundant in active region loops of the solar

corona than in the photosphere, and this phenomenon is usually referred to as “FIP bias”. While the hot loops (3-4 MK) of active regions with high magnetic field display FIP bias, the low-temperature ($\sim$1 MK) non-active corona has nearly photospheric abundances. However, there are no observations available for the abundances of coronal features namely X-ray Bright Points (XBPs) associated with intermediate magnetic fields and temperatures.

The *Solar X-ray Monitor* (XSM) on board the Chandrayaan-2 mission carried out spectroscopic observations of the Sun in soft X-rays during the 2019-20 solar minimum, providing a unique opportunity to study soft X-ray spectra of the quiescent solar corona in the absence of any active regions. Figure no. 1 shows the XSM light curve during this period where the blue shaded intervals correpond to the times when no active region like feature was present on the solar disk. We carried out spectral analysis of the quiet Sun spectrum in these intervals, excluding periods of microflares. The spectra were fitted with an isothermal plasma emission model based on CHIANTI atomic database to obtain temperature, emission measure, and abundances of Mg, Al, and Si, as shown in Figure no. 3.

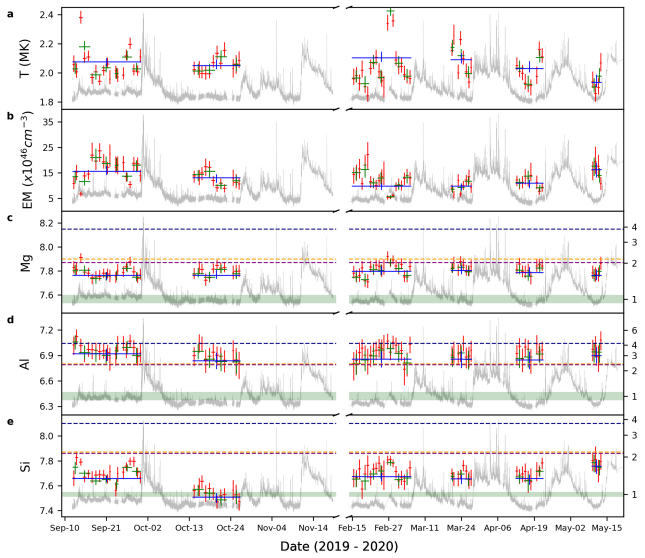

Figure no. 3: The five panels show the results of the fitting of quiet Sun spectrum with XSM, viz. Temperature (a), EM (b), as well as the absolute abundances of Mg (c), Al (d), and Si (e) in logarithmic scale with A(H)=12. XSM light curves for the entire duration are shown in gray in the background. Dashed lines show reported values of abundances in active regions and the range of photospheric abundances is shown as green bands. The right y-axis in panels c-e show the FIP bias values for the respective elements with respect to average photospheric abundances.

We find that the derived parameters remain nearly constant over time with a temperature around 2 MK and that the FIP bias is $\sim$2, which is lower than the values observed in active regions. X-ray images obtained by Hinode XRT during these periods suggest that most of the emission in the XSM energy range arises from XBPs, which is also reflected in the observed temperature around 2 MK. Thus, we conclude that the intermediate FIP bias observed by XSM most likely corresponds to the XBPs having lower magnetic fields than active regions, which is consistent with the expectations from the widely considered Pondermotive force model for FIP bias.

doi : https://doi.org/10.3847/2041-8213/abf35d

(S. Vadawale, N. P. S. Mithun, B. Mondal, A. Sarkar, P. Janardhan, B. Joshi, A. Bhardwaj, M. Shanmugam, A. R. Patel, H. L. Adalja, S. K. Goyal, T. Ladiya, N. K. Tiwari, N. Singh, S. Kumar)

Interstellar comet 2I/Borisov (C/2019 Q4)

On 30 August 2019, Gennady Borisov discovered a cometary object using his self-built 0.65 m telescope. Initially designated as C/2019 Q4, this object was later identified to be the first ever interstellar comet to be observed passing through the Solar system. It was redesignated as 2I/Borisov. The comet possessed a very large eccentricity of e = 3.379 and a very high hyperbolic excess velocity of v $\sim$ 32 Km/s, confirming the interstellar origin. Multiple groups across the globe observed the comet in spectroscopic method to detect the presence of CN and C_2, similar to that in Solar system comets. The comet was identified to be depleted in carbon chain molecules due to the less abundance in C_2 with respect to CN. As the comet approached perihelion, an increase in the relative abundance of C_2 was observed.

In our work, we report the spectroscopic results of the Interstellar comet 2I/Borisov, with observations before and after perihelion using two Indian observatories, the Mount Abu Infrared Observatory (MIRO) and the Himalayan Chandra Telescope (HCT operated by IIA). The pre and post perihelion spectroscopic observations were made using the HFOSC instrument at HCT to observe an optical spectrum of the Interstellar comet as illustrated in Figure no. 4. Clear detections of CN, C_2 and C_3 were made on both the epochs.

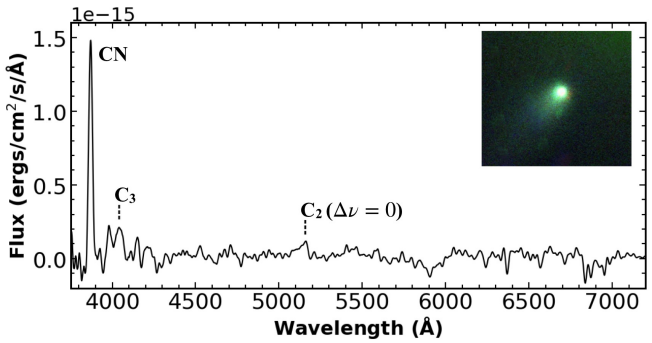

Figure no. 4: Optical spectrum of 2I/Borisov observed with the HFOSC instrument on HCT on 2019-12-22.965 UT. Inset shows the RGB colour composite view of the comet on the same night using images taken with HFOSC.

Along the orbit of the comet, based on the relative abundance of C_2 radical, the behaviour has changed from highly depleted to moderately depleted as it approached perihelion. Surprisingly, the abundance dropped post-perihelion, once again making the comet highly depleted in carbon-chain molecules. We also noticed an asymmetry in the production rate (molecules/s) of CN and C_3 post-perihelion. Generally, such asymmetries in production rates are observed among the short period comets of our Solar system close to perihelion. Using photometric observations made using both MIRO and HCT, we infer the dust-to-gas ratio to be consistent with the numbers observed for Solar system comets depleted in carbon chain molecules. The possible size of the nucleus was deduced to be $0.18 \leq r \leq 3.1$ km. Our observations show that 2I/Borisov's behaviour is analogous to that of the Solar system comets. Considering all the observational evidences, we infer that the comet 2I/Borisov was formed in a proto-stellar

system undergoing a very inhomogeneous mixing of various volatile compounds beyond the CO ice line.

This work was carried out in collaboration with Kumar Venkataramani (AU, USA), D. K. Sahu (IIA), D. Angchuk(IIA), T. Sivarani(IIA), and A. Unni(IIA)

doi : https://doi.org/10.1093/mnras/stab084

(K. Aravind and S. Ganesh)

Modelling heterogenous dust particles: an application to cometary polarization

In this work, we put forward a comet dust model, which considers multiple dust morphology having inhomogeneous mixture of silicate minerals and carbonaceous compounds. Taking into account the results from Rosetta/MIDAS and COSIMA instruments, we develop high porosity hierarchical aggregates (HA), low porosity Solids and moderately porous fluffy solids (FS). Light scattering simulations are executed using the multi-sphere T-matrix code (MSTM-v3.0) and the Discrete Dipole Approximation (DDSCAT-v7.3.3) over the modelled dust particles in order to extract the degree of linear polarization, phase function, depolarization ratio and anisotropy parameter. All computations related to this study are executed using the Vikram-100 HPC at PRL, Ahmedabad.

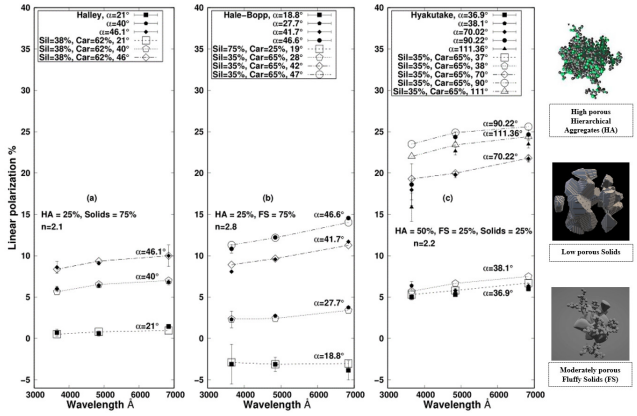

Figure no. 5: Wavelength dependence of polarisation in comets Halley, Hale-Bopp and Hyakutake. Last column shows the dust grains with different morphologies considered in our model.

Under power-law size distribution (n = 2.0 to 3.0) and inhomogeneous composition having silicate minerals and carbonaceous materials, we study the polarimetric response for the mixing combinations (HA + Solids), (HA + FS) and (HA + FS + Solids) for different sets of mixing percentage of silicate minerals and carbonaceous compounds. The flexibility of the model, allows us to control a large number of physical parameters like size, shape, porosity and composition of the dust particles. This enables us to replicate the standard polarization phase curve observed in several comets having different dynamical age. Apart from the polarimetric response, the model also recreates the strong wavelength dependence of polarization observed in the case of comet Hale-Bopp and the moderate dependence for comets Halley and Hyakutake (see Figure no. 5). Our dust model indicates that long-period comets may have a high percentage of loose particles, retaining the morphology from the proto-planetary phase, while the short-period comets possess a high percentage of solid particles with low porosity. This difference in the dust properties could be due to frequent and/or higher magnitude of weathering by solar radiation during the relatively more frequent passages close to the Sun by the short-period comets.

doi : https://doi.org/10.1093/mnras/staa3647

(P. Halder and S. Ganesh)

Probing the physical conditions and star formation processes in the Galactic H II region S305

Massive OB-stars ($\geq$ 8 $M_{\odot}$) have a profound impact on their immediate environment through the radiative and mechanical energy they inject from their formation phase until their death. Hence, these stars have the ability to trigger the birth of young stellar objects (YSOs) and young massive stars. However, understanding the formation mechanisms of massive OB-stars and their feedback process are still far from complete. In this context, we analyzed multi-scale and multi-wavelength observations of the Galactic H II region S305 (distance ~ 3.7 kpc), which is excited by massive O8.5V and O9.5V stars. In Figure no. 6a, infrared images reveal an extended sphere-like shell (extension $\sim$7.5 pc; at T_d = 17.5–27 K) enclosing the S305 H II region (size $\sim$5.5 pc; age $\sim$1.7 Myr). The extended structure observed in the *Herschel* temperature map indicates that the molecular environment of S305 is heated by the massive O-type stars. Regularly spaced molecular condensations and dust clumps are investigated toward the edges of the infrared shell (see Figure no 6b), where the polycyclic aromatic hydrocarbon (PAH) and H_2 emission is also observed. The molecular line data show a signature of an expanding shell of molecular gas in S305. GMRT 610 and 1280 MHz continuum maps reveal overdensities of the ionized emission distributed around two O-type stars (see blue contours in Figure no 6a), which are surrounded by the horseshoe envelope (extension $\sim$2.3 pc). A molecular gas deficient region/cavity is identified toward the center of the horseshoe envelope, which is well traced with PAH, H_2, molecular, and dust emission.

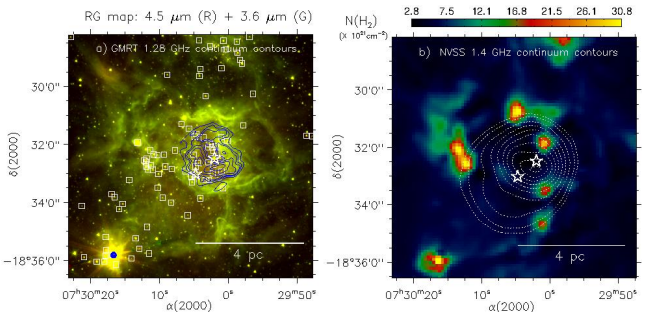

Figure no. 6: a) Two-color composite image (Red: *Spitzer* 4.5 μm and Green: *Spitzer* 3.6 μm) of the S305 H ii region. The GMRT 1.28 GHz continuum emission contours (in blue) and the positions of YSOs (see squares) are also overlaid on the color-composite image. b) *Herschel* column density map overlaid with the NVSS 1.4 GHz contours. In each panel, the positions of previously known massive O-type stars are marked by star symbols. A scale bar referring to 4 pc (at a distance of 3.7 kpc) is also displayed.

The edges of the infrared shell are found to be located in the front of the horseshoe envelope. All these outcomes provide the observational evidence of the feedback of O-type stars in S305. Moreover, non-thermal radio emission is detected in S305 with an average spectral index $\alpha \sim -0.45$. The variations in α range from -1.1 to 1.3. We interpret that this spectrum corresponds to a combination of soft synchrotron emission and thermal emission from the ionized gas. We show that suppression of low-frequency emission by the Razin-Tsytovich effect can be relevant in the context of H ii regions. We estimated the magnetic field in the H ii region to be ∼0.2–1 mG. The high content of relativistic particles needed to produce the observed emission requires them to be accelerated *in situ*. Finally, the soft radio emission is consistent with a low Mach number shock with $V_{sh} \sim 30$ km s^{-1}. Future observations exploring the unobserved frequency ranges below 600 MHz and above 1.4 GHz are expected to further constrain these values.

This work was done in collaboration with Saurabh Sharma (ARIES, India), Rakesh Pandey (ARIES, India), S. del Palacio (IAR, Argentina), D. K. Ojha (TIFR, India), P. Benaglia (IAR, Argentina), T. Baug (KIAA-PKU, China), and S. R. Das (IIST-Trivandrum, India).

doi : https://doi.org/10.3847/1538-4357/ab9c27

(L. K. Dewangan)

Star-forming sites IC 446 and IC 447: an outcome of end-dominated collapse of Monoceros R1 filament

After the launch of the *Herschel* Space Observatory, filamentary structures have been commonly found in star-forming regions. Filaments having various physical scales, spanning from the scale of the molecular cloud to the scale of protostellar envelope (i.e., ∼100–0.1 pc), have been reported in the literature, and are often found to nurture star formation activities along their major axis.

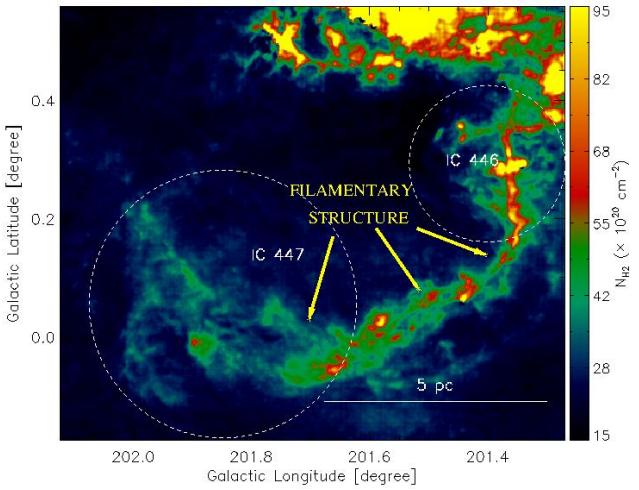

Figure no. 7: *Herschel* column density map of an area hosting IC 446 and IC 447. Broken circles indicate the extent of IC 446 and IC 447. A scale bar corresponding to 5 pc is shown in the figure.

The observational and theoretical studies suggest that filamentary clouds break into fragments of dense clumps and cores, which can further collapse to form young stellar objects (YSOs) as well as massive stars ($>$ 8 M$_\odot$). However, the physical processes that govern the filamentary fragmentation and the formation of massive clumps/cores and clusters of YSOs are still debatable. In this relation, we carried out an analysis of multi-wavelength observations of Monoceros R1 (Mon R1) complex (at d ∼760 pc). An elongated filament (length ∼14 pc, mass ∼1465 M$_\odot$) is investigated in the complex, which is the most prominent structure in the *Herschel* column density map (see Figure no. 7). An analysis of the FUGIN ^{12}CO(1–0) and ^{13}CO(1–0) line data confirms the existence of the filament traced in a velocity range of [−5, +1] km s^{-1}. The filament is found to host two previously known sites IC 446 and IC 447 at its opposite ends. A massive young stellar object (YSO) is embedded in IC 446, while IC 447 contains several massive B-type stars. The *Herschel* temperature map reveals the extended warm dust emission (at $T_d \sim$ 15–21 K) toward both the ends of the filament. The *Spitzer* ratio map of 4.5 μm/3.6 μm emission suggests the presence of photo-dissociation regions and signature of outflow activity toward IC 446 and IC 447. Based on the photometric analysis of point-like sources, clusters of YSOs are traced mainly toward the filament ends. The filament is found to be thermally supercritical showing its tendency of fragmentation, which is further confirmed by the detection of a periodic oscillatory pattern (having a period of ∼3–4 pc) in the velocity profile of ^{13}CO. Our outcomes suggest that the fragments distributed toward the filament ends have rapidly collapsed, and had formed the known star-forming sites. Overall, the elongated filament in Mon R1 is a promising sample of the "end-dominated collapse" scenario.

This work was done in collaboration with L. E. Pirogov (IAPRAS, Russia) and D. K. Ojha (TIFR, India).

doi : https://doi.org/10.3847/1538-4357/aba2c6

(N. K. Bhadari and L. K. Dewangan)

New insights in the H ii region G18.88−0.49: hub-filament system and accreting filaments

Understanding the formation process of massive OB-type stars ($\gtrsim$ 8 M$_\odot$) is still far from complete. Dust and molecular filaments are often associated with dense massive star-forming clumps, H ii regions excited by massive stars, and young stellar clusters. It is thought that massive stars and clusters of young stellar objects (YSOs) commonly form within parsec-scale massive clumps/clouds such as hub-filament systems (e.g., Monoceros R2) and ridges (e.g., DR 21). Hub-filament systems are known as a junction of multiple filaments. Such investigation requires the knowledge of molecular gas motion in the hub-filament system. In this context, we performed an analysis of multi-wavelength observations of an area of 0°.27 × 0°.27 around the Galactic H ii region G18.88−0.49, which is powered by an O-type star (age ∼10^5 years). In Figure no. 8, the *Herschel* column density map reveals a shell-like feature of extension ∼12 pc × 7 pc and mass ∼2.9 ×10^4 M$_\odot$ around the H ii region; its existence is further confirmed by the distribution of molecular (^{12}CO, ^{13}CO, C^{18}O, and NH_3) gas at [60, 70] km s^{-1}. Four subregions are studied toward this shell-like feature, and show a mass range of ∼0.8–10.5 ×10^3 M$_\odot$. These subregions associated with dense gas are dominated by non-thermal pressure and supersonic non-thermal motions. The shell-like feature is associated with the H ii region, Class I protostars, and a massive protostar candidate, illustrating the

ongoing early phases of star formation (including massive stars). The massive protostar is found toward the position of the 6.7 GHz methanol maser, and is associated with an outflow activity. Five parsec-scale filaments are identified in the column density and molecular maps, and appear to be radially directed to the dense parts of the shell-like feature. This configuration is referred to as a "hub-filament" system. Significant velocity gradients (0.8–1.8 km s^{-1} pc^{-1}) are observed along each filament, suggesting that the molecular gas flows towards the central hub along the filaments. Overall, our observational findings favor a global non-isotropic collapse scenario as discussed in Motte et al. (2018), which can explain the observed morphology and star formation in and around the H ii region G18.88−0.49. This work was done in collaboration with D. K. Ojha (TIFR, India), Saurabh Sharma (ARIES, India), S. del Palacio (IAR, Argentina), and A. Das (University of Hyderabad, India)

doi : https://doi.org/10.3847/1538-4357/abb827

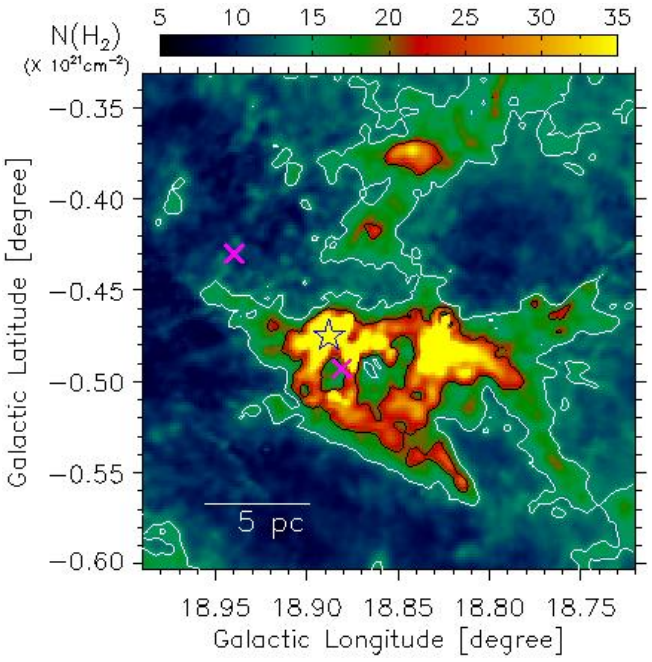

Figure no. 8: *Herschel* column density ($N(H_2)$) map of the Hii region G18.88−0.49. Filamentary structures are traced in the column density map at a contour level of 14.1 × 10^{21} cm^{-2} (white contour). A solid contour (in black), at $N(H_2)$ = 21 × 10^{21} cm^{-2}, traces a shell-like feature in the figure. The scale bar referring to 5 pc (at a distance of 5.0 kpc) is shown. The position of a 6.7 GHz methanol maser is marked by a star. Crosses show the positions of two H ii regions G18.937−0.434 and G18.88−0.49.

(L. K. Dewangan and N. K. Bhadari)

Unveiling the Importance of Magnetic Fields in the Evolution of Dense Clumps Formed at the Waist of Bipolar H II Regions: A Case Study of Sh 2-201 with JCMT SCUBA-2/POL-2

In this regard, we present the properties, structures, and morphologies of magnetic fields (B-fields) in two clumps (clump 1 and clump 2), located at the waist of the bipolar H ii region Sh2-201, based on JCMT SCUBA-2/POL-2 observations of 850 μm polarized dust emission. We find that B-fields in the direction of the clumps are bent and compressed, showing bow-like morphologies (see Figure no. 9), which we attribute to the feedback effect of the H ii region on the surface of the clumps. Using the modified Davis-Chandrasekhar-Fermi method we estimate B-fields strengths of 266 μG and 65 μG for clump 1 and clump 2, respectively. From virial analyses and critical mass ratio estimates, we argue that clump 1 is gravitationally bound and could be undergoing collapse, whereas clump 2 is unbound and stable. We hypothesize that the interplay between thermal pressure imparted by the H ii region, B-field morphologies, and the various internal pressures of the clumps (such as magnetic, turbulent, and gas thermal pressure), has the following consequences: (a) formation of clumps at the waist of the H ii region; (b) progressive compression and enhancement of the B-fields in the clumps; (c) stronger B-fields will shield the clumps from erosion by the H ii region and cause pressure equilibrium between the clumps and the H ii region, thereby allowing expanding I-fronts to blow away from the filament ridge, forming bipolar H ii regions; and (d) stronger B-fields and turbulence will be able to stabilize the clumps. A study of a larger sample of bipolar H ii regions would help to determine whether our hypotheses are widely applicable.
This work has been done in collaboration with Chakali Eswaraiah, Di Li, Yuehui Ma (CAS, China), Jia-Wei Wang, Shih-Ping Lai (NTHU, Taiwan), and other team members from various national and international institutes/organizations.

doi : https://doi.org/10.3847/1538-4357/ab83f2

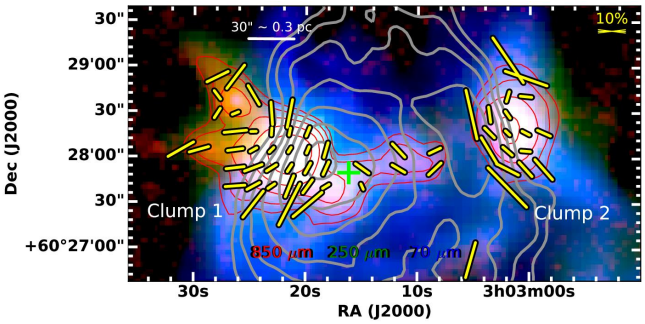

Figure no. 9: B-field vector maps are overlaid on the color composite of JCMT/SCUBAPOL2 850 μm Stokes I (red), *Herschel* SPIRE/250 μm (green), and *Herschel* PACS/70 μm (blue) images. Red contours correspond to JCMT/SCUBAPOL2 850 μm Stokes I map and are drawn at [3, 6, 12, 24, 48, 96, 192] × the rms noise of 14 mJy/beam. Gray contours, corresponding to the VLA/21 cm continuum emission representing the distribution of the ionized medium of H ii region, are drawn at [1, 3, 6, 12, 24, 48, 96, 206] × the rms noise of 2.3×10^{-4} mJy/beam. In the map, reference vectors with a B-field orientation of 90 degrees, along with mean uncertainty of 7 degrees are shown.

(Manash Samal)

The PDR structure and kinematics around the compact H ii regions S235 A and S235 C with C ii, ^{13}C ii, O i and HCO$^+$ line profiles

Understanding structure and gas kinematics of the photodissociation regions (PDRs) around the H ii regions are of great importance for the understanding the evolution of H ii regions. In this work,

we investigated compact H ii regions S235 A and S235 C of the S235 complex. We observe the C ii, ^{13}C ii and O i line emission, using SOFIA/upGREAT and complement them by data of HCO^+ and CO. We use the ^{13}C ii line to measure the optical depth of the C ii emission, and find that the C ii line profiles are influenced by self-absorption, while the ^{13}C ii line remains unaffected by these effects. Hence, for dense PDRs, ^{13}C ii emission is a better tracer of gas kinematics. The optical depth of the C ii line is up to 10 in S235 A. We find an expanding motion of the C ii-emitting layer of the PDRs into the front molecular layer in both regions. Comparison of the gas and dust columns shows that gas components visible neither in the C ii nor in low-J CO lines may contribute to the total column across S235 A. We test whether the observed properties of the PDRs match the predictions of spherical models of expanding H ii region + PDR + molecular cloud. Integrated intensities of the ^{13}C ii, C ii and O i lines are well-represented by the model, but the models do not reproduce the double-peaked C ii line profiles due to an insufficient column density of C^+. The model predicts that the O i line could be a more reliable tracer of gas kinematics, but the foreground self-absorbing material does not allow using it in the considered regions.
This work has been done in collaboration with M. S. Kirsanova (RAS, Russia), V. Ossenkopf-Okada (Universitatzu Koln, Germany), L. D. Anderson (West Virginia University, USA) and other team members from various internationl institutes/organizations.

doi : https://doi.org/10.1093/mnras/staa2142

(Manash Samal)

CHIMPS2: Survey description and ^{12}CO emission in the Galactic Centre

The latest generation of Galactic-plane surveys is enhancing our ability to study the effects of galactic environment upon the process of star formation. We present the first data from CO Heterodyne Inner Milky Way Plane Survey 2 (CHIMPS2). CHIMPS2 is a survey that will observe the Inner Galaxy, the Central Molecular Zone (CMZ), and a section of the Outer Galaxy in ^{12}CO, ^{13}CO, and $C^{18}O$ ($J = 3 \rightarrow 2$) emission with the Heterodyne Array Receiver Program on the James Clerk Maxwell Telescope (JCMT). The first CHIMPS2 data presented here are a first look towards the CMZ in ^{12}CO J = 3→2 and cover $-3^\circ \leq \ell \leq 5^\circ$ and $|b| \leq 0^\circ 5$ with angular resolution of 15 arcsec, velocity resolution of 1 km s^{-1}, and rms $\Delta T_A^* = 0.58$ K at these resolutions. Such high-resolution observations of the CMZ will be a valuable data set for future studies, whilst complementing the existing Galactic Plane surveys, such as SEDIGISM, the *Herschel* infrared Galactic Plane Survey, and ATLASGAL. In this paper, we discuss the survey plan, the current observations and data, as well as presenting position-position maps of the region. The position-velocity maps detect foreground spiral arms in both absorption and emission.
noindent This work has been done in collaboration between D. J. Eden, T. J. T. Moore (Liverpool John Moores Universit, UK), M. J. Currie (East Asian Observatory, USA), A. J. Rigby (Cardiff University, UK) and other team members from various international institutes/organizations.

doi : https://doi.org/10.1093/mnras/staa2734

(Manash Samal)

Testing the star formation scaling relations in the clumps of the North American and Pelican cloud complexes

The processes which regulate the star-formation within molecular clouds are still not well understood. Various star-formation scaling relations have been proposed to explain this issue by formulating a relation between star-formation rate surface density ($\Sigma_{\rm SFR}$) and the underlying gas surface density ($\Sigma_{\rm gas}$). In this work, we test various star formation scaling relations, such as Kennicutt-Schmidt relation, volumetric star-formation relation, orbital time model, crossing time model, and multi free-fall time scale model towards the North American and Pelican Nebulae complexes and in cold clumps associated with them. Measuring stellar-mass from young stellar objects and gaseous mass from CO measurements, we estimated mean $\Sigma_{\rm SFR}$, star formation rate per free-fall time, and star formation efficiency (SFE) for clumps to be 1.5 $M_\odot yr^{-1} kpc^{-2}$, 0.009, 2.0%, respectively, while for the entire NAN complex the values are 0.6 $M_\odot yr^{-1} kpc^{-2}$, 0.0003, and 1.6%, respectively. For clumps, we notice that the observed properties are in line with the correlation obtained between $\Sigma_{\rm SFR}$ and $\Sigma_{\rm gas}$, and between $\Sigma_{\rm SFR}$ and $\Sigma_{\rm gas}$ per free-fall time (see Figure no. 10) and orbital time for Galactic clouds. At the same time, we do not observe any correlation with $\Sigma_{\rm gas}$ per crossing time and multi free-fall time. Even though we see correlations in former cases, however, all models agree with each other within a factor of 0.5 dex, and discriminating between these models is not possible due to the current uncertainties in the input observables. We also test the variation of $\Sigma_{\rm SFR}$ versus the dense gas, but due to low statistics, a weak correlation is seen in our analysis.
This work has been done in collaboration with Swagat R. Das, Jessy Jose (IISER, Tirupati), Shaobo Zhang (CAS, China), Neelam Panwar (ARIES, Nainital) and other team members from various internationl institutes/organizations.

doi : https://doi.org/10.1093/mnras/staa3222

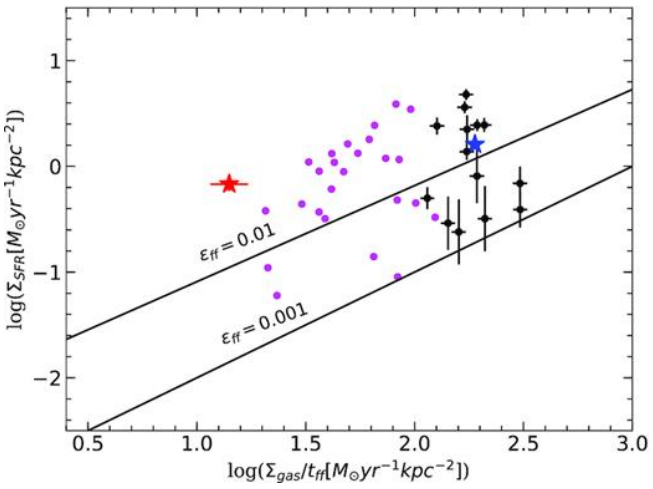

Figure no. 10: The variation of $\Sigma_{\rm SFR}$ with Σ_{gas}/t_{ff}. The two solid lines correspond to the volumetric star formation relation with $\epsilon_{\rm ff} = 0.01$ (top) and $\epsilon_{\rm ff} = 0.001$ (bottom). The black filled circles show the values within the 14 clumps from our study. The red and blue stars represent the values obtained over the entire NAN complex and the average value of all the clumps. Magenta dots are for the sources of Evans et al. (2014).

(Manash Samal)

Asteroseismology of SZ Lyn using multiband high time resolution photometry from ground and space

Z Lyn is a Delta Scuti type pulsating star in a single line spectroscopic binary system. The star is identified as a radial pulsator with a fundamental radial mode of 8.296 d^{-1}. The Delta Scuti stars show radial and non-radial oscillations with periods of less than 1 day. Therefore, m v = 9.1 mag. SZ Lyn was investigated in multi-band photometry using 50 cm CDK reflector at Mount Abu for frequencies of radial and non-radial modes.

The observations were carried out between December 2013 and November 2016. A total of 4328 frames in B, 4569 in V and 6836 in R during the seven nights covering at least one pulsation cycle of SZ Lyn in each night. In addition, the analysis includes data from two ground based observatories, APT (Arizona), Super WASP and space based mission of TESS. The well resolved light curves and power spectra (Figure no. 11) of data from ground and space reveal the presence of 23 frequencies with four independent modes, 13 harmonics of the fundamental radial mode. The frequency 8.296 d^{-1} is identified as the fundamental radial mode by amplitude ratios of UBVR bands. The frequencies 14.535 d^{-1}, 32.620 d^{-1} and 4.584 d^{-1} are newly discovered independent modes of SZ Lyn. Out of these three, 14.535 d^{-1} and 32.620 d^{-1} are identified as low order p-modes and 4.584 d^{-1} as medium order g-mode.

The mode identification of oscillation frequencies leads to redefine the physical parameters of SZ Lyn with a proper modeling. Our work shows that even after the very well sampled high quality photometry from the space based TESS mission, the multi-wavelength coverage from the ground (such as from the MIRO) are very important to have a better understanding of the models. A best model is resulted for SZ Lyn through the optimization of stellar evolutionary and pulsation models with observed frequencies. The model corresponds to 7500 K ¡ T_{eff} ¡ 7800 K, log (g) 3.81±0.06 and mass 1.7-2.0 M_{sun}.

This work was carried out in collaboration with Janaka Adassuriya (ACC, Sri Lanka), J. L. Gutierrez (UPC, Spain), G. Handler (NCAC, Poland), S. Joshi (ARIES, India), K P S C Jayaratne (UC, Sri Lanka).

doi : https://doi.org/10.1093/mnras/staa3923

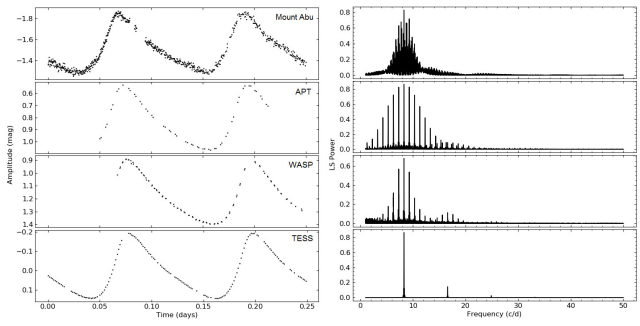

Figure no. 11: Light curves and power spectra of the observations.

(S. Ganesh and K S Baliyan)

CK Vulpeculae: Revealing a Remarkably Powerful Blast from the Past

CK Vulpeculae which erupted in AD 1670-71 which was long considered to be the first well documented nova outburst. It is an iconic object which was studied by some of the most distinguished astronomers of that era like Hevelius, Cassini and Haley. However, recent observations have required that alternative scenarios be considered for its explosion. Long slit infrared spectroscopy of a forbidden line of iron reported here has revealed high line-of-sight velocities ($\sim \pm$ 900 km/s) of the ansae at the tips of the bipolar lobes imaged in H_α in 2010 (see Figure no. 12). The deprojected velocities of the tips are approximately $\pm$ 2130 km/s assuming the previously derived inclination angle of 65o for the axis of cylindrical symmetry of the bipolar nebula. Such high velocities are in stark contrast to previous reports of much lower expansion velocities in CK Vul. Based on the deprojected velocities of the tips and their angular expansion measured over a 10-year baseline, we derive a revised estimate, with estimated uncertainties, of 3.2 kpc for the distance to CK Vul. This implies that the absolute visual magnitude at the peak of the 1670 explosion was M_V = -12.4, indicating that the 1670 event was far more luminous than previous estimates and brighter than any classical nova or any Galactic stellar merger. We propose that CK Vul belongs to the class of Intermediate Luminosity Optical Transients (ILOTs), objects which bridge the luminosity gap between novae and supernovae. While eruptions in lower luminosity ILOTs are attributed to merger events, the origin of the highly luminous ILOT outbursts is currently not known.

This work is done in collaboration with T. R. Geballe (Gemini Observatory, USA), A. Evans(Astrophysics Group, Lennard Jones Laboratories, Keele University, UK), M. Shahbandeh (Minnesota Institute for Astrophysics, University of Minnesota, USA), C.

doi : https://doi.org/10.3847/2041-8213/abc885

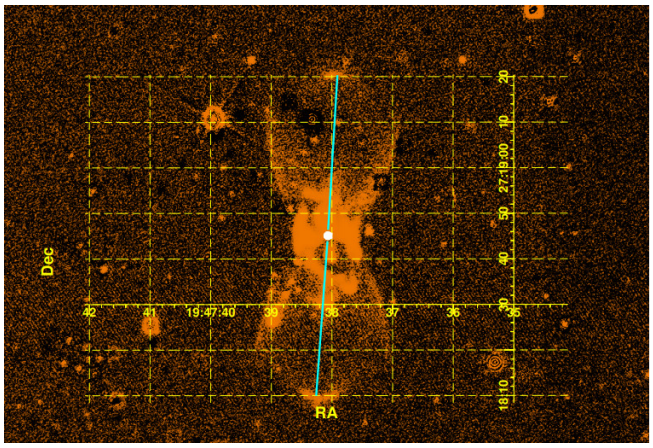

Figure no. 12: H_α continuum-subtracted image of CK Vul observed on 2010 June 22 with the Gemini North Telescope. The position of the compact radio source is indicated by the white dot. The slit (cyan line) was centered on this source and passes through the tips of the ansae located near the top and bottom center of the image.

(D P K Banerjee)

Ultra-violet Spectroscopy from AstroSat confirms the symbiotic nature of SU Lyn

The ultra-violet(UV) spectroscopy data from Ultra-Violet imaging telescope (UVIT) onboard India's AstroSat space observatory has been used, for the first time, to resolve the nature of a peculiar star named SU Lyn. SU Lyn had long been known as an ostensibly unremarkable red giant star. However, it was noticed in 2016 that hard X-ray emission was emanating from SU Lyn. This raised the suspicion that the star harboured a hidden, hot companion assumed to be a white dwarf. A definite way to establish the presence of a white dwarf is through ultra-violet (UV) observations since white dwarfs are hot and emit radiation mostly in the UV range. The PRL team had been observing SU Lyn since 2016 with various Indian observing facilities and a suite of instruments, most notably with the UVIT. From the ground, the star was observed with the HESP instrument on the IIA-HCT telescope, with the indigenous in-house developed MFOSC-P spectrograph and with the Near-Infrared Camera and Spectrometer on the PRL 1.2 m telescope at Mount Abu.

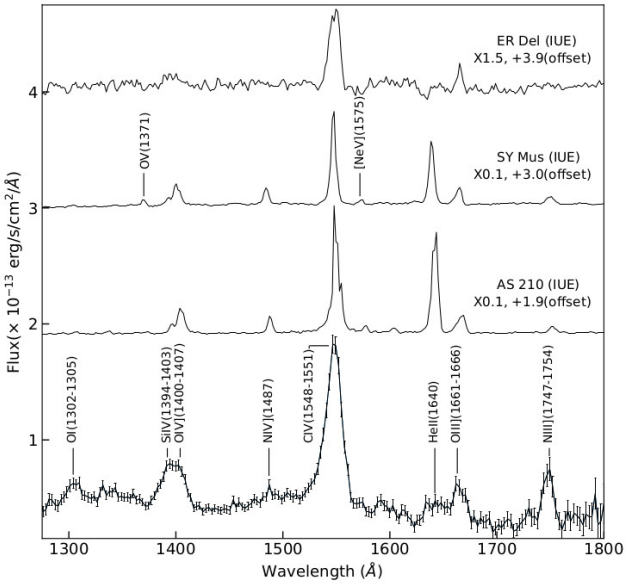

Figure no. 13: The AstroSat-UVIT spectrum of SU Lyn with the emission lines identified. Archival spectra of three other symbiotic systems (ER Del, SY Mus and AS 210) are also shown for comparison.

The Far-UV (1300-1800 Angstroms) spectrum of SU Lyn (Figure no. 13), obtained with the AstroSat-UVIT instrument, showed emission lines of silicon (Si IV), carbon (C IV), oxygen (OIII), and nitrogen (N III) in a spectrum typical of symbiotic stars – the binary star systems consist of a red giant and a white dwarf. Thus, it confirmed the existence of a hidden white dwarf, thereby making SU Lyn a rare member of the class of symbiotic systems. Further, the UV, optical, and NIR spectra together were used to conclude that the white dwarf is not sufficiently hot to produce the typical emission lines in the optical spectrum. This was the reason that SU Lyn had not shown any signatures of hosting a white dwarf from ground-based observations. This study also proved that most of the UV radiation was not coming from the white dwarf. Instead, it originated from the material which the white dwarf was fetching from the red giant companion in the form of an accretion disk.

doi : https://doi.org/10.1093/mnrasl/slaa159

(Vipin Kumar, Mudit K. Srivastava, Dipankar P.K. Banerjee, and Vishal Joshi)

Revisiting the spectral and timing properties of 4U 1909+07 with NuSTAR and Astrosat

High mass X-ray binaries (HMXBs) are known to consist of a compact object (mostly a neutron star) and a massive ($>$10 solar-mass) OB optical companion in a close binary. The material from the companion primarily gets accreted onto the neutron star by falling into its deep gravitation potential. This process releases an enormous amount of energy, mostly in the X-ray range of the electromagnetic spectrum. Depending on the nature of the optical companion, the mass transfer can take place differently between two sub-classes of HMXBs viz. super-giant X-ray binaries and Be/X-ray binaries. The compact object in super-giant X-ray binaries (SGXBs) captures sporadically a small fraction of the stellar wind from its super-giant companion. The luminosity of the compact object reaches as high as 10^{35} erg/s in most of SGXBs. Luminosity with one to three orders of magnitude higher has also been observed from a couple of SGXB systems. Strong magnetic field of the neutron stars, with a field strength of B$\sim$10^{12} G in HMXBs, guides the accreted matter beyond the magnetospheric radius. The field lines funnel the plasma onto a confined region at the magnetic poles forming hot spots and accretion columns on the neutron star surface. X-ray pulsations from the neutron star are observed when the hot spot rotates around the spin axis of the system. Pulse profiles of these pulsating neutron stars (pulsars) provide information on emission geometry and also on the distribution of matter in its close proximity. A typical energy spectrum of a pulsar is shaped by thermal and bulk Comptonization processes in the accretion column that can be described by an empirical power law model modified with a high energy cutoff.

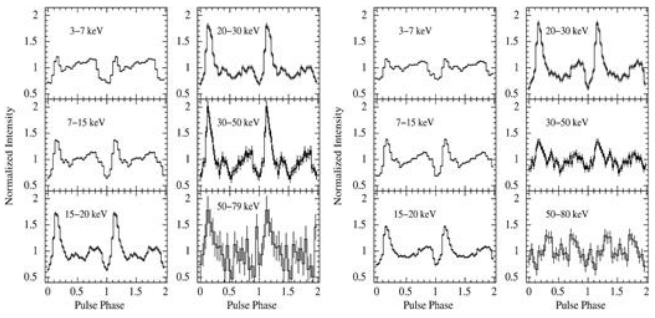

Figure no. 14: Energy resolved pulse profiles of 4U 1909+07 obtained by folding the light curves from NuSTAR (left) and Astrosat/LAXPC (right) observations with the estimated spin periods. Two pulses are shown in each panel for clarity. The error-bars represent 1σ uncertainties.

We carried out a detailed study of the high-mass X-ray binary pulsar 4U 1909+07 using NuSTAR and Astrosat observations in July 2015 and 2017, respectively. X-ray pulsations at 604 s are clearly detected in our study. Based on the long-term spin-frequency evolution, the source is found to spun-up in the last 17 yr. We observed a strongly energy-dependent pulse profile that evolved from a complex broad structure in soft X-rays into a profile with a narrow emission peak

followed by a plateau in energy ranges above 20 keV (Figure no. 14). This behaviour ensured a positive correlation between the energy and pulse fraction. The pulse profile morphology and its energy evolution are almost similar during both the observations, suggesting a persistent emission geometry of the pulsar over time. The broad-band energy spectrum of the pulsar is approximated by an absorbed high-energy exponential cut-off power-law model with iron emission lines. In contrast to the previous report, we found no statistical evidence for the presence of cyclotron absorption features in the X-ray spectra. We performed phase-resolved spectroscopy using data from the NuSTAR observation. Our results showed a clear signature of absorbing material at certain pulse phases of the pulsar. These findings are discussed in terms of stellar wind distribution and its effect on the beam geometry of this wind-fed accreting neutron star. We also reviewed the subsonic quasi-spherical accretion theory and its implication on the magnetic field of 4U 1909+07 depending on the global spin-up rate.

This work was done in collaboration with Gaurava K. Jaisawal of National Space Institute, Technical University of Denmark, Denmark.

doi : https://doi.org/10.1093/mnras/staa2604/

(Neeraj Kumari and Sachindra Naik)

Timing and Spectral Properties of Newly Discovered Black hole Transient MAXI J1348-630

Transient black hole X-ray binaries (BHXRBs) generally spend most of the time in quiescent state with occasional outbursts. During X-ray outbursts, a significant amount of matter from the companion star gets accreted onto the central black hole via accretion disk. During the accretion process, the gravitational potential energy of the accreted matter gets converted to heat and radiation which is emitted in the entire electromagnetic wavebands. Recently discovered black hole candidate (BHC) MAXI J1348-630 went into an outburst in January 2019.

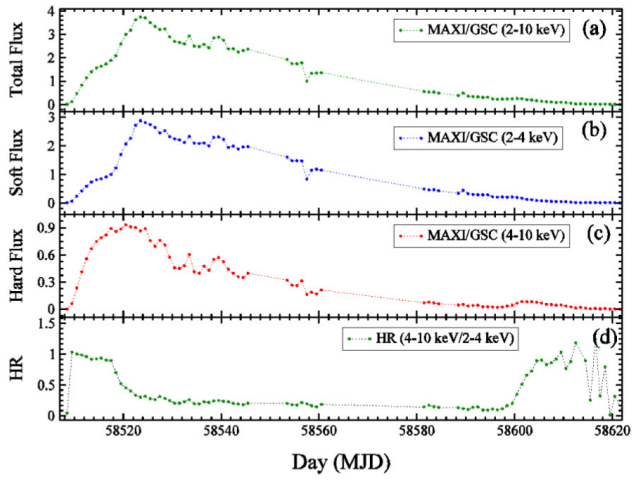

Figure no. 15: X-ray light curves of the recently discovered black hole transient MAXI J1348-630. The source flux (in Crab units) during the 2019 outburst, in 2-10 keV (a), 2-4 keV (b) and 4-10 keV (c) ranges are shown. The hardness ratio (ratio between the light curves in 4-10 keV range and 2-4 keV range) curve is shown in bottom panel (d).

The outburst was simultaneously discovered by MAXI/GSC and Swift/BAT on 26 January, 2019. It was also observed with other X-ray satellites such as INTEGRAL, NICER andHXMT. The BHC was also observed in other wavebands such as optical and radio. The 2019 outburstcontinued for about 4 months. After that, the source went to the quiescent state. Since then, the BHC was observed to re-brightened briefly twice. The 2019 outburst started on 26 January, 2019 (MJD = 58509). In the rising phase, the $2 - 10$ keV X-ray intensity increased rapidly till February 9 2019 (MJD = 58523). After that, it decreased slowly (Figure no. 15). Thus, the outburst can be termed as 'slow-rise-slow-decay' type. We have studied the spectral and timing properties of MAXI J1348-630 in details during the 2019 outburst. We used simultaneous observation of Swift/XRT, Swift/BAT and MAXI/GSC in the energy range of 1-150 keV. We carry out the spectral analysis with the two component advective flow (TCAF) solution. With this, we extracted flow parameters such as Keplerian disk rate, sub-Keplerian halo rate, shock location and shock compression ratio. Based on the variation of accretion rates and hardness ratio, we classified the entire outburst as follows : HS (rising phase) $\rightarrow$ HIMS (rising phase) $\rightarrow$ SIMS (rising phase) $\rightarrow$ SS $\rightarrow$ SIMS (decay phase) $\rightarrow$ HIMS (decay phase) $\rightarrow$ HS (decay phase). During the outburst, we observed quasi periodic oscillation (QPO) only in 2 observations. From the spectral analysis, we estimated the mass of the black hole is 9.1 solar-mass.

doi : https://doi.org/10.3847/1538-4357/ab9696

(Arghajit Jana, Neeraj Kumari and Sachindra Naik)

Probing Nuclear and Circumnuclear Properties of NGC 6300 using X-ray Observations

Active galactic nuclei (AGNs) are the most energetic persistent objects in the universe. The AGNs are powered by the accreting supermassive black holes (SMBH) which reside at the centre of each galaxy. The matter from the surrounding medium is accreted in the form of a geometrically thin, optically thick accretion disc around the blackhole, also known as the standard disc. The accretion disc, in case of AGNs, predominately radiates in the UV/optical wavebands and creates the so-called 'big-blue-bump' in the broadband spectral energy distribution (SED). The X-rays, on the other hand, are emitted from a Compton cloud located within a few tens of Schwarzschild radii around the central engine. The X-rays can be produced by the inverse-Compton scattering of the UV/optical photons originating from the accretion disc. The hard X-ray photons are reflected at the relatively cold matter and produce Fe fluorescent line. Thus, along with the primary X-ray continuum, a reflection hump at $\sim$15-30 keV energy range, and a Fe fluorescent line at $\sim$ 6.4 keV are observed in the X-ray spectrum of AGNs. An additional soft X-ray ($<$ 2 keV) component, known as 'soft excess' is often observed in the AGN spectra. The 'soft excess' could have a completely different origin than the primary continuum, and is often associated with the host galaxy. AGNs are classified as type-I or type-II based on the observation of broad line emission (originate in the broad line emitting region or BLR) or narrow line emission (originate from narrow line emitting region or NLR) in the optical wavebands. In type-I AGN, both broad lines and narrow lines are observed, while in type-II AGN, only narrow lines are observed in the optical spectra. Seyfert 2 galaxies are the radio-quiet type-II AGNs. In this case, a dusty torus, located far away (a few parsecs) from the nucleus, surrounds the circumnuclear region.

We carried out a detailed X-ray timing and spectral analysis of the Seyfert 2 galaxy NGC 6300 by using observations from the Suzaku observatory, theChandra X-ray Observatory and the Nuclear Spectroscopic Telescope Array (NuSTAR) mission between 2007 and 2016. We calculate the variance and the rms fractional variability of the source in different energy bands and we find variabilities in various energy bands. Spectral properties of the source are studied by using various phenomenological and physical models. The properties of the Compton clouds, reflection, Fe K_α line emission and soft X-ray excess are studied in detail. Several physical parameters of the source are extracted and investigated to establish the presence/absence of any correlation between them. We also investigate the nature of the circumnuclear 'torus' and we find that the torus is not uniform, but clumpy. The observed changes in the line-of-sight column density (Figure no. 16) can be explained in terms of transiting clouds. The iron line-emitting region is found to be different in the different epochs of observations. We also observe that the torus and the nucleus independently evolve over the years.

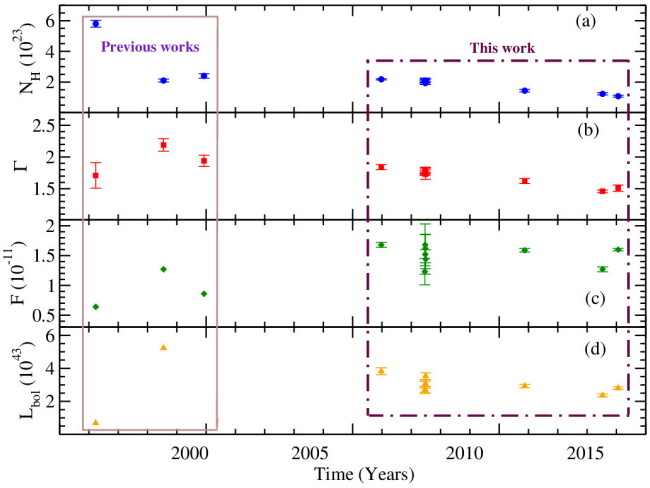

Figure no. 16: Variation of (a) line-of-sight column density (N_H) in 10^{23} cm^{-2} unit, (b) photon index (Γ), (c) 2−10 keV absorbed flux (F) in 10^{-11} ergs cm^{-2} s^{-1} unit and (d) 2 − 10 keV bolometric luminosity (Lbol) in 10^{43} ergs/s unit are shown over the years.

doi : https://doi.org/10.1093/mnras/staa2552

(Arghajit Jana, Neeraj Kumari and Sachindra Naik)

AstroSat Observations of the first Galactic ULX Pulsar Swift J0243.6+6124

Ultra-luminous X-ray sources (ULXs) are non-nuclear point-like objects with apparent luminosities exceeding 10^{39} erg/s. A majority of the ULXs are found in external galaxies and are often considered promising candidates to host heavier than stellar-mass black holes. Coherent X-ray pulsations were discovered from a ULX in M82, thanks to the fast timing capability of NuSTAR, making it the first Ultra-luminous X-ray pulsar (ULP). A new transient X-ray source, Swift J0243.6+6124 was detected in outburst by Swift-BAT on October 3, 2017 and X-ray pulsations at ∼9.86 s were detected with Swift-XRT in the 0.2-10 keV band. This outburst lasted for about five months, and several multi-wavelength observations were performed from radio to hard X-rays. The optical spectroscopic observations revealed that the optical counterpart in the system is a late Oe- or early Be-type star. Later, the Be/X-ray binary (BeXRB) nature of the source was confirmed. The peak X-ray luminosity of the pulsar exceeds the Eddington limit for a neutron star (NS) by a factor of ∼ 40, thus, making the pulsar the first Galactic X-ray pulsar to belong to the recently discovered family of ULPs. AstroSat observed the pulsar twice as part of the Target of Opportunity (ToO) program.

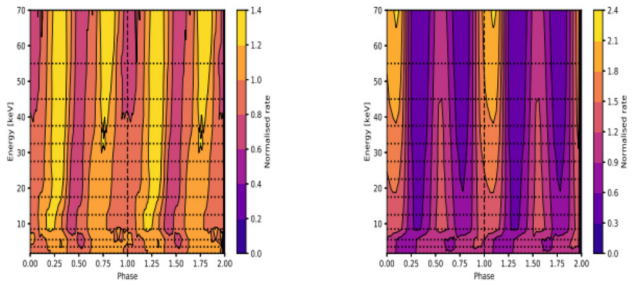

Figure no. 17: Energy-resolved pulse profiles for Swift J0243.6+6124 from SXT and LAXPC data of first AstroSat observation (Left) and second observation (Right). Yellow (Purple) colour correspond to higher (lower) count rates at different phases and energies. Horizontal cuts are pulse profiles for the selected energy range while the vertical cut represent spectra during one complete rotation cycle.

Our broadband timing and spectral observations from AstroSat data show that X-ray pulsations at ∼ 9.85 s have been detected up to 150 keV when the source was accreting at the super-Eddington level. The pulse profiles are a strong function of both energy and source luminosity, showing a double-peaked profile (Figure no. 17) with pulse fraction increasing from ∼ 10% at 1.65 keV to 40-80% at 70 keV. The pulse profiles show a strong energy and luminosity dependence which is consistent with results from NICER and Fermi–GBM. The continuum X-ray spectra are well-modeled with a high energy cut-off power law (Γ ∼ 0.6-0.7) and one or two blackbody components with temperatures of ∼ 0.35 keV and 1.2 keV, depending on the accretion level. No iron line emission is observed at sub-Eddington level, while a broad emission feature at around 6.9 keV is observed at the super-Eddington level, along with a blackbody radius (121 - 142 km) that indicates the presence of optically thick outflows. Our study of broad-band X-ray spectra does not show any dip-like feature indicative of a cyclotron line. Spectral data from observations made at the sub-Eddington level could be modeled well using an absorbed high energy cut-off power law and a blackbody. Data obtained during the super-Eddington phase of the source, however, requires additional components such as another blackbody and a Gaussian component for the iron emission line.

This work was done in collaboration with Aru Beri of IISER, Mohali.

doi : https://doi.org/10.1093/mnras/staa3254

(Sachindra Nayak)

VHE gamma-ray detection of FSRQ QSO B1420+326 and modeling of its enhanced broadband state in 2020

QSO B1420+326 is a blazar classified as a flat-spectrum radio quasar (FSRQ) which was found to be in an enhanced flux state at the beginning of the year 2020. Our aim was to search for

very high-energy (VHE) gamma-ray emission from the blazar during this flaring state and trace the flare evolution via an extensive multiwavelength (MWL) campaign.

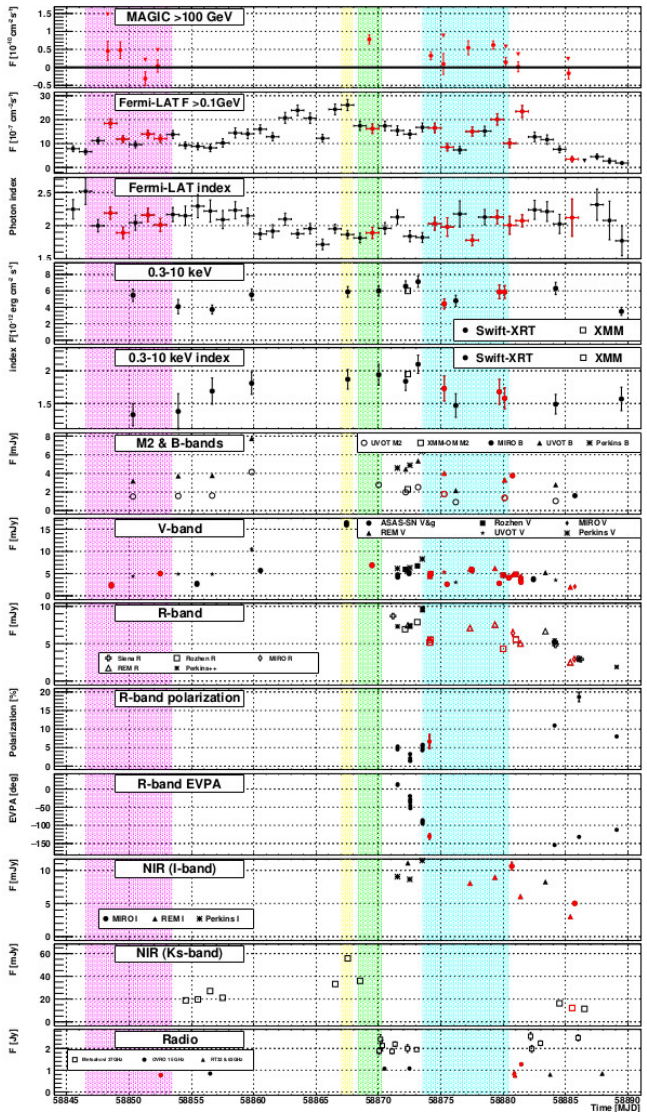

Figure no. 18: MWL light curve of QSO B1420+326 between Dec 28, 2019 and Feb 11, 2020 (see titles and legends of individual panels). Optical and UV observations are corrected for the Galactic attenuation. The points in red are contemporaneous ($\pm 12\ hr$) with MAGIC observations. The shaded regions show the time ranges of the four considered flare evolution periods. Flux upper limits in the first two panels are shown with downward triangles.

The source was observed with a number of instruments in radio, near-infrared, optical (including polarimetry and spectroscopy), ultraviolet, X-ray, and gamma-ray bands. Among these, we carried out photometric optical observations with the MFOSC-P instrument, used in imaging mode, mounted on the $1.2\ m$ telescope of Mount Abu IR Observatory. This blazar was observed in B, V, R, and I bands (Johnson-Cousins filters) on MJD 58880 and MJD 58885. The data was reduced (including bias subtraction, flat-fielding, and cosmic-ray correction) and analyzed using standard photometry packages from Image Reduction and Analysis Facility (IRAF). For each image the PSF value was measured and aperture photometry was applied. Standard stars from the SDSS DR12 and VizieR catalogs were used for photometric calibration. In Figure no. 18, we present the MWL light curve summarizing the evolution of the flare. Based on the VHE state of the source we defined three periods selected for further analysis: A: MJD 58846.5 - 58853.5 (without VHE gamma-ray detection), C: MJD 58868.3 - 58870.3 (VHE gamma-ray flare), D: MJD 58873.5 - 58880.5 (detection over longer time scale). In addition, we defined the fourth period: B: MJD 58867 - 58868, which does not have simultaneous gamma-ray data from MAGIC telescopes but contains the peak of the optical and IR flare as well as one of the local peaks of HE emission.

Further, dedicated optical spectroscopy results were used to estimate the accretion disk and the dust torus luminosity. Spectral energy distribution modeling was performed in the framework of combined synchrotron-self-Compton and external Compton scenario in which the electron energy distribution is partially determined from acceleration and cooling processes. Based on the MWL study it is noticed that during the enhanced state, the flux of both SED components of QSO B1420+326 drastically increased and the peaks were shifted to higher energies. Follow-up observations with the MAGIC led to the detection of VHE gamma-ray emission from this source, making it one of only a handful of FSRQs known in this energy range.

This work was done in collaboration with J. Sitarek (UL, Poland) et al. for the MAGIC and F. D'Ammando (INAF, Italy) et al. for the Fermi-LAT collaboration.

doi : https://doi.org/10.1051/0004-6361/202039687

(Prachi Prajapati, Parveen, S. Ganesh)

The Relativistic jet orientation and host galaxy of the peculiar blazar PKS 1413+135

PKS 1413+135 is one of the most peculiar blazars known with its strange properties that led to the hypothesis almost four decades ago that it is gravitationally lensed by a mass concentration associated with an intervening galaxy. It exhibits symmetric achromatic variability, a rare form of variability that has been attributed to gravitational milli-lensing. It has been classified as a BL Lac object, and is one of the rare objects in this class with a visible counterjet.

BL Lac objects have jet axes aligned close to the line-of-sight. Based on high resolution radio observations it has also been classified as a compact symmetric object - objects that have jet axes not aligned close to the line of sight. Intensive efforts to understand this blazar have hitherto failed to resolve even the questions of the orientation of the relativistic jet and the host galaxy. Answering these two questions is important because they challenge our understanding of jets in active galactic nuclei and the classification schemes we use to describe them. We show that the jet axis is aligned close to the line-of-sight and PKS 1413+135 is almost certainly not located in the apparent host galaxy, but is a background object in the redshift range $0.247 < z < 0.5$. The intervening spiral galaxy at $z = 0.247$ provides a natural host for the putative lens responsible for symmetric achromatic variability and is shown to be a Seyfert 2 galaxy (see Figure no. 19). We also show that a multizone model is needed to account for the high-energy emission.

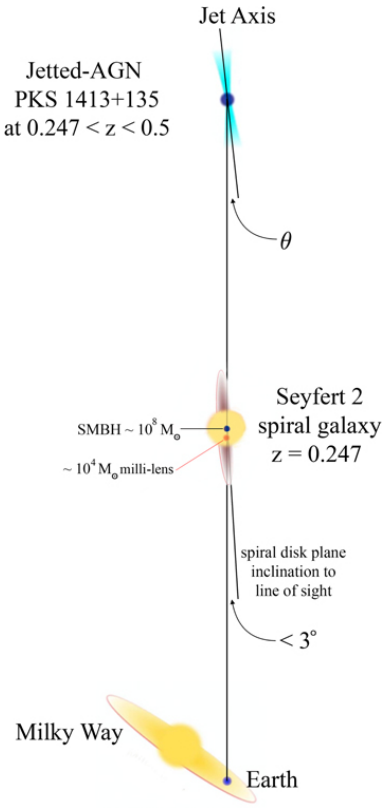

Figure no. 19: The orientation of the blazar PKS 1413+135 and the Seyfert 2 spiral active galaxy at z = 0.247. The angle θ indicates the angle between the jet axis and the line-of-sight. Three gravitational lensing systems considered are : (i) the nuclear bulge of the spiral galaxy, (ii) the SMBH powering the spiral AGN, and (iii) the putative milli-lens.

This work has been done in collaboration with Prof. Anthony C.S. Readhead and Dr. Vikram Ravi (Owens Valley Radio Observatory, California Institute of Technology, Pasadena, USA) and other team members from various international organizations.

doi : https://doi.org/10.3847/1538-4357/abd08c

(Veeresh Singh)

uGMRT detection of HI 21-cm absorption in a radio AGN at z = 3.5

Using upgraded Giant Metrewave Radio Telescope we detect HI 21-cm absorption associated with a radio active galactic nucleus (AGN) 8C 0604+728 at $z = 3.53$. The source is at the highest redshift for which associated HI 21-cm absorption has been discovered till date, surpassing earlier known absorber at $z = 3.39$. The uGMRT observations towards the target were conducted using the 250−500 MHz receiver and software correlator. We used a bandwidth of 4.17 MHz centred at 313.6 MHz, and subdivided into 512 channels, which provided a velocity resolution of 7.8 km s^{-1} and a coverage of 3994 km s^{-1}. Figure no. 20 shows the HI 21-cm absorption spectrum towards 0604+728. This source also shows UV variability on the timescales of years and we estimate ultraviolet luminosities of 3.2 $\times$ 10^{23} W Hz^{-1} and 6.2 $\times$ 10^{23} W Hz^{-1}, and ionizing photon rates of 1.8 $\times$ 10^{56} s^{-1} and 5.0 $\times$ 10^{56} s^{-1}, using data of two different epochs. The UV luminosity and photon rate in later epoch are nearly 6.2 and 1.7 times higher than thresholds suggested in the literature above which all the neutral hydrogen in the AGN host galaxy is expected to be ionized. The detection demonstrates that neutral hydrogen can survive in the host galaxies of AGNs with high ultraviolet luminosities. Optical spectrum shows a high equivalent width ratio of 15.2 for the Lyman-α (Ly α) and He I emission lines, which is consistent with AGN photoionization models. However, a significant contribution from young stellar populations to the excess Lyα flux cannot be ruled out.

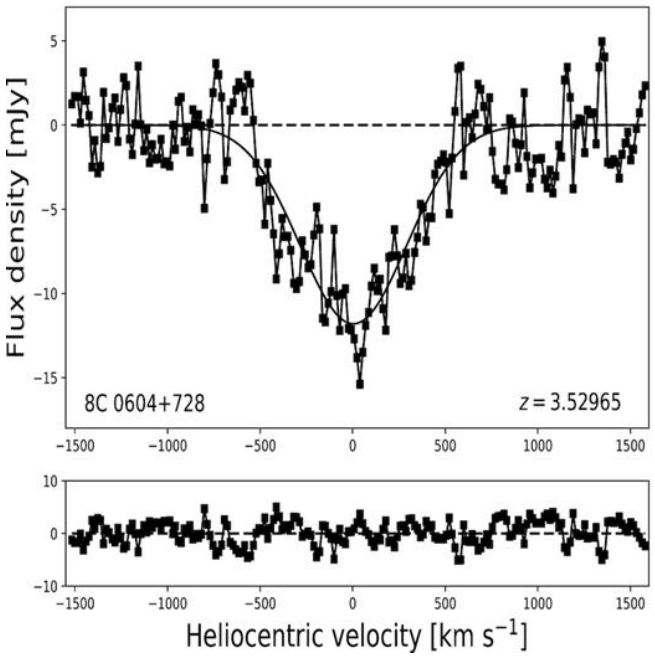

Figure no. 20: The HI 21-cm absorption spectrum towards 0604+728, at z = 3.53. The top panel shows a Gaussian fit to thee absorption feature, while the bottom panel shows the residual after the fit is subtracted from the spectrum.

This work has been done in collaboration with Dr. Regina Jorgenson (Maria Mitchell Observatory Nantucket USAA), Prof. Tao An (Shanghai Astronomical Observatory China) and Dr. Yogesh Chandola (Purple Mountain Observatory Nann jing China).

doi : https://doi.org/10.1093/mnras/staa3306

(JNHS Aditya, Vishal Joshi, Veeresh Singh)

The PRL 2.5m Telescope Project and PARAS-2 project

PRL is developing a new facility of state-of-the-art 2.5m telescope. The telescope will have most advanced active optics system and tip/tilt mechanism for first order seeing correction for the first time in the country. The telescope was built by M/s. AMOS,S.A., Belgium and in the month of October 2020 the Factory Acceptance Test took place. Figure no. 21a below shows the complete telescope being tested at the Factory and Figure no. 21b shows many millisecond exposure star images being stacked together.

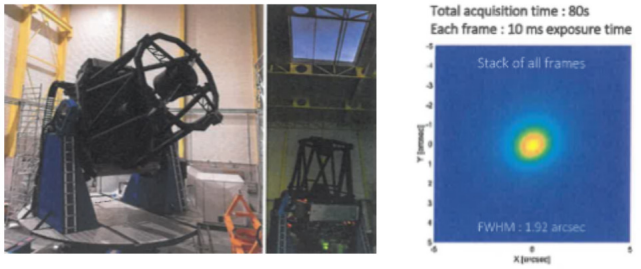

Figure no. 21: The telescope being tested on sky (left panel) and stack of star images (right panel).

The individual images had about 10millisec exposers a time under which the atmosphere is partially frozen and hence ideal test the telescope optics using star light. The graph (Figure no. 22) below shows the best individual exposure frames showed an star FWHM of 0.31 arcsecs which is very close of encircled enclosed energy of 80% with in 0.35 arcecs.

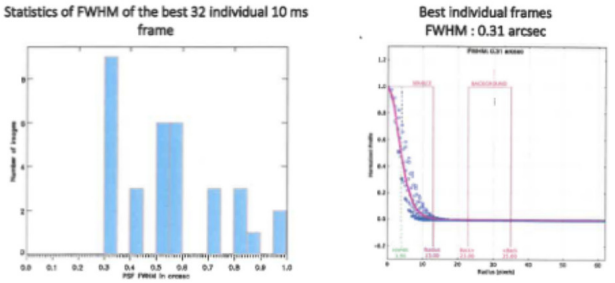

Figure no. 22: Left graph shows star PSF FWHM versus total number of images, while the right graph shows the best star FWHM achieved by the telescope optics in spite of large atmospheric turbulence and bad seeing of 2arcsecs in Belgium.

At Gurushikar, Mt. Abu the actual telescope site we have median seeing of better than 1.4arcsecs and hence the star images are expected to be excellent. The demonstration of 0.31arcsecs star FWHM shows that the telescope optics are excellent with most precise polished primary mirror in the country (rms 26 nanometres polishing errors) in the country. The telescope boxes have arrived at the site after the successful completion of FAT at Belgium. The telescope is expected to see first light from Gurushikar, Mt. Abu late 2021 or early 2022.

PARAS-2 (PRL Advanced Radial-velocity Abu-sky Search) is one of the first light instrument for the 2.5m telescope. PARAS-2 is an optical fiber-fed, temperature and vacuum stabilized high resolution (R 100,000) spectrograph with dedicated time on the 2.5m telescope for exoplanet sciences namely discoveries and characterizations. PARAS-2 was developed in PRL-Ahmedabad campus and has demonstrated resolution of 100,000 between 380nm and 700nm wavelengths. This is for the first time such a spectrograph has been developed in the country that has capacity of 100,000 resolution. Figure no. 23 below shows a snapshot of the spectrograph inside the vacuum chamber along with test solar spectra.

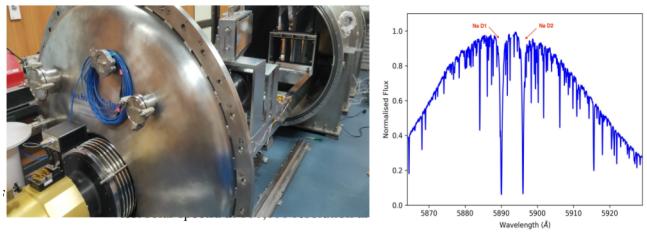

Figure no. 23: The spectrograph will be ready for doing science along with the 2.5m telescope late 2021 or early 2022.

(Abhijit Chakrborty)

NISP instrument development work

etector with $2\mathrm{K} \times 2\mathrm{K}$ pixels) will be used with SIDECAR ASIC and its control board. Both H2RG and ASIC along with optics and filter wheels will be inside a LN2 cooled vacuum dewar. Various developments related to this work are summarized below.

Temperature servo control

The infrared detector has to be maintained at a stable temperature of ~ 79 K to minimize thermal noise. At the same time the SIDECAR ASIC which controls the detector, is maintained at a stable temperature of ~ 85 K.

To stabilize the detector temperature within tens of mK, Proportional-Integral-Derivative (PID) active control can be used. For this, a laboratory experiment was performed inside a closed chamber with a heat sink at the top as shown in Figure no. 24.

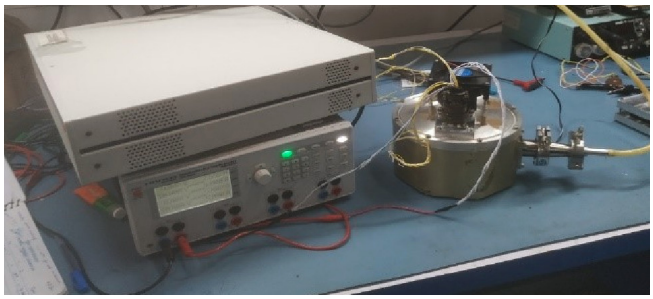

Figure no. 24: Experimental setup for PID active control of temperature.

The setup included a thermocouple type E as a temperature sensor and a resistor of $25\ \Omega$, 100 W as a heating element. The experiment was conducted at room temperature. A Lakeshore temperature controller (model 336) was used for recording sensor temperature and activating closed loop control by setting P, I, & D parameters interactively. For closed loop control, the heater was powered by controlled output and the thermocouple sensor signal was taken as input signal. Different control combinations P, PI, and PID techniques were tested by setting P, I, & D coefficient values.

Initially, we started with PID coefficients as shown in Figure no. 25.

At these values, oscillations of 300 mK were recorded. To minimise these oscillations we performed auto-tuning.

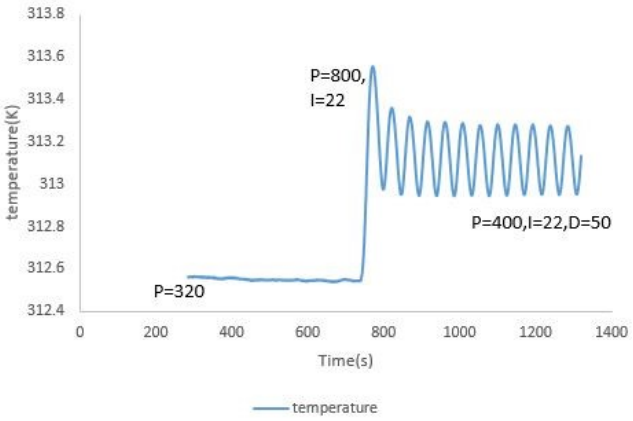

Figure no. 25: Temperature plot vs. data when the coefficients are set interactively.

The controller provides PID control using an 'Autotune' option where it generates the P, I, and D values automatically. Figure no. 26a shows the set point and the temperature variation to determine the P, I, and D values obtained from autotuning. Peak-peak fluctuations of 170 mk were recorded around setpoint temperature of 306 K in the auto-tuning mode. The system parameters (P, I, and D values) achieved from autotune were provided as fixed inputs to the controller to observe the temperature profile shown in the right panel of Figure no. 26. Stability was achieved at the set point temperature and the peak to peak fluctuations were reduced to 30 mk. In conclusion, better stability was achieved using fixed values of the PID parameters.

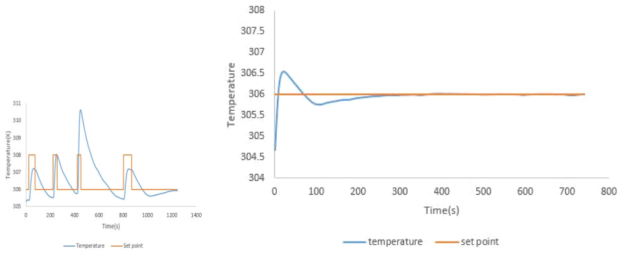

Figure no. 26: Temperature plot vs. data for auto tuning (Left) and with coefficients obtained from auto tune (Right).

Thermal testing of the NISP detector assembly

Detector assembly setup:

As mentioned earlier, the NISP detector is to be operated in vacuum at cryo temperature. For this purpose, a housing was designed and fabricated in the PRL workshop (see Figure no. 27a). The entire detector assembly (Figure no. 27b) is enclosed inside this aluminium detector housing. The assembly is cooled by a Copper cold finger from a cold plate at the base of an LN2 tank. The detector assembly and the detector housing are thermally isolated from surrounding structures. Temperature values are monitored at various locations in the vacuum dewar: on the dummy detector, the Aluminium base plate, the detector housing and the LN2 tank. A vacuum level of 2×10^{-6} mbar and LN2 volume is maintained throughout the test. The temperature values are measured and recorded using Lakeshore temperature controller and the pressure values are also recorded using a full range active pirani/cold cathode gauge.

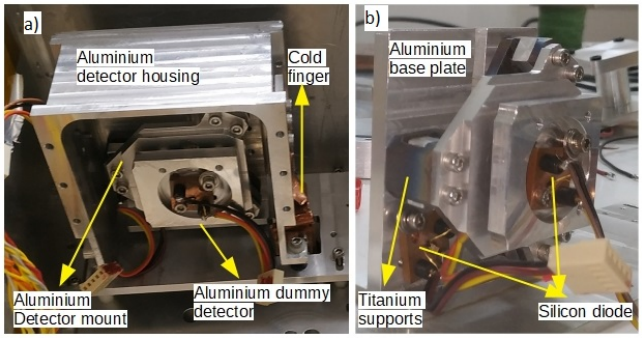

Figure no. 27: a) Detector housing with cold finger connection from LN2 tank. b) Detector assembly with silicon diode

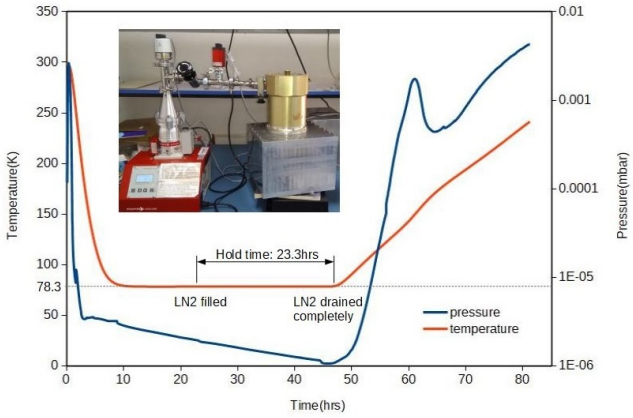

Figure no. 28: Temperature at the location of the dummy detector and Pressure inside the Dewar during cold test

Maximum cooling rate at the location of the dummy detector was observed as 0.864 K/min with stable temperature under no load of 78.3 K at Ahmedabad (corresponding to 76.8 K at Gurushikar, Mt.Abu, Rajasthan, India - with the difference being due to the difference in altitude). The measured temperature stability is ± 0.003 K. LN2 hold time from the above experiment is measured as 23.3 hrs.

Validation of thermal numerical model with experimental results:

A numerical model was developed to determine the cooling rate of the detector assembly (detector, Al base plate and titanium supports combined). The maximum cooling rate from the numerical model was 0.928 K/min whereas 1.01 K/min was observed in our test setup which is within the range required for cooling the infrared detector.

Vacuum Dewar characterisation:

Charcoal getter testing: Different type of getters are used to maintain vacuum levels in Dewar. Depending on the gases to be removed getter

pumps will be selected. Based on the pressure rise profile, gases present inside the Dewar can be found. Major factors for pressure rise inside Dewar are 1. Leak 2. Permeability 3.Out-gassing and 4. Virtual leaks. Volatile compounds and water vapours deposited on the surfaces are the major contributors for out-gassing. Baking, cleaning with ethyl alcohol and increased pumping time will drastically decrease the effect of outgassing and virtual leaks. Leak and permeability are the external contributors where gas molecules in atmosphere enters chamber through material and minute pores. As Nitrogen and oxygen contributes to 99% of air by volume the major portion of the molecules that enters chamber through leak and permeability is nitrogen and oxygen.

Nitrogen, oxygen and water vapour present on surfaces inside Dewar are to be removed to maintain vacuum inside Dewar. To remove water vapours, entire Dewar needs to be baked to 150-300°C for 24-48 hrs under constant pumping condition. Since the Dewar encloses sensitive optics and detector, baking of the Dewar is not possible. As it is very difficult to remove water vapours without baking, cold surfaces inside the Dewar are used for solidification of water vapours which decreases the pressure. The same can be observed in Figure no. 29, where the drop in pressure can be noted with LN2 being filled. The getter which can adsorb nitrogen and oxygen gases at cryogenic temperature and re-activates at room temperature is to be used. Charcoal getter satisfies the above conditions. To characterise the working of getter, two tests were conducted in the test Dewar with and without getter. Pressure in the Dewar with and without getter is 2×10^{-6} mbar and 1×10^{-4} mbar. It can be observed from Figure no. 30, that getter is not only used to maintain vacuum for long durations, it also improves the vacuum level. Average pumping speed of the charcoal getter is calculated as 1.46 l/s (at 10^{-6} mbar).

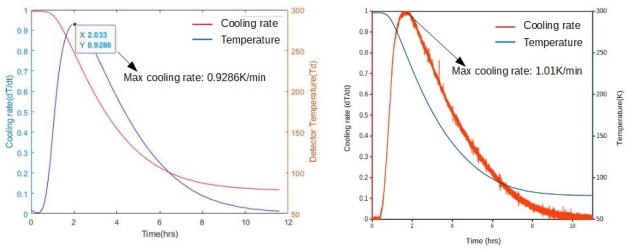

Figure no. 29: Temperature and cooling rate of detector assembly from numerical method (left) and experimental setup (right)

Vacuum leak rate characterisation of the Dewar

The characterisation of the vacuum Dewar used in the above tests is carried out by estimating the vacuum leak rate of the Dewar in the absence of charcoal getter. The leak rate is independently estimated by monitoring the rise in the pressure (left panel of Figure no. 31) in the chamber and also by using an mass-spectrometer leak detector (MSLD – right panel of Figure no. 31). We estimate a leak rate from the pressure profile at the level of 2.93×10^{-6} mbar.l/s while the value estimated from the MSLD is 1.97×10^{-6} mbar.l/s. The source of this nominal leak is the gas permeation through the Viton O-rings (with a permeability rate of 6.6×10^{-7} mbar.l/s-m) used in sealing the joints of the chamber surfaces.

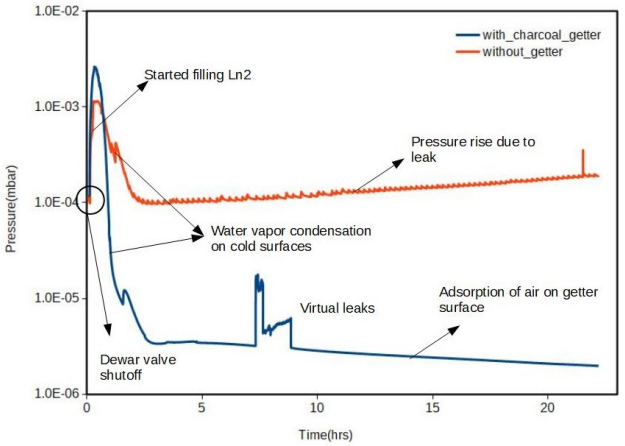

Figure no. 30: Pressure profiles in the chamber with and without charcoal getter.

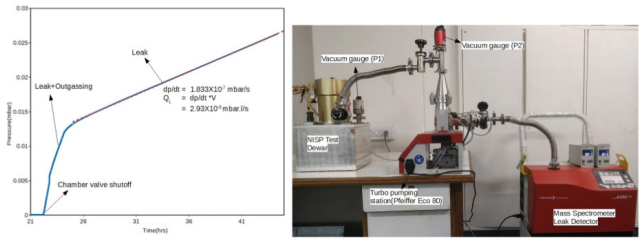

Figure no. 31: Pressure rise profile (left) and Leak test using Mass Spectrometer Leak Detector (right).

(The NISP team: Alka, A B Shah, A Rai, D Sarkar, H Adalja, K S Baliyan, P S Patwal, P Prajapati, P Kasarla, S Naik, S N Mathur, and S Ganesh)

In-flight Calibration of Chandrayaan-2 Solar X-ray Monitor

The *Solar X-ray Monitor* (XSM) on board India's Chandrayaan-2 mission is designed to carry out broadband spectroscopy of the Sun from lunar orbit. It observes the Sun as a star and measures the spectrum every second in the soft X-ray band of 1 – 15 keV with an energy resolution better than 180 eV at 5.9 keV. The Chandrayaan-2 mission was launched on 22 July 2019, and the XSM began nominal operations, in lunar orbit, from September 2019. In-flight observations of the on-board calibration source, background, and the Sun are used to establish the sensitivity and calibration of the XSM.

Spectra obtained with the calibration source over the course of in-flight oeprations have shown that the spectral performance of the instrument has remained constant and identical to that on the ground. Using observations when the Sun is outside the field of view of the instrument, the background spectrum measurements were obtained. It is seen that the the background is approximately 35 times lower than the count rate from the Sun, the lowest observed levels of solar activity, showing that the XSM is sensitive enough to detect solar activity well below A-class.

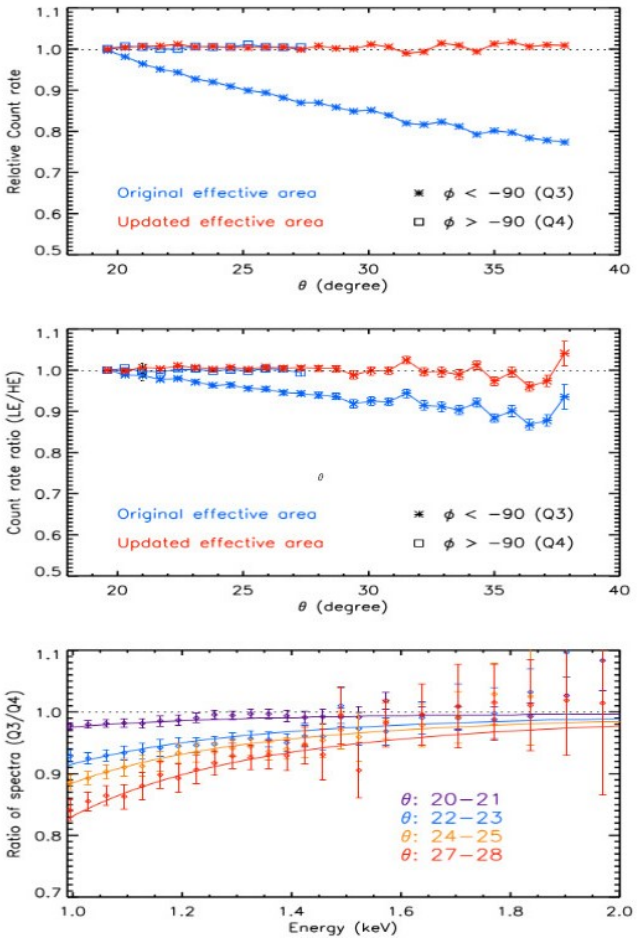

Figure no. 32: Top panel shows normalized XSM count rates during quiet Sun observations as a function of angle for observations over two quadrants of XSM, corrected with the original and updated effective areas. Middle panel is similar to the top panel, but shows the ratio of count rates in lower (1–1.2 keV) and higher (1.2–1.5) energy ranges. Bottom panel shows the ratio of observed spectra in two different quadrants and best fit models of additional absorption are overplotted.

Generally, X-ray spectrometers utilize observations of the standard source Crab for in-flight calibration of effective area, but this is not feasible for the XSM due to its very small aperture area and large field of view and thus we used quiet Sun observations when the inherent source variability was minimum. As the angle between the Sun and the XSM boresight varies with time, the observed raw count rates are expected to be varying even if the source flux remains constant, but these modulations are expected to be corrected after taking into account the angle-dependant effective area. However, it was found that the effective area corrected count rates still show an angle dependance for observations over one quadrant of the XSM detector as shown in Figure no 32a. On further analysis, it was identified that this effect has an energy dependance as demonstrated in Figure no 32b, suggesting an additional absorption factor that depends on angle. We determine this additional absorption factor empirically from the observed spectral ratios shown in Figure no 32c by modeling it as absorption by beryllium. After incorporating this factor in the effective area, the corrected count rates were found to be constant with angle. Thus the on-ground estimate of the effective area has been refined and the uncertainty in the effective area with angle is shown to be within 1%. These correction have been incorporated into the XSM Data Analysis Software and calibration data base for scientfic use of the XSM data.

A part of the ground calibration of XSM was carried at RRCAT, Indore in collaboration with M. K. Tiwari, M. H. Modi and T. Ganguli.

doi : https://doi.org/10.1007/s11207-020-01712-1

(N. P. S. Mithun, S. V. Vadawale, A. Sarkar, M. Shanmugam, A. R. Patel, B. Mondal, B. Joshi, P. Janardhan, H. L. Adalja, S. K. Goyal, T. Ladiya, N. K. Tiwari, N. Singh, S. Kumar)

Adaptive Optics(AO) Test Bench: AO Simulation Software Development

An AO laboratory test bench is being developed as a precursor of a near-infrared (NIR) Adaptive Optics (AO) system for the upcoming PRL 2.5m telescope. The test bench would be used to validate the performance of various components, e.g. wavefront sensor, deformable mirror, tip-tilt mirror etc., to be used in the AO system. The design of a complex optical system like adaptive optics relies heavily on end-to-end simulations to predict the expected performance of the system, residual wavefront errors, response of each of the subsystems etc. The simulation software is utilized to identify the optimal hardware components and predict the instrument's behaviour in different sky conditions. Moreover, the software would also be useful in troubleshooting hardware related issues, which otherwise would be a complex and tedious problem. As a part of our AO system development efforts, we have developed a user-friendly, modular, portable and desktop computer-based software package that runs on the Python programming environment.

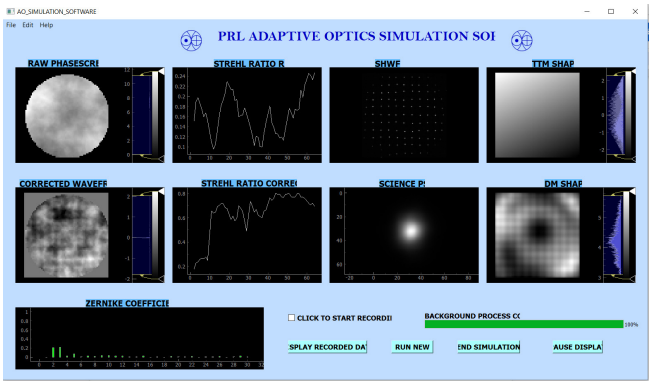

Figure no. 33: Screenshot of PRL Adaptive Optics Test Bench Simulation Software

A user-friendly front end user interface (UI) is developed to set the initial parameters and visualize the temporal behaviour of wavefront propagation within the system. Figure no. 33 shows a screenshot of the UI. All simulation related parameters can be easily set in the "Edit" menu. Different sub-window plots represent output/behaviour of different modules viz. wavefront generation, Shack-Hartmann wavefront sensor, tip-tilt mirror, deformable mirror, wavefront reconstruction and science camera at the same time instant. The simultaneous display is highly advantageous in accessing performance and troubleshooting purpose.

The UI can be used for starting a new simulation or retrieve an older simulation. The underlying algorithm is novel in the sense that GUI front end code which works on multi-threading mode, invokes back-end code that runs on multi-processing mode. There is a total of 13 back-end processes running in parallel. The data is shared between the processes using multi-processing queues. The Hierarchical Data Format(HDF5) is used to store and process the data. The software is being further optimized in order to make it faster. Likewise, the software accuracy is being tested with different validation metrics.

(Vaibhav Dixit, Ankita Patel and Mudit K. Srivastava)

DarpanX: A python package for modeling X-ray reflectivity of multilayer mirrors

We have initiated the development of hard X-ray optics for future Indian X-ray astronomy missions, and in this context, we have developed a program, DarpanX, to calculate X-ray reflectivity for single and multilayer mirrors. Multilayer X-ray mirrors consist of a coating of a large number of alternate layers of high Z and low Z materials with a typical thickness of 10 – 100 Å, on a suitable substrate.

Such coatings play an important role in enhancing the reflectivity of X-ray mirrors by allowing reflections at angles much larger than the critical angle of X-ray reflection for the given materials. Coating with an equal thickness of each bilayer (constant period multilayers) enhances the reflectivity at discrete energies, satisfying Bragg condition for the given thickness. However, by systematically varying the bilayer thickness in the multilayer stack (depth graded multilayers), it is possible to design X-ray mirrors having enhanced reflectivity over a broad energy range. Such depth graded multilayer mirrors are essential to realize the hard X-ray telescope for astronomical observations.

DarpanX is an essential step in Design of such multilayer X-ray mirrors and their characterization with X-ray reflectivity measurements. It can be used as a stand-alone tool for designing multilayer mirrors with required characteristics. But more importantly, it has been implemented as a local model for the popular X-ray spectral fitting program, XSPEC, and thus can be used for accurate fitting of the experimentally measured X-ray reflectivity data.

It is developed in python3 and is publicly distributed as an open source software on GitHub `https://github.com/biswajitmb/DarpanX.git`.

This work is carried out in collaboration with C. Karmakar, M. R. Pate, R. B. Upadhyay (SAC, Ahmedabad), S. Panini (IIA, Bangalore), and V. Navalkar (CBS, Mumbai).

doi : `https://doi.org/10.1016/j.ascom.2020.100446`

(B. Mondal, S. Vadawale, N. P. S. Mithun, C. S. Vaishnava, N. K. Tiwari, and S. K. Goyal)

MFOSC-EP for PRL 2.5m Telescope: Optical Design of the Echelle Spectro-Polarimeter

Mt. Abu Faint Object Spectrograph and camera – Echelle Polarimeter (MFOSC-EP) is an instrument currently being designed for the upcoming PRL 2.5m telescope. MFOSC-EP would operate in visible wavelengths (3800-9500Å) and is envisaged as a general user's observatory instrument. The instrument incorporates the functionalities of a low-resolution FOSC (faint object spectrograph and camera) kind of instrument and intermediate resolution spectro-polarimeter. These two modules would use a common collimator. The complete system architecture and optical design of low-resolution part, including the collimator optics, was described in previous years' annual report. Here we discuss the optical design of the spectro-polarimeter section of the instrument.

The collimated beam from the collimator optics enters into the polarimeter section. It consists of an MgF_2 Wollaston prism as a polarizer and a half-wave plate of PMMA material. Collimator makes the pupil of diameter $\sim$41mm within polarimeter optics chain. The Wollaston prism decomposes the beam in the form of ordinary and extra-ordinary beams, which is focused by the polarimeter camera optics (designed with two achromatic doublets and a single lens) on to the entrance of the echelle spectrometer (separated by $\sim$500μm) for their simultaneous spectroscopy. The Collimator+Polarimetr optics provides magnification of $\times$1. Thus, the f/8 beam of the telescope remains intact and enters into the spectrometer section.

The echelle spectrometer is designed with the f/8 collimator (designed with two doublet and one singlet lenses) and f/3.5 camera optics. The system provides magnification of $\times$0.45 to the slit width. The echelle-collimator makes pupil at an echelle grating (79 line-pair(lp)/mm). The dispersed beam is then cross-dispersed by the grating cross-dispersers. Two plane rules reflection gratings (600 lp/mm blazed at 4000Å and 300 lp/mm blazed at 7600Å) are used for two wavelength ranges $\sim$3900-5520Å and 5470-9000Å respectively. The echelle-camera optics is designed with two achromatic doublet and three singlet lenses. It finally records the cross dispersed multi-order spectra on to a 2K$\times$2K CCD detector with 13.5μm pixel size. The projected slit is sampled by 3.5 pixels, and the designed spectral resolution is $\sim$12000. The spectra traces for ordinary and extra-ordinary beams on the CCD detector are shown in Figure no. 34 for red and blue cross-dispersers for all the orders.

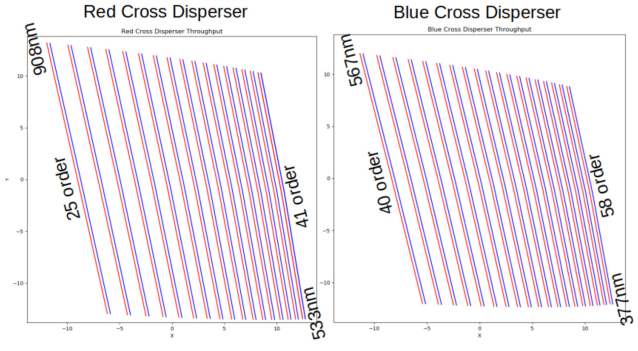

Figure no. 34: The echellogram showing the footprints of cross dispersed spectra on the CCD detector. The ordinary and extra-ordinary beam's traces are shown in red and blue respectively.

(Vipin Kumar, Vaibhav Dixit and Mudit K. Srivastava)

Solar Physics

Evidence that magnetic-jerk accompanying major solar flares can drive seismic emissions in the sunspots

Recently, it was proposed that abrupt changes in the solar magnetic fields observed during the major flares can drive seismic waves in the Sun. Therefore, we have performed a detailed analysis of acoustic enhancements in sunspots accompanying M- and X-class solar flares and the associated changes in the magnetic fields.

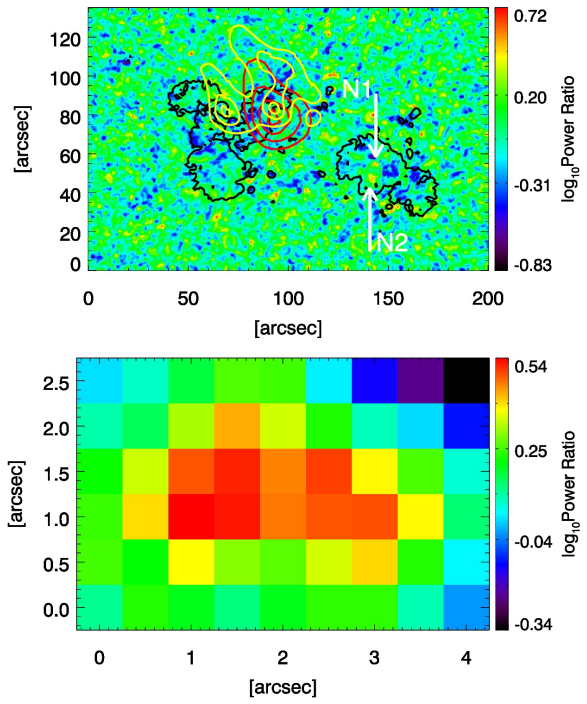

Figure 1.: A brief illustration of results obtained for the active region NOAA 11882. In the top panel, we show the ratio of acoustic power maps estimated for spanning flare and pre-flare epochs in the 2.5-4 mHz band (p-modes). Here, black contours represent the outer boundary of the sunspot penumbra, whereas the yellow contours represent flare-ribbon locations from the H_α observations from GONG. The red contours represent hard X-ray footpoints as observed in 12-25 keV band from RHESSI. The bottom panel illustrates the blow-up region of 'N1' enhanced location in the sunspot as indicated in the power map ratio.

For this purpose, we have used high-resolution Dopplergrams and line-of-sight magnetograms at a cadence of 45 s, along with vector magnetograms at a cadence of 135 s obtained from HMI instrument on board the SDO space mission.

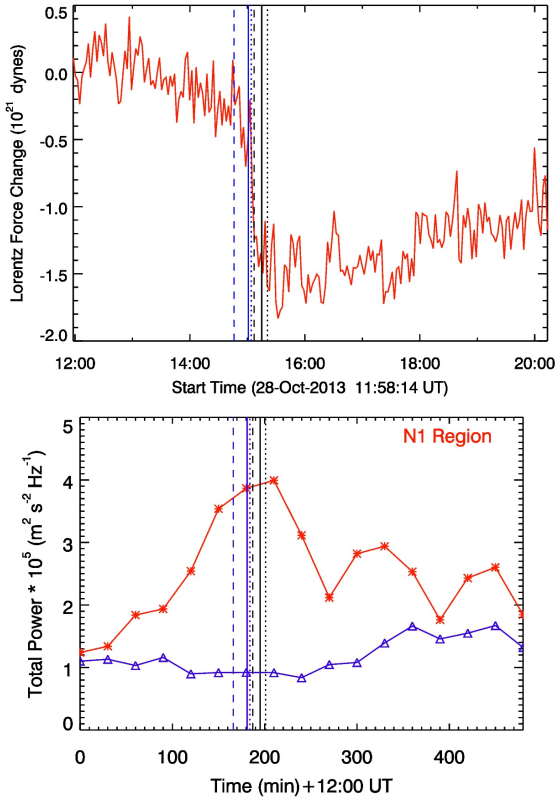

Figure 2.:Top panel: plot in red color shows the temporal evolution of change in horizontal component of Lorentz force in the 'N1' location. The dashed, solid, and dotted blue and black vertical lines represent the onset, peak, and decay time of M2.7 and M4.4-class flares, respectively, in the active region NOAA 11882. Bottom panel: plots showing the temporal evolution of integrated acoustic power over the 'N1' location (red color with asterisks) whereas that shown in blue color with triangles represents evolution of total power in an unaffected region in the same sunspot.

In order to identify the location of flare ribbons and hard X-ray footpoints, we have also used H_α observations obtained from GONG instruments and hard X-ray images in 12–25 keV energy band from the RHESSI spacecraft. Acoustic velocity power maps in 2.5–4 mHz band (p-modes) are constructed for pre-flare, spanning flare, and post-flare epochs for the identification of seismic emission locations in the sunspots. In the power maps, we have selected only those locations which are away from the flare ribbons and hard X−ray footpoints. These regions are believed to be free from any flare related artefacts in the observational data. We have identified concentrated locations of acoustic power enhancements in sunspots

(c.f., Figure 1) accompanying major flares. Our investigation provides evidence that abrupt changes in the magnetic fields and associated impulsive changes in the Lorentz force (known as 'magnetic-jerk') are the driving source for these seismic emissions in the sunspots during the flares (c.f., Figure 2) These seismic emissions in the sunspots are essential to study because these enhanced locations can provide better information about the deep dynamics in the active regions during the flare. In addition, since these 'magnetic-jerk' driven seismic waves can also propagate from photosphere to higher solar atmospheric layers along the magnetic field lines in the form of magneto-acoustic waves, hence these can contribute to the heating of the solar atmosphere.

doi : https://doi.org/10.1093/mnras/staa1974

(H. Kumar and B. Kumar)

The Formation of an Atypical Sunspot Light Bridge as a Result of Large-scale Flux Emergence

Light Bridges (LBs) are bright, extended structures within the umbrae of sunspots/pores. LBs are often seen during the early stages of sunspot formation or during the late phase of sunspot decay and are located along lanes where individual spots coalesce or fragment. Their formation is generally regarded to stem from vigorous overturning convection within a sunspot. We explore the above premise in this investigation by analysing the formation, structure, and evolution of an atypical LB in a regular sunspot, using a combination of full-disk data from NASA's Solar Dynamics Observatory (SDO) and high-resolution data from the 76 cm Dunn Solar Telescope (DST) of the National Solar Observatory in New Mexico, USA. The LB results from the emergence of magnetic flux with one footpoint rooted in a pore outside the parent sunspot that appears about 17 hr before the LB.

The pore has a polarity opposite to that of the sunspot and recedes from it at a speed of about 0.4 km/s. This is accompanied by the development of an elongated magnetic channel in the outer penumbra that triggers the formation of the LB when it reaches the inner penumbral boundary. The LB is a nearly horizontal structure with a field strength of about 1.2 kG that exhibits long-lived photospheric blueshifts of about 0.85 km/s along its entire length. The thermal inversion of chromospheric spectra from the DST reveal the LB to be about 600–800 K hotter than the umbra. Our results indicate that the LB formation is part of a flux emergence event with the LB envelope reaching a height of about 29 Mm before dissolving after about 13 hr. We conclude that the existence of persistent, large-scale photospheric blueshifts in LBs is the most likely criterion for distinguishing between flux emergence events and overturning convection in field-free umbral intrusions.

This work was done in collaboration with Christian Beck (National Solar Observatory, USA), and Debi Prasad Choudhary (California State University, USA).

doi : https://doi.org/10.3847/1538-4357/abc618

(R. E. Louis)

Homologous Flaring Activity over a Sunspot Light Bridge in an Emerging Active Region

Sunspot light bridges are known to exhibit a variety of dynamic and persistent phenomena such as surges, small-scale jets, etc., in the chromosphere and transition region. While it has generally been proposed that magnetic reconnection is responsible for this small-scale dynamism, persistent flaring activity lasting several hours from the same spatial location on a sunspot light bridge has rarely been reported. We combine observations from the Atmospheric Imaging Assembly and the Helioseismic Magnetic Imager on board the Solar Dynamics Observatory to investigate homologous flaring activity over a small sunspot light bridge in an emerging flux region. The homologous flares all produced broad, collimated jets, including a B6.4 class flare. The jets rise at a speed of about 200 km/s and emerge from the same spatial location for nearly 14 hrs, after which they cease completely. A nonlinear force-free (NLFF) extrapolation of the photospheric magnetic field shows a low-lying flux rope connecting the light bridge to a remote opposite-polarity network. The persistent flares occur as a result of the rapid horizontal motion of the leading sunspot that causes the relatively vertical magnetic fields in the adjacent umbra to reconnect with the low-lying flux rope in the light bridge. Our results indicate that the flaring ceases once the flux rope has lost sufficient twist through repeated reconnections.

This work was done in collaboration with Julia Thalmann (University of Graz, Austria).

doi : https://doi.org/10.3847/2041-8213/abd478

(R. E. Louis)

Evolutionary Stages and Triggering Process of a Complex Eruptive Flare with Circular and Parallel Ribbons

We report a multi-wavelength study of a complex M-class solar eruptive flare that consists of three different sets of flare ribbons, viz. circular, parallel, and remote ribbons. Magnetic field modeling of source active region NOAA 12242 exhibits the presence of 3D null-point magnetic topology that encompasses an inner bipolar region (Figure 3). The event initiates with the faint signatures of the circular ribbon along with remote brightening right from the pre-flare phase that points toward the ongoing slow yet persistent null-point reconnection. We first detected flux cancellation and an associated brightening, which are likely signatures of tether-cutting reconnection that builds the flux rope near the polarity inversion line (PIL) of the inner bipolar region. In the next stage, with the onset of M8.7 flare, there is a substantial enhancement in the brightening of circular ribbon, which essentially suggests an increase in the rate of ongoing null-point reconnection. Finally, the eruption of underlying flux rope triggers 'standard flare reconnection' beneath it producing an abrupt rise in the intensity of the parallel ribbons as well as enhancing the intensity of circular ribbon brightening (Figure 4), suggesting an increase in the rate of null-point reconnection by external forcing. We show that within the fan dome, the region with magnetic decay index $n>1.5$ borders the null-point quasi-separatrix layer. Our analysis suggests that both the torus instability and the breakout model have played role toward the triggering mechanism for the eruptive flare. This event is a nice example of the dynamical evolution of a flux rope initially confined in a null-point topology that subsequently activates and erupts with the progression of the circular-cum-parallel ribbon flare.

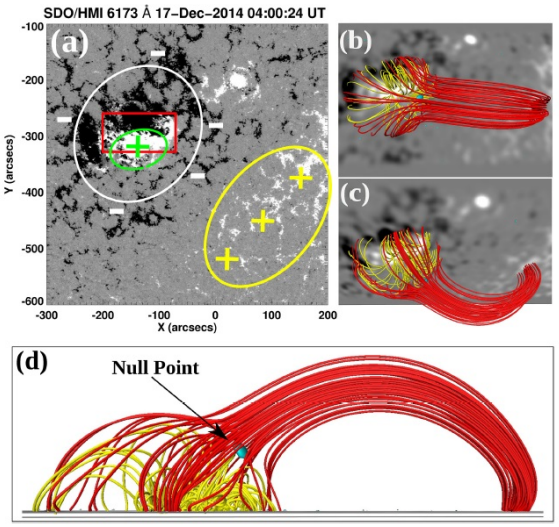

Figure 3.: Panel (a): SDO/HMI LOS photospheric magnetogram at 04:00:24 UT on 2014 December 17. The central positive polarity and the surrounding negative polarity regions are represented by the green and white ellipse, respectively. The flux rope formation and remote brightening regions are marked by the red box and yellow ellipse, respectively. Panels (b)–(d): Zoomed views of the coronal field lines showing the null-point topology in three different projections. The yellow and red lines represent the inner dome and outer dome lines, respectively. The cyan patch lying in between the yellow and red field lines in panels (b)–(d) represents an iso-surface of 4G, which consists a magnetic null-point.

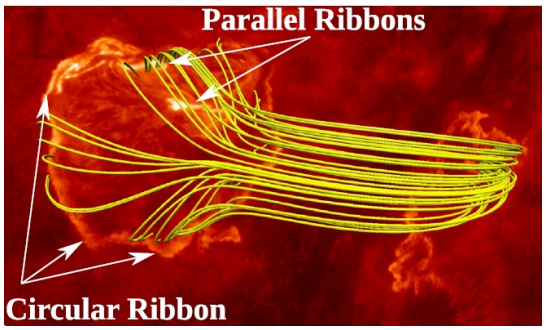

Figure 4.: SDO/AIA 304 Å image showing different sets of flare ribbons, overplotted with the NLFFF extrapolated field lines (shown in yellow color).

This work was done in collaboration with Navin Chandra Joshi (SRM University, Delhi-NCR, India).

doi : https://doi.org/10.1093/mnras/staa3480

(P. K. Mitra and B. Joshi)

Eruptive–Impulsive Homologous M-class Flares associated with Double-decker Flux-rope configuration in Minisigmoid of NOAA 12673

We present a multi-wavelength analysis of two homologous, short-lived, impulsive flares of GOES class M1.4 and M7.3 that occurred from a very localized minisigmoid region (Figures5(a), (b)) within the active region NOAA 12673 on 2017 September 7.

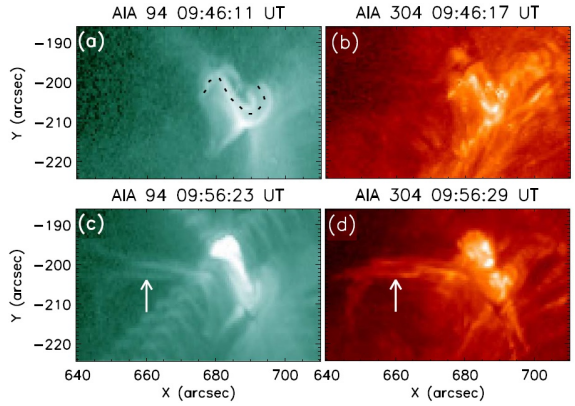

Figure 5.: Panel (a): AIA 94 Å image showing the minisigmoid structure (highlighted by the dashed curve). Panel (b): AIA 304 Å image showing the minisigmoid structure in low temperature. Panels (c)-(d): AIA 94 and 304 Åimages showing the jet-like eruption from the minisigmoid (indicated by the white arrows).

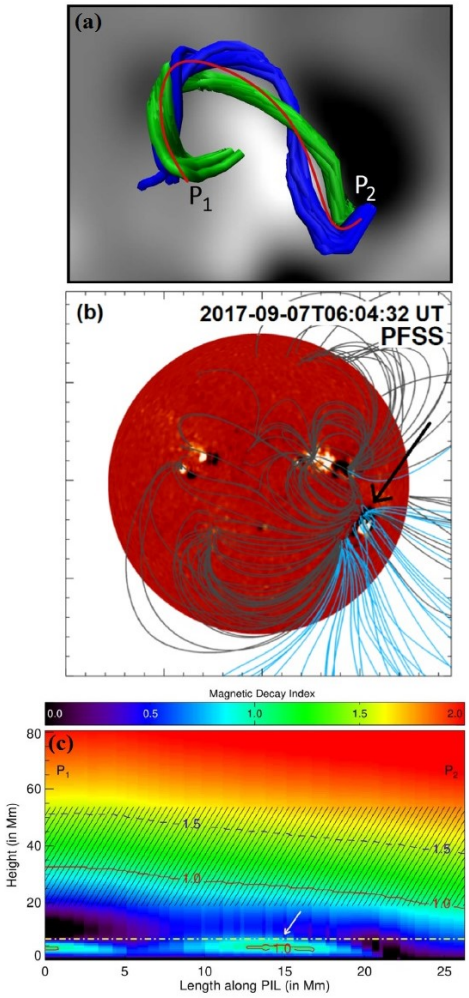

Figure 6.: Panel (a): NLFFF extrapolation results showing a double-decker configuration at the core of the minisigmoid. Panel (b): Global PFSS extrapolation results showing a set of open field lines originating close to the active region. Panel (c): Distribution of magnetic decay index above the PIL of the double-decker system, indicated by the red curve in panel (a).

Both flares were associated with initial jet-like plasma ejection that for a brief amount of time moved toward the east (Figures5(c), (d)) in a collimated manner before drastically changing direction toward the southwest. Nonlinear force-free field (NLFFF) extrapolation reveals the presence of a compact double-decker flux rope configuration in the minisigmoid region (Figure 6(a)) prior to the flares. A set of open field lines originating near the active region (Figure 6(b)) that were most likely responsible for the anomalous dynamics ofthe erupted plasma gave the earliest indication of an emerging coronal hole near the active region. The horizontal field distribution suggests a rapid decay of the field above the active region, implying high proneness of the flux rope system toward eruption (Figure 6(c)). In view of the low coronal double-decker flux ropes and compact extreme ultraviolet brightening beneath the filament, along with associated photospheric magnetic field changes, our analysis supports the combination of initial tether-cutting reconnection and subsequent torus instability for driving the eruption.

This work was done in collaboration with Astrid M. Veronig(Univ. of Graz, Austria), Ramesh Chandra (Kumaun Univ., India), K. Dissauer (Univ. of Graz, Austria), and Thomas Wiegelmann (Max-Planck Institute, Germany).

doi : https://doi.org/10.3847/1538-4357/aba900

(P. K. Mitra and B. Joshi)

Development of a confined Circular-cum-ParallelRibbon Flare and associated Pre-Flare activity

We study a complex GOES M1.1 circular ribbon flare and related pre-flare activityon 26 January 2015 [SOL2015-01-26T16:53] in the solar active region NOAA 12268.This circular ribbon flare activity (Figure 7(a)) was observed by the Atmospheric Imaging Assembly (AIA) on board Solar Dynamics Observatory (SDO) and the Reuven Ramaty High Energy Solar Spectroscopic Imager (RHESSI). The examination of photospheric magnetograms during the extended period, prior to the event, suggests the successive development of a so-called “anemone” type magnetic configuration (Figure 7(b)). The Nonlinear Force Free Field (NLFFF) extrapolation reveals afan-spine magnetic configuration with the presence of a coronal null-point (Figure 7(c)-(d)). We found that the pre-flare activity in the active region starts ≈15 min prior to the main flare in the form of localized bright patches at two locations. A comparison of locations and spatial structures of the pre-flare activity with magnetic configuration of the corresponding region suggests onset of magnetic reconnection at the null-point along with the low-atmosphere magnetic reconnection caused by the emergence and the cancellation of the magnetic flux. The main flareof M1.1 class is characterized by the formation of a well-developed circular ribbon along with a region of remote brightening. Remarkably, a set of relatively compact parallel ribbons formed inside the periphery of the circular ribbon which developed lateral to the brightest part of the circular ribbon. During the peak phase of the flare, a coronal jet is observed at the north-east edge of the circular ribbon, which suggests interchange reconnection between large-scale field lines and low-lying closed field lines. Our investigation suggests a combination of two distinct processes in which ongoing pre-flare null-point reconnection gets further intensified as the confined eruption along with jet activity proceeded from within the circular ribbon region which results to the formation of inner parallel ribbons and corresponding post-reconnection arcade. *This work was done in collaboration with Pooja Devi (Kumaun Univ., India), Ramesh Chandra (Kumaun Univ., India), Astrid M. Veronig(Univ. of Graz, Austria), and Reetika Joshi (Kumaun Univ., India).*

doi : https://doi.org/10.1007/s11207-020-01642-y

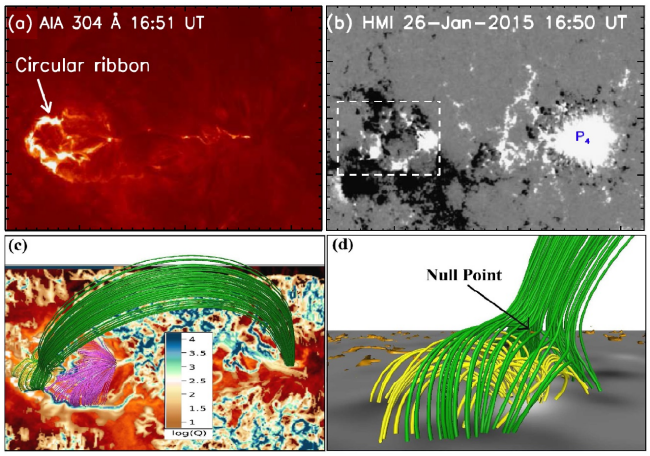

Figure 7.: Panel (a): AIA 304 Å image showing the circular ribbon flare. Panel (b): Co-temporal LOS HMI magnetogram showing the magnetogram associated with the circular ribbon (indicated by the white dashed box) and the region of remote brightening (marked by P4). Panel (c): NLFFF extrapolation results showing a fan-spine configuration and distribution of log(Q) over the background AIA 304 Å image. A close up of the fan region is shown in panel (d) where the location of the null-point is indicated by an arrow.

(P. K. Mitra and B. Joshi)

Successive occurrences of Quasi-Circular Ribbon Flares in a Fan-Spine-Like Configuration involving Hyperbolic Flux-tube

We carried out a comprehensive analysis of the formation and the evolution of a fan-spine-like configuration that developed over a complex photospheric configuration where dispersed negative polarity regions were surrounded by positive polarity regions. This unique photospheric configuration, analogous to the geological ‘atoll’ shape (Figure 8(a)), hosted four homologous flares within its boundary. Computation of the degree of squashing factor (Q) maps clearly revealed an elongated region of high Q-values between the inner and outer spine-like lines, implying the presence of a hyperbolic flux tube (HFT, Figure 9). The coronal region associated with the photospheric atoll configuration was distinctly identified in the form of a diffused dome-shaped bright structure directly observed in Extreme Ultraviolet (EUV) images (Figure 8(b)). A filament channel resided near the boundary of the atoll region (indicated by the dashed curve in Figure 8(b)). The activation and eruption of flux ropes from the filament channel led to the onset of four eruptive homologous quasi-circular ribbon flares within an interval of ≈11 h. During the interval of the four flares, we observed continuous decay and cancellation of negative polarity flux within the atoll region. Accordingly, the apparent length of the HFT gradually reduced to a null-point-like configuration before the fourth flare. Prior to each flare, we observed localized brightening beneath the filaments which, together with flux cancellation, provided support for

the tether-cutting model of solar eruption. The analysis of magnetic decay index revealed favorable conditions for the eruption, once the pre-activated flux ropes attained the critical heights for torus instability.

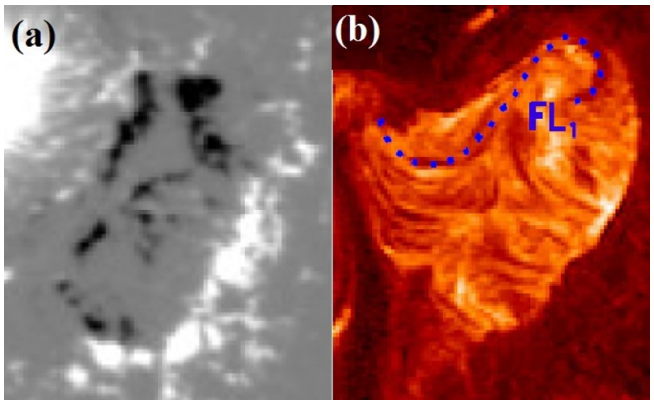

Figure 8.: Panel (a): HMI line-of-sight (LOS) magnetogram showing the photospheric morphology of the magnetic atoll region. Panel (b): Co-temporal AIA 304 Å image associated with the magnetic atoll region, showing an elongated dome-shaped bright structure. The dashed curve (marked as 'FL1') indicates a filament channel situated along the northern boundary of the atoll region.

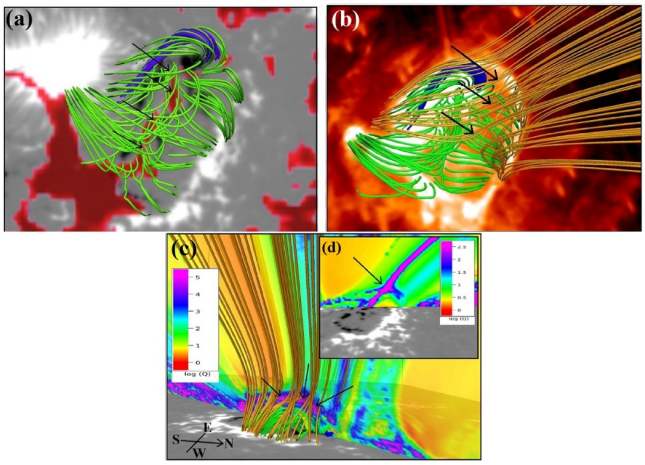

Figure 9.: Panel (a)-(b): Non-linear force-free field (NLFFF) extrapolation results of the magnetic atoll showing the presence of a flux rope (blue lines) and closed magnetic loops within the region (the green lines) besides large open field lines originating from the outer magnetic patches of the atoll region (yellow lines). Panel (c): A Y-Z tilted vertical surface drawn along the yellow lines representing the distribution of Q-values, suggesting the presence of a hyperbolic flux tube(HFT; Indicated by the arrows). In panel (d), the distribution of Q is shown along a plane passing across the magnetic atoll region, i.e. along X-Z plane. The arrow in panel (d) indicates an 'X'-shape formed by the regions of high Q, further providing evidence for the HFT.

doi : https://doi.org/10.1093/mnras/stab175

(P. K. Mitra and B. Joshi)

First detection of HXR coronal channel evidencing activated magnetic flux rope structure in solar corona

The conditions governing the formation and development of flux ropes is dependent upon the local coronal magnetic field topology and magnetic flux evolution through the photosphere below. To explore the underlying mechanisms in detail, we conduct a comprehensive multi-wavelength analysis of a major M6.6 long duration solar event with special emphasize on its pre-flare phase. The event occurred in active region NOAA 12371 on 2015 June 22. A remarkable aspect of the event was an active pre-flare phase lasting for about an hour during which a hot EUV coronal channel was in the build-up stage and displayed co-spatial hard X-ray (HXR) emission up to energies of 25 keV. The coronal magnetic field configuration based on nonlinear-force-free-field (NLFFF) modeling clearly exhibited a magnetic flux rope (MFR) oriented along the polarity inversion line (PIL) (Figure 10) and co-spatial with the HXR coronal channel (Figure 11(b)). This is the first detection of an MFR through direct HXR imaging, signifying the MFR to be in the hot, activated stage. We also obtain high coronal loops (HCL) and low-lying coronal loop (LLCL) structures from magnetic field modelling conforming EUV 171 Å observations (Figures 10(a) and 11(a)).

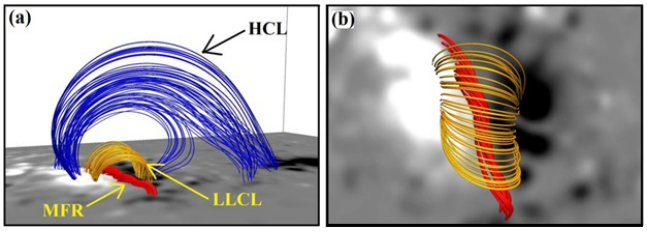

Figure 10.: (a) NLFFF modeling of the active region corona reveals the existence of magnetic flux rope (MFR), low-lying coronal loops (LLCL), and high-lying coronal loops (HCL) in the flaring region. (b) The position of the MFR along the PIL of the active region and the overlying LLCLs are shown.

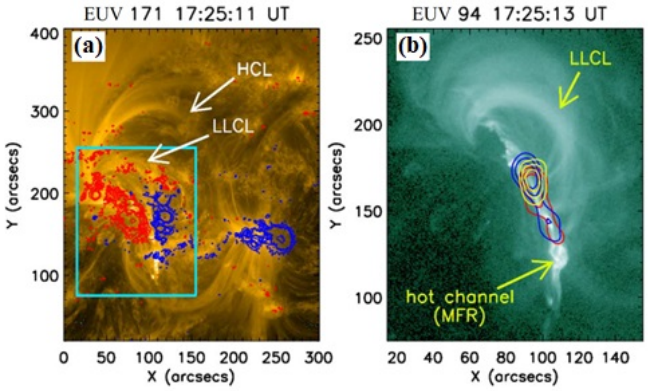

Figure 11.: (a) EUV 171 Å image of the active region is shown during the pre-flare phase, overplotted with the photospheric line-of-sight magnetogram. The positive and negative polarities of the magnetogram are denoted by red and blue contours, respectively. The rectangular box indicates a hot core region, whose enlarged view is shown in EUV 94 Å channel in panel (b) overplotted with X-ray contours in 5–10 keV (red), 10–15 keV (blue), and 15–25 keV (yellow).

It is to be noted that the significant changes in the active region's photospheric magnetic field during an extended period of ≈42 hr was observed in the form of rotation of sunspots, moving magnetic features, and flux cancellation along the PIL. Prior to the flare onset, the MFR underwent a slow rise phase (≈14 km s^{-1}) for ≈12 minutes, which we attribute to the faster build-up and activation of the MFR by tether-cutting reconnection occurring at multiple locations along the MFR itself. The sudden transition in the kinematic evolution of the MFR from the phase of slow to fast rise (≈109 km s^{-1} with acceleration

≈110 m s^{-2}) precisely divides the pre-flare and impulsive phase of the flare (Figure 12), which points toward the feedback process between the early dynamics of the eruption and the strength of the flare magnetic reconnection.

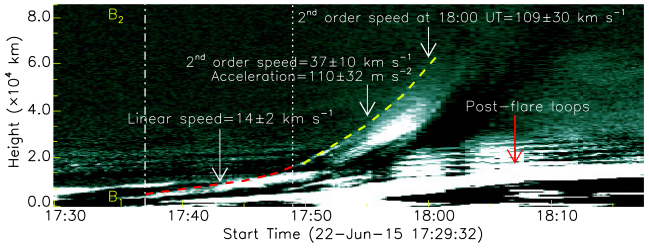

Figure 12.: Time-slice diagram of the erupting hot channel shows the slow rise (speed ≈14 km s^{-1}) phase between ≈17:37 UT and ≈17:49 UT (shown by the red dashed line), which is followed by another phase of its fast eruption (shown by yellow dashed line) between ≈17:49 UT to ≈18:00 UT.

This work has been done in collaboration with Astrid M. Veronig (University of Graz, Austria) and VasylYurchyshyn (New Jersey Institute of Technology, USA).

doi : https://doi.org/10.3847/1538-4357/ab962b

(S. Sahu, B. Joshi and P. K. Mitra)

Radio-loud and radio-quiet CMEs: solar cycle dependency, influence on cosmic ray intensity, and geo-effectiveness

Coronal mass ejections (CMEs) largely influence the space weather and cause geomagnetic perturbations. Hence, the statistical studies pertaining to the occurrence of CMEs over the solar cycles and their consequence at the near-Earth region are extremely important.

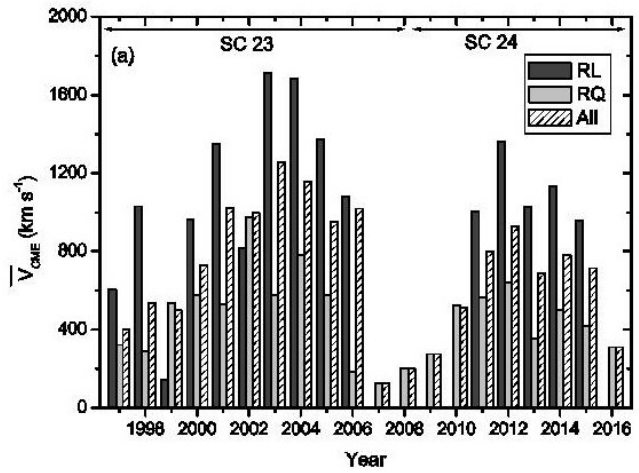

Figure 13.: Histogram showing yearly average speed of RL, RQ, and all Earth-reaching CMEs at near-Sun region for solar cycles 23 and 24.

For an in-depth understanding, such studies need to be carried out considering various observational aspects of CMEs. With this motivation, we carried out a statistical study of radio-loud (RL) and radio-quiet (RQ) CMEs during solar cycles 23 and 24. We also assess their geo-effectiveness and analyze their influence on cosmic ray intensity (CRI). The RL and RQ CMEs constitute 40% and 60% cases, respectively, of the total population of CMEs that arrive the near-Earth region at 1 AU. The mean speed of RL CMEs (≈1170 km/s) is found to be significantly higher (almost twice) than the mean speed of RQ CMEs (≈519 km/s) in the low corona (Figure 13) while their speed became comparable (≈536 km/s for RL and ≈452 km/s for RQ CMEs) at near-Earth region (Figure 14).

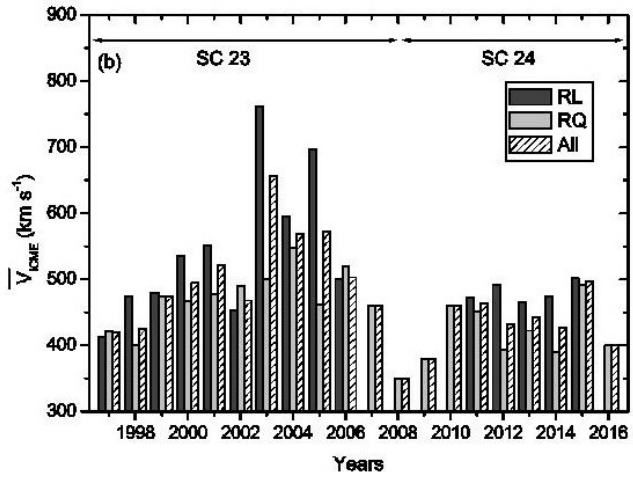

Figure 14.: Histogram showing yearly average speed of RL, RQ, and all Earth-reaching CMEs at near-Earth region.

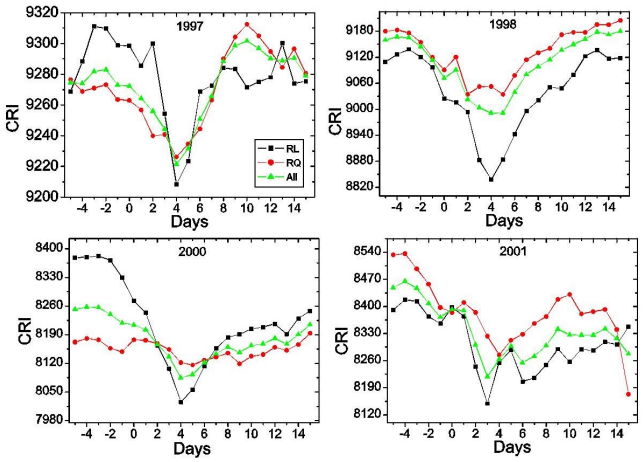

Figure 15.: Yearly plots of superposed epoch analysis showing the variation of CRI during the period of 21 days with respect to CME onset day (5 days before and 15 days after the epoch day) during 1997-2001.

The yearly-averaged speeds of Earth-reaching CMEs follow solar cycle variations. The CRI and geomagnetic Dst index are found to have good negative correlation with speed of Earth-reaching CMEs. RL CMEs were found to be more effective in producing CRI depressions (Figure 15) and geomagnetic storms (GSs) in comparison to RQ CMEs; in about 70% cases RL CMEs produced CRI depression and GSs earlier than the RQ CMEs. Superposed epoch analysis

suggests strongest depression in CRI occurs 2-5 days and 4-9 days after the onset of RL and RQ CMEs, respectively. Further, GS events show a time-lag of 1-5 days and 3-8 days, respectively, with respect to RL and RQ CMEs.

This work has been done in collaboration with Ramesh Chandra from Kumaun University, Nainital, India.

doi : https://doi.org/10.1007/s10509-021-03930-w

(H. Kharayat and B. Joshi)

On the relationship between hemispheric asymmetry in solar coronal rotation and solar activity during solar cycle 24

Sun's differential rotation produces stretches and twists in the solar magnetic fields, as a result creates sunspots and most of the solar activities in the solar atmosphere. Thus, the study of evolution of solar rotation with the progress of solar activity cycle is important for better understanding of the variations in solar activity.

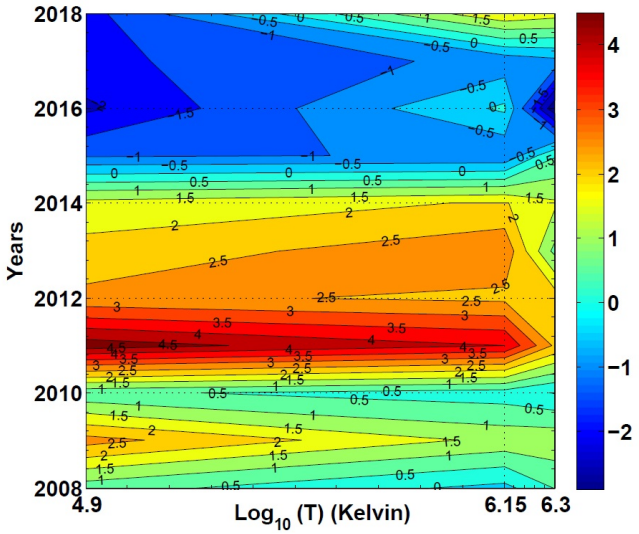

Figure 16.: The contour plot of the temporal variation of hemispheric asymmetry index (AI) as a function of temperature using observations of the STEREO space mission. It is seen that the AI is high during the solar maximum (2011-2014) phase of the solar cycle 24. The bar on right shows the color code for AI (%).

In this work, we have studied the relationship between hemispheric asymmetry in solar coronal rotation and solar activity during solar cycle 24. We find an evidence of very high and statistically significant relationship between hemispheric asymmetry in solar coronal rotation rate and solar activity. Our approach is based on cross correlation of hemispheric asymmetry index (AI) in rotation rate with annual solar activity indicators. To obtain hemispheric asymmetry in solar rotation rate, we use solar full disk (SFD) images at 30.4 nm, 19.5 nm and 28.4 nm wavelengths for 24^{th} solar cycle i.e., for the period from 2008 to 2018, as recorded by the Solar Terrestrial Relations Observatory (STEREO) space mission. Our analysis shows that hemispheric asymmetry in rotation rate is high during the solar maxima from 2011 to 2014 (c.f., Figure 16). On the other hand, hemispheric asymmetry drops gradually on both sides (i.e., from 2008 to 2011 and from 2014 to 2018). The results further show that asymmetry index (AI) leads sunspot numbers by $\sim$ 1.56 years (c.f., Figure 17). This gives a clear indication that hemispheric asymmetry triggers the formation of sunspots working together with the differential rotation of the Sun.

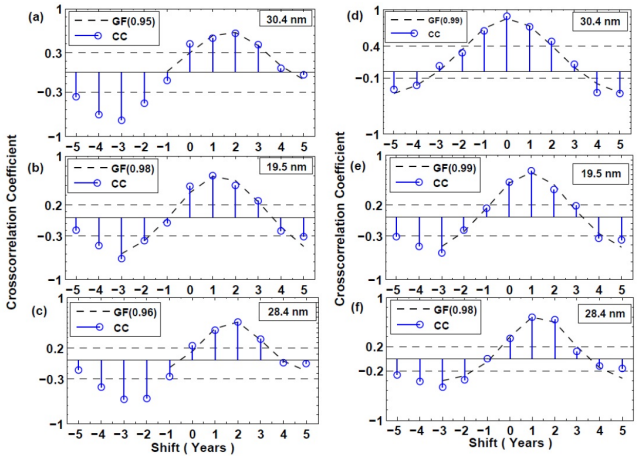

Figure 17.: Cross-correlation of hemispheric asymmetry index (AI) in rotation rate as observed in 30.4 nm, 19.5 nm and 28.4 nm wavelengths from STEREO mission and annual sunspot numbers as a function of shift (years) are shown in the panels (a), (b) and (c). The panels (d), (e) and (f) depict the cross-correlation of AI in rotation rate for 30.4 nm, 19.5 nm and 28.4 nm and the individual extracted EUV flux as a function of shift in years. The horizontal dashed lines show 95% confidence levels.

This work has been done in collaboration with Jaidev Sharma and Anil Malik of CCSU, Meerut and H.O. Vats of SERF, Ahemedabad.

doi : https://doi.org/10.1093/mnras/staa2863

(B. Kumar)

Magnetic and Velocity Field Topology in Active Regions of Descending Phase of the Solar Cycle 23

Solar active regions (ARs) are three-dimensional magnetic structures extending from the interior below the photosphere to the coronal heights. The sub-photospheric medium is an excellent conductor where frozen-in-field condition may satisfy. Over a period of time, plasma flows may evolve with magnetic fieldlines near the photosphere, and may swirl around them. Therefore, we can expect topological association between the sub-photospheric flows and photospheric magnetic fields. We have analysed the topology of photospheric magnetic fields and sub-photospheric flows of a sample of 189 active regions observed during the peak to descending phase of solar cycle 23. Our analysis shows clear evidence of hemispheric preferences in topological parameters such as the magnetic, current and kinetic helicities, and the 'curl-divergence'. We found 68% (67%) ARs in the northern (southern) hemisphere with negative (positive) magnetic helicities (ref. Figure 18). Hemispheric preferences are found to exist statistically for all the time except in few ARs observed during the peak and the end phases of the solar cycle. This means that magnetic fields are dominantly left (right)-helical in scales smaller than individual ARs of northern(southern) hemisphere. We found that magnetic and current helicity parameters show equator-ward propagation similar to the sunspot cycle (Figure 19), suggesting that

solar dynamo could be helical in nature. An AR with larger area and stronger field may have larger helicities. Therefore, such patterns of helicities could also be due to variations of areas and magnetic fields of sunspots during a solar cycle from larger areas with stronger fields regions to smaller areas with weaker field regions.

Kinetic helicity exhibited similar hemispheric trend to that of magnetic and current helicity parameters. There are 65%(56%) ARs with negative (positive) kinetic helicity as well as divergence-curl, at the depth of 2.4 Mm, in the northern (southern) hemisphere. The hemispheric distribution of the kinetic helicity became more evident at larger depths, e.g, 69%(67%) at the depth of 12.6 Mm. Similar hemispheric trend of kinetic helicity to that of the current helicity supports the mean field dynamo model. We also found that the hemispheric distribution of all the flow parameters increased with the field strength of ARs. The topology of photospheric magnetic fields and near surface sub-photospheric flow fields did not show good association, but the correlation between them enhanced with depth, which could be indicative of more aligned flows at deeper layers of ARs (Figure 20).

This work has been carried out in collaboration with Ram Ajor Maurya (National Institute of Technology, Calicut).

doi : https://doi.org/10.1007/s11207-020-01666-4

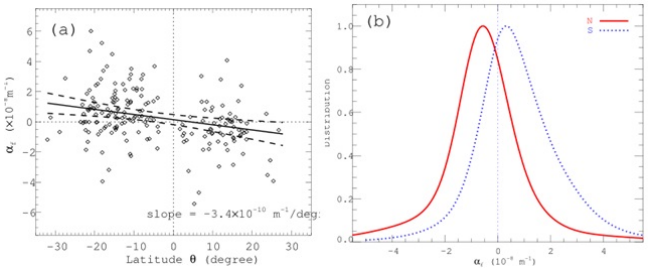

Figure 18.: (a) Latitudinal distribution of force-free parameter α_f , where solid lines represent the linear least square fitting between the parameter α_f and latitude, and dashed lines correspond to 95% confidence intervals. (b) Probability distribution function of α_f for the northern hemisphere (solid & red) and southern hemisphere (dotted & blue).

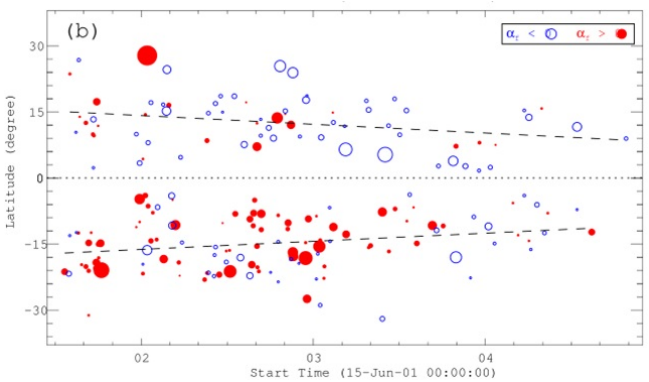

Figure 19.: Latitudinal distribution of magnetic helicity parameter α_f as a function of time, where sizes of opened (filled) circles represent magnitudes of negative (positive) values of the parameter α_f and dashed lines represent the linear regression lines through ARs latitude.

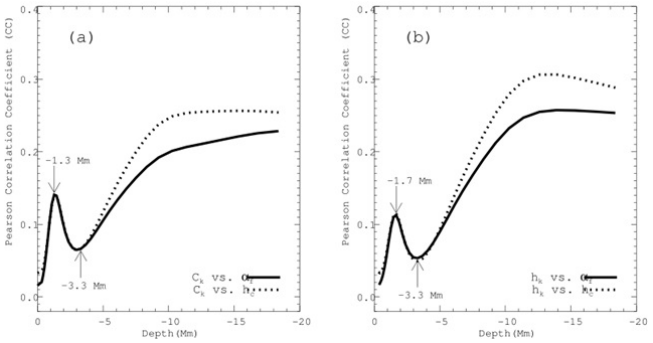

Figure 20.: Depth dependent correlation coefficients between kinetic helicity and magnetic helicity parameters: (a) C_k& α_f (solid line), C_k&h_c (dashed line), (b) h_k& α_f (solid line), h_k&h_c (dashed line).

(A. Ambastha)

Magnetohydrodynamic Simulation of Magnetic Null-point Reconnections and Coronal Dimmings during the X2.1 Flare in NOAA AR 11283

The magnetohydrodynamics of active region NOAA 11283 is simulated using an initial non-force-free magnetic field extrapolated from its photospheric vector magnetogram. We focus on the magnetic reconnections at a magnetic null point that participated in the X2.1 flare on 2011 September 6 around 22:21 UT (SOL2011-09-06T22:21X2.1) followed by the appearance of circular flare ribbons and coronal dimmings.

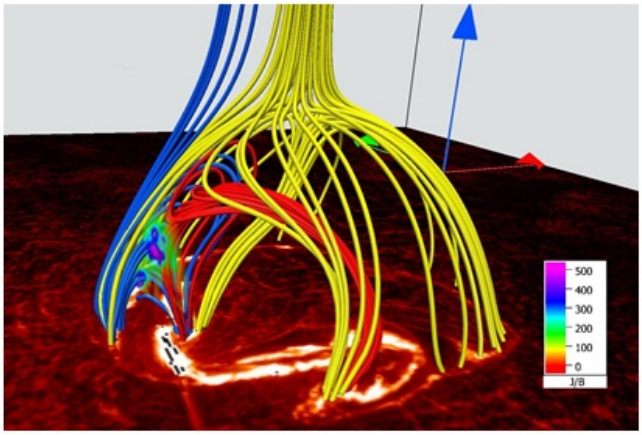

Figure 21.: Comparison of magnetic field topology with the flare ribbons observed in the SDO/AIA 304 Å channel which show an excellent agreement with the field lines constituting the dome of the 3D null and the circular flare ribbons, while the foot points of the X-type field lines correspond well to the parallel flare ribbons.

The initial magnetic field from extrapolation displays a three-dimensional (3D) null topology overlying a sheared arcade. Prior to the flare, magnetic loops rise due to the initial Lorentz force, and reconnect at the 3D null, leading to expansion and loss of confined plasma that produce the observed pre-flare coronal

dimmings. Further, the simulated dynamics documents the transfer of twist from the arcade to the overlying loops through reconnections, developing a flux rope. The nonparallel field lines comprising the rope and lower-lying arcades form an X-type geometry. Importantly, the simultaneous reconnections at the 3D null and the X-type geometry can explain the observed circular and parallel flare ribbons. Reconnections at the 3D null transform closed inner spine field lines into open field lines of the outer spine. The footpoints of these open field lines correspond to a ring-shaped coronal dimming region, tracing the dome. Further, the flux rope bifurcates because of these reconnections, which also results in the generation of open magnetic field lines. The plasma loss along the open field lines can potentially explain the observed coronal dimming.

This work was done in collaboration with Avijeet Prasad (The University of Alabama in Huntsville, USA), Karin Dissauer (University of Graz, Austria), Qiang Hu (The University of Alabama in Huntsville, USA), A. M. Veronig (University of Graz, Austria) and Sanjay Kumar (Patna University, India).

doi : https://doi.org/10.3847/1538-4357/abb8d2

(R. Bhattacharyya and Bhuwan Joshi)

Magnetic Reconnections in the Presence of Three-Dimensional Magnetic Nulls and Quasi-Separatrix Layers

Magnetic reconnection (MR) is believed to be the physical process central to the solar eruptive events such as solar flares, CMEs, and prominence eruption.

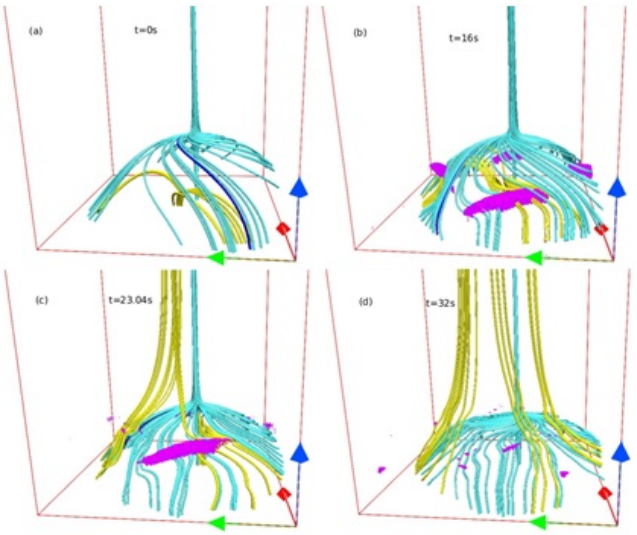

Figure 22.: Evolution of a 3D null along with the fan surface (represented by cyan field lines). The figure is overlaid with the yellow field lines under the dome and the isosurface of electric currents with a high isovalue (in pink). The movement of field lines of the dome is marked by a blue field line. Important are the appearances of the current at the fan surface and subsequent change in the connectivities of the yellow field lines through reconnections.

The potential locations for the reconnections are three-dimensional (3D) magnetic nulls, separator, quasi-separatrix layers (QSLs), and quasi-separator. In this work, we numerically explore magnetic reconnections, initiated by the presence of 3D nulls and QSLs by performing magnetohydrodynamics (MHD) simulations. The suitable initial magnetic fields are obtained by superposing uniform vertical magnetic fields of two different magnitudes on a linear force-free field. The interior of the computational box has two 3D nulls (morphologically similar to the ones observed in the solar corona) with separatrix domes separated by a quasi-separator (or hyperbolic flux tube) with QSLs. The first simulation corresponds to the uniform field with a larger magnitude, leading to the nulls at lower heights and the separate domes. Under forcing, the resultant dynamics originates strong electric currents and strong torsional fan reconnection at the 3D nulls. The formation of the currents and subsequent torsional fan reconnection are depicted in Figure 22. In addition, weak QSL reconnections at the hyperbolic flux tube are also simulated. Flipping or slipping of field lines is obtained in both cases. The second simulation, with a weaker vertical field, supports larger domes. The separatrix surfaces meet at the hyperbolic flux tube and their rotation leads to QSL reconnection which is stronger than the first simulation.

This work has been done in collaboration with S. Kumar (Patna University, India) and A. Prasad (The University of Alabama in Huntsville, USA).

doi : https://doi.org/10.1007/s11207-021-01768-7

(S. S. Nayak, R. Bhattacharyya)

Magnetohydrodynamics model of an X-class flare in NOAA active region 12017 initiated with non-force-free extrapolation

The solar flares are one of the transient phenomena on the solar atmosphere where huge amount of energy releases owing to magnetic reconnection: a change in the magnetic topology, relaxation of stressed magnetic energy into heat and kinetic energy, along with an acceleration of charge particles. One of the preferable sites of reconnection are three dimensional (3D) magnetic nulls (points where $|B|$=0). The work explores the reconnection at such a null located above the flaring active region AR12017 through numerical simulation. The flare lasts from $\sim$17:30 UT to $\sim$18:10 UT on 2014 March 29. The simulation is initiated with a coronal magnetic field constructed from photospheric vector magnetogram using the non-force-free-field (NFFF) extrapolation technique. The constructed coronal magnetic field is depicted in Figure 23 (a); showing a 3D null with its signature spine axis and fan plane (field lines in color sky blue and pink) along with a pair of flux ropes (drawn in red and chartreuse colors) which co-locate with the observed filaments. A set of sheared arcades, in ultramarine color, are found below the null. Also, a set of connecting field lines, drawn in golden color are existing in the extrapolated coronal magnetic field. The numerical simulation is carried out in the Vikram-100 HPC cluster at the PRL using 168 processors (each having 8 cores) for a wall time of 192 hours. The simulation covers 30 minutes of the observed flare, panels b - d showing the evolution of the field lines during the flare with reconnection initiated at the null point. Importantly, the panel c depicts foot points of field lines overlay the flare brightening that agrees with the general perception. Foot points at the other end of the spine also overlap with the observed remote brightening, attributing the flare to be triggered by the magnetic reconnection at the 3D null. The shearing arcades also participate in the reconnection at 3D null. The flux ropes lose their twist under

suitable Lorentz force and became visibly less twisted post-flare loops (in red and chartreuse colors at panel d, marked with black arrow. The estimated free energy released during the computed evolution was of the order of 10^{31} ergs and matches with the corresponding observational value. The novelty of this work is in the realization that a complex active region can have more than one magnetic structure and their interplay can initiate magnetic reconnection and hence, flares.

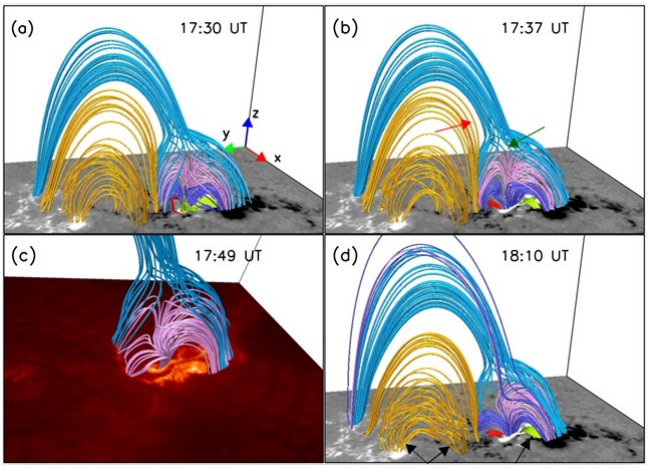

Figure 23.: The figure shows the evolution of the flare hosted by the active region AR12017. Different colors represent magnetic field lines near the flaring region. The flare spans from ∼17:30 UT – ∼18:10 UT on 2014 March 29. Different color field lines represent the connectivity in the vicinity of the flaring region. The green arrow in the panel b highlights the location of null point and others mark the changes in the topologies.

This work has been done in collaboration with Dr. Sanjay Kumar at Patna University, India.

doi : https://doi.org/10.1063/5.0035086

(S. S. Nayak and R. Bhattacharyya)

Evolution of Three-Dimensional Coherent Structures in Hall Magnetohydrodynamics

Hall Magnetohydrodynamics (HMHD) is important to explore physical systems undergoing fast magnetic reconnection at the order of the ion inertial length scale. Examples include solar transients along with reconnections in magnetosphere, magnetotail, and laboratory plasmas. We have extended the computational model EULAG-MHD to include Hall forcing. In addition to successful benchmarking of the numerical Hall MHD model initiated with unidirectional sinusoidal magnetic field, the HMHD simulations emphasize the complexity of three-dimensional (3D) evolution over its two-dimensional counterpart. The magnetic reconnections onset significantly earlier in HMHD. Importantly, the magnetic field generated by the Hall term breaks any inherent symmetry, ultimately making the evolution 3D. The resulting 3D reconnections develop magnetic flux ropes (MFRs) and magnetic flux tubes (MFTs). Projected on the reconnection plane, the ropes and tubes appear as magnetic islands, which later break into secondary islands, and finally coalesce to generate an X-type neutral point. These findings are in agreement with the theory and contemporary simulations of HMHD. We have executed the simulations to understand the influence of the Hall forcing on generation and ascend of an MFR from sheared magnetic arcades-a novel scenario instructive in understanding the coronal transients. The rope evolves through intermediate complex structures, ultimately breaking locally because of reconnections (Figure 24). Interestingly, the breakage occurs earlier in the presence of the Hall term, signifying faster dynamics leading to magnetic topology favorable for reconnections.

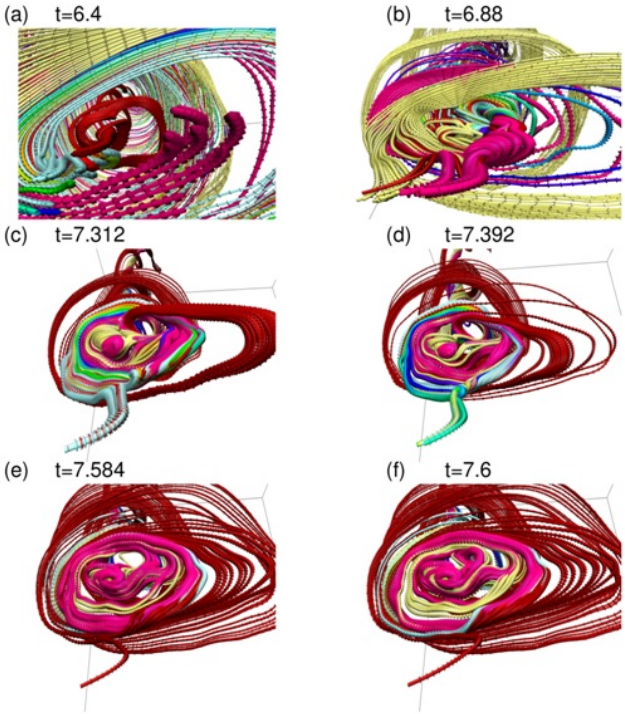

Figure 24.: The zoomed instances of internal reconnection within the flux rope during the HMHD evolution of the solar-like magnetic flux rope.

This work has been done in collaboration with P.K. Smolarkiewicz (National Center for Atmospheric Research, Boulder, CO, USA.)

doi : https://doi.org/10.3847/1538-4357/abc8f7

(K. Bora and R. Bhattacharyya)

Development of a low-order Adaptive optics system at Udaipur Solar Observatory

Resolution of any ground-based telescope is limited by the atmospheric turbulence commonly known as seeing. To enhance the resolution of a seeing limited telescope to its diffraction limit, it is necessary to employ image restoration techniques. Adaptive Optics (AO) is one such technique that corrects the distorted wavefront in real time, thereby improving image quality. An adaptive optics system is developed at USO for Multi-Application Solar Telescope (MAST).

The main components of the system are (a) a stand-alone image stabilization for compensation of global tilt of the distorted wavefront and (b) a Shack-Hartmann wavefront sensor along with a 37-channel

membrane mirror for sensing and correction of local tilts of the distorted wavefront. Optical setup is shown in Figure 25.

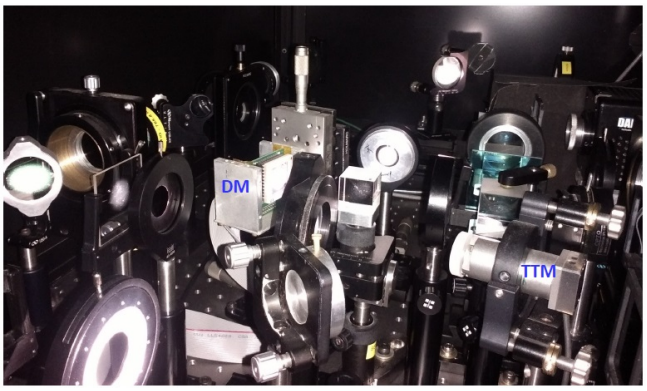

Figure 25.: Optical setup of the AO system showing the Tip-Tilt mirror (TTM) and the Deformable Mirror (DM).

Closed-loop update rate of the system is about 1 kHz and the correction bandwidth is 80-100 Hz. The corrected field of view of the adaptive optics system is about 15-20 arcsec. Capability of the adaptive optics system is demonstrated by obtaining the high-resolution observations of recent solar activity, particularly active region 12781 during its passage on the solar disk. Observations show considerable improvement in the image quality and the SNR due to adaptive optics system. These high-resolution observations (Figure 26) were obtained in both chromosphere (Ca II 8542) and photosphere (Fe I 6173) simultaneously. These observations will allow us to understand chromospheric transients and the related phenomena in the lower solar atmosphere.

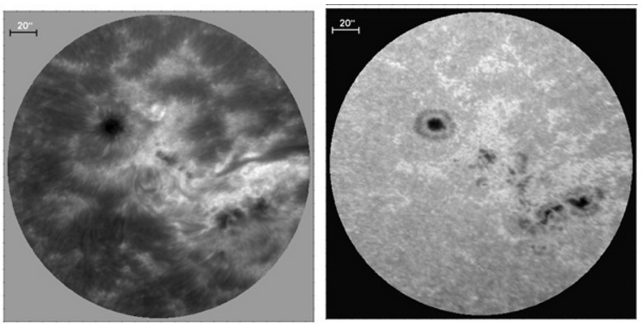

Figure 26.: Observations of the active region 12781 obtained with narrow-band spectral imager on MAST while adaptive optics system in operation. FOV is 236×236 arcsec^2. These images are corresponding to the line cores of CaII8542 (left) and FeI 6173 (right), which are formed in chromosphere and photosphere, respectively.

This work has been done in collaboration with R. Sridharan IIA, Bangalore.

(A. Raja Bayanna, S. K. Mathew, B. Rmaya, R. E. Louis, A. Kulhari and B. Kumar)

Planetary Sciences

Modelling of Planetary Atmosphere, Simulations and Interstellar Medium

The strength of lightning on the Venus inferred from ionospheric whistler-mode waves

Lightning produces an extremely low frequency (ELF) radio wave that propagates along magnetic field lines to higher altitudes in the ionosphere. The Interplanetary Magnetic Field (IMF) induces currents in the ionosphere that generate an opposing field. The field lines tend to be nearly horizontal to the surface around much of the planet, except in the tail where it is more radial. A dual fluxgate magnetometer onboard Venus Express (VEX) was able to detect ELF signals up to 64 Hz at various altitudes throughout the mission. We searched all available data within the ionosphere for lightning-generated whistler-mode waves. The mission was in orbit from 2006-2014 and in that time, there were nearly 7 cumulative hours of whistler observations below 400 km. In some cases, there was continuous activity for over a minute, implying a connection to an electrical storm below. These signals were most frequently seen when the spacecraft was at $\sim$ 250 km altitude. Most signals were observed within 200-350 km altitude with a rate of $\sim$ 3% of the time the spacecraft spent at these altitudes. Because the ionosphere becomes strongly magnetized during solar minimum, detection rates are about twice as high compared to solar maximum. The Poynting flux during solar maximum shows a decrease with increasing altitude, providing an evidence that the waves were generated below the ionosphere. This conclusion is less clear during solar minimum. Pioneer Venus (PVO) was able to detect the electric component of lightning-generated waves at 100 and 700 Hz, but on the nightside and at lower latitudes in contrast to the North polar orbit of VEX. The improved capability of VEX over PVO has greatly increased our knowledge of Venus lightning.

This work was done in collaboration with Pr. C. T. Russell, Department of Earth, Planetary, and Space Sciences, University of California, Los Angeles, USA.

doi : https://doi.org/10.5194/epsc2020-483

(J. P. Pabari)

Photoelectron distribution on sunlit surface of the Moon

We propose an analytical formulation describing the characteristic energy distribution of the photoelectrons over the sunlit regolith of the Moon. In deriving the distribution function, Fowler's approach based on fermionic lattice electrons for the photoemission has been coupled with observed solar spectra, photoelectric quantum yield, and latitude dependent surface temperature. It is noticed that the dominant contribution in the photoelectron distribution function comes from EUV photons (3 eV – 300 eV) of the solar spectra. The analysis also illustrates that the photoelectron distribution for the observed solar spectra is significantly different from the spectrum based on Planck's radiation law. The photoelectron distribution is found a significant function of the lunar surface potential – the photoelectron distribution in the steady state considerably differs from that of the uncharged surface. In calculations, the variation in photoelectron distribution function with the lunar latitude, quantum yield, and work function of the surface material has been parametrically analyzed, and it is found sensitive to the constituent parameters.

doi : https://doi.org/10.1063/5.0016411

(S. K. Mishra)

Electrostatic charging of permanently shadowed craters on the Moon

An open question of the electrostatic charge development on the lunar surface in the electron-rich region within the permanently shadowed craters (PSCs) is addressed. We propose that the fine dust grains on the crater surface may act as efficient field emission centers generating electrons via quantum field tunneling. This return current may be sufficient to establish a steady state dynamical equilibrium for the surface-plasma system. This leads to the crater surface attaining a finite electric potential. Our analysis illustrates that the PSC having $\sim$ 100 nm dust, covering 1% of the surface area within the electron-rich region, may acquire $\sim$ 100's V negative potential in the steady state condition. This phenomenon is also pertinent with a fine irregular structure on the crater surface to dust scale (e.g., the amorphous ice within polar craters). This concept also suggests a solution for the moving object near the leeward face and electron-rich region, where it suffers strong charging effects with large dissipation time – this can be hazardous for the instrument and human operations in the lunar exploration. This excessive charging can be remediated by introducing the hemispherical microstructure tips (via surface engineering) on the plasma-facing surface of the moving object. These micro tips might act as FE centers, generating a sufficient return current to avoid the high electrostatic potential development and efficiently facilitate the charge dissipation. This work enriches the understanding of charge/

potential development on the crater (or moving object) surface in the electron-rich regions within PSC's and potentially useful for campaign design in forthcoming Moon exploration robotic/ human missions.

doi : https://doi.org/10.1093/mnrasl/slaa082

(S. K. Mishra and A. Bhardwaj)

Role of photoelectric charge fluctuation in dust detachment from the lunar surface

Electrostatic processes are argued to be of fundamental importance in understanding the particle dynamics and complex dusty plasma environment over airless bodies—the Moon has been of particular interest. Based on the theory of electrostatic charge fluctuation corresponding to the photoemission current, the fundamental problem of dust detachment from the lunar surface is addressed. By applying the charge fluctuation at the microscopic scale, we have quantified the magnitude of fluctuating charge density over the sunlit lunar surface and illustrated that it could induce a sufficient electric field to overcome the dust–surface adhesive van der Waals bonding through the electrostatic Coulomb repulsion. The analysis takes into account the dynamic equations for the statistical variables, viz., the mean charge and the variance, corresponding to the charge distribution over the microscopic spots exposed to the solar radiation. The photoemission under the influence of extreme ultraviolet Lyman a radiation in the solar spectrum and subsequent collection of the emitted photoelectrons are accounted for as the dominant charging processes of the lunar surface. Based on analysis and calculations, the fluctuating charge is illustrated to be a significant function of the spot size, which may induce significantly high electric field fluctuations locally. As an illustrative example, it is shown that one square micrometer spot may acquire 15 electronic charges and might induce a local electric field equivalent to 10 kV/m, which can support the detachment of the submicrometer dust particles from the lunar surface.

doi : https://doi.org/10.1063/5.0009741

(S. K. Mishra)

Recurrent solar energetic particle flux enhancements observed near the Earth and Mars

The period 01 Aug to 15 Nov, 2016 was characterized by the presence of corotating interaction regions (CIRs) and a few weak coronal mass ejections (CMEs) in the heliosphere. We show recurrent energetic electron and proton enhancements observed near the Earth (1 AU) and Mars (1.43–1.38 AU) during this period. The observations near the Earth use data from instruments on board the Advanced Composition Explorer, the Solar and Heliospheric Observatory, and Solar Dynamics Observatory and those near Mars are from the Solar Energetic Particle, Solar Wind Ion Analyzer, and Magnetometer instruments on board the Mars Atmosphere and Volatile EvolutioN (MAVEN). During this period, the energetic electron fluxes observed near the Earth and Mars showed prominent periodic enhancements over four solar rotations, with major periodicities of $\sim$ 27 days and $\sim$ 13 days. Periodic radar blackouts/weakenings of radar signals at the Mars were observed by the Mars Advanced Radar for Subsurface and Ionosphere Sounding/Mars Express, and are associated with these solar energetic electron enhancements. During this period, a weak CME and a high-speed stream (HSS)-related interplanetary shock could have interacted with the CIR and enhance energetic proton fluxes near 1.43–1.38 AU, causing $\sim$ 27 days periodicity in proton fluxes to be significantly diminished at 1.43–1.38 au. These events also have an unexpected impact on the Martian topside ionosphere, such as topside ionospheric depletion and compression observed by the Langmuir Probe and Waves and Neutral Gas and Ion Mass Spectrometer on board MAVEN. These observations are unique not only because of the recurring nature of electron enhancements seen at two vantage points, but also because they reveal the unexpected impact of the weak CME and interplanetary shock on the Martian ionosphere, which provides new insights into the impact of CME–HSS interactions on the Martian plasma environment.

This work is done in collaboration with C. Krishnaprasad, Smitha V. Thampi, K. Kishore Kumar, and Tarun K. Pant of Space Physics Laboratory, VSSC, Trivandrum, and Christina O. Lee of Space Sciences Laboratory, University of California Berkeley, USA.

doi : https://doi.org/10.3847/1538-4357/abb137

(A. Bhardwaj)

Search for the Martian Schumann resonances

Active dust devils or dust storms occur on the Mars during southern hemisphere summer, when the planet is near periapsis. Within dust storms, dust particles undergo triboelectric charging. The charge transfer leads to charge separation and a lightning discharge is expected to occur when the charge exceeds the breakdown strength of the media present. The electric discharges produce ELF waves in the surface-ionosphere waveguide that encircles the globe. These waves give rise to Schumann resonances in the waveguide resonant cavity. In a heterogeneous cavity, Schumann resonance modes are observable using an $in-situ$ instrument. Recently it has been possible to search for these electromagnetic waves from the Mars surface using the UCLA-provided InSight fluxgate magnetometer. The weakness of the vertical component of ULF waves at the Mars suggests that the subsurface is electrically conducting, allowing trapping of electromagnetic energy between the subsurface and the ionosphere. The fundamental mode of Schumann resonance carries high energy and various values of the first mode are predicted in the literature for Mars like 13-14 Hz or between 9-14 Hz and 17.5 Hz. Even if the fundamental mode is above 10 Hz, the 20 Hz sampling rate can allow detection of an aliased signal. We examine the data obtained during Martian sandstorms for the possible existence of such waves. A large dust storm was detected on Mars beginning on InSight sols 40 to 50, and ending during sols 50 to 90. Examining the 20 Hz InSight magnetometer data during this period reveals no clearly identifiable Schumann Resonance signals within the bandwidth of the magnetometer.

This work has been led by Pr. C. T. Russell, Department of Earth, Planetary, and Space Sciences, University of California, Los Angeles, USA.

doi : https://doi.org/10.5194/epsc2020-541

(S. A. Haider and J. P. Pabari)

Thermal emission spectra on the Mars: observations and modeling

The thermal emission spectrum is very useful to understand the atmosphere and its surface. It gives us information about atmospheric temperature, pressure, mineralogy and presence of atmospheric constituents including their isotopes. We have analyzed thermal emission data obtained from Planetary Fourier Spectrometer (PFS) onboard Mars Express (MEX) for MY28 when a global dust storm occurred in the southern hemisphere at low latitudes from 0° to 30°S between Ls $\sim$ 280° and 300°. We have also studied thermal emissions in absence of dust storm between Ls $\sim$ 240° and 320° at low latitudes. The PFS observed emission spectra between wave numbers 250-1400 cm^{-1}. In this spectrum two broad features at wave number 600-750 cm^{-1} and 900-1200 cm^{-1} have been observed by CO_2 and dust respectively. We have also estimated brightness temperature from thermal emission spectra by inverting the Planck function. The maximum brightness temperature $\sim$ 280°K was measured at Ls=240° when the Mars received a large amount of solar radiation at perihelion. The minimum brightness temperature $\sim$ 220°K was observed at Ls=320° in the absence of dust storm. In presence of dust storm, thermal emission spectra and brightness temperatures were reduced by factors of $\sim$ 3.0 and $\sim$ 1.3, respectively, between wave numbers 900-1200 cm^{-1} in comparison to that observed in absence of dust storm.

doi : http://nopr.niscair.res.in/handle/123456789/54918

(S. A. Haider and J. Masoom)

X-ray flare responses in the D and E region ionosphere of the Mars

We report responses of two X-ray flares that occurred on 6 April 2001 and 17 March 2003 in the ionosphere of the Mars. The Mars Global Surveyor (MGS) observed these flare effects from radio occultation experiment in the E region of the Mars at Solar Zenith Angle (SZA) 71°. The D region of the Mars cannot be observed below 80 km by radio occultation method. We have estimated Ionospheric Electron Content (IEC) from flare and non-flare electron density profiles obtained at different Universal Time (UT) in the D and E regions of the Mars' ionosphere due to impact of X-rays (0.5-90 A) at SZA 71°. Figure 1a represents the calculated time series of IEC for 6 April 2001 in the D region ionosphere of the Mars. Figure 1b shows the same IEC profile but for 17 March 2003. The maximum IEC on 6 April 2001 is calculated to be 15 $\times$ 10^{10} cm^{-2} at 19:27 UT.

On 17 March 2003 peak IEC is estimated $\sim$ 7.5 $\times$ 10^{10} cm^{-2} at 19:11 UT. MGS observed the E-region flare profiles on 6 April 2001 and 17 March 2003 after about 46 min and 27 min delay from the peak X-ray flux at Mars i.e. 20:13 UT and 19:38 UT. In Figure 1c we have plotted the IEC of E region at latitude 84.8°N using 11 electron density profiles observed by MGS on 6 April 2001. In Figure 1d we have plotted the IEC of E region at latitude 82.0°N using 7 electron density profiles observed by MGS on 17 March 2003. These IEC were obtained by integrating the observed electron density profiles from lowest altitude (88 km) to E-F valley (115 km) (beyond this altitude the F layer starts in the measurements of MGS profiles). In these figures we have also plotted estimated IEC of E region ionosphere for comparison with MGS observations. It is found that simulated value of IEC is higher than the measured IEC of MGS by factors of $\sim$ 2 to 3 at the flare peak. There are no flare electron density measurements on the exact flare time. The IEC peak in the E region is observed $\sim$ 1.5 $\times$ 10^{11} cm^{-2} and $\sim$ 1.2 $\times$ 10^{11} cm^{-2} during the flare decay period at 20:30 UT and 19:38 UT on 6 April 2001 and 17 March 2003 respectively. It is calculated$\sim$ 6.2 $\times$ 1011 cm^{-2} on 6 April 2001 at 19:27 UT. On 17 March 2003 it is lowere by a factor of $\sim$ 2 than that estimated on 6 April 2001. The estimated and measured IEC of the E region shows good agreement during the decay phase of each flare.

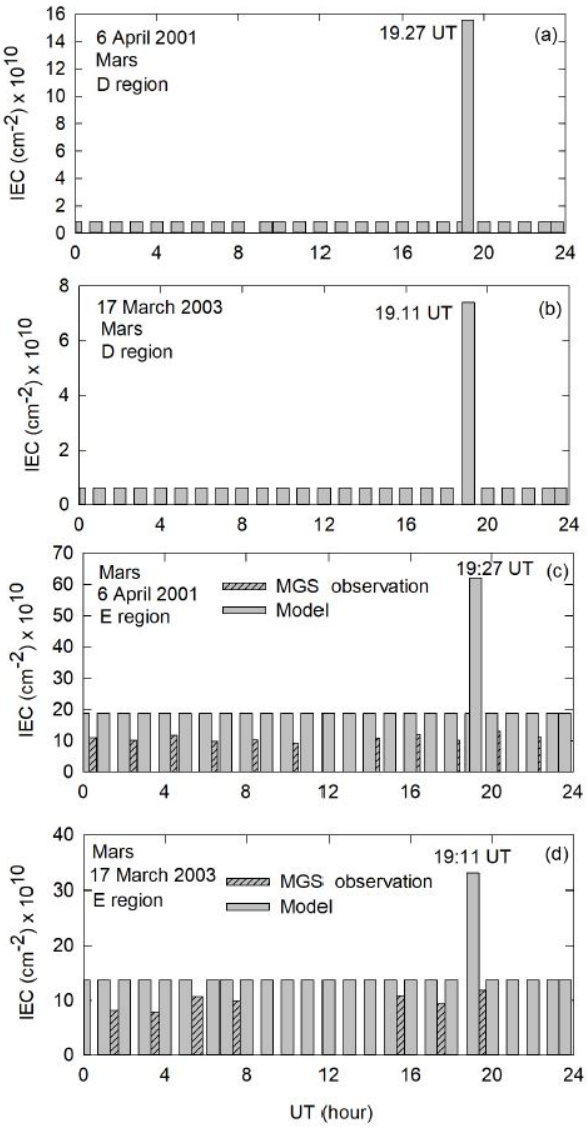

Figure 1: (a) Time series of estimated iec in Mars' D region on 6 April 2001, (b) same spectrum as shown in figure 1a but for 17 March 2003, (c) Time series of estimated IEC in Mars' E region ionosphere on 6 April 2001, (d) same spectrum as shown in in figure 1c but for 17 March 2003.

doi : https://doi.org/10.1016/j.icarus.2021.114403

(S. A. Haider and Y. Siddhi)

CO^+ first-negative band emission: A tracer for CO in the Martian upper atmosphere

Recently, Imaging Ultraviolet Spectrograph (IUVS) on-board Mars Atmosphere and Volatile EvolutioN (MAVEN) satellite observed CO^+ first-negative band limb emission in the Martian upper atmosphere. We aim to explore the photochemical processes in the Martian upper atmosphere, which drives this band emission.

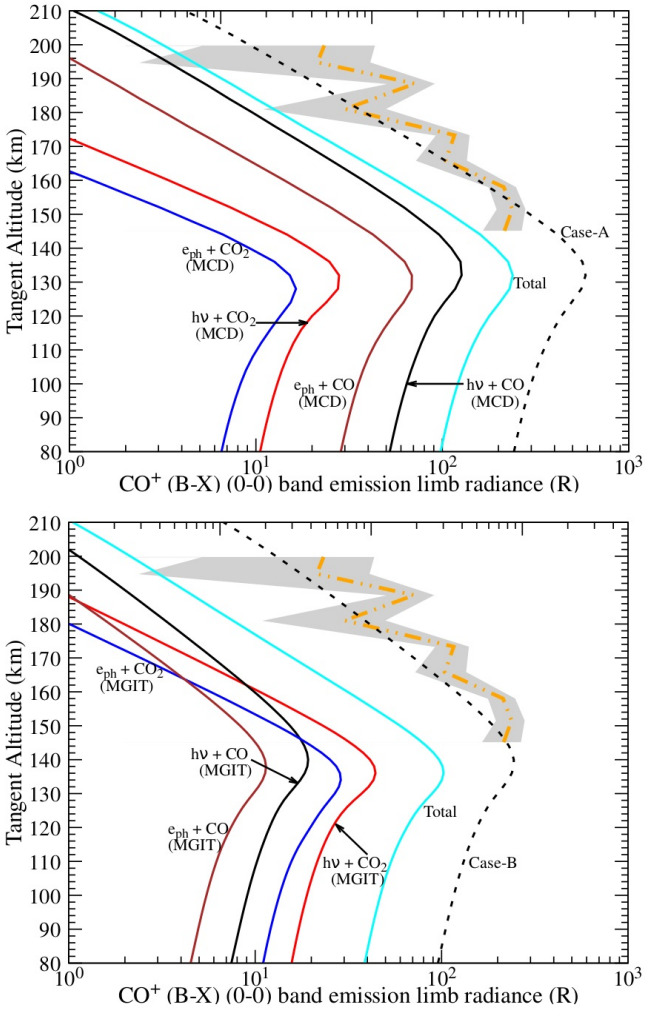

Figure 2: Comparison between modelled CO+ first-negative (0–0) band emission limb intensity profiles using neutral densities from MCD (top panel), and MGIT (bottom panel) models as well as the IUVS/MAVEN observation. The dashed, double-dotted orange curve represents the IUVS/MAVEN observed average intensity of CO+ first-negative (0–0) band emission on 7 April 2016 and the grey shaded area is its 1s uncertainty (taken from Stevens et al. 2019). Here Case-A and Case-B are the modelled limb intensity profiles by increasing the CO density in the MCD and MGIT models by a factor of 3 and 8, respectively.

A photochemical model is developed to study the excitation processes of CO^+ first-negative band emission ($B^2\Sigma^+ \rightarrow X^2\Sigma^+$) in the upper atmosphere of Mars. The number density profiles of CO_2 and CO from two different models, viz., Mars Climate Database (MCD) and Mars Global Ionosphere-Thermosphere (MGIT) are used to determine the limb intensity of this band emission. On increasing the CO density by a factor of 4 and 8 in MCD and MGIT models, respectively, the modelled CO^+ first-negative band limb intensity profile is found to be consistent with IUVS/MAVEN observation (see the top and bottom panels of Figure 2). In this case, the intensity of this band emission is significantly determined by the ionization of CO by solar photons and photoelectrons, and the role of dissociative ionization of CO_2 is negligible. Since CO is the major source of the $CO^+(B^2\Sigma^+)$, we suggest that the observed CO^+ first-negative band emission intensity can be used to retrieve the CO density in the Martian upper atmosphere for the altitudes above 150 km.

doi : https://doi.org/10.1051/0004-6361/202038147

(S. Raghuram and A. Bhardwaj)

Forbidden atomic oxygen emissions in the Martian dayside upper atmosphere.

Recently, Nadir and Occultation for Mars Discovery (NOMAD) ultraviolet and visible spectrometer instrument on board the European Space Agency's ExoMars Trace Gas Orbiter (TGO) simultaneously measured the limb emission intensities for both [OI] 2972 and 5577 Å (green) emissions in the dayside of Martian upper atmosphere. But the atomic oxygen red-doublet emission lines ([OI] 6300 and 6364 Å), which are expected to be observed along with [OI] 5577 and 2972 Å emissions, are found to be absent in the NOMAD-TGO dayside observed spectra.

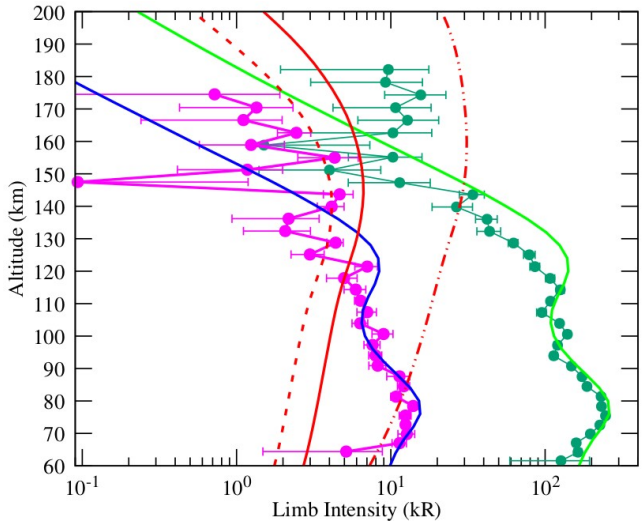

Figure 3: Comparison between modelled and observed limb intensity profiles of [OI] 2972, 5577, and 6300 Å emissions. Magenta and thick green curves with x-error bars represent the respective NOMAD-TGO observed limb intensity profiles for [OI] 2972 and 5577 Å emissions on 28 April 2019 (taken from Gérard et al., 2020). Blue, green and red curves are the modelled limb intensity profiles for [OI] 2972, 5577 and 6300 Å emissions, respectively. These limb intensities are calculated by decreasing the Fox (2004) modelled neutral density profiles for solar minimum condition by a factor of 2. Dashed and dash double-dotted red curves represent the calculated limb intensity profiles for [OI] 6300 Å emission by reducing the Fox (2004) modelled atomic oxygen density by a factor of 10 and for solar maximum condition, respectively.

We aim to explore the photochemistry of all these forbidden atomic oxygen emissions ([OI] 2972, 5577, 6300, 6464 Å) in the Martian daylight upper atmosphere and suitable conditions for the simultaneous detection of these emissions lines in the dayside visible spectra. A photochemical model is developed to study the production and loss processes of $O(^1S)$ and $O(^1D)$, which are the respective

excited states of green and red-doublet emissions, by incorporating various chemical reactions of different O-bearing species in the upper atmosphere of Mars. By reducing Fox (2004) modelled neutral density profiles by a factor of 2, the calculated limb intensity profiles for [OI] 5577 and 2972 Å emissions are found to be consistent with the NOMAD-TGO observations. In this case, at altitudes below 120 km, our modelled limb intensity for [OI] 6300 Å emission is smaller by a factor 2 to 5 compared to that of NOMAD-TGO observation for [OI] 2972 Å emission, and above this distance it is comparable with the upper limit of the observation. We studied various parameters which can influence the limb intensities of these atomic oxygen forbidden emission lines. Our calculated limb intensity for [OI] 6300 Å emission, when the Mars is at near perihelion and for solar maximum condition, suggests that all these forbidden emissions should be observable in the NOMAD-TGO visible spectra taken on the dayside of Martian upper atmosphere. More simultaneous observations of forbidden atomic oxygen emission lines will help to understand the photochemical processes of oxygen-bearing species in the dayside Martian upper atmosphere.

This work was done in collaboration with Sonal Kumar Jain of Laboratory for Atmospheric and Space Physics, University of Colorado, Boulder, USA.

doi : https://doi.org/10.1016/j.icarus.2021.114330

(S. Raghuram and A. Bhardwaj)

Model calculation of ionization efficiency in the Martian dayside ionosphere using MAVEN observations

The ionization efficiency (η), which is defined as the ratio of the electron impact to the photon impact ionization rates, is calculated for the dayside Martian ionosphere using Mars Atmosphere Volatile EvolutioN (MAVEN) observations of neutral density and solar flux as input to the model. To calculate the secondary (electron impact) ionization rates, the photoelectron flux is computed using the Analytical Yield Spectrum (AYS) approach. Model calculations suggest that η should increase consistently as altitude decreases in the lower ionosphere. However, when the secondary ionization rates are calculated using the SWEA/MAVEN measured photoelectron flux, the ionization efficiency remains constant in the region 160–250 km. This behaviour is not in agreement with the theory of the altitude variation of ionization efficiency. The reason for this discrepancy is examined in detail. It is suggested that this disagreement is caused by the altitude independent nature of MAVEN measured photoelectron flux. In two MAVEN deep dip orbits SWEA measured flux showed an altitudinal variation and the η curve estimated using these observations showed the variation in agreement with the theory. This suggests that the ionization efficiency calculated using SWEA/MAVEN measured photoelectron flux will show an altitude dependent behaviour only when the instrument can resolve the altitudinal variation in the electron flux. We also calculated the ionization efficiency for two MAVEN dayside deep dip campaigns. The efficiency of CO_2 and O showed an increase of 30 percent and 60 percent, respectively, at 130 km as compared to its value at 200 km.

This work was done in collaboration with Vrinda Mukundan, Smitha V. Thampi and C. Krishnaprasad of Space Physics Laboratory, VSSC, Trivandrum.

doi : https://doi.org/10.1093/mnras/staa2123

(A. Bhardwaj)

A physico-chemical model to study the ion density distribution in the inner coma of comet C/2016 R2 (Pan-STARRS)

The recent observations show that comet C/2016 R2 (Pan-Starrs) has a unique and peculiar composition when compared with several other comets observed at 2.8 AU heliocentric distance.

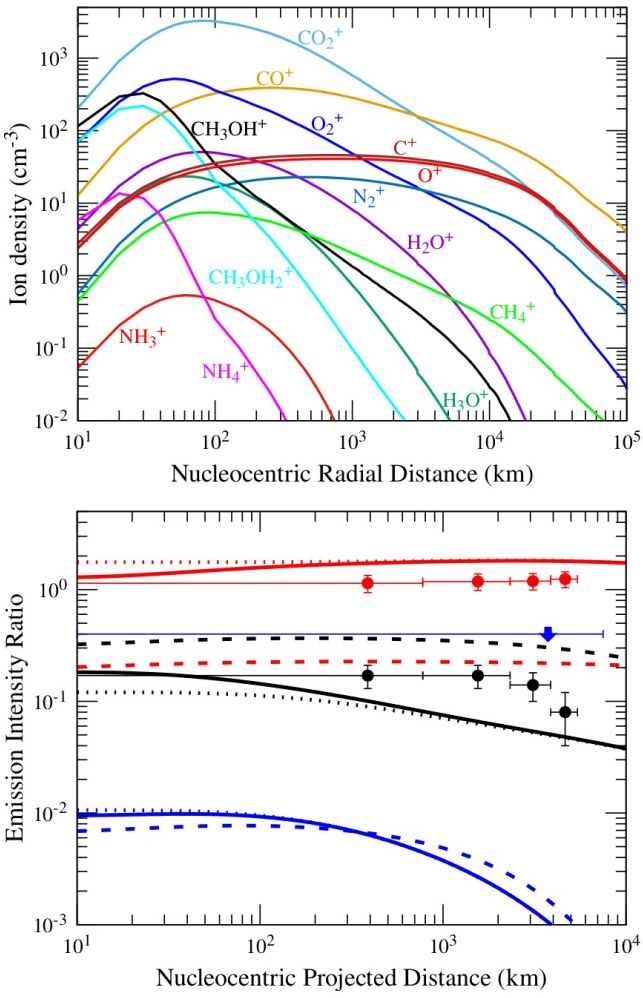

Figure 4: The modelled density profiles for different ions in the coma of comet C/2016 R2 (top panel). Modelled emission intensity ratios of N_2^+/CO^+ (red), CO_2^+/CO^+ (black), and H_2O^+/CO^+ (blue) as a function of projected distance (bottom panel). Solid curves are the modelled ratio profiles by accounting for all excitation processes. Dashed and dotted curves represent the modelled emission intensity ratios profiles by accounting for only ionization of neutrals and only solar resonance fluorescence mechanisms, respectively. The observed flux ratios are plotted with corresponding colours with vertical error bars. The blue horizontal line with a downward arrow represents the derived upper limit of H_2O^+/CO^+ emission intensity ratio.

Assuming solar resonance fluorescence is the only excitation source,

the observed ionic emission intensity ratios are used to constrain the corresponding neutral abundances in this comet. We developed a physico-chemical model to study the ion density distribution in the inner coma of this comet by accounting for photon and electron impact ionization of neutrals, charge exchange and proton transfer reactions between ions and neutrals, and electron-ion thermal recombination reactions. Our calculations show that CO_2^+ and CO^+ are the major ions in the inner coma, and close to the surface of nucleus CH_3OH^+, $CH_3OH_2^+$ and O_2^+ are also important ions (see Top panel of Figure 4). By considering various excitation sources, we also studied the emission mechanisms of different excited states of CO^+, CO_2^+, N_2^+, and H_2O^+. We found that the photon and electron impact ionization and excitation of corresponding neutrals significantly contribute to the observed ionic emissions for radial distances smaller than 300 km, and at larger distances solar resonance fluorescence is the major excitation source. Our modelled ion emission intensity ratios are consistent with the ground-based observations (see bottom panel of Figure 4). Based on the modelled emission processes, we suggest that the observed ion emission intensity ratios can be used to derive the neutral composition in the cometary coma only when the ion densities are significantly controlled by photon and photoelectron impact ionization of neutrals rather than by the ion-neutral chemistry.

This work was done in collaboration with Damien Hutsemékers, Jean Manfroid, and Emmanuel Jehin of STAR Institute, University of Liege, Belgium, and Cyrielle Opitom of European Southern Observatory, Santiago, Chile.

doi : https://doi.org/10.1093/mnras/staa3885

(S. Raghuram and A. Bhardwaj)

Remote Sensing and Data Analysis

Geologic context and potential EVA targets at the lunar south pole

The lunar south pole is being targeted for exploration, in part, because it contains topographical high points with >50% illumination needed for solar power. Additionally, the south pole is being targeted because it contains permanently shadowed regions (PSRs), which may sequester resources in the form of volatile materials. Geologically, the pole lies on the rim of ∼ 21 km diameter Shackleton crater, which is located on the topographic rim of the ∼ 2,500 km diameter South Pole-Aitken (SPA) basin, is the largest and oldest basin on the Moon [Figure 5].

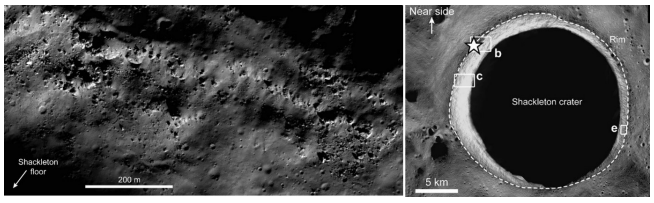

Figure 5: The Shackleton crater and the layered stratigraphy in the inner wall with exposed boulders.

To prepare for future missions, we conducted a photogeologic analysis of the walls, rim, and ejecta of Shackleton crater. Two types of underlying (target) terrains were identified. The impact penetrated and exposed (1) purest anorthosite (PAN) representative of primitive crust and (2) a layered terrain that is likely a series of impact ejecta deposits that stratigraphically cover the crystalline crust. Crew performing extravehicular activities (EVAs) near the south pole may be able to sample PAN; impact melt from Shackleton, SPA, and other pre-Nectarian and Nectarian-age impacts; and polar regolith, including material from small PSRs that may contain volatile components. The topography in the south polar region is dramatic, often producing slopes in excess of 15°, creating mobility challenges for astronauts during EVAs.

This work was done in collaboration with A. J. Gawronska, N. Barrett, S.J. Boazman, C.M. Gilmour, S.H. Halim, K. McCanaan, A.V. Satyakumar, J. Shah, H.M. Meyer, D.A. Kring of LPI Intern program.

doi : https://doi.org/10.1016/j.asr.2020.05.035

(Harish)

Numerical modeling of the formation of the Shackleton crater at the lunar south pole

The lunar south pole, on the rim of Shackleton crater, is the target for the next human landing on the Moon. We use numerical modeling to investigate the formation of that crater and the distribution of ejecta around the south pole. We find that a 1.5 km diameter asteroid with a chondrite-like composition, vertically impacting a gabbroic anorthositic target at 15 km/s, forms a crater morphologically similar to Shackleton. If the impact had a shallower 45-degree trajectory, the asteroid may have had a diameter of 1.75 km and velocity of 15 km/s or a diameter of 1.5 km and velocity of 20 km/s. Impact melt is generated during the impact, with most of the melt volume ponding on the crater floor. We introduce a water-bearing layer at various depths in the target and find that the burial depth of a volatile layer influences the final crater morphology and may explain the morphology of Shackleton [Figure 6].

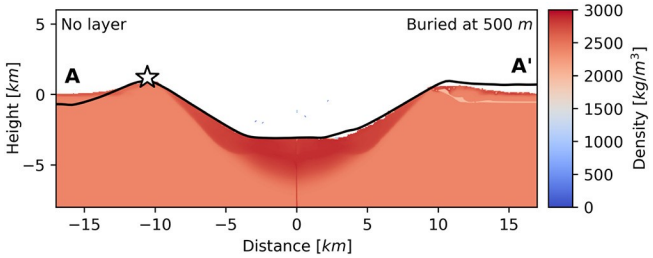

Figure 6: Density plot to represent the asymmetric surface structure at the impact site. The final crater morphology for a target surface with a homogenous target layer (left) and a target layer with a 100 m thick volatile layer buried at 500 m (right) are displayed.

This work was done in collaboration with Samuel H. Halim, Natasha Barrett, Sarah J. Boazman, Aleksandra J. Gawronska, Cosette M. Gilmour, Katie McCanaan, Animireddi V. Satyakumar, Jahnavi Shah, David A. Kring of LPI Intern program.

doi : https://doi.org/10.1016/j.icarus.2020.113992

(Harish)

Thermophysical behaviour of the lunar surface

Observations from recent missions have completely changed the existing perception about the lunar heat flow and thermophysical behavior. Deep Moon quakes (>500km), observations of surface shrinkage (Graben)/tectonic activity, reports about young volcanism, dry granular flows and mass movements point towards the possible existence of accumulated internal heat. Also, significant to mention at this point are the recent observations of distinct thermo physical behaviour of morphologically distinct lunar terranes with significant variations in lunar day-night temperatures. If the global heat flow of the Moon is planned to be estimated in future either by $in-situ$ investigations or through remote sensing observations or numerical modeling, precise estimation of equilibrium boundary between external and internal heat fluxes is necessary to infer the net heat flow on the Moon. This requires an in-depth understanding of the lunar near surface thermophysical behaviour. However, the understanding of lunar surface thermophysical behavior is not straight forward and has several inter-dependencies and therefore a systematic and numerous detailed in-depth investigations are needed. Even after numerous efforts carried out for several decades, very little is known and thus necessitates the planning of a series of geo-physical experiments on the Moon in near future. The current state of knowledge about lunar surface thermophysical behaviour comes from ground-based observations, orbiter observations and laboratory experiments conducted on samples returned by Apollo missions. The remote sensing observations when integrated with numerical models, mostly one dimensional in nature, and combined with Apollo sample return measurements have provided information about surface and subsurface temperatures and their variations. Lunar surface and subsurface temperatures of the Moon are dictated by a complex interplay of number of parameters. These surface and subsurface temperatures also manifest significant latitudinal, stratigraphic and topographical variability.

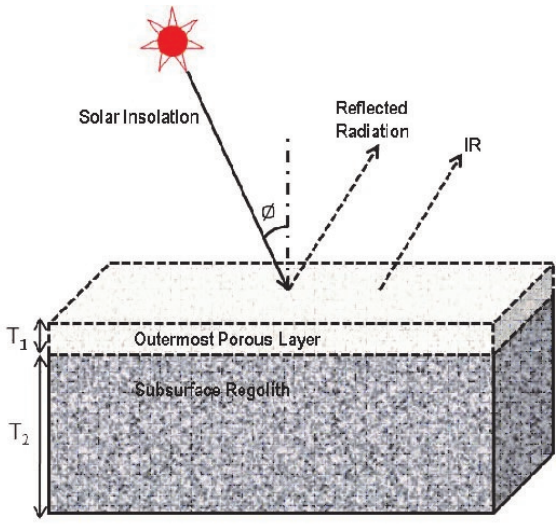

Figure 7: Schematic representation of two-layer nature of lunar surface from present understanding

Due to the large day-night temperature gradients of $\sim$ 300K on the Moon, the basic thermophysical properties viz. thermal conductivity and specific heat also exhibit significant variations. Based on the present understanding and in-depth modelling work being carried out at PRL, the lunar surface can be best thought to be represented by a two layer model having two distinct thermal regimes as shown in figure 7. It consists of an uppermost porous layer of extremely low thermal conductivity followed by a regolith layer beneath with relatively higher thermal conductivity. However, the nature and extent of this surficial pororus layer is not well-constrained particularly at high and polar latitudes. Since this porous layer principally dictates the propagation of solar heat influx to the interior layers, an in-depth understanding of the thermo physical behaviour of lunar surficial layer and its stratigraphic and spatial variation is needed for a better estimation of the equilibrium boundary due to external and internal heat fluxes. Although some efforts are being made, extensive studies are needed. However, laboratory experiments have certain limitations in terms of simulating parametric variation and long-term variability. This can be overcome by augmenting the laboratory experiments with comprehensive numerical simulations. Apart from these, the most prospective thing to accomplish in future would be to plan for a series of geophysical measurements through international cooperation, possibly through establishing an international lunar network.

doi : https://doi.org/10.1007/978-3-319-05546-6_200-1

(K. Durga Prasad)

Processes governing the VIS/NIR spectral reflectance behavior of lunar swirls

Based on the analysis of Moon Mineralogy Mapper (M^3) on-board Chandrayaan-1, we investigated six swirls associated with magnetic anomalies of variable strength. Swirls are characterized by high albedo patterns of a complex shape co-located with localized magnetic fields. One of the most commonly accepted hypotheses for the explanation of lunar swirls is magnetic shielding from charged solar wind particles, thus preventing the darkening of the surface material that occurs outside a magnetic field due to the differential solar wind bombardment, resulting in lighter and darker albedo variations. However, magnetic shileding does not imply a specific mode of swirl formation and the formation of swirl still remains unexplained. In this work, we used calibrated M^3 data and constructed regional maps of the integrated 3 μm band depth and the soil compaction map for six swirls. To quantify the similarity of an observed spectral trend to reduced space-weathering vs. soil compaction, we use the compaction-significance spectral index (CSSI), a positive real number defined by a pair of spectra located on a bright and a dark surface, respectively. Small values of CSSI are typical of fresh impact craters, whereas large values indicate a spectral trend inconsistent with reduced space-weathering alone. The CSSI maps of swirls and surroundings suggest presence of an additional physical process beyond magnetic shielding. As a possible external mechanism, the interaction between the regolith and cometary gas has been suggested which might be similar to the effect of a landing rocket jet. This mechanism can explain the observed on-swirl vs. off-swirl spectral trends.

This work was done in collaboration with Marcel Hess, TU Dortmund, Germany.

doi : https://doi.org/10.1051/0004-6361/201937299

(M. Bhatt and A. Bhardwaj)

Geology of the Grimaldi Basin on the Moon: Evidence for volcanism and tectonism during the Copernican period

The availability of high-resolution datasets from various missions has significantly improved our understanding of the Moon by revealing volcanic and tectonic activities that have occurred in the recent past. We have found evidence of such events in the Grimaldi Basin, a Pre-Nectarian basin located near the western edge of the Oceanus Procellarum. Moon Mineralogy Mapper (M^3), FeO wt%, and TiO2 wt % data have been used to study the compositional make-up of the Grimaldi mare basalt. Additionally, morphological studies and crater chronology have been carried out using moderate to very high-resolution images from Lunar Reconnaissance Orbiter (LRO) to decipher the geological evolution of the Grimaldi Basin. In this study (Fig. 8), we have found that in the south-central part, the basin experienced Copernican aged volcanism $\sim$ 700 Ma ago, resulting in the formation of olivine-bearing basalts with high FeO and TiO_2 contents. Cross-cutting of small Copernican craters by fresh wrinkle ridges and lobate scarps has been observed at several places, suggesting that tectonic activities also occurred in the basin during the past $\sim$ 50 Ma-1 Ga.

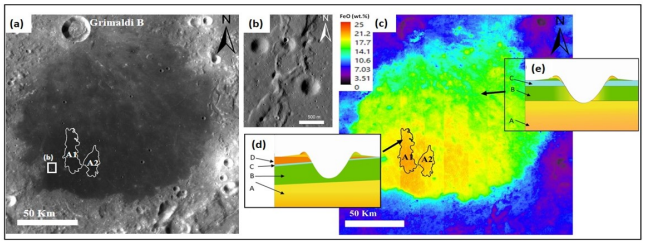

Figure 8: (a) LROC WAC mosaic of Mare Grimaldi showing the location of young mare unit A1 and A2 that formed $\sim$ 700 Ma ago and location of the distorted craters enclosed within a square; (b) A blown-up view of the tectonically distorted small impact craters during recent times; (c) A FeO wt % map of the Mare Grimaldi showing the deciphered stratigraphic sequences (d) and (e). Here, A is the lowermost strata with high FeO content, B is the immediately overlying strata with intermediate FeO content, C is the ejecta unit of varying thickness deposited from crater Grimaldi B with very low FeO content, and D is the $\sim$ 80 m thick uppermost strata with very high FeO content emplaced during the Copernican period.

doi : https://doi.org/10.1016/j.icarus.2020.113921

(T. Singh and N. Srivastava)

Water-Ice exposing scarps within the northern midlatitude craters on the Mars

New exposures of water ice along the scarps wall located within craters in the northern midlatitude region of Mars have been made using high-resolution imagery and spectral data of Mars Reconnaissance Orbiter. The exposed water-ice deposits appear in bluish-white color and have absorptions at 1.5 and 2 μm [Figure 9]. These scarps are located on the pole-facing walls and equator-facing wall origin floor deposits which formed over the latitude dependent mantle. Our observations advance in bracketing the younger ice deposits through the crater size-frequency distributions of host craters, which formed around $\sim$ 25 and $\sim$ 95 Myr and exposed around $\sim$ 1 Myr. This reveals that ice transportation, accumulation, compaction, and ice-dust mixing occurred in recent epochs. Our study complements the earlier studies that shallow water ice is spatially widespread and consistent with subsurface water-ice detection by neutron spectrometer. We interpret that the ice remnants are likely to be preserved along, craters pole wall and equator-facing walls and associated floor deposits, which demonstrates widespread water-ice resources on Mars.

This work was done in collaboration with Nicolas Mangold of Laboratoire de Planétologie et Géodynamique, Nantes, CNRS.

doi : https://doi.org/10.1029/2020GL089057

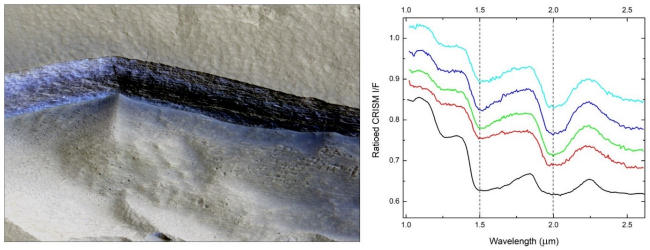

Figure 9: The False-colored HiRISE images with bluish-white contrast represent the water-ice-rich regions. The corresponding spectrum with 1.5 and 2 μm absorption confirms the water-ice deposit.

(Harish, S. Vijayan and A. Bhardwaj)

Global documentation of overlapping lobate deposits in the Martian gullies

Gullies on the surface of the Mars are linear-to-sinuous channels linking an alcove at the top to a fan at the bottom (Figure 10). The most interesting interpretation of the past two decades has been that the Martian gullies were carved by the flow of liquid water. However, the recent images revealed that the Martian gullies are active today and that sublimation of seasonal carbon dioxide frost – not liquid water – could have played an important role in their formation. In order to bring new information on this intriguing aspect, HiRISE images of gullies between 30-75° in both north and south were analyzed. We analyzed 1726 impact craters (988 craters in the northern hemisphere and 738 craters in the southern hemisphere) between 30° and 75° latitude range. It was found that the gullies formed in 20 craters (6 in the northern hemisphere and 14 in the southern hemisphere) are dominated by the overlapping lobate deposits (Figure 10), showing that a debris-flow like process may be responsible for gully formation. The lobate deposits were not observed to be forming today, so it still remains under investigation as to whether the sublimation of carbon dioxide frost can create such lobate deposits and therefore whether it can explain the formation of the Martian gullies.

This work was done in collaboration with Tjalling De Haas of Department of Physical Geography, Universiteit Utrecht, Princetonlaan, Utrecht, the Netherlands and Susan J. Conway of CNRS, Laboratoire de Planétologie et Géodynamique, Université de Nantes, France.

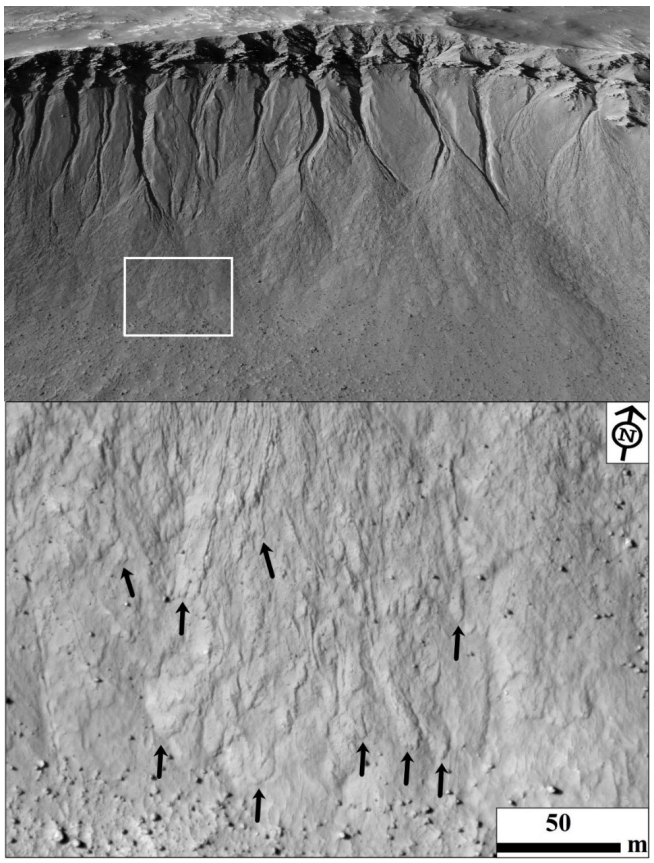

Figure 10: Top panel: 3D view of gullies on the pole-facing wall of $\sim$ 8 km diameter Los crater (35.08° S, 76.22° W) on Mars. The box shows the location of bottom panel. Bottom panel: Image shows the gully fan surface within Los with overlapping lobate deposits (arrows), including convex-up and tongue shaped terminal lobes with lateral levees.

doi : https://doi.org/10.1016/j.icarus.2020.113979

(R. K. Sinha and D. Ray)

Boulder fall activity in the Jezero crater, Mars

NASA Mars 2020 Perseverance rover landed inside the Jezero crater on February 18, 2021 (Figure 11). We report 63 boulder fall tracks within the crater using High-Resolution Imaging Science Experiment (HiRISE) images. The boulder tracks have both fresh and faded morphologies similar to those reported elsewhere on the Mars, but reported for the first time in Jezero crater. We combine observations from 16 boulder-tracks on the western delta deposit with 47 in the surrounding regions to infer possible process(es) of boulder destabilization, which can be tested with rover observations. We propose that this newly found hazard should be taken into account for rover operations. Boulders associated with tracks are geologically "recent falls," so it is possible that the surfaces of these boulders may provide an opportunity to sample material less exposed to radiation than other rocks at the martian surface and could be ideal targets to analyze for organics.

This work was done in collaboration with Susan J. Conway, Marion Massé, and Nicolas Mangold of CNRS, Laboratoire de Planétologie et Géodynamique, Université de Nantes, France.

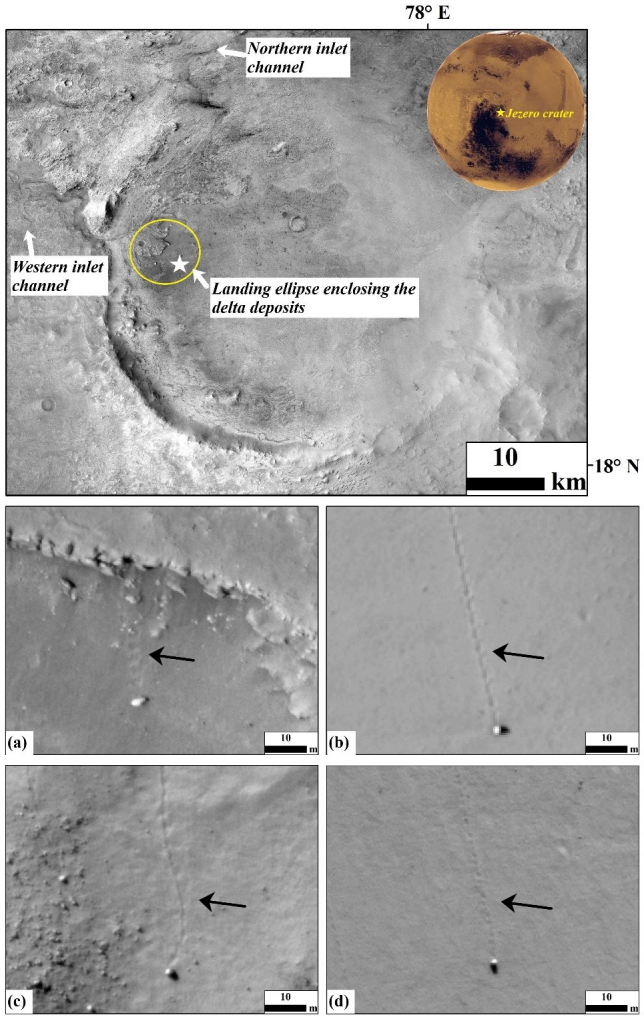

Figure 11: Top panel: Landing site (Jezero crater; centered at 18.42°N, 77.67°E) of the Mars 2020 Perseverance Rover. The landing ellipse is shown in yellow. The white star inside the landing ellipse shows the location of the Perseverance rover. Bottom panel: (a-d) HiRISE image based zoomed views of the boulder fall tracks (marked by arrows) found inside the crater.

doi : https://doi.org/10.1029/2020GL090362

(R. K. Sinha, A. Rani, S. Vijayan , A. B. Sarbadhikari and A. Bhardwaj)

Meteorite, Analogue and Laboratory Studies

Experimental studies on temperature dependent thermal conductivity of lunar analogues under simulated lunar environment

It is well accepted that the laboratory measurements of physical properties of planetary materials provide key support to the definition of science and measurement objectives of ground-based, orbital,

and lander observations; instrument design and calibration; mission planning; and analysis and interpretation of retrieved data. The role of laboratory studies under simulated lunar environment in understanding physical properties of materials and their behaviour is multifold. One such aspect is related to the studies of temperature dependent thermal properties. For example, in order to properly understand the lunar surface and subsurface thermophysical behaviour, appropriate parameter values for density, thermal conductivity, specific heat etc. and initial boundary conditions for temperatures and incident heat flux are needed. In situ measurements and laboratory analysis of returned samples from Apollo missions showed that these parameters are not constant and are inter-dependent. It was shown earlier that under ambient pressure or stress-free conditions, a trend of temperature independent (or less dependent) thermal conductivity was observed. However, the same is expected to be significantly dependent on temperature under vacuum conditions, but no systematic measurements exist in literature. Towards this understanding we are carrying out several experiments on lunar analogous samples under simulated lunar environment. A small chamber for creating simulated lunar environment (pressure and temperatures) has been custom-designed and constructed in order to carry out such experiments, the details of which were already reported earlier. The present setup provided an opportunity to take such measurements under lunar conditions (under vacuum) at different temperatures.

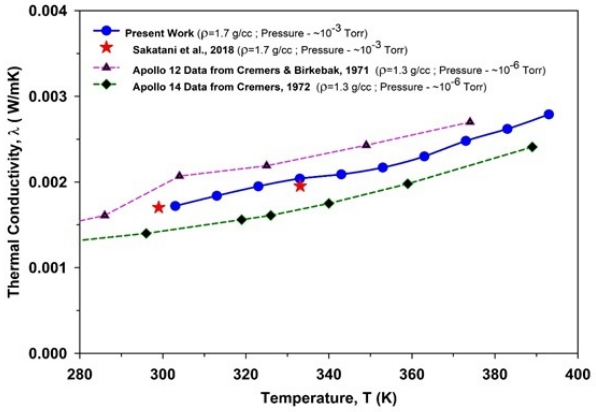

Figure 12: Temperature dependent thermal conductivity of 100 μm basalt powder under vacuum conditions ($\sim 10^{-3}$ Torr) and its comparison with some earlier data

Figure 12 shows the experimental estimation of the variation in thermal conductivity of 100 μm basalt powder as a function of temperature measured under vacuum conditions using the developed chamber. For comparison, figure 12 also shows two experimentally estimated values by Sakatani et al., (2018) using JSC-1A basalt sample of similar grain size and environmental conditions. As shown in figure 12, thermal conductivity has a significant dependence on the temperature of the sample. This effect is expected to be more prominent as the pressure decreases. According to literature, the combined effect of temperature dependent thermal conductivity and Specific heat account for $\sim$ 20-50% of the diurnal variation of thermal Inertia of lunar surface. Also, to account for radiative and conduction components in porous media, temperature dependent thermal conductivity and specific heat needs to be considered in all numerical studies (Cremers et al., 1971). However, such a behaviour under lunar environmental conditions is not understood at all. Earlier, few experiments were conducted on the powdered Apollo returned samples in order to understand the variation in temperature dependent thermal conductivities under vacuum conditions (Cremers and Birkebak, 1971; Cremers, 1972). Two such experimental plots from Apollo 12 and Apollo 14 samples are also shown in figure 12. While the physical parameters and experimental conditions are completely different for Apollo samples, the plots are shown only to compare the trend of temperature dependent thermal conductivity obtained from the present work. It may be noted that the data from literature used in figure 12 for comparison is from a specific and limited set of experiments conducted for the purpose. Several other experiments are underway to investigate these aspects.

doi : https://doi.org/10.1016/j.pss.2020.105038

(K. Durga Prasad, S. V. S. Murty and V. Rai)

Jhuran sandstone of Kutch has hematite concretions (aka "Blueberries") like Mars: Implications for warm, watery early Mars

Spheroidal hematite concretions also known as "Blueberries" (looks similar to blueberries in a muffin) is one of the most exciting discoveries on Mars by the Opportunity rover. Current condition on Mars is inhospitable for liquid water to exist, while finding of hematite concretions suggest there was definite involvement of water with the rocks (and diagenesis) in the ancient past on Mars when the condition was warm and wet. Though argument existed that the spherical objects could be the pieces of meteorite or could be a result of volcanic accretion, however, the claim is still inconclusive.

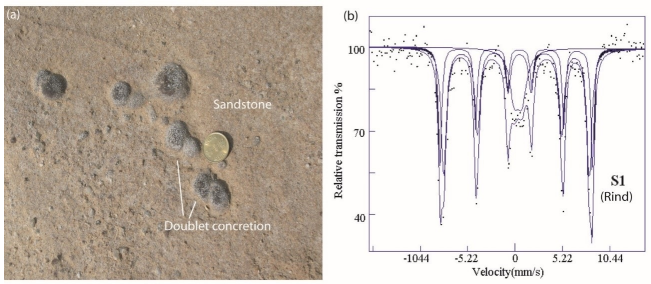

Figure 13: (a) Hematite concretions from Jhuran formation, Kutch, India (b) Mössbauer spectroscopy of hematite rind from Jhuran concretion

The recent findings of diagenetic hematite concretions in Jhuran sandstone of the Upper Jurassic of Kutch district, Gujarat, western India, show striking resemblance with the setting of the Martian spherules (Fig. 13a). The concretions occur as $in-situ$ or erosional lag deposits, similar to what has been inferred by Opportunity on Mars. This study examines the mineralogy, spectroscopy (VNIR and Mössbauer) and whole-rock chemistry of hematite concretions and the host Jhuran sandstone (Fig. 13b). We suggest that after burial, reducing fluids, either derived from the underlying sedimentary units, or from within the pore-spaces of the sandstone itself, removed the iron oxides and bleached parts of the sandstone, giving rise to the variety of colours observed. In the final stage, these reducing

fluids eventually interacted with oxidizing groundwater that most likely infiltrated during a later fluid flux event and thus facilitated the precipitation of iron concretions.

A near perfect terrestrial analogue locality to the Mars that mimics the concretions is still elusive on the Earth. However, continued research on terrestrial analogue sites helps to better understand the geologic evolution and near-surface processes on Mars. The Kutch area in India is already known as a potential Martian analogue locality. It has been argued that the transformation from the wet and humid to dry and arid environment on Mars is mimicked by the Cenozoic history of Kutch. This further indicates that the Cenozoic environment of Kutch may be similar to the conditions that prevailed during the Noachian to Hesperian (epochs) transition on Mars. We argue that the concretions in the Jhuran Formation of Kutch represent another data point that reinforces the need to use the Kutch area for further analogue studies of the Martian surface. Many parts of Kutch remain to be explored from this angle, and therefore call for detailed investigation in the near future.

This work was done in collaboration with Space Applications Center, Ahmedabad, Indian Institute of Technology, Kharagpur and University of Rajasthan, Jaipur

doi : https://doi.org/10.1016/j.pss.2021.105163

(D. Ray and A.D. Shukla)

Presolar silicate and oxide grains found in lithic clasts from Isheyevo and the fine-grained matrix of northwest Africa 801

Presolar stardust grains are the direct snapshots of the stellar nucleosynthesis, and laboratory analyses of these grains provide excellent opportunity to better understand stellar and interstellar processes of grain formation, alteration and destruction. We report on the discovery of 33 oxygen-anomalous grains from two carbonaceous chondrite meteorites, namely the CH3/CBb3 chondrite Isheyevo and the CR2 chondrite Northwest Africa (NWA) 801. Oxygen isotopic compositions indicate that the majority of grains formed in the outflows of low mass ($\sim$ 1.2 to $\sim$ 2.2 M$\odot$), solar metallicity red giant or asymptotic giant branch stars, while two highly 17O enriched grains likely have nova origins. Eight grains with 18O-rich compositions, including an extremely 18O-rich grain ($\sim$ 16 times solar 18O/16O ratio) probably formed in type-II supernova explosion. Close-to-normal silicon, magnesium and calcium isotopic compositions of grains are consistent with the isotope exchange in the interstellar medium or the meteorite parent body, while several grains with Si and Mg isotopic anomalies reflect the galactic chemical volution (GCE). An Isheyevo clast showed several hot-spots with moderate to high 15N-enrichments, including a hot-spot with extreme 15N-excess of (7225 $\pm$ 316)%. However, no correlation was observed between 15N-enrichment and presolar oxygen-rich grain abundance. Grain shape and morphological study by high resolution secondary electron images point towards several differences in grain formation conditions in different stellar environments. Several grains with elliptical shapes likely indicate primary condensation feature. Couple of complex grains display decoupling of the isotopic and elemental compositions in the grain formation environments. Low silicate-to-oxide abundance ratio for the fine-grained chondrule rims (FGRs) in NWA 801 likely reflect the preferential destruction of silicates due to terrestrial weathering.

This work was done in collaboration with Hsiao S. S. Y., Peeters Z., Shang H., Lee D. C., and Bizzarro M. of Tawian University & University of Copenhagen

doi : https://doi.org/10.3847/1538-4365/abdbab

(M. N. Sanghani and K. K. Marhas)

Amorphisation of presolar grains in the interstellar medium (ISM) due to interaction with Glactic Cosmic Rays (GCR).

Most of the presolar SiC grains analysed in the laboratory have been observed/reported to be crystalline and even spectroscopically detected as 11-micron feature in ISM. Absence of amorphous SiC in both laboratory and spectroscopically has been under discussion since last two decades, especially because, majority of presolar silicate grains studied in the laboratory have amorphous structure, and both amorphous and crystalline ($<$10%) silicates have been observed around AGB star and young main-sequence stars. There are studies indicating the possibility of 9-micron feature correlating with the amorphous SiCs. As for the laboratory measurements, this difference between presolar silicates and SiC mainly arises due to the different identification/separation methods. Presolar silicates have been identified based on in-situ measurement, whereas, SiCs are chemically separated. The in-situ measurements within the meteorite sections have very less effect on morphology of the grains, and hence the amorphous grains remain unaltered/intact. Whereas, harsh chemicals used in chemical separation method could lead to destruction of presolar grains especially amorphous grains (disordered structure) in comparison to crystalline ones (ordered crystals). On the other hand, in ISM, the grains travelling in low density and temperature region allows molecules to be adsorbed on the grain, eventually forming an ice mantle on the grain. These ice mantles have been proposed to be the protective layer for the presolar grains from the external destructive processes. The composition of ice in a molecular cloud varies with the local conditions depending on various factors like shock waves, the collision of grains, absorption of photons etc. The sputtering of grains in the interstellar medium also occurs due to galactic cosmic rays(GCRs). In the present study, sputtering rate of presolar Silicon Carbide (SiC) grains, of different sizes and different thickness of ice-mantle, in ISM due to GCRs have been calculated for their experimentally deducted lifetime ($\sim$ 1Gyr) using an ion target simulator SDTrimSP (freeware). The model simulations indicate galactic cosmic ray(s) with energy range from 10 MeV to 1 GeV are just capable of sputtering/ destructing $\sim$13-15% of the grain itself. This value, stretched over 1 billion years is not as significant as the other destruction processes and therefore can be classified as a minor destruction process. The effect of the galactic cosmic ray on ice mantle and core is also noted with particular emphasis on amorphisation/recoils generated inside the SiC core and their distribution within the grain.

doi : https://doi.org/10.3847/1538-4357/abc25b

(A. Garg, K. K. Marhas and V. Goyal)

Mineralogy, petrology and geochemical studies of recently fallen Mahadeva Meteorite

A single stone weighing $\sim$ 15 kg fell on July 22, 2019 (14:30 IST) at Mahadeva village (lat: N26°28'56.28" long: 86°35'53.17"E) nearly 6 km east of the Laukahi Police station, Madhubani district, Bihar. Macroscopic features of Mahadeva meteorite well resembles ordinary chondrite, typically covered with thin fusion crusts of different textures and thickness as in Fig 14. Mineralogical, Petrology and geochemical studies were carried out using JEOL SEM coupled with EDS and Cameca EPMA. The modal abundances of olivine varied between 36.1 to 38.4%; low-Ca pyroxene: 34.8 - 38.4%; high-Ca pyroxene: 5.1 - 6.7%; feldspar 7.2 - 8.3%; metal (Fe-Ni alloy) and sulphide (troilite): 10.3 -14.0% and accessories phases like chromite and merrilite vary from 0.6 to 1.1%. The matrix is coarsely crystallised and chondrule-matrix integration are common throughout the studied section. The chondrule size ranges 250-600 μm, except in one case exceeds 2 mm across. Type of chondrules includes barred, porphyritic and cryptocrystalline variety. Feldspars ($<$70 μm) are common in matrix, occasionally occur as interstitial phase within chondrule.
Based on petrochemical studies, Mahadeva is classified as H-chondrite. Homogeneous olivine (Fa: 19.3 mol %) (Per cent mean deviation $<$4%) and low-Ca pyroxene (Fs:17.6 mol%) composition further suggest that Mahadeva is highly equilibrated chondrite (resembles petrologic type 5/6), a few relict chondrules still can be recognised. The temperature of equilibration is estimated $\sim$780°C and 828°C, respectively (olivine-chromite and two pyroxene thermometry), in association with evidences of moderate shock metamorphism.

doi : https://doi.org/10.1016/j.pss.2020.105111

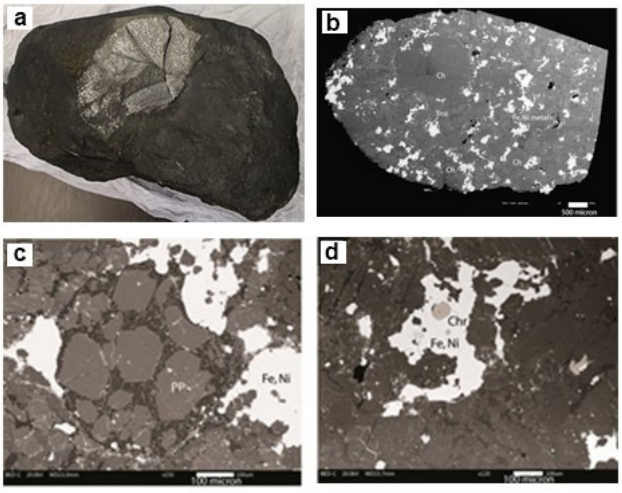

Figure 14: (a) Hand specimen of Mahadeva meteorite (b) BSE image of Mahadeva meteorite (c, d) BSE image of chondrule and matrix of the Mahadeva meteorite section.

(D. K. Panda, D. Ray and A. D. Shukla)

The Mukundpura CM2: Significance on asteroidal process and analog for near Earth asteroids

The Mukundpura CM2 (Fall June 6, 2017) was classified to be a carbonaceous chondrite and considered one of the most primitive meteorites and a remnant of the first solid bodies to accrete in the Solar system. The type of the meteorite is rare and only to fifth reported carbonaceous meteorite fall in India. In view of very high degree of phyllosilicate content ($\sim$ 90 vol%) the overall extent of aqueous alteration is variegated and extensive. The phyllosilicate fraction of Mukundpura is estimated $>$0.9. The differences of FeO/SiO_2 and S/SiO_2 ratios of matrices also correspond brecciated nature of clast underwent different extent of alteration (as shown in Fig. 15a). The chemical composition of matrix is consistent with progressive aqueous alteration (as shown in Fig. 15b). The extent of alteration also appears pervasive due to overabundance of phyllosilicate, rarity of metals and presence of sulphate. The mineralogy of Mukundpura resembles surface of the near-Earth asteroids Ryugu and Bennu. Further, Infrared spectroscopy correspond that spectral properties of the surface of these B and C type asteroids are consistent with CM carbonaceous meteorites. Therefore, a better understanding of the nature and aqueous and thermal evolution of such primitive group of meteorites will help considerably in the interpretation of results of these ongoing and upcoming missions to Asteroids (e.g. Hayabusa 2 and OSIRIS-REx).

This work was done in collaboration with Space Applications Center, Ahmedabad and Indian Institute of Technology, Kharagpur.

doi : https://doi.org/10.1016/j.chemer.2020.125729

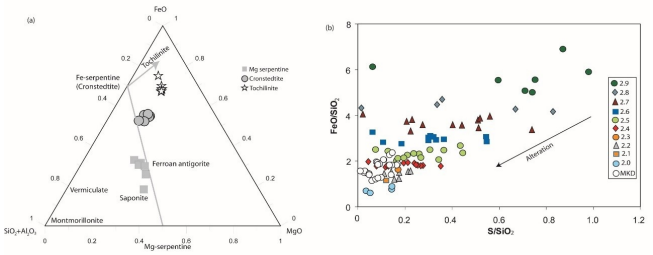

Figure 15: a. SiO_2+Al_2O_3)-FeO-MgO ternary plot to show different clast of matrix corresponding to Mg-serpentine, Cronstedtite and Tochilinite. b. FeO/SiO_2 versus S/SiO_2 of matrices clasts with subtype ranging 2.0 to 2.9.

(S. Baliyan, D. Ray, D.K. Panda and A.D. Shukla)

Pre-compaction exposure and heterogeneous nitrogen isotopic systematics in chondrules

Chondrules are the major constituents of primitive meteorites, which formed as molten objects. The pre-compaction exposure is identified by means of an excess of cosmogenic isotopes relative to what has been produced during the recent space travel of the meteorite from its parent body to the Earth. The excess cosmogenic nuclide is from the additional episode of earlier production. This occurred during the time between chondrule formation and chondrite accretion. Chondrules from Dhajala H3.8 chondrite was studied for this purpose. The type 3 unequilibrated ordinary chondrite is chosen since it is unaltered material from the early solar system. Isotopes of noble gases and nitrogen were studied in chondrules. The solar wind

is absent in the chondrules. The cosmic ray exposure ages of all the chondrule studied are similar to the bulk sample analysis of the Dhajala chondrite. No excess of cosmogenic noble gas concentration is detected. There is no evidence of pre-compaction irradiation in the individual chondrules from Dhajala chondrite. The trapped nitrogen isotopic ratio is determined for each chondrule. It is observed that the nitrogen signatures in chondrules differ from nebular composition. It is also dissimilar to the phase Q present in primitive chondrites. Large range is observed for the nitrogen isotopic ratio $^{15}N/^{14}N$ in the chondrules. This indicates that there are more than one trapped component present in the chondrules. The observed 15N enrichment is local and indicates that certain process affects the nitrogen inventory in the nebula.

doi : https://doi.org/10.1111/maps.13565

(R. R. Mahajan)

Cosmic ray exposure history and neutron effects in Karimati (L5) chondrite

Meteorites, before they fall to the Earth, are exposed to energetic cosmic ray radiation that induce nuclear reactions. The cosmogenic nuclide produced in this interaction is used to understand the exposure history of the meteorite. The cosmic ray exposure age of a meteorite measures the time interval in space between formation of a meteoroid as a meter-sized object and its capture by the Earth. It is a useful parameter to understand the dynamics in the interplanetary region of asteroids orbits. Karimati was witness to fall in the village Karimati, Upper Pradesh, India. It was classified as L5 ordinary chondrite. The exposure age is determined using noble gases. The cosmogenic noble gases yield the age of 16.4 Ma. That is the time period when this meteoroid separated from its parent body. The trapped noble gases are of Q-type in Karimati chondrite. Excess of 82Kr, which is produced by neutron capture on 81Br is observed. Presence of neutron effect suggest larger size of the meteoroid.

doi : https://doi.org/10.1007/s11038-020-09532-w

(R. R. Mahajan)

Nitrogen isotopes in metal separates from ordinary chondrites

Understanding the origin of chondritic metal and its relationship with the associated silicates are critical to know the processes that produced chondrites in the protoplanetary disk in the early solar system. Metal separates from the ordinary chondrites Katol (L6), Itawa Bhopji (L3-5) and Portales Valley (H6) were investigated for nitrogen composition, its variation and association with noble gases. Anomalous nitrogen is observed in the metal separates of Portales Valley H6 chondrite. This leads to the conclusion that there exists heterogeneity of nitrogen in it. This confirms unusual formation mechanism of the parent body of Portales Valley. Nitrogen isotopic signature in Katol and Itawa Bhopji chondrites are distinct from Q, solar wind and cometary nitrogen. The recognition of non-solar, non-cometary and non-Q nitrogen signatures in metal separates from ordinary chondrites appear to record evolutionary processes occurred on the parent objects and/or in the nebula.

doi : https://doi.org/10.1007/s10509-020-03845-y

(R. R. Mahajan)

Development of Payloads for Planetary Mission

VODEX Development

The dust particles of the size bigger than $\sim$ 0.1 μm travel inward toward Sun and can encounter various planets during their travel. The flux of these Interplanetary Dust Particles (IDPs) is not measured at Venus, except a few spot measurements at larger distances from Venus.

Figure 16: Photograph of the dust detector

The study of IDP at Venus is important to understand the third meteor ion layer in the electron density profile of the Venusian atmosphere. This is because the IDPs are ablated in the atmosphere and leave metal ions behind. A Venus Orbiter Dust Experiment (VODEX) is proposed for future Venus orbiter to study flux and distribution of high-altitude dust at and around the Venus and also between the Earth and Venus. The engineering model of VODEX is under development for the demonstration using PS4 of PSLV. The optimized detector meets the vibration levels of the PS4 and its Proto-Flight Model (PFM) is initiated. The front-end electronics of the detector is developed and tested for the model under development. The processing electronics using FPGA is demonstrated in the laboratory and its further development is underway. Thermal analysis of the detector was carried out from the available information regarding analysis. A photograph of the detector is shown in Figure 16 and the results of its thermal analysis are depicted in Figure 17. The results show that the temperature remains in the allowable limits, except few places, which is resolved using rearrangement of the devices on the main and power PCB. Further work on the engineering model is ongoing.

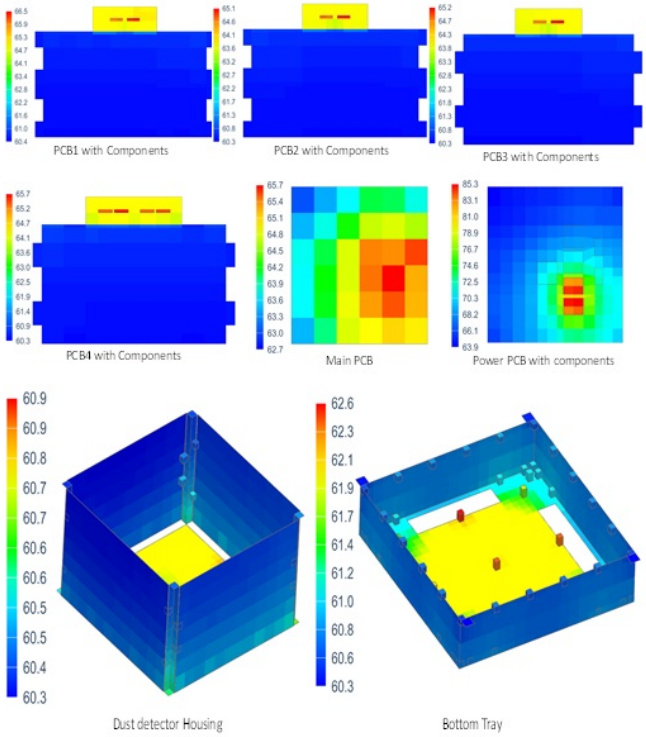

Figure 17: Preliminary thermal analysis of the dust detector for PS4.

(J. P. Pabari, S. Nambiar, S. Jitarwal, Rashmi, K. Acharyya, V. Sheel, R. Mahajan, A. Bhardwaj, S. M. K. Praneeth, B. Shah, J. Rami, V. Singh, R. Singh, S. A. Haider and Team)

Study of high-energy particle generated noise in VODEX

The solar wind acts as noise for the dust detector and therefore, it needs to be studied for various high-energy particles coming through the solar wind and also, GCR. We have used ACE and GOES data of the solar wind particles for a solar cycle of 11 year, starting from 2006 to 2017. The SEP flux closest to the average of eleven-year events was taken, which falls during December 2006. The proton flux of normal solar condition and the SEP event occurred during December 2006 were utilized in the analysis through the Geant4 software. Figure 18 shows the detector response of the high-energy solar wind particles. Further, the response to GCR was studied and the results are depicted in Figure 19. One can observe from the results in Figure 18 and Figure 19 that the effect of high-energy particles is to produce secondary electrons, which appear in the electron channel of dust detector, as a background noise. Whenever a dust particle makes an impact on the target, it creates electrons and ions both, which are used in the coincidence analysis for identification of the dust impact. Hence, the dust impact can be differentiated from the background noise.

Proton Energy Band* (MeV)	Average percentage of detached electrons for given energy range	Proton flux during normal solar condition for the detector (#/s)	Detached electrons for detector during normal solar condition	Proton flux during SEP for the detector (#/s)	Detached electrons for detector during SEP
0.74-4.2	0	208863.39	0	86897997.05	0
4.2-8.7	0.0012	511.10	0.0061	30055596.87	360.67
8.7-14.5	0.0128	1149.07	0.1471	9416674.73	1205.33
15-40	0.0203	367.15	0.0745	14298441.02	2902.58
38-82	0.0198	378.74	0.0750	1343630.69	266.04
84-200	0.6883	775.20	5.3357	136377.71	938.69
110-900	3.8582	3059.69	118.0490	184740.92	7127.67
Total			**123.69**	-	**12800.98**

Figure 18: Dust detector response to high-energy solar wind particles, obtained through Geant4 software.

GCR Energy (MeV)	GCR Flux (Fallaize, 2007) (# s^{-1})	Average Percentage of Detached Secondary Electrons	Detached Electrons for Dust Detector
10	0.0302	0.0031	9.36×10^{-7}
100	0.1056	0.0135	1.43×10^{-5}
1000	0.1811	5.5746	0.0101
10000	0.0030	6.2189	0.0002
Total			**0.0103**

Figure 19: Dust detector response to GCR, obtained through Geant4 software.

(J. P. Pabari, S. Nambiar, S. Jitarwal, Rashmi, K. Acharyya, V. Sheel, A. Bhardwaj, R. K. Singh, K. A. Lad, J. M. Jakhariya and Team)

HV biasing of VODEX, plasma capture and detector capacitance

In order to capture the impact plasma in two channels, viz., electron channel and ion channel, the detector needs to be biased using HV. Optimization of detector bias was carried out using SIMION software and the plasma capture was studied. The results are shown in Figure 20, from which one can observe that the dust impact generated plasma species are captured effectively on the respective channels. There is marginal loss of ions in the grid mounted at the top of detector, which is necessary for the protection of detector from solar wind electrons. Only the effective captured ions and electrons are taken in the analysis and hence, the marginal loss can be covered in the calibration part. The impact plasma is captured and processed in the charge sensitive preamplifier for derivation of particle parameters. The detector capacitance plays a vital role in the signal conditioning as it appears at the input to the electronics chain. Since, the dust detector is a customized instrument (not commercially available), we need to know its capacitance through modelling and compare it with the measurement. We have made a detector structure in COMSOL and modelled it, whose results

are shown in Figure 21. The modelling results show the detector capacitance to be 28 pF, while the measurement show it to be 32 pF. The results match broadly and a small difference between the two comes from the stray capacitance nearby, during the measurement.

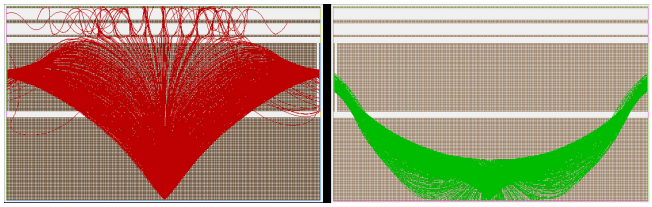

Figure 20: Capturing the impact plasma species in respective channels (ions on left and electrons on right).

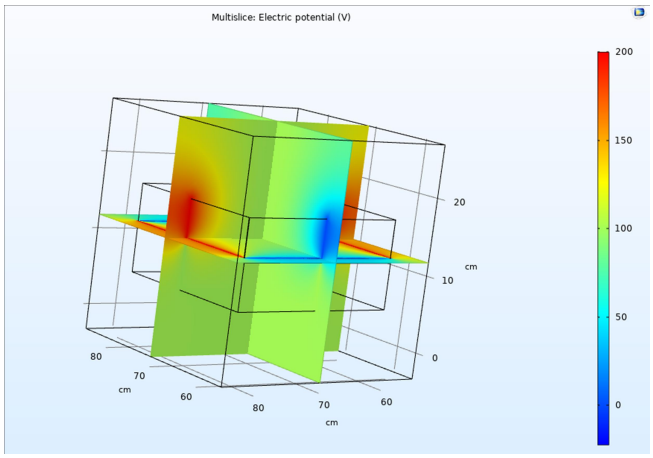

Figure 21: Modelling of detector in COMSOL, giving the electric potential slice plot. From this, the detector capacitance is derived to be 28 pF.

(J. P. Pabari, S. Nambiar, S. Jitarwal, Rashmi, K. Acharyya, V. Sheel, A. Bhardwaj, R. K. Singh, K. A. Lad, J. M. Jakhariya and Team)

Design and realization of diplexer for radio occultation experiment

Atmospheric density profile of a planet is studied by a Radio Occultation (RO) experiment using a satellite-based transmitter. A microwave signal is sent by the transmitter and it is received at the ground station. The frequency change occurred during the transmission from the planetary atmosphere and subsequent information are retrieved through the modelling and data analysis. A diplexer is useful device when two signals are transmitted for the RO experiment. The microwave diplexer was designed and developed. The diplexer was tested at 6.7 GHz and 8.4 GHz frequencies, whose results are depicted in Figure 22. One can observe from the results that the device can easily handle both the signals separately.

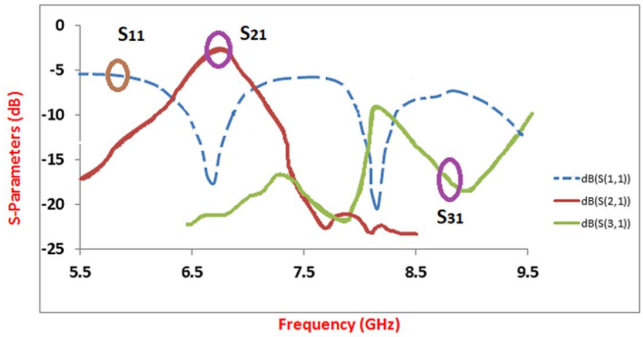

Figure 22: Testing results of microwave diplexer at 6.7 GHz and 8.4 GHz, showing effective handling of both the signals.

This work has been led by Dr. Trushit Upadhyaya, Department of Electronics Engineering, CHARUSAT, Changa, Nadiad.

doi:https://doi.org/10.1016/j.aeue.2020.153497

(J. P. Pabari, V. Sheel and S. Jitarwal)

LIVE Development

A Lightning Instrument for VEnus (LIVE) is being developed at PRL for detection of lightning on Venus. Various aspects were studied, which are as follows.

A. Non-Foster active impedance matching of short dipole antenna for a lightning instrument: Electrically small antenna suffers from high Q impedance such as narrow bandwidth and poor gain. To improve them, passive impedance is often used but it is restricted to the Bode-Fano limit. Active matching network incorporating non-foster circuits could overcome the shortcoming of passive impedance matching. We have proposed an instrument called Lightning Instrument for VEnus (LIVE) to detect Venusian lightning using future mission. In this work, an active impedance matching network to transfer the maximum power from an electrically small antenna to the load is presented. Without the proper impedance matching, signal reflections can exist along the path from the source to the load. Matching the impedances throughout the circuit yields a desired Voltage Standing Wave Ratio (VSWR). Low VSWR circuits transfer the maximum amount of power from the source to the load. Impedance Matching can eliminate or minimize the reactance in a wide frequency range. In the present work, matching of short dipole antenna to the load by using Non-Foster Active Impedance matching network is realized using negative Impedance Converter. The simulation results of the Active matching network prototype is presented.

B. LIVE Design, Mounting, Background Noise, Spectrum and Antenna: The engineering model of the LIVE has been initiated, whose design blocks are shown in Figure 23. It consists of an electrically short antenna, preamplifier, various filters and automatic gain control system, before the signal is processed in the back-end electronics. In another option of the design, the filters are not present, instead the signal from the preamplifier is sampled at the sufficient sampling rate and then processed in a digital signal processor for

getting further information. The accommodation study of LIVE has been carried out as well. The antenna and the front-end electronics may be kept on the boom, away from the spacecraft; while the processing electronics can be kept on the deck. The sensor should look downward towards Venus from where the signals are expected to come, after passing through the Venusian ionosphere.

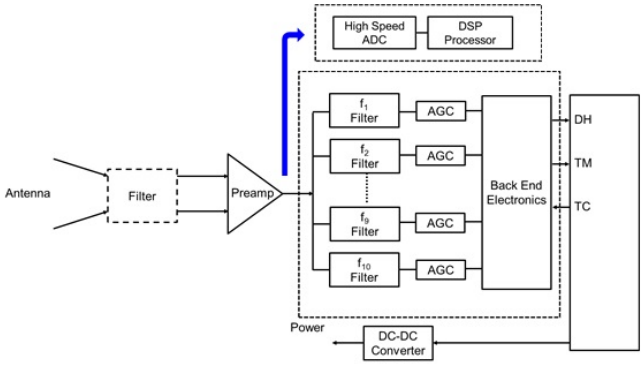

Figure 23: Design blocks of LIVE

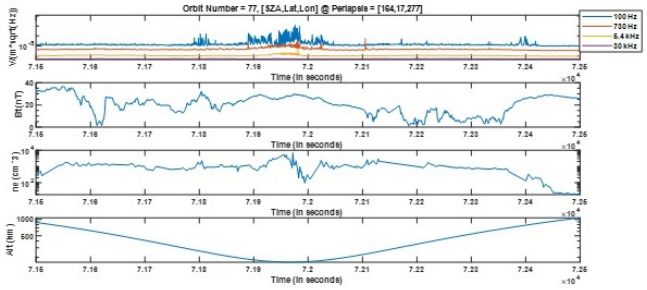

Figure 24: Observed parameters by PVO in shadow region of Orbit 77. The signal burst signal corresponds to lightning in the top panel, detected by OEFD.

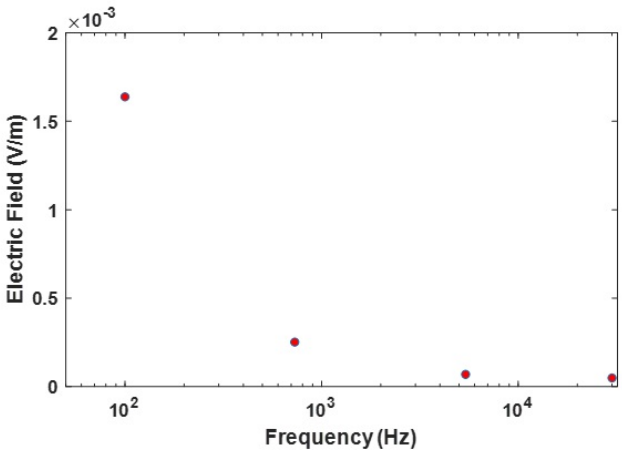

Figure 25: Electric Field Spectrum provided by OEFD at time instance t = 71965.5 s of Orbit 77 of PVO.

In addition, the background calculation for the LIVE has been carried out using data analysis of the earlier observations by PEFD on PVO. The observations are shown in Figure 24. The nightside background was found much less than that on the dayside on Venus. Based on the background, the requirements for the sensitivity was obtained. Further, lightning data were analyzed, which are provided by OEFD on PVO. A lightning spectrum of four points, retrieved from four channel measurements of PVO is shown in Figure 25, from which, it can be seen that the received spectrum decays similar to that of Earth. A comparison of the OEFD antenna versus the LIVE antenna is depicted in Figure 26, from which, it can be seen that the length of the LIVE antenna needs to be larger and/or the angle between the two arms of the vee antenna should be more, as compared to that of the OEFD.

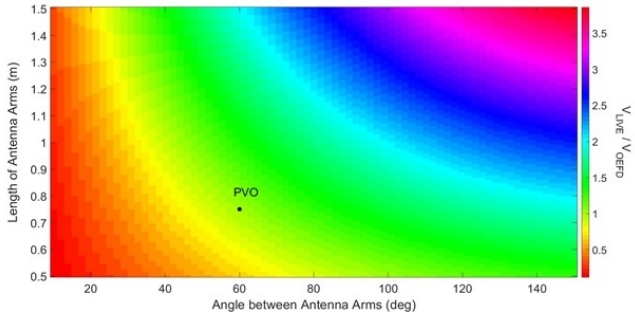

Figure 26: Ratio of induced voltage in the antenna of LIVE to that of the OEFD as a function of antenna length and the angle between two arms. The dot marked shows the parameters of the PVO instrument. The antenna length of 1.5 m along with the separation angle of 120° to 150° is suggested for LIVE, having larger processing bandwidth, in order to achieve the similar level of sensitivity as that of OEFD on PVO.

Further, in case of Venusian lightning, the flow of electrons within the discharge channels constitutes electric current and efforts have been made to model these electric currents within the discharge channel. Using the electric currents within the discharge channels, it is possible to model the expected time domain and frequency domain characteristics of electric fields generated by lightning. The expected streamer speeds in Venus middle clouds are on the order of 10^6 m/s when the electric field at the streamer tip is about ten times the breakdown field. If the field at the streamer tip is higher, then the streamer speeds can reach speeds as high as 10^8 m/s. For these streamer speeds, the expected peak frequency of the lightning spectrum is between 1 kHz and 11 kHz. Using a normalized current amplitude and a given streamer speed, we calculate the expected peak frequency for different electric current rise time and total duration combinations. With increasing streamer speeds, the peak frequency increases. For the expected streamer speeds in Venus middle clouds and peak frequency constraints, the duration of the current waveform and the rise time of the current waveform are found to be within the range from $\sim$ 30-100 μs and $\sim$ 1-30 μs, respectively. The lightning spectrum for a bi-exponential discharge current is shown in Figure 27, which can be useful for the design of LIVE. Moreover, preliminary design related to antenna boom and deployment was carried out. A baseline design of the LIVE antenna deployment is shown in Figure 28. Modal analysis has been performed for stowed and deployed condition of antenna with the main purpose of optimising the antenna mass without placing frequencies in the undesired range. Antenna also must support the launch environment without suffering any structural alteration. Further developmental work is ongoing.

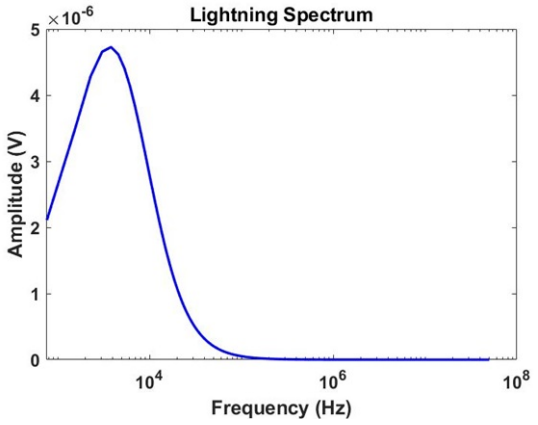

Figure 27: The lightning spectrum, based on bi-exponential discharge current, obtained after the Fourier transformation. The peak frequency where the amplitude is maximum is 3.8 kHz.

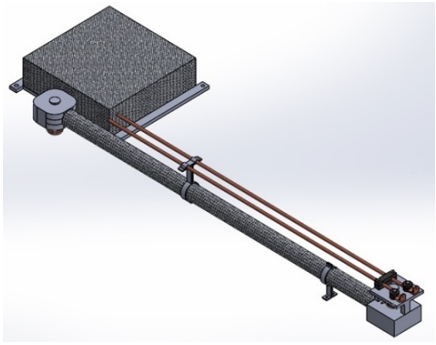

Figure 28: Baseline design of the LIVE antenna deployment system.

(J. P. Pabari, S. Jitarwal, D. Kumar, S. Nambiar, Rashmi, K. Acharyya, N. Upadhyaya, Janmejay Kumar, G. Dhote, T. Upadhyaya, V. Sheel and A. Bhardwaj)

Field testing of electrically short dipole antenna

An electrically short dipole antenna has been designed to receive the lightning pulse possible to occur in the Venusian environment for the ongoing lightning project. Waveforms of the electromagnetic signal received by the antenna shall be converted to electric voltage and it shall be sent back to the Earth as digital data for further analysis. It is advantageous to use an electrically short dipole antenna compared to other multipole antenna configurations because it weighs less, has lower power consumption and can deliver all the scientific outcomes which a multipole antenna systems are able to deliver. The antennas were simulated and multiple iterations were carried out to meet the optimal antenna performance. The electrically short dipole antenna having the arm length of 0.75m were design to integrate with the existing electronics of the project. Upon the prototype development, the initial measurement of the antennas were conducted at PRL, using Vann de Graff generator. As a next step, the antenna test setup is done in the far field vicinity at Charotar University of Science and Technology (CHARUSAT) campus, Changa, Anand. The 150 kV discharge unit is being utilized for performing sensitivity analysis of the Vee dipole antenna at CHARUSAT University, as visible in Figures 29 and 30. The signal reception was detected at a distance of 250 m. The sensitivity analysis is an ongoing activity.

This work has been led by Dr. Trushit Upadhyaya, Department of Electronics Engineering, CHARUSAT, Changa, Nadiad.

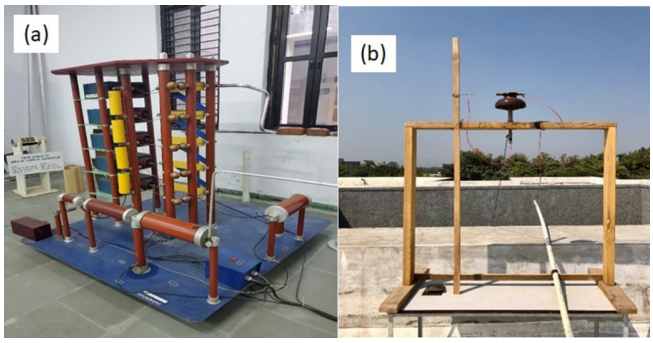

Figure 29: Initial testing set up of ground-based testing at the terrace of CHARUSAT (a) Capacitor-Banked based (b) 150 kV discharge unit.

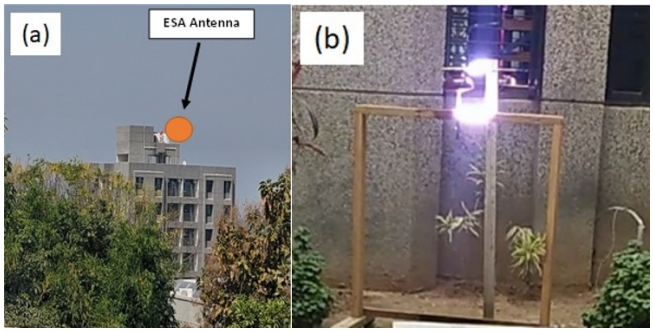

Figure30: (a) Electrically Small antenna (ESA) kept at 250 m from the source (b) Spark captured after the discharge using 150 kV unit

(J. P. Pabari, K. Acharyya, S. Jitarwal, D. Kumar, S. Nambiar, Rashmi and team)

Study of natural lightning using LIVE Laboratory model: Time-frequency localization

Lightning is well studied on the Earth; however, it is yet to be understood fully on other planets like the Venus and Mars. The flash rate, strength, cloud model etc are yet to be known for the Venus. A Lightning Instrument for Venus (LIVE) is proposed for future orbiter to study the lightning on Venus in ELF-VLF frequency range. A laboratory model of LIVE has been in use for few years for detection of natural lightning on the Earth. The signals were captured at PRL and were analysed using different transformations. The Short Time Fourier transformation (STFT), Hilbert-Huang transformation (HHT), Wigner-Ville distribution (WVD) and continuous Wavelet transformation (CWT) were applied to understand the better suitability of a given transformation. The signal is shown in Figure 31, which is captured by the laboratory model of LIVE and the results in the

transformed domain are depicted in Figures 32 and 33 for the four transformations. It can be seen from the results that the HHT gives easiness of interpretation or better resolution as compared to other transformations. Also, the realization complexity of the HHT is not very high. Thus, the HHT provides higher resolution with lesser implementation complexity. (18^{th} VEXAG Meeting 2020, No. 8010)

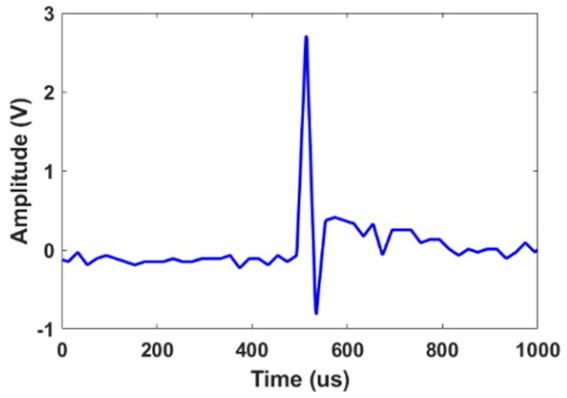

Figure 31: Natural lightning discharge pulse acquired at PRL Thaltej campus using laboratory model of LIVE.

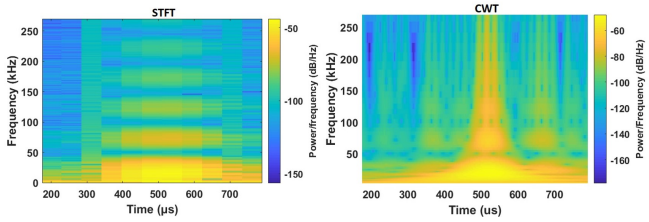

Figure 32: Results of natural lightning signal after applying STFT and CWT transformations.

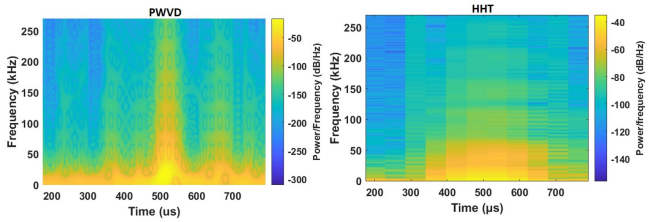

Figure 33: Results of natural lightning signal after applying PWVD and HHT transformations

(S. Jitarwal, J. P. Pabari, D. Kumar, G. Dhote, S. Nambiar, Rashmi, T. Upadhyaya, K. Acharyya, V. Sheel, A. Bhardwaj and team)

Neutral & ion mass spectrometer (NIMS)

Neutral and ion mass spectrometer is being developed for $in-situ$ measurements of neutral and ion species for future planetary exploration missions. This quadrupole mass spectrometer will operate in dual mode, i.e., neutral mode and ion mode in the mass range of 2 to 200 m/q. The instrument consists of ionizer section based on the electron impact ionization (EI) technique, quadrupole filter and ion detector. Both CEM and Faraday cup are used for the ion detection. First version of engineering model has been realized which includes the mechanical detector head and in-house designed electronics. The electronics controls the EI energy, ionization current, focus voltage. The default operating energy is 70 eV. Quadrupole filter section is working on 2.76 MHz frequency. CEM detector has been biased to -2.2 kV. The realized model is undergoing the cross-calibration with the commercial mass spectrometer. Figure 34 shows the test setup where both commercial quadrupole mass spectrometer and NIMS have been assembled.

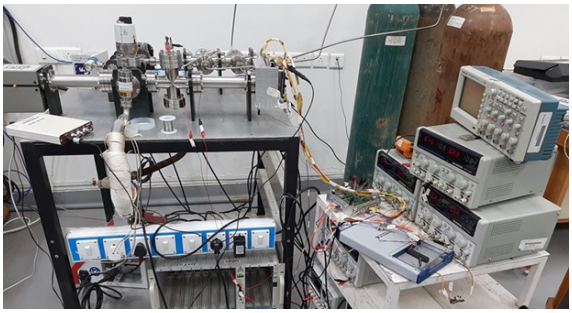

Figure 34: Test setup for commercial and PRL designed mass spectrometers.

In this setup, neutrals are measured by both the mass spectrometers and results are compared. Ions are also generated and measured using NIMS. During ions measurements, filament of the NIMS is kept off. Figure 35 shows the preliminary results acquired during ions' measurements. In this measurements, Argon gas was injected and the peak shown at 40 is from Ar+ ions. The tuning of the electronics is going on. The next version of engineering model will be realized after all the planned measurements are over.

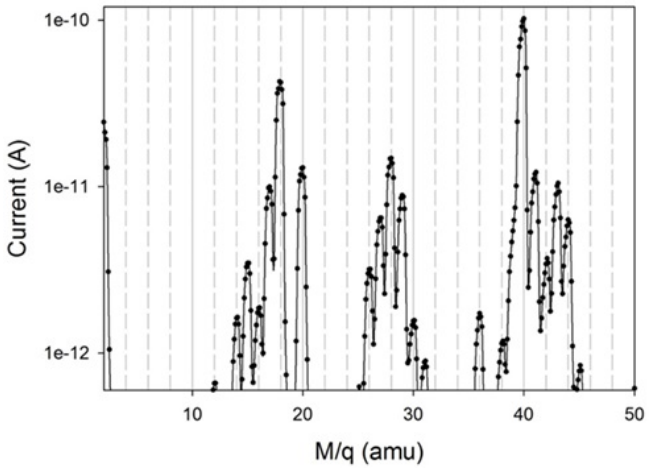

Figure 35: Plot shows the raw data for CEM_counts with m/q during ion mode of the mass spectrometer.

(S. K. Goyal, R. R. Mahajan, A. Auknoor, P. Sharma, J. Mehar, N. K. Upadhyay, V. Sheel and A. Bhardwaj)

Development of an EUV instrument for monitoring solar spectral irradiance onboard future missions to Mars and Venus

The Solar irradiance in the Ultra-violet (soft x-rays, EUV and FUV) is one of the primary energy inputs that dictates the chemistry and dynamics of the entire ionosphere and upper atmosphere of the Mars and Venus. EUV radiation is an important source of heating and ionisation in the atmosphere and affects all the regions of the Mars and Venus. While Solar EUV significantly influences photochemistry at lower altitudes and dictates the locations of ionopause at both Mars and Venus, it plays an equally significant role in dictating the dynamics of the upper atmosphere/thermosphere as well. As the solar UV intensity varies continuously as a function of wavelength on all time scales such as diurnal, seasonal, solar flares etc., a significant variability in these processes is also observed. Of all the solar UV lines (28.4 nm- Fe XV, 30.4 nm – He II, 58.4 nm – He I, 62.5 nm – O V and 97.5 – C III), He II (30.4 nm) is the most intense line followed by He I (58.4 nm) line that causes most of the ionisation at both Mars and Venus. Furthermore, the entire range of UV flux from $\sim$ 0.1 – 100 nm also contributes significantly to the CO_2 ionisation. Therefore, the Solar EUV flux $<$ 100 nm becomes an important parameter that goes into the model calculations to understand the chemistry and dynamics. While, no direct measurement of solar EUV flux is available at Venus till date, only broadband measurements are available at Mars from recent MAVEN mission.

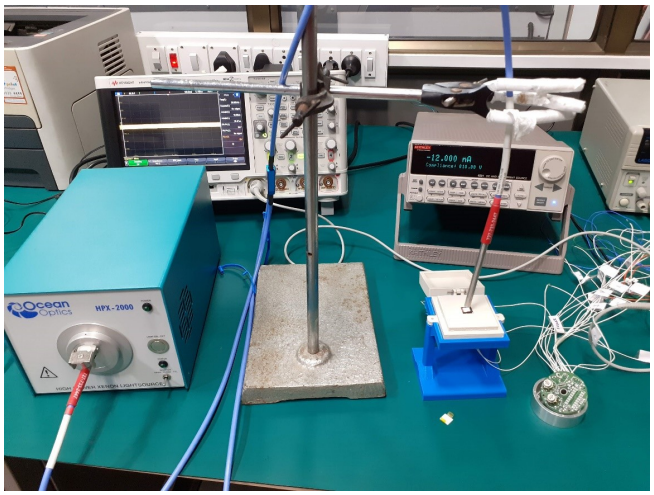

Figure 36: Front-end test setup of EUV front-end with a fibre-based UV source

Because of the lack of such measurements, Earth-based EUV measurements at 1 AU scaled to Mars and Venus distances are still used for interpretation of plasma observations or deducing photochemistry. For this purpose, a miniaturised broadband UV photometer is being developed to be flown on a future mission to the Mars and Venus. The photometer being developed will carryout observations in both broadband and at around certain specific wavelengths regions to reconstruct the EUV/UV spectral irradiance at Mars and Venus. These measurements will also aid interpreting the plasma measurements through other companion instruments such as Langmuir probe and Retarding Potential analyser planned to be flown on the same orbital platform. The EUV monitor consists of three major parts: the sensor package, the front-end electronics and the backend package. The three packages combine to form the final instrument package. The sensor package consists of the EUV sensors, the spectral filters and the optical assembly. Design of such a photometer includes several challenges viz. selection of detector and filter assembly, design of sensitive front-end, processing electronics etc. The developed UV photometer consists of a sensor package, front-end electronics and a microcontroller/FPGA based back-end electronics. A proto-type system is under development at PRL. We are developing and simultaneously testing the front end electronics which consists of conversion of sensor current into voltages by applying appropriate signal conditioning technique. We have carried out initial characterization of the sensing front-end. Further testing and characterisation are underway.

(K. Durga Prasad, C. Kumar, S. Mishra, P. K. S. Reddy, J. Kumar, M. Bhatt, V. Sheel, S. A. Haider and A. Bhardwaj)

Development of a simple and effective gas mixing scheme for PETC

A large-scale Planetary Environment Test Chamber (PETC) is envisaged to be developed at Physical Research Laboratory, Ahmedabad which will serve as a useful multi-purpose facility for carrying out various experiments and tests related to planetary science and exploration. The first step towards this is the realisation of a start-up system as detailed in the earlier report. Here we report the design and development of a simple and yet effective gas mixing scheme for the start-up PETC. A simple and effective system for creating gaseous environment inside a controlled chamber has been envisaged, which forms a crucial sub-system of the PETC gas mixing. A predetermined amount of gas needs to be injected into the control chamber at a given pressure so that a gaseous mixture of required composition can be maintained to simulate the required planetary atmospheres. Instead of using a complex and high-cost gas flow controllers, we have developed a methodology to achieve the same by utilising simple and discrete components. This alternate method aims to achieve a desired mass ratio of gases via flow-controlled gas mixing. This methodology assumes the gases being used are ideal gases which is mostly true considering the gas pressures inside the chamber which will be sufficiently low to assume an ideal gas behaviour. By allowing the gas, at a known temperature and pressure, to flow at an estimated flow rate for a fixed amount of time, we will be able to control the mass flow rate there by the mass injected into the chamber. This also requires time-controlled opening and closing of valves which can be done using “Shut-off” valves. Here in the setup, a fixed amount of each gas is introduced directly into the chamber. No separate mechanical mixing is required. As the gas undergoes free expansion (high pressure gas in the line to a vacuum inside the chamber), the turbulence caused by the injection of gases by itself causes a homogeneous mixing and can hold the homogeneity at least for the time scales of few hours. Due to the simplicity of design and the nature of the individual components being used to control each parameter of the gas flow, optimisation is feasible and the system can be customized readily to suit any subsequent requirements. After certain delay due to COVID related lockdown, resources and budgetary issues, the system is currently being realised with the available resources and expect to soon have a functional demonstration. Once the set-up is fully assembled and functional it will be a standalone system for any type of gas mixing.

(K. Durga Prasad, P. K. S. Reddy, J. Kumar, C. Kumar, S. Mishra, V. Patel, H. R. Vaghela, V. Sheel, S. A. Haider and A. Bhardwaj)

FPGA based processing electronics for ASPEX payload onboard Aditya L-1 Mission

Aditya Solar wind Particle EXperiment (ASPEX) is one of the payload onboard Aditya-L1 mission which is aimed to measure particles in the energy range of 100 eV to 20 MeV. ASPEX has two subsystems namely Solar Wind Ion Spectrometer (SWIS) and Supra-Thermal Energetic Particle Spectrometer (STEPS). SWIS works in the energy range of 100 eV to 20 keV and the STEPS works in the energy range of 20 keV to 20 MeV. The FPGA based processing electronics is designed and configured such that it controls and receives the data from these two subsystems independently. The processing electronics package contains the FPGA and its interfaces, power sub-system and telemetry & tele-command interfaces. Mechanically, the PE package is common for SWIS and STEPS, but electrically it is independent.

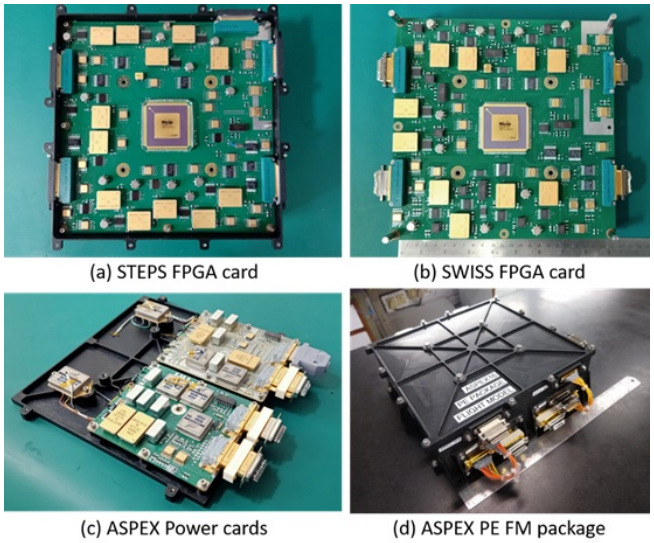

Figure 37: ASPEX Processing electronics flight model photographs

The SWIS subsystem is Top-Hat analyser based design with resistive encoder/anode readout. It has two Top-Hat analysers namely to THA1 and THA2, THA1 is designed with magnetic mass analyser. FPGA PCB has interface with 5 chains (four from THA1 for four quadrants and one from THA2) from the front-end electronics which gives 10 shaping amplifier outputs (2 outputs per quadrant of resistive anode). The STEPS instrument is configured with nine silicon detectors and three scintillator detectors to measure the particles from six different directions. Twelve shaping amplifier outputs from these detectors come to STEPS FPGA card for further processing. Figure-37 shows the flight model PCBs which are stacked together in single package as shown in Figure-37(d). Both the processing electronics PCBs contain Microsemi make RTAX2000 one-time programmable FPGA to process the signal from the analog chains of both SWIS and STEPS, convert into digital form and carry out the data processing onboard and also control the peripheral devices. FPGAs are fulfilling the functional requirements like data command decode, onboard data processing, spectral data generation, storing the data, packetizing, health parameter readout, controlling the operational modes, digital telemetry interface, generation of control signals for devices like Peak detector, ADC, DAC etc. The HDL code design, verification and data pack writing for both SWIS and STEPS are completed. The power subsystem contains two PCBs, one each for SWIS and STEPS. These PCBs accommodate EMI filter, DC-DC converter modules, relays and relay drivers providing necessary biases and their control for these subsystems. High power dissipating DC-DC converters are directly mounted on base plate of package for better heat transfer. The GP250 relays are used to switch ON/OFF the power lines going to front-ends and processing electronics subsystems. Fabrication and assembly of this package is completed and tested with SWIS and STEPS front-end electronics for their functional and performance measurements. The test and evaluation of processing electronics package with STEPS subsystem is completed. The weight of package is $\sim$ 3 Kg and consumes about 14 W power.

(A. Patel, T. Ladiya, M. Shanmugam, H. Adalja, P. Adhyaru, S. K. Goyal, M. Shah, P. Kumar, S. Vadawale, D. Chakrabarty and team)

Supra thermal & energetic particle spectrometer (STEPS) - Subsystem of ASPEX payload

Aditya Solar wind Particle EXperiment (ASPEX) is one of the seven scientific experiments onboard the Aditya - L1 mission, to be placed in a halo orbit around the Sun-Earth L1 Lagrangian point. ASPEX is going to measure the slow and fast solar wind, supra-thermal particles and solar energetic particles. ASPEX has been devised into two independent sub-systems named as Solar Wind Ion Spectrometer (SWIS) and Supra Thermal & Energetic Particle Spectrometer (STEPS). SWIS measures the angular and energy distribution of solar wind ions in the energy range of 100 eV to 20 keV while STEPS covers the high-energy spectrum of the particles i.e. 20 keV/n to 5 MeV/n from six directions. The STEPS subsystem has been configured into three packages in order to cover the six directional measurements i.e. STEPS-1, STEPS-2A & STEPS-2B. STEPS-1 package houses four detector units (SR, IM, PS and NP) and their front-end electronics (FEE). STEPS-2A package has one detector unit (EP) and FEE for EP and SP (STEPS-2B) detector units. ASPEX-PE is a processing electronics package, common for both SWIS and STEPS. Flight models of the STEPS and ASPEX-PE have been developed and tested. Test & Evaluation (T&E) tests i.e. Burn-In test, Vibration test (Sine, Random) at the levels of proto-flight model, Thermo-vacuum test (storage and active cycles) have been successfully completed. EMI/EMC test is going to be conducted for both SWIS & STEPS together. The scientific calibration of instrument is going on. Figure 38 shows three packages i.e. STEPS-1, STEPS-2A & STEPS-2B and ASPEX-PE. Figure 39 shows the photograph taken during thermo-vacuum test.

Silicon Photomultiplier (SiPM) which is being used along with Scintillation detector in STEPS for the high-energy particle measurements has been successfully qualified for the space application. The following tests were conducted on the multiple sets of the devices: baking, short and extended thermal cycling, burn-In, vibration (sine, random), mechanical shock test, thermo-vacuum test, radiation test. Life test of SiPM is going on. Qualification models (QM) for STEPS and ASPEX-PE have also been developed and tested. T&E of these packages is going on. STEPS instrument provides data of particle measurements in CDF format in three levels: Level0, Level1 and Level2. Level0 is the raw data from the instrument. Level1 is derived from Level0, which provides direction wise separated particle counts vs ADC channel. Level 2 is the energy-calibrated data, derived from Level1. The software for the same has been developed and is in final stage.

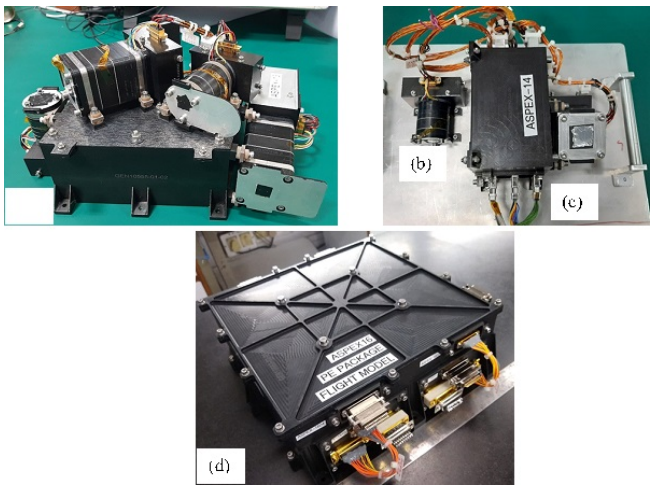

Figure 38: Flights models of (a) STEPS-1, (b) STEPS-2B, (c) STEPS-2A (c) and (d) ASPEX-PE.

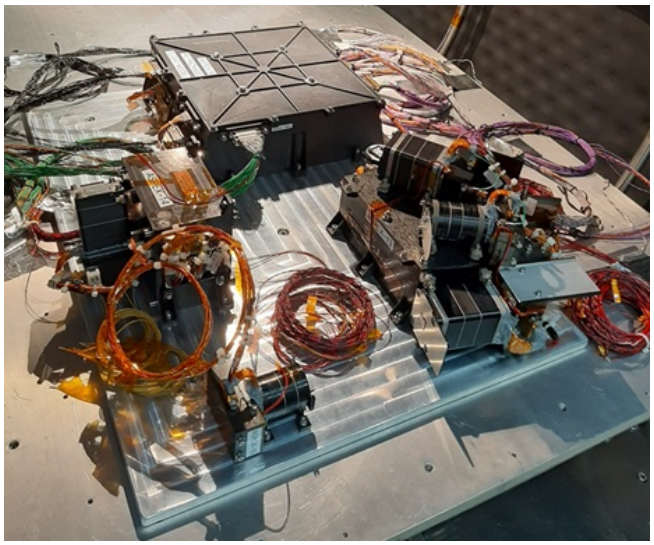

Figure 39: Thermo-vacuum test of FM hardware (STEPS + ASPEX-PE)

(S. K. Goyal, M. Shanmugam, A. R. Patel, N. K. Tiwari, P. Sharma, A. Auknoor, T. Ladiya, S. V. Vadawale, P. Janardhan, D. Chakrabarty, A. Sarada, Bijoy, Ayisha, Sushil, Deepak, Nishant and Team)

Planetary rock sampling technology project

The Directorate of Technology Development and Innovation (DTDI), ISRO HQ has invited technology ideas from ISRO/DOS centers under the MyVision2030 theme during the first technology workshop of DTDI, held on 14th and 15th November 2019. Among the several ideas received from the centers, DTDI has identified a few prospective ones based on a set of criteria that are used to formulate futuristic projects, such as novelty, relevance, and value addition to the Indian Space Programme. One such project formulated by DTDI is 'Planetary Rock Sampling Technology' based on our idea of automated drilling and coring of planetary sub-surfaces for $in-situ$ and sample return missions. In this project, the science team from PRL is working out the scientific requirements and VSSC is involved in the designing and realization of the hardware. The project will be executed in a phased manner wherein during the Phase 1, drilling, coring, and sample analysis will be carried out in-situ using the lander/rover platform and sample return will be achieved in the subsequent phases. While Phase-1 will be in execution, subsequent technological and scientific developments will go on in parallel directed towards achieving technology readiness levels for the advanced phases. Currently, the Baseline Design Review (BDR) Report is being prepared.

This project is jointly pursued with VSSC

(A. J. Verma, N. Srivastava, N. Upadhyay, R. R. Mahajan, K. Durga Prasad, V. Sheel and A. Bhardwaj)

Functional testing and delivery of ChaSTE Front-End Electronics for Chandrayaan-3

Chandra's Surface Thermophysical Experiment (ChaSTE) aims to study the thermophysical properties of Lunar subsurface by deploying a 10 cm thermal probe. The experiment for Chandrayaan-3 is similar to the one developed for the Vikram lander on Chandryaan-2 mission. We had developed a Flight Spare Model for Chandrayaan-2 mission which is being used for Chandrayaan-3 mission. The fabricated electronics card kept under controlled environment conditions at SAC was withdrawn. As per the guidelines provided by TEG/SRA, SAC, various tests such as visual inspection, thermal soak and functional verification tests were conducted at SAC QA and clean room at PRL. As per guidelines provided, active thermal Soak tests were carried out at suggested ChaSTE payload temperature levels as per ISRO ETLS document for Chandrayaan-2. The PRL thermal chamber facility was used for this thermal testing with proper ESD and grounding facilities available at the work bench. The package was kept inside the chamber with thermistors placed on the package and the base plate for temperature monitoring. Pre- and Post-Thermal Final FT was carried out with the package kept under ambient lab conditions as per the procedure described earlier. Functional verification tests were carried out using a custom-made setup in an ESD safe workbench placed in a Class 1000 clean room of PRL. All the functional tests were carried out for a standard input temperature for all channels. The output of each channel is monitored for its stability for each input temperature. The acceptable level of stability is achieved during all the tests. The results show that the functional performance of the ChaSTE FE FM card is within the acceptable limits and the package has been cleared for further activity. Qualitative verification of Science data of temperature monitoring at five different temperatures (223.15 K, 248.15 K, 273.15 K, 298.15 K and 323.15 K) using a Thermowel/Temperature Calibrator was also carried out to ascertain satisfactory performance of the FE card. The Chandrayaan-3 ChaSTE front-end electronics was then flagged of by the Director, PRL, in presence of Dean and other PRL members, for delivery to SPL/VSSC, Trivandrum, for integration, T&E and delivery of ChaSTE payload to the Chandrayaan-3 project.

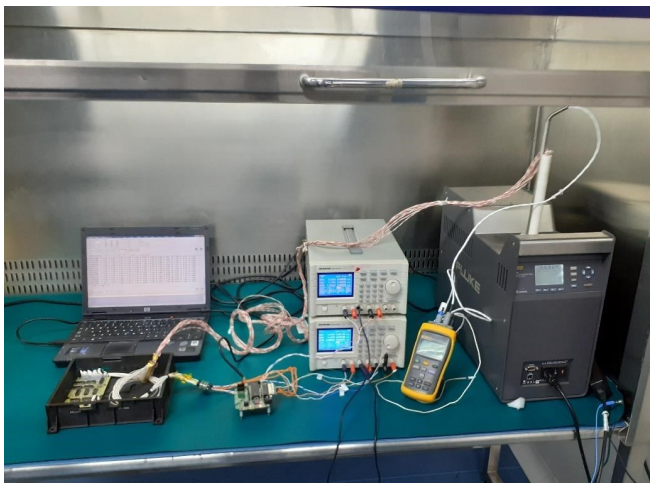

Figure 40: Test set-up used for ChaSTE FE FM functional verification at PRL Clean lab

Figure 41: Flag-off of ChaSTE FE Package by the Director, PRL

(K. Durga Prasad, C. Kumar, S. Mishra, P. K. S. Reddy, T. Ladiya, A. Patel, M. Shanmugam, N. P. S. Mithun and A. Bhardwaj)

Assessment of radiation damage effects on Silicon Drift Detector based X-ray spectrometer onboard Chandrayaan-2 mission

In recent years, Silicon Drift Detector (SDD) based X-ray spectrometers are widely flown onboard space/planetary missions due to its superior spectroscopic performance. The solar X-ray Monitor (XSM) onboard Chandrayaan-2 mission uses SDD for the detection of solar X-rays around the lunar orbit. The XSM instrument is designed to provide the energy resolution of $\sim$ 175 eV at 5.9 keV for the detector operating temperature of $\sim$ -35°C. XSM also has stable spectral performance for the count rates up to $\sim$ 105 counts/s. It is well known that the performance of any silicon detector, and hence its energy resolution, degrades, due to environmental effects as well as radiation damage. The energy resolution of the SDD based X-ray spectrometer mainly depends on the leakage current and the noise contributed by the readout electronics. The electronic noise associated with the readout electronics will not change significantly as the space instruments are designed using space grade components, which are designed to withstand higher radiation dose levels. Hence, any change in the instrument performance will mainly depend on the detector leakage current for the given detector operating temperature. In the space based systems, the increase in the detector leakage current is mainly due to the radiation damage while the temperature of the detector is being actively controlled. In our previous work, it was demonstrated that, one can estimate the change in the performance of the SDD based X-ray spectrometer by measuring the detector leakage current. A new and novel technique was used to measure the detector leakage current. This is achieved by counting the ramp signal frequency from the output of the detector readout electronics with the use of Reset type Charge Sensitive Pre-Amplifier (CSPA) configuration. When there is no X-ray interaction with the detector, ramp signal frequency is mainly due to the detector leakage current. The same technique was implemented in XSM onboard Ch-2 and we are continuously monitoring the detector performance since launch, July, 2019.

Before Ch-2 launch, the measured ramp signal frequency is $\sim$ 1.5 Hz from November 2017 to July 2019 and increased to about 6 Hz when the instrument was in the radiation belt en-route to the Moon. After reaching the lunar orbit, there is slow and steady increase in the ramp signal frequency which is about 11 Hz as on March 2021. The data points were taken from the spectral data received from XSM onboard Ch-2 when there is no X-ray events in the data packets. This is to make sure that the ramp signal frequency measurement is mainly due to the detector leakage current. We derived the leakage current using the below equation

$$\mathrm{I}_o = \mathrm{C} \times \frac{\mathrm{V_{RAMP}}}{\mathrm{T_{RAMP}}}$$

Where I_o is the leakage current, C is the charge integrating capacitor in the CSPA, $\mathrm{V_{RAMP}}$ is the ramp signal amplitude and $\mathrm{T_{RAMP}}$ is the ramp signal period ($\mathrm{T_{RAMP}}$ = 1/$\mathrm{F_{RAMP}}$). The value of the charge integration capacitor was estimated independently, which is about 60 fF. The ramp signal amplitude is set between -2V to 4V. By substituting these values in the above equation gives the leakage current values as 0.54 pA at 1.5 Hz, 2.16 pA at 6 Hz, 3.96 pA at 11 Hz. We also measured the energy resolution and the peak energy position of the XSM using onboard calibration source and observed that there is no degradation in the performance as shown in Fig. 42. Even though the leakage current increased from 0.54 pA to 4 pA, the energy resolution remains same at around 175 eV. It was earlier demonstrated that, at

lower leakage currents, the energy resolution is mainly determined by the readout electronics noise and at higher leakage currents, the energy resolution degrades with increase in the leakage current. The same behaviour has been observed from the onboard measurements as well. From these measurements, it can also be seen that the radiation damage effects on the SDD is minimal even after 1.5 years of operation in the lunar orbit. This is mainly due to additional shielding provided to the detector during Earth to Moon transit and also due to solar minimum conditions.

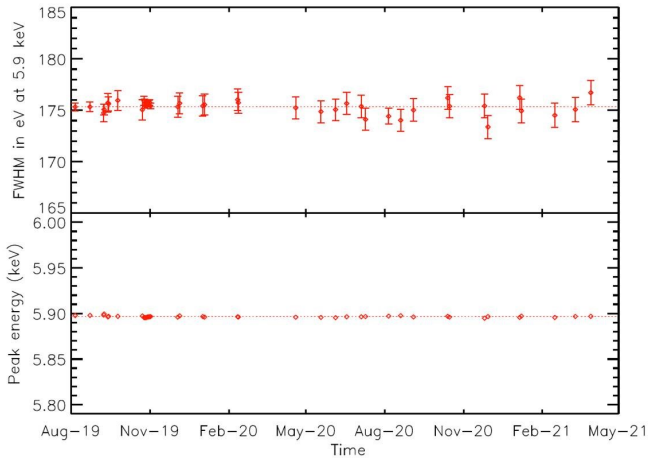

Figure 42: XSM instrument performance, energy resolution (top panel) and peak energy position (bottom panel) measured from August, 2019 to March, 2021.

(M. Shanmugam, A. Patel, N. P. S. Mithun and S. Vadawale)

Look up table based digital temperature controller using Field Programmable Gate Arrays (FPGA) for the Silicon Drift Detectors

Silicon Drift Detectors (SDD) are often used in the planetary missions as solid-state X-ray detectors in different types of spectrometer applications. They have low detector capacitance, low leakage current and reduced noise due to integrated FETs, hence providing very good energy resolution at high count rates. One of the main parameters that dictates the performance of the SDD spectrometer is temperature of the detector chip and hence it is desirable to maintain the detector temperature to a particular value during the measurements. Peltier or Thermo-electric cooler (TEC) is used to maintain the temperature of SDD which is generally embedded with the detector chip. SDD from KETEK has inbuilt thermistor which monitors the detector chip temperature and a peltier for cooling the device. Often analog circuits are used to maintain the SDD temperature but they take up larger room and require more power in order to incorporate different set point temperatures, hence FPGA based temperature control presents better alternative going forward.

In our design we have chosen a look-up table-based implementation in a Field Programmable Gate Array (FPGA) to control the temperature of the SDD. The temperature reading from the TEC is monitored using Analog to digital convertor (ADC) and is given to the FPGA. Based on the circuit simulation of the temperature readout circuit, a lookup table is generated and stored in FPGA for output voltage of readout circuits at different temperature. Depending on output from the readout circuit and set point value at that temperature, FPGA decides whether to increase or decrease the gate voltage of the FET driver which allows sufficient current to the peltier to achieve desired detector temperature. The provision has been made to change the desired temperature of the detector chip using command. With this design, we are able to measure and control the detector chip temperature with an accuracy of $\pm 0.5^{\circ}$C and achieved a resolution of 173 eV @5.9 KeV. In continuation to this, we plan to incorporate dynamic control such as Proportional-Integral-Derivative (PID) to further improve the temperature stability of the detector chip.

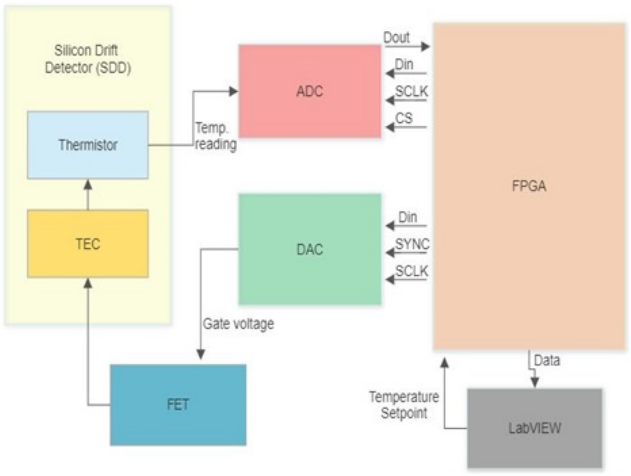

Figure 43: Block diagram of proposed digital temperature controller

(N. Singh, A. Patel, M. Shanmugam, T. Ladiya, S. Kumar and D. Kumar)

Alpha Particle Spectrometer (APS) for future lunar Lander/Rover mission

It is proposed to develop an Alpha Particle Spectrometer (APS) for the upcoming ISRO-JAXA Lander/Rover mission to study the volatile transport on the Moon. The existence of permanently shadowed areas in the polar regions of the moon implies that these areas can act as cold traps for water molecules and other volatiles that will be transported from the hot sunlit side of the moon to these colder areas. The proposed APS instrument is aimed to detect 5.49 MeV and 5.304 MeV alpha particles from ^{222}Rn and ^{210}Po near permanently shadowed areas in lunar polar region, to understand the transport of volatiles on the lunar surface. In this direction, we have established an APS experiment in the laboratory as shown in fig. 44. This experiment uses 450 mm^2 ion-implanted silicon based charged particle detector with depletion depth of 100 μm. The entrance window of the detector is an extremely thin ($\sim$500Å) with boron implantation which results in very low attenuation of alpha particles and hence one can achieve low energy threshold. The proposed experiment requires active area of $\sim$10 cm^2 as the signal is very feeble.

In the laboratory setup, the detector and the source are kept inside a small vacuum chamber. The charge output from the detector is read by a Charge Sensitive Pre-Amplifier (CSPA) which converts it in to voltage pulse. The output of the CSPA is fed to the shaping amplifier

to improve the signal to noise ratio. The peak height information of the Gaussian pulse is read using Multichannel Analyzer (MCA), which provides the spectrum of counts vs energy. A sample spectrum acquired using the laboratory APS setup is shown in fig. 45. It provides the energy resolution of $\sim$ 20 keV at 5.486 MeV. The leakage current of the detector was also measured at different biasing voltages. The leakage current is $\sim$ 2.8 nA for the typical detector bias of $\sim$ 50V.

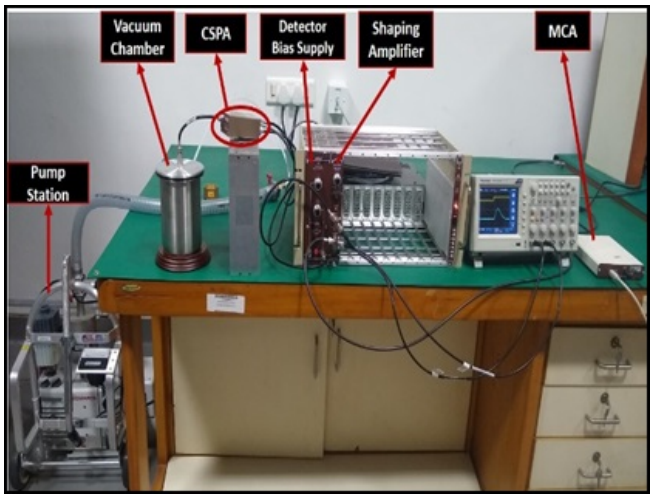

Figure 44: Lab-Based Setup for Alpha Particle Spectrometer

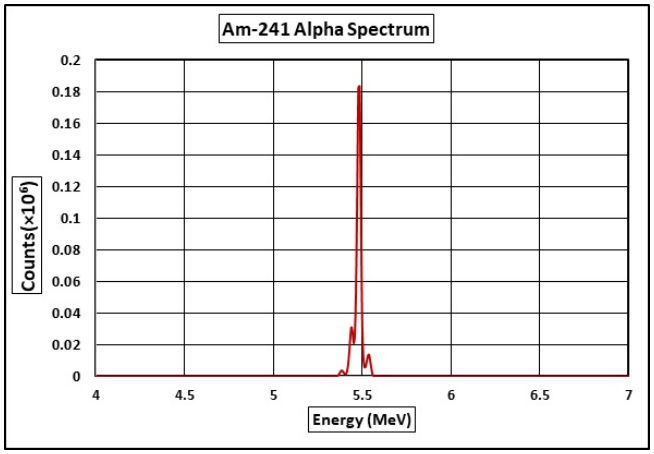

Figure 45: Am-241 Spectrum showing alpha decay at $\sim$5.486 MeV

(S. Kumar, M. Shanmugam, A. Patel, N. Singh, D. K. Painkra, T. Ladiya and D. Banerjee)

Design and evaluation of integrated LP electronics of LPEX experiment for MOM-2

The evaluation details of the design verification model of the Langmuir Probe and Electric Field experiment (LPEX) has been reported earlier. Based on these evaluation results and suggestions provided by the payload review committee, a first version of the Langmuir probe engineering model (EM-1) PCB for the integrated electronics is designed, fabricated and populated. The EM PCB includes a common LP electronics with Electrometer, sweep bias and digitisation, all included together. The EM-1 PCB was designed which aims to measure current from 01.pA – 0.1mA with sweep bias capability form -90V to +90V. The sweep bias design accommodates a 12-bit DAC which is amplified and programmed to provide variable time steps and variable bias steps with respect to varying regimes of ionosphere. The digitisation circuit has a 8-channel 12 bit ADC and reference voltage circuit. The PCB was designed with a provision of guard along transimpedance amplifier to reduce the leakage current and improve noise immunity. The fabricated and wired undergoing testing is shown in figure 46. The electrometer testing is completed and sweep bias and ADC testing is in pipeline.

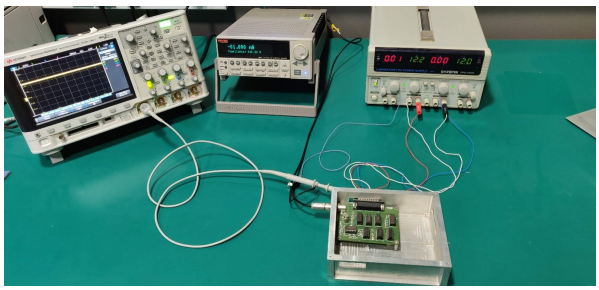

Figure 46: Testing of the EM-1 Fabricated LP FE board

(K. Durga Prasad, C. Kumar, S. Mishra, P. K. S. Reddy, J. Kumar, V. Sheel, S. A. Haider and A. Bhardwaj)

Mechanical analysis of boom and deployment mechanism for LPEX payload

LPEX Payload is selected payload for MOM-2 mission. LPEX Payload has two instruments LP and EF (1) EF has two probes and (2) LP has one probe. The requirement of keeping the LPEX probes $\sim$1m away from the spacecraft demands that a boom deployment mechanism needs to be developed.

Table: Comparison of theoretical calculation with FEM analysis

Parameter	Theoretical Result	Present Work
Max Stress(Von-Mises) (Mpa)	3.7	3.5133
Probe end deflection (mm)	0.02103	0.0205
First Mode Frequency (Hz)	-	457.31

LPEX boom deployment mechanism is a torsion spring hinged based mechanism in which the strain energy stored in the torsion spring is utilized for deploying the boom. A frangibolt or a suitable locking mechanism will be used for holding the boom sub-assembly in stowed state during flight. A micro-switch will be used as a deployment confirmation system and preload in torsion spring will be used for retain the boom sub-assembly in the deployed state. In order to assess the suitability of the design for flight conditions, structural analysis has been carried out using a finite element package. The material of boom has been considered to be CFRP. A fixed joint is

considered boom-mechanism interface. Static and modal analysis of boom sub-assembly has been carried out using finite-element analysis. Preliminary analysis of the results obtained from static and modal analysis of the boom sub assembly appears to be under permissible limits as per design parameter and material specification of boom. The modal analysis gives the first mode of frequency as 457.31 Hz. The end deflection in stowed state has been found to be 0.02 mm and maximum stress (Von mises) is around 3.5 Mpa which are within the permissible limit.

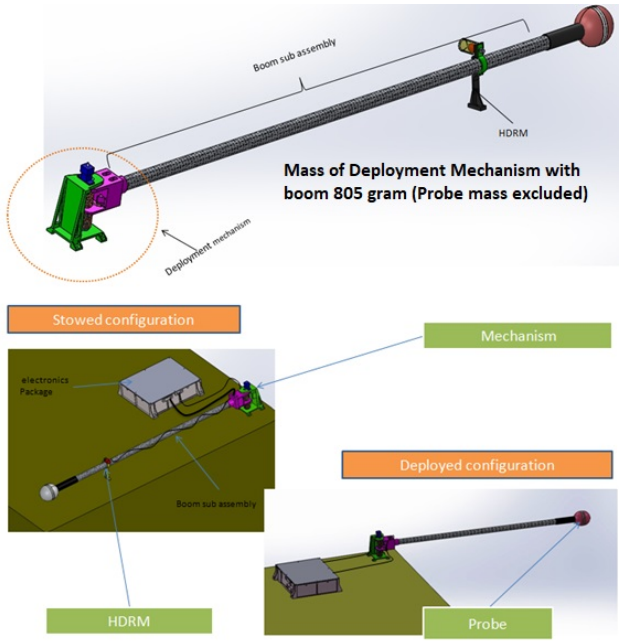

Figure 47: CAD design of the proposed deployment mechanism in stowed and deployed conditions

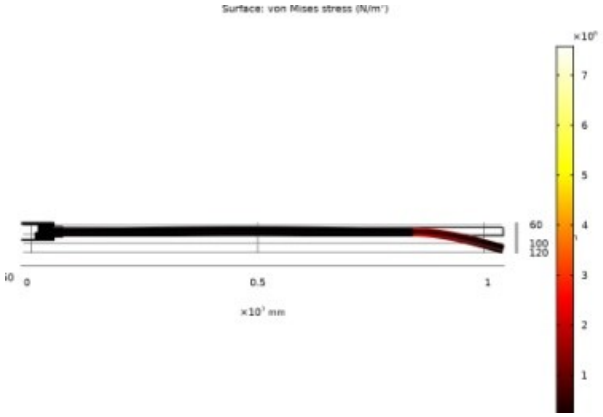

Figure 48: Simulation results from static analysis: Max stress 3.5Mpa

(K. Durga Prasad, J. Kumar, P. K. S. Reddy, C. Kumar and S. Mishra)

Development of a numerical model to study atomosphere of exoplanets

The study of exoplanets is one of the fastest-growing branches of modern-day astronomy. To study atmospheric composition of exoplanets, we require a numerical model that can deal with the different chemical and physical processes, namely chemical equilibrium, transport processes, and photochemistry. We have developed a Fortran-based numerical model to study the effect of the exoplanet's physical and chemical parameters on the atmospheric composition of the exoplanet. The model uses the plane-parallel approximation and divides the atmosphere into N layers equally separated in the log pressure scale. The T-P profile of the exoplanet is used to assign the temperature of each layer. In each layer, the model solves the mass continuity equation for each species, and this equation includes chemical kinetics, photochemistry, and transport terms. The chemical kinetics uses the chemical reaction network to calculate the forward and backward reaction rates, to find the source and loss terms in the mass continuity equation. The photochemistry required the photon flux in each layer, and this photon flux is calculated by the two-stream approximation of the radiative transfer. The scattering and absorption are used to find the total optical depth, and stellar flux at the stellar surface is given as the input for calculation. In the transport processes which allow the interaction between different layers, we have included Eddy diffusion and molecular diffusion. Integration of the mass continuity equation, as defined by the model, gives the mixing ratios of the different atmospheric species. The benchmarking of the model is done by calculating the mixing ratio of the HD18933b exoplanet and comparing it with published results for this planet.

(V. Soni and K. Acharyya)

MERCURY code simulation of IDP evolution in inner solar system

Asteroid belt is a main source of Interplanetary Dust Particles (IDPs) in our solar system. The other sources are Kuiper belt and occasional comets entering the solar system.

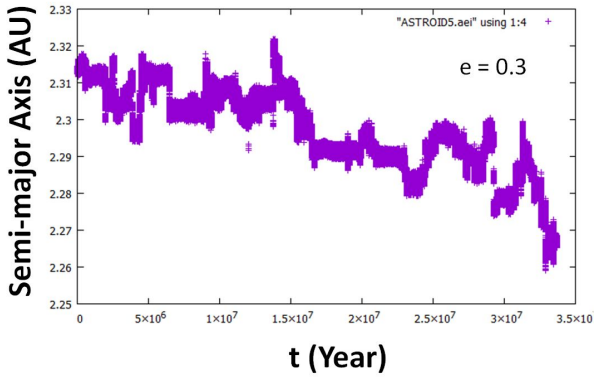

Figure 49: Variation of semi-major axis of IDP, initially attached to Asteroid belt, for the eccentricity of 0.3. The semi-major axis starts deviating whenever the eccentricity exceeds 0.25 and the particle is detached from Asteroid belt.

It is expected that all size of particles starting from few hundreds of nanometers to big asteroids are present in the belt. The belt particles have been bound to it, either from the time of formation of the solar system or they might have been produced due to the collisions of bigger objects. The dust particles remain attached to the system as long as the gravitational influence of the Sun, planets and other minor

objects balance one another. The IDP evolves dynamically over the geological time scale and starts to deviate from their original orbit. Mathematically, this is an N-body problem, in which, we simulate the dynamical system of particles under the influence of physical forces like gravity. The dynamics of IDP is studied based on N-body problem using MERCURY code. The exercise was carried out to study the deviation in the semi-major axis as well as the inclination of the IDP, which are major parameters for the particles to spiral in toward Sun. Our results show that the IDPs are detached from the asteroid belt when the eccentricity is greater than 0.25. This has been found to occur within 33 My, which corresponds to 0.1 AU distance, inward towards Sun. The deviation of semi-major axis for the eccentricity of 0.3 can be observed from results in Figure 49. It is expected that IDPs can reach Mars in about 264 My after getting detached from the belt.

(J. P. Pabari, Rashmi, K. Acharyya, S. Nambiar, S. Jitarwal, V. Sheel, Anil Bhardwaj and D. Kumar)

Development of a multifluid model to study the coma of comets

Comets show a general diversity in their volatile composition, but in most cases H_2O is observed to be the dominant volatile. This is followed by CO and CO_2, and trace amounts of other species such as CH_4, CH_3OH, O_2, and NH_3 are also present. However, the observed ratio of any species with respect to water varies considerably from one comet to another. Also, few comets have been observed to have a CO/H_2O ratio > 1. We have constructed a state-of-the-art multifluid numerical model to study how the chemistry and dynamics of the coma of a comet changes for varying abundances of the major volatiles. The model is described using the fluid conservation equations for number density, mass, momentum and energy. Active chemistry occurs in the coma and the energy that is released due to chemical reactions is non-uniformly distributed amongst the volatile species in the coma, resulting in different temperatures. Hence, for a complete description of the coma, we have used a multifluid model whereby the neutrals, ions and electrons are considered as three separate fluids. Apart from chemical reactions, we have also considered the exchange of energy between the three fluids due to elastic and inelastic collisions. The fluid conservation equations can be written as a set of first order differential equations in species number density, velocity and temperature. Numerical integration of these equations gives the temperature and velocity profiles of the coma, for varying cometocentric distances. We can also obtain the number density profiles of the different ionic and neutral species that are created in the coma. We have successfully benchmarked the model by testing our model results with other published results.

(S. Ahmed and K. Acharyya)

Development of analytical model to specify dielectric permittivity of the Martian subsurface using orbiter sounding radars

Sounding orbiter radars is proven to be an efficient tool to identify the subsurface properties of planetary bodies. These instruments generally use long wavelength (kHz to GHz) radio signals to probe the subsurface and carry the material information in terms of the physics parameters like dielectric permittivity, loss tangent and reflectance – for instance, Shallow RADar (SHARAD) operates at mean frequency of $\sim$20MHz (15-25 MHz). The basis of the mechanism is that electromagnetic (or radio) signal possesses reflection and transmission from any dielectric discontinuity. Since, the subsurface may correspond to multilayer deposits, each layer might contribute in designing the effective signal that is received by orbiter radar after subsurface reflection. For instance, as an electromagnetic (em) radio wave signal emitted by orbiting radar interact with top crust of the planetary surface, it exhibits partial reflection, scattering via rough surface and transmittance. The transmitted wave propagates further deeper within the sub-surface and goes again for a partial reflection /transmittance at another dielectric discontinuity; during propagation, the radio waves also suffer the amplitude attenuation and phase change on account of absorption within medium. This process continues until the wave completely diminishes. These partial reflections from surface and sub-surfaces are usually recorded by the radar in terms of the power at different time delays which eventually infers the cumulative inherent effects of the dielectric characteristics and sublayer widths. In order to model these features, we initiate with a three layer model which could be generalized to n-layer deposits by including the layer properties and recurrence formulation. For the purpose, we consider the radio wave reflection from two consecutive interfaces of surface and sub-surface, and assume the sublayer (of width l) is sandwiched between the surface materials. We utilize linear theory of em wave propagation to obtain the intensity and phase after reflection /transmission of the wave signal. For simplicity, the two mediums (surface /sub-surface materials) may be considered homogeneous and nondispersive, while the subsurface layer is characterized by low-loss medium. Under these physical conditions, we have derived the expressions for coefficient of power reflection in terms of physical properties of the subsurface and surface layers. As the sounding radars gives information of power reflectance as output, the dielectric permittivity might be obtained using the derived relation. The model for multilayer deposits is under development phase.

(R. R. Bharti and S. K. Mishra)

SIMION based simulation of two and three channel hypervelocity dust detectors

Ever-evolving interplanetary dust particles are a great source of knowledge about the history of our solar system. A dust detector is proposed for future planetary missions, which will study the dust properties like mass, velocity and flux in interplanetary space in our solar system. The detector design allows the capture of ions and electrons generated on the impact of a particle, using biased electrostatic collectors. The efficiency to capture these impact generated particles depends on the bias voltage applied and the configuration in which they are applied, other than the detector geometry. In this work, simulation is carried out using SIMION software to compare two channel and three channel detector configurations. In two channel configuration, the target is grounded and all collector plates are biased either negatively or positively. While in three channel configuration, the target is grounded with two positively biased collector plates and two negatively biased collector plates. It is found that the two-channel configuration gives higher capture efficiency. However, a limitation of this configuration compared to three channel detector is the lack of third channel information, which provides the indication of the start of event and also helps in distinguishing real events from noise.

(S. Nambiar, J. P. Pabari, Rashmi, S. Jitarwal, K. Acharyya, S. M. K. Praneeth, R. Singh, D. Kumar and team)

Space and Atmospheric Sciences

Contribution of light-absorbing aerosols to absorption over the Indo-Gangetic Plain and Himalayas

Analyzing new and high quality in situ observations, for the first time, the individual contributions of light-absorbing aerosols (black carbon (BC), brown carbon (BrC) and dust) to aerosol absorption are quantified over the Himalayan region (Figure 1), a relatively poorly studied region with several sensitive ecosystems of global importance, as well as highly vulnerable populations.

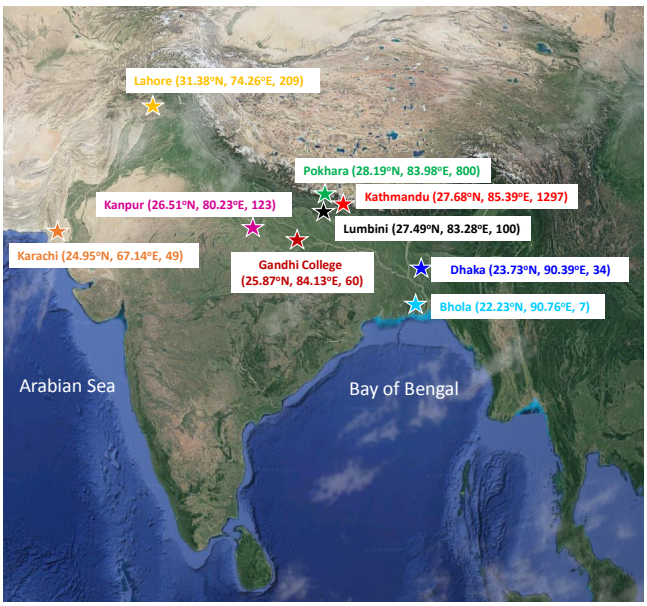

Figure 1: Details of the study locations in the IGP and the Himalayan foothills in South Asia (the background map was generated with Google maps (https://www.google.com/maps). The latitude, longitude and elevation (in meters above sea level, m a.s.l.) of each location are given.

The annual and seasonal average single scattering albedo (SSA) over Kathmandu is the lowest of all the locations. The SSA over Kathmandu is $<$0.89 during all seasons, which confirms the dominance of light-absorbing carbonaceous aerosols from local and regional sources over Kathmandu. The SSA decreases with increasing elevation over the Himalayas, confirming the dominance of light absorbing carbonaceous aerosols at higher elevations. In contrast, the SSA over the Indo-Gangetic Plain (IGP) did not exhibit a pronounced spatial variation. BC dominates ($\geq$75%) the aerosol absorption over the IGP and the Himalayas throughout the year (Figure 2).

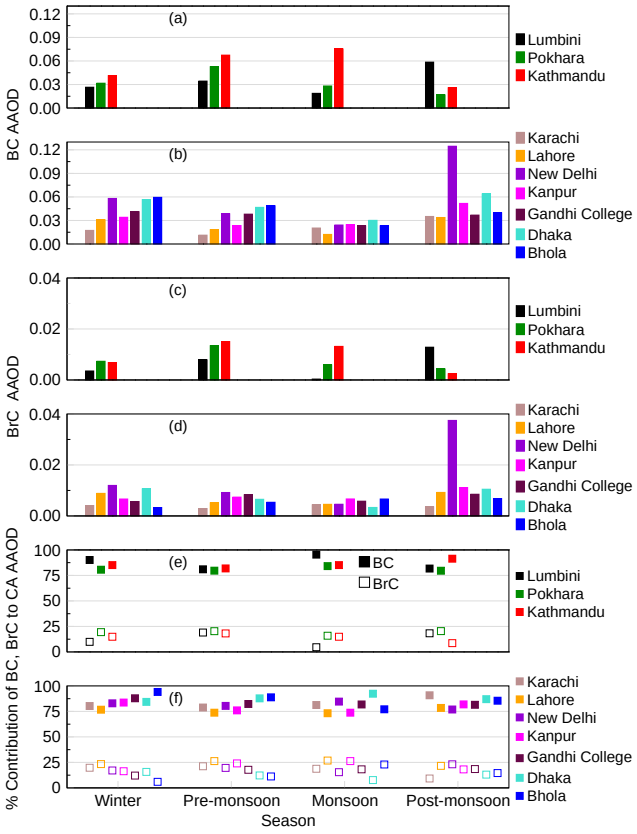

Figure 2: Black carbon (BC) and brown carbon (BrC) over the IGP and the Himalayan Foothills: Seasonal mean values of: (a, b) BC AAOD, (c, d) BrC AAOD, and (e, f) percentage contribution of BC and BrC to CA AAOD corresponding to a wavelength of 550nm

Higher BC concentration at elevated locations in the Himalayas leads to lower SSA at elevated locations in the Himalayas. The contribution of dust to aerosol absorption is higher throughout the year over the IGP than over the Himalayas. The aerosol absorption over South Asia is very high, exceeding available observations over East Asia, and previous model estimates. This quantification will be valuable as observational constraints to help improve regional simulations of climate change, impacts on the glaciers and the hydrological cycle, and will help to direct the focus towards BC as the main contributor to aerosol-induced warming in the region.

This work was done in collaboration with Maheswar Rupakheti and Mark G. Lawrence, Institute for Advanced Sustainability Studies, Potsdam, Germany.

doi : https://doi.org/10.1016/j.envint.2020.105814

(S. Ramachandran)

Asian Aerosol Dipole - Changing Content, Composition and Atmospheric Heating

Aerosol emissions from human activities have been extensive and changing rapidly over Asia. Model simulations and satellite observations indicate a dipole pattern in aerosol emissions and loading between South Asia and East Asia, two of the most heavily polluted regions of the world (Figure 3).

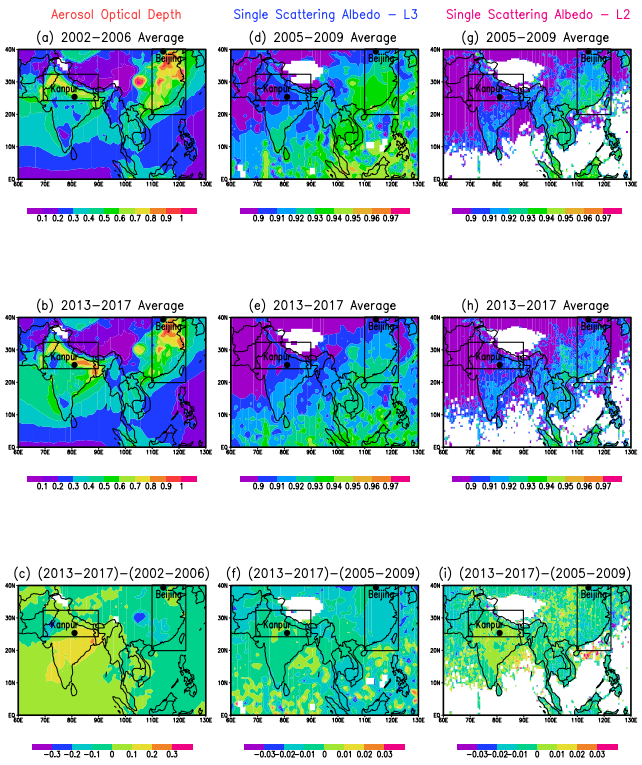

Figure 3: Changing aerosol patterns over South Asia and East Asia: MODIS Terra version 6.1 level-3 monthly AOD at a wavelength of 0.55 μm averaged for (a) 2002-2006 and (b) 2013-2017. OMI OMAERUV v003 level-3 SSA at a wavelength of 0.388 μm averaged for (d) 2005-2009 and (e) 2013-2017, and OMI OMAERO v003 level-2 SSA at a wavelength of 0.388 μm averaged for (g) 2005-2009 and (h) 2013-2017. The spatial differences in AOD and SSA between the two periods are shown in (c), (f), and (i) respectively.

We examine the previously unexplored diverging trends in the existing dipole pattern of aerosols between East and South Asia using the high quality, two-decade long ground-based time series of observations of aerosol properties from the Aerosol Robotic Network (AERONET), from satellites (Moderate Resolution Imaging Spectroradiometer (MODIS) (Figure 3) and Ozone Monitoring Instrument (OMI)) (Figure 3), and from model simulations (Modern-Era Retrospective Analysis for Research and Applications, version 2 (MERRA-2). The data cover the period since 2001 for Kanpur (South Asia) and Beijing (East Asia), two locations taken as being broadly representative of the respective regions. Since 2010 a dipole in aerosol optical depth (AOD) is maintained (Figure 3), but the trend is reversed-the decrease in AOD over Beijing (East Asia) is rapid since 2010, being 17% less in current decade compared to first decade of twenty- first century, while the AOD over South Asia increased by 12% during the same period (Figure 4).

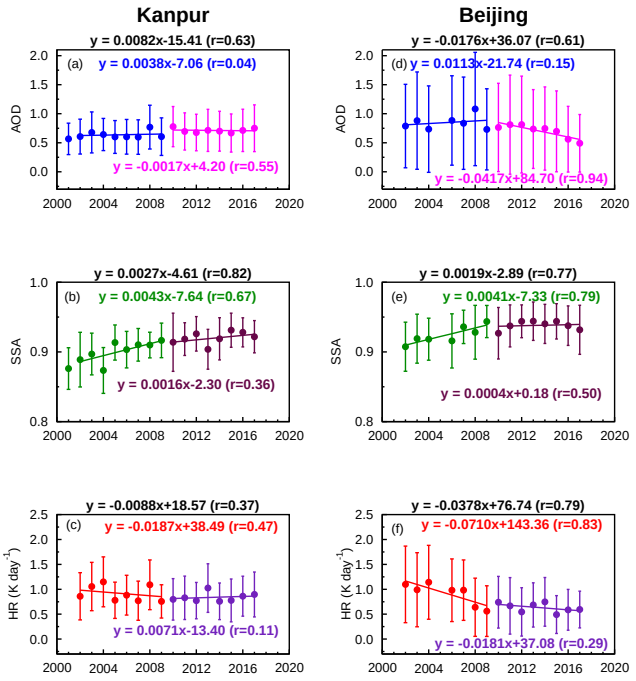

Figure 4: Aerosol optical properties and heating rate over Kanpur and Beijing during 2001-2017 derived from the AERONET observations: Annual mean (a, d) aerosol optical depth (AOD) and (b, e) single scattering albedo (SSA) over Kanpur and Beijing, respectively, at a wavelength of 0.50 μm. (c, f) atmospheric solar heating rate due to aerosols (HR) (K day^{-1}) estimated using the aerosol radiative forcing (Wm^{-2}) of the atmosphere over Kanpur and Beijing. Vertical bars indicate $\pm 1\sigma$ (standard deviation) from the mean. Trend lines and equations are drawn for two different periods: 2002-2009, and 2010-2017 respectively. The equations for the overall trend (2002-2017) for the respective aerosol parameter are given (in black) at the top of each figure.

Furthermore, we find that the aerosol composition is also changing over time. The single scattering albedo (SSA), a measure of aerosol's absorption capacity and related to aerosol composition, is slightly higher over Beijing than Kanpur, and has increased from 0.91 in 2002 to 0.93 in 2017 over Beijing and from 0.89 to 0.92 during the same period over Kanpur, confirming that aerosols in this region have on an average become more scattering in nature (Figure 4). The spatial patterns in level-2 (unaffected by the row anomaly in OMI) and level-3 (affected by the row anomaly) SSA and their differences are similar (Figure 3). These changes have led to a notable decrease in aerosol-induced atmospheric heating rate (HR) over both regions between the two decades, decreasing considerably more over East Asia ($-$ 31%) than over South Asia ($-$ 9%). The annual mean HR is lower now, it is still large ($\geq$ 0.6 K per day), which has significant climate implications. The seasonal trends in AOD, SSA and HR are more pronounced than their respective annual trends over both regions. The seasonal trends are caused mainly by the increase/decrease in anthropogenic aerosol emissions (sulfate, black carbon and organic carbon) while the natural aerosols (dust and sea

salt) did not change significantly over South and East Asia during the last two decades. The MERRA-2 model was able to simulate the observed trends in AODs well but not the magnitude, while it also did not simulate the SSA values or trends well. These robust findings based on observations of key aerosol parameters and previously unrecognized diverging trends over South and East Asia need to be accounted for in current state-of-the-art climate models to ensure accurate quantification of the complex and evolving impact of aerosols on the regional climate over Asia. The findings open up a new area for research such as how the diverging trends might contribute to climate change and large-scale changes in regional atmospheric stability, circulation and hydrological cycle over both regions.

This work was done in collaboration with Maheswar Rupakheti and Mark G. Lawrence, Institute for Advanced Sustainability Studies, Potsdam, Germany.

doi : https://doi.org/10.1038/s41598-020-76936-z

(S. Ramachandran)

Optical and physical characteristics of aerosols over the Pokhara Valley in the Himalayan foothills

Seasonal and inter-annual variations of aerosol optical, and physical properties over Pokhara Valley in the foothills of central Himalayas in Nepal utilizing the high-quality multi-year columnar aerosol data observed recently from January 2010 to December 2017 were comprehensively analyzed.

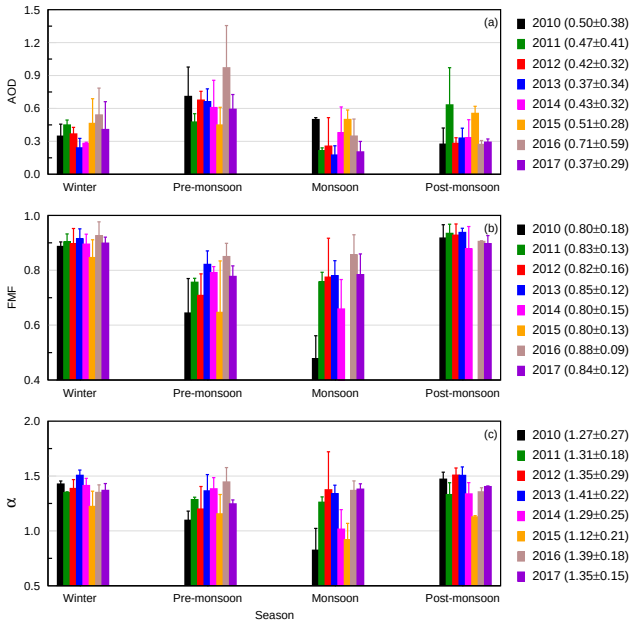

Figure 5: Seasonal mean (a) aerosol optical depth (AOD) at 0.55 μm, (b) fine mode fraction (FMF) in AOD and (c) Ångström exponent (α) computed from the AODs in the 0.44-0.87 μm wavelength region for the years 2010 to 2017. The annual mean values of the above aerosol parameters and their $\pm 1\sigma$ standard deviation from the mean are given for each year.

The influence of forest fires and agro-residue fires on aerosol properties were also investigated. Seasonal average aerosol optical depth (AOD) over Pokhara was $\geq$0.3 during the year, highest in pre-monsoon and lowest during monsoon. AOD exhibits a consistent seasonal cycle every year with a peak in pre-monsoon (Figure 5). Fine mode fraction contributing to AOD and Ångström exponent (α) corroborate seasonal pattern of AODs. AODs showed good correlation with fire counts. The aerosol volume size distributions are bimodal. The peaks in volume size distribution and volume concentrations obtained in 2016 pre-monsoon are the highest during the 8-year observation period which coincided with peaks in the occurrence of highest number of fires in the Pokhara Valley and surrounding region. Effective radius of coarse mode aerosols was an order of magnitude larger than fine mode aerosols. The analysis of optical and physical properties of aerosols over the Pokhara Valley suggest that the aerosols observed over the Himalayan foothills are of urban/industrial, biomass burning and dust origin with proportional contributions varying in different seasons. The study provides observational constraints on aerosol properties that can serve as inputs for model simulation of aerosol physiochemical processes and quantification of impacts on air quality, climate and sensitive ecosystems.

This work was done in collaboration with Maheswar Rupakheti, Institute for Advanced Sustainability Studies, Potsdam, Germany.

doi : https://doi.org/10.1016/j.atmosres.2020.105254

(S. Ramachandran)

Radiative effects of aerosols over the Pokhara Valley in the Himalayan foothills

A comprehensive analysis of seasonal and inter-annual variations of aerosol properties (optical, physical and chemical) and radiative effects over Pokhara Valley in the foothills of central Himalayas utilizing the high-quality multi-year columnar aerosol data observed recently from January 2010 to December 2017 was performed. The single scattering albedo (SSA) either decreases as a function of wavelength or remains independent of wavelength (Figure 6).

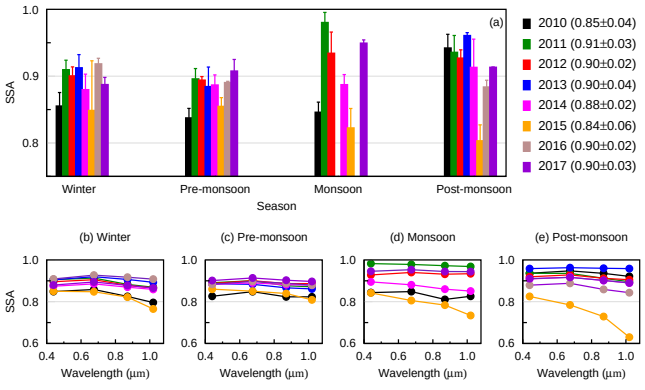

Figure 6: Seasonal variation of single scattering albedo (SSA) corresponding to a wavelength of 0.55 μm during 8-year period (2010-17). The annual average SSA with standard deviation for each year is shown on the right side of panel (a). SSA spectra in the wavelength range of 0.44-1.02 μm during 2010-2017 for different seasons – (b) winter, (c) pre-monsoon, (d) monsoon and (e) post-monsoon

The seasonal aerosol absorption optical depth (AAOD) exhibits a

behavior opposite to that of SSA. Carbonaceous aerosols (CA) dominate ($\geq$60%) aerosol absorption during whole year. Black carbon (BC) alone contributes $>$60% to $AAOD_{CA}$ while brown carbon (BrC) contributes the rest. The absorbing aerosol types are determined to be BC, and mixed (BC and dust) only. Dust as absorbing aerosol type is absent over the Himalayan foothills. The aerosol radiative forcing (ARF) at the surface (ARF_{SFC}) was $\geq$-50 Wm^{-2} except in monsoon almost every year. The ARF of the atmosphere (ARF_{ATM}) was $\geq$50 Wm^{-2} during winter and pre-monsoon in all the years (Figure 7).

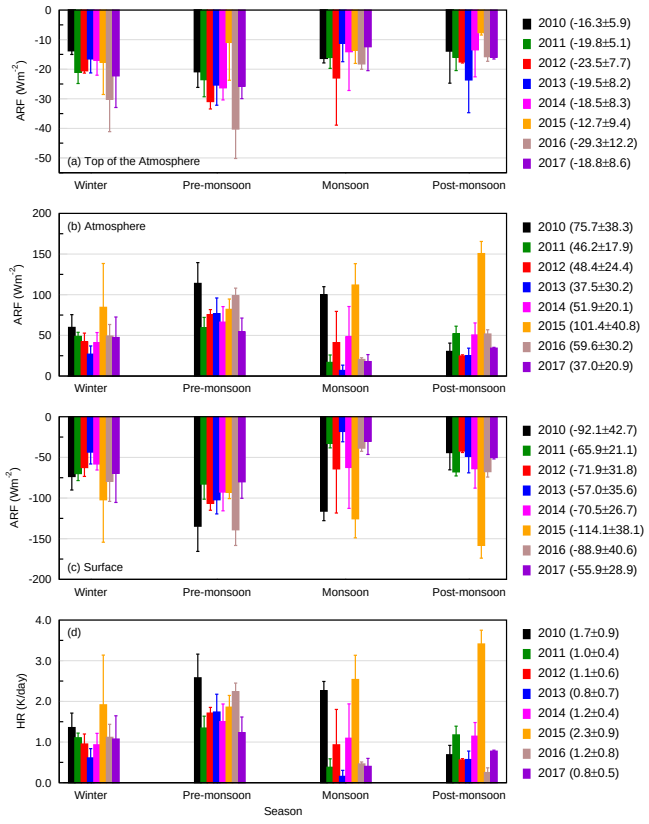

Figure 7: The observed seasonal aerosol radiative forcing (ARF) over Pokhara Valley from winter to post-monsoon for each year during 2010-17 (a) at the top of the atmosphere, (b) in the atmosphere, and (c) at the surface of the earth. (d) Seasonal mean atmospheric solar heating rate (HR) estimated using the aerosol radiative forcing (Wm^{-2}) in the atmosphere (ARFATM). The numbers on the right hand side of each panel are the annual average and standard deviation for each year.

The aerosol radiative forcing efficiency (ARFE) at the surface, top of the atmosphere (TOA) and the atmosphere followed a similar pattern as that of ARF. High values of ARFE at SFC, TOA and ATM (except during monsoon when values are slightly lower) suggest that aerosols are efficient in significantly modulating the incoming solar flux throughout the year. The annual average aerosol-induced atmospheric heating rate (HR) over Pokhara was nearly 1 K day^{-1} every year during 8-year observation, and was highest in 2015 ($\sim$2.5 K day^{-1}) (Figure 7). In comparison, the HR was about 1 K day^{-1} or more over all the locations in IGP during the year. These quantitative results can be used as inputs in global/regional climate models to assess the climate impact of aerosols, including on regional temperature, hydrological cycle and melting of glaciers and snowfields in the region.

This work was done in collaboration with Maheswar Rupakheti, Institute for Advanced Sustainability Studies, Potsdam, Germany.

doi : https://doi.org/10.1016/j.envpol.2020.114799

(S. Ramachandran)

Aerosol characteristics and radiative effects in South Asian pollution outflow over a background site

Aerosol characteristics and radiative effects using recently available high-quality columnar aerosol data collected at several AERONET sites in South Asia, with a focus on pollution outflow from continental South Asia observed over Hanimaadhoo in Maldives, a small island in northern Indian Ocean were quantified. The seasonal average aerosol optical depth (AOD) over Hanimaadhoo was $\geq$0.3 (except ca. 0.2 during monsoon season), and single scattering albedo (SSA) is $>$0.90 in all seasons (Figure 8).

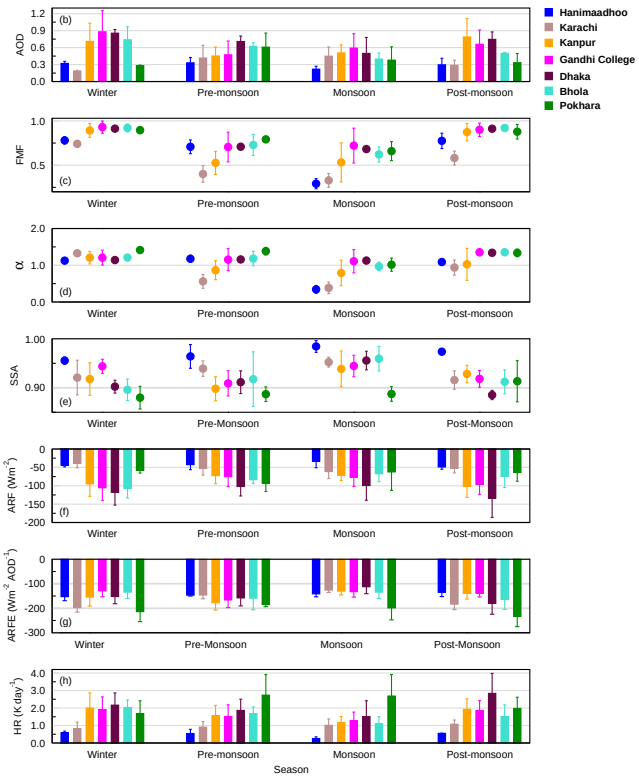

Figure 8: Seasonal mean aerosol characteristics: (b) AOD, (c) FMF, (d) α and (e) SSA obtained over Hanimaadhoo in comparison on a regional scale with other locations across the Indo-Gangetic Plain (IGP), a major source region for aerosols over Hanimaadhoo. (f) Aerosol radiative forcing (ARF), (g) efficiency (ARFE) and (h) atmospheric solar heating rate (HR) are also plotted. Vertical bars correspond to $\pm 1\sigma$ (standard deviation) from the mean.

Fine mode aerosols contribute dominantly to AOD. SSA decreases as a function of wavelength due to influence of continental aerosols, except during monsoon when its spectral trend reverses due to increase in dust. Carbonaceous aerosols dominate ($>$90%) contribution to absorption AOD (AAOD). Black carbon (BC) and brown carbon (BrC) contribute $>$75% and $<$25%, respectively, to AAOD due to carbonaceous aerosols. The observed seasonal aerosol

radiative forcing (ARF) at surface (ARF_{SFC}), at top of atmosphere (ARF_{TOA}) and in atmosphere (ARF_{ATM}) was >-25 Wm^{-2}, >-20 Wm^{-2} and ∼+20 Wm^{-2}, respectively (Figure 8). Aerosol loading and atmospheric warming have increased over this background site over the last decade. A regional-scale analysis of aerosol properties and radiative effects across and surrounding the Indo-Gangetic Plain (IGP) showed that AOD was ≥0.3 over entire region, and aerosols reduce seasonally 30-50 Wm^{-2} of solar radiation reaching the surface, contributing significantly to solar dimming effect. Such high regional values of ARF, $ARFE_{SFC}$ and HR, and increasing trends have significant implications to climate and hydrological cycle over South Asia and beyond.

This work was done in collaboration with Maheswar Rupakheti, Institute for Advanced Sustainability Studies, Potsdam, Germany.

doi : https://doi.org/10.1016/j.atmosenv.2020.117813

(S. Ramachandran)

Widespread enhancement in fine particulate matter over the Indo-Gangetic Plain towards winter

Fine particulate matter ($PM_{2.5}$) influences the visibility, climate, and air quality. The Indo-Gangetic Plain (IGP) region, home to about one-seventh of the world's population, experiences strongly enhanced $PM_{2.5}$ pollution every post-monsoon and winter. We performed high-resolution modelling to unravel the role of dynamics and regional emissions over this region. Model, in agreement with measurements, shows that the $PM_{2.5}$ distribution having patches of enhanced concentrations (≥100 μgm^{-3}) during post-monsoon, evolves dramatically into widespread enhancement across IGP during winter (Figure 9).

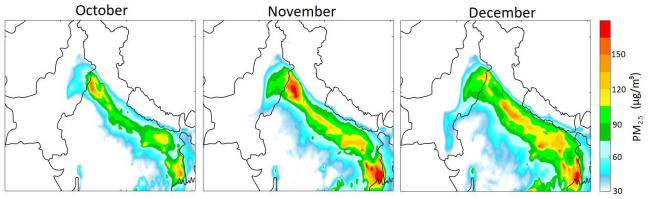

Figure 9: Mean distribution of $PM_{2.5}$ over the northern Indian region during October, November, and December 2016, as simulated by the WRF-Chem model.

Sensitivity simulation and satellite-based measurements revealed a dominant role of biomass-burning over northwest IGP during post-monsoon. Whereas, in contrast, towards winter, a large-scale decline in temperature, shallow atmospheric boundary layer, and weaker winds drastically reduced ventilation confining anthropogenic influences near the surface. The study highlights a west-east gradient in terms of sources, with western IGP dominated by biomass-burning and eastern IGP dominated by anthropogenic sources in post-monsoon. This gradient weakens in winter when entire IGP is dominated by anthropogenic sources. We argue that a generic emission reduction policy will not yield desired results, and advocate for a season-based source-focused policy taking unfavourable atmospheric dynamics into account, to minimize the air quality and climate impacts.

This work is done in collaboration with A. Sharma, S. Gunthe of IIT Madras, M. Kumar, A. Pozzer of MPI-Chemistry, Germany, I. Girach of SPL Trivandrum, N. Singh of ARIES Nainital, T. U. Ansari of Lancaster University, UK.

doi : https://doi.org/10.1038/s41598-020-62710-8

(Narendra Ojha and Som Kumar Sharma)

Impact of COVID-19 lockdown on ozone build up over Ahmedabad

COVID-19 lockdown created a rare opportunity to study the air quality responses to dramatic reduction in man-made emissions. In contrast with the precursor species, the build-up of ozone has been observed to be enhanced by ∼39% over Ahmedabad.

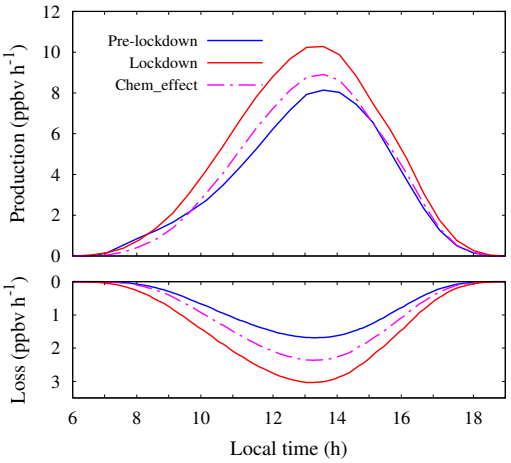

Figure 10: Model derived production and loss rates of ozone for pre-lockdown and lockdown conditions. Chem_effect is an additional simulation with chemical inputs of lockdown but meteorological inputs of pre-lockdown.

To explain this observation, we incorporated the measurements of chemical species and prescribed environmental conditions of this region into a photochemical box model (NCAR Master Mechanism). Model, in a good agreement with measurements, reproduced the observed ozone enhancement during the lockdown. Sensitivity simulations unravelled that the ozone enhancement was contributed by both the non-linear chemistry (by ∼25%) as well as the changes in meteorological conditions (by ∼16%). We estimated that the net ozone production rate was higher by up to 1.2 ppbv h^{-1} during the lockdown as compared to the pre-lockdown (Figure 10). Our analyses highlight that the lockdown impacts can be modulated profoundly by the complex chemistry plus meteorological changes, offsetting the benefits of lower precursor levels in the context of ozone pollution. The findings could prove valuable in planning strategies to curb ozone pollution in future by considering the effects of chemistry and meteorological variations in this semi-arid urban environment.

This work is done in collaboration with I. Girach of Space Physics Laboratory, Trivandrum.

doi : https://doi.org/10.18520/cs/v120/i2/376-381

(Meghna Soni and Narendra Ojha)

Elevated levels of biogenic non-methane hydrocarbons in the marine boundary layer of the Arabian Sea during the inter-monsoon

Ocean surface acts as a source or sink for several trace gases including N_2O, CH_4, CO, and volatile organic compounds (VOCs). Among these gases, VOCs have profound effects in the marine atmosphere as their air-sea exchange can significantly influence the composition and chemistry of the marine atmosphere. The Arabian Sea is one of the most biologically productive ocean regimes, and hence possesses a perennially intense oxygen minimum zone. High productive oceans can potentially modify the production and sea-to-air exchange of trace gases including VOCs (Figure 11).

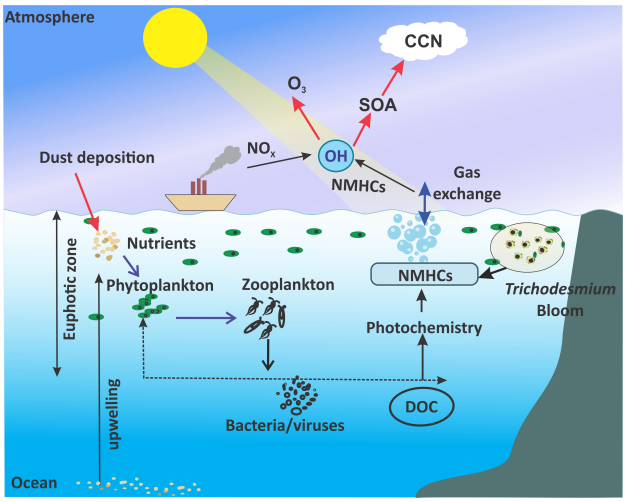

Figure 11: Emission from phytoplankton and dissolved organic carbon (DOC) present in seawater is an important natural source of many non-methane hydrocarbons (NMHCs) in the marine boundary layer (MBL).

We measured non-methane hydrocarbons (NMHCs) in the marine air and characterized the phytoplankton species in seawater of the Arabian Sea during the pre-monsoon season of the year 2017. The light alkenes namely ethene and propene were the dominant VOCs in the marine air with average mixing ratios of 8.92$\pm$3.5 and 3.38$\pm$1.3 ppbv, respectively. The high levels of alkenes were associated with the higher abundances of *Trichodesmium* and *Thalassiosira* species. We have calculated the emission fluxes of ethene using "top-down" and "bottom up" approaches and found the large discrepancies using these two methods. In the bottom-up approach, among the several sources of uncertainty, the major cause of lower fluxes (one order of magnitude) than those estimated using the top-down approach could be the emissions of alkenes from the sea surface microlayer. The estimated emission flux of ethene using "bottom-up" approach (2.0-6.9$\times10^9$ molecules cm^{-2} s^{-1}) was higher than those reported for several other oceanic regions. Such high emission rates of NMHCs in remote regions can significantly affect the regional tropospheric oxidation chemistry. Several studies reported that the emission of NOx from shipping over the northern Indian Ocean has increased significantly during last two decades. In the presence of NOx, VOCs act as an important source of atmospheric pollutant such as ozone, secondary organic aerosol and peroxy-acetyl nitrate. Our observations highlight the need to evaluate the biogeochemical processes controlling the oceanic emissions of NMHCs over the northern Indian Ocean.

This work is done in collaboration with Ravi Yadav from Indian Institute of Tropical Meteorology (IITM), Pune and Meenu P. from CSIR-National Institute of Oceanography, Regional Centre, Kochi.

doi : https://doi.org/10.1029/2020JD032869

(Nidhi Tripathi, L. K. Sahu, Arvind Singh, Anil Patel and Kashyap Patel)

Emissions and atmospheric concentrations of α-pinene at an urban site of India: Role of changes in meteorology

The measurements of a monoterpenes (mainly α-pinene) were performed by the PTR-TOF-MS instrument at an urban site of India from mid-January to March 2014.

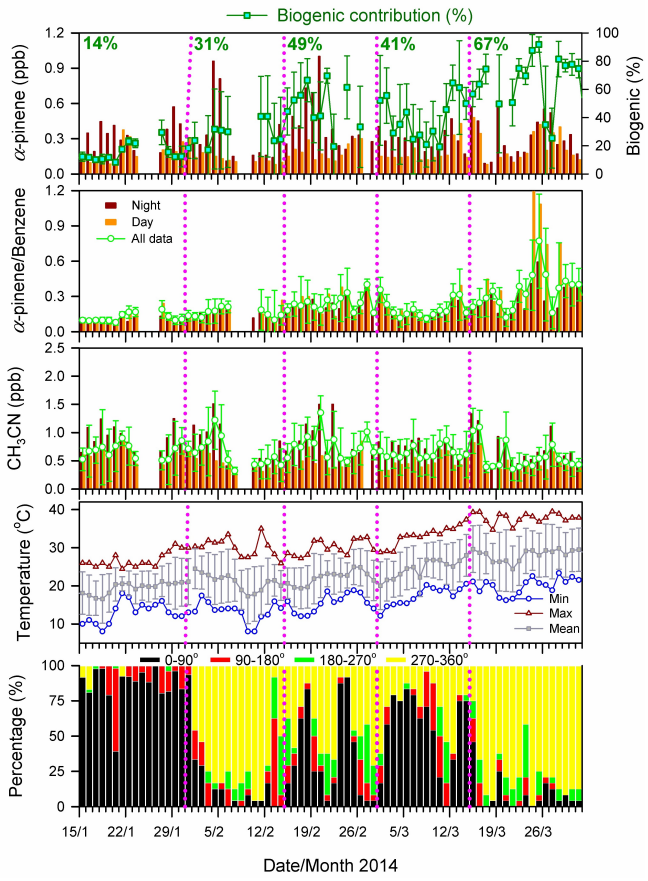

Figure 12: The time series of α-pinene, α-pinene/benzene ratio (ppb ppb^{-1}), CH_3CN, biogenic contribution, daily air temperatures (minimum, maximum and mean), and percentage occurrence of winds from the different sectors.

The daytime concentration increased from 0.15 ppb in the second-half of January to 0.40 ppb in the second-half of March. Both the nighttime and daytime ratios of α-pinene/benzene in the second-half of March were 2-3 times higher their respective values from mid-January to first-half of February. The ratios of α-pinene/benzene increased from $\sim$0.27 ppb ppb^{-1} at lower temperatures to $\sim$0.51 ppb ppb^{-1} at higher temperatures indicating the increase of biogenic emissions in March. The concentration of α-pinene exhibited exponential decline with wind speed, but the rate of decrease in

February was about twice that for March. The nighttime ratios of α-pinene/isoprene were greater than those measured in the daytime, suggesting temperature-dependent biogenic emissions of α-pinene. From mid-January to March, the increase of $\sim$53% in the biogenic contributions of α-pinene were associated with the change in meteorological conditions (Figure 12). Our analysis suggests that the combined effect of the northwest wind flow and higher air temperatures in March favored the emissions of BVOCs from local vegetation. The exceptionally high concentrations of α-pinene up to 6 ppb were measured during the Holi bonfire festival. This is the first study reporting the change in α-pinene during winter-summer transition over India. In the urban regions of developing countries, high emissions of BVOCs from vegetation and of NOx from anthropogenic sources can act as a source of ozone.

doi : https://doi.org/10.1016/j.chemosphere.2020.127071

(Nidhi Tripathi and L. K. Sahu)

Emissions of non-methane volatile organic compounds from a landfill site in a major city of India: Impact on local air quality

The concentrations of C_2-C_8 NMVOCs were measured at 21 different sites in the downwind of the largest landfill (Pirana) in Ahmedabad city during a pre-monsoon month of year 2017.

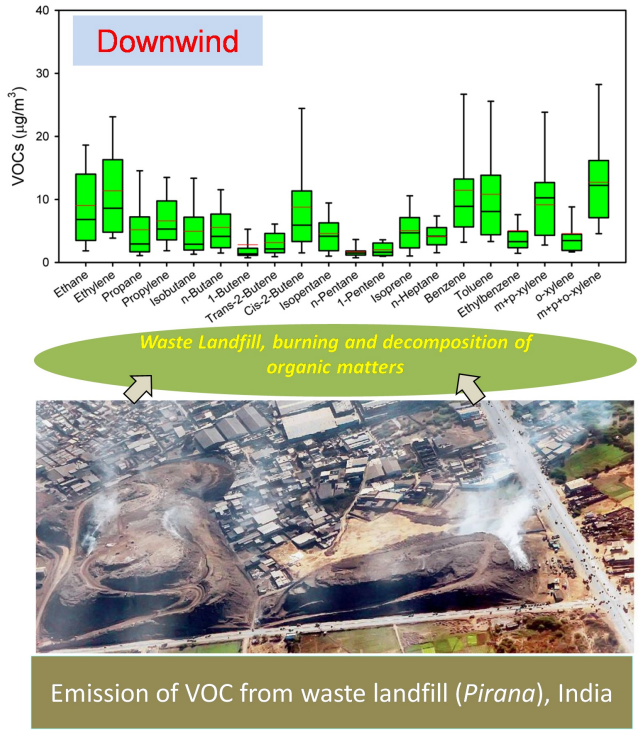

Figure 13: Emissions of non-methane volatile organic compounds (NMVOCs) from the largest landfill of Pirana in the western India located in Ahmedabad city. The measurements of various NMVOCs were conducted in the downwind regions during the pre-monsoon season to characterize the emissions and their impact on air quality.

The residential areas were the major receptors because of predominant NW and SW wind flows during the study period. The concentrations of almost all NMVOCs measured at nearby sites within 800 m from the landfill were higher than their concentrations at the greater distances. The concentrations of all NMVOCs show substantial variations with the distance from the landfill site (Figure 13). The values of the total BTEX (ΣBTEX) in the upwind regions were 18-84% higher than the mean value measured at the upwind sites. The meteorological parameters and inferences of other sources played an important role in varying influences of the landfill emissions. The relative abundances of NMVOCs did not change much with the distance. Alkane and aromatic compounds made the major contributions to ambient concentrations. The contributions of biogenic emission from the decomposition of the landfill organic materials at nearby sites were higher than those at far downwind sites. Although air sampling covered the distances of up to $\sim$2.5 km, the impact of landfill emissions in the downwind regions covering greater distances were simulated using the dispersion model. Among NMVOCs, cis-2-Butene, m+p-xylenes, propylene/ethylene, and trans-2-Butene explain $\sim$75% of the total Prop-Equiv concentrations. In the OFP scale, except for ethylene and isoprene, VOCs show similar relative contributions to those of Propy–Equiv concentrations. In reality, in addition to the values of Propy–Equiv concentration/OFP of ambient VOCs, the concentrations of NOx are important in controlling the ozone level. In the past few decades, application of proton transfer reaction- mass spectrometry (PTR-MS) technique has gained popularity for the real-time measurements of many VOCs at low concentrations. Our future studies will involve a comprehensive measurement of NMVOCs using PTR-ToF-MS in different seasons.

This work is done in collaboration with Pragnesh N. Dave from Sardar Patel University, Vallabh Vidyanagar, Samiksha Bajaj from Amity University, Noida and Ravi Yadav from Indian Institute of Tropical Meteorology (IITM), Pune.

doi : https://doi.org/10.1016/j.heliyon.2020.e04537

(L. K. Sahu, Nidhi Tripathi and Kashyap Patel)

Aromatic compounds in a semi-urban site of western India: Seasonal variability and emission ratios

Ambient concentrations of benzene, toluene, and CO were measured at a semi-urban site of Udaipur in western India during the year 2015. Monthly mixing ratios of benzene, toluene, and CO were in the ranges of 0.58-1.18, 0.62-1.48, and 218-548 ppbv, respectively. In wintertime, the higher concentrations of aromatic VOCs and CO were due to shallower boundary layer depths and transport from polluted Indo-Gangetic Plain. The Δtoluene/Δbenzene slope of 1.18$\pm$0.41 ppb ppb^{-1} characterizes vehicle exhaust emissions. The higher values of Δtoluene/Δbenzene in May coincided with the higher ambient temperatures (average $\sim$35°C) indicating emissions from evaporative sources. The emission ratios of Δbenzene/ΔCO (1.82$\pm$0.47 ppb ppm^{-1}) and Δtoluene/ΔCO (2.2$\pm$0.72 ppb ppm^{-1}) in the winter season are comparable to those for several urban regions of the world. The ozone formation potential and propylene-equivalent concentration of aromatics were lower than those of alkanes and alkenes measured during the same study period. Ethane (4.4$\pm$3 ppbv), propane (3.4$\pm$2 ppbv), and *n*-Butane (3.9$\pm$2 ppbv), ethene (5.8$\pm$3 ppbv), and propene (1.6$\pm$1 ppbv) were the dominant alkane and alkene compounds measured during the study period. The

composition of non-methane volatile organic compounds shows small change with the photochemical age suggesting the contributions of several other sources in addition to vehicular exhaust. The positive matrix factorization analysis suggests relatively high loadings of benzene (∼30%), toluene (45%), and CO (32%), respectively from vehicle exhaust. The study highlights major contributions of vehicle exhaust, but emissions from other sources such as biomass burning, industries, evaporative loss, and biogenic are also significant (Figure 14).

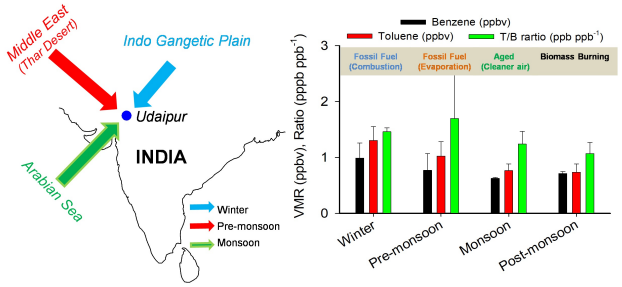

Figure 14: Measurement site in Udaipur city in western India is influenced by the winds from NE in the winter, NW in the pre-monsoon and SW in the monsoon season. The seasonal comparison of mean mixing ratios of aromatic VOCs and toluene to benzene (T/B) ratio indicate predominance of air masses influenced by different emission sources.

This work is done in collaboration with Ravi Yadav from Indian Institute of Tropical Meteorology (IITM), Pune.

doi : https://doi.org/10.1016/j.atmosres.2020.105114

(L. K. Sahu and Nidhi Tripathi)

Observations of Trace Gases in Earth's Lower Atmosphere: Instrumentation and Platform

The earth's atmosphere is a complex mixture of many gases and their observations are incorporated in chemistry-climate models. Atmospheric observations have been the backbone of recent progress in atmospheric science, particularly about our understanding of the sun-atmosphere interaction causing chemical and radiative forcing linked to the environment and climate change. In terms of technology, there has been significant progress in both in-situ and remote sensing measurements of various variables in the lower atmosphere. Among many variables, trace gases play important role in climate change and several environmental problems. The recent progress in both in-situ and remote sensing based instrumentations has enabled the researchers to investigate various atmospheric processes in great detail. For example, Gas chromatography (GC) based instrumentation provides the detection from simple to complex species present in the atmosphere at very low concentrations. The laser-based spectroscopic instruments are emerging tools for fast response measurements of trace gases, which are important to understand rather short-term processes. The proton transfer reaction-mass spectrometry (PTR-MS) is regarded as one of the great technologies for the detection of numerous but specific types of trace gases namely volatile organic compounds (VOCs). However, there are advantages and disadvantages of any instrument in terms of quality of data, comprehensiveness, and cost. In this paper, we have discussed the recent progress in instrumentation used for the measurements of trace gases in the lower atmosphere using space, aircraft and satellite based platforms as well as some laboratory techniques (Figure 15). We have also briefly highlighted the progress during the past couple of decades, present status, and future scenarios of trace gas measurements in the South Asia region.

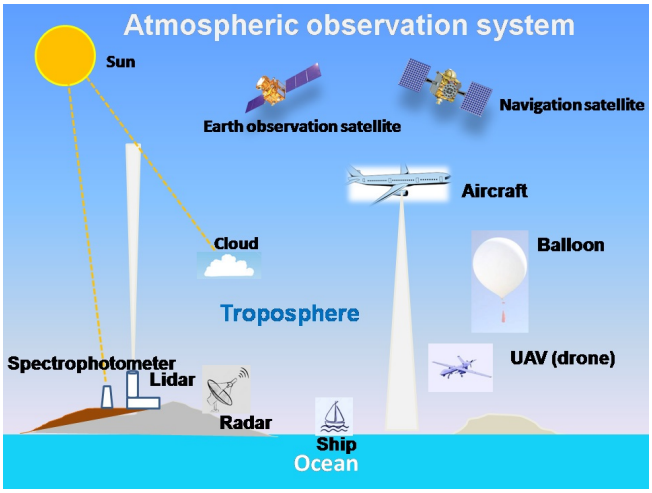

Figure 15: A pictorial representation of the atmospheric observation system consists of a multitude of individual surface-, air-, and space-based instruments used for the in-situ and remote sensing measurements of trace gases in the lower atmosphere. The integrated national and international strategies will be necessary to make comprehensive measurements of trace gases in the Earth's lower atmosphere.

This work is done in collaboration with. Ravi Yadav from Indian Institute of Tropical Meteorology (IITM), Pune.

doi : https://wwwops.currentscience.ac.in/Volumes/118/12/1893.pdf

(L. K. Sahu and Nidhi Tripathi)

Mixing ratios of SO_2 and NO_2 in tropical rural environment

Sulphur dioxide is a toxic pollutant in the atmosphere emitted from natural sources and human activities. We analysed the surface mixing-ratio of SO_2 and NO_2 measured over the time period from January 2010 to April 2012 at Gadanki, in Andhra Pradesh and found that SO_2 and NO_2 mixing-ratio are very low over this region. However, during January to May relatively higher concentrations of SO_2 are observed, mainly coming from power plants located in southern and eastern India as indicated by higher SO_2/NO_2 ratios of greater than 0.5. In one instance, on June 20th, 2011, it is found that the OMI SO_2 value was a factor of 13 higher than 2011 annual mean. Using the FLEXible PARTicle dispersion model (FLEXPART) and satellite data, it is found that the observed higher SO_2 value on 20^{th} June was due to intercontinental transport of SO_2 from Nabro volcanic eruption. Using the FLEXPART model with ECLIPSE-v5 emission inventory, the observed seasonal variation of SO_2 could be well reproduced; however, the mixing ratios are found to be overestimated, possibly due to incorrect vertical profile used in the model.

This work was done in collaboration with A. Jayaraman of Bangalore University, Benguluru and S. V. B. Rao Ritesh of Sri Venkateswara University, Tirupati.

doi : https://doi.org/10.1007/s12040-020-1366-4

(K. Renuka, Harish Gadhavi and Shyam Lal)

Aerosol size distribution in rural environment and implications for cloud droplet formation

Aerosol number size distributions in the diameter range of 5 nm-34 μm were measured in tropical southern India during the transition season from May (pre-monsoon) to June-July (monsoon). Averaged over the entire measurement period, the particle number size distributions were bimodal with a total particle number concentration of $N_{tot} = (4.5 \pm 2.7) \times 10^3$ cm^{-3} (arithmetic mean $\pm$ standard deviation). The ratio of Aitken to accumulation mode particle number concentrations (N_{ait}/N_{acc}) ranged from 1.06 to 2.07, increasing from May to June-July due to a pronounced decrease in the accumulation mode particles with the onset of the monsoon. Cloud condensation nuclei concentrations at 0.4% supersaturation ($CCN_{0.4}$) were calculated under the assumption of an average continental hygroscopicity parameter of $\kappa = 0.3$. The calculated $CCN_{0.4}$ concentrations are mostly sensitive to variations in N_{acc} and vary accordingly between the May and June-July. Using a cloud parcel model, we investigated the formation of cloud droplets using the measured average particle number size distributions, updraft velocities up to 20 ms^{-1}, and initial aerosol particle number concentrations up to 25,000 cm^{-3}. We found different regimes of CCN activation and cloud formation for the month of May (shifting from aerosol-limited regime to transitional regime) and for June-July (transitional regime), which was primarily due to the variability of particle number concentrations in the accumulation mode.

This work was done in collaboration with S. S. Gunthe, Ravikrishna, S. Shika, and M. N. S. Sai Suman of IIT Madras.

doi : https://doi.org/10.1007/s42452-020-2804-2

(Harish Gadhavi)

Can Quasi-Periodic Gravity Waves Influence the Shape of Ice Crystals in Cirrus Clouds?

The study of gravity waves and their impact on the microphysical changes in cirrus clouds over the subtropical Indian region using Raman lidar, satellite, model simulations, and reanalysis data sets has been done. It is found that the cirrus clouds are formed from the convective outflow of large-scale convergence zone extending from south-west to north-east Indian region. These clouds are modulated by the upward propagating gravity waves with time periods ~40 min (at ~8.0-8.5 km) and ~20 min (at ~9.0-9.5 km) over the Raman lidar observational site as shown in Figure 16. The wave-induced enhancement of moisture leads to supersaturation, thereby controlling the ice crystals' size and shape through depositional freezing. The ice crystals size increases and they transform to irregular shapes in the presence of wave activity. Therefore, the present work is unique and will have implications toward the uncertainties associated with cirrus clouds in both regional and global climate models.

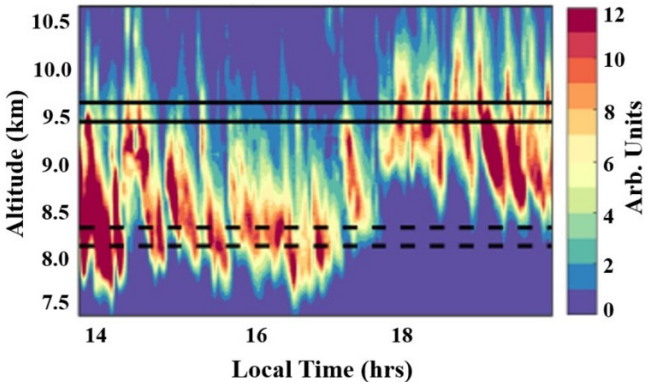

Figure 16: Modulation of Cirrus cloud patch (7.5-10.5km) by quasi-periodic gravity waves observed in range corrected signals (RCS) obtained at 532-nm using Raman Lidar. Horizontal lines (Dashed and solid) represent the regions of noticeable wave activity. (Sourita et al., GRL 2020. Doi:10.1029/2020GL087909)

This work was done in collaboration with Kumar, P., (SAC, ISRO, Ahmedabad) and Kumar, K. N., (NCMRWF, Noida, U.P.).

doi : https://doi.org/10.1029/2020GL087909

(Sourita Saha and Som Sharma)

Environmental impacts of fireworks on aerosol characteristics and radiative properties over a mega city, India

Present study investigates the variations in aerosol characteristics, concentrations, and radiative properties due to the burning of firecrackers during the Diwali festival event followed by New year festival celebrations over a representative urban environment. A six day's long intensive in situ measurements of Black Carbon (BC), Particulate Matter (PM), and Aerosol Optical Depth (AOD) were collected to capture pre to post-Diwali and New Year festival celebrations marked with massive fireworks. We observed an increase of 286%, 89.5%, and 60.5% in BC, PM10, and PM2.5 concentrations, respectively, on the festival night as compared to pre-event days. An increase in in-situ measured AOD is comparable with concurrent satellite-derived AOD. Angstrom exponent, $\alpha > 1.0$ along with high turbidity coefficient; β estimated for the festival period clearly implies the abundance of fine-mode particles, probably the smoke aerosols loading from fireworks. The Mie-scattered return signals received by the ground-based Raman LiDAR at 532 nm showed an increased concentration of 'anthropogenic aerosols', attributed to the increased cracker's activity. Space-based CALIPSO LiDAR observations also validate the presence of 'polluted dust' and 'smoke' types of aerosols at the near-surface to 5 km altitude over the study area. A sharp increase in gaseous air pollutants like SO_2 and NOx concentrations exceeding the National Ambient Air Quality Standards is also observed. The COART model run simulations in the SWIR region showed an increased 'cooling' at the surface (-125 Wm^{-2} to -185Wm^{-2}) as compared to 'warming' in the atmosphere during the event period.

A maximum heating rate (1.9 Kday^{-1}) due to total aerosol radiative forcing is also estimated. These investigations provide useful insights into the impact of burning firecrackers on urban air quality besides radiative impacts at a regional scale. Such celebration-induced air pollution events may lead to severe health impacts, particularly respiratory and cardiovascular ailments in the resident population.

This work was done in collaboration with Chhabra, A. (SAC, ISRO), Turakhia, T. and Iyer, R. (St. Xavier's College, Ahmedabad) and Chauhan, P. (IIRS, ISRO), Dehradun.

doi : https://doi.org/10.1016/j.cacint.2020.100049

(Som Sharma and Sourita Saha)

Effects of solar flux versus compositional variation on the variability of daytime oxygen optical emission rates over low- and mid-latitudes

Daytime oxygen airglow emission rate variability provides us with a means of remote investigations of the upper atmospheric behavior.

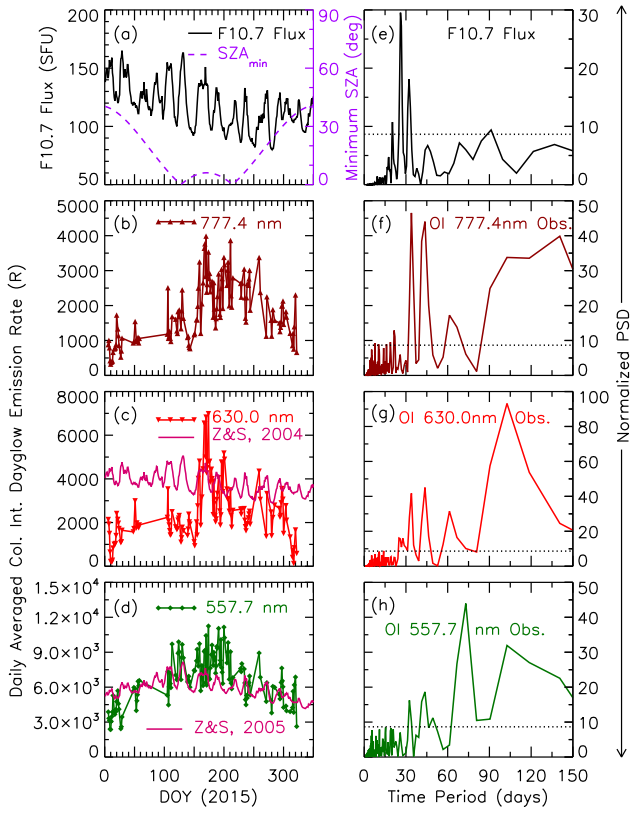

Figure 17 (a): The solar F10.7 cm flux in solar flux units (SFU) (dark solid line) along with the lowest value of solar zenith angle, SZAmin, for a given day (dashed blue line) for the observational location, Hyderabad as a function of the day of the year (DOY). (b)-(d) Daily averaged dayglow emission rates at all the three wavelengths. The plots (c, d) also show the peak empirical dayglow emission rates (pink line) as given by the empirical model. (e-h): Results of spectral analyses showing similar periodicities (e) in solar flux and (f-h) three OI dayglow emission rates obtained over Hyderabad.

Dayglow emission rates typically show a diurnal pattern with a peak at around noon, especially during geomagnetic quiet conditions. The photochemical and empirical models show that the emission rates typically vary as a function of solar zenith angle (SZA) and solar flux. Thus, both, larger solar flux magnitudes and smaller solar zenith angles, contribute to larger dayglow emission rates as the yield of excited oxygen atoms is expected to be greater in those conditions. However, variability in the annual dayglow emission rates obtained from measurements at low-latitudes (Hyderabad, India; 17°N, 80°E; 8.7°N Mag. Lat.) and mid- latitudes (Boston, USA; 42.2°N, 71°W; 48.3°N Mag. Lat.) show different behavior with regard to solar flux variation. The variability in the low-latitude dayglow emission rates at OI 777.4 nm, OI 630.0 nm and OI 557.7 nm is primarily dependent on the variations in the solar flux (Figure-17). However, such primary dependence on the solar flux is not reflected on the emission rate variability seen over mid-latitudes. This discrepancy is understood to be due to the relative effects of solar flux and the globally changing compositional variability, characterized by the oxygen to molecular density ratios (O/N_2), that show varying behavior from mid- to low-latitudes. Seasonal compositional variation due to transport processes is attributed to be the cause for the observed discrepancy which is also confirmed by independent satellite measurements. An empirical model of O/N_2 as a function of day of the year and latitude obtained using satellite based ultraviolet measurements to quantify the compositional variation.

This work was done in collaboration with former PRL students D. K. Karan, F. I. Laskar, who are now at Laboratory for Atmospheric and Space Physics, University of Colorado, CO, USA, T. Vijayalakshmi, at JNTU, Hyderabad and S. Chakrabarti at Univ. of Massachusetts, Lowell, USA.

doi : https://doi.org/10.1016/j.jastp.2020.105293

(D. Pallamraju)

Effects of solar flux variation on the neutral wave dynamics over low and equatorial latitudes

Gravity waves play an important role in the redistribution of energy and momentum in the atmosphere. As they propagate, they manifest as wave-like fluctuations in both neutrals and plasmas. Therefore, by monitoring such fluctuations, information on the wave characteristics in the thermosphere can be derived. Present investigations have been carried out using the innovative method of deriving vertical propagation characteristics of gravity waves that has been evolved at in PRL. It is found that the wave propagation characteristics depend on the atmospheric background conditions. Variation in the solar flux (characterized by F10.7 cm flux index) directly alters the thermospheric conditions, which, in turn, affects the prevailing atmospheric dynamics. Correspondingly, variation in the vertical propagation speeds of these gravity waves has been found to be similar to the changes in F10.7 cm flux, as can be seen in Figure 18(a). In order to quantify these similarities, 20-day averaged values of vertical phase speeds and F10.7 cm solar flux have been considered taking into account the thermospheric lethargy of ∼20 days, which seem to be correlated as seen in Figure-18(b). Linear relation has been established between the two, which can be used in global scale modelling of thermospheric wave dynamics.

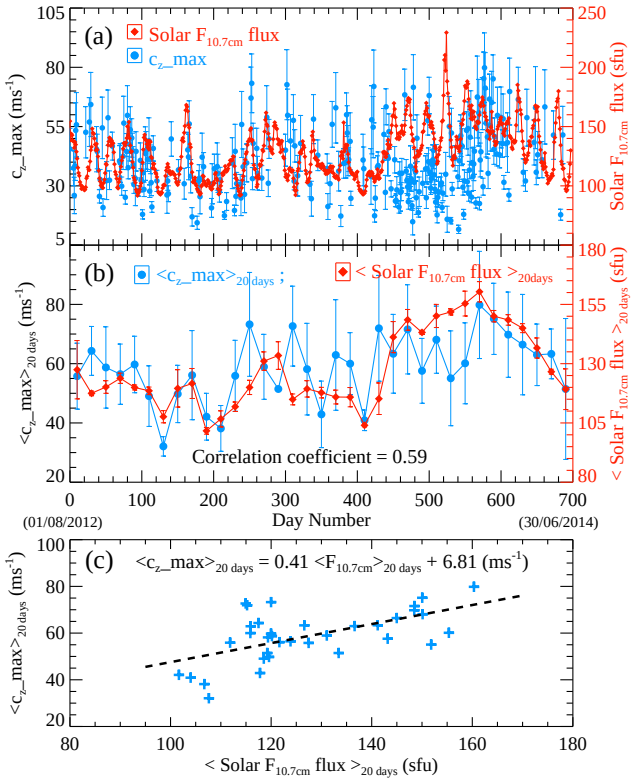

Figure 18: a) Distribution of daily maximum values of vertical phase propagation speeds (cz) (cyan colored circles) along with variation in Solar F10.7cm flux (red colored diamonds). (b) Maximum values of cz over 20 days window (cyan colored curve with circles) and 20-day averaged values of the Solar F10.7cm flux (red colored curve with diamonds). (c) Maximum cz in every 20 day window is plotted as a function of 20- day averaged values of Solar F10.7cm flux. The least- square fit between these two is shown as a dashed line.

doi : https://doi.org/10.1016/j.jastp.2020.105414

(Subir Mandal, D. Pallamraju, and P. Suryawanshi)

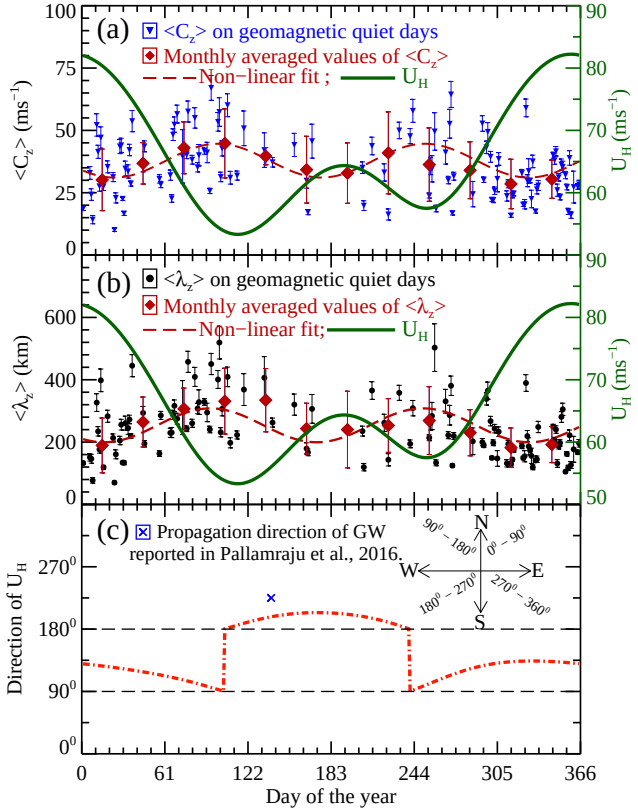

Figure 19: (a) Quiet time seasonal variability in daily vertical phase speeds (<cz>) of GWs are shown as filled inverted triangle, which shows two maxima annually. Filled diamonds represent monthly averaged values (<cz monthly>) along with their standard deviations. The dashed curve represents non-linear fit that represents variations in monthly averaged values. The solid curve represents noon-time resultant horizontal wind over Ahmedabad. (b) Same as in (a) but for the <λz>. (c) Directions of propagations of noon-time resultant horizontal winds (UH) over Ahmedabad are shown as a dash-dotted curve. Horizontal dashed lines are drawn for angles of 90° and 180°. Winds are either north- westward or south-westward, depending on the direction of meridional winds. Blue-coloured cross represents an earlier reported propagation direction of GW in the daytime obtained using large field-of-view optical measurements.

Evidence of high to low latitude coupling in the neutral wave dynamics during geomagnetic storms

The variation in the vertical propagation characteristics of gravity waves, both during geomagnetically quiet and disturbed conditions, are investigated. During geomagnetically quiet times, the vertical propagation speeds and scale sizes have been found to be anti-correlated with modelled thermospheric neutral winds with two peaks annually, one each in the equinoxes (Figure-19). Such anti-correlation indicates that over Ahmedabad the thermospheric gravity waves propagate mostly in the westward direction. Non-linear fit has been arrived at to characterize the seasonal variation of gravity waves over low- and equatorial-latitudes. Also, it has been observed that during geomagnetic storms, these gravity wave parameters are different from those observed during quiet times. The differences in their values indicate a response to the extra energy that becomes available in the high-latitudes during geomagnetic storms. During geomagnetically storms, high energy particles precipitate in the auroral regions. During such events, the magnitudes of currents increase which causes Joule heating at the high-latitudes.

Auroral electrojet index (AE) is a proxy of the heat generated at the auroral regions. Further, these differences in the gravity wave parameters during geomagnetically disturbed times have been found to be excellently correlated with the integrated values of the auroral electrojet (AE) indices of 28 h prior to the observation of vertical propagation of gravity waves (as can be seen in Figure 20).

Thus, we have obtained a direct evidence of neutral wave coupling between high- to low-latitudes, hitherto not reported earlier. Based on such results, linear relation has been derived between the two, using which one can estimate the changes in the vertical speeds of gravity waves during geomagnetically disturbed times.

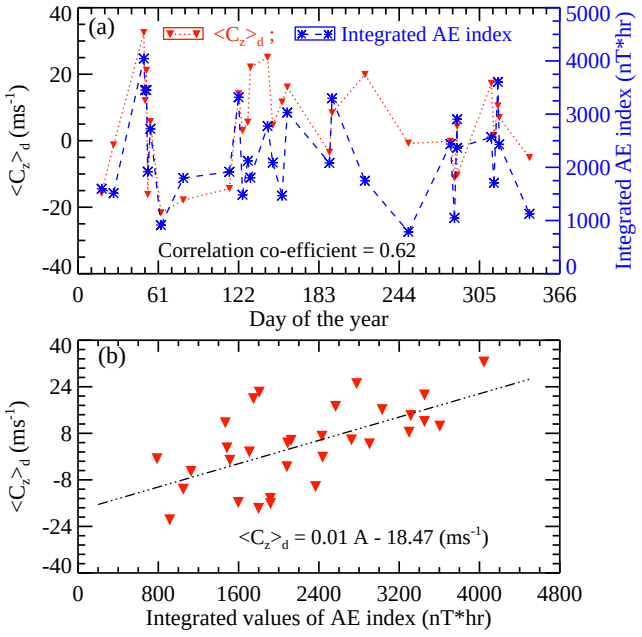

Figure 20: (a) <cz>d values of 31 (out of 40) days of geomagnetic disturbed conditions are shown (red-coloured inverted triangles). Values of the AE index integrated over 4 h around the peak value of the AE index of past 28 h with respect to 14 LT on the day of observation for those days are shown (blue-coloured asterisks). (b) Scatter plot between <cz>d and integrated AE index values showing a linear relationship (dash-dotted line).

doi : https://doi.org/10.1016/j.jastp.2020.105470

(S. Mandal and D. Pallamraju)

Signature of the 27-day oscillation in the MLT tides and its relation with solar radiation at low latitudes

The modulation of the dominant atmospheric tides, (i.e. diurnal, semidiurnal and terdiurnal) in the mesosphere and lower thermosphere (MLT) is investigated using long-term meteor wind database from three Southern hemispheric low-latitude locations, São João do Cariri (7.4°S, 36.5°W), Cachoeira Paulista (22.7°S, 45°W) and Santa Maria (29.7°S, 53.7°W). The spectral analysis reveals an evident and intermittent signature of a 27-day oscillation in the tidal amplitudes. Relationship between the 27-day tidal modulation in the MLT and solar rotation is looked into utilizing solar UV flux (Lyman-α) that indicates a conspicuous linkage of the tides with the solar short-term variability. The strong correlation between the solar variability and tidal modulation in the concerned period with positive lags at certain intervals may indicate predominate solar influence on the MLT tides. Potential involvement of the lower, middle and upper atmospheric dynamics and chemistry to support the observed oscillation feature is deemed plausible (Figure 21).

The research work was done in collaboration with P. P. Batista, National Institute for Space Research, São José dos Campos, São Paulo, Brazil, R. A. Buriti, Federal University of Campina Grande, Campina Grande, Paraiba, Brazil,V. F. Andrioli, State Key Laboratory of Space Weather, National Space Science Center, Chinese Academy of Sciences, Beijing, China, N. J. Schuch, Southern Regional Space Research Center-CRCRS, COCRE/INPE-MCTIC, Santa Maria, Brazil.

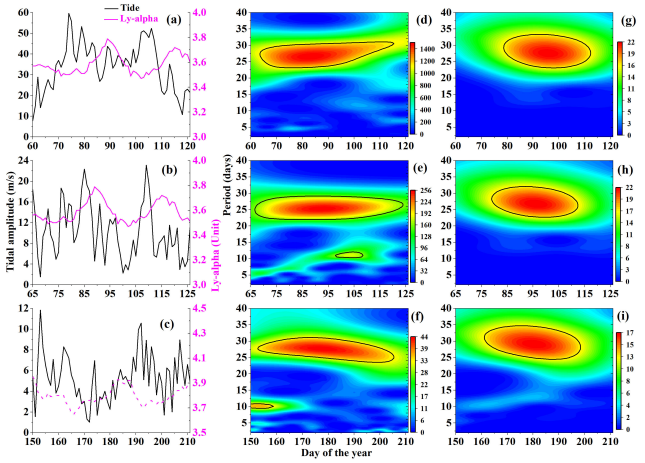

Figure 21: Daily tidal amplitudes and Ly-α flux (unit = 10^{11} photonscm^{-2}s^{-1}) at 90 km for (a) diurnal tide during 060-121 DY, 2008 at CP, (b) semidiurnal tide during 065-126 DY, 2008 at CA and (c) terdiurnal tide during 150-211 DY, 2006 at SM. Corresponding wavelet spectra estimated from the daily amplitude in the zonal wind for (d) diurnal tide, (e) semidiurnal tide and (f) terdiurnal tide. Wavelet spectra computed from the daily Ly-α data shown in plots (g), (h) and (i) corresponding to the intervals of a, b and c, respectively.

doi : https://doi.org/10.1186/s40623-020-01149-7

(Amitava Guharay)

Signature of a 120-day oscillation in the MLT winds and tides over São João do Cariri (7.4°S, 36.5°W)

A conspicuous and intermittent signature of a 120-day oscillation is found in the winds and tides in the mesosphere and lower thermosphere (MLT) over a Southern hemispheric equatorial station, São João do Cariri (7.4°S, 36.5°W) for the first-time using meteor radar observations during the interval 2004-2008. The intermittent 120-day modulation can be as high as 10 ms^{-1} in the MLT winds. However, the seasonal component of the concerned periodicity, i.e. terannual oscillation is relatively smaller in amplitude ($<$ 4 ms^{-1}) than the instantaneous component. The oscillation feature is also investigated for the dominant tides. The 120-day modulation amplitude is higher (maximum $\sim$5 ms^{-1}) in the diurnal and semidiurnal tides and relatively smaller in the terdiurnal tide (peak $\sim$2 ms^{-1}). The intermittent behavior of the particular oscillation in wind and absence in temperature may imply it to be a feature of the MLT wind circulation. Proximity of period may also indicate a possible contribution from the lower atmospheric intraseasonal oscillation to some extent at times. Furthermore, existence of the same periodicity in the solar UV flux may indicate a plausible indirect solar connection with the MLT circulation although direct solar influence cannot be ascertained (Figure 22).

The research work was done in collaboration with P. P. Batista, National Institute for Space Research, São José dos Campos, São Paulo, Brazil, R. A. Buriti, Federal University of Campina Grande, Campina Grande, Paraiba, Brazil,V. F. Andrioli, State Key Laboratory of Space Weather, National Space Science Center, Chinese Academy of Sciences, Beijing, China, N. J. Schuch, Southern Regional Space Research Center-CRCRS, COCRE/INPE-MCTIC, Santa Maria, Brazil.

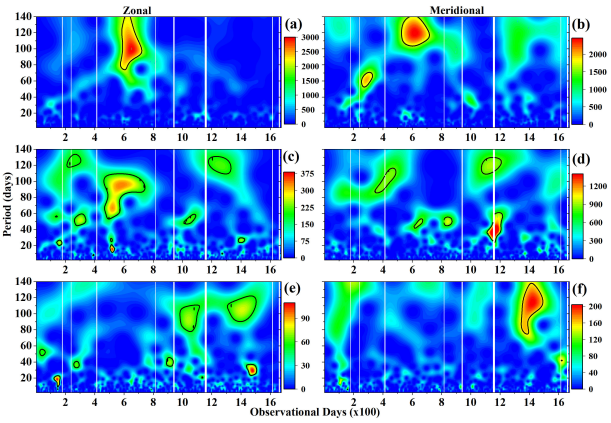

Figure 22: Wavelet power ($m^2 s^{-2} day^{-1}$) spectra estimated using daily tidal amplitudes at 90 km for diurnal tide (a-zonal, b-meridional), semidiurnal tide (c-zonal, d-meridional) and terdiurnal tide (e-zonal, f-meridional).

doi : https://doi.org/10.1016/j.jastp.2020.105337

(Amitava Guharay)

Evidence for distinctive changes in the solar wind helium abundance in solar cycle 24

The relative abundance of alpha particles with respect to protons, usually expressed as A_{He} = $(n_\alpha/n_p)*100$, is known to respond to solar activity, although changes in its behaviour in the last four solar cycles are not known.

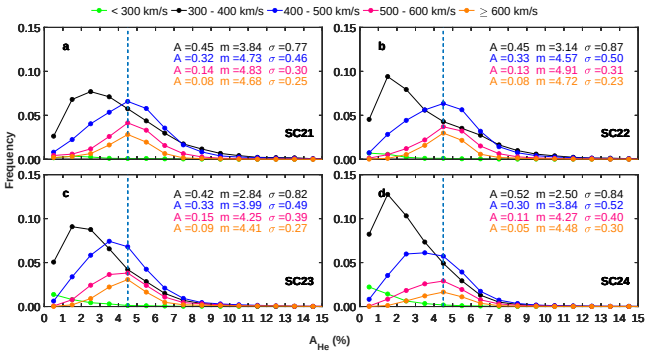

Figure 23: Frequency distribution of A_{He} events with 1% bin size for four velocity bins, viz. (1). 300 km/s (2) 300-400 km/s (3) 400-500 km/s (4) 500-600 km/s (6) > 600 km/s in solar cycles 21 (a), 22 (b), 23 (c) and 24 (d). The frequency distributions are approximated by log-normal distributions wherein A, σ and m are the fit parameters namely normalization coefficient, standard deviation and median in linear scale respectively. The vertical dashed lines mark A_{He} of 4.5%.

By systematically analysing inter-calibrated A_{He} data obtained from the first Lagrangian point of the Sun-Earth system, it is shown that the A_{He} variations are distinctively different in solar cycle 24 as compared to the last three cycles. The frequency of A_{He} = 2-3 per cent events is significantly higher (Figure 23) in slow/intermediate solar winds in solar cycle 24 as opposed to the dominance of the typical A_{He} = 4-5 per cent events in the previous three cycles. Further, the occurrence of $A_{He} > 10$ per cent events is significantly reduced in cycle 24. Not only that the changes in delay of A_{He} with respect to peak sunspot numbers are less sensitive to changes in solar wind velocity in cycle 24. The investigation suggests that the coronal magnetic field configuration started undergoing systematic changes starting from cycle 23 and this altered magnetic field configuration affected the way helium got processed and depleted in the solar atmosphere.

doi : https://academic.oup.com/mnrasl/article/503/1/L17/6134760?login=true

(Yogesh, D. Chakrabarty and N. Srivastava)

Van Allen probe observations of disappearance, recovery and patchiness of plasmaspheric hiss following two consecutive interplanetary shocks: First results

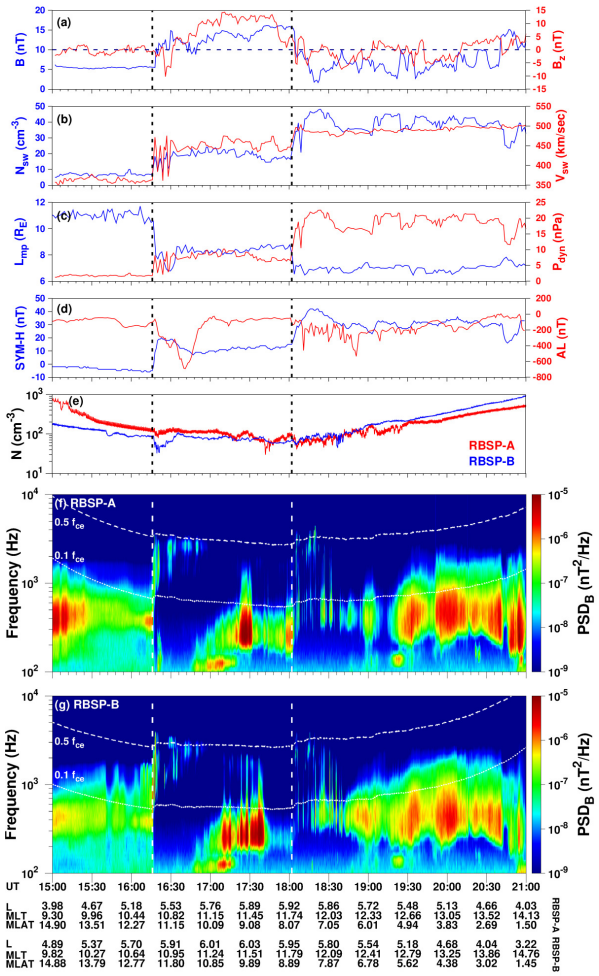

Figure 24: Overview of the plasmaspheric hiss event on December 19, 2015: (a) solar wind magnetic field magnitude (B) and the z-component of the magnetic field (B_z) in GSM coordinates; (b) solar wind proton number density (N_{sw}) and solar wind velocity (V_{sw}); (c) magnetopause location (L_{mp}) and solar wind dynamic pressure (P_{dyn}); (d) geomagnetic activity indices SYM-H and AL; (e) cold electron densities calculated from the EFW (Electric Fields and Waves) probe potentials for RBSP-A (red) and RBSP-B (blue); magnetic field power spectral density (PSD) in the waveform receiver (WFR) channels observed by (f) RBSP-A and (g) RBSP-B. The arrivals of the two IP shocks are shown by the two vertical dashed lines. The dashed and dotted curves in panels f and g represent 0.5 f_{ce} and 0.1 f_{ce} respectively. f_{ce} is electron cyclotron frequency.

A plasmaspheric hiss event (Figure 24), observed by the Van Allen probes in response to two successive interplanetary (IP) shocks occurring within an interval of ∼2 h on December 19, 2015, are presented for the first time. The first shock arrived at 16:16 UT and caused disappearance of hiss for ∼30 min. Combined effect of plasmapause crossing, significant Landau damping by suprathermal electrons and their gradual removal by magnetospheric compression led to the disappearance of hiss. Calculation of electron phase space density and linear wave growth rates showed that the shock did not change the growth rate of whistler waves within the core frequency range of plasmaspheric hiss (0.1-0.5 kHz) during this interval making conditions unfavorable for the generation of hiss. The recovery began at ∼16:45 UT which is attributed to an enhancement in local plasma instability initiated by the first shock-induced substorm and additional possible contribution from chorus waves. This time, the wave growth rate peaked within the core frequency range (∼350 Hz). The second shock arrived at 18:02 UT and generated patchy hiss persisting up to ∼19:00 UT. It is shown that an enhanced growth rate and additional contribution from shock-induced poloidal Pc5 mode (periodicity ∼240 s) ultralow frequency (ULF) waves resulted in the excitation of hiss waves during this period. The hiss wave amplitudes were found to be additionally modulated by background plasma density and fluctuating plasmapause location. The investigation highlights the important roles of IP shocks, substorms, ULF waves, and background plasma density in the variability of plasmaspheric hiss.

This work is done in collaboration with G. D. Reeves and B. A. Larsen of Space Science and Applications Group, Los Alamos National Laboratory, Los Alamos, NM, USA, D. N. Baker Laboratory for Atmospheric and Space Physics, University of Colorado, Boulder, CO, USA, S. G. Claudepierre Space Sciences Department, The Aerospace Corporation, El Segundo, CA, USA; Department of Atmospheric and Oceanic Sciences, University of California, Los Angeles, CA, USA, A. W. Breneman School of Physics and Astronomy, University of Minnesota, Minneapolis, MN, USA and D. P. Hartley Department of Physics and Astronomy, University of Iowa, Iowa City, IA, USA.

doi : https://doi.org/10.1029/2020JA028873

(S. Chakraborty and D. Chakrabarty)

Evidence for the significant differences in response times of equatorial ionization anomaly crest corresponding to plasma fountains during daytime and post-sunset hours

Based on 10 years' (2010-2019) of vertical total electron content (VTEC) data from Ahmedabad (23.0°N, 72.6°E, dip angle 35.2°) and campaign based OI 630.0 nm airglow intensity measurements from Mt. Abu (24.6°N, 72.7°E, dip angle 38.0°), it is shown that plasma density over the equatorial ionization anomaly (EIA) crest region increases in varying degrees during post-sunset hours (2000-2100 LT) in magnetically quiet periods. The post-sunset peak in VTEC precedes the corresponding peak in airglow intensity. By comparing post-sunset VTEC enhancements with ionosonde observations from Tirunelveli (8.7°N, 77.7°E, dip angle 1.7°), it is shown that pre-reversal enhancement (PRE) of the zonal electric field causes these enhancements over the EIA crest region. These observations are supported by TEC measurements by GAGAN (GPS Aided Geo Augmented navigation), the Indian Satellite-based Augmentation . Comparison of average VTEC variations with global empirical model drifts reveals that the post-sunset enhancements in VTEC occurs ∼1.7 h after the PRE and are significant only during December solstice and equinoctial months in high solar activity years (Figure 25) similar to seasonal variations in PRE amplitudes. This time delay (response time of EIA crest) is almost half compared to the average response time (3-4 h) associated with the daytime fountain. Based on the latitudinal gradient in SBAS-TEC, it is proposed that the PRE drives plasma from 5°N to 10°N magnetic latitudes to the EIA crest region leading to shorter response time. These results show the important role of the PRE in conditioning the EIA crest region.

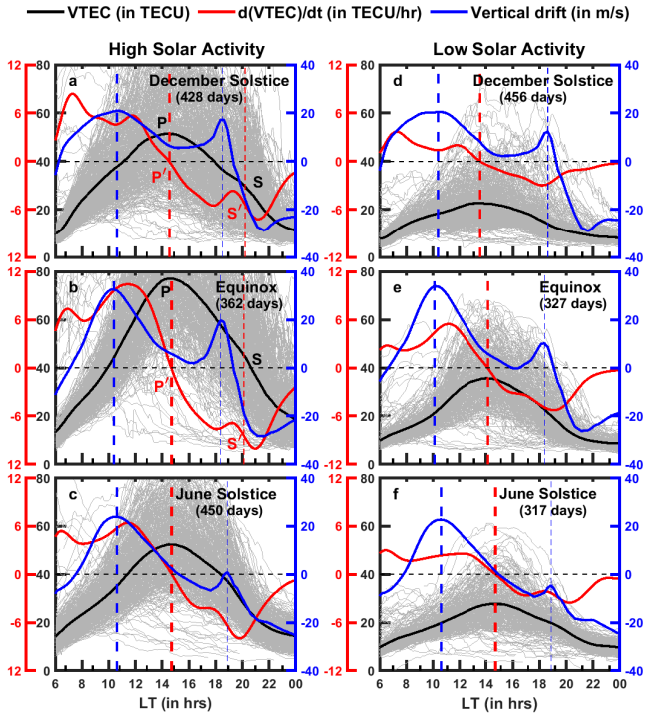

Figure 25: Variation of individual days' VTEC over Ahmedabad (gray), average of seasonal VTEC (black), temporal derivative of seasonal VTEC (red), and model-derived vertical drift (blue) in December solstice (top), Equinox (middle), and June solstice (bottom) under high (left panel) and low (right panel) solar activity years. The number of days used to calculate the seasonally averaged VTEC curve is also mentioned in each subplot. The points P and S represent primary (afternoon) and secondary (post-sunset) maxima of VTEC. P and S are determined based on P' and S' that are overall and local zero crossing points of d(VTEC)/dt. The intervals between the thick and thin vertical dashed lines (blue and red) are the response times of the EIA crest region during noon and post-sunset hours respectively.

doi : https://doi.org/10.1029/2020JA028628

This work is done in collaboration with B. G. Fejer of Utah State University, Logan, UT, USA, S. Sunda of Airport Authority of India, Ahmedabad, India, G. K. Seemala and S. Sripathi of Indian Institute of Geomagnetism, Navi Mumbai, India.

(A. Kumar, D. Chakrabarty, K. Pandey, and A. K. Yadav)

Effects of IMF By on ring current asymmetry under southward IMF Bz conditions observed at ground magnetic stations: case studies

In this work, the role of interplanetary magnetic field (IMF) By on the asymmetry of the ring current during the main phase of

geomagnetic storms is evaluated. The mean H variations have been calculated using 31 ground magnetic stations over magnetic latitudes of 09-45° following the methodology of Li et al. (2011, https://doi.org/10.1029/2011JA016886). Further, the magnetic local time (MLT) variations in the H component at these stations w.r.t. the mean H were investigated for three cases of geomagnetic storms with varying southward IMF Bz and IMF By conditions. Significant ring current asymmetries were observed during the main phase of geomagnetic storms. The primary role of IMF Bz on the asymmetry of the ring current is observed from these cases. More importantly, the investigation brings out for the first time, the additional role of IMF By in influencing the MLT distribution of ring current observed at ground magnetic stations. Under southward IMF Bz conditions, it is shown based on SuperDARN and AMPERE data that IMF By can alter the MLT distribution of ring current under suitable conditions. The timescales of IMF By also play very important role in determining the asymmetry in the ring current. Under steady convection state, IMF By can rotate the convection cells based on its polarity, which in turn can change the MLT distribution of ring current observed by low-latitude ground stations. This investigation, thus, brings out the important role of IMF By on the asymmetric MLT distribution of ring current under southward IMF Bz.

This work is done in collaboration with B. Veenadhari and S. Tulasi Ram of Indian Institute of Geomagnetism, Navi Mumbai, India, and T. Kikuchi of Research Institute for Sustainable Humanosphere, Kyoto University, Uji, Japan, and Y. Miyoshi of Institute for Space-Earth Environmental Research, Nagoya University, Nagoya, Japan.

doi : https://doi.org/10.1029/2019JA027493

(S. Kumar and D. Chakrabarty)

Investigation on longitudinal and decadal variations of the equatorial electrojet using a physical model

A detailed investigation on longitudinal and decadal variations of general characteristics (amplitude, width, peak altitude) of the equatorial electrojet (EEJ) is carried out using a physics-based model of electrojet. A few important aspects that emerge from this investigation include (i) changes in the half-width of EEJ with longitude and it's dependence on the rate of change of dip-angle with latitude, (ii) changes in EEJ strength as large as 10-20% over the Peruvian and Brazilian sectors from 1960 to 2020 associated with significant changes in the local geomagnetic field, (iii) wave-4 structure in the EEJ current density and integrated EEJ current. In addition, it is shown that the peak EEJ current density over different longitudes inversely depends on the strength of geomagnetic field. More importantly, relationships of EEJ parameters (such as half-width, peak current density, integrated current) with ionospheric electric field, electron density, and geomagnetic field are brought out. These relationships are verified using EEJ observations carried out earlier using sounding rocket and ground based magnetometers. This comprehensive account of the longitudinal and decadal variations of EEJ along with the expressions to calculate EEJ characteristics can be used in observational and modelling studies to understand the low-latitude ionospheric electrodynamics in greater detail.

doi : https://doi.org/10.1016/j.asr.2021.02.040

(K. Pandey, R. Sekar, D. Chakrabarty, and B. G. Anandarao)

Mid-Latitude Spread-F Structures Over the Geomagnetic Low-Mid Latitude Transition Region: An Observational Evidence

An observational evidence of a unique plasma depletion event was captured by an O(1D) 630.0 nm airglow imager on 13 June 2018 over a transition region of geomagnetic low-mid latitude, Hanle, Leh Ladakh, India (32.77°N, 78.97°E; Mlat. $\sim$24.1°N). The observed plasma depletion structures are tilted at an angle of 13° $\pm$ 2° west of the geomagnetic north and drifted toward west. Collocated Global Navigation Satellite System-Total Electron Content measurements confirm that the structures are indeed associated with TEC depletions. Simultaneous ionosonde measurements from Delhi, India (28.70°N, 77.10°E; Mlat. $\sim$20.2°N) shows spread-F signatures confirming that these structures are associated with the ionospheric irregularities. Interestingly, radar observations over the geomagnetic low-latitude station Gadanki, India (13.5°N; 79.2°E; Mlat. $\sim$6.5°N) reveal the absence of equatorial plasma bubbles on this night. Therefore, these observations strongly suggest that the observed structures in the airglow images over Hanle are associated with mid-latitude spread-F (MSF). These MSF structures are possibly affected by the shear in the zonal plasma drift that forces the field aligned plasma irregularity structures to tilt toward west. These observations, for the first time, bring out the presence of MSF structures over geomagnetic low-mid latitude transition region. It is suggested that the plasma distribution over low latitudes plays an important role in the occurrence of MSF structures over this transition region. Understanding the source and characteristics of the plasma irregularity structures over this transition region can help in understanding the spatio-temporal evolution of global L-band scintillation in a better way.

This work is done in collaboration with S. Mondal, S. Sarkhel and M. V. Sunil Krishna of Department of Physics, Indian Institute of Technology Roorkee, Roorkee, India], P. Pavan Chaitanya and A. K. Patra of National Atmospheric Research Laboratory, Gadanki, Andhra Pradesh, India], R. K. Choudhary and T. K. Pant of Ionosphere Thermosphere Magnetosphere Physics Branch, Space Physics Laboratory, Vikram Sarabhai Space Centre, Thiruvananthapuram, India, A. K. Upadhayaya of Environmental Sciences and Biomedical Metrology Division, CSIR National Physical Laboratory, New Delhi, India, and T. Sori of Institute for Space-Earth Environment Research (ISEE), Nagoya University, Nagoya, Japan.

doi : https://doi.org/10.1029/2019JA027531

(M. Sivakandan and D. Chakrabarty)

Altitude of two-stream irregularities in equatorial E region using sounding rocket experiments from Thumba

Amplitudes of two-stream irregularities and equatorial electrojet (EEJ) current are known to peak around the same altitude. Sounding rocket-borne magnetometer experiments have consistently shown that the EEJ current density maximizes around 105-km altitude whereas the theoretical models predict the EEJ peak around 100 km. One of the propositions to bridge this difference in the altitude has been based on the inclusion of small-scale turbulence (wavelength of $<$100 m) with the largescale dynamics (kilometer size). This proposition is examined based on in situ measurements of E region electron density and plasma irregularities (two-stream and gradient-drift irregularities)

obtained at different times of the day and night. These measurements were obtained based on sounding rocket flight experiments conducted from Thumba Equatorial Rocket Launching Station (8.54° N, 76.86° E), a facility in the vicinity of the dip equator. Whenever two-stream irregularities are present, the minimum electrojet current density is estimated based on the threshold velocity required for generation of these plasma irregularities. This method provides estimates of nighttime E region current also, which is difficult to measure. It is found that amplitudes of both two-stream irregularities and the estimated EEJ current peak around 105-km altitude irrespective of the presence or absence of the gradient-drift irregularities at the base of electrojet (95 to 100 km altitude).

doi : https://doi.org/10.1029/2019JA027195

(K. Pandey and S. P. Gupta)

Development of data acquisition software for a Short Wave Infrared (SWIR) InGaAs Camera

A new imaging system for SWIR range is being developed using InGaAs 320x256 sensor array that has a spectral response in the range of 950 to 1650 nm wavelength region. This Short wave Infrared Imager (SIRI) will be used to image the brightest OH bands that have emission in this wavelength region to investigate smaller scale features at the OH emission altitude (∼87 km). SIRI uses a commercial camera that is equipped with three-stage thermoelectric cooler. The functions related to camera operations are provided in Camera's Software Development Kit (SDK). By making use of these functions, a console based application software has been developed using C++ for data acquisition that can be scheduled as per the requirement. This software customizes the data acquisition mechanism as per the user's requirement. In order to execute the data acquisition we have created following three files:

1) Camera Setting file[.xcf]: It comes with camera installation and contains various parameter that can be programmed. 2) Profile files[.txt]: It is user defined file and contains some parameters with required values that define the operational conditions of the camera, like Location, Integration time, Temperature, name of the camera setting file, etc. 3) Schedule file[.txt]: It is user defined file and contains the date time range and name of Profile files to customize the camera settings accordingly during runtime.

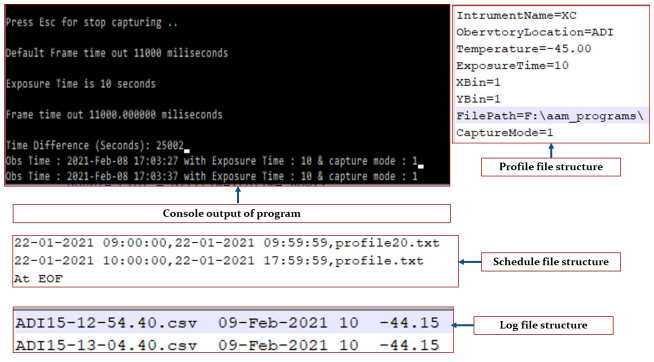

Figure 26: Screenshots of File structure and output.

This program is executed with one command line argument i.e. "schedule.txt" The screenshots of file structures of above mentioned files and console output are shown in Figure 26. After execution, it initialises the camera with specific configurations and settings and then starts the data acquisition as per the schedule and stores the image in a pre-defined format (.csv). The software then creates the data catalog file (log.txt) in the required format. The software will automatically create/update the directory structure. The camera is being operated using the newly developed software from optical aeronomy laboratory, Thaltej Campus. Further work towards the optimization of the imager and its data analysis is under progress.

(Atul A. Manke and Ravindra P. Singh)

Development of front-end and processing electronics using bare C650 Chip

The airglow photometer payloads projected by PRL for the Venus and the Earth missions will deploy 2D array detector. As part of our developmental effort, we have designed a laboratory model for a typical airglow payload and selected the SCMOS CAPELLA-CIS120 chip considering optimization of field of view (FOV), signal to noise ratio (SNR) etc. Since this chip is not available with us presently, we have explored the bare C650 chip available in the laboratory to design the prototype of the front-end and processing electronics. This R&D activity is important for future developments of airglow payloads at PRL for terrestrial and planetary applications. Note that this chip has already been used in HySIS payload (Chandrayaan-1 mission) and LiVHySI payload (YouthSat mission). Through an independent effort, we have now developed the required understanding at PRL on how to use this chip (and other detector chips) for our space-based experiments. The prototype (Figure 28) developed in the laboratory consists of front-end, processing, and ground checkout systems. The front-end card consists of all analog and digital power supply components along with the C650 chip. It also includes parameter control pins such as gain control, dark voltage cancelation, ADC external input selection, and data output mode of the C650 chip. The front end card is interfaced through FPGA proASIC3 A3P250 with a buffer resistor card.

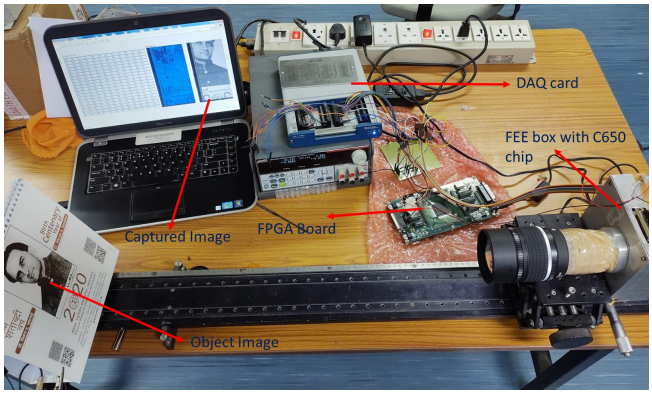

Figure 28: Laboratory set up for the front-end, processing, and ground checkout systems for the bare C650 chip. The captured image is of Prof. Vikram Sarabhai.

The dimensions of the front card are 13.3 cm x 11.1 cm. The C650 chip is controlled (e.g. clock logic and other parameters) through

a FPGA. All analog and digital power inputs along with these clock pulses to the chip constitute the 12-bit parallel output data. In the ground checkout segment, this 12-bit parallel data are taken through DAQ card 6363 and processed in Labview software. This 12-bit parallel data are converted into decimal values, arranged into a 1D array and subsequently converted into a 2D array in Labview. This 2D array is then used to construct a gray-scale image. The time for a single frame capture is 0.3ms. In the future, similar exercise will be carried out for the scientific SCMOS CAPELLA -CIS120.

(R. Pathak, A. Sarda, A. Yadav, and D. Chakrabarty)

Geosciences

Hydrometeorological processes and evaporation from falling rain in Indian sub-continent:Insights from stable isotopes and meteorological parameters

Rigorous analysis of measured isotopic composition (δ^{18}O and δD) of 556 daily rainwater samples collected at four Indian stations viz., Jammu, Jorhat, Hyderabad and Ahmedabad, is done in conjunction with satellite and model derived meteorological and isotopic parameters to discern prominent hydrometeorological processes and factors in four different climatic zones in the Indian subcontinent (Figure 1).

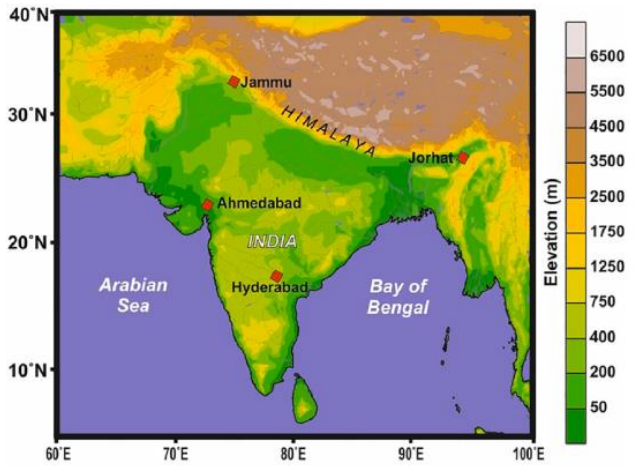

Figure no. 1: Elevation map of the Indian subcontinent and locations of four sampling stations.

A new Indian Meteoric Water Line (IMWL), better representing the different climatic zones, including the semi-arid western India, has been defined:[δD = (7.6$\pm$0.1) δ^{18}O + (8$\pm$1); R2 = 0.96; P$<$0.05; N = 556]. The lower slope of IMWL compared to the Global Meteoric Water Line signifies the role of evaporation from falling rain throughout the Indian sub-continent, though it is surrounded by large marine water body, and bordered by lofty Himalayan mountains in the north obstructing the monsoonal winds.

This study provides new quantitative insights about various hydrometeorological processes across the Indian subcontinent, where rain formation and post-precipitation processes involve either advection within in saturated or unsaturated air column, or convection within in saturated/unsaturated air column (Figure 3).

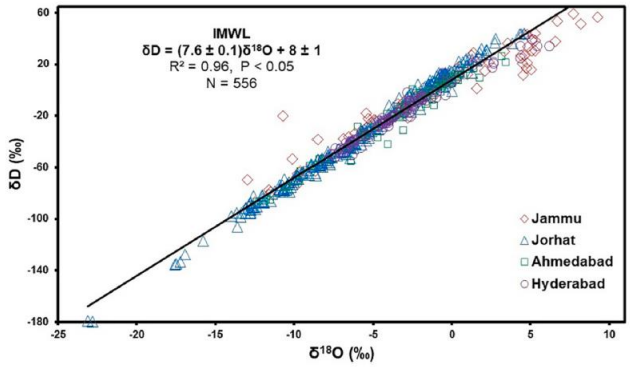

Figure no. 2: Composite δ^{18}O - δD regression line based on daily rainfall samples collected from all the four stations.

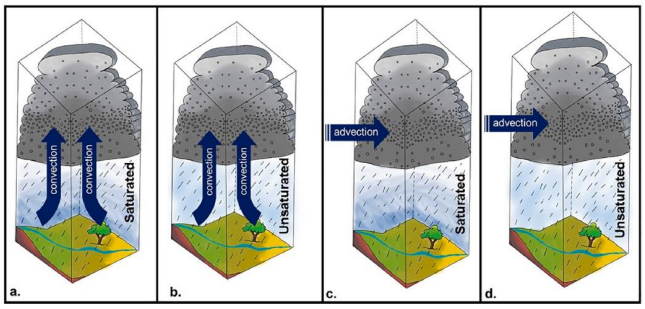

Figure no. 3: A schematic diagram showing **a)** convection within saturated air column; **b)** convection within unsaturated air column; **c)** advection over saturated air column; and **d)** advection over unsaturated air column.

Some of the important inferences drawn from this study are: (i) The estimated evaporative losses from falling raindrops for the four stations are [Jammu: Maximum 52% and Minimum 8%; Jorhat: Max 15% and Min 4%; Ahmedabad Min 8% and Hyderabad Max 29% and Min 15%]. (ii) Increased availability of surface waters due to flood in Brahmaputra River and high value (88%) of column averaged RH results in the lowest evaporative loss from falling raindrops at Jorhat in Northeast. (iii) The high Cloud Liquid Water Content (CLWC) over a longer span of altitude facilitates the interaction of falling raindrop with isotopically depleted ambient vapor and results in isotopically depleted rain. (iv) The observed inverse relationship between the evaporative loss from falling raindrop and the column averaged RH confirms that the post condensation kinetic processes are realistically accounted in

this study. (v) Validation with measured isotope data of rain shows that the LMDZ-iso modelled rain fails to incorporate evaporative isotopic enrichment and generates negative bias.

doi : https://doi.org/10.1016/j.jhydrol.2020.125601

(H. Oza, A. Gangulya, V. Padhya and R.D. Deshpande)

Sources and processes of groundwater arsenic mobilization in upper Jhelum basin, western Himalayas

Arsenic concentration in groundwater is one of the worst problems we are facing owing to its carcinogenic effect. The problem should therefore be addressed scientifically.

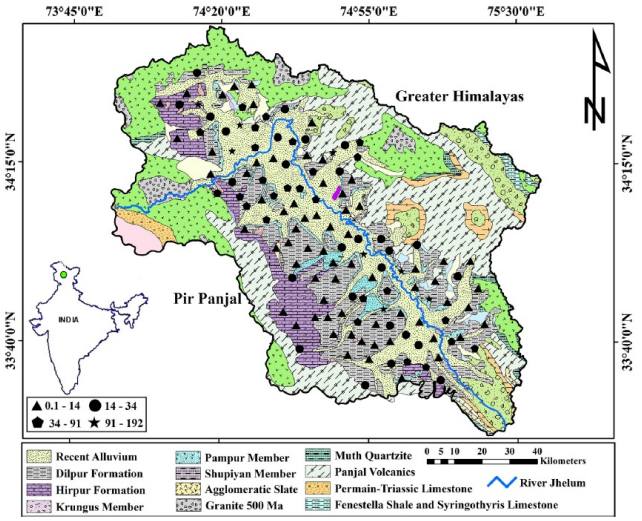

Figure no. 4: Lithological map of upper Jhelum basin with sampling locations (Kashmir Valley; Arsenic values are reported in μgL^{-1})

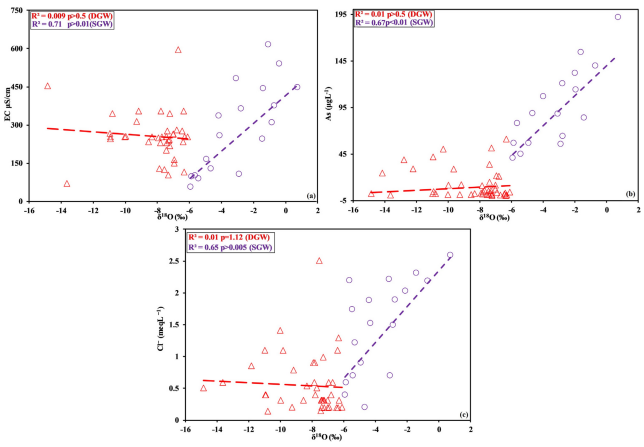

Figure no. 5: The study suggests that the source of Arsenic is from quaternary deposits of unconsolidated aquifers with their provenance from the volcanic, sedimentary and metamorphic rocks of Himalayan orogeny.

Although groundwater Arsenic enrichment is reported in many basins across the globe, still scientists have long way to go. In the present study we present new Arsenic data in groundwater to understand the processes and aquifer environment responsible for the Arsenic mobilization in groundwater of upper Jhelum basin, western Himalayas (Figure 4). The groundwater in the unconsolidated aquifers is less mineralized, with low electric conductivity, moderate pH and is mainly of Ca-Mg-HCO_3 type.The results suggest that carbonate dissolution, silicate weathering and active cation exchange is controlling the ionic composition of groundwater. Arsenic concentration in groundwater showed a wide range (0.14 μg L^{-1} to 192 μg L^{-1}), with 45% of water samples having Arsenic $>$10 μgL^{-1} (WHO guidelines for drinking water). The shallow groundwater wells were more Arsenic enriched than deep groundwater wells. Groundwater Arsenic showed significant correlation with redox sensitive parameters including Fe, Mn, pH, NH_4–N, HCO^{3-} and poor correlation with NO^{3-} and SO_4^{2-}. Besides the lower slope (w.r.t. GMWL) and higher isotopic values (δ^{18}O and δ^{2}H), a significant correlation of δ^{18}O with Arsenic, EC and Cl^- is observed in shallow groundwater.

doi : https://doi.org/10.1016/j.jhydrol.2020.125292

This work is done in collaboration with Dr. Gh.Jeelani, Kashmir University and Team.

(R.D. Deshpande)

Monsoon variability over the last 46 kyr inferred from Bay of Bengal ocean sediments

Freshwater-induced stratification in the upper ocean of the Bay of Bengal is linked to the changes in the Indian monsoon.

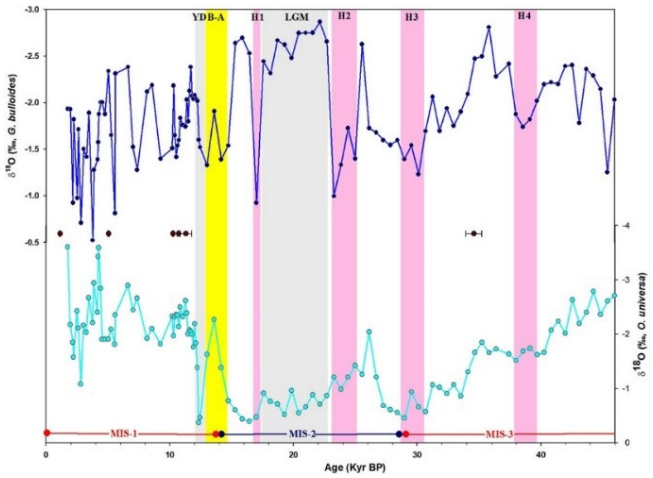

Figure no. 6: δ^{18}O variability record of planktic foraminifera Globigerina bulloides (blue) and Orbulina universa (cyan) obtained from core SK-170/2 recovered from the southwestern Bay of Bengal.

Variability in δ^{18}O and δ^{13}C of selected planktonic foraminifera species along length of a sediment core retrieved from the southwestern Bay of Bengal covering the last 46 kyr was reconstructed (Figure 6). Results show that the northeast monsoon was dominant during the Last Glacial Maximum.Remarkable

signatures were observed during the Marine Isotope Stage (MIS) 3 to MIS^{-1}. Results suggest that Indian monsoon variability is controlled by a complex of factors such as solar insolation, North Atlantic climatic shifts, and coupled ocean–atmospheric variability during the last 46 kyr. Regional correlation of the δ^{18}O records suggests that the processes that have controlled the hydroclimate in the southwestern Bay of Bengal were similar to those that occurred in other parts of the Bay of Bengal and the Andaman Sea. The variabilities observed in this study are in broad agreement with the other monsoon reconstructions from Bay of Bengal, which suggests that the forcing mechanisms of monsoon appear to be similar in the entire north Indian Ocean.

doi : https://doi.org/10.1002/jqs.3263

This work was carried out in collaboration with Prof. A.C. Narayana of University of Hyderabad.

(P. Kiran Kumar & M.G. Yadava)

Marine Reservoir Age Correction for the Andaman basin

Marine reservoir age is important for radiocarbon dating of marine and coastal samples. Radiocarbon concentration in pre-bomb marine samples of known ages are used to derive marine reservoir age of a region. Annually banded coral from Landfall island in the northern Andaman has been analyzed for its radiocarbon concentration between 1948-1951. Radiocarbon age and reservoir effect (ΔR) are reported for these pre-bomb coral samples from the northern Andaman region. The mean radiocarbon age of 331$\pm$61 yr BP was obtained for the period 1948-1951 with an average reservoir age correction of -138$\pm$61 yr. This reservoir age correction is lowest reported from the northern Indian Ocean. The ΔR values obtained using mollusk shells and coral from Andaman region show a large variation in ΔR values. ΔR value of the northern Andaman and the Bay of Bengal appears lower than that of southern Andaman. As Landfall Island is situated in the northern part of the Andaman archipelago, the lower reservoir age correction could result due to freshwater flux and reduced upwelling in the region.

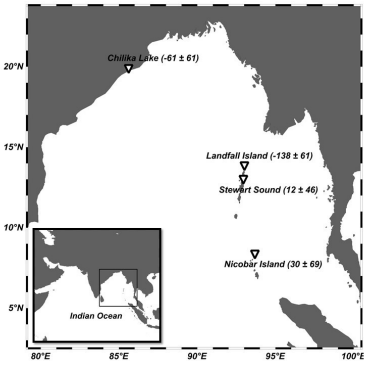

Figure no.7: Map of north-eastern Indian Ocean with reservoir age correction values from Landfall Island, Chilika lake, Stewart sound and Nicobar Island (Inset: Study location marked by rectangle in northern Indian Ocean)

doi : https://doi.org/10.1017/RDC.2020.91

(H. Raj, R. Bhushan, M. Muruganantham & A.J. Dabhi)

Hydroclimate variability during the last two millennia from the mudflats of Diu Island, Western India

The climate variability over western India has been significantly influenced by the perturbations in the Indian summer monsoon (ISM) and thus, provides a crucial platform to investigate the paleomonsoon variations, weathering intensity, and sediment source.

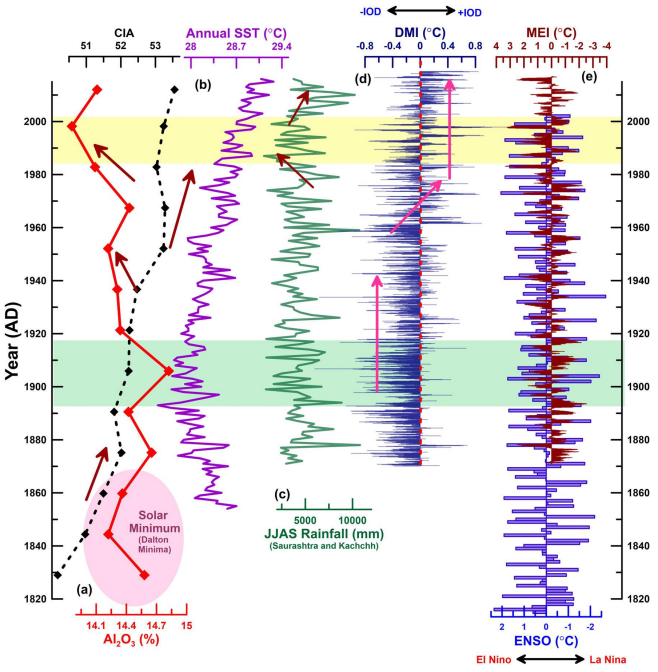

Figure no. 8: Comparison of Al_2O_3 and CIA with the available instrumental data such as SST and rainfall along with DMI and MEI indices for the last two centuries. Green and yellow band indicates ISM intensification and weakening phase. CIA and SST followed similar trend indicating crucial role of temperature on the intensity of chemical weathering.

The mudflats of southern Saurashtra, western India are deprived of perennial rivers, but the region receives terrestrial contribution exclusively due to activation of seasonal rivers during the monsoon. In the present study, an attempt has been made to investigate the paleomonsoon and palaeoweathering using various geochemical proxies (detrital, productivity, redox, and weathering) on the mudflat sediment core of southern Saurashtra, western Gujarat. The core is chronologically constrained by ^{14}C, ^{210}Pb, and ^{137}Cs dating techniques. The study suggests ISM strengthening during 2000-1800 cal yr BP with intermittent marginal ISM weakening during 1950-1970 cal yr BP and 1930-1890 cal yr BP associated with the reduced solar irradiance. Further, ISM weakening has been invoked during Dark Age Cold period (1800-1300 cal yr BP) and Little Ice Age (800-200 cal yr BP) interrupted by a marginal ISM strengthening during Medieval Warm period and the last two centuries witness climate warming. In spite of changes in the geochemical proxies as a function of ISM fluctuations, the palaeo-weathering intensities has remained nearly consistent wherein the chemical weathering was less operative and accompanied by the deposition of texturally immature sediments. The sediments of Diu mudflat indicate mafic signatures thereby underscoring a major contribution of the Deccan basalts along with other variable sources.

This work was done in collaboration with Drs. Upasana S. Banerji, National Center of Earth Science Studies, Trivandrum and Prof. A.J.T. Jull, NSF-AMS Facility, University of Arizona, Tucson, USA.

doi : https://doi.org/10.1002/gj.4116

(R. Bhushan)

^{210}Pb dating of recent sediments from the continental shelf of western India: factors influencing sedimentation rates

Several cores from the continental shelf of the Arabian Sea along the Indian Coast were investigated for change in sedimentation rates duly constrained for chronology based on ^{210}Pb and ^{137}Cs dating techniques. The emphasis was to look for spatial and temporal variation in the sedimentation rate along the continental shelf of eastern Arabian Sea between Goa to Kochi for water depth $\leqslant$ 150 m. This study showed varying sedimentation rates in coastal and distant sediment cores. Both ^{210}Pb and ^{137}Cs dating techniques showed comparable sedimentation rate in most sediment cores. The sedimentation in the continental shelf region of the coastal Arabian Sea is primarily controlled by discharge of sediments from rivers during Indian summer monsoon. Increased sedimentation rate from the north (off Goa) to the south (off Kochi) was triggered by high riverine flux and longshore sediment transport.

doi : https://doi.or/10.1007/s10661-020-08415

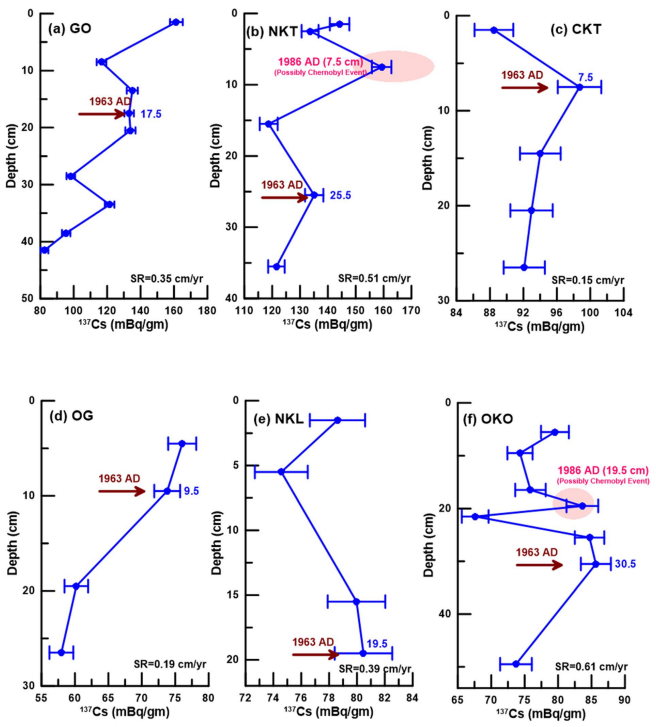

Figure no. 9: Downcore variation of ^{137}Cs for the sediment cores raised during SM-29. 1963 AD and 1986 AD corresponding to nuclear test and Chernobyl accident has been marked

(C. Shah, U.S. Banerji, K.R.Chandana & R.Bhushan)

Assessment of contaminants in the northwestern Bay of Bengal

The coastal sediments in the northern Bay of Bengal has undergone contamination due to the heavy metal contribution from rivers. To evaluate the status of contamination in the inner shelf region of the Bay of Bengal, a sediment core chronologically constrained using ^{210}Pb dating technique from the northwest Bay of Bengal was investigated for several trace elements. To assess sediment quality, enrichment factor (EF), geo-accumulation index (Igeo), and Modified Nemerow Pollution Index (MPI) were derived. The influence on ecology by individual contaminants and combined contaminants was evaluated using the potential ecological risk factor (Eri) and modified ecological risk index (MRI). The single-element pollution indices indicated that the sediment has no significant pollution by individual elements. However, the multi-elemental approach shows slight pollution in the sediment core. The ecology is at low risk by contaminants present in the sediment. Comparison of the elemental values of shelf sediment with adjacent riverine and estuarine samples demonstrates the role of estuarine environment and/or high riverine flux of sediments causing either removal or dilution of trace elements during its transport from the river to the sea.

This work was done in collaboration with Ms. Romi Nambiar and Dr. P.S. Shrivastava from Department of Chemistry, Gujarat University, Ahmedabad.

doi : https://doi.org/10.1007/s11356-020-09576-5

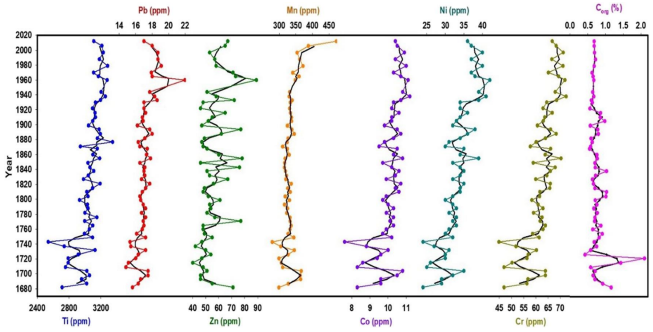

Figure no. 10: Down-core variation of Ti, Pb, Zn, Mn, Co, Mo, and Ni in SM 24/14 core (black lines are 3 points running average)

(C. Shah, J. Kumar & R. Bhushan)

Mid-late Holocene evolutionary history and climate reconstruction of Vellayani lake, south India

The lake sediments received significant wide attention for archiving paleoclimate and paleo sea-level variability during late Quaternary period.It has been extensively used to disentangle the interrelationships existing among the regional and the global climate systems. In the present study,the applicability of lake sediments has been the major impetus to delineate the mid-late Holocene climate and sea level variability using a $\sim$10 m sediment core retrieved

from a protected freshwater lake-the Vellayani lake, southern Kerala, southwest India. The sediment core was studied using multiproxy approach and was chronologically supported by AMS radiocarbon dates. The results show monsoon intensification and a high sea level during 6430 - 4390 cal yr BP led to the formation of a coastal lagoon system in the area. Study demonstrated marginal reduction in monsoon during 4390 - 2600 cal yr BP interspersed by an intensified phase during 3800 - 2600 cal yr BP. Concurrently, a sea regression during 4390 - 2600 cal yr BP restricted sea water influence in the study area. Proxies indicated a significant monsoon reduction during 2600 - 1000 cal yr BP followed by monsoon intensification post -1000 cal yr BP. After 2600 cal yr BP, the deposition of a thick pile of alluvium by the Karamana river might have hindered the tidal influence and later the basin has been transformed in to a freshwater lake. The present lake configuration was attained after 440 cal yr BP. Further, comparison of paleoclimate reconstructed from the present study with the global records revealed the existence of a teleconnection of Indian monsoon with the global climate system.

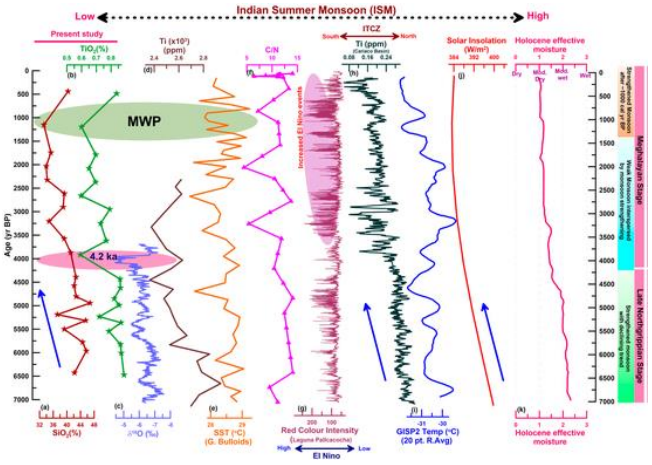

Figure no. 11: Comparison of detrital proxies with other paleoclimatic records. **(a)** SiO_2 and **(b)** TiO_2 of the present study, **(c)** Mawmluh Cave *(Berkelhammer et al., 2012)* **(d)** off Srilanka marine sediment core *(Chandana et al., 2017)* **(e)** Arabian Sea SST reconstruction *(Saraswat et al., 2013)* **(f)** Kukkal Lake, Karnataka *(Rajmanickam et al., 2017)* **(g)** ENSO events recorded in Peruvian lake (Laguna Pollacacocha) *(Moy et al., 2002)* **(h)** Titanium concentration in Cariaco basin *(Haug et al., 2001)* **(i)** GISP2 ice core temperature *(Alley, 2004)* **(j)** Solar insolation (0°June) *(Berger and Loutre, 1991)* **(k)** Holocene effective moisture *(Herzschuh, 2006)*.

doi : https://doi.org/10.1016/j.quaint.2021.03.018

This work was done in collaboration with Drs. Upasana S. Banerji and Dr. D. Padmanlal from National Center of Earth Science Studies, Trivandrum.

(A.J. Dabhi, A. Shivam & R. Bhushan)

Paleoenvironment of the Central Himalaya during late MIS 3

Marine Isotope Stage (MIS) 3 was an interstadial stage in the climate history of the Earth where the last phase (40 to 30 ka) showed relatively warmer climate over the northwest China, Tibetan Plateau, and northwestern India compared to other regions of the world. However, not many studies are reported for climate variability during this period from the Himalayan region. In this study, an attempt was made to understand the paleoenvironment of the Central Himalaya during 45 - 29 ka using stable isotopic compositions of carbon ($\delta^{13}C_{TOC}$) and nitrogen ($\delta^{15}N_{TN}$) along with their elemental ratios (TOC/TN) in bulk organic matter and occluded organic matter within diatom frustules ($\delta^{13}C_{Diatom}$) of a paleolake sequence.The variabilities in $\delta^{13}C_{Diatom}$, $\delta^{13}C_{TOC}$, and TOC/TN ratios indicated intermittent changes in the lake carbon dynamics from bicarbonate dominated system to carbon dioxide dominated regime. These changes in lacustrine carbon cycling provided evidence for existence of sporadic dry events in the Central Himalaya during 45 - 29 ka. In agreement with the records from the northwest China, Tibetan Plateau, and northwestern India, our results also confirm the existence of a relatively wet and humid period during 40 - 32 ka in the Central Himalaya. Therefore, it appeared that compared to other parts of the world, relatively wet and humid climate existed throughout this region. However, the mechanism behind this wet and humid phase remains to be explored and warrants a high-resolution paleoclimate study in the Himalaya.

doi : https://doi.org/10.1016/j.quaint.2020.08.024

(A. Rahman and S. Kumar)

Carbon biogeochemistry of two contrasting estuarine ecosystems

Comprehensive understanding and quantification of different aspects of estuarine carbon (C) cycle are essential to decipher regional and global changes. In this study, premonsoon C biogeochemistry of two contrasting estuarine systems (Hooghly - anthropogenically influenced and Sundarbans - mangrove dominated) located in the deltaic region of Ganges,India was investigated. The DIC concentration in the Hooghly (2.27 $\pm$ 0.22 mmol L^{-1}) was higher than the Sundarbans (1.77 $\pm$ 0.06 mmol L^{-1}) with relatively depleted $\delta^{13}C_{DIC}$. The mixing model analysis suggested DIC chemistry in the Hooghly to be principally regulated by respiration of estuarine algae, whereas Sundarbans showed evidences for DIC removal and mangrove derived DIC contribution. The DOC behaved non-conservatively in both the estuaries. The POC in the Hooghly showed signatures of estuarine algae and marine plankton in the mixing and marine zones, whereas dominance of terrestrial organic matter was found in the freshwater zone of the Hooghly and estuaries of Sundarbans. Both pCO_2 (556 - 5002 μatm) and CH_4 (15.4 - 445.7 nmol L^{-1}) varied over a wider range in the Hooghly compared to the Sundarbans (pCO_2: 268 - 418 μatm; CH_4: 41.6 - 71.5 nmol L^{-1}). The Sundarbans acted as a net sink for CO_2, whereas the Hooghly was a significant source to the regional atmosphere. Both the estuaries acted as source of CH_4 with comparable exchange fluxes. Overall, the Sundarbans was a net C sink and the Hooghly was a net source to regional atmosphere via cumulative fluxes of CO_2 and CH_4.

doi : https://doi.org//10.1007/s12237-021-00908-3

(M.K. Dutta and S. Kumar)

Effects of the type of forest alteration on gross nitrogen mineralization in soils

Change in land-use practices can result in major shifts in the cycling of various elements, particularly nitrogen (N), which is prone to

anthropogenic perturbations. For quantifying these shifts, accurate measurements of rates of biogeochemical transformations of N are needed. In this study, ^{15}N isotope dilution technique to understand the effects of the types of forest alteration on N transformation rates by comparing gross N mineralization and ammonium (NH_4^+) consumption rates in soils of a managed forest, an unmanaged forest, and a rubber plantation in Kerala, India, was used. Overall, nitrate (NO_3^-) dominated soils of the managed and unmanaged forests, whereas soils in the rubber plantation showed relatively higher NH_4^+ concentration. Total N (TN) and total organic carbon (TOC) concentrations were the highest under the rubber canopy. In soils of all three forest types, gross N mineralization rates were higher compared to NH_4^+ consumption rates. Despite high TN and TOC concentrations, the rates of gross N mineralization and NH_4^+ consumption were considerably lower in the rubber plantation compared to the managed and unmanaged forests. The lower NH_4^+ consumption rates in the rubber plantation led to significantly higher residence time of NH_4^+ ($\sim$4 days) compared to the managed and unmanaged forests ($<$2 days), possibly contributing to acidification of rubber soils (pH $\sim$4.8). These results together suggest that replacement of naturally grown forests with a mono-cropped plantation such as rubber negatively impact rates of N transformation processes in tropical soils and imply that change in tree species composition of naturally grown forests can adversely affect soil microbial activity. We recommend intercropping these plantations with commercial crops to maintain soil microbial diversity and biogeochemical cycling for sustainable forest management.

doi : https://doi.org/10.1007/s11676-020-01225-4

(N. Sharma and S. Kumar)

Nitrogen transformation rates in the Himalayan soils at different temperature and elevation conditions

Vast expanses of climatically sensitive ecosystems, such as tropical montane, remain unstudied in terms of factors controlling nitrogen (N) availability and in turn productivity. Temperature and elevation are two important, yet understudied, factors which decide the fate of N in montane ecosystems. Therefore, this study aimed to quantify and understand changes in rates of N transformation processes in tropical montane soils of the Himalayas under different temperature-elevation conditions.

The ^{15}N isotope dilution technique was employed to quantify the rates of gross N transformations in soils collected at two depth intervals (0 - 20 cm and 20 - 40 cm) from five elevations (3000m, 2500m, 2000m, 1500m, and 1000m above sea level) of the Garhwal Himalayas. The rates were measured at low (10°C) and high temperature (23°C) conditions to decipher the effect of temperature change on N cycling in montane soils. The results indicated a significant increase in gross N mineralization rates under the high temperature condition compared to the low. Interestingly, gross nitrification rates remained unaffected of temperature change. Increase in gross N mineralization at high temperature condition was accompanied with increased ammonium (NH_4^+) consumption, which was largely in the form NH_4^+ immobilization. In general, gross N transformation rates in the top soils showed higher response to change in temperature and elevation conditions than the bottom soils. Increase in rates of N mineralization and other soil N cycling processes at higher temperature suggests potential acceleration in N turnover due to warming in the Himalayan soils. Increased NH_4^+ immobilization and poor sensitivity of nitrification to temperature is likely to increase soil N conservation at higher temperature. The inconsistent variation in N transformation rates with elevation suggested higher control of edaphic factors on soil N cycling at a particular elevation.

doi : https://doi.org/10.1007/s11368-020-02722-z

(N. Sharma and S. Kumar)

Nitrogen dynamics in soils of a global biodiversity hotspot

Being one of the important nutrients required by plants during photosynthesis, nitrogen (N) exerts a significant control on primary productivity and carbon dioxide sequestration. Therefore, it is essential to quantify the rates of N cycling processes, such as gross N mineralization and nitrification, to understand the flow and availability of N in different ecosystems. Lack of such data in tropical regions, particularly the Indian subcontinent, has constrained our understanding of N dynamics in soils of the subcontinent. In this study, we reported the gross N transformation rates from the hot and humid tropical forest soils of the Western Ghats, one of the global biodiversity hotspots located in India. The experiments conducted using the ^{15}N isotope dilution technique showed higher average gross N mineralization and gross nitrification rates in the top soil layers (0 - 20 cm), which decreased significantly with depth (20 - 40 cm) indicating potential for higher microbial activity in the top soils. The overall consumption rate of mineral N exceeded its production rate with higher consumption of ammonium (NH_4^+) than nitrate ($NO^3{}_-$) suggesting NH_4^+ as a preferred N source for microbes. The consumption of NH_4^+ was higher through NH_4^+ immobilization than nitrification indicating active N conservation mechanism and an efficient microbial adaptation. Despite high rates of consumption, accumulation of NH_4^+ and NO_3^- in soils of the Western Ghats suggested additional sources of mineral N other than internal recycling of N. Long residence time of NH_4^+ and NO_3^- in soils implied longer availability of unutilized mineral N leading to high soil acidity and potential for loss of N through leaching and denitrification.

doi : https://doi.org/10.1002/jpln.201900126

(N. Sharma and S. Kumar)

Chemical and isotopic characteristics of PM_{10} over the Bay of Bengal: Effects of continental outflow on a marine environment

Pollutants transport from South and Southeast Asia can profoundly affect the marine atmospheric boundary layer (MABL) over the Bay of Bengal (BoB). This study presents chemical and stable isotopic composition of PM_{10} collected at Port Blair Island (11.6°N, 92.7°E) located in the middle of the BoB during the late northeast monsoon (February - April), a period when the BoB receives considerable continental outflow. The dominance of continental inputs over a marine realm was evident by a significant amount of nss-$SO_4{}^{2-}$ (range: 1.8 to 16.9 μg m^{-3}), which accounts for $\sim$65% of the total water-soluble inorganic constituents. The impact of anthropogenic emissions was further evident from the widespread

depletion of chloride (range: 57-100%, avg: 98±7%) from sea-salt aerosols. Carbonaceous species (elemental carbon and organic matter) contributed nearly 35% to PM_{10}. Further, average $\delta^{13}C$ (-25.6‰± 0.5) and $\delta^{34}S$ (4.5‰± 1.3) values observed over the marine study region were similar to those found in typical urban environments. $\delta^{15}N$ values (13.7‰± 5.1) show the significant presence of combustion sources along with the effect of atmospheric processing. Aerosol $\delta^{13}C$ values correlate positively with the ratio of water-soluble organic carbon to total organic carbon, indicating the aging of organic aerosols during the transport. In aggregate, this study provides newer insights into sources of carbonaceous species and their chemical processing in MABL of BoB.

This study was carried out in collaboration with Dr. Rajesh Agnihotri (BSIP, Lucknow), Late Mr. Ravi Sawlani (NPL, Delhi), and, Dr. S. Suresh Babu (SPL, Thiruananthpuram)

doi : https://doi.org/10.1016/j.scitotenv.2020.138438

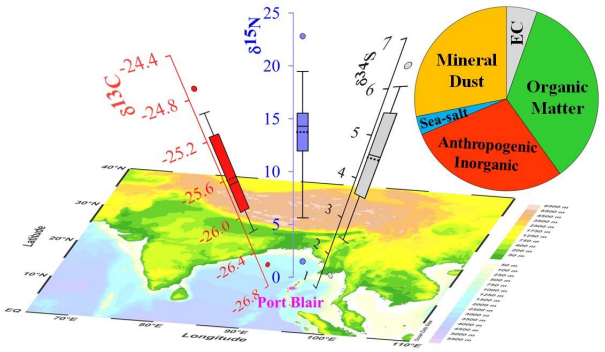

Figure no. 12: Average chemical composition and isotopic composition of C, N, and, S over the Port Blair Island, Bay of Bengal.

(N. Rastogi, A. Patel & R.V. Satish)

Effect of COVID-19 lockdown on the concentration and composition of NR-$PM_{2.5}$ over Ahmedabad, a big city in western India

To investigates the impact of reduced anthropogenic emissions during the lockdown period on the concentration, composition, and characteristics of non-refractory particular matter $\leq$2.5 μm aerodynamic diameter (NR-$PM_{2.5}$) and black carbon (BC) at Ahmedabad, a big city in western India, online measurements were performed from February 29 to March 23 (before lockdown, P1), April 10 to May 01 (during the lockdown, P2), and June 1 to June 16 (post lockdown, P3) using a high-resolution time-of-flight aerosol mass spectrometer (HR-ToF-AMS) and an Aethalometer. In summary, the NR-$PM_{2.5}$ was dominated by OA during study period and on average, organic aerosols (OA), NO_3^-, SO_4^{2-}, NH_4^+, Cl^-, BC at 370 nm (BC_{370}), and BC at 880 nm (BC_{880}) were reduced by 52, 64, 43, 62, 86, 52, and 57%, respectively, during P2 compare to P1. However, the diurnal trends of species were similar during the lockdown and no-lockdown periods. Source apportionment of OA using positive matrix factorization analysis revealed three factors: hydrocarbon-like organic aerosol (HOA), low volatile oxygenated OA (LV-OOA), and semi-volatile oxygenated OA (SV-OOA), contributing 26%, 44% and, 30%, respectively, to the total OA during the study period. This study is essential in understanding and assessing the effects of reduced anthropogenic emissions on the air quality of Ahmedabad, which in turn shall be very useful in planning appropriate mitigation strategies. Atmospheric abundances and diurnal variability during lockdown, representing regional background concentrations, may also be very useful for regional modelling studies.

doi : https://doi.org/10.1016/j.uclim.2021.100818

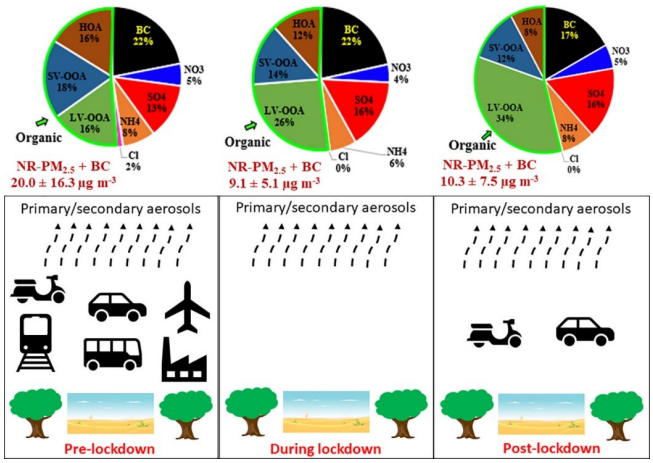

Figure no. 13: Average composition of $PM_{2.5}$ species (NR-$PM_{2.5}$ including black carbon (BC)) and PMF-derived OA factors during pre-lockdown, during lockdown, and post-lockdown period over Ahmedabad.

(J. Dave, R. Meena, A. Singh & N. Rastogi)

Oxidative Potential of Ambient PM and Related Health Endpoints over South Asia: A Review

South Asia occupies only about 3.5% of the world's area but, about 25% of the average world's population lives here and is continuously exposed to severe air pollution. Unprecedented development activities in most of the South Asian cities emit primary and secondary pollutants into the atmosphere. Particulate matter (PM), a principal air pollutant, are tiny enough to remain suspended in the atmosphere for a long time (about a week). They can penetrate the human nasal airway and damage the lungs. PM effects on human health are assessed based on their mass concentration, size distribution, and chemical composition. Despite being critically important, studies related to PM effects on human health are limited over South Asia. In recent years, only a few South Asian research groups started studying the ability of atmospheric PM to cause human health hazards by generating in situ reactive oxygen species (ROS). The capability of atmospheric PM to produce ROS and/or deplete antioxidants is termed as their oxidative potential (OP). Though limited, efforts are made to identify particular species with the higher OP. Atmospheric aging of PM can alter their OP. No studies from South Asia, except a few from India, investigated how the atmospheric aging changes the chemical and

physical properties of PM and affect their OP (both volume-normalized OP (OP_V) and mass-normalized OP (OP_M) over South Asia. These studies showed that OP depends more on PM composition rather than its concentrations. Therefore, mitigation strategies for reducing PM mass concentrations alone may not be sufficient, and linking PM OP with significant health effects may be a better way to regulate specific sources of PM rather than overall PM mass. This review reports the necessities and limitations for PM OP studies in South Asia and future directions.

doi : https://doi.org/10.5572/ajae.2020.123

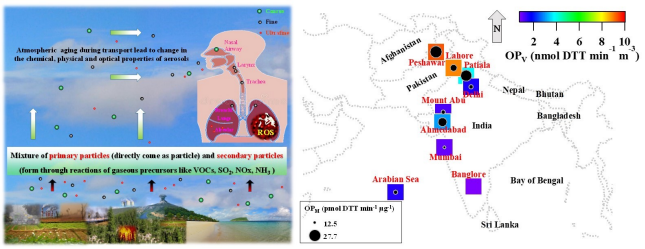

Figure no. 14: **(a)** A schematic representation of sources of atmospheric PM and their reach in the human body where they can generate reactive oxygen species and affect human health, and **(b)** Dithiothreitol (DTT)-based average volume-normalized oxidative potential (OP_V, color scale) and average mass-normalized oxidative potential (OP_M, size of bubbles) over South Asia.

(A. Patel and N. Rastogi)

Oxidative Potential of Atmospheric PM_{10} at Five Different Sites of Ahmedabad, a Big City in Western India

This study presents the oxidative potential (OP) as well as a wide range of chemical speciation of PM_{10} at the five sites representing different environments in a big city, Ahmedabad, of western India. On average, PM_{10} mass concentrations were 116±36, 228±43, 133±29, 101±21 and 70±20 μg m^{-3}, volume-normalized OP (OP_V) were 2.51±0.71, 5.62±0.68, 2.69±0.76, 2.14±0.41 and 1.55±0.51 nmol DTT min^{-1} m^{-3}, and mass-normalized OP (OP_M) were 22±3, 25±5, 21±6, 21±2 and 22±3 pmol DTT min^{-1} μg^{-1} over Bapunagar (Backward Residential Area), Narol (Industrial), Paldi (Bus Transport Hub), Income Tax (Huge Running Traffic) and Science City (Posh Residential Area), respectively. Overall, OP_V showed a significant linear correlation with PM_{10} mass, whereas OP_M remained more or less uniform with increasing PM_{10}. Although the OP_M values were similar, the variability in PM_{10} mass concentration from site-to-site reflects the corresponding health risks associated with PM_{10} exposure for the people living in these areas. Further, a noticeable temporal variation in OP_M at Narol and Paldi suggests that sources (species) with diverse OP_M contributed to PM_{10} on different days. A strong linear relationship between OP_{OC} (ratio of OP_V to the mass concentration of organic carbon) and f43 (ratio of m/z 43 signal to total water-soluble organic aerosols (WSOA) signal) suggests that the fossil-fuel combustion derived WSOA have higher OP. Furthermore, the relationships of OP with water-soluble trace metals and brown carbon are also investigated and discussed. Nitrogenous organic compounds particularly emitted from the traffic-related sources (Paldi and Income Tax) have higher OP_{OC} than those emitted from other sources over Bapunagar, Narol, and Science City.

Aerosol sampling was thankfully assisted by Mr. Utsav Gandhi and Dr. Nitasha Khatri from Gujarat Environment Management Institute, Gandhinagar.

doi : https://doi.org/10.1016/j.envpol.2020.115909

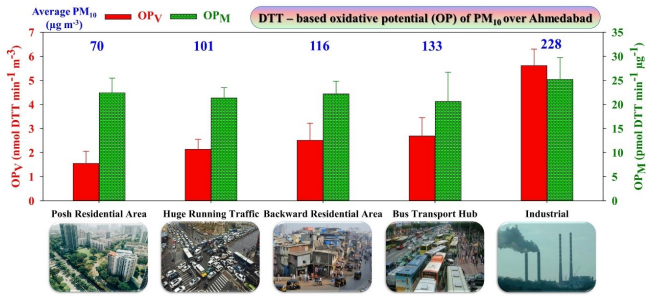

Figure no. 15: Volume normalized oxidative potential (OP_V) and mass-normalized OP (OP_M) over five different sites of Ahmedabad.

(A. Patel and N. Rastogi)

Sources and characteristics of light-absorbing fine particulates over Delhi through the synergy of real-ime optical and chemical measurements

Carbonaceous aerosols are mainly comprised of black carbon (BC) and organic carbon (OC) that contribute considerably to the global climate. Until recently, it was believed that BC was the only light-absorbing aerosol component that leads to positive radiative forcing, and OC was considered to be a scattering-type aerosol. However, recent studies reported that some fraction of organics also shows light absorption characteristics from the near UV to the visible region, labeled as brown carbon (BrC). In comparison to BC, the properties of BrC are least understood as they may consist of thousands of organic compounds with complicated molecular compositions. In this context, the present study examines the light absorption characteristics of fine atmospheric particulates (PM_1) using the co-located real-time measurements of chemical and optical aerosol characteristics at a site located in Delhi (28.54°N, 77.19°E) during winter (January 01 to February 10, 2019). The contribution of absorption by BC and BrC to the total absorption (b_{abs}) is computed using the absorption ÅAngström exponent (AAE) method. The period average contribution of BrC absorption ($b_{abs-BrC}$) to b_{abs} is found to be highest at 370 nm (23%) that decreased exponentially with increasing wavelengths, i.e.,18, 12, 10, and 4% at 470, 520, 590, and 660 nm, respectively. The absorption spectrum of BrC is used to study the bulk composition of BrC, which indicates that primary BrC was dominant during morning and night time, whereas secondary BrC was significant during the rest of the time. Further, organic aerosols (OA) were divided into different factors using positive-matrix factorization (PMF) analysis, and the mass absorption efficiency (E_{abs}) of each factor was assessed through multivariate linear regression of $b_{abs-BrC}$ with OA factors. The biomass burning

OA (BBOA) exhibited the highest E_{abs} at 370nm (0.86 m^2 g^{-1}), followed by semi-volatile oxygenated OA (SVOOA; 0.67 m^2 g^{-1}) and hydrocarbon-like OA (HOA; 0.42 m^2 g^{-1}). Further, although the composition of OA was dominated by LVOOA (32%) and BBOA (32%), followed by SVOOA (22%), and HOA (14%) (Fig. 16a), their contribution to b_{BrC} followed different order due to differences in their mass absorption efficiencies. The BBOA contributed almost half (48%) of $b_{abs-BrC}$ followed by SVOOA (26%), and HOA (10%) (Fig.16b). This study provides quantitative information on the sources of BrC and their relative contribution to BrC absorption over a heavily polluted region, which is still lacking in the literature. These results have implications in understanding the source-specific BrC absorption.

PRL lead this study with the collaborative support of researchers from IIT-Kanpur, IIT-Delhi, and Paul Scherrer Institute, Switzerland

doi : https://doi.org/10.1016/j.atmosenv.2021.118338

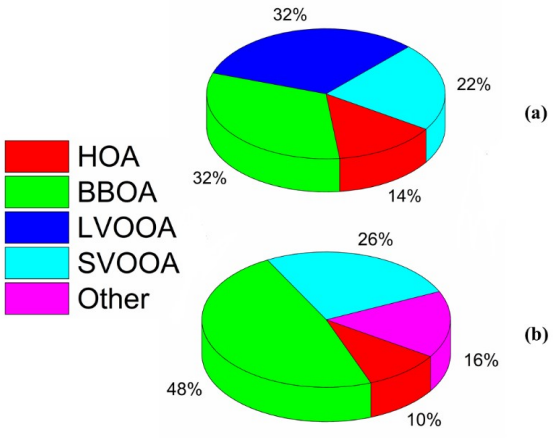

Figure no.16: Relative contribution of organic aerosol (OA) component loadings (a) to OA mass and (b) to brown carbon absorption at 370 nm (b_{BrC}).

(A. Singh and N. Rastogi)

Microbes as a boon for the bane of heavy metals

Modern globalization has escalated anthropocentric sources for heavy metal contamination in diverse natural habitats. Pernicious nature of heavy metals poses a major threat to all life forms in the environment. Heavy metals are not degradable like the organic pollutants but could be transformed to be persistent in a less toxic form. Microbes are the cheap tool as they evolve rapidly to combat heavy metal stress by developing various survival strategies, for instance sequestration or active transportation of metal. Their short generation time, large surface area and ease of genetic manipulation make them ideal candidates to use for the bioremediation process. Many heavy metal resistant microbes such as species of Bacillus, Pseudomonas, Acidothiobacillus, Saccharomyces, Geobacter and Rhizophus have been used for remediation of heavy metal contaminated sites. The effectiveness of bioremediation technique depends upon various factors, including biotic as well as abiotic, which mainly determine bio-availability of metal for remediation.The different metal microbe interactions such as sorption, accumulation, mineralization, transformation and solubilization are responsible for tapering heavy metal concentration at various loci or sites. The review emphasizes on the different interactions of the microbes with heavy metals, their survival strategies and the applications of the resistant strains in remediation.

This study was done in collaboration with Dr.M. Saraf, Gujarat University, Ahmedabad.

doi : https://doi.org/10.1007/s42398-020-00112-2

(A.D. Shukla)

Role of fluid in strain softening within the Main Central thrust in Sikkim: The origin of quartz-rich mylonites

The presence of fluids promotes strain softening, and profoundly affects the evolution of shear zones.The Main Central thrust (MCT) is a major shear zone that accommodated at least 90 km of shortening, and played a significant role in Cenozoic evolution of the Himalaya. Surprisingly, no information exists on the role of fluid in evolution of the MCT. This study integrates mineralogical, and geochemical analyses with mass-balance calculations to explore the role of fluids in evolution of the MCT shear zone from four exposures, which span ∼40 km distance along the transport direction in Sikkim, eastern India. Our analyses reveal significant fluid-induced strain softening in the investigated exposures, attested by retrogression of biotite to chlorite, and feldspar to muscovite, and quartz. The retrogressed feldspar grains are surrounded by recrystallized quartz, and the muscovite, and chlorite produced due to retrogression define the mylonite foliations, which indicate fluid activity was syn-tectonic. We propose a three-stage conceptual model to analyze the role of fluid in the evolution of the MCT in Sikkim: First,the shear zone nucleated along pre-existing structurally weak, and compositionally distinct zones. Following which, the proto shear zone developed in closed-system conditions, and deformation localized by dynamic recrystallization, and dislocation creep resulting in formation of ∼200 - 1000 m-thick protomylonites. Then, fluids infiltrated the shear zone, and induced retrogression, and element mobility. In the hinterland- most exposures, significant fluid-induced retrogression transformed the calc-silicate and paragneiss protoliths to mylonites resembling micaceous quartzites. In the frontal-most, and structurally intermediate exposures, the muscovite and chlorite grains underwent further dissolution, leaving behind a quartz-rich residue; thus, transforming tonalite orthogneiss, and paragneiss protoliths to mylonites resembling monomineralic quartzites. The deformation front narrowed through time, and became progressively localized within the ∼120 - 410 m-thick strain-softened mylonites at the shear zone core, whereas, deformation ceased or continued slowly in the ∼100-880 m-thick protomylonites at the margins. The study improves our understanding of the strain softening mechanisms operative within the MCT, and the origin of quartz-rich mylonites.

This study was done in collaboration with Dr. S. Chakraborty, IIT, Mumbai and Dr. A.S. Majumdar, IIT (ISM), Dhanbad.

doi : https://doi.org/10.1016/j.jsg.2020.104145

(A.D. Shukla)

Serpentinization and sustenance of life at slow-spreading ridges in Central Indian Ocean ridges

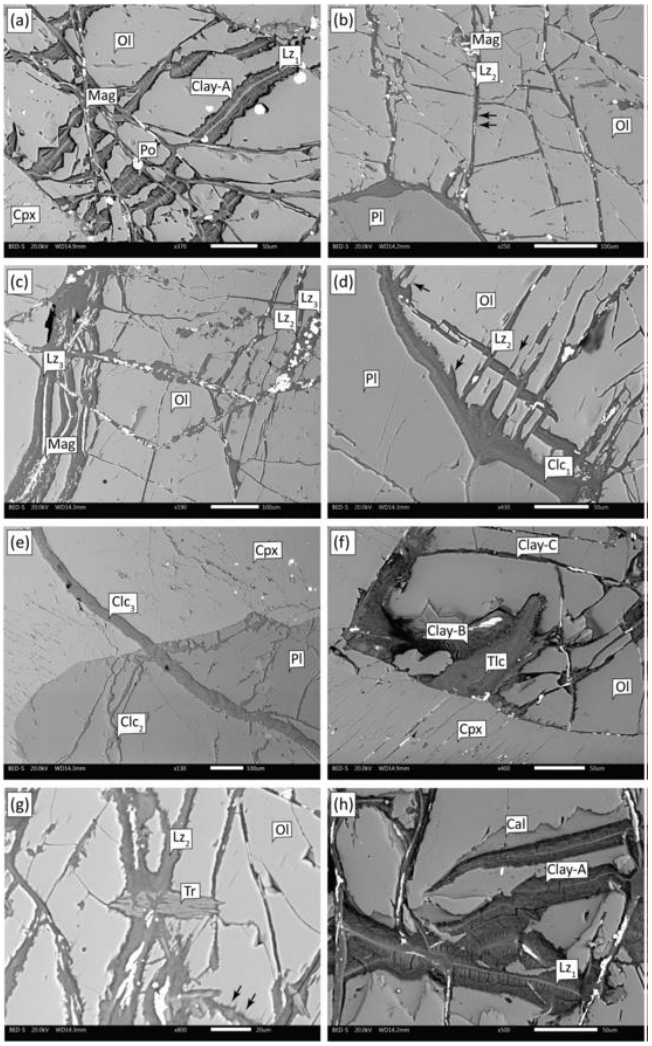

Figure no. 17: Typical BSE–SEM images of different olivine replacement textures in studied CIR olivine–gabbro samples. **(a)** Compositionally–zoned type–1 pseudomorphic mesh texture replacing olivine (Ol), showing the development of lizardite (Lz_1) layer $\pm$ magnetite (Mag) and the central part of the rim and clay–A towards the olivine interface. Presence of pyrrhotite (Po) is evident within olivine grains. Cp_x = clinopyroxene. **(b)** Compositionally - homogeneous type–1 rim replacing olivine (Ol), composed of Lz_2 lizardite $\pm$ magnetite (Mag). Presence of wedge-shaped depression (marked by black arrow) is also evident at Ol–Lz_2 grain boundary. **(c)** Type–2 vein texture, showing the development of Lz_3 serpentine + magnetite (Mag) replacing primary olivine (Ol). Note the cross–cutting relation of Lz_3 layer with respect to Lz_2 serpentine. **(d)** Replacement texture at the olivine (Ol) – plagioclase (Pl) grain boundary, showing the development of clinochlore (Clc_1) and lizardite (Lz_2) towards the plagioclase and olivine interfaces, respectively. Evidence of wedge–shaped cracks (marked by black arrow) are distinct here at the Ol–Lz_2 interface. **(e)** Replacement texture showing the formation of Clc_3 chlorite transgressing through plagioclase (Pl) and clinopyroxene (Cp_x) grains. Development of Clc_2 chlorite replacing plagioclase (Pl), cross–cut by Clc_3, is also evident.**(f)** Replacement texture at the olivine (Ol) - clinopyroxene (Cp_x) grain boundary, showing the development of talc (Tlc) in contact with Cp_x and clay-B toward the Ol grain. Formation of clay-C replacing Ol grain is also evident.**(g)** Compositionally-homogeneous type-1 replacement texture replacing olivine (Ol), evidencing the presence of tremolite (Tr), cross–cut by Lz_2 serpentine. Presence of wedge-shaped depression (marked by black arrow) is distinct at Ol–Lz_2 grain boundary. **(h)** Compositionally–zoned type–1 rim, showing the development of calcite (Cal) layer replacing primary olivine (Ol), towards the inner interface of previously formed clay–A and Lz_1 layer.

An alteration history through the textural-compositional characteristics across olivine mineral at its interfaces in inconsistently serpentinized olivine-gabbro rock samples from the "Vityaz Megamullion" in the northern Central Indian Ridge (CIR) were studied. The geochemical data and petrographical observations used to understand the role played by temperature and different chemical properties in infiltrating fluid (e.g. seawater/hydrothermal solution) which might have played on the pattern of compositional evolution during such processes. The two distinct types of replacement rims (i.e. type-1 and type-2) are conspicuous in our samples (Fig.17).

Type-1 pseudomorphic mesh rim, that formed within individual olivine grains, occurs in two different textural modes: (a)as successive layers of Fe-rich (X_{Mg} = 0.89 $\pm$ 0.02) lizardite $\pm$ magnetite, clay and calcite towards the olivine interface, and (b)as homogeneous rim of comparatively Fe-poor lizardite (X_{Mg} = 0.93 $\pm$ 0.01) $\pm$ magnetite. Replacement of olivine by talc and chlorite is evident towards the clinopyroxene and plagioclase grain boundaries, respectively. Local precipitation of clay minerals is also observed at the inner interface of talc layer and within intra-olivine fractures. Type-2 rim is characterized by the development of inter-olivine Mg-rich lizardite (X_{Mg} = 0.97 $\pm$ 0.01) + magnetite layer cross-cutting type-1 veins; thus, post-dates type-1 replacement. The process of CIR olivine-gabbro alteration records at least two stages of serpentinization. Any presence of brucite has not been observed, suggesting relatively higher silica activity at reacting interfaces during olivine-gabbro alteration than that of peridotite serpentinization at temperature $< 330^{\circ}$C.

The pattern of compositional evolution across olivine interface implies a micrometer-scale variation in different chemical properties in reacting fluid (i.e. log $a_{SiO_2(aq)}$, log a_{H_2O}, log $a_{Al^{3+}}$ / $a^3{}_{H^{+3}}$ and log $a_{Ca^{2+}}/a^2{}_{H^{+2}}$) and/or temperature during progressive alteration of olivine. Type-2 replacement attests greater extent of magnetite precipitation as compared to type-1 serpentinization, which may indicate increasing fluid-rock ratio in the system and/or decreasing magnitude of Fe intake into serpentine structure with ongoing alteration. Importantly, it implies release of H_2(*aq*) during olivine-gabbro serpentinization, which is consistent with that observed during peridotite serpentinization. This corroborates that alteration in the deepest part of the oceanic crust may play an important role on the sustenance of biosphere in slow-spreading ridges.

doi : https://doi.org/10.1016/j.lithos.2020.105730

This study was done in collaboration with Dr.D. Ray, PSDN, PRL and with Dr. A.S. Majumdar, IIT (ISM) Dhanbad.

(A.D. Shukla)

Mid- to Late Holocene relative sea-level change in the Gulf of Kachchh, western India

The Holocene sea level is modulated by a combination of factors such as tectonic instability, coastal configuration changes, proximity of the sites to meltwater discharge, sediment flux, and most importantly the post-last glacial maximum (LGM) glacio-isostatic adjustment (GIA) in the higher latitudes (Newman et al., 1989; Shennan and Horton, 2002). Therefore, a generalized global time/depth Holocene sea-level curve would be misleading (Pirazzoli, 1991). Along the Indian coast, studies suggest significant changes in the magnitude of the Holocene sea level (e.g. Pant and Juyal, 1993; Banerji et al., 2015). Thus, using multiproxy data (sedimentology, trace elements, organic geochemistry, ichnology, and pollen) supported by optical and radiocarbon dating

we aimed to determine the Relative Sea Level (RSL)–the change in sea level relative to land at a particular time and site from intertidal deposits from Gulf of Kachchh (Figure 18). Specifically, the magnitude and causes of Mid- to Late Holocene RSL changes were determined and also its influence, if any, was investigated on coastal Harappan settlements.

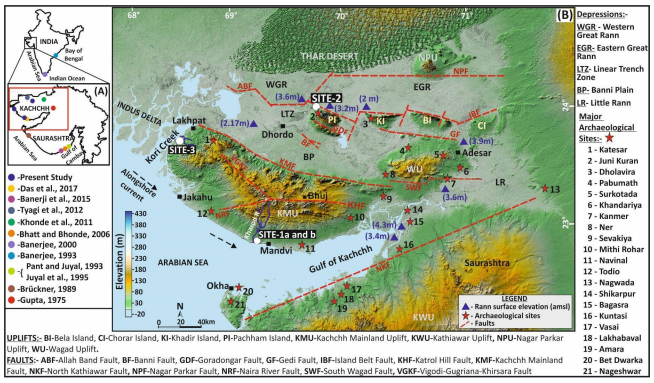

Figure no.18: In the inset map of India and (A) Gulf of Kachchh region, the colored dots mark the locations of various studies. The red rectangle marks the location of the enlarged map. (B) Digital Elevation Map of Kachchh peninsula showing major and minor thrusts (modified after Biswas, 2016). Sites investigated in the present study are marked in white circles: the Kharod Estuary (Site-1a), the river section (Site-1b), the India Bridge section (Site-2), and the Nani Cher Estuary section (Site-3).

The study suggests the dominance of fluvial activity between 16.5 $\pm$ 1.6 and 9.9 $\pm$ 0.7 ka. After $\sim$7 ka (7.3 $\pm$ 0.4, 6.8 $\pm$ 0.5 ka), the sea level rose until 4.7 $\pm$ 0.2 ka; where, tectonically corrected Mid-Holocene RSL change is estimated as 1.45 $\pm$ 0.33 m between $\sim$7 and $\sim$5 ka (Figure 19). The Mid-Holocene RSL high is attributed to the meltwater contribution from the Himalayan cryosphere, with subordinate contribution from glacio-isostatic adjustment and crustal subsidence. The second marginally high Late Holocene tectonically corrected RSL change at $\sim$1 ka (1.1 $\pm$ 0.1 ka and 1045 $\pm$ 175 cal yr BP) is estimated as 0.53 $\pm$ 0.43m. This is ascribed to monsoon wind-driven tidal ingression during Medieval Warming Period that might have affected the tidal amplitude positively. The study suggests that the Mid-Holocene RSL change did not play a deterministic role in the abandonment of the Harappan coastal settlements.

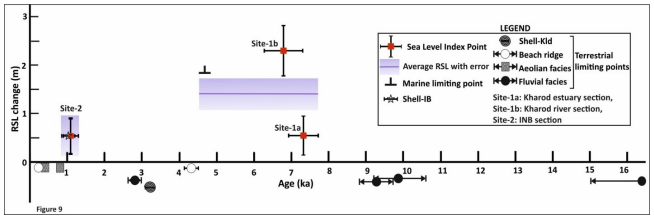

Figure no. 19: Age-elevation plot of the mid and late sea-level index points (SLIPs) and terrestrial and marine limiting points. The associated errors in RSL and chronology are shown by vertical and horizontal bars, respectively. The Mid-Holocene RSL ($\sim$7–5 ka) (blue stippling) is the average of RSL based on SLIPs at Sites-1a and -1b. Based on terrestrial limiting data points, we suggest that the negative tendency might have begun $\sim$4.5 ka. The Late Holocene RSL ($\sim$1 ka) (blue stippling) is marked from SLIP at Site-2.

doi : https://doi.org/10.1017/qua.2020.86

This study was done in collaboration with Gaurav Chauhan, M. Dhabi, S. Bhandari, B. Bhosle, A. Lakhote from The K.S.K.V. Kachchh University, Bhuj; S. Pandey BSIP, Lucknow and B.S. Desai from MS University Vadodara.

(S. Sharma, A.D. Shukla, R. Nambiar, R. Bhushan & N. Juyal)

Evidence for brown carbon absorption over the Bay of Bengal during the southwest monsoon season: a possible oceanic source

The near UV-visible light-absorbing organic carbon (OC) of ambient aerosols, referred as brown carbon (BrC), influences the atmospheric radiative forcing on both regional and global scales. We documented BrC absorption in the aqueous and methanol extracts of marine aerosols over the Bay of Bengal (BoB: September - October 2017) and a city, Visakhapatnam (May - June2018), in southern India during the southwest monsoon. The absorption spectra of BrC over the BoB showed several peaks around 300|400 nm and differ from those observed over Visakhapatnam. The absorption coefficient of BrC over the BoB, unlike Visakhapatnam data, does not seem to covary with other chemical proxies of biomass burning (non-sea-salt or nss-K^+) and coal combustion (nss-$SO_4{}^{2-}$) in the continental outflows, suggesting a different source of BrC over the BoB. Besides, we observed higher proportions of water-insoluble organic carbon (WIOC/OC: 0.89 $\pm$ 0.02) and significant enrichment of Mg^{2+} over Na^+ (relative to seawater) in BoB aerosols. This result and the backward air mass trajectories both indicate their major source of OC from marine-derived organic matter. In contrast, the absorption spectra of BrC over Visakhapatnam are like those from biomass burning emissions in the Indo-Gangetic Plain. This observation is further supported by the satellite-based fire counts and backward air mass trajectories. Therefore, this study underscores the significance of BrC aerosols from the oceanic sources that was not reported.

This work was carried out in collaboration with Dr. Poonam Bikkina and Dr. Srinivas Bikkina, CSIR-NIO, Goa.

doi : https://doi.org/10.1039/D0EM00111B

(A.K. Sudheer and M. Gaddam)

Present, past, and future of the oxygen minimum zone (OMZ) in the northern Indian Ocean

Decreasing concentrations of dissolved oxygen in the ocean are considered as one of the main threats to marine ecosystems as they jeopardize the growth of higher organisms. They also alter the marine nitrogen cycle, which is strongly bound to the carbon cycle and climate. Results obtained from the global atmosphere-ocean Kiel Climate Model and eddy resolving regional models indicate that a decreasing inflow of oxygen-enriched water masses from the south intensified the Arabian Sea OMZ during the last 6000 years, whereas a decreasing oxygen concentration within inflowing Persian Gulf Water intensifies the OMZ in response to global warming. These trends significantly affect benthic and pelagic ecosystems. The regular occurrence of Noctiluca is an example of a new phenomenon that

is assumed to herald a regime shift within the pelagic ecosystem of the Arabian Sea in response to declining concentrations of dissolved oxygen. Comprehensive studies investigating possible repercussions on the OMZ through e.g. impacts on the export production and vertical migration and distributions of zooplankton are missing. Accordingly, these recent changes augment the problems that arise when trying to represent the Indian Ocean OMZ in models, and thus in projecting the impact of the changing monsoon system on productivity and OMZ development under global change scenarios.

This work was done in collaboration with Tim Rixen, Leibniz Centre for Tropical Marine Research (ZMT), Bremen, Germany.

doi : https://doi.org/10.5194/bg-17-6051-2020

(A. Singh)

Dinitrogen fixation rates in the Bay of Bengal during summer monsoon

Biological dinitrogen (N_2) fixation exerts an important control on oceanic primary production by providing bioavailable form of nitrogen (such as ammonium) to photosynthetic microorganisms. N_2 fixation is dominant in nutrient poor and warm surface waters. The Bay of Bengal is one such region where no measurements of phototrophic N_2 fixation rates exist. The surface water of the Bay of Bengal is generally nitrate-poor and warm due to prevailing stratification and thus, could favour N_2 fixation. We commenced the first N_2 fixation study in the photic zone of the Bay of Bengal using $^{15}N_2$ gas tracer incubation experiment during summer monsoon 2018. We collected seawater samples from four depths (covering the mixed layer depth of up to 75m) at eight stations. N_2 fixation rates varied from 4 to 75 μmol N m^{-2} d^{-1}. The contribution of N_2 fixation to primary production was negligible ($<$1%, Figure 20). However, the upper bound of observed N_2 fixation rates is higher than the rates measured in other oceanic regimes, such as the Eastern Tropical South Pacific, the Tropical Northwest Atlantic, and the Equatorial and Southern Indian Ocean.

doi : https://doi.org/10.1088/2515-7620/ab89fa

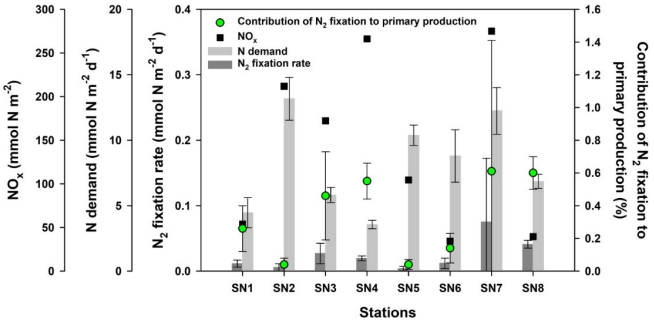

Figure no. 20: Euphotic zone integrated NO_x, N demand, N_2 fixation rate and contribution of N_2 fixation to primary production at all the stations

(H. Saxena, D. Sahoo, M. Atif Khan, S. Kumar, A.K. Sudheer & A. Singh)

Non-Redfieldian C:N:P ratio in the inorganic and organic pools of the Bay of Bengal during the summer monsoon

Nitrogen (N) and phosphorus (P) determine the strength of the ocean's biological carbon (C) pump and variation in N:P ratio is key to phytoplankton growth. A fixed C:N:P ratio (106:16:1) in organic matter and deep-water nutrients was observed by Alfred C. Redfield. However, recent studies have challenged the concept of Redfield Ratio and this remains to be examined in oceanic basins like the Bay of Bengal. For this purpose, we sampled the water in the Bay of Bengal for C, N, and P content in the organic and inorganic pools from surface to 2000 m. Overall, C:N:P ratio deviated greatly from the Redfield Ratio (Figure 21). The C:N:P ratio in particulate organic matter varied from 232:25:1 in the top layer (surface to the depth of chlorophyll maximum) to 966:72:1 in the deep water (300 – 2000 m). In dissolved organic matter, the ratio varied from 357:30:1 in the top layer to 245:66:1 in the deep water. The N:P ratio in nutrients varied from 3 in the top layer to 12 in the deep water. The nutrient depleted top layer (average nitrate + nitrite $\sim$ 0.7 μmol L^{-1}) with low N:P ratio coupled with reported low primary production rates in the Bay suggested that the production was N limited. Concurrent N_2 fixation rates were not significant to alter the observed C:N:P ratio. Eddies showed a mixed effect on C:N:P ratio. Our C:N:P ratios in particular organic matter are comparable to other tropical basins and supports the nutrient supply hypothesis for low latitude ecosystems.

doi : https://doi.org/10.3354/meps13498

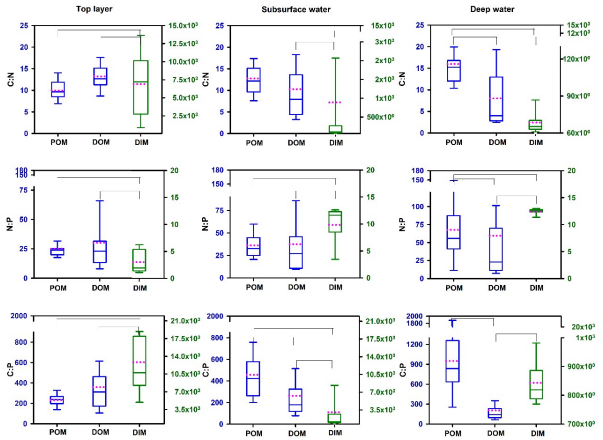

Figure no. 21: C:N, N:P and C:P ratios in top layer, subsurface water, and deep water

(D. Sahoo, H. Saxena, N. Tripathi, M. Atif Khan, A. Rahman, S. Kumar, A.K. Sudheer & A. Singh)

Assessment of role of vehicular catalytic converter temperature in emission of pollutants using stable isotopes

Air pollution caused by vehicular emission has been an issue of public concerns because of rapid increase in the emission from transport sector. Alternative technologies (e.g., biofuel, electric and hybrid vehicles) have been proposed but in the existing set up,

enhancing the efficiency of catalytic converters in fossil fuelled engines is probably the easiest way of controlling the harmful emissions and are implemented by manufacturers due to strict government rules. Catalytic converters reduce toxic and harmful compounds in exhaust gases into less harmful/inert species. The efficiency, however, is largely affected by the operating temperature of a converter which is set by the hot exhaust gas released from the combustion chamber. Using multiple isotope ratio analyses in exhaust CO_2 ($\delta^{13}C$, $\delta^{17}O$, $\delta^{18}O$, and Δ_{47}) and N_2O ($\delta^{15}N$, $\delta^{18}O$ and Site Preference) in diesel and gasoline powered vehicles, we observed that the degree of N_2O reduction to N_2 in gasoline powered vehicle is high when the converter temperature is above 200°C (temperature estimated from Δ_{47} values). In contrast, diesel vehicles produce N_2O in abundance, a consequence of selective catalytic reduction of NO_x, and the reduction efficiency depends on the converter temperature. Therefore, the catalytic converters act as sinks and sources of N_2O to the atmosphere in gasoline and diesel operated vehicles, respectively. We also carried out the isotopic analyses inside a highway tunnel and observed elevated N_2O concentration indicating that the vehicular exhaust is a net source of N_2O to the atmosphere. The combined study of clumped isotopes and N_2O concentration in the exhaust gas suggests that it is useful in probing the operational temperature of catalytic converters and monitoring the pollution level in operation, thus providing an opportunity for manufacturers to optimize the catalytic efficiency to reduce the level of toxic pollutants to the environment.

The work was done in collaboration with Prof. Mao-Chang Liang, Academia Sinica, Taiwan.

doi : https://doi.org/10.1021/acs.est.0c07430

(A.H. Laskar)

Contribution of pollutants in Delhi from crop residue burning using the triple oxygen isotope technique in atmospheric CO_2

Air quality in the megacity Delhi is a major concern not only because of emissions from local sources but also due to pollutants from crop residue burning in the surrounding areas of the city, particularly the rice straw burning in the post monsoon season. Isotopes in CO_2, a major burning product, provide an alternative way to characterize the impact of biomass burning from a new perspective that other common tracers such as particulate matters are limited because of their physical and chemical reactiveness. Using conventional ([CO_2], $\delta^{13}C$, and $\delta^{18}O$) and unconventional ($\Delta^{17}O$) isotope ratios at a site in Delhi, and two surrounding remote regions during a field campaign in October 18-20, 2017, anthropogenic CO_2 has been found to vary between 4 and 40%. Further analysis done by employing isotopic mixing model with constraints from the $\Delta^{17}O$ values yields that rice straw burning contributes as much as ∼70% of the total anthropogenic CO_2, which is more than double of the fossil fuel contribution (30%), during the study days.

The work was done in collaboration with Dr. A.S. Maurya, IIT Roorkee and Prof. Mao-Chang Liang, Academia Sinica, Taiwan.

doi : https://doi.org/10.1016/j.envpol.2020.114542

(A.H. Laskar)

Thermoregulation of Late Cretaceous dinosaurs inferred using clumped isotope thermometry in fossil eggshell carbonates

The thermal physiology of dinosaurs, especially the warm blooded (endothermic) or cold blooded (ectothermic) nature of their metabolism, inferred indirectly using body mass, biophysical modelling, bone histology and growth rate, has long been a matter of debate. Clumped isotope thermometry, based on the thermodynamically driven preference of ^{13}C - ^{18}O bonds in carbonate minerals of fossilized eggshells, yields temperature of egg formation in the oviduct and can delineate the nature of thermoregulation of some extinct dinosaur taxa. In the present study, the clumped isotope thermometry was applied to the eggshells of a several species of modern birds and reptiles to show that it is possible to obtain the body temperatures of these species. The technique was then used to the fossil eggshells of Late Cretaceous sauropods and theropods recovered from western and central India to estimate the body temperatures of these extinct species. The distribution of body temperatures of dinosaurs along with modern birds and reptiles are shown in (Figure 22). The dinosaur body temperatures varied between 29°C and 46°C, with an overall average of 37°C. The analyses suggest that these late Cretaceous giant species were endowed with a capacity of variable thermoregulation to control their body temperature.

The work was done in collaboration with Dr. D.M. Mohabey, Geological Survey of India and Prof. Mao-Chang Liang, Academia Sinica, Taiwan.

doi : https://doi.org/10.1016/j.heliyon.2020.e05265

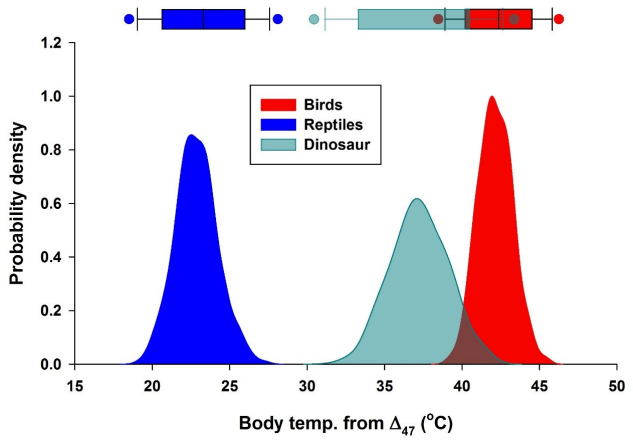

Figure no. 22: Box-and-whisker plots (top) and bootstrap probability density distributions (bottom) of the mean body temperatures of modern birds and reptiles and Late Cretaceous Indian dinosaurs estimated from measured Δ_{47} values in fossil eggshell carbonates.

(A.H. Laskar and S.K. Bhattacharya)

Constraining the formation age of the crude oil (NIST RM 8505) by Re-Os geochronometry: significance of analytical method and uncertainties

Crude oil (also known as Petroleum) is composed of different components: various hydrocarbon phases, and organic compounds

containing major proportions of nitrogen, sulfur, and oxygen, and different abundances of different trace elements. Different organic compounds present in crude oil can be characterized by their volatility, viscosity, and specific gravity. In addition to understanding the geochemistry of the crude oils, another critical aspect has been to constrain their formation age. Both Re and Os have a strong affinity towards organic phases; this organophilic nature of both these trace metals can be used to estimate the crude oil formation age. Here, we present the results for Re-Os dating of NIST RM 8505 crude oil (Venezuelan crude oil). The average Re and Os concentrations in NIST RM 8505 crude oil are 2.43 $\pm$ 0.15 ng/g and 30.0 $\pm$ 0.7 pg/g Os, respectively. While the Re concentration of the crude oil is relatively enriched over the crustal component, the average Os abundance is very similar to the upper continental crust. For dating the crude oil by the Re-Os geochronometry, the Re-Os isotopic analyses were done after separating different crude oil components: maltene (n-alkane soluble) and asphaltene (n-alkane insoluble). Several asphaltene precipitations using different n-alkane solvents (pentane, heptane and decane) provide a Model 1 age of 75 $\pm$ 24 Ma for RM 8505 crude oil. Using the maltene-crude oil-asphaltene triplets extracts from RM 8505 yields a more precise Model 1 age 78.5 $\pm$ 2.3 Ma, with an initial $^{187}Os/^{188}Os$ of 0.88 $\pm$ 0.02. These results suggest that Re-Os dating of maltene-crude oil-asphaltene triplets can provide precise constraints to the formation age of the crude oil.

doi : https://doi.org/10.1016/j.chemgeo.2019.119381

(V. Goswami)

Programmable Automated Field Deployable High Frequency Rainwater Sample

Uncertainties in weather forecasting, especially for the rainfall event, makes it difficult and inconvenient to collect rain water samples in manual sampling system. Collection of the rainwater samples at desire time interval or cumulative sample over a certain time duration is an essential perquisite for modern hydro meteorological and environmental applications.

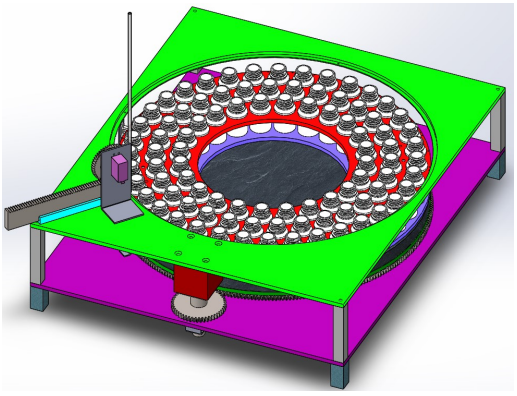

Figure no. 23: Sample Tray Structure design of the instrument

Automated High frequency Rain Water Sampler is an instrument to facilitate automatic sampling of runoff during rainfall events. The objectives of the instrument are to collect rainwater sample accumulated over a certain time duration, continuously measure the amount of rainfall (cm) from volume of rainwater collected (cm^3), detect the isolated rain events and store the samples after collecting the rainwater for such events. It has to facilitate remote monitor and control through real time program. The prototype of this instrument has been developed. It mainly comprises of input funnel structure, motorized sample tray mechanism, electronic control system, valves and sensors. The sample tray structure accommodates 90 sample bottles (Max. 60 ml) which get filled during rainfall event sequentially as per control algorithm. The data log is generated to time tag the sample bottle associated with rainfall event. The performance of the instrument has been verified during last monsoon season at PRL campus and based on that different sampling strategy for sampling is being worked out in order to accommodate in control program.

(M. Shah, H. Vaghela, R.D. Deshpande & L. Chavda)

Depositional history of the Mesoproterozoic Chhattisgarh Basin

The Chhattisgarh Basin is one of the most important Proterozoic basins of peninsular India. Owing to its deposition in the Mesoproterozoic, the largely undeformed and unmetamorphosed sedimentary sequence of this basin is believed to hold vital clues to our understanding of the evolution of the Indian craton subsequent to the disintegration of the supercontinent Columbia. Despite its importance, only limited studies have been carried out to decipher the depositional history of the basin and to correlate various litho-units in it. Here, we present results of quantitative provenance analysis of the sediments in the basin using trace element and Nd isotopic ratios and discuss their implications for the evolution of the basin in the context of regional tectonics. The sediment provenance analysis reveals that the spatially extensive $\sim$2.5 Ga old granitoids of the Bastar craton were the major contributors (45% to 65%) of the total sediment budget into the basin during its initial stage of evolution. As sedimentation progressed the contribution from the Bastar granitoids was restricted to less than 30% of the total budget with the remaining supplied by younger 1.6 - 1.7 Ga magmatic rocks. The overall provenance of sediments appears to have remained constant throughout the evolutionary history of the basin; however, the relative contributions of various sources did change with time. The latter is highly conspicuous across the stratigraphic boundary between the Singhora and Chandarpur groups, in the lower part of the Chhattisgarh Supergroup. The geochemical data suggest that the basin developed as a result of either rift or sag into which the sea incursion occurred through the adjacent grabens during the Mesoproterozoic marine transgression.

doi : https://doi.org/10.1080/00206814.2020.1712557

(B.G. George and J.S. Ray)

Provenance of the Oligocene Sediments in the Andaman Forearc

Finding provenance of the siliciclastic turbidites deposited in the Andaman Trench-Forearc Basin had remained contentious with most indicators pointing towards major sediment sourcing either from eastern Myanmar or from nascent Himalayan mountain belt. Whereas the palaeo-Irrawaddy River was considered as the main transporting agent for sediments originating in Myanmar, the Himalayan sediments were believed to have been recycled from the earliest Bengal

Fan. Here, we examine existing Sr–Nd isotopic data for Oligocene sediments deposited in the basin and exposed today on the Andaman Accretionary Prism (AAP) to determine their provenance and transport pathways. We also present new data for sediments in the Barail Group, Bengal Basin and use them to test the sediment recycling hypothesis. Results of our study confirm that material from the Himalayan sources, transported through the submarine Bengal Fan, contributed significantly to the Andaman basin during the Oligocene. Sr-Nd isotopic compositions considered along with published U-Pb detrital zircon age data reveal that both the Tethys Himalaya and Higher Himalaya were the major sediment suppliers to the basin, with a minor contribution coming from juvenile source(s) in the Indo-Myanmar ophiolite belt and/or the central Myanmar volcanic arc. We propose that the large Himalayan contribution was a result of rapid exhumation and high rate of erosion in the north-eastern Himalaya and Tibet during Late Eocene and Oligocene and sediment transport by the palaeo-channels of the Yarlung-Siang-Brahmaputra river system via the Bengal Basin/Fan.

doi : https://doi.org/10.1007/978-3-030-39843-9_5

(N. Awasthi, B.G. George & J.S. Ray)

Theoretical Physics

Effects of hadronic repulsive interactions on the fluctuations of conserved charges

We investigate the effect of repulsive interaction between hadrons on the fluctuations of the conserved charges. We calculate the baryon, the electric charge, and the strangeness susceptibilities within the ambit of hadron resonance gas model extended to include the short range repulsive interactions. The repulsive interactions are included through a mean-field approach where the single particle energy gets modified due to mean-field interactions between hadrons proportional to the number density of hadrons. We assume different mean-field interactions for mesons and baryons. It is shown that the repulsive interactions play a very crucial role to describe hadronic matter near transition temperature. We also show that in order to consistently describe higher order conserved charge fluctuations mesonic repulsive interactions cannot be neglected. Further, we demonstrate that the repulsive interaction of baryons is essential to describe the lattice simulation results at finite baryon chemical potential for higher order fluctuations.

This work was done in collaboration with [Somenath Pal, A. Bhattacharyya] of Calcutta University and [Guruprasad Kadam] of Sivaji University Kolhapur.

doi : https://doi.org/10.1103/PhysRevD.103.054015

(Hiranmaya Mishra)

An Equation of State for Magnetized Neutron Star Matter and Tidal Deformation in Neutron Star Mergers

We derive an equation of state (EOS) for magnetized charge-neutral nuclear matter relevant for a neutron star (NS). The calculations are performed within an effective chiral model based on the generalization of the σ model with nonlinear self-interactions of the σ mesons along with the $\rho - \sigma$ cross-coupling term. This model is extended by introducing the contributions of a strong magnetic field on the charged particles. The contributions arising from the effects of the magnetic field on the Dirac sea of charged baryons are also included. The resulting EOS for the magnetized dense matter is used to investigate the NS properties like its mass, radius, and tidal deformability. The magnitude of the magnetic field at the core of the NS considered here is in the range of 10^{15}–10^{18} G, for which the relative deformation from spherical symmetry turns out to be less than cwone percent, giving a post facto justification for the spherically symmetric treatment of the NS structure. The dimensionless tidal deformability $\Lambda_1.4$ is 526 for an NS with mass 1.4 $\mathrm{M}_{\odot}$, which is consistent with the recent observation of GW 170817. The maximum mass of the NS in the presence of a strong magnetic field is consistent with the observational constraints on the mass of the pulsar PSR J0348–0432, and its radius at a mass of 1.4$\mathrm{M}_{\odot}$ is also in agreement with the empirical bounds.

This work was done in collaboration with [N.K. Patra, T. Mallik and T. Jha] of BITS Pilani, Goa.

doi : https://doi.org/10.3847/1538-4357/aba8fc

(Hiranmaya Mishra)

Magneto-Seebeck coefficient and Nernst coefficient of a hot and dense hadron gas

We discuss the thermoelectric effect of hot and dense hadron gas within the framework of the hadron resonance gas model. Using the relativistic Boltzmann equation within the relaxation time approximation we estimate the Seebeck coefficient of the hot and dense hadronic medium with a gradient in temperature and baryon chemical potential. The hadronic medium in this calculation is modeled by the hadron resonance gas (HRG) model with hadrons and their resonances up to a mass cutoff $\Lambda \sim 2.6$ GeV. We also extend the formalism of the thermoelectric effect for a nonvanishing magnetic field. The presence of magnetic field also leads to a Hall type thermoelectric coefficient (Nernst coefficient) for the hot and dense hadronic matter apart from a magneto-Seebeck coefficient. We find that generically in the presence of a magnetic field the Seebeck coefficient decreases while the Nernst coefficient increases with the magnetic field. At higher temperature and/or baryon chemical potential these coefficients approach to their values at vanishing magnetic field.

This work was done in collaboration with [A. Das] of Institute of Nuclear Physics, Krakow, Poland and [Ranjita K. Mahapatra] of Banki Autonomous College, Cuttack.

doi : https://doi.org/10.1103/PhysRevD.102.014030

(Hiranmaya Mishra)

HQ Collisional energy loss in a magnetized medium

We study the effect of the magnetic field on the collisional energy loss of heavy quark (HQ) moving in a magnetized thermal partonic medium. This is investigated in the strong field approximation where the lowest Landau level (LLL) becomes relevant. We work in the limit $g\sqrt{e\mathrm{B}}$.

doi : https://doi.org/10.1007/JHEP05(2020)068

(B. Singh,, S. Mazumder and H. Mishra)

Low energy constraints from absolute neutrino mass observables and lepton flavor violation in left-right symmetric model

We have studied the correlations among the three absolute neutrino mass observables - the effective Majorana mass governing neutrino-less double beta decay, the electron neutrino mass which is measured in single beta decay experiments and the sum of the light neutrino masses constrained from cosmological observations, in the context of minimal left-right symmetric model. Two phenomenologically interesting cases of type-I seesaw dominance as well as type-II seesaw dominance have been considered. We have taken into account the independent constraints coming from lepton flavour violation, single beta decay, cosmology and neutrino-less double beta decay and have determined the combined allowed parameter space that can be probed in the future experiments. We have also analyzed the correlations and tensions between the different mass variables. In addition, the constraints on the masses of the heavy particles coming from lepton flavor violation and the bounds on three absolute neutrino mass observables are also determined. We show that these constraints can rule out some of the parameter space which are not probed by the collider experiments.

doi : https://doi.org/10.1103/PhysRevD.103.055016

(Srubabati Goswami and Vishnudath, K.N.)

Implications of the dark large mixing angle solution and a fourth sterile neutrino for neutrinoless double beta decay

We analyze the effect of the dark large mixing angle (DLMA) solution on the effective Majorana mass governing neutrino-less double beta decay in the presence of a sterile neutrino. We consider the 3+1 picture, comprised of one additional sterile neutrino. We check that the Mikheyev-Smirnov-Wolfenstein resonance in the Sun can take place in the DLMA parameter space in this scenario. Next, we investigate how the values of the solar mixing angle corresponding to the DLMA region alter the predictions of effective neutrino mass governing neutrino-less double beta decay, by including a sterile neutrino in the analysis. We also compare our results with three-generation cases for both standard large mixing angle (LMA) and DLMA. Additionally, we evaluate the discovery sensitivity of the future Xe based experiments in this context.

This work was done in collaboration with D. Kuchibatla of School of Natural Sciences, Mahindra Ecole Centrale, Hyderabad.

doi : https://doi.org/10.1103/PhysRevD.102.015020

(Srubabati Goswami , Vishnudath, K.N. , Poddar, Tanmay)

Realization of the minimal extended seesaw mechanism and the TM_2 type neutrino mixing

We worked on the phenomenology of sterile neutrino mass matrices in the minimal extended seesaw mechanism with me. We considered a neutrino mass model based on the flavour symmetry group $\mathrm{A}_4 \times \mathrm{C}_4 \times \mathrm{C}_6 \times \mathrm{C}_2$ which accommodates a light sterile neutrino. We also introduced a U(1) gauge symmetry in the sterile sector and also impose CP symmetry. The vacuum alignments of the scalar fields in the model spontaneously break these symmetries and generates the fermion mass matrices. We obtained the light neutrino masses and the mixing observables. In the active neutrino sector, we obtained the TM_2 mixing pattern with non-zero reactor angle. The appeal of the model lies in minimal number of free parameters and also ability to explain both active and sterile neutrino parameters.

This work was done in collaboration with R. Krishnan of Saha Institute of Nuclear Physics, Kolkata.

doi : https://doi.org/10.1007/JHEP09(2020)050

(Srubabati Goswami, Ananya Mukherjee)

The impact of nonminimal Universal Extra Dimensional model on $\Delta\mathrm{B} = 2$ transitions

In a five dimensional Universal Extra Dimensional scenario, the masses and couplings of many Kaluza-Klein excitations are significantly modified compared to the minimal set up. Within such a Universal Extra Dimensional scenario, the Kaluza-Klein contributions of quarks, gauge bosons and charged Higgs to $\Delta\mathrm{B} = 2$ transitions leading to B-$\bar{\mathrm{B}}$ mixing are evaluated at one loop order, and their impact on Unitarity Triangle are studied in detail. This allows to set stringent limits $geq 1.48$ TeV on the inverse of the radius of compactification of the extra dimension.

doi : https://doi.org/10.1140/epjc/s10052-021-08937-9

(Avirup Shaw)

Phenomenology of $\tau^- \to \pi^- \nu_\tau \gamma$ using light cone sum rules

The radiative tau decay, $\tau^- \to \pi^- \nu_\tau \gamma$, is studied within the light cone sum rule approach. This mode involves non-perturbative form factors in the time like region unlike the radiative pion decay, leading to resonant contributions. The leading order results for the

form factors are derived and the branching ratio for the mode is presented. This is the first application of light cone sum rules to a decay mode like this and the results provide an independent check on the non-perturbative quantities, including the structure dependent parameter at zero momentum transfer.

doi : https://doi.org/10.1103/PhysRevD.103.056017

(Anshika Bansal, Namit Mahajan)

Impact of soft photons on $\mathrm{B} \to \mathrm{K}\ell^+\ell^-$

The modes, $\mathrm{B} \to \mathrm{K}\ell^+\ell^-$, with $\ell = e, \mu$, have attracted a lot of theoretical and experimental attention as the ratio of the muon to electron final states presents a very clean observable in the quest for physics beyond the Standad Model (SM). Experimentally, this ratio deviates from unity as expected from SM (universality between electrons and muons) by about 15%. However, the theoretical calculations don't inlcude the corrections due to Quantum Electrodynamics (QED). Proper inclusion of these turns out to be notorious due to the fact that unless the measurements are made photon inclusive, there are large logarithmic factors, dependent on the lepton mass, that affect the modes significantly, and worsen the ratio to some degree. Detailed theoretical expressions are presented to enable a comparison with the experimental results once the energy and angular cuts adopted in the experiments are provided, making the theoretical predictions more robust.

doi : https://doi.org/10.1103/PhysRevD.103.056022

(Dayanand Mishra, Namit Mahajan)

Unification and Higgsino dark matter in the GUT scale supersymmetry

We have carried out a detailed study of a scenario in which supersymmetry is broken at the Grand Unification (GUT) scale leaving the two-Higgs-doublet model as an effective low energy theory along with superpartners of Higgs and gauge boson, namely Higgsinos and Gauginos, at the intermediate scale. The Higgsino at TeV scale can account for the observed Dark Matter in the universe provided that the gauginos are not heavier than 10^5 GeV. Such a scenario is termed as split-supersymmetry and it provides precision gauge coupling unification consistent with the proton lifetime. However, light gauginos lead to the Higgs mass larger than its experimentally observed value. We show that splitting the gauginos circumvent this problem. The investigation is carried out through two-loop renormalization group evolution and one-loop corrected matching conditions between the various scales present in the framework.

doi : https://doi.org/10.1103/PhysRevD.101.115008

(V. S. Mummidi and Ketan M. Patel)

Neutrino oscillations in the presence of gravitational lensing

Neutrino oscillation in flat spacetime is a well understood, both theoretically and experimentally. It is well-known in this case the oscillation probabilities depend on the difference of square of neutrino masses and not on the individual mass or absolute mass scale. We show that this picture substantially gets modified in the presence of gravitational lensing. If neutrinos pass by a gravitating object (a star or black-hole), their effective path length is changed resulting into interference effect. We observe that such interference effects depend on the absolute mass of neutrinos and one can infer the absolute neutrino mass scale from the lensing effects. Various quantitative aspects of this are investigated in two and three flavour case.
This work was carried out in collaboration with Himanshu Swami and Kinjalk Lochan from IISER, Mohali.

doi : https://doi.org/10.1103/PhysRevD.102.024043

(Ketan M. Patel)

Inflation and long-range force from a clockwork D term

Cosmic inflation driven by the vacuum energy associated with the D term of a supersymmetric Abelian gauge group and a possible existence of long-range force mediated by an ultralight gauge boson Z' are two extreme examples of models based on extra U(1) symmetries. Large vacuum energy sets the scale of inflation while the scales of long-range forces induced by anomaly free extra gauged U(1) symmetries are constrained by neutrino oscillations, binary pulsar timings, and invisible neutrino decay. There exists a difference of about 40 orders of magnitude between the scales of these two. Also, gauge couplings associated with the long-range forces are very small compared to the standard model couplings and the one required for inflation. We propose a framework based on clockwork mechanism in which these vastly different scales and associated new physics can coexist without invoking any arbitrarily small or large parameter in the fundamental theory.

doi : https://doi.org/10.1103/PhysRevD.103.035008

(Anjan S. Joshipura, Subhendra Mohanty, Ketan M. Patel)

Scope of unveiling compressed supersymmetric scenario using boosted jet techniques

Search for compressed supersymmetry at multi-TeV scale, in the presence of a light gravitino dark matter, can get sizeable uplift while looking into the associated fat-jets with missing transverse momenta as a signature of the boson produced in the decay process of much heavier next-to-lightest sparticle. We perform the detailed background study adopting a multivariate analysis using a boosted decision tree to provide a robust investigation to explore the discovery potential for

such signal at 14 TeV LHC considering different benchmark points satisfying all the theoretical and experimental constraints.

This work was done in collaboration with Ms A. Bhardwaj, PRL, B. Mukhopadhyaya, IISER-Kolkata S.K. Rai, HRI, Prayagraj, and J. Dutta, University of Hamburg.

doi : https://doi.org/10.1007/JHEP10(2020)083

(Partha Konar)

Deep learning approach to probe the invisible decay of Higgs

Vector boson fusion proposed initially as an alternative channel for finding heavy Higgs has now established itself as a crucial search scheme to probe different properties of the Higgs boson or for new physics.

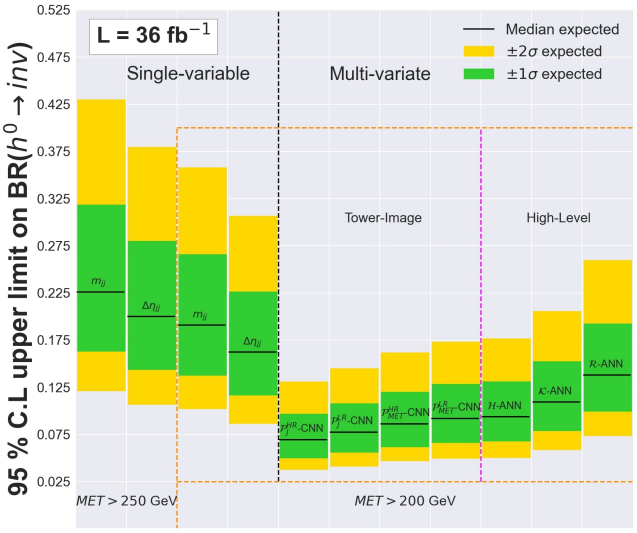

Figure No. 1: The median expected upper limit on the invisible branching ratio of SM Higgs at 95% CL along with the one and two sigma error bands are shown for integrated luminosities of 36 fb^{-1}. Comparing the performance of present experimental reach (Single-variable) together with possible Multi-variate reach both with respect to high-level and low-level feature spaces, clearly demonstrate the capability of deep-learning (CNN) framework just using low-level calorimeter data.

We explore the merit of deep-learning entirely from the low-level calorimeter data in the search for invisibly decaying Higgs. Such an effort supersedes decades-old faith in the remarkable event kinematics and radiation pattern as a signature to the absence of any color exchange between incoming partons in the vector boson fusion mechanism. We investigate among different neural network architectures, considering both low-level and high-level input variables as a detailed comparative analysis. To have a consistent comparison with existing techniques, we closely follow a recent experimental study of CMS search on invisible Higgs with 36 fb^{-1} data. We find that sophisticated deep-learning techniques have the impressive capability to improve the bound on invisible branching ratio by a factor of three, utilizing the same amount of data. Without relying on any exclusive event reconstruction, this novel technique can provide the most stringent bounds on the invisible branching ratio of the SM-like Higgs boson. Such an outcome has the ability to constraint many different BSM models severely.

This work was done in collaboration with Ng, V., A. Bhardwaj, PRL and A. Nayak IOP, Bhubaneswar.

doi : https://doi.org/10.1140/epjc/s10052-020-08629-w

(Partha Konar)

Linking the pseudo-Dirac dark matter and radiative neutrino mass in a singlet doublet scenario, and A dark clue to seesaw and leptogenesis in singlet doublet scenario with (non)standard cosmology

We developed a simple extension of the standard model with a pair of fermions, a singlet and a doublet, in a common thread linking the dark matter problem with the smallness of neutrino masses associated with several exciting features. In the presence of a small bare Majorana mass term, the singlet fermion brings in a pseudo-Dirac dark matter capable of evading the strong spin-independent direct detection bound by suppressing the dark matter annihilation processes mediated by the neutral current. In consequence, the allowed range of a mixing angle between the doublet and the singlet fermions gets enhanced substantially. The presence of the same mass term in an association with singlet scalars also elevates tiny but nonzero masses radiatively for light Majorana neutrino satisfying observed oscillation data. Using extension of this model, we also worked out an alternative scenario of leptogenesis assisted by dark sector which leads to the baryon asymmetry of the Universe satisfying all theoretical and experimental constraints. In the presence of a (non)standard thermal history of the Universe, we perform the detailed dark matter phenomenology adopting the suitable benchmark scenarios, consistent with direct detection and neutrino oscillations data. Besides, we have demonstrated that the singlet scalars can go through CP-violating out of equilibrium decay, producing an ample amount of lepton asymmetry. Unconventional thermal history of the Universe can thus aspire to lend a critical role both in the context of dark matter as well as in realizing baryogenesis.

These works were done in collaboration with A. Mukherjee, A.K. Saha, and S Show at PRL.

doi : https://doi.org/10.1103/PhysRevD.102.015024

(Partha Konar)

Modelling the influence of progressive social awareness, lockdown and anthropogenic migration on the dynamics of an epidemic

The basic Susceptible-Infected-Recovered (SIR) model is extended to include effects of progressive social awareness, lockdowns and anthropogenic migration. It is found that social awareness can effectively contain the spread by lowering the basic reproduction

rate R_0. Interestingly, the awareness is found to be more effective in a society which can adopt the awareness faster compared to the one having a slower response. The paper also separates the mortality fraction from the clinically recovered fraction and attempts to model the outcome of lockdowns, in absence and presence of social awareness. It is seen that staggered exits from lockdowns are not only economically beneficial but also helps to curb the infection spread. Moreover, a staggered exit strategy with progressive social awareness is found to be the most efficient intervention. The paper also explores the effects of anthropogenic migration on the dynamics of the epidemic in a two-zone scenario. The calculations yield dissimilar evolution of different fractions in different zones. Such models can be convenient to strategise the division of a large zone into smaller sub-zones for a disproportionate imposition of lockdown, or, an exit from one. Calculations are done with parameters consistent with the SARS-COV-2 pathogen in the Indian context.

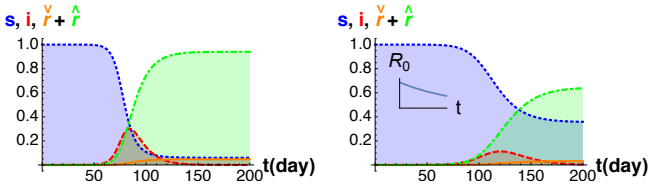

Figure No. 2: Dashed red line is the history of the infection fraction (Left plot) in absence of Progressive Social Awareness and (Right plot) in presence of Progressive Social Awareness. Progressive Social Awareness is modelled with time dependent R_0 as shown in inset.

doi : https://doi.org/10.1007/s40435-020-00692-1

(R. Bhattacharyya, P. Konar)

One-loop amplitudes for Higgs+4-partons with full mass effects

Compact analytic expressions for the one-loop Higgs+4-partons helicity amplitudes are calculated when the circulating particle in the loop is a massive coloured quark. A close relationship is unveiled with the scalar theory in which a massive colour triplet scalar circulates inside the loop. Many advanced techniques like on-shell recursion relations, momentum twistors *etc.* are employed to achieve simple and compact expressions for the scattering amplitudes. Such calculations not only ensure fast computation and numerical stability, but also reveal interesting analytic properties inherent in these amplitudes.

This work was done in collaboration with Lucy Budge, Giuseppe De Laurentis & R. Keith Ellis of IPPP, Durham University, UK and John M. Campbell of Fermilab, USA.

doi : https://doi.org/10.1007/JHEP05(2020)079

(Satyajit Seth)

Study of warm inflationary models and their parameter estimation from CMB

Warm inflation is a natural and well-motivated description of cosmic inflation which accounts for the inflaton dissipation and radiation production during the inflationary phase, neglected in the standard cold description. Considering $\lambda\phi^4$ and $\lambda\phi^6$ inflaton potentials, the self coupling parameter λ and the dissipative parameter Q_P are determined using the CosmoMC numerical code by demanding consistency with Cosmic Microwave Background (CMB) observations. These inflaton potentials yield the tensor to scalar ration, r, in the weak dissipative regime that is consistent with the observations and can be probed in the future experiments.

This work was done in collaboration with [Raghavan Rangarajan] of School of Arts and Sciences, Ahmedabad University.

doi : https://doi.org/10.1142/S0218271820500558

(Richa Arya)

Formation of Primordial Black Holes from Warm Inflation

Primordial Black Holes (PBH) can serve to be a useful probe of the early cosmic history, particularly the phase of inflation. The collapse of density perturbations into PBHs generated during warm inflation scenario is studied. Some very interesting features like red (blue) tilted spectrum of the curvature perturbations is found at large (small) scales. These can be ascribed to the coupling of the inflaton to other fields that plays a crucial role in warm inflation. Evaporation constraints on the initial mass fraction of the generated PBHs and the possibility of Planck mass PBH relics to constitute the dark matter are also discussed.

doi : https://doi.org/10.1088/1475-7516/2020/09/042

(Richa Arya)

A theory of resistivity in Kondo lattice materials: memory function approach

We have theoretically analyzed DC resistivity ρ in the Kondo-lattice materials using the powerful memory function formalism. The complete temperature evolution of ρ is investigated using the Wolfle-Gotze expansion of the memory function. The resistivity in this model originates from spin-flip magnetic scattering of conduction s-electron off the quasi-localized d or f electron spins. We find the famous resistivity upturn in lower temperature regime ($k_B T > \mu_D$) we discover that resistivity scales as cube root of T ($\rho \propto T^{\frac{3}{2}}$). Our results are in reasonable agreement with the experimental results reported in the literature.

This work was done in collaboration with Komal Kumari and Raman Sharma of HP university Shimla, H.P.

doi : https://doi.org/10.1088/1361-648X/aba382

(Navinder Singh)

Conditional q-normal form for wavefunction structure in quantum many-fermion systems with k-body interactions

For finite quantum many-particle systems modeled with say m fermions in N single particle states and interacting with k-body interactions ($k \leq m$), the wavefunction structure is studied using random matrix theory. Hamiltonian for the system is chosen to be $\mathrm{H} = \mathrm{H}_0 + \lambda \mathrm{V}$ with the unperturbed H_0 Hamiltonian being a t-body operator and V a k-body operator with strength λ. Representing H_0 and V by independent Gaussian orthogonal ensembles (GOE) of random matrices in t and k particle spaces respectively, first four moments, in m-particle spaces, of the strength functions $\mathrm{F}_\kappa(\mathrm{E})$ are derived; strength functions contain all the information about wavefunction structure. With E denoting the H energies or eigenvalues and κ denoting unperturbed basis states with energy E_κ, the $\mathrm{F}_\kappa(\mathrm{E})$ give the spreading of the κ states over the eigenstates E.

It is shown that the first four moments of the strength functions are essentially same as that of the conditional q-normal distribution given in: P.J. Szabowski, Electronic Journal of Probability **15**, 1296 (2010). This naturally gives asymmetry in strength functions with respect to E as E_κ increases and also the peak value changes with E_κ. Thus, we have the remarkable result that wavefunction structure in quantum many-fermion systems with k-body interactions follows in general the conditional q-normal distribution.

This work is carried out with Manan Vyas (UNAM, Cuernavaca, Mexico).

doi : https://doi.org/10.1088/1742-5468/ababfc

(V.K.B. Kota)

Multiple $\mathrm{SU}(3)$ algebras in nuclei: Results for (β, γ) bands and scissors 1^+ band

Shell model and interacting boson model spaces admit multiple $\mathrm{SU}(3)$ algebras generating the same rotational spectra but different $\mathrm{E2}$ decay properties, depending on the phases in the quadrupole generator of $\mathrm{SU}(3)$. In the ground (g) $\mathrm{K} = 0^+$ bands in nuclei this is demonstrated recently using systems with nucleons in a single oscillator shell [Kota, Sahu and Srivastava, Bulg. J. Phys. **46**, 313 (2019); Eur. Phys. J. Special Topics **229**, 2389 (2020)]. Going beyond these studies, this year results are obtained for $\mathrm{E2}$ decay properties of β and γ bands members, as generated by multiple $\mathrm{SU}(3)$ algebras, using sdgIBM and $sdgi$IBM examples. In addition, results are presented for the $\mathrm{E2}$ and $\mathrm{M1}$ decay properties of the levels of the 1^+ scissors band in heavy nuclei using sdgIBM-2 and $sdgi$IBM-2.

The scissors 1^+ band properties are also studied using a shell model example with six protons in (pf) shell and twelve neutrons in (sdg) shell. These results establish that: (i) with multiple $\mathrm{SU}(3)$ algebras, it is possible to have rotational bands with very weak $\mathrm{E2}$ strengths among the levels where normally one expects strong strengths; (ii) $\mathrm{E2}$ decay of the levels of β and γ bands to the ground band are quite different for some of the $\mathrm{SU}(3)$ algebras with strong dependence on the phases in the quadrupole generator; (iii) it is possible to have the scissors 1^+ band with the $\mathrm{E2}$ and $\mathrm{M1}$ decay of the lowlying levels of this band to the g band are strong or weak depending on the phases.

This work is carried out with R. Sahu (NIST, Berhampur).

doi : https://doi.org/10.1140/epjst/e2020-000088-4

(V.K.B. Kota)

Event Rates for the Scattering of Weakly Interacting Massive Particles from ^{23}Na and ^{40}Ar

Detection rates for the elastic and inelastic scattering of weakly interacting massive particles (WIMPs) off ^{23}Na are calculated within the framework of Deformed Shell Model (DSM) based on Hartree-Fock states. At first, the spectroscopic properties of the detector nucleus, like energy spectra and magnetic moments, are calculated and compared with experimental data. Following the good agreement of these results, DSM wave functions are used for obtaining elastic and inelastic spin structure functions, nuclear structure coefficients and so forth for the WIMP-^{23}Na scattering. Then, the event rates are also calculated with a given set of supersymmetric parameters. In the same manner, using DSM wavefunctions, nuclear structure coefficients and event rates for elastic scattering of WIMPs from ^{40}Ar are also obtained. These results for event rates and also for annual modulation will be useful for the $ongoing$ and future WIMP detection experiments involving $detector\ materials$ with ^{23}Na and ^{40}Ar nuclei.

This work is carried out with R. Sahu (NIST, Berhampur) and T.S. Kosmas (University of Ioannina, Ioannina, Greece).

doi : https://doi.org/10.1103/PhysRevC.102.035501

(V.K.B. Kota)

Edited special issue of EPJST

A special issue of European Journal of Physics: Special Topics (EPJST) on the topic "Role of SYmmetries in Nuclear Physics" was broughtout with a PRL scientist (V.K.B. Kota) as the editor (along with A.K. Jain of Amity University, Noida). The editors invited 14 scientists with 7 from India and 7 from abroad. All the manuscrpits are refereed by two refereees. The articles in the issue covered current topics such as: (i) point group symmetries in light odd-mass nuclei; (ii) new directions in $\mathrm{SU}(3)$ symmetry for rotational nuclei; (iii) sympletic $Sp(6,\mathrm{R})$ symmetry for no-core shell model; (iv) partial dynamical symmetries generating shape coexitance in medium mass nuclei; (v) a solvable model for octupole collectivity in nuclei; (vi) developemens in pairing sympletic symmetry and its various extentions including deformed mean-field single particle part, many-body pairing and so on; (vii) general features of dual symmetry breaking, i.e. simultaneous dynamical and spontaneous breaking in various algebraic models of nuclei; (viii) symmetry restoration in mean-field theories; (ix) isospin in compound nuclear fusion-fission reactions; (x) applications of random matrix theory giving information on symmetries via the statistical energy level fluctuations.

This work is carried out with A.K. Jain (Amity, Noida).

doi : https://doi.org/10.1140/epjst/e2020-000209-2

(V.K.B. Kota)

Atomic, Molecular and Optical Physics

Episodically Volatile High Energy Non-Cohesive River-Floodplain Systems: The Ping River, Thailand

Volatile rivers involve floodplain stripping and subsequent floodplain reconstruction by vertical accretion. Not much is known about such rivers and their behavior through time. The Ping River of northern Thailand provided a good case study. Stratigraphic and morphostratigraphic analysis along with optical dating of sediments, helped elucidate the manner in which river behaved and helped delineate and the arrival time for stripping events of about three centuries. The stripping events occurred due to varied combinations of wet periods, tropical lows, typhoons, and atmospheric rivers. It was suggested that increase in intensity of extreme rainfall would increases due to warming of Earth, which in turn would lead to increase in the frequency of floodplain stripping events, leading to changes in the fluvial landscapes and flood mitigation strategies.

This work was done in by a consortium led by R.J. Wasson, A. Zeigler, H.S. Lim and others from National University of Singapore. The Optical dating work was carried out by H.S. Lim and E. Teo at PRL and, by T. Rittenour at Utah State University. USA

doi : https://doi.org/10.1016/j.geomorph.2021.107658

(A.K.Singhvi)

Surface paleothermometry using low-temperature thermo - luminescence of feldspar

Thermoluminescence (TL) of feldspar was explored for its potential to extract temperature histories experienced by rocks on Earth's surface. TL signals from feldspar in the laboratory arise from the release of trapped electrons from a continuous distribution of trapping energies that have a range of thermal stabilities. The distribution of trapping energies, or thermal stabilities implies that the lifetime of trapped electrons at room temperature ranges from less than a year to several billion years. Shorter lifetimes are associated with low-temperature TL signals, or peaks, and longer lifetimes are associated with high temperature TL signals. Lower-temperature TL signals (i.e. between 200 and 250° C) were sensitive to temperature fluctuations occurring at Earth's surface over quaternary timescales and it was demonstrated that it is possible to reconstruct past surface temperature histories in terrestrial settings by exploiting the continuous distribution of trapping energies. The potential of this suggestion was tested through theoretical experiments, in which a periodic temperature history was applied to a kinetic model that encapsulated the kinetic characteristics of TL thermometry. A Bayesian approach was then used to invert TL measurements into temperature histories of rocks, assuming that past temperature variations follow climate variations observed in the δ^{18}O records. Studies on samples collected at the Mer de Glace (Mont Blanc massif, European Alps) gave similar temperature histories for both samples. Confirming that the TL of feldspar may be used as a paleothermometer.

This study was done in collaboration with R. H. Biswas, F. Herman, G. E. King, B. Lehmann of Institute of Earth Studies at the University of Laussane

doi : https://doi.org/10.5194/cp-2019-173

(A.K. Singhvi)

Watt-level, ultrafast, tunable yellow source based on single-pass, fourth-harmonic generation of Cr^{2+}:ZnS laser at 2360 nm

We report a compact source of high power, tunable, ultrafast yellow radiation using fourth-harmonic generation of a mid-IR laser in two-stage frequency-doubling processes. Using Cr2CVZnS laser at 2360 nm frequency-doubled in a multi-grating MgO:PPLN crystal, we have generated near-IR radiation tunable across 1137-1200 nm with average output power as high as 2.4 W and pulse width of $\sim$60 fs. Subsequently, the near-IR radiation is frequency-doubled using a bismuth triborate (BIBO) crystal to produce coherent yellow radiation tunable across 570-596 nm with a maximum average power of $\sim$1 W. The source has a maximum mid-IR to yellow (near-IR to yellow) single pass conversion efficiency as high as $\sim$29.4% ($\sim$47%). Without any pulse compression, the yellow source has output pulses at a repetition rate of 80 MHz with a pulse width of $\sim$130 fs in Gaussian-shaped and a spectral width of $\sim$4 nm corresponding to a time-bandwidth product of 0.45. The generated output beam has a Gaussian transverse beam profile with measured M2 values of M_x^2 $\sim$1.07 and M_y^2 $\sim$1.01.

doi : https://doi.org/10.1364/OL.404358

(Deepika Yadav, Anirban Ghosh, Ravi K. Saripalli, and G. K. Samanta)

Multi-structured-beam optical parametric oscillator

Structured beams, conventionally generated through the spatial mode conversion of the Gaussian laser beams, have attracted great

interest in recent years. Optical parametric oscillators (OPOs) have demonstrated the potential for the generation of tunable structured beams directly from an input pump source. However, to date, a particular OPO design has been shown to produce such beams only in a specific configuration and different spatial structured beams require different system architectures. Here, we report the generation of multiple-structured beams from a single OPO device. Using a vortex-beam-pumped ultrafast OPO in singly-resonant oscillator design and through the control of the mode structure of the resonant beam using a simple intracavity aperture, we generate vortex, Airy, vortex Airy, and Gaussian signal beams over a tunable wavelength range across 1457-1680 nm, simultaneous with vortex beam in the non-resonant idler across 2902-3945 nm, from different ports of the device. The signal and idler vortices have output power in excess of 1 W and maximum vortex order of $l_i = 2$, while the Airy beam and vortex Airy beam have output power of more than 200 mW. The generic experimental design can be used to provide multi-structured spatial beams with broad tunability across different spectral regions by proper selection of pump laser and nonlinear material and in all times-scales from continuous-wave to ultrafast femtosecond domain.

This work was done in collaboration with Majid Ebrahim-Zadeh and his group from the Institute of Photonic Sciences, Barcelona

doi : https://doi.org/10.1364/OE.398011

(Varun Sharma and G. K. Samanta)

Nonlinear frequency conversion of 3D optical bottle beams generated using a single axicon

We demonstrate a novel experimental scheme to generate and study the nonlinear frequency conversion of a three dimensional (3D) optical Bessel bottle beam (BBB). Using a single axicon and standard optical components and controlling the spot size and divergence of the input Gaussian beam to the axicon, we have generated stable micron-size, high-power optical BBB with tunable spatial characteristics. The BBB has a series of low-intensity regions surrounded by high intensity with diameters of $\sim$30 μm and 17 μm, respectively, at a variable period of 2.3 to 6.4 mm along with the beam propagation. Using the single-pass second harmonic generation (SHG) of femtosecond BBB at 1064 nm in a bismuth triborate nonlinear crystal, we have generated BBB at 532 nm with output power as high as 75 mW and single-pass SHG efficiency of 1.9%. We also observed the self-healing of the BBB at both pump and SHG wavelengths. It is interesting to note that the pump beam truncation shows self-healing in the SHG beam. Such observation proves the direct transfer of the pump's spatial characteristics to the SHG beam in the nonlinear process, potentially useful for imaging even in the turbid medium in biology. This generic scheme can be used at different wavelengths and timescales (continuous-wave to ultrafast).

doi : https://doi.org/10.1364/OL.413899

(A. Srinivasa Rao, Deepika Yadav and G. K. Samanta)

Selective tuning of Hilbert spaces in states encoded with spatial modes of light

Spatial modes of light directly give the most easily accessible degree of freedom that span an infinite dimensional Hilbert space. The higher dimensional spatial mode entanglement realized using spontaneous parametric down conversion (SPDC) process is generally restricted to the subspace defined by a single spatial mode in pump. Access to other modal subspaces can be realized by pumping beams carrying several easily tunable transverse modes. As a proof of principle experiment, we generate twin-photon states in an SPDC process with pump as a superposition of first order Laguerre-Gaussian (or Hermite-Gaussian) modes. We show that the generated states can be easily tuned between different subspaces by controlling the respective modal content in the pump superposition.

doi : https://doi.org/10.1088/1367-2630/abc783

(A. Anwar, N. Lal, S. Prabhakar, R. P. Singh)

Optical-vortex diagnostics via Fraunhofer slit diffraction with controllable wavefront curvature

Far-field slit diffraction of circular optical-vortex (OV) beams is efficient for measurement of the topological charge (TC) magnitude but does not reveal its sign. We show that this is because in the common diffraction schemes the diffraction plane coincides with the incident OV waist plane. Based on the examples of Laguerre-Gaussian incident beams containing a spherical wavefront component, we demonstrate that the far-field diffracted beam profile possesses an asymmetry depending on the incident wavefront curvature and the TC sign. This finding enables simple and efficient ways for the simultaneous diagnostics of the TC magnitude and sign, which can be useful in many OV applications, including OV-assisted metrology and information processing.

doi : https://doi.org/10.1364/JOSAA.388926

(S. Patil, V. Kumar, R.P. Singh in collaboration with A Bekshaev, L Mikhaylovskaya from Physics Research Institute, I. I. Mechnikov National University, Ukraine)

Tunable ultraslow light propagation in ruby

Ruby is one of the best solids for generation of slow light at room temperature. Ultraslow light propagation to $\sim$2.8 m/s has been demonstrated experimentally in ruby rod of length 7.6 cm. The systematic variation of optical delay with the modulation frequency, laser power and depth of focus has been studied. Fine tuning from $\sim$12 ms to $\sim$20 ms has been achieved by using laser power and depth of focus as a knob. These studies suggest that ruby rod may find potential applications in developing the tunable optical delay-based devices.

doi : https://doi.org/10.1016/j.optcom.2020.125913

(V. Kumar, S. G. Reddy, R.P. Singh in collaboration with S. Kumari from Department of Applied Physics, Central University of Jharkhand)

Effect of laser beam propagation through the plasmonic nanoparticles suspension

Gold nanoparticles are excellent light absorbers at the surface plasmon resonance wavelength. This absorption process generates highly energetic electrons near the surface that enhances the local electric field on the gold nanoparticles surface, and results in modification of the refractive index. The present work focuses on interaction of the laser, both near and far from the resonance wavelength, with colloidal solution of plasmonic nanoparticles. For the laser beam interaction, we first prepared the gold nanoparticles by sol gel method and characterized the absorption spectrum in terms of particle size and morphology. The absorption peak in visible range confirmed to the formation of Au nanoparticles. Therefore, a laser at 532 nm was selected to study light matter interaction with Au nanoparticles in solution. The interaction produced diffraction rings, which changed shape over time due to convection of colloidal nanoparticles. In another experiment, a 405 nm laser with the same power produced only a laser spot on the screen. Thus, the 532 nm is closer to the surface plasmon excitation and is responsible for producing a pattern of diffraction rings in the far-field region. The produced diffraction rings provide a very simple and sensitive technique to find out induced nonlinear refractive index for the plasmonic nanoparticles. Finding plasmonic resonances holds importance for variety of applications in plasmonic sensing and these rings could be used to characterize the resonances.

doi : https://doi.org/10.1016/j.rio.2021.100081

(A. Kumar, R.P. Singh in collaboration with A. Taneja from Department of Chemistry, Dr. Bhimrao Ambedkar University, Agra and T. Mohanty from School of Physical Sciences, Jawaharlal Nehru University, New Delhi)

Strong-field ionization of polyatomic molecules: ultrafast H atom migration and bond formation in the photodissociation of CH_3OH:

The H-atom migration and bond formation in CH_3OH induced by intense femtosecond laser pulses are investigated using a Velocity Map Imaging (VMI) spectrometer. Various laser parameters like intensity (1.5×10^{13}Wcm^{-2}–12.5×10^{13}Wcm^{-2}), pulse duration (29 fs and 195 fs), wavelength (800 nm and 1300 nm), and polarization (linear and circular) can serve as a quantum control for hydrogen migration and the yield of H_n^+ (n = 1–3) ions which have been observed in this study. Further, in order to understand the ejection mechanism of the hydrogen molecular ions H^{2+} and H^{3+} from singly-ionized CH_3OH, quantum chemical calculations were employed. The dissociation processes of CH3OH+ occurring by four dissociative channels to form $CHO^+ + H_3, H_3^+ + CHO, CH_2^+ + H_2O$ and $H_2O^+ + CH_2$ are studied. Using the combined approach of experiments and theory, we have successfully explained the mechanism of intramolecular hydrogen migration and predicted the dissociative channels of singly-ionized CH_3OH. The laser intensity dependence of H_n^+ ion formation is shown in figure 1.

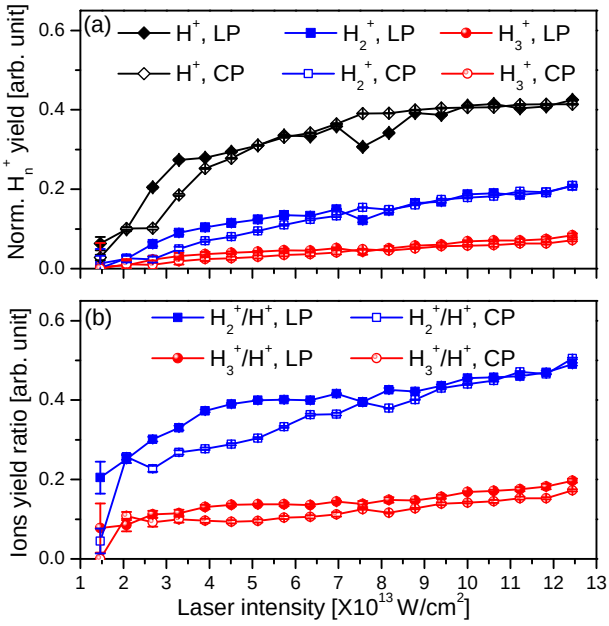

Figure no. 1: Normalized H_n^+ (n = 1-3) ion yield as a function of laser intensity for CH_3OH (maximum error is 7%). (b) Ratio of bond formation to bond breakup in CH_3OH as a function of laser intensity (maximum error is 6%). Solid symbols stand for linear polarization while hollow symbols stand for circular polarization in both (a) and (b).

doi : https://doi.org/10.1039/D0FD00129E

(R. Das, Deepak K Pandey, V. Nimma, P Madhusudhan, P. Bhardwaj, P. Chandravanshi, Muhammed Shameem KM, Dheeraj K Singh, R. K. Kushawaha)

Improving the Signal Strength and Detection Limits of Laser-Induced Breakdown Spectroscopy

The role of nanoparticles in improving the LIBS signal intensity has been investigated and highlighted using silver nanoparticles on brass substrates. A 0.5 μl of Ag colloidal nanoparticles solution having a 10 nm particle size was introduced onto the substrate surface in order to perform nanoparticle LIBS measurements.

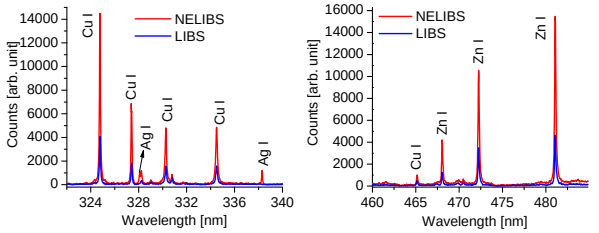

Figure no. 2:Comparison of LIBS and nanoparticle-LIBS spectra of brass substrate over two different spectral regions.

The nanoparticle-coated substrate shows up to 4-times intensity

enhancement compared to normal surface. This enhancement in signal intensity is attributed to the localized surface plasmons. The linewidth of the spectral lines is found to be identical in both LIBS and nanoparticle LIBS. Figure 2 manifests the LIBS spectra recorded from a pure brass and nanoparticle coated brass surface over two spectral regions of 320 – 340 nm and 460-480nm, respectively (small spectral range of LIBS spectra are shown here to avoid the complexity). Brass is an alloy of zinc and copper, and all the major emission lines observed from the LIBS spectra belongs to these elements. It is evident from the spectra that the NPs coated LIBS spectrum shows an average enhancement of LIBS intensity up to 4 times than the conventional LIBS spectrum.

doi : https://doi.org/10.1007/978-981-33-6084-6_12

(KM Muhammed Shameem, R. Das, V. Nimma, S. Soumyashree, P. Kumar, R. K. Kushawaha)

New Cold Target Recoil-Ion Momentum Spectrometer (COLTRIMS) in PRL

This year, the commissioning of a new Cold Target Recoil-Ion momentum Spectrometer in the femtosecond laser lab, AMOPH PRL, has been performed. This spectrometer is indigenously developed in PRL's workshop to study the ultrafast processes in atomic and molecular systems. PRL's COLTRIMS setup consists of 9 plates on either side of the ionization region and is operates under the Wiley McLaren condition. An 80 mm diameter MCP-DLD (Roentdek) on the ion side and a 40 mm diameter MCP (Roentdek) on the ion side is installed to detect the electrons and ions. Calibration was performed using photoionization of Xenon. A photoionization experiment of CH_3Cl has been performed to investigate the fragmentation dynamics of ionized CH_3Cl. The COLTRIMS setup is shown in the left panel of figure 3. The first result of this new setup is shown in the right panel of figure 3 for demonstration purposes only. The PRL's new COLTRIMS setup is functional and used to study the strong-field ionization of atoms and molecules.

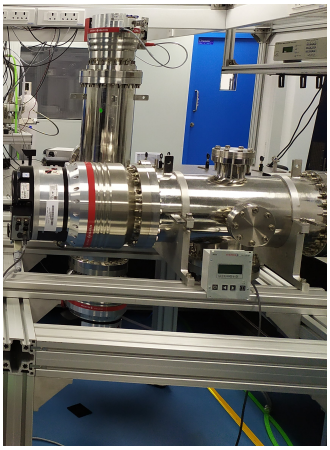

Figure no. 3: PRL's Cold Target Recoil-Ion Momentum Spectrometer, Femtosecond laser lab, AMOPH.

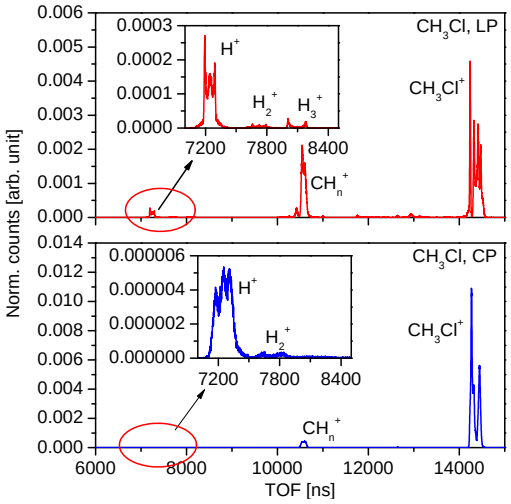

Figure no. 4: Strong field ionization of CH_3Cl, a TOF spectrum of CH_3Cl at 70mW of average power for linear and circular polarized light pulses having 29 fs pulse duration, 800nm wavelength.

(Madhusudhan P, P. Bhardwaj, R. Das, S. Soumyashree, P. Chandravanshi, V. Nimma, P. Kumar, R. K. Kushawaha)

Triatomic molecules as the prospective candidates to search for electric dipole moment of an electron

In search of suitable molecular candidates for probing the electric dipole moment (EDM) of the electron (d_e), a property that arises due to parity and time-reversal violating (P,T-odd) interactions, we investigated the triatomic mercury hydroxide (HgOH) molecule.The impetus for this proposal is based on previous works on two systems: the recently proposed ytterbium hydroxide (YbOH) experiment that demonstrates the advantages of polyatomics for such EDM searches, and the finding that mercury halides provide the highest enhancement due to d_e compared to other diatomic molecules. We identified the ground state of HgOH as being in a bent geometry, and showed that its EDM enhancement factor is comparable to the corresponding value for YbOH. Along with the theoretical results, we discussed plausible experimental schemes for an EDM measurement in HgOH. Furthermore, we provided pilot calculations of the EDM enhancement factors due to d_e for $HgCH_3$ and $HgCF_3$, that are natural extensions of HgOH.

This work was carried out in collaboration with Dr. V. Srinivasa Prasannaa [Centre for Quantum Engineering, Research and Education (CQuERE), TCG CREST, Salt Lake, Kolkata 700091, India], Dr. Nicholas R. Hutzler [Division of Physics, Mathematics, and Astronomy, California Institute of Technology, Pasadena, CA 91125, USA], Dr. Minori Abe [Department of Chemistry, Tokyo Metropolitan University, 1-1, Minami-Osawa, Hachioji-city, Tokyo 192-0397, Japan] and Prof. B. P. Das [Department of Physics, Tokyo Institute of Technology, 2-12-1-H86 Ookayama, Meguro-ku, Tokyo 152-8550, Japan].

doi : https://doi.org/10.3390/atoms9010007

(R. Mitra and B. K. Sahoo)

Laser spectroscopy of indium Rydberg atom bunches by electric field ionization

We reported application of a novel electric field-ionization setup for high-resolution laser spectroscopy measurements on bunched fast atomic beams in a collinear geometry. In combination with multi-step resonant excitation to Rydberg states using pulsed lasers, the field ionization technique demonstrates increased sensitivity for isotope separation and measurement of atomic parameters over previous non-resonant laser ionization methods.The set-up was tested at the Collinear Resonance Ionization Spectroscopy experiment at ISOLDE-CERN to perform high-resolution measurements of transitions in the indium atom from the $5s^2 5d\ ^2D_{5/2}$ and $5s^2 5d\ ^2D_{3/2}$ states to $5s^2 np\ ^2P$ and $5s^2 nf\ ^2F$ Rydberg states, up to a principal quantum number of $n = 72$. The extracted Rydberg level energies were used to re-evaluate the ionization potential of the indium atom to be 46,670.107(4) cm^{-1}. The nuclear magnetic dipole and nuclear electric quadrupole hyperfine structure constants and level isotope shifts of the $5s^2 5d\ ^2D_{5/2}$ and $5s^2 5d\ ^2D_{3/2}$ states were determined for ^{113,115}In. The results are compared to calculations using relativistic coupled-cluster theory. A good agreement is found with the ionization potential and isotope shifts, while disagreement of hyperfine structure constants indicates an increased importance of electron correlations in these excited atomic states. With the aim of further increasing the detection sensitivity for measurements on exotic isotopes, a systematic study of the field-ionization arrangement implemented in the work was performed at the same time and an improved design was simulated and is presented. The improved design offers increased background suppression independent of the distance from field ionization to ion detection.

This work was carried out along with ISOLDE-CERN Collaboration.

doi : https://doi.org/10.1038/s41598-020-68218-5

(B.K.Sahoo)

Charge radii of exotic potassium isotopes challenge nuclear theory and the magic character of $N = 32$

Nuclear charge radii are sensitive probes of different aspects of the nucleon–nucleon interaction and the bulk properties of nuclear matter, providing a stringent test and challenge for nuclear theory. Experimental evidence suggested a new magic neutron number at $N = 32$ in the calcium region, whereas the unexpectedly large increases in the charge radii open new questions about the evolution of nuclear size in neutron-rich systems. By combining the collinear resonance ionization spectroscopy method with β-decay detection, we were able to extend charge radii measurements of potassium isotopes beyond $N = 32$. We provided a charge radius measurement of ^{52}K by combining high accuracy atomic calculations with the precise isotope shift measurements. It did not show a signature of magic behaviour at $N = 32$ in potassium. The results were interpreted with two state-of-the-art nuclear theories. The coupled-cluster theory reproduces the odd–even variations in charge radii but not the notable increase beyond $N = 28$. This rise was well captured by Fayans nuclear density functional theory, which, however, overestimated the odd–even staggering effect in charge radii. These findings highlight our limited understanding of the nuclear size of neutron-rich systems, and expose problems that are present in some of the best current models of nuclear theory.

This work was carried out along with ISOLDE-CERN collaboration.

doi : https://doi.org/10.1038/s41567-020-01136-5

(B.K.Sahoo)

Optical-lattice based Cs active clock with continual superradiant lasing signal

We demonstrated state-of-the-art technique of an active clock to provide a continuous superradiant lasing signal using an ensemble of trapped Cs atoms in the optical lattice. A magic wavelength of the proposed $|7S_{1/2}; F = 4, M_F = 0\rangle \rightarrow |6P_{3/2}; F = 3, M_F = 0\rangle$ clock transition in Cs atom was identified at 1181 nm for constructing the optical lattice. Pertinent optical lines were also found for pumping and repumping atoms from their ground states. A fractional uncertainty about 10^{-15} level to the clock frequency has been predicted by carrying out rigorous calculations of several atomic properties. The bad-cavity operational mode of the active clock is anticipated to improve its short-term stability remarkably by suppressing intrinsic thermal fluctuations. Thus, a composite clock system with better in both short-term and long-term stabilities can be built by combining the above proposed active clock with another high-accuracy passive optical clock.

This work was carried out in collaboration with Duo Pan and Jingbiao Chen of State Key Laboratory of Advanced Optical Communication Systems and Networks, Department of Electronics, Peking University, Beijing 100871, China; Bindiya Arora of Department of Physics, Guru Nanak Dev University, Amritsar, Punjab 143005, India; Y. -M. Yu of Beijing National Laboratory for Condensed Matter Physics, Institute of Physics, Chinese Academy of Sciences, Beijing 100190, China.

doi : https://doi.org/10.1103/PhysRevA.102.041101

(B.K.Sahoo)

Precise determination of g_j factors of the Cd^+, Yb^+ and Hg^+ ions

Accurate calculations of g_j factors of the ground state of the Cd^+, Yb^+ and Hg^+ ions were presented by employing the normal order unrelaxed Λ-approach relativistic coupled-cluster (Λ-RCC) theory. Contributions from the quantum electrodynamics (QED) are estimated from the free electron QED contributions and roles of electron correlation effects were analyzed with different cut-off of occupied and virtual active orbitals in the Λ-RCC method. Our final g_j factors came out to be $2.002291(4)$, $2.002798(113)$ and $2.003128(41)$ for the Cd^+, Yb^+ and Hg^+ ions, respectively. Our result for Hg^+ agreed up to the fourth decimal places with its experimental value 2.0031745(74) indicating that our calculations of the other ions are of similar accuracies. These reported g_j factors can be used to scrutinize the background noise related to the stray magnetic fields in the laser-cooled microwave ion clocks using the above ions.

This work was done in collaboration with Yan-mei Yu of Beijing National Laboratory for Condensed Matter Physics, Institute of Physics, Chinese Academy of Sciences, Beijing 100190, China and B. B. Suo of Institute of Modern Physics, Northwest University, Xi'an, Shanxi 710069, China

doi : https://doi.org/10.1103/PhysRevA.102.062824

(B.K.Sahoo)

Electric dipole and quadrupole properties of Cd atom for atomic clock applications

Accurate values of atomic properties of Cd atom that are sensitive to an external electric field in an experiment, such as static electric dipole and quadrupole polarizabilities, hyperpolarizabilities, and quadrupole moments, were reported by carrying out calculations using the four-component relativistic coupled-cluster theory. The finite-field approach was adopted to estimate the above quantities from the evaluated energies. The roles of electron correlation effects in the calculations were demonstrated by giving results with different approximations. Precise knowledge of the above spectroscopic properties is useful for estimating typical systematics of the optical clocks built using the Cd atoms.

This work was carried out in collaboration with X. T. Guo of Beijing National Laboratory for Condensed Matter Physics, Institute of Physics, Chinese Academy of Sciences, Beijing 100190, China; Y. -M. Yu of University of Chinese Academy of Sciences, 100049 Beijing, China; Y. Liu of State Key Laboratory of Metastable Materials Science and Technology & Key Laboratory for Microstructural Material Physics of Hebei Province, School of Science, Yanshan University, Qinhuangdao, 066004, China and B. B. Suo of Institute of Modern Physics, Northwest University, Xi'an, Shanxi 710069, China.

doi : https://doi.org/10.1103/PhysRevA.103.013109

(B.K.Sahoo)

CP violating effects in ^{210}Fr and prospects for new physics beyond the Standard Model

We reported theoretical results of the electric dipole moment (EDM) of ^{210}Fr which arises from the interaction of the EDM of an electron with the internal electric field in an atom and the scalar-pseudoscalar electron-nucleus interaction; the two dominant sources of CP violation in this atom. Employing the relativistic coupled-cluster theory, we evaluated the enhancement factors for these two CP violating interactions to an accuracy of about 3% and analyzed the contributions of the many-body effects. These two quantities in combination with the projected sensitivity of the ^{210}Fr EDM experiment could provide constraints on new physics beyond the Standard Model. Particularly, we demonstrated that their precise values are necessary to account for the effect of the bottom quark in models in which the Higgs sector is augmented by nonstandard Yukawa interactions such as the two-Higgs doublet model.

This work was carried out in collaboration with Nanako Shitara and B. P. Das of Department of Physics, School of Science, Tokyo Institute of Technology, Ookayama, Meguro-ku, Tokyo, 152-8550, Japan; N. Yamanaka of Amherst Center for Fundamental Interactions, Department of Physics, University of Massachusetts, Amherst, MA, 01003, USA, and Toshio Watanabe of Global Scientific Information and Computing Center, Tokyo Institute of Technology, Ookayama, Meguro-ku, Tokyo, 152-8550, Japan.

doi : https://doi.org/10.1007/JHEP02(2021)124

(B.K.Sahoo)

Reappraisal of P, T-odd parameters from the improved calculation of electric dipole moment of ^{225}Ra atom

By employing the recently developed relativistic normal coupled-cluster theory, we obtained the electric dipole moment (EDM) of ^{225}Ra due to nuclear Schiff moment (NSM) and tensor-pseudotensor (T-PT) electron-nucleus (e-N) interaction as $-6.3(5)\times10^{-17}S|e|cm/(|e|fm^3)$ and $-13(1)\times10^{-20}C_T\langle\sigma_N\rangle|e|cm$, respectively, for the NSM S, T-PT coupling coefficient C_T and nuclear Pauli spinor σ_N. This is corroborated by analyzing the dipole polarizability value of ^{225}Ra, which is obtained as 257(8) ea_0^3. Our EDM results, in combination with the measurement[Phys. Rev. Lett. $\mathbf{114}$, 233002 (2015)], are about 8% and 28% improvements over the limits that were reported using the relativistic coupled-cluster theory for the NSM and T-PT e-N coupling coefficient, respectively. Further combining with the nuclear calculations, we infer limits on the EDM of neutron $d_n < 1.15\times10^{-23}|e|cm$, the EDM of proton $d_p < 1.1\times10^{-22}|e|cm$, the quantum chromodynamics parameter $|\bar{\theta}| < 2.46\times10^{-10}$ and the combined up- and down- quark chromo-EDMs $|\tilde{d}_u - \tilde{d}_d| < 1.36\times10^{-26}|e|cm$. Though these bounds are not competitive at present with the current-best limits acquired from ^{199}Hg atom, they can be bettered when the measurement of EDM in ^{225}Ra improves by four orders.

doi : https://doi.org/10.1088/1361-6455/aba6aa

(V. S. Prasannaa, R. Mitra and B. K. Sahoo)

Determination of the dipole polarizability of the alkali-metal negative ions

We determined electric dipole polarizabilities (α_d) of the alkali-metal negative ions, from H^- to Fr^-, by employing four-component relativistic many-body methods. Differences in the results were shown by considering Dirac-Coulomb (DC) Hamiltonian, DC Hamiltonian with the Breit interaction, and DC Hamiltonian with the lower-order quantum electrodynamics interactions. At first, these interactions were included self-consistently in the Dirac-Hartree-Fock (DHF) method, and then electron correlation effects are incorporated over the DHF wave functions in the second-order many-body perturbation theory, random phase approximation and coupled-cluster (CC) theory. Roles of electron correlation effects and relativistic corrections were analyzed using the above many-body methods with size of the ions. We finally quoted precise values of α_d of the above negative ions by estimating uncertainties to the CC results, and compared them with other calculations wherever available.

doi : https://doi.org/10.1103/PhysRevA.102.022820

(B.K.Sahoo)

Investigating properties of Cl^- and Au^- ions using relativistic many-body methods

We investigated ground state properties of singly charged chlorine (Cl^-) and gold (Au^-) negative ions by employing four-component relativistic many-body methods. In our approach, we attach an electron to the respective outer orbitals of chlorine (Cl) and gold (Au) atoms to determine the Dirac-Fock (DF) wave functions of the ground state configurations of Cl^- and Au^-, respectively. As a result, all the single-particle orbitals see the correlation effects due to the appended electron of the negative ion. After obtaining the DF wave functions, lower-order many-body perturbation methods, random-phase approximation, and coupled-cluster (CC) theory in the singles and doubles approximation are applied to obtain the ground state wave functions of both Cl^- and Au^- ions. Then, we adopt two different approaches to the CC theory – a perturbative approach due to the dipole operator to determine electric dipole polarizability and an electron detachment approach in the Fock-space framework to estimate ionization potential. Our calculations are compared with the available experimental and other theoretical results.

doi : https://doi.org/10.1088/1361-6455/abd91b

(B.K.Sahoo)

Analysis of an Optical Lattice Methodology for Detection of Atomic Parity Nonconservation

We analyzed an experimental scheme for detecting atomic parity violation. The experimental concept was supported by obtaining *ab initio* data necessary for assessing the plausibility of the approach and for an analysis of the wavelength-dependent light shift in Cs. A range of experimental details were investigated, combined with a survey of realistic lasers parameters. These were adopted to project the feasibility of the scheme to eventually be capable of delivering data beyond the standard model of particle physics.

This work was done in collaboration with A. Kastberg of Institute de Physique de Nice, Université Côte d'Azur, CNRS, 06108 Nice, France; T. Aoki of Institute of Physics, Graduate School of Arts and Sciences, The University of Tokyo, Tokyo, Japan; Y. Sakemi of Center for Nuclear Study, The University of Tokyo, Wako, Japan, and B. P. Das of International Education and Research Center of Science and Department of Physics, Tokyo Institute of Technology, Tokyo, Japan.

doi : https://doi.org/10.3390/sym12060974

(B.K.Sahoo)

Evidence of episodically accelerated denudation on the Tibetan Namche Barwa massif by megafloods

Megafloods cause widespread mobilization of sediments that have strong potential to control the geodynamic evolution of the Namche Barwa (NB) massif by changing the landscape morphology within a short time. However, the impact of catastrophic events on the denudation of the massif over the longer time scale has not been explored in detail. This contribution assesses the impact of catastrophic floods on the denudation style of the Namche Barwa (NB) massif over millennial time scales. Towards this, 21 optical ages and $\sim$1700 detrital thermochronometric ages of zircon and apatite minerals extracted from paleoflood sediments downstream of the massif, were integrated with decadal sediment load and aggradation data to estimate the minimum denudation rate during paleoflood events. The results indicate that the 7 ka flood eroded $\sim$71 m of material from the NB massif. This denudation is equivalent to the material that would be produced over $\sim$8000 years of erosion at a rate of $\sim$9 mm/a. The 3.5 ka flood eroded $\sim$24 m of material equaling $\sim$2500 years' worth of erosion at a rate of $\sim$9 mm/a. Such relatively instantaneous denudations are three orders of magnitude higher than averaged denudation rates over million-year time scale. This study, therefore, provides the first evidence of the strong interplay of catastrophic flood events and tectonics for the rapid exhumation of the Namche Barwa massif. Megafloods from the failure of dammed lakes provide valuable information to understand the flood surge risk for human settlements in the Siang and the Assam valleys.

This work was done in collaboration with Biraj Borgohain; George Mathew, IIT Mumbai and Vikrant Jain, IIT Gandhinagar

doi : https://doi.org/10.1016/j.quascirev.2020.106410

(N. Chauhan and A. K. Singhvi)

Bleaching of blue light stimulated luminescence of quartz by moonlight

Moonlight is sunlight reflected from the moon's surface. It is additionally modulated by the Earth's atmosphere, dust and pollutants on its way to the surface of the Earth. This contribution reports the bleaching rates of blue light stimulated luminescence (BLSL) signal of Quartz under full moonlight exposure at the Earth's surface. Quartz BLSL reduced to 70% by an exposure of 5 hrs moonlight, is in contrast to $\sim$90% reduction in $<$ 3 s with daylight. This was anticipated due to (a) reduced moonlight flux by about a factor of half a million, (b) inverse power law dependence of bleaching efficiency on wavelength and (c) moonlight and daylight have spectral peaks around 650 and 550 nm, respectively. Deconvolution of OSL components suggests that moonlight affects the fast component of OSL signal the most. This has ramification for the application in polar regions, where the availability of daylight is at a premium during the winter months. Within a given context, it is conjectured that this could be used to infer the seasonality of sediment transport.

doi : https://doi.org/10.1007/s12040-020-01474-1

(H.M. Rajapara, V. Kumar, N. Chauhan and A. K. Singhvi)

Publications in Journals

Astronomy and Astrophysics

1. Acciari V. A., S. Ansoldi, L. A. Antonelli, A. Arbet Engels, M. Artero, K. Asano, . . . , P. Prajapati, P. Kumar, S. Ganesh,..., T. J. Pearson, 2021, *"VHE gamma-ray detection of FSRQ QSO B1420+326 and modeling of its enhanced broadband state in 2020"*, Astronomy & Astrophysics, v.647, p.19, doi :https://doi.org/10.1051/0004-6361/202039687.
2. Adassuriya, J., S. Ganesh, J. L. Gutiérrez, G. Handler, S. Joshi, K. P. S. C. Jayaratne, and K. S. Baliyan, 2021, *"Asteroseismology of SZ Lyn using multiband high time resolution photometry from ground and space."*, Monthly Notices of the Royal Astronomical Society, v.502, p. 541-555, doi :https://doi.org/10.1093/mnras/staa3923.
3. Aditya J.N.H.S., R. Jorgenson, V., Joshi V. Singh, A. Tao, and Y. Chandola, 2021, *"uGMRT detection of associated H I 21-cm absorption at z = 3.5"*, Monthly Notices of the Royal Astronomical Society, v. 500, p. 998-1002, doi :https://doi.org/10.1093/mnras/staa3306.
4. Aravind, K., S. Ganesh, K. Venkataramani, D. Sahu, D. Angchuk, T. Sivarani, and A. Unni, 2021, *"Activity of the first interstellar comet 2I/Borisov around perihelion: results from Indian observatories"*, Monthly Notices of the Royal Astronomical Society, v.502, p. 3491-3499, doi :https://doi.org/10.1093/mnras/stab084.
5. Banerjee, D. P. K., T. R. Geballe, A. Evans, M. Shahbandeh, C. E. Woodward, R. D. Gehrz, S. P. S. Eyres, S. Starrfield, Zijlstra, A. Zijlstra, 2020, *"Near-infrared Spectroscopy of CK Vulpeculae: Revealing a Remarkably Powerful Blast from the Past"*, The Astrophysical Journal Letters, v. 904, p. 5, doi :https://doi.org/10.3847/2041-8213/abc885.
6. Beri A., S. Naik, K. P. Singh, G. K. Jaisawal, ..., H. Raichur, 2021, *"AstroSat Observations of the first Galactic ULX Pulsar Swift J0243.6+6124"*, Monthly Notices of the Royal Astronomical Society, v. 500, p. 565-575, doi :https://doi.org/10.1093/mnras/staa3254.
7. Bhadari, N. K., L. K. Dewangan, L. E. Pirogov, and D. K. Ojha, 2020, *"Star-forming sites IC 446 and IC 447: an outcome of end-dominated collapse of Monoceros R1 filament"*, The Astrophysical Journal, v. 899, p. 1-13, doi :https://doi.org/10.3847/1538-4357/aba2c6.
8. Bisht, D., Q. Zhu, R. K. S. Yadav, S. Ganesh, G. Rangwal, A. Durgapal, D. P. Sariya, and I.-G. Jiang, 2021, *"Multi-colour photometry and Gaia EDR3 astrometry of two couples of binary clusters (NGC 5617 and Trumpler 22) and (NGC 3293 and NGC 3324)"*, Monthly Notices of the Royal Astronomical Society, **v. 503**, P. 5929-5947, doi :https://doi.org/10.1093/mnras/stab691.
9. Chatterjee K., Debnath, D., Chatterjee, D., Jana, A., Chakrabarti, S. K, 2020, *"Inference on accretion flow properties of XTE J1752-223 during its 2009-10 outburst"*, Monthly Notices of the Royal Astronomical Society, v. 493, p. 2452-2462, doi :https://doi.org/10.1093/mnras/staa391.
10. Das S. R., J. Jose, M. R. Samal, S. Zhang, N. Panwar, 2021, *"Testing the star formation scaling relations in the clumps of the North American and Pelican nebulae cloud complex"*, Monthly Notices of the Royal Astronomical Society, v. 500, p. 3123-3141, doi :https://doi.org/10.1093/mnras/staa3222.
11. Debnath D., D. Chatterjee, A. Jana, S. K. Chakrabarti, K. Chatterjee, 2020, *"Accretion flow properties of XTE J1118+480 during its 2005 outburst"*, Research in Astronomy and Astrophysics, v. .20, p. 175, doi :https://doi.org/10.1088/1674-4527/20/11/175.
12. Dewangan, L. K., D. K. Ojha, S. Sharma, S. del Palacio, N. K. Bhadari, and, A. Das, 2020, *"New insights in the HII region G18.88-0.49: hub-filament system and accreting filaments"*, The Astrophysical Journal, v. 903, p. 1-17, doi :https://doi.org/10.3847/1538-4357/abb827.
13. Dewangan, L. K., S. Sharma, R. Pandey, S. del Palacio, D. K. Ojha, P. Benaglia, T. Baug, and, S. R. Das, 2020, *"Probing the physical conditions and star formation processes in theGalactic HII region S305"*, The Astrophysical Journal, v. 898, p. 1-16, doi :https://doi.org/10.3847/1538-4357/ab9c27.
14. Dewangan, L. K., T. Baug, and D. K. Ojha, 2020, *"Uncovering distinct environments in an extended physical system around the W33 complex"*, Monthly Notices of the Royal Astronomical Society, v. 496, p. 1278-1294, doi :https://doi.org/10.1093/mnras/staa1526.
15. Dewangan, L. K., T. Baug, L. E. Pirogov, and D. K. Ojha, 2020, *"Investigating the physical conditions in extended system hosting mid-infrared bubble N14"*, The Astrophysical Journal, v. 898, p. 1-20, doi :https://doi.org/10.3847/1538-4357/ab964c.
16. Eden D. J., T. J. T. Moore, M. J. Currie, A. J. Rigby, E. Rosolowsky, Y. Su, K.-T. Kim, . . . , M. R. Samal . . . , J J Zhou, 2020, *"CHIMPS2: survey description and ^{12}CO emission in the*

Galactic Centre", Monthly Notices of the Royal Astronomical Society, v. 498, p. 5936-5951, doi :https://doi.org/10.1093/mnras/staa2734.

17. Eswaraiah C., Li D., M. R. Samal, J.-W. Wang, Y. Ma, S.-P. Lai, A. Zavagno,. . . ,D. K. Ojha, 2020, *"Unveiling the Importance of Magnetic Fields in the Evolution of Dense Clumps Formed at the Waist of Bipolar H II Regions: A Case Study of Sh 2-201 with JCMT SCUBA-2/POL-2"*, The Astrophysical Journal, v. 897, p. 90, doi :https://doi.org/10.3847/1538-4357/ab83f2.

18. Halder, P., 2021, *"JaSTA-3: Light scattering simulations for heterogeneous aggregates"*, Computer Physics Communications, v 261, 107818, doi :https://doi.org/10.1016/j.cpc.2020.107818.

19. Halder, P. and S. Ganesh, 2021, *"Modelling heterogeneous dust particles: an application to cometary polarization"*, Monthly Notices of the Royal Astronomical Society, v.501, p. 1766-1781, doi :https://doi.org/10.1093/mnras/staa3647.

20. Jaisawal G. K., S. Naik, W. C. G. Ho, N. Kumari, P. Epili, and G. Vasilopoulos, 2020, *"Revisiting the spectral and timing properties of 4U 1909+07 with NuSTAR and Astrosat"*, Monthly Notices of the Royal Astronomical Society, v.498, p. 4830-4838, doi :https://doi.org/10.1093/mnras/staa2604.

21. Jana A., A. Chatterjee, N. Kumari, P. Nandi, S. Naik, D. Patra,, 2020, *"Probing Nuclear and Circumnuclear Properties of NGC 6300 using X-ray Observations"*, Monthly Notices of the Royal Astronomical Society, v. 499, p. 5396-5409, doi :https://doi.org/10.1093/mnras/staa2552.

22. Jana A., D. Debnath, D. Chatterjee, K. Chatterjee, S. K. Chakrabarti, S. Naik, R. Bhowmick, N. Kumari, 2020, *"Accretion flow evolution of a new blackhole candidate MAXI J1348-630 during the 2019 outburst"*, The Astrophysical Journal, v. 897, p. 1-13, doi :https://doi.org/10.3847/1538-4357/ab9696.

23. Kaur, H., S. Sharma, L. K. Dewangan, D. K. Ojha, A. Durgapal, and, N. Panwar, 2020, *"Unveiling the physical conditions in NGC 6910"*, The Astrophysical Journal, v. 896, p. 1-17, doi :https://doi.org/10.3847/1538-4357/ab9122.

24. Kirsanova M. S., V. Ossenkopf-Okada, L. D. Anderson, P. A. Boley, J. H. Bieging, Y. N. Pavlyuchenkov, M. Luisi,N. Schneider, M. Andersen, M.R.Samal, A. M. Sobolev, C. Buchbender, R. Aladro, Y. Okada, 2020, *"The PDR structure and kinematics around the compact H II regions S235 A and S235 C with [C II], [13C II], [O I], and HCO+ line profiles"*, Monthly Notices of the Royal Astronomical Society, v. 497, p. 2651-2669, doi :https://doi.org/10.1093/mnras/staa2142.

25. Kumar, V, M. K. Srivastava, D P. K. Banerjee and V. Joshi, 2021, *"UV spectroscopy confirms SU Lyn to be a symbiotic star"*, Monthly Notices of the Royal Astronomical Society - Letters, v. 500, p. L12-L16, doi :https://doi.org/10.1093/mnrasl/slaa159.

26. Mazarbhuiya, A., H. S. Das, P. Halder, 2021, *"The Umov effect in cosmic dust analogue fluffy aggregates"*, Monthly Notices of the Royal Astronomical Society, v.502, p. 3491-3499, doi :https://doi.org/10.1093/mnras/stab084.

27. Mithun, N. P. S., S. V. Vadawale, A. R. Patel, M. Shanmugam, Chakrabarty D., P. Konar, T. N. Sarvaiya, G. D. Padia, A. Sarkar, P. Kumar, P. Jangid, A. Sarda, M. S. Shah, A. Bhardwaj, 2021, *"Data processing software for Chandrayaan-2 Solar X-ray Monitor"*, Astronomy and Computing, v. 34, p. 100449, doi :https://doi.org/10.1016/j.ascom.2021.100449.

28. Mithun, N. P. S., S. V. Vadawale, M. Shanmugam, A. R. Patel, N. K. Tiwari, H. L. Adalja, S. K. Goyal, T. Ladiya, N. Singh, S. Kumar, M. K. Tiwari, M. H. Modi, B. Mondal, A. Sarkar, B. Joshi, P. Janardhan, A. Bhardwaj, 2021, *"Ground calibration of Solar X-ray Monitor on board the Chandrayaan-2 orbiter"*, Ground calibration of Solar X-ray Monitor on board the Chandrayaan-2 orbiter, V. 51, p. 33-60, doi :https://doi.org/10.1007/s10686-020-09686-5.

29. Mithun, N. P. S., S. V. Vadawale, M. Shanmugam, A. R. Patel, N. Singh, S.Kumar, N. K. Tiwari, S. K. Goyal, A. B. Sarbadhikari, G. Arora, Y. Srivastava, H. K. Adalja, T. Ladiya, D. K. Painkra, S. B. Banerjee, V. R. Patel, A. Bhardwaj, 2020, *"Ground calibration of Alpha Particle X-ray Spectrometer (APXS) on- board Chandrayaan-2 Pragyaan rover: An empirical approach"*, Planetary and Space Science, v. 187, p. 104923, doi :https://doi.org/10.1016/j.pss.2020.104923.

30. Mithun, N. P. S.,S. V. Vadawale, A. Sarkar, M. Shanmugam, A. R. Patel, B. Mondal, B. Joshi, P. Janardhan, H. L. Adalja, S. K. Goyal, T. Ladiya, N. K. Tiwari, N. Singh, S. Kumar, M. K., M. H. Modi, A. Bhardwaj, 2020, *"Solar X-Ray Monitor on Board the Chandrayaan-2 Orbiter: In-Flight Performance and Science Prospects"*, SolarPhysics, v..295, p.139, doi :https://doi.org/10.1007/s11207-020-01712-1.

31. Mondal, B., S. V. Vadawale, N. P. S. Mithun, C. S. Vaishnava, N. K. Tiwari, S. K. Goyal, S. S. Panini, V. Navalkar, C. Karmakar, M. R. Patel, R.B. Upadhyay, 2021, *"DarpanX: A python package for modeling X-ray reflectivity of multilayer mirrors"*, Astronomy and Computing, v. 34, p. 100446, doi :https://doi.org/10.1016/j.ascom.2020.100446.

32. Panwar, N., S. Sharma, D. K. Ojha, T. Baug, L. K. Dewangan, B. C. Bhatt, and, R. Pandey, 2020, *"Star formation and evolution of blister-type HII region Sh 2-112"*, The Astrophysical Journal, v. 905, p. 1-14,, doi :https://doi.org/10.3847/1538-4357/abc42e.

33. Pavlenko, Y. V., A. Evans, D. P. K. Banerjee, T. R. Geballe, U. Munari, R.D. Gehrz, C. E. Woodward, S. Starrfield, 2020, *"Isotopic ratios in the red giant component of the recurrent nova T Coronae Borealis"*, Monthly Notices of the Royal Astronomical Society, v. 498, p.4853-4863, doi :https://doi.org/10.1093/mnras/staa2658.

34. Readhead A. C. S., V. Ravi, I. Liodakis, M. L. Lister, V. Singh, M. F. Aller, R. D. Blandford, . . . ,J. A. Zensus, 2021, *"The Relativistic Jet Orientation and Host Galaxy of the Peculiar Blazar PKS 1413+135"*, The Astrophysical Journal, v. 907, p. 61-89, doi :https://doi.org/10.3847/1538-4357/abd08c.

35. Rho, J., A. Evans, T. R. Geballe, D. P. K. Banerjee,..., Joshi, V.,...,S. Yan, 2021, *"Near-infrared and Optical Observations of Type Ic SN 2020oi and Broad-lined Type Ic SN 2020bvc: Carbon Monoxide, Dust, and High-velocity Supernova Ejecta"*, The Astrophysical Journal, v. 908, p. 21, doi :https://doi.org/10.3847/1538-4357/abd850.

36. Sharma, V., S. Iyyani, D. Bhattacharya, T. Chattopadhyay, S. V. Vadawale, V. B. Bhalerao, 2020, *"Spectropolarimetric analysis of prompt emission of GRB 160325A: jet with evolving environment of internal shocks"*, Monthly Notices of the Royal Astronomical Society, v.493, p.5218-5232, doi :https://doi.org/10.1093/mnras/staa570.

37. Venkataramani, K., S. Ganesh, and K. S. Baliyan, 2020, *"Ionic emissions in comet C/2016 R2 (Pan-STARRS)"*, Monthly Notices of the Royal Astronomical Society, v.495, p. 3559-3570, doi :https://doi.org/10.1093/mnras/staa1141.

Solar Physics

38. Bhattacharyya, R. and P. Konar, 2021, *"Modelling the influence of progressive social awareness, lockdown and anthropogenic migration on the dynamics of an epidemic"*, Int. J. Dynam. Control, v. 9, p. 797-806, doi :https://doi.org/10.1007/s40435-020-00692-1.

39. Bora, K., R. Bhattacharyya and P. K. Smolarkiewicz, 2021, *"Evolution of Three-dimensional Coherent Structures in Hall Magnetohydrodynamics"*, The Astrophysical Journal, v. 906, pp. 16, doi :https://doi.org/10.3847/1538-4357/abc8f7.

40. Devi, P., B. Joshi, R. Chandra, P. K. Mitra, A. M. Veronig and R. Joshi, 2020, *"Development of a Confined Circular-Cum-Parallel Ribbon Flare and Associated Pre-Flare Activity"*, Solar Physics, v. 295, pp. 22, doi :https://doi.org/10.1007/s11207-020-01642-y.

41. Devi, P., P. Demoulin, R. Chandra, R. Joshi, B. Schmieder and B. Joshi, 2021, *"Observations of a prominence eruption and loop contraction"*, Astronomy and Astrophysics, v. 647, pp. 15, doi :https://doi.org/10.1051/0004-6361/202040042.

42. Joshi, N. C., A. C. Sterling, R. L. Moore and B. Joshi, 2020, *"Sequential Lid Removal in a Triple-decker Chain of CME-producing Solar Eruptions"*, The Astrophysical Journal, v. 901, pp. 15, doi :https://doi.org/10.3847/1538-4357/abacd0.

43. Joshi, N. C., B. Joshi and P. K. Mitra, 2021, *"Evolutionary stages and triggering process of a complex eruptive flare with circular and parallel ribbons"*, Monthly Notices of the Royal Astronomical Society, v. 501, p. 4703–4721., doi :https://doi.org/10.1093/mnras/staa3480.

44. Kharayat, H., B. Joshi, and R. Chandra, 2021, *"Radio-loud and radio-quiet CMEs: solar cycle dependency, influence on cosmic ray intensity, and geo-effectiveness"*, Astrophysics and Space Science, v. 366, pp. 13, doi :https://doi.org/10.1007/s10509-021-03930-w.

45. Kumar, H. and B. Kumar, 2020, *"On the seismic emission in sunspots associated with Lorentz force changes accompanying major solar flares"*, Monthly Notices of the Royal Astronomical Society, v. 497, p. 976-987., doi :https://doi.org/10.1093/mnras/staa1974.

46. Kumar, S., S. S. Nayak, A. Prasad and R. Bhattacharyya, 2021, *"Magnetic Reconnections in the Presence of Three-Dimensional Magnetic Nulls and Quasi-Separatrix Layers"*, Solar Physics, v. 296, pp. 23, doi :https://doi.org/10.1007/s11207-021-01768-7.

47. Louis, R. E. and J. K. Thalmann, 2021, *"Homologous Flaring Activity over a Sunspot Light Bridge in an Emerging Active Region"*, The Astrophysical Journal Letters, v. 907, pp. 8, doi :https://doi.org/10.3847/2041-8213/abd478.

48. Louis, R. E., C. Beck and D. P. Choudhary, 2020, *"The Formation of an Atypical Sunspot Light Bridge as a Result of Large-scale Flux Emergence"*, The Astrophysical Journal, v. 905, pp. 22, doi :https://doi.org/10.3847/1538-4357/abc618.

49. Maurya, R. A. and A. Ambastha, 2020, *"Magnetic and Velocity Field Topology in Active Regions of Descending Phase of Solar Cycle 23"*, Solar Physics, v. 295, pp. 26, doi :https://doi.org/10.1007/s11207-020-01666-4.

50. Mitra, P. K. and B. Joshi, 2021, *"Successive occurrences of quasi-circular ribbon flares in a fan-spine-like configuration involving hyperbolic flux tube"*, Monthly Notices of the Royal Astronomical Society, v. 503, p. 1017-1035, doi :https://doi.org/10.1093/mnras/stab175.

51. Mitra, P. K., B. Joshi, A. M. Veronig, R. Chandra, K. Dissauer and T. Wiegelmann, 2020, *"Eruptive-Impulsive Homologous M-class Flares Associated with Double-decker Flux Rope Configuration in Minisigmoid of NOAA 12673"*, The Astrophysical Journal, v. 900, pp. 20, doi :https://doi.org/10.3847/1538-4357/aba900.

52. Nayak, S. S., R. Bhattacharyya and S. Kumar, 2021, *"Magnetohydrodynamics model of an X-class flare in NOAA active region 12017 initiated with non-force-free extrapolation"*, Physics of Plasmas, v. 28, pp. 6, doi :https://doi.org/10.1063/5.0035086.

53. Prasad A., K. Dissauer, Q. Hu, R. Bhattacharyya, A. M. Veronig, S. Kumar and B. Joshi, 2020, *"Magnetohydrodynamic Simulation of Magnetic Null-point Reconnections and Coronal Dimmings during the X2.1 Flare in NOAA AR 11283"*, The Astrophysical Journal, v. 903, pp. 17, doi :https://doi.org/10.3847/1538-4357/abb8d2.

54. Sahu, S., B. Joshi, P. K. Mitra, A. M. Veronig and V. Yurchyshyn, 2020, *"Hard X-Ray Emission from an Activated Flux Rope and Subsequent Evolution of an Eruptive Long-duration Solar Flare"*, The Astrophysical Journal, v. 897, pp. 19, doi :https://doi.org/10.3847/1538-4357/ab962b.

55. Sharma, A., D. Tripathi, R. Erdelyi, G. R. Gupta and G. A. Ahmed, 2020, *"Wave amplitude modulation in fan loops as observed by AIA/SDO"*, Astronomy and Astrophysics, v. 638, pp. 11, doi :https://doi.org/10.1051/0004-6361/201936667.

56. Sharma, J., A. K. Malik, B. Kumar and H. O. Vats, 2020, *"Evidence of a strong relationship between hemispheric asymmetry in solar coronal rotation and solar activity during solar cycle 24"*, Monthly Notices of the Royal Astronomical Society, v. 499, p. 5442-5446, doi :https://doi.org/doi:10.1093/mnras/staa2863.

Planetary Sciences

57. Baliyan, S., H. Moitra, S. Sarkar, D. Ray, D. K. Panda, A. D. Shukla, S. Bhattachrya, and S. Gupta, 2020, *"Mineralogy and Spectroscopy (Visible Near Infrared and Fourier Transform Infrared) of Mukundpura CM2: Implications for asteroidal aqueous alteration"*, Geochemistry, v. 81, pp. 125729, doi :https://doi.org/10.1016/j.chemer.2020.125729.

58. Durga Prasad, K. and S. V. S. Murty, 2020, *"Development of a chamber to simulate lunar surface environment"*, Planetary and Space Science, v. 191, p. 105038, doi :https://doi.org/10.1016/j.pss.2020.105038.

59. Garg A., Marhas K. K. and Goyal V., 2020, *"Sputtering of presolar grains via Galactic Cosmic Rays in the Interstellar medium"*, The Astrophysical Journal, v. 905, p. 80, doi :https://doi.org/10.3847/1538-4357/abc25b.

60. Gawronska, A. J., N. Barrett, S.J. Boazman, C.M. Gilmour, S.H. Halim, Harish, K. McCanaan, A.V. Satyakumar, J. Shah, H.M. Meyer, D.A. Kring, 2020, *"Geologic context and potential EVA targets at the lunar south pole"*, Advances in Space Research, v. 66, p. 1247-1264, doi :https://doi.org/10.1016/j.asr.2020.05.035.

61. Halim, S. H., N. Barrett, S. J. Boazman, A. J. Gawronska, C. M. Gilmour, Harish, K. McCanaan, A. V. Satyakumar, J. Shah and D. A. Kring, 2021, *"Numerical modeling of the formation of Shackleton crater at the lunar south pole"*, Icarus, v. 354, p. 113992, doi :https://doi.org/10.1016/j.icarus.2020.113992.

62. Harish and Vijayan S., 2020, *"Craters in the vicinity of Valles Marineris region, Mars: Chronological implications to the graben and pits activities"*, Icarus, v. 343, p. 113704, doi :https://doi.org/10.1016/j.icarus.2020.113704.

63. Harish, S. Vijayan, N. Mangold and A. Bhardwaj, 2020, *"Water-Ice Exposing Scarps Within the Northern Midlatitude Craters on Mars"*, Geophysical Research Letters, v. 47, p. 14, doi :https://doi.org/10.1029/2020GL089057.

64. Hess M., Wöhler C., Bhatt M., Berezhnoy A. A., Grumpe A., Wohlfarth K., Bhardwaj A., and Shevchenko V. V., 2020, *"Processes governing the VIS/NIR spectral reflectance behavior of lunar swirls"*, Astronomy & Astrophysics, v. 639, pp. 1-18, doi :https://doi.org/10.1051/0004-6361/201937299.

65. Jha, P., P. Das and D. Ray, 2021, *"Understanding genesis of iron oxide concretions present in Dhandraul (Vindhyan) Sandstone: Implications in formation of Martian hematite spherules"*, Journal of Earth System Science, v. 130, pp. 49, doi :https://doi.org/10.1007/s12040-020-01542-6.

66. Krishnaprasad C., Smitha V. Thampi, Anil Bhardwaj, Christina O. Lee, K. Kishore Kumar, and Tarun K. Pant, 2020, *"Recurrent Solar Energetic Particle Flux Enhancements Observed near Earth and Mars"*, Astrophysical Journal, v. 902, pp. 1-11, doi :https://doi.org/10.3847/1538-4357/abb137.

67. Mahajan R. R., 2020, *"Laser microprobe noble gases and nitrogen analysis of chondrules form the Dhajala chondrite"*, Meteoritics & Planetary Science (MAPS), v. 55, p. 2141-2156, doi :https://doi.org/10.1111/maps.13565.

68. Mahajan R. R., 2020, *"Exposure ages, noble gases and nitrogen in the ordinary chondrite Karimati (L5)"*, Earth, Moon, and Planets (EMP), v. 124, p. 3-13, doi :https://doi.org/10.1007/s11038-020-09532-w.

69. Mahajan R. R., 2020, *"Noble gases and nitrogen in metal from the ordinary chondrites Katol (L6), Itawa Bhopji (L3-5) and Portales Valley (H6)"*, Astrophysics and Space Science, v. 365, p. 1-10, doi :https://doi.org/10.1007/s10509-020-03845-y.

70. Majumder, A. S., D. Ray and A. D. Shukla, 2020, *"Serpentinization of olivine–gabbro in Central Indian ridge: Insights into H2 production during alteration in lower oceanic crust and sustenance of life at slow–spreading ridges"*, Lithos, V. 374-375, pp. 105730, doi :https://doi.org/10.1016/j.lithos.2020.105730.

71. Masoom, J., S. A. Haider and Macro Giuranna, 2019, *"Response of dust on thermal emission spectra observed by Planetary Fourier Spectrometer (PFS) onboard Mars express (MEX)"*, Indian Journal of Radio & Space Physics, v. 48, p. 38-44, doi :http://nopr.niscair.res.in/handle/123456789/54918.

72. Mishra, S. K., 2020, *"Photoelectron distribution on sunlit surface of the Moon: A formalism"*, Physics of Plasmas, v. 27, p. 082906, doi :https://doi.org/10.1063/5.0016411.

73. Mishra, S. K., 2020, *"Role of photoelectric charge fluctuation in dust detachment from the lunar surface"*, Physics of Plasmas, v. 27, p. 052901, doi :https://doi.org/10.1063/5.0009741.

74. Mishra, S. K. and A. Bhardwaj, 2020, *"Electrostatic charging of permanently shadowed craters on the Moon"*, Monthly Notices of Royal Astronomical Society – Letters (MNRASL), v. 496, p. L80, doi :https://doi.org/10.1093/mnrasl/slaa082.

75. Misra, S., A. Smith, D. Ray and W.A. Hastie, 2020, *"Geochemical evidence of mixing between A-type rhyolites and basalts from Southern Lebombo, South Africa: Implications for evolution of the Northern Karoo Igneous Province"*, Geological Journal, v. 56, p. 1072-1108, doi :http://dx.doi.org/10.1002/gj.3970.

76. Mukundan V., S. V. Thampi, A. Bhardwaj and C. Krishnaprasad, 2020, *"Model calculation of ionization efficiency in the Martian dayside ionosphere using MAVEN observations"*, Monthly Notices of the Royal Astronomical Society, v. 497, pp. 2239–2249, doi :https://doi.org/10.1093/mnras/staa2123.

77. Nickerson, S., N. Rangwala, S. Colgan, C. DeWitt, X. Huang, K. Acharyya et al., 2021, *"The First Mid-Infrared Detection of HNC in the Interstellar Medium: Probing the Extreme Environment Towards the Orion Hot Core"*, The Astrophysical Journal, v. 907, pp. 51, doi :https://doi.org/10.3847/1538-4357/abca36.

78. Panda, D. K., D. Ray, A. Shukla, 2020, *"The petrochemical constraint and cosmogenic records of Mahadeva (H5) chondrite: a new fall in India"*, Planetary Space Science, v. 194, p. 105111, doi :https://doi.org/10.1016/j.pss.2020.105111.

79. Pillai, N. S., S. Narendranath, K. Vadodariya, S. P. Tadepalli, Radhakrishna V., A. Tyagi, R. Yadav, B. Singh, V. Sharan, P.S. Athiray, P. Sreekumar, K. Sankarasubramanian, M. Bhatt, A. Basu Sarbadhikari, N.P.S. Mithun, S. Vadawale, 2021, *"Chandrayaan-2 Large Area Soft X-ray Spectrometer (CLASS): Calibration, In-flight performance and first results"*, Icarus, 363, 114436, doi :https://doi.org/10.1016/j.icarus.2021.114436.

80. Ray, D., A. D. Shukla, S. Bhattacharya, S. Gupta, P. Jha and U. Chandra, 2021, *"Hematite concretions from the late Jurassic Jhuran sandstone, Kutch, Western India: Implications for sedimentary diagenesis and origin of "blueberries" on Mars"*, Planetary and Space Science, v. 197, p. 105163, doi :https://doi.org/10.1016/j.pss.2021.105163.

81. Ray, D., S. Misra and D. R. Nelson, 2021, *"Lunar feldspathic meteorite Dhofar 081- Petrochemical constraints on petrogenesis"*, Journal of Earth System Science, v. 130, pp. 39, doi :https://doi.org/10.1007/s12040-020-01499-6.

82. Sanghani M. N., Marhas K. K., Hsiao S. S. Y., Peeters Z., Shang H., Lee D. C., and Bizzarro M., 2020, *"Presolar silicate and oxide grains found in lithic clasts from Isheyevo and fine grained matrices of NWA 801"*, The Astrophysical Journal Supplement Series (APJS), v. 253, p. 41, doi :https://doi.org/10.3847/1538-4365/abdbab.

83. Sathiyaseelan, S., D. K. Panda, D. Banerjee, D. Ramesh and A. D. Shukla, 2021, *"Chronology of coastal dune ridges in Vaigai Prodelta Region, South-Eastern Tamil Nadu, India"*, Current Science, v. 120, p. 382-388, doi :https://www.currentscience.ac.in/Volumes/120/02/0382.pdf.

84. Shah, S. Y., S. A. Haider, G. J. Molina-Cuberos, M. A. Abdu and I. S. Batista, 2021, *"A coupled model of the D and E regions of Mars' ionosphere and flare and non-flare electron density profiles"*, Icarus, v. 361, pp. 114403, doi :https://doi.org/10.1016/j.icarus.2021.114403.

85. Shreedevi P. R., R. K. Choudhary, Smitha V. Thampi, Sneha Yadav, T. K. Pant, Yiqun Yu, Ryan McGranaghan, Evan G. Thomas, Anil Bhardwaj and A. K. Sinha, 2020, *"Geomagnetic storm induced plasma density enhancements in the southern polar ionospheric region: A comparative study using St. Patricks day storms of 2013 and 2015"*, Space Weather, v. 18, pp. 1-20, doi :https://doi.org/10.1029/2019SW002383.

86. Singh, T. and N. Srivastava, 2020, *"Geology of Grimaldi Basin on the Moon: Evidence for volcanism and tectonism during the Copernican period"*, ICARUS, v. 351, pp. 113921, doi :https://doi.org/10.1016/j.icarus.2020.113921.

87. Sinha, R. K., A. Rani, S. J. Conway, S. Vijayan, A. Basu Sarbadhikari, M. Massé, N. Mangold, and Anil Bhardwaj, 2020, *"Boulder fall activity in the Jezero crater, Mars"*, Geophysical Research Letters, v. 47, pp. 1-10, doi :https://doi.org/10.1029/2020GL090362.

88. Sinha, R. K., D. Ray, T. De Haas, and S. J. Conway, 2020, *"Global documentation of overlapping lobate deposits in Martian gullies"*, ICARUS, v. 352, p. 1-23, doi :https://doi.org/10.1016/j.icarus.2020.113979.

89. Susarla R. and A. Bhardwaj, 2020, *"CO+ First-negative band emission: A tracer for CO in the Martian upper atmosphere"*, Astronomy and Astrophysics, v. 639, pp. 1-6, doi :https://doi.org/10.1051/0004-6361/202038147.

90. Susarla R., A. Bhardwaj, D. Hutsemékers, C. Opitom, J. Manfroid, and E. Jehin, 2021, *"A physicochemical model to study the ion density distribution in the inner coma of comet C/2016 R2 (Pan-STARRS)"*, Monthly Notices of the Royal Astronomical Society, v. 501, pp. 4035–4052, doi :https://doi.org/10.1093/mnras/staa3885.

91. Susarla R., S. K. Jain, A. Bhardwaj, 2021, *"Forbidden atomic oxygen emissions in the Martian dayside upper atmosphere"*, Icarus, v. 359, p. 114330, doi :https://doi.org/10.1016/j.icarus.2021.114330.

92. Upadhyaya, T., J. Pabari, V. Sheel, A. Desai, R. Patel and S. Jitarwal, 2020, *"Compact and high isolation microstrip diplexer for future radio science planetary applications"*, AEU - International Journal of Electronics and Communications, Elsevier, v. 127, pp. 1-7, doi :https://doi.org/10.1016/j.aeue.2020.153497.

Space and Atmospheric Sciences

93. Chakraborty, S., Chakrabarty, D., Reeves, G. D., Baker, D. N., Claudepierre, S. G., Breneman, A. W., Hartley, D. P., and Larsen, B. A., 2021, *"Van Allen probe observations of disappearance, recovery and patchiness of plasmaspheric hiss following two consecutive interplanetary shocks: First results"*, Journal of Geophysical Research: Space Physics, v. 126, e2020JA028873, doi :https://doi.org/10.1029/2020JA028873.

94. Chhabra, A., Turakhia, T., Sharma, S., Saha, S., Iyer, R., and Chauhan, P., 2020, *"Environmental impacts of fireworks on aerosol characteristics and radiative properties over a mega city, India"*, City and Environment Interactions, v. 7, 100049, doi :https://doi.org/10.1016/j.cacint.2020.100049.

95. Chutia, L., Ojha, N., Girach, I. A., Pathak, B., Sahu, L. K., and Bhuyan, P. K., 2020, *"Seasonal Evolution of Sulfur Dioxide Over the Indian Subcontinent"*, URSI Radio Science Letters, v. 2, ., doi :https://doi.org/10.46620/20-0046.

96. Dave, P. N., Sahu, L.K., Tripathi, N., Bajaj, S., Yadav, R., and Patel, K., 2020, *"Emissions of non-methane volatile organic compounds from a landfill site in a major city of India: Impact on local air quality"*, Heliyon, v. 6, e04537, doi :https://doi.org/10.1016/j.heliyon.2020.e04537.

97. Girach, I. A., Nair, P. R., Ojha, N., and Sahu, L. K., 2020, *"Tropospheric carbon monoxide over the northern Indian Ocean during winter: Influence of inter-continental transport"*, Climate Dynamics, v. 54, p. 5049–5064, doi :https://doi.org/10.1007/s00382-020-05269-4.

98. Girach, I. A., Tripathi, N., Nair, P. R., Sahu, L. K., and Ojha, N., 2020, *"O_3 and CO in the South Asian outflow over the Bay of Bengal: Impact of monsoonal dynamics and chemistry"*, Atmospheric Environment, v. 233, p. 117610, doi :https://doi.org/10.1016/j.atmosenv.2020.117610.

99. Guharay, A., Batista, P. P., and Buriti, R. A., 2020, *"Signature of a 120-day oscillation in the MLT winds and tides over São João do Cariri (7.4° S, 36.5° W)"*, Journal of Atmospheric and Solar-Terrestrial Physics, v. 207, 105337, doi :https://doi.org/10.1016/j.jastp.2020.105337.

100. Guharay, A., Batista, P. P., Buriti, R. A., and Schuch, N. J., 2020, *"Signature of the 27-day oscillation in the MLT tides and its relation with solar radiation at low latitudes"*, Earth, Planets and Space, 72:, 51, doi :https://doi.org/10.1186/s40623-020-01149-7.

101. Jindal, P., Thapliyal, P. K., Shukla, M. V., Sharma, S. and Mitra, D., 2020, *"Trend analysis of atmospheric temperature, water vapour, ozone, methane, and carbon-monoxide over few major cities of India using satellite data"*, Journal of Earth System Sciences, v. 129, 60, doi :https://www.ias.ac.in/article/fulltext/jess/129/0060.

102. Kumar, A., Chakrabarty, D., Pandey, K., Fejer, B. G., Sunda, S., Seemala, G. K., Sripathi, S., and Yadav, A. K., 2021, *"Evidence for the significant differences in response times of equatorial ionization anomaly crest corresponding to plasma fountains during daytime and post-sunset hours"*, Journal of Geophysical

Research: Space Physics, v. 126, e2020JA028628, doi :https://doi.org/10.1029/2020JA028628.

103. Kumar, S., Veenadhari, B., Chakrabarty, D., Tulasi Ram, S., Kikuchi, T., and Miyoshi, Y., 2020, *"Effects of IMF By on Ring Current Asymmetry Under Southward IMF Bz Conditions Observed at Ground Magnetic Stations: Case Studies"*, Journal of Geophysical Research: Space Physics, v. 125, e2019JA027493, doi :https://doi.org/10.1029/2019JA027493.

104. Mandal, S., and Pallamraju, D., 2020, *"Thermospheric gravity wave characteristics in the daytime over low-latitudes during geomagnetic quiet and disturbed conditions"*, Journal of Atmospheric and Solar-Terrestrial Physics, v. 211, 105470, doi :https://doi.org/10.1016/j.jastp.2020.105470.

105. Mandal, S., Pallamraju, D., and Suryawanshi, P., 2020, *"Changes in the daytime thermospheric gravity wave propagation characteristics over low-latitudes in response to the variation in solar flux"*, Journal of Atmospheric and Solar-Terrestrial Physics, v. 209, 105414, doi :https://doi.org/10.1016/j.jastp.2020.105414.

106. Ojha, N., Sharma, A., Kumar, M., Girach, I., Ansari, T. U., Sharma, S. K., Singh, N., Pozzer, A., and Gunthe, S. S., 2020, *"On the widespread enhancement in fine particulate matter across the Indo-Gangetic Plain towards winter"*, Scientific Reports, v. 10, p. 5862, doi :https://doi.org/10.1038/s41598-020-62710-8.

107. Pallamraju, D., Karan, D. K., Laskar, F. I., Vijaya Lakshmi, T., and Chakrabarti, S., 2020, *"Effect of solar flux versus compositional variations on the variability of daytime oxygen optical emission rates over low- and mid-latitudes"*, Journal of Atmospheric and Solar-Terrestrial Physics, v. 205, 105293, doi :https://doi.org/10.1016/j.jastp.2020.105293.

108. Pandey, K., and Gupta, S. P., 2020, *"Altitude of twostream irregularities in equatorial E region using sounding rocket experiments from Thumba"*, Journal of Geophysical Research: Space Physics, v. 125, e2019JA027195, doi :https://doi.org/10.1029/2019JA027195.

109. Pandey, K., Sekar, R., Chakrabarty, D., and Anandarao, B. G., 2021, *"Investigation on longitudinal and decadal variations of the equatorial electrojet using a physical model"*, Advances in Space Research, v. 68, p. 182-200, doi :https://doi.org/10.1016/j.asr.2021.02.040.

110. Patra, P. K., Krol, M. C., Prinn, R. G., Takigawa, M., Mühle, J., Montzka, S. A., Lal, S., Yamashita, Y., Stijn Naus, Chandra, N., Weiss, R. F., Krummel, P. B., Fraser, P. J., O'Doherty, S., and J. W. Elkins, 2021, *"Methyl Chloroform continues to constrain the hydroxyl (OH) reactivity of the troposphere"*, Journal of Geophysical Research: Atmospheres, v. 126, e2020JD033862, doi :https://doi.org/10.1029/2020JD033862.

111. Ramachandran, S., and Rupakheti, M., 2020, *"Inter-annual and seasonal variations in columnar aerosol characteristics and radiative effects over the Pokhara Valley in the Himalayan foothills – Composition, radiative forcing, and atmospheric heating"*, Environmental Pollution, v. 264, p. 114799, doi :https://doi.org/10.1016/j.envpol.2020.114799.

112. Ramachandran, S., and Rupakheti, M., 2020, *"Year-round aerosol characteristics and radiative effects in the South Asian pollution outflow over a background site in the Maldives"*, Atmospheric Environment, v. 240, p. 117813, doi :https://doi.org/10.1016/j.atmosenv.2020.117813.

113. Ramachandran, S., and Rupakheti, M., 2021, *"Inter-annual and seasonal variations in optical and physical characteristics of columnar aerosols over the Pokhara Valley in the Himalayan foothills"*, Atmospheric Research, v. 248, p.105254, doi :https://doi.org/10.1016/j.atmosres.2020.105254.

114. Ramachandran, S., Rupakheti, M., and Lawrence, M. G., 2020, *"Black carbon dominates the aerosol absorption over the Indo-Gangetic Plains and the Himalayan foothills"*, Environment International, v. 142, p.105814, doi :https://doi.org/10.1016/j.atmosenv.2020.105814.

115. Ramachandran, S., Rupakheti, M., and Lawrence, M. G., 2020, *"Aerosol-induced atmospheric heating rate decreases over South and East Asia as a result of changing content and composition"*, Scientific Reports, v. 10, p. 20091, doi :https://doi.org/10.1038/s41598-020-76936-z.

116. Rawat, P., Naja, M., Thapliyal, P. K., Srivastava, S., Bhardwaj, P., Kumar, R., Bhatacharjee, S., Venkatramani, S., Tiwari, S. N., and Lal, S., 2020, *"Assessment of vertical ozone profiles from INSAT-3D Sounder over the Central Himalayas"*, Current Science, v. 119, p. 1113-1122, doi :http://dx.doi.org/10.18520/cs/v119/i7/1113-1122.

117. Renuka, K., Gadhavi, H., Jayaraman, A., Rao, S. V. B., and Lal, S., 2020, *"Study of mixing ratios of SO_2 in a tropical rural environment in south India"*, Journal of Earth System Science, 129:, 124, doi :https://doi.org/10.1007/s12040-020-1366-4.

118. Saha S., Kumar N. K., Sharma S., Kumar P., and Joshi V., 2020, *"Can QuasiPeriodic Gravity Waves Influence the Shape of Ice Crystals in Cirrus Clouds?"*, Geophysical Research Letters, v. 47, e2020GL087909, doi :https://doi.org/10.1029/2020GL087909.

119. Sahu, L. K., Tripathi, N., and Yadav, R., 2020, *"Observations of trace gases in the earth's lower atmosphere: instrumentation and platform"*, Current Science, v. 118, p. 1893-1902, doi :https://wwwops.currentscience.ac.in/Volumes/118/12/1893.pdf.

120. Sahu, L. K., Yadav, R., and Tripathi, N., 2020, *"Aromatic compounds in a semi-urban site of western India: Seasonal variability and emission ratios"*, Atmospheric Research, v. 264, p. 105114, doi :https://doi.org/10.1016/j.atmosres.2020.105114.

121. Shika, S., Gadhavi, H., Suman, M. N. S., Ravikrishna, R., and Gunthe, S. S., 2020, *"Atmospheric aerosol properties at a semirural location in southern India: particle size distributions and implications for cloud droplet formation"*, SN Applied Sciences, 2:, 1007, doi :https://doi.org/10.1007/s42452-020-2804-2.

122. Shukla, K. K., Phanikumar, D. V., Kumar, N. K., Kumar, A., Naja, M., Sharma, S., and Attada, R., 2021, *"Micro-Pulse Lidar observations of elevated aerosol layers over the Himalayan region"*, Journal of Atmospheric and Solar-Terrestrial Physics, v. 213, 105526, doi :https://doi.org/10.1016/j.jastp.2020.105526.

123. Singh, J., Singh, N., Ojha, N., Sharma, A., Pozzer, A., Kiran Kumar, N., Rajeev, K., Gunthe, S. S., and Kotamarthi, V. R., 2021, *"Effects of spatial resolution on WRF v3.8.1 simulated*

meteorology over the central Himalaya", Geoscientific Model Development, v. 14, p.1427-1443, doi :https://doi.org/10.5194/gmd-14-1427-2021.

124. Sivakandan, M., Mondal, S., Sarkhel, S., Chakrabarty, D., Sunil Krishna, M. V., Chaitanya, P. P., Patra, A. K., Choudhary, R. K., Pant, T. K., Upadhayaya, A. K., and Sori, T., 2020, *"Mid-latitude spread-F structures over the geomagnetic low-mid latitude transition region: An observational evidence"*, Journal of Geophysical Research: Space Physics, v. 125, e2019JA027531, doi :https://doi.org/10.1029/2019JA027531.

125. Soni, M., Ojha, N., Girach, I., 2021, "Impact of COVID-19 lockdown on surface ozone build-up at an urban site in western India based on photochemical box modelling", Current Science, v. 120, No. 2, p.376-381, doi:https://doi.org/10.18520/cs/v120/i2/376-381

126. Stewart, G. J., Acton, W. J. F., Nelson, B. S., Vaughan, A. R., Hopkins, J. R., Arya, R., Mondal, A., Jangirh, R., Ahlawat, S., Yadav, L., Sharma, S. K., Dunmore, R. E., Yunus, S. S. M., Hewitt, C. N., Nemitz, E., Mullinger, N., Gadi, R., Sahu, L. K., Tripathi, N., Rickard, A. R., Lee, J. D., Mandal, T. K., and Hamilton, J. F., 2021, *"Emissions of non-methane volatile organic compounds from combustion of domestic fuels in Delhi, India"*, Atmospheric Chemistry and Physics, v. 21, p. 2383-2406, doi :https://doi.org/10.5194/acp-2020-892.

127. Stewart, G. J., Nelson, B. S., Acton, W. J. F., Vaughan, A. R., Farren, N. J., Hopkins, J. R., Ward, M. W., Swift, S. J., Arya, R., Mondal, A., Jangirh, R., Ahlawat, S., Yadav, L., Sharma, S. K., Yunus, S. S. M., Hewitt, C. N., Nemitz, E., Mullinger, N., Gadi, R., Sahu, L. K., Tripathi, N., Rickard, A. R., Lee, J. D., Mandal, T. K., and Hamilton, J. F., 2021, *"Emissions of intermediate-volatility and semi-volatile organic compounds from domestic fuels used in Delhi, India"*, Atmospheric Chemistry and Physics, v. 21, p. 2407-2426, doi :https://doi.org/10.5194/acp-2020-860.

128. Stewart, G. J., Nelson, B. S., Acton, W. J. F., Vaughan, A. R., Hopkins, J. R., Yunus, S. S., Hewitt, C. N., Nemitz, E., Mandal, T. K., Gadi, R., Sahu, L. K., Rickard A. R., Lee, J. D., and Hamilton, J. F., 2021, *"Comprehensive organic emission profiles, secondary organic aerosol production potential, and OH reactivity of domestic fuel combustion in Delhi, India"*, Environmental Science: Atmospheres, v. 1, p. 104-117, doi :https://doi.org/10.1039/D0EA00009D.

129. Tripathi, N., and Sahu, L. K., 2020, *"Emissions and atmospheric concentrations of α-pinene at an urban site of India: Role of changes in meteorology"*, Chemosphere, v. 256, p. 127071, doi :https://doi.org/10.1016/j.chemosphere.2020.127071.

130. Tripathi, N., Sahu, L. K., Singh, A., Yadav, R., Patel, A., Patel, K., and Meenu P., 2020, *"Elevated levels of biogenic nonmethane hydrocarbons in the marine boundary layer of the Arabian Sea during the intermonsoon"*, Journal of Geophysical Research: Atmospheres, v.125, e2020JD032869, doi :https://doi.org/10.1029/2020JD032869.

131. Yadav, V., Rathi, R., Gaur, G., Sarkhel, S., Chakrabarty, D., Sunil Krishna, M. V., Pavan Chaitanya, P., Patra, A. K., and Choudhary, R. K., Pant, T. K., Upadhayaya, A. K., 2021, *"Interaction between nighttime MSTID and mid-latitude field-aligned plasma depletion structure over the transition region of geomagnetic low-mid latitude: First results from Hanle, India"*, Journal of Atmospheric and Solar-Terrestrial Physics, v. 217, 105589, doi :https://doi.org/10.1016/j.jastp.2021.105589.

132. Yadav, V., Rathi, R., Sarkhel, S., Chakrabarty, D., Sunil Krishna, M. V. and Upadhayay, A. K., 2021, *"A unique case of complex interaction between MSTIDs and midlatitude fieldaligned plasma depletions over geomagnetic lowmid latitude transition region"*, Journal of Geophysical Research: Space Physics, v. 126, e2020JA028620, doi :https://doi.org/10.1029/2020JA028620.

133. Yogesh, Chakrabarty, D., and Srivastava, N., 2021, *"Evidence for distinctive changes in the solar wind helium abundance in solar cycle 24"*, Monthly Notices of the Royal Astronomical Society: Letters, v. 503, p. L17-L22, doi :https://doi.org/10.1093/mnrasl/slab016.

Geosciences

134. Awasthi, N. and Ray, J.S., 2020, *"Tracking Indian monsoon variability from changes in sediment provenance"*, Current Science, v. 119, p. 291-306, doi :https://doi.org/10.18520/cs/v119/i2/291-306.

135. Banerji, U.S., J. Shaji, P. Arulbalaji, K. Maya, S. Vishnu Mohan, A.J. Dabhi, A. Shivam, R. Bhushan and D. Padmalal, 2021, *"Mid-late Holocene evolutionary history and climate reconstruction of Vellayani lake, south India"*, Quaternary International, v. 592, In press, doi :https://doi.org/10.1016/j.quaint.2021.03.018.

136. Banerji, U.S., R. Bhushan, K. Batuk Joshi, J. Shaji and A.J.T. Jull, 2021, *"Hydroclimate variability during the last two millennia from the mudflats of Diu Island, Western India"*, Geological Journal, v. 1, pp. 1-21, doi :https://doi.org/10.1002/gj.4116.

137. Bhowmik, H.S., S. Naresh, D. Bhattu, N. Rastogi, A.S.H. Prévôt and S.N. Tripathi, 2021, *"Temporal and spatial variability of carbonaceous species (EC; OC; WSOC and SOA) in $PM_{2.5}$ aerosol over five sites of Indo-Gangetic Plain"*, Atmospheric Pollution Research, v. 12, p. 375-390, doi :https://doi.org/10.1016/j.apr.2020.09.019.

138. Bikkina, P., S. Bikkina, K. Kawamura, A.K. Sudheer, G. Mahesh and and S. Kuswanth Kumar, 2020, *"Evidence for brown carbon absorption over the Bayof Bengal during the southwest monsoon season: a possible oceanic source"*, Environmental Science Processes & Impacts, v. 22, p. 1743-1758, doi :https://doi.org/10.1039/D0EM00111B.

139. Chakraborty, S., A.S. Majumdar and A.D. Shukla, 2020, *"Role of fluid in strain softening within the Main Central thrust in Sikkim: The origin of quartz-rich mylonites"*, Journal of Structural Geology, v. 140, 104145, doi :https://doi.org/10.1016/j.jsg.2020.104145.

140. Chaudhuri, A., A. Chatterjee, S. Banerjee and J.S. Ray, 2020, *"Tracing multiple sources of sediments using trace element and Nd isotope geochemistry: provenance of the Mesozoic succession in the Kutch Basin, western India"*, Geological Magazine, v. 158, pp. 359 - 374, doi :https://doi.org/10.1017/S0016756820000539.

141. Dave, D., S. Sarma, P. Parmar, A. Shukla, D. Goswami, A.D. Shukla and M. Saraf, 2020, *"Microbes as a boon for the bane of*

heavy metals", Environmental Sustainability, v. 3, p. 233-255, doi :https://doi.org/10.1007/s42398-020-00112-2.

142. Dave, J., R. Meena, A. Singh and N. Rastogi, 2021, *"Effect of COVID-19 lockdown on the concentration and composition of NR-$PM_{2.5}$ over Ahmedabad, a big city in western India"*, Urban Climate, v. 37, 100818, doi :https://doi.org/10.1016/j.uclim.2021.100.

143. Diwate. P., N.K. Meena, R. Bhushan, S. Pandita, K.R. Chandana and P. Kumar, 2020, *"Sedimentation rate (^{210}Pb and ^{137}Cs), grain Size, organic matter and bathymetric studies in Renuka Lake, Himachal Pradesh, India"*, Himalayan Geology, v. 41, p. 51-62, doi :https://www.himgeology.com/volume_abstract.php?abstract=910.

144. Dutta, M.K., S. Kumar, R. Mukherjee, N. Sharma, R. Bhushan, P. Sanyal, M. Paul and S. Mukhopadhyay, 2021, *"Carbon biogeochemistry of two contrasting estuarine ecosystems during premonsoon"*, Estuaries and Coasts, v. 115, p., doi :https://doi.org/10.1007/s12237-021-00908-3.

145. Gautam, P.K., A.C. Narayana, P. Kiran Kumar, P.G. Bhavani, M.G. Yadava and A.J.T. Jull, 2021, *"Indian monsoon variability during the last 46 kyr: isotopic records of planktic foraminifera from southwestern Bay of Bengal"*, Journal of Quaternary Science, v. 36, p., doi :https://doi.org/10.1002/jqs.3263.

146. Ghosh, S., P. Sanyal, S. Roy, R. Bhushan, S.P Sati, A. Philippe and N. Juyal, 2020, *"Early Holocene Indian summer monsoon and its impact on vegetation in the Central Himalaya: Insight from δD and $\delta^{13}C$ values of leaf wax lipid"*, The Holocene, v. 30, p. 1063-1074, doi :https://doi.org/10.1177/0959683620908639.

147. Gupta, G.V.M., R. Jyothibabu, Ch.V. Ramu, A.Y. Reddy, K.K. Balachandran, V. Sudheesh, S. Kumar, N.V.H.K. Chari, K. F. Bepari, P.H. Marathe, B. Reddy and A.K. Vijayan, 2021, *"Is the world's largest coastal deoxygenation zone not anthropogenically driven?"*, Environment Research Letters, v. 16, 054009, doi :https://doi.org/10.1088/1748-9326/abe9eb.

148. Jeelani, G., S.A. Lone, A.U. Nisa. A. Mukherjee and R.D. Deshpande, 2020, *"Sources and processes of groundwater arsenic mobilization in upper Jhelum basin, western Himalayas"*, Journal of Hydrology, v. 591, 125292, doi :https://doi.org/10.1016/j.jhydrol.2020.125292.

149. Kiko, R., D. Bianchi, C. Grenz, H. Hauss, M. Iversen, S. Kumar, A. Maas and C. Robinson, 2020, *"Zooplankton and Nekton: Gatekeepers of the Biological Pump"*, Frontiers in Marine Science, v. 7, 00545, doi :https://doi.org/10.3389/fmars.2020.00545.

150. Lalchandani, V., V. Kumar, A. Tobler, N.M. Thamban, S. Mishra, J.G. Slowik, D. Bhattu, P. Rai, R. Satish, D. Ganguly, S. Tiwari, N. Rastogi, G. Močnik, A.S.H. Prévôt and S.N. Tripathi, 2021, *"Real-time characterization and source apportionment of fine particulate matter in the Delhi megacity area during late winter"*, Science of the Total Environment, v. 770, 145324, doi :https://doi.org/10.1016/j.scitotenv.2021.145324.

151. Laskar, A.H., S.K. Bhattacharya, D.M. Mohabey and M.C. Liang, 2020, *"Variable thermoregulation of Late Cretaceous dinosaurs inferred by clumped isotope analysis in fossil eggshell carbonates"*, Heliyon, v. 6, p. e05265, doi :https://doi.org/10.1016/j.heliyon.2020.e05265.

152. Nambiar, R., C. Shah, J. Kumar, P.S. Shrivastav and R. Bhushan, 2020, *"Assessment of contaminants in the northwestern Bay of Bengal"*, Environmental Science and Pollution Research, v. 27, pp. 34090-34098, doi :https://doi.org/10.1007/s11356-020-09576-5.

153. Oza, H., A. Ganguly, V. Padhya and R.D. Deshpande, 2020, *"Hydrometeorological processes and evaporation from falling rain in Indian sub-ontinent: Insights from stable isotopes and meteorological parameters"*, Journal of Hydrolog, v. 591, 125601, doi :https://doi.org/10.1016/j.jhydrol.2020.125601.

154. Patel, A., N. Rastogi, U. Gandhi and N. Khatri, 2021, *"Oxidative Potential of Atmospheric PM10 at Five Different Sites of Ahmedabad, a Big City in Western India"*, Environmental Pollution, v. 268, 115909, doi :https://doi.org/10.1016/j.envpol.2020.115909.

155. Patra A., A.D. Shukla, S. Kumar and B.P. Singh, 2021, *"Signatures of hyperthermal events in the Late Paleocene-Early Eocene limestone succession of the Jaisalmer basin, India"*, Carbonates and Evaporites, v. 36, p., doi :https://doi.org/10.1007/s13146-020-00666-6.

156. Puthussery, J., A. Singh, P. Rai, V.K. Bhattu, P. Vats, M. Furger, N. Rastogi, J. Slowik, D. Ganguly, A.S.H. Prévôt, S.N. Tripathi and V. Verma, 2020, *"Real-Time Measurements of $PM_{2.5}$ Oxidative Potential using Dithiothreitol (DTT) Assay in Delhi, India"*, Environmental Science and Technology Letters, v. 7, p. 504-510, doi :https://doi.org/10.1021/acs.estlett.0c00342.

157. Rahman, A., S. Sarkar and S. Kumar, 2020, *"Paleoenvironment of the central Himalaya during mid to late MIS 3 using stable isotopic composition of lacustine organic matter occluded in diatoms and sediments"*, Quaternary International, v. 558, pp. 1-9, doi :https://doi.or/10.1016/j.quaint.2020.08.024.

158. Rai, P, M. Furger, I. El Haddad, V. Kumar, S. Visser, L. Wang, A. Singh, K. Dixit, D. Bhattu, J.E. Petit, D. Ganguly, N. Rastogi , U. Baltensperger, S.N. Tripathi, J.G. Slowik and A.S.H. Prévôt, 2020, *"Real-time measurement and source apportionment of elements in Delhi's atmosphere"*, Science of the Total Environment, v. 742, 140332, doi :https://doi.org/10.1016/j.scitotenv.2020.140332.

159. Rai, P., J.G. Slowik, M. Furger, I. El. Haddad, S. Visser, Y. Tong, A. Singh, G. Wehrle, V. Kumar, A.K. Tobler, D. Bhattu, L. Wang, D. Ganguly, N. Rastogi, R. Huang, J. Necki, J. Cao, S.N. Tripathi, U. Baltensperger, and A.S.H. Prévôt, 2021, *"Highly time-resolved measurements of element concentrations in PM_{10} and $PM_{2.5}$: Comparison of Delhi, Beijing, London, and Krakow"*, Atmospheric Chemistry and Physics, v. 21, p. 717-730, doi :https://acp.copernicus.org/articles/21/717/2021.

160. Raj, H., R. Bhushan, M. Muruganantham and R. Nambiar, 2020, *"Marine Reservoir Age correction fir the Andaman Basin"*, Radiocarbon, v. 62, p. 1339-1347, doi :https://doi.org/10.1017/RDC.2020.91.

161. Rastogi, N., R. Agnihotri, R. Sawlani, A. Patel, S. Suresh Babu and R. Satish, 2020, *"Chemical and isotopic and characteristics of PM_{10} over the Bay of Bengal: Effects of continental outflow on a marine environment"*, Science of the Total Environment, v. 726, 138438, doi :https://doi.org/10.1016/j.scitotenv.2020.138438.

162. Ray, D., A.D. Shukla, S. Bhattacharya, S. Gupta, P. Jha, A. Patra and U. Chandra, 2021, *"Hematite concretions from the Late Jurassic Jhuran sandstone, Kutch, western India: implications for sedimentary diagenesis and origin of "blueberries" on Mars"*, Planetary & Space Sciences, v. 197, 105163, doi :https://doi.org/10.1016/j.pss.2021.105163.

163. Rixen, T., G. Cowie, B. Gaye, J. Goes, H.R. Gomes, R.R Hood, Z. Lachkar, H. Schmidt, J. Segschneider and A. Singh, 2020, *"Reviews and syntheses: Present, past, and future of the oxygen minimum zone in the northern Indian Ocean"*, Biogeosciences, v. 17, p. 6051-6080, doi :https://doi.org/10.5194/bg-17-6051-2020.

164. Sahoo D., H. Saxena, N. Tripathi, M. Atif Khan, A. Rahman, S. Kumar, A.K. Sudheer and A. Singh, 2020, *"Non-Redfieldian C: N: P ratio in the inorganic and organic pools of the Bay of Bengal during the summer monsoon"*, Marine Ecology Progress Series, v. 653, p. 41-55, doi :https://doi.org/10.3354/meps13498.

165. Satish, R., N. Rastogi, A. Singh and D. Singh, 2020, *"Change in Characteristics of Water-soluble and Water-Insoluble Brown Carbon Aerosol during a Large-Scale Biomass Burning"*, Environmental Science and Pollution Research, v. 27, p. 33339-33350, doi :https://doi.org/10.1007/s11356-020-09388-7.

166. Saxena H., D. Sahoo, M.A. Khan, S. Kumar, A.K. Sudheer and A. Singh, 2020, *"Dinitrogen fixation rates in the Bay of Bengal during summer monsoon"*, Environment Research Communications, v. 2, 051007, doi :https://doi.org//10.1088/2515-7620/ab89fa.

167. Sebastian, S., R. Bhutani, S. Balakrishnan, J.K. Tomson and A.D. Shukla, 2021, *"Geochemical and isotopic studies of potassic granite from the western Dharwar craton, southern India: Implications for crustal reworking in the Neoarchean"*, Geological Journal, v. 56, p. 2930-2949, doi :https://doi.org/10.1002/gj.4085.

168. Shah, C., U. Banerji, K.R. Chandana and R. Bhushan, 2020, *"^{210}Pb dating of recent sediments from the continental shelf of western India: factors influencing sedimentation rates"*, Environmental Monitoring and Assessment, v. 192, p. 468, doi :https://doi.org/10.1007/s10661-020-08415.

169. Sharma, N. and Kumar S.,, 2021, *"Nitrogen transformation rates in the Himalayan Soils at different temperature and elevation conditions"*, Journal of Soils and Sediments, v. 21, p. 13-26, doi :https://doi.org/10.1007/s11368-020-02722-z.

170. Sharma, N. and Kumar, S, 2020, *"Gross rates of nitrogen transformation in soils of a global biodiversity hotspot (Western Ghats, India)"*, Journal of Plant Nutrition and Soil Science, v. 183, p. 579-591, doi :https://doi.org/10.1002/jpln.201900126.

171. Sharma, N. and Kumar, S, 2020, *"Effects of forest type alteration on gross nitrogen mineralization in soils of Southern India"*, Journal of Forestry Research, v. 120, 1007-662X, doi :https://doi.org/10.1007/s11676-020-01225-4.

172. Sharma, S., G. Chauhan, A.D. Shukla, R. Nambiar, R. Bhushan, B.G. Desai, S. Pandey, M. Dhabi, S. Bhandari, S. Bhonsle, A. Lakhote and N. Juyal, 2020, *"Causes and implication of mid to late Holocene relative sea-level change in the Gulf of Kachchh, western India"*, Quaternary Research, v. 100, p. 98-121, doi :https://doi.org/10.1017/qua.2020.86.

173. Sheikh Nawaz A., A. Sharma, S. Agrawal, M.G. Yadava, R.A. Jani, J. Dubey and P. Morthekai, 2020, *"Oxygen and deuterium isotope characteristics of Teesta river catchment from Sikkim Himalaya, India: Implications of different moisture sources"*, Geochemical Journal, v. 54, p. 327-336, doi :https://doi.org/10.2343/geochemj.2.0604.

174. Sheikh Nawaz A., S. Agrawal, A. Sharma, B. Phartiyal, P. Morthekai, P. Govil, R. Bhushan, S. Farooqui, P.S. Jena and A. Shivam, 2020, *"Holocene hydroclimatic variability in the Zanskar Valley, Northwestern Himalaya, India"*, Quaternary Research, v. 97, pp. 1-17, doi :https://doi.org/10.1017/qua.2020.

175. Singh, A., N. Rastogi, V. Kumar, J. Slowik, R. Satish, V. Lalchandani, N. Thamban, P. Rai, D. Bhattu, P. Vats, D. Ganguly, S.N. Tripathi and A.S.H. Prévôt, 2021, *"Sources and characteristics of light-absorbing fine particulates over Delhi through the synergy of real-time optical and chemical measurements"*, Atmospheric Environment, v. 252, 118338, doi :https://doi.org/10.1016/j.atmosenv.2021.118338.

176. Wang, L., J.G. Slowik, N. Tripathi, D. Bhattu, P. Rai, V. Kumar, P. Vats, R. Satish, U. Baltensperger, D. Ganguly, N. Rastogi, L.K. Sahu, S.N.Tripathi and A.S.H. Prévôt, 2020, *"Source characterization of volatile organic compounds measured by PTR-ToF-MS in Delhi, India"*, Atmospheric Chemistry and Physics, v. 20, p. 9753-9770, doi :https://doi.org/10.5194/acp-20-9753-2020.

Theoretical Physics

177. Abdallah, W., A. Kumar, and A.K. Saha, 2020, *"Soft leptogenesis in the NMSSM with a singlet right-handed neutrino superfield"*, Journal of High Energy Physics, 2104, 065, doi :https://doi.org/10.1007/JHEP04(2020)065.

178. Arya, R., 2020, *"Formation of Primordial Black Holes from Warm Inflation"*, JCAP, 09, 042, doi :https://doi.org/10.1088/1475-7516/2020/09/042.

179. Arya, R., and R. Rangarajan, 2020, *"Study of warm inflationary models and their parameter estimation from CMB"*, Int. J. Mod. Phys. D, 29, 2050055, doi :https://doi.org/10.1142/S0218271820500558.

180. Bai R, D Gaur, H Sable, S Bandyopadhyay, K Suthar, D Angom, 2020, *"Segregated quantum phases of dipolar bosonic mixtures in two-dimensional optical lattices"*, Physical Review A, 102, 043309, doi :https://doi.org/10.1103/PhysRevA.102.043309.

181. Banerjee, S., R. S. Gupta, J. Y. Reiness, S. Seth, M. Spannowsky, 2020, *"Towards the ultimate differential SMEFT analysis"*, Journal of High Energy Physics, 2009, 170, doi :https://doi.org/10.1007/JHEP09(2020)170.

182. Bansal, A. and N. Mahajan, 2021, *"Phenomenology of $\tau^- \to \pi^- \nu_\tau \gamma$ using light cone sum rules"*, Phys. Rev. D, 103, 056017, doi :https://doi.org/10.1103/PhysRevD.103.056017.

183. Bera, S., Haldar, S.K., Chakrabarti, B., Trombettoni, A., and Kota, V.K.B., 2020, *"Relaxation of Shannon entropy for trapped interacting bosons with dipolar interactions"*, Eur. Phys. J. D, 74, 73/1-10, doi :https://doi.org/10.1140/epjd/e2020-100358-5.

184. Bhardwaj, A., A. Das, P. Konar, T. Mandal, and A. Thalapillil, 2020, *"Looking for Minimal Inverse Seesaw scenarios at the LHC with Jet Substructure Techniques"*, J. Phys. G, 47, 075002, doi :https://doi.org/10.1088/1361-6471/ab7769.

185. Bhardwaj, A., J. Dutta, P. Konar, B. Mukhopadhyaya, S.K. Rai, 2020, *"Boosted jet techniques for a supersymmetric scenario with gravitino LSP"*, Journal of High Energy Physics, 2010, 083, doi :https://doi.org/10.1007/JHEP10(2020)083.

186. Bhattacharya S., S. Mohanty and P. Parashari, 2021, *"Implications of the NANOGrav result on primordial gravitational waves in nonstandard cosmologies"*, Phys. Rev. D, 103, 063532, doi :https://doi.org/10.1103/PhysRevD.103.063532.

187. Bhattacharya S., S. Mohanty and P. Parashari, 2020, *"Primordial black holes and gravitational waves in nonstandard cosmologies"*, Phys. Rev. D, 102, 043522, doi :https://doi.org/10.1103/PhysRevD.102.043522.

188. Bhattacharya, S., P. Ghosh, A.K. Saha, and A. Sil, 2020, *"Two component dark matter with inert Higgs doublet: neutrino mass, high scale validity and collider searches"*, Journal of High Energy Physics, 2103, 090, doi :https://doi.org/10.1007/JHEP03(2020)090.

189. Borah, D., S.J. Das, and A.K. Saha, 2021, *"Cosmic inflation in minimal* $\mathrm{U}(1)_{\mathrm{B?L}}$ *model: implications for (non) thermal dark matter and leptogenesis"*, European Physical Journal C, 81, 169, doi :https://doi.org/10.1140/epjc/s10052-021-08944-w.

190. Budge, L., J. M. Campbell, G. D. Laurentis, R. K. Ellis, S. Seth, 2020, *"The one-loop amplitudes for Higgs + 4 partons with full mass effects"*, Journal of High Energy Physics, 2005, 079, doi :https://doi.org/10.1007/JHEP05(2020)079.

191. Das,A., H. Mishra and R. K. Mohapatra, 2020, *"Magneto-Seebeck coefficient and Nernst coefficient of a hot and dense hadron gas"*, Phys. Rev. D, 102, 014030, doi :https://doi.org/10.1103/PhysRevD.102.014030.

192. Deepthi, K.N. Goswami, S , Vishnudath, K. N. and Poddar, T.K., 2020, *"Implications of the dark large mixing angle solution and a fourth sterile neutrino for neutrinoless double beta decay"*, Phys. Rev. D, 102, 015020, doi :https://doi.org/10.1103/PhysRevD.102.015020.

193. Goswami, Srubabati and Vishnudath, K.N., 2021, *"Low energy constraints from absolute neutrino mass observables and lepton flavor violation in left-right symmetric model"*, Phys. Rev. D, 103, pp. (1- 15), doi :https://doi.org/10.1103/PhysRevD.103.055016.

194. Joshipura, A. S., S. Mohanty and K. M. Patel, 2021, *"Inflation and long-range force from a clockwork* D *term"*, Phys. Rev. D, 103, 035008, doi :https://doi.org/10.1103/PhysRevD.103.035008.

195. Konar, P., A. Mukherjee, A.K. Saha, and S. Show, 2020, *"Linking the pseudo-Dirac dark matter and radiative neutrino mass in a singlet doublet scenario"*, Phys. Rev. D, 102, 015024, doi :https://doi.org/10.1103/PhysRevD.102.015024.

196. Konar, P., A. Mukherjee, A.K. Saha, and S. Show, 2021, *"A dark clue to seesaw and leptogenesis in singlet doublet scenario with (non)standard cosmology"*, Journal of High Energy Physics, 2103, 044, doi :https://doi.org/10.1007/JHEP03(2021)044.

197. Kota, V.K.B., and Jain, A.K., 2020, *"Role of Symmetries in Nuclear Physics"*, Eur. Phys. J. Special Topics, 229, 2349-2352, doi :https://doi.org/10.1140/epjst/e2020-000209-2.

198. Krishnan, R, Mukherjee, Ananaya and Goswami, Srubabati, 2020, *"Realization of the minimal extended seesaw mechanism and the TM$_2$ type neutrino mixing"*, Journal of High Energy Physics, 09, pp (1-21), doi :https://doi.org/10.1007/JHEP09(2020)050.

199. Kumar R, S Chattopadhyay, D Angom, BK Mani, 2021, *"Fock-space relativistic coupled-cluster calculation of a hyperfine-induced* $^1\mathrm{S}_0 \rightarrow {}^3\mathrm{P}_0^o$ *clock transition in* $\mathrm{A}l^+$*"*, Physical Review A, 103, 022801, doi :https://doi.org/10.1103/PhysRevA.103.022801.

200. Kumari, K., R. Sharma and N. Singh, 2020, *"A theory of resistivity in Kondo lattice materials: memory function approach"*, Journal of Physics: Condensed Matter, 32, 425603, doi :https://doi.org/10.1088/1361-648X/aba382.

201. Malakar M, S Ray, Subhasis Sinha, D Angom, 2020, *"Phases and collective modes of bosons in a triangular lattice at finite temperature: A cluster mean field study"*, Physical Review B, 102, 184515, doi :https://doi.org/10.1103/PhysRevB.102.184515.

202. Mazumdar A., S. Mohanty and P. Parashari, 2020, *"Inflation models in the light of self-interacting sterile neutrinos"*, Phys. Rev. D, 101, 083521, doi :https://doi.org/10.1103/PhysRevD.101.083521.

203. Mishra, A. K., 2020, *"Lightening the Dark Matter from its Viscosity and Explanation of EDGES Anomaly"*, JCAP, 05, 034, doi :https://doi.org/10.1088/1475-7516/2020/05/034.

204. Mishra, D. and N. Mahajan, 2021, *"Impact of soft photons on* $\mathrm{B} \rightarrow \mathrm{K}\ell^+\ell^-$*"*, Phys. Rev. D, 103, 056022, doi :https://doi.org/10.1103/PhysRevD.103.056022.

205. Mukherjee K, S Bandyopadhyay, D Angom, A Martin, S Majumder, 2021, *"Dynamics of the Creation of a Rotating Bose-Einstein Condensation by Two Photon Raman Transition Using a Laguerre-Gaussian Laser Pulse"*, Atoms, 9, 14, doi :https://doi.org/10.3390/atoms9010014.

206. Mummidi, V. S., and K. M. Patel, 2020, *"Precision unification and Higgsino dark matter in GUT scale supersymmetry"*, Phys. Rev. D, 101, 115008, doi :https://doi.org/10.1103/PhysRevD.101.115008.

207. Ng, V., A. Bhardwaj, P. Konar, and A. Nayak, 2020, *"Invisible Higgs search through Vector Boson Fusion: A deep learning approach"*, Eur. Phys. J. C, 80, 1055, doi :https://doi.org/10.1140/epjc/s10052-020-08629-w.

208. Pal,S., Guruprasad Kadam, Hiranmaya Mishra, Abhijit Bhattacharyya, 2021, *"Effects of hadronic repulsive interactions on the fluctuations of conserved charges"*, Physical Review D, 103, 054016, doi :https://doi.org/10.1103/PhysRevD.103.054015.

209. Patra, N.K., T. Malik, D. Sen, T. K. Jha and H. Mishra, 2020, *"An Equation of State for Magnetized Neutron Star Matter and Tidal Deformation in Neutron Star Mergers"*, Astrophys. J. 900, 1, 49, doi :https://doi.org/10.3847/1538-4357/aba8fc.

210. Poddar T.K. and S. Mohanty, 2020, *"Probing the angle of birefringence due to long range axion hair from pulsars"*, Phys. Rev. D, 102, 083029, doi :https://doi.org/10.1103/PhysRevD.102.083029.

211. Poddar T.K., S. Mohanty and S. Jana, 2020, *"Constraints on ultralight axions from compact binary systems"*, Phys. Rev. D, 101, 083007, doi :https://doi.org/10.1103/PhysRevD.101.083007.

212. Rao, K., S. Rindani, P. Sarmah, 2021, *"Study of anomalous gauge-Higgs couplings using Z boson polarization at LHC"*, Nuclear Physics B, 964, 115317, doi :https://doi.org/10.1016/j.nuclphysb.2021.115317.

213. Roy A, S Pal, S Gautam, D Angom, P Muruganandam, 2020, *"FACt: FORTRAN toolbox for calculating fluctuations in atomic condensates"*, Computer Physics Communications, 256, 107288, doi :https://doi.org/10.1016/j.cpc.2020.107288.

214. Sahu, R., Kota, V.K.B. and Kosmas, T.S., 2021, *"Event Rates for the Scattering of Weakly Interacting Massive Particles from ^{23}Na and ^{40}Ar"*, Particles (MDPI), 4, 75-92, doi :https://doi.org/10.3390/particles4010010.

215. Sahu, R., Kota, V.K.B., and Srivastava, P.C., 2020, *"Quadrupole properties of the eight* $\mathrm{SU}(3)$ *algebras in* $(sdgi)$ *space"*, Eur. Phys. J. Special Topics, 229, 2389-2403, doi :https://doi.org/10.1140/epjst/e2020-000088-4.

216. Sahu, R., Papoulias, D.K., Kota, V.K.B. and Kosmas, T.S., 2020, *"Elastic and inelastic scattering of neutrinos and weakly interacting massive particles on nuclei"*, Phys. Rev. C, 102, 035501/1-21, doi :https://doi.org/10.1103/PhysRevC.102.035501.

217. Shaw, A., 2021, *"The impact of nonminimal Universal Extra Dimensional model on* $\Delta \mathrm{B} = 2$ *transitions"*, Eur. Phys. J. C, 81, 137, doi :https://doi.org/10.1140/epjc/s10052-021-08937-9.

218. Singh, N, 2021, *"Leading theories of the cuprate superconductivity: A critique"*, Physica C: Superconductivity and its Applications, 580, 1353782, doi :https://doi.org/10.1016/j.physc.2020.1353782.

219. Singh,B., S. Mazumder and H. Mishra, 2020, *"HQ Collisional energy loss in a magnetized medium"*, Journal of High Energy Physics, 2005, 068, doi :https://doi.org/10.1007/JHEP05(2020)068.

220. Suthar K, H Sable, R Bai, S Bandyopadhyay, S Pal, D Angom, 2020, *"Supersolid phase of the extended Bose-Hubbard model with an artificial gauge field"*, Physical Review A, 102, 013320, doi :https://doi.org/10.1103/PhysRevA.102.013320.

221. Suthar K, R Kraus, H Sable, D Angom, G Morigi, J Zakrzewski, 2020, *"Staggered superfluid phases of dipolar bosons in two-dimensional square lattices"*, Physical Review B, 102, 214503, doi :https://doi.org/10.1103/PhysRevB.102.214503.

222. Swami, H., K. Lochan and K. M. Patel, 2020, *"Signature of neutrino mass hierarchy in gravitational lensing"*, Phys. Rev. D, 102, 024043, doi :https://doi.org/10.1103/PhysRevD.102.024043.

223. Vyas, Manan and Kota, V.K.B., 2020, *"Bivariate q -normal distribution for transition matrix elements in quantum many-body systems"*, J. Stat. Mech.: Theory and Experiment, 2020, 093101/1-17, doi :https://doi.org/iopscience.iop.org/article/10.1088/1742-5468/ababfc.

Atomic, Molecular and Optical Physics

224. A. Anwar, N. Lal, S. Prabhakar and R.P. Singh, 2020, *"Selective tuning of Hilbert spaces in states encoded with spatial modes of light"*, New Journal of Physics, v. 22, p. 113020, doi :https://doi.org/10.1088/1367-2630/abc783.

225. A. Bekshaev, L. Mikhaylovskaya, S. Patil, V. Kumar and R.P. Singh, 2020, *"Optical-vortex diagnostics via Fraunhofer slit diffraction with controllable wavefront curvature"*, Journal of Optical Society of America A, v. 37, p. 780, doi :https://doi.org/10.1364/JOSAA.388926.

226. A. Kastberg, B. K. Sahoo, T. Aoki, Y. Sakemi and B. P. Das, 2020, *"Analysis of an optical lattice methodology for detection of atomic parity nonconservation"*, Symmetry, v. 12, p. 974, doi :https://doi.org/10.3390/sym12060974.

227. A. Koszors, W. G. Jiang, X. F. Yang, S. W. Bai, J. Billowes, C. L. Binnersley, T. E. Cocolios, M. L. Bissell, B. S. Cooper, R. P. de Groote, A. Ekstrm, K. T. Flanagan, C. Forssn , S. Franchoo, R. F. Garcia Ruiz, F. P. Gustafsson, G. Hagen, G. R. Jansen, A. Kanellakopoulos, M. Kortelainen, W. Nazarewicz, G. Neyens, S. Novario, T. Papenbrock, P.-G. Reinhard, B. K. Sahoo, C. Ricketts, A R. Vernon, S. G. Wilkins and H. Z. Yu, 2021, *"Charge radii of exotic potassium isotopes challenge nuclear theory and the magic character of* $\mathrm{N} = 32$*"*, Nature Physics, v. 17, p. 439-443, doi :https://doi.org/10.1038/s41567-020-01136-5.

228. A. Kumar, A. Taneja, T. Mohanty and R.P. Singh, 2021, *"Effect of laser beam propagation through the plasmonic nanoparticles suspension"*, Results in Optics, v. 3, p. 100081, doi :https://doi.org/10.1016/j.rio.2021.100081.

229. A. R. Vernon, C. M. Ricketts, J. Billowes, T. E. Cocolios, B. S. Cooper, K. T. Flanagan, R. F. Garcia Ruiz, F. P. Gustafsson,G. Neyens, H. A. Perrett, B. K. Sahoo, Q. Wang, F. J. Waso, and X. F. Yang, 2020, *"Laser spectroscopy of indium Rydberg atom bunches by electric field ionization"*, Scientific Reports, v. 10, p. 12306, doi :https://doi.org/10.1038/s41598-020-68218-5.

230. A. Srinivasa Rao, Deepika Yadav and G. K. Samanta, 2021, *"Nonlinear frequency conversion of 3D optical bottle beams generated using a single axicon"*, Optics Letters, v. 46, p. 657-660, doi :https://doi.org/10.1364/OL.413899.

231. A.K. Singhvi, 2020, *"Future Geosciences"*, Journal of the Geological Society of India, v. 96, p. 533-538, doi :https://doi.org/10.1007/s12594-020-1600-3.

232. B. Borgohain,G. Mathew,N.Chauhan,V. Jain and A.K. Singhvi, 2020, *"Evidence of episodically accelerated denudation on the Namche Barwa massif (Eastern Himalayan syntaxis) by megafloods"*, Quaternary Science Reviews, v. 245, p. 106410, doi :https://doi.org/10.1016/j.quascirev.2020.106410.

233. B. K. Sahoo, 2021, *"Investigating properties of Cl^- and Au^- ions using relativistic many-body methods"*, Journal of Physics B: Atomic, Molecular and Optical Physics, –, –, doi :https://doi.org/10.1088/1361-6455/abd91b.

234. B. K. Sahoo, 2020, *"Determination of dipole polarizabilities of the alkali-metal negative ions"*, Physical Review A, v. 102, p. 022820, doi :https://doi.org/10.1103/PhysRevA.102.022820.

235. Deepika Yadav, Anirban Ghosh, Ravi K. Saripalli, and G. K. Samanta, 2020, *"Watt-level, ultrafast, tunable yellow source based on single-pass, fourth-harmonic generation of Cr^{2+}:ZnS laser at 2360 nm"*, Optics Letters, v. 45, p. 5109-5112, doi :https://doi.org/10.1364/OL.404358.

236. Duo Pan, B. Arora, Y. -M. Yu, B. K. Sahoo, and J. Chen, 2020, *"Optical-lattice based Cs active clock with continual superradiant lasing signal"*, Rapid Communication, v. 102, p. 041101, doi :https://doi.org/10.1103/PhysRevA.102.041101.

237. E. Shivakarthik, J.K. Meka, Harish ,V.S. Surendra, K.K. Rahul, R. Thombre, H. Hill, S. Vijayan and B. Sivaraman, 2020, *"Sticking dust and micrometeorite particles on to ices at high impact velocities - Implications for astrochemical ice enrichment"*, Planetary and Space Science, v. 190, p. 104972, doi :https://doi.org/10.1016/j.pss.2020.104972.

238. H. M. Rajapara,V.Kumar,N. Chauhan,P. N. Gajjar and A. K. Singhvi, 2020, *"Bleaching of blue light stimulated luminescence of quartz by moonlight"*, Journal of Earth System Science, v. 129, p. 212, doi :https://doi.org/10.1007/s12040-020-01474-1.

239. M. Elowitz, B. Sivaraman, A Hendrix, J –I Lo, S –L Chou, B –M Cheng, B N Raja Sekhar and N J Mason, 2021, *"Possible detection of hydrazine on Saturn's moon Rhea"*, Science Advances, v. 7, –, doi :https://doi.org/10.1126/sciadv.aba5749.

240. M. Kaur, D. F. Dar, B. K. Sahoo and B. Arora, 2021, *"Radiative Transition Properties of Singly Charged Magnesium,Calcium, Strontium and Barium ions"*, Atomic Data and Nuclear Data Tables, v. 137, p. 101381, doi :https://doi.org/10.1016/j.adt.2020.101381.

241. N. Shitara, N. Yamanaka, B. K. Sahoo, T. Watanabe and B. P. Das, 2021, *"CP violating effects in ^{210}Fr and prospects for new physics beyond the Standard Model"*, Journal of High Energy Physics, v. 2021, p. 124, doi :https://doi.org/10.1007/JHEP02(2021)124.

242. Oman. G. Kocurek, R. Westerman, C. Hern, D. Tatum, H. M. Rajapara, A.K. Singhvi, 2020, *"Aeolian dune accommodation space for Holocene Wadi Channel avulsion strata, Wahiba dune field"*, Sedimentary Geology, v. 399, p. 105612, doi :https://doi.org/10.1016/j.sedgeo.2020.105612.

243. P. Kumar, S. Soumyashree,, N. R. Epuru, S. B. Banerjee, R.P. Singh and K.P. Subramanian, 2020, *"Determination of Stark Shifts and Widths Using Time Resolved Laser-Induced Breakdown Spectroscopy (LIBS) Measurements"*, Applied Spectroscopy, v. 74, p. 913, doi :https://doi.org/10.1177/0003702819891172.

244. R. Das, D. K. Pandey, V. Nimma, P. Madhusudhan, P. Bhardwaj, P. Chandravanshi, Muhammed Shameem KM, D. K. Singh and R. K. Kushawaha, 2021, *"Strong-field ionization of polyatomic molecules: ultrafast H atom migration and bond formation in the photodissociation of CH_3OH"*, Faraday Discussions, 228, 432-450, doi :https://doi.org/10.1039/D0FD00129E.

245. R. J. Wasson, A. Ziegler, H.S. Lim, E. Teo, D. Lam, D. Higgitt, T. Rittenour, K. N. B. M. Ramdzan, C. C. Joon, A. K. Singhvi, 2021, *"Episodically volatile high energy non-cohesive river-floodplain systems: New information from the Ping River, Thailand, and a global review"*, Geomorphology, v. 382, p. 107658, doi :https://doi.org/10.1016/j.geomorph.2021.107658.

246. R. Mitra, V. S. Prasannaa, B. K. Sahoo, N. Hutzler, M. Abe and B. P. Das, 2021, *"Study of HgOH to Assess its Suitability for Electron Electric Dipole Moment Searches"*, ATOMS, v. 9, –, doi :https://doi.org/10.3390/atoms9010007.

247. R.H.Biswas,F. Herman,G. E. King,B. Lehmann and A.K.Singhvi, 2020, *"Surface paleothermometry using low-temperature thermoluminescence of feldspar"*, Climate of the Past, v. 16, p. 2075-2093, doi :https://doi.org/10.5194/cp-16-2075-2020.

248. S. Chakraborty, J. Gowrishankar, A. Joshi, P. Kannan, R. K. Kohli, S. C. Lakhotia, G. Misra C. M. Nautiyal, K. Ramasubramanian, N. Sathyamurthy and A. K. Singhvi, 2020, *"Suggestions for a National Framework for Publication of and Access to Literature in Science and Technology in India"*, Current Science, v. 118, p. 1026-1034, doi :https://doi.org/10.18520/cs/v118/i7/1026-1034.

249. S. Dutt, S. Singh, A. Mahajan, B. Arora and B. K. Sahoo, 2020, *"van der Waals coefficients of the multi-layered MoS_2 with alkali metals"*, Physica Scripta, v. 95, p. 095506, doi :https://doi.org/10.1088/1402-4896/abae20.

250. S. Kumari, V. Kumar, S.G. Reddy and R.P. Singh, 2020, *"Tunable ultraslow light propagation in ruby"*, Optics Communications, v. 473, p. 125913, doi :https://doi.org/10.1016/j.optcom.2020.125913.

251. S. Singh, Jyoti, B. Arora, B. K. Sahoo, and Y.-M. Yu, 2020, *"Magic wavelengths for optical-lattice based Cs and Rb active clocks"*, ATOMS, v. 8, p. 79, doi :https://doi.org/10.3390/atoms8040079.

252. V. S. Prasannaa, B. K. Sahoo, M. Abe and B. P. Das, 2020, *"Significance of Non-Linear Terms in the Relativistic Coupled-Cluster Theory in the Determination of Molecular Properties"*, Symmetry, v. 12, p. 811, doi :https://doi.org/10.3390/sym12050811.

253. V. S. Prasannaa, R. Mitra and B. K. Sahoo, 2020, *"Reappraisal of P, T-odd parameters from the improved calculation of electric dipole moment of ^{225}Ra atom"*, Journal of Physics B: Atomic, Molecular and Optical Physics, v. 53, p. 195004, doi :https://doi.org/10.1088/1361-6455/aba6aa.

254. V. S. Surendra, V. Jayaram,J.K. Meka, S. Vijayan,V. Chandrasekaran, R. Thombre, Thiruvenkatam,A. Mallya, B. N. Raja Sekhar, M .Muruganantham,A. Datey,H. Hill, A. Bhardwaj, G. Jagadeesh, K. P. J. Reddy, N. J. Mason and B. Sivaraman, 2020, *"Shock processing of amino acids leading to complex structures - Implications to the Origin of Life"*, Molecules, v. 25, p. 5634, doi :https://doi.org/10.3390/molecules25235634.

255. Varun Sharma, S. Chaitanya Kumar, G. K. Samanta and M. Ebrahim-Zadeh, 2020, *"Multi-structured-beam optical parametric oscillator"*, Optics Express, v. 28, p. 21650-21658, doi :https://doi.org/10.1364/OE.398011.

256. X. T. Guo, Y. -M. Yu, Y. Liu, B. B. Suo, and B. K. Sahoo, 2021, *"Electric dipole and quadrupole properties of Cd atom for atomic clock applications"*, Physical Review A, v. 103, p. 013109, doi :https://doi.org/10.1103/PhysRevA.103.013109.

257. Y. -M. Yu, B. K. Sahoo, and B. B. Suo, 2020, *"Ground state g_j factors of the Cd^+, Yb^+ and Hg^+ ions"*, Physical Review A, v. 102, p. 062824, doi :https://doi.org/10.1103/PhysRevA.102.062824.

Publications in Proceedings of Conference/ Symposia/ Workshops

Solar Physics

1. Maurya, R. A. and Ambastha, A., 2021, *"Inversion of solar sub-surface flows using high-degree acoustic modes"*, AIP Conference proceedings, v. 2336, 020001, 10 pp.
2. Upadhyay, K., Joshi, B., Mitra, P. M., Bhattacharyya, R., Oberoi, D., and Monstein, C., 2020, *"Solar radio observation using CALLISTO at the USO/PRL, Udaipur"*, 2019 IEEE MTT-S International Microwave and RF Conference (IMARC), p. 1-6.

Planetary Sciences

3. Bhatt M., Wöhler C., Aravind K., Ganesh S. and Bhardwaj A., 2021, *"Regolith characteristics of the Reiner Gamma swirl as revealed by polarimetric observations"*, 52^{nd} Lunar and Planetary Science Conference, The Woodlands, Texas, Abstract No. 2430.
4. Bhattacharya, A., J. P. Pabari and S. Jitarwal, 2021, *"Schumann resonance in Venus: Dependence on volcanism and tracer for lightning activity"*, 52^{nd} Lunar and Planetary Science Conference, The Woodlands, Texas, Abstract No. 1398.
5. Bhattacharya, A., S. Jitarwal, J. P. Pabari and V. Sheel, 2021, *"Proposed model for estimation of atmospheric dust and cloud mass loading on Mars"*, 52^{nd} Lunar and Planetary Science Conference, The Woodlands, Texas, Abstract No. 1547.
6. Bhattacharya, A., V. Sheel, J. P. Pabari, T. Imamura and K. McGouldrick, 2020, *"Flow instabilities in Venus clouds explored by Akatsuki radio science experiment"*, 18^{th} VEXAG Meeting 2020, Abstract No. 8008.
7. Dhingra D., Chauhan P., Bhatt M., Kumar A., Thangjam G., Patil A., Bhattacharya S., Chauhan M., Dagar A., 2021, *"Spectral observations from imaging infrared spectrometer (IIRS) onboard Chandrayaan-2 orbiter: radiance data comparisons"*, 52^{nd} Lunar and Planetary Science Conference, The Woodlands, Texas, Abstract No. 2436.
8. Kumar, D. V. R., J. P. Pabari, K. Acharyya, S. Jitarwal, S. Nambiar, Rashmi and T. Upadhyaya, 2021, *"Constraint on Discharge Current Parameters and Streamer Speeds of Venusian Lightning"*, 52^{nd} Lunar and Planetary Science Conference, The Woodlands, Texas, Abstract No. 1768.
9. Kumar, D. V. R., J. Pabari and K. Acharyya, 2020, *"Is GCR induced ionization the prime driving force for Venus Lightning?"*, 18^{th} VEXAG Meeting 2020, Abstract No. 8004.
10. Jaiswal S., R. R. Mahajan and M. Ngangom, 2021, *"Heavy noble gas in eucrites and diogenites: an attempt to understand the trapped components"*, 52^{nd} Lunar and Planetary Science Conference, The Woodlands, Texas, Abstract No. 1183.
11. Jitarwal, S., J. P. Pabari, D. Kumar, G. Dhote, S. Nambiar, Rashmi, T. Upadhyaya, K. Acharyya, V. Sheel and Anil Bhardwaj, 2020, *"Time-frequency localization of electrostatic discharge for lightning study"*, 18^{th} VEXAG Meeting 2020, Abstract No. 8010.
12. Jitarwal, S., T. Upadhyaya, J. P. Pabari, S. Nambiar, D. Kumar, Rashmi and K. Acharyya, 2021, *"Non-foster active impedance matching of short dipole antenna for a lightning instrument"*, 52^{nd} Lunar and Planetary Science Conference, The Woodlands, Texas, Abstract No. 2162.
13. Kumar A., R. R. Mahajan and A. B. Sarbadhikari, 2021, *"Neon isotopic study in ordinary chondrites"*, 52^{nd} Lunar and Planetary Science Conference, The Woodlands, Texas, Abstract No. 1421.
14. Lajaunie L., M. N., Sanghani, W. D. A. Rickard, J. J. Calvino, K. K. Marhas and M.Bizzarro, 2020, *"Combined multi-isotopic and (S)TEM study of pre-solar silicates to probe the solar system's prenatal history"*, European Geophysical Union, Online Meeting, May 2020, Vol.14, EPSC2020-23.
15. Mahajan R. R., S. K. Goyal, N. Upadhyay, A. Auknoor, P. Sharma, J. Kaur, V. Sheel, A. Bhardwaj and SAC team, 2020, *"Mass spectrometric study of planetary atmospheres in future missions: a case study, Venus neutral and ion mass analyzer (VENIMA)"*, 18^{th} VEXAG Meeting 2020, Abstract no. 8026.
16. Mahajan, R. R. and A. B. Sarbadhikari, 2021, *"Nitrogen and noble gases in martian meteorite Tissint"*, 52^{nd} Lunar and Planetary Science Conference, The Woodlands, Texas, Abstract No. 1041.
17. Nambiar, S., J. P. Pabari, Rashmi, S. Jitarwal, K. Acharyya, S. M. K. Praneeth, R. Singh and D. Kumar, 2021, *"Comparative analysis of two and three channel hypervelocity dust detectors"*, 52^{nd} Lunar and Planetary Science Conference, The Woodlands, Texas, Abstract No. 1904.
18. Narendranath S., N. S. Pillai, K. Vadodariya, D. Dhingra, M. Bhatt, G. Thangjam, V. Radhakrishna and V. Tyagi, 2021, *"New insights from Chandrayaan-2 large area soft X-ray spectrometer"*, 52^{nd} Lunar and Planetary Science Conference, The Woodlands, Texas, Abstract No. 2230.
19. Pabari, J. P., Rashmi, K. Acharyya, S. Nambiar, S. Jitarwal, V. Sheel, A. Bhardwaj and D. Kumar, 2021, *"Detachment of Interplanetary Dust Particles from Asteroid Belt"*, 52^{nd} Lunar and Planetary Science Conference, The Woodlands, Texas, Abstract No. 1430.

20. Rani, A., A. B. Sarbadhikari, D. R. Hood, S. Karunatillake and S. Nambiar, 2021, *"Synthesis of chemical provinces on Mars and their geologic interpretations"*, 52^{nd} Lunar and Planetary Science Conference, The Woodlands, Texas, Abstract No. 2353.

21. Srivastava, P., S. Ghosh, A.K. Das, S.K. De, S. Misra and D. Ray, 2021, *"An evaluation of the size of Ramgarh crater, India: Clues from satellite gravity data"*, 52^{nd} Lunar and Planetary Science Conference, The Woodlands, Texas, Abstract No. 1906.

Space and Atmospheric Sciences

22. Chutia, L., Ojha, N.,Girach, I. A., Pathak, B., Sahu, L. K., and Bhuyan, P. K., 2020, *"Distribution of sulfur dioxide over Indian subcontinent: Remote sensing observations and model reanalysis"*, 2020 XXXIIIrd General Assembly and Scientific Symposium of the International Union of Radio Science, 29 August - 5 September, 2020 held in Rome, Italy, pp. 1-4.

Theoretical Physics

23. Poddar T. K. and S. Mohanty, 2020, *"Astronomical Probes of Ultra Light Dark Matter"*, Springer Proceedings in Physics, volume 248, pp 221-227.

24. Poddar T. K., S. Mohanty and S. Jana, 2020, *"Constraints on Ultra Light Dark Matter from Compact Binary Systems"*, Springer Proceedings in Physics, volume 248, pp 317-320.

25. Sarmah, P., K. Rao, S. Rindani, 2020, *"Polarization of Z Boson as a Probe of Anomalous Gauge-Higgs Couplings"*, Springer Proceedings in Physics, Workshop on Frontiers in High Energy Physics 2019, v. 248, pp. 213-217.

Atomic, Molecular and Optical Physics

26. Ghosh, A., D. Yadav, R. K. Saripalli, and G. K. Samanta, 2020, *"High power, tunable, ultrafast yellow laser using cascaded second harmonic generation of mid-IR Cr^{2+}: ZnS laser in MgO: PPLN crystals"*, Nonlinear Frequency Generation and Conversion: Materials and Devices XIX, 11264.

27. Ghosh, A., R. K. Saripalli, K. Subith, N. A. Chaitanya, V. Sharma, I. De Leon, and G. K. Samanta, 2020, *"Generation of non-collinear Poincaré beam through the spin-orbit interaction in Epsilon-Near-Zero film"*, Frontiers in Optics, FM7C. 3.

28. Rao, A. S., and G. K. Samanta, 2020, *"High Peak Power, Non-diffractive and Micro-size Optical Bottles Generation in Bessel Beams"*, Laser Applications Conference, JTh2A. 9.

29. Biswas, A., Banerji, A., Lal, N., Chandravanshi, P., and Singh, R. P., 2020, *"Coincidence detection based quantum key distribution protocol"*, Quantum 2.0, QTu8B. 17.

30. Biswas, A., Lal, N., Banerji, A., and Singh, R. P., 2020, *"Entanglement Duality Assisted Secure Key Distribution"*, Frontiers in Optics, OSA Technical Digest (Optical Society of America, 2020), JTu1A.48.

31. Yadav, D., A. Ghosh, R. K. Saripalli, G. K. Samanta, 2020, *"High-power, femtosecond, coherent yellow source using two-stage second harmonic generation of Cr^{2+}: ZnS laser"*, Nonlinear Optics and its Applications, 11358, 1135823.

32. Subith, K., R. K. Saripalli, A. Ghosh, and G. K. Samanta, 2020, *"Frequency-doubling characteristics of non-collinear Poincaré beams"*, Frontiers in Optics, FM7C. 2.

33. Saripalli, R. K., A. Ghosh, A. C. Nellikka, and G. K. Samanta, 2020, *"Frequency conversion of ultrafast, higher order vector vortex beams"*, Nonlinear Frequency Generation and Conversion: Materials and Devices XIX, 11264.

34. Saripalli, R. K., N. A. Chaitanya, A. Ghosh, V. Sharma, I. De Leon, and G. K. Samanta, 2020, *"Experimental verification of vortex generation through spin-orbit coupling in epsilon-near-zero films"*, CLEO: QELS_Fundamental Science, FM2B. 81.

35. Kumar, V., V. Sharma, S. Singh, and G. K. Samanta, 2020, *"Direct observation of topological charge of single photon using a tilted-lens commonly used for classical vortex beams"*, Laser Science, JTu1A. 27.

Books Edited / Review Articles / Other Publications

Books Edited

1. Yadav, R., Trivedi, P., Sahu, L. K., Beig, G., and Tripathi, N., 2020, *"Air Pollution Modeling"*, Air Pollution and Environmental Health, Part of the Environmental Chemistry for a Sustainable World (ECSW) book series, Springer, Singaporev. 20, p. 37-55, https://doi.org/10.1007/978-981-15-3481-2_3
2. Dave, P. N., Chaturvedi, S. and Sahu, L. K., 2021, *"Impact of polychlorinated biphenyls on environment and public health"*, Handbook of Advanced Approaches Towards Pollution Prevention and Control: Volume 1: Conventional and Innovative Technology, and Assessment Techniques for Pollution Prevention and Controlp. 261-280, https://doi.org/10.1016/B978-0-12-822121-1.00013-8
3. Mohanty, S., 2020, *"Astroparticle Physics and Cosmology"*, Springer: Lecture Notes in Physicsp. 1-287, doi:10.1007/978-3-030-56201-4
4. Kota, V. K. B., 2020, *"*$\mathrm{SU}(3)$ *Symmetry in Atomic Nuclei"*, Springer Nature, Singapore289 pages; ISBN:978-981-15-3602-1
5. Kota, V. K. B., and Jain, A. K. (Editors), 2020, *"Role of Symmetries in Nuclear Physics"*, Eur. Phys. J. Special Topicsvolume 229, number 14-15, p. 2349-2628
6. Das R., Muhammed Shameem K. M.,Nimma V., Soumyashree S., Kumar P. and Kushawaha, R. K., 2021, *"Improving the Signal Strength and Detection Limits of Laser-Induced Breakdown Spectroscopy (Modern Techniques of Spectroscopy: Basics, Instrumentation, and Applications)"*, Springer SingaporeP. 307-320, ISBN - 978-981-33-6084-6
7. Madhusudhan P., Das R., Bharadwaj, P.,Chandravanshi P., Soumyashree S., Nimma V. and Kushawaha R. K., 2021, *"Modern Experimental Techniques in Ultrafast Atomic and Molecular Physics (Book: Modern Techniques of Spectroscopy: Basics, Instrumentation, and Applications)"*, Springer Singaporep. 257- 285, ISBN -978-981-33-6084-6
8. Singhvi, A. K., 2020, *"A life with Men, Women and Molecules by M. Vijayan"*, Indian National Science Academy, Bahadur Shah Zafar Marg, New Delhi330 pp,ISBN - 978-81-939482-6-2
9. Ray, J. S, 2020, *"The Andaman Islands and Adjoining Offshore: Geology, Tectonics and Paleoclimate"*, 36^{th} IGC Commemorative Volume and Society of Earth Scientists Series by Springer ISBN 978-3-030-39842-2
10. Bhattacharya, S., Pande, K., Kumar, A., Kingson, O. and Ray, J. S., 2020, *"Timing of formation and obduction of the Andaman Ophiolite"*, The Andaman Islands and Adjoining Offshore: Geology, Tectonics and Paleoclimatepp. 19-42, doi.org/10.1007/978-3-030-39843-9_2.
11. Awasthi, N., George, B. G. and Ray, J. S., 2020, *"Tracing the sources and depositional pathways for the Oligocene sediments in the Andaman Forearc"*, The Andaman Islands and Adjoining Offshore: Geology, Tectonics and Paleoclimatepp. 93-106, doi.org/10.1007/978-3-030-39843-9_5.

Review Articles

1. Kumari, K., N. Singh, 2020, *"The memory function formalism: an overview"*, Eur. J. Phys., v.v. 41, p. 053001
2. Sahu, L. K., Tripathi, N., and Yadav, R., 2020, *"Observations of trace gases in the earth's lower atmosphere: instrumentation and platform"*, Current Science, v.118(12), 1893
3. Shiokawa, K., Dasso, S., Miteva, R., Pallamraju, D., and S-R. Zhang, 2021, *"Preface of the special issue: Variability of the Sun and Its Terrestrial Impact (VarSITI) Completion Symposium 2019 and the SCOSTEP 14th Quadrennial Solar-Terrestrial Physics Symposium (STP14)"*, J. Atmos. Sol. Terr. Phys., v.v. 215, p. 105593
4. Anand M., Russell S., Lin Y., Wadhwa M., Marhas K. K. and Tachibana S., 2020, *"Role of Sample Return in Addressing Major Questions in Planetary Sciences"*, Space Science Review, Springer, v.v. 216, no. 101
5. Band, S. and Yadava, M. G., 2020, *"Addressing past monsoon variability from speleothems, special section, Paleoclimate studies in India"*, Current Science, v.v. 119, no. 2
6. Patel, A. and Rastogi, N., 2021, *"Oxidative Potential of Ambient PM and Related Health Endpoints over South Asia: A Review"*, Asian Journal of Atmospheric Environment, v.v. 15, p. 40-50.

Bulletin/Digest/magazine Articles

7. Saxena P., Sonwani S., Sharma S., Kumar P., Chandra N., 2020. Carbonaceous aerosol variations in foggy fays: A critical analysis during the fireworks festival. Fresenius Environmental Bulletin Volume 29 – No. 08/2020 pages 6639-6656.
8. Banerji, U.S., R. Bhushan and D. Padmalal, 2020, Hydroclimate variability during the last two millennia and imprints of forcing factors: A study from western India, Ocean Digest, 7(2), 4-10.

Technical Reports

9. Kushwaha, P. K., S. Urmalia, D. Pallamraju, R. P. Singh, and P. Suryawanshi, (2021). Design and Development of Filter Wheel Controller Card, Temperature Controller and Automated Software using Labview for CMAP Instrument authored by PRL Technical Note, 2021. PRL-TN-2021-112.

Papers Presented in National/ International Conferences

International 25

1. A. Bhattacharya, Sheel V., Pabari J. P., Imamura T., McGouldrick K., "Flow instabilities in Venus clouds explored by Akatsuki radio science experiment", 18^{th} VEXAG Meeting 2020, 16-17 Nov, 2020.
2. A. Raja Bayanna, "Chromospheric observations of Solar activity with MAST", workshop 4 of 39^{th} meeting of the Astronomical Society of India meeting, 18 — 23 Feb, 2021.
3. B. Karthikeyan, K. K. Marhas, V. Goyal and D. K. Panda, "Silicon carbide polytype distribution in circumstellar condition: A Raman Spectroscopic study", 2^{nd} Indian Planetary Science Conference, PRL, Ahmedabad, 25-26 Feb, 2021.
4. B. Joshi, "A low intensity, long-duration solar eruptive flare and associated solar radio storm: SDO and PRL-CALLISTO observations", 39^{th} meeting of the Astronomical Society of India, 18 — 23 Feb, 2021.
5. C. P. Pabari, S. Nambiar, J. P. Pabari, K. Acharyya, S. Jitarwal and Rashmi, "Analysis of IDP flux from Galileo Dust Detector", 2^{nd} Indian Planetary Science Conference, PRL, Ahmedabad, 25-26 Feb, 2021.
6. Chandan Kumar, "Development of Langmuir Probe Electronics for LPEX payload for future Mars mission", 2^{nd} Indian Planetary Science Conference, PRL, Ahmedabad, 25-26 Feb, 2021.
7. D. K. Panda and A. D. Shukla, "Alteration of Fe-Ni-S metal phase in Mukundpura meteorite", 2^{nd} Indian Planetary Science Conference, PRL, Ahmedabad, 25-26 Feb, 2021.
8. Dinesh Kumar V. R., J. P. Pabari, K. Acharyya, S. Nambiar, S. Jitarwal, Rashmi, "Current Status of Venus Lightning Research", 2^{nd} Indian Planetary Science Conference, PRL, Ahmedabad, 25-26 Feb, 2021.
9. Duggirala Pallamraju and Subir Mandal, "New insights into the daytime thermospheric wave dynamics over low-latitudes obtained using radio technique: response to the solar flux and seasonal variations", AGU 2020, 01-17 Dec, 2020.
10. Duggirala Pallamraju and Subir Mandal, "Recent results on the low- latitudinal gravity wave behavior obtained through innovative approach using a radio technique", 43^{rd} COSPAR Scientific Assembly, 28 Jan-4 Feb, 2021.
11. Duggirala Pallamraju, Subir Mandal, and Deepak K Karan, "New developments in the understanding of the daytime low-and equatorial-latitudinal electrodynamics and wave dynamics obtained using optical and radio techniques", 43^{rd} COSPAR Scientific Assembly, 28 Jan-4 Feb, 2021.
12. Durga Prasad K., "Monitoring solar spectral irradiance at Mars and Venus by using an EUV instrument onboard future missions", 43^{rd} COSPAR Scientific Assembly, Sydney, Australia, 28 Jan-03 Feb, 2021.
13. Durga Prasad K., "Thermophysical Behaviour of the Moon - Current understanding and future implications", 2^{nd} Indian Planetary Science Conference, PRL, Ahmedabad, 25-26 Feb, 2021.
14. Durga Prasad, K., and Kalyan Reddy, P., "An insight into the Thermophysical Behaviour of Apollo 17 and Chandrayaan-2 Landing Sites on the Moon", 43^{rd} COSPAR Scientific Assembly, Sydney, Australia, 28 Jan-03 Feb, 2021.
15. Durga Prasad, K., Chandan Kumar, Sanjeev Mishra, Kalyan Reddy, P. and Janmejay Kumar, "Design and Evaluation of Langmuir Probe and Electric Field Experiment (LPEX) for Indian Mars Orbiter Mission-2", 43^{rd} COSPAR Scientific Assembly, Sydney, Australia, 28/01/2021- 03/02/2021.
16. D. Ray, "Anatomy of iron meteorite: Understanding core of a differentiated asteroid", 2^{nd} Indian Planetary Science Conference, PRL, Ahmedabad, 25-26 Feb, 2021.
17. F. Joshi and J. P. Pabari, "Mathematical Modelling of Martian Dust Storm", 2^{nd} Indian Planetary Science Conference, PRL, Ahmedabad, 25-26 Feb, 2021.
18. H. Kharayat, "Origin of fast coronal mass ejection and associated M-class flare from transient coronal sigmoid in active region NOAA 11909", 39^{th} meeting of the Astronomical Society of India, 18 — 23 Feb, 2021.
19. H. Kharayat, "Origin, activation and blowout expansion of pre-CME coronal arcade from the active region NOAA 11947", IIA-50 international conference on "Advances in Observations and Modelling of Solar Magnetism and Variability", 1 — 4 March, 2021.
20. H. Kumar, "Magnetic-jerk driven seismic emission in sunspots accompanying major solar flares", IIA-50 international conference on "Advances in Observations and Modelling of Solar Magnetism and Variability", 1 — 4 March, 2021.
21. H. Kumar, "Study of seismic emission in sunspots associated with Lorentz force changes accompanying major solar flares", 39^{th} meeting of the Astronomical Society of India, 18 — 23 Feb, 2021.
22. J. P. Pabari, K. Acharyya, S. Nambiar, S. Jitarwal, Rashmi, S. M. K. Praneeth, B. Shah, J. B. Rami, V. Singh, R. R. Mahajan, R. K. Singh, T. Upadhyaya, V. Sheel, S. A. Haider and Anil Bhardwaj, "Interplanetary dust at Venus and its detection", 43^{rd} COSPAR Scientific Assembly, Sydney, Australia, 28 Jan-03 Feb, 2021.

23. J. P. Pabari, K. Acharyya, V. Sheel, Anil Bhardwaj, S. Nambiar, S. Jitarwal, Rashmi, S. M. K. Praneeth, B. Shah, V. K. Singh, R. Singh, D. Kumar and Team, "Status of IDP flux models and observations in the inner solar system", 2^{nd} Indian Planetary Science Conference, PRL, Ahmedabad, 25-26 Feb, 2021.

24. K. Sharma, Girach, I., Sharma, N., Singh, N., and Ojha, N., "Ozone variations in central Himalayan valleySeasonal changes and impact of biomass-burning", International Conference on Aerosol Air Quality, Climate Change and Impact on Water Resources and Livelihoods in the Greater Himalayas, ARIES, Nainital, 14-16 Sept, 2020.

25. K. Upadhyay, "Observations of solar activities at low radio frequencies by CALLISTO at USO/PRL", 39^{th} meeting of the Astronomical Society of India meeting, 18 $-$ 23 Feb, 2021.

26. M. Bhatt, Wöhler C., Aravind K., Ganesh S., Bhardwaj A., "First results of polarimetric observations of the Reiner Gamma swirl using EMPOL of Mount Abu observatory", 2^{nd} Indian Planetary Science Conference, PRL, Ahmedabad, 25-26 Feb, 2021.

27. M. Hess, Wohlfarth, K., Wöhler, C., Berezhnoy, A. A., Bhatt, M. and Bhardwaj, A., "Space Weathering Trends at the Mare Moscoviense Swirl", European Planetary Science Congress 2020, 21 Sept-09 Oct, 2020.

28. M. N. Sanghani, L. Lajaunie, S.Y. Hsiao, W. D.A. Rickard, J. J.Calvino, V. Goyal, K.K. Marhas and M. Bizzarro, "Combined Isotopic, Microstructural and (S)TEM Investigations of Presolar Silicates", 2^{nd} Indian Planetary Science Conference, PRL, Ahmedabad, 25-26 Feb, 2021.

29. Meghna Soni, Girach, I., and Ojha, N., "Chemistry and dynamics of reactive trace gases over India", International Conference on Aerosol Air Quality, Climate Change and Impact on Water Resources and Livelihoods in the Greater Himalayas, ARIES, Nainital, 14-16 Sept, 2020.

30. N. Panwar, "Hematite detection in lunar high latitudes using Chandrayaan-1 HySI data", 2^{nd} Indian Planetary Science Conference, PRL, Ahmedabad, 25-26 Feb, 2021.

31. N. Rastogi, "Characterization and Source Apportionment of Organic Aerosols in Delhi, India", EGU General Assembly 2020, 4-8 May, 2020.

32. N. Rastogi, "Effect of Biomass Burning, Firework Emissions, and Haze Events on the Oxidative Potential of Ambient Particulate Matter in Delhi, India", American Geophysical Union (AGU) Fall Meeting 2020, 1-17 Dec, 2020.

33. Nandita Srivastava, "IP Flux rope simulator (INFROS) : Predicting the magnetic field vectors of ICMEs", COSPAR 2021, Jan 29 $-$ Feb 3, 2021.

34. Nandita Srivastava, "Lorentz force reveals the energy build up processes in recurrent solar flare", COSPAR 2021, Jan 29 $-$ Feb 3, 2021.

35. P. Halder, "Comet dust model based on the findings from the Rosetta mission", 39th Annual Meeting of the Astronomical Society of India, 18 $-$ 23 Feb, 2021.

36. P. K. Mitra, "Multi-wavelength Analysis and Modeling of the Largest Solar Flare in the Solar Cycle 24", International Workshop on Space Science, 18 $-$ 21 May, 2020.

37. P. K. Mitra, "Successive Occurrences of Quasi-circular Ribbon Flares in a Fan-spine-like Configuration Involving Hyperbolic Flux Tube", IIA-50 international conference on "Advances in Observations and Modelling of Solar Magnetism and Variability", 1 $-$ 4 March, 2021.

38. Parveen Kumar, "Optical micro-variability in radio-loud narrow line Seyfert 1 galaxies", 39th Annual Meeting of the Astronomical Society of India, 18 $-$ 23 Feb, 2021.

39. R. E. Louis, "Formation of an Atypical Sunspot Light Bridge as a Result of Large-scale FluxEmergence", workshop 4 of 39^{th} meeting of the Astronomical Society of India, 18 $-$ 23 Feb, 2021.

40. R. E. Louis, "Inferring Magnetic and Velocity Fields in the Solar Atmosphere", High-End workshop on "Solar Activities and their Influences in the Heliosphere and Planetary Atmospheres", 8 $-$ 14 March, 2021.

41. R. E. Louis, "Spectro-polarimetric Diagnostic Tools for Investigating Solar Magnetic Flux Emergence", workshop 6 of 39^{th} meeting of the Astronomical Society of India, 18 $-$ 23 Feb, 2021.

42. R. Hart, C. Russell, J. Pabari and T. Zhang, "The Strength of Lightning on Venus Inferred from Ionospheric Whistler-Mode Waves", European Planetary Science Congress 2020, 21 Sept-09 Oct, 2020.

43. R. R. Bharti, I. B. Smith, S. K. Mishra and N. Srivastava, "SHARAD detection of subsurface reflection near Mangala Fossa, Mars", 2^{nd} Indian Planetary Science Conference, PRL, Ahmedabad, 25-26 Feb, 2021.

44. R. R. Mahajan, "Ordinary Chondrites: nitrogen systematics", The 11^{th} Symposium on Polar Science, National Institute of Polar Science, Tokyo, Japan., 01-03 Dec, 2020.

45. R. R. Mahajan and PRST Team, "New insights from the isotopic analysis of returned lunar samples at higher depth", 2^{nd} Indian Planetary Science Conference, PRL, Ahmedabad, 25-26 Feb, 2021.

46. R. R. Mahajan, K. K. Marhas, N. Upadhyay, A. Verma, J. Pabari, S. K. Goyal, M. Bhatt, A. D. Shukla, N. Srivastava, D. Panda, D. Ray, A. Basu Sarbadhikari, R. Sinha and Team, "Indian sample curation and processing facility", 2^{nd} Indian Planetary Science Conference, PRL, Ahmedabad, 25-26 Feb, 2021.

47. R. Sanwari, J. P. Pabari and R. Garg, "Venus Lightning: Data Analysis with Mathematical Approach", 2^{nd} Indian Planetary Science Conference, PRL, Ahmedabad, 25-26 Feb, 2021.

48. S. Jitarwal, J. P. Pabari, V. Sheel, S. Nambiar and Rashmi, "Design and Testing of X-Band Radio Occultation Transmitter and Receiver for future Mars Mission", 2^{nd} Indian Planetary Science Conference, PRL, Ahmedabad, 25-26 Feb, 2021.

49. S. K. Goyal, "Aditya Solar wind & Particle Experiment (ASPEX) onboard Aditya-L1 mission", 43^{rd} COSPAR Scientific Assembly, Sydney, Australia, 28 Jan-03 Feb, 2021.

50. S. K. Goyal, "Proposed measurements of high energy particles from a future Indian Mars orbiter and en-route Mars using an Energetic Ion Spectrometer", 43^{rd} COSPAR Scientific Assembly, Sydney, Australia, 28 Jan-03 Feb, 2021.

51. S. K. Goyal, "Proposed measurements of supra-thermal and energetic particles from the Sun-Earth L1 point and Martian orbit", 2^{nd} Indian Planetary Science Conference, PRL, Ahmedabad, 25-26 Feb, 2021.

52. S. K. Mishra, “Development of In-situ Measurement Technique for Water Ice Detection for Planetary Applications”, 2^{nd} Indian Planetary Science Conference, PRL, Ahmedabad, 25-26 Feb, 2021.

53. S. Natrajan and K. K. Marhas, “The origin of Insoluble organic matter: A multi-technique study”, 2^{nd} Indian Planetary Science Conference, PRL, Ahmedabad, 25-26 Feb, 2021.

54. S. S. Nayak, “Exploring the X1.0 flare on 2014 Mar 29 via non-force-free-field extrapolation and its MHD evolution”, AAS/Solar Physics Division Meeting, 18 $-$19 August, 2020.

55. S. Saha and Sharma, S., “Classification of Aerosols over Ahmedabad using Ground-based Raman Lidar and HYSPLIT and MACC-II Model”, National Symposium on Remote Sensing for Environment Monitoring & Climate Change Assessment: Opportunities and Challenges conducted by ISRS at SAC, Ahmedabad, 18-19 Dec, 2020.

56. S. Sahu, “First detection of HXR emission from an activated flux rope and initiation process of the associated coronal mass ejection”, 39^{th} meeting of the Astronomical Society of India, 18 $-$ 23 Feb, 2021.

57. S. Sharma, Kundu, S., Saha, S. and Raju, P. L. N., “Investigations of Atmospheric Clouds and Boundary Layer over India using Ground-based Lidar”, TROPMET-2020 conducted by NESAC, 14-17 Dec, 2020.

58. S. Uttam, V. Sheel, S. K. Mishra, “Dust distribution within a vortex and its significance for Mars”, 2^{nd} Indian Planetary Science Conference, PRL, Ahmedabad, 25-26 Feb, 2021.

59. Sana T., J. P. Pabari and V. Sheel, “Dust storm-driven lightning existence on Mars”, 2^{nd} Indian Planetary Science Conference, PRL, Ahmedabad, 25-26 Feb, 2021.

60. Sushant Dutta, “Population of remnant radio galaxies in deep radio surveys”, 39th Annual Meeting of the Astronomical Society of India, 18 $-$ 23 Feb, 2021.

61. T. Singh, “Geology of the Crüger-Sirsalis Basin: Evidence of prolonged mare volcanism on the Moon”, 2^{nd} Indian Planetary Science Conference, PRL, Ahmedabad, 25-26 Feb, 2021.

62. Y. Yu, C. T. Russell, P. J. Chi, S. A. Haider, J. Pabari, J. G. Luhmann, “Search for Martian Schumann Resonances”, European Planetary Science Congress 2020, 21 Sept-09 Oct, 2020.

Various Events, and Outreach Activities at PRL

Vikram Jayanti Celebrations

The year 2019-2020 was the Birth Centenary year of Dr. Vikram Sarabhai, the founder of PRL, and 12^{th} August 2020 was his 101st Birth Anniversary. In the normal circumstances, PRL would have celebrated this momentous occasion with great fervour, but due to COVID-19 pandemic situation, it was not possible. Nevertheless, PRL had organized a Webinar on "Dr. Vikram Sarabhai and Physical Research Laboratory (PRL)", on Monday, 10 August 2020. Shri A.S. Kiran Kumar, Chairman, PRL Council of Management, was the Guest of Honour, of this Webinar. The two very learned speakers, Dr. K. Kasturirangan, Honorary Distinguished Advisor, ISRO, and Shri Kartikeya Sarabhai, Director, Centre for Environment Education; shared their reminiscences on "Dr. Vikram Sarabhai and PRL" based on their personal association with both Dr. Sarabhai and the PRL. The webinar was broadcasted on YouTube and PRL Facebook page, which was viewed by around 5000 persons.

The traditional event of garlanding the statue of Dr. Vikram Sarabhai at main campus and bust at Thaltej campus and tree plantation to commemorate Vikram Jayanti, 12 August 2020 was arranged. The event was arranged in the presence of a very limited number of PRL colleagues and Sarabhai family members by following the COVID-19 protocols, precautions, and social distancing. In view of the unprecedented situation, the event was recorded which was made available on the PRL website soon after the event. The event was also celebrated with great enthusiasm at the Udaipur Solar Observatory keeping in view all the protocols and precautions.

The 39^{th} Meeting of the Astronomical Society of India

The 39^{th} Meeting of the Astronomical Society of India commenced on 18^{th} February 2021 with four online Workshops. Workshop 4 (WS4), titled Recent Insights into Solar Active Region Dynamics was co-hosted by the Udaipur Solar Observatory-PRL and IIT-BHU. The focus of the Workshop was to provide students and early career scientists a common platform to share their research on solar active region dynamics, and initiate a direction to channel our efforts, both observationally and theoretically, into understanding our magnetic star comprehensively. The talks covered the interior of the Sun to the interplanetary medium with emphasis on synoptic and high-resolution observations from both ground and space, specialized diagnostic techniques, and advanced numerical simulations. There were a total of 18 presentations, which included 5 invited talks.

WS4 comprised of 4 sessions which were dedicated to the;

1. Physics of the Solar Dynamo and Sub-Photospheric Flows in Active Regions

2. Magnetic Flux Emergence and Transport

3. Solar Eruptions and their Propagation in the Interplanetary Medium

4. Numerical Simulations and Machine Learning to Investigate Active Region Dynamics

The Workshop was attended by nearly 60 participants.

2^{nd} Indian Planetary Science Conference (IPSC-2021) organised online by PRL

Following a grand success of the 1^{st} Indian Planetary Science Conference (IPSC-2020) with a overwhelming response and participation, the 2^{nd} Indian Planetary Science Conference (IPSC-2021) was successfully organized by PRL during 25-26 February, 2021 in a virtual mode, through WebEx platform. The conference highlighted the recent results and various studies related to the atmosphere, surface and interior of solar system objects and their satellites including various planetary processes and the early solar system. Papers on modeling studies, remote sensing and in-situ observations using planetary missions, planetary analogues and laboratory studies were invited and presented.

Response to the call for abstracts was tremendous with over 200 registrations and nearly 130 abstracts submitted for presentation at IPSC02021. Over 70 contributions were scheduled for oral talks and nearly 50 submissions were scheduled as poster presentations. The conference was inaugurated online by Shri. A.S. Kiran Kumar (Chairman, Apex Science Board and Chairman, PRL Council of Management). Dr. Anil Bhardwaj, Director, PRL presented the welcome address while Dr. Varun Sheel, Convener (IPSC-2021), provided an overview of the conference. The two-day conference included eight sessions under the following themes: Atmospheres of terrestrial planets, Astrobiology and Astrochemistry, Terrestrial planets- Geology and Surface Processes, Solar Science and Lunar Science, Comets and Solar System Processes, Instrumentation and Laboratory Studies, Meteorites and Small bodies. One of the uniqueness of the conference was to provide an opportunity to all the poster authors to present their work in a crisp one-minute presentation mode which was highly successful. Each technical session was supported by a team of moderators to oversee the smooth execution and transition of talks during that session. The second in the series of IPSC conferences, initiated by PRL, witnessed exhaustive deliberations and was smoothly conducted in online mode.

National Science Day 2021

National Science Day (NSD) in India is celebrated on 28 February each year to mark the discovery of the Raman Effect. The primary focus of the NSD celebration is to widely spread the message about the importance of science in the daily lives of people. As a result, this event is celebrated all over the country in schools, colleges, universities and other academic, scientific, technical, medical and research institutions. This year due to the constraints posed by the COVID-19 pandemic the NSD -2021 events Scholarship, as well as Aruna Lal Scholarship examination and interviews, were conducted via online mode. The event and efforts were unconventional this time, but due to the efforts, the vision, concept, foresight and execution with the support of NSD committee and other PRL colleagues, the NSD 2021 event was conducted in a seamless manner.

PRL celebrated NSD on 28 February 2021 by conducting various ONLINE competitive events among the students selected through a screening test held on 16th January 2021. Five students were awarded the Aruna Lal scholarship selected through personal interview which were also held in ONLINE mode. In NSD-2021, a total of around 780 students appeared in the ONLINE screening test. In total, 104 students were selected to participate in various events organized by PRL.

Additionally, to popularize education of the girl child, PRL invited 87 girl students from schools across Gujarat to attend the ONLINE NSD event. Twelve prizes for poster/model competition were given to the students and winners presented their models/posters on the topics i) Innovative ideas on space tourism and space habitat (poster theme), ii) Recycled waste to demonstrate science (model theme) on 28 February 2021 via ONLINE mode.

International Women's Day (IWD) - 2021 Celebration at PRL

The International Women's Day (IWD) - 2021 was celebrated at PRL on 08^{th} March 2021. The event commenced with an opening song. Dr. Anil Bhardwaj, Director PRL addressed the audience on the occasion. The invited speaker Dr. Vibhuti Patel, Former Professor, from Tata Institute of Social Sciences and SNDT Women's University, Mumbai delivered a talk on "Gender Implications of COVID19 Pandemic: Intersection of Inequalities". A poem was recited after the lecture. Shri. C.V.R.G. Deekshitulu gave closing remarks. The programme ended with the vote of thanks.

Astrobiology Webinar @ PRL

Astrobiology is one of the interdisciplinary areas of science that is rapidly evolving and has the potential to reveal the mystery that shrouds the Origin of Life. The research carried out in India in this trans-disciplinary field is developing, and there is a lot of interest to engage with astrobiology research at various levels. There are a few courses works in astrobiology taught in academic institutions. Many students are interested in carrying out short and long term projects in astrobiology. The unforeseen circumstances that we are facing now due to COVID19 pandemic has heavily affected the summer projects at various levels, especially for emerging research area, such as astrobiology. However, it is imperative that the momentum is to be kept up, hence, PRL has organized a webinar series of astrobiology lectures from international and national academics who are currently carrying out astrobiology research and teaching.

Independence Day - 2020 Celebrations @ PRL

The 74th Independence Day was celebrated with the hoisting of the National Flag by Dr. Anil Bhardwaj, Director, PRL at 10.00 hrs. near library lawns of PRL Main Campus. Due to the present condition of COVID-19 pandemic and the MHA Guidelines, the Independence Day was celebrated following the protocols, precautions & social distancing measures with the restriction of 50 PRL Members. The event saw an inspiring speech by the Director, PRL. Exceptionally good CISF personnel were awarded for their services. The entire function was telecast live on the YouTube for all the staff members. The event was also celebrated at Udaipur Solar Observatory keeping in view all the social distancing norms.

The Foundation Day of the Udaipur Solar Observatory (USO)

The Foundation Day was commemorated on 22nd September 2020. This year the event was conducted online with a live stream on Youtube. The USO Foundation Day 2020 was a special occasion as it celebrated 25 years of the GONG project. GONG or the Global Oscillation Network Group is one of the flagship synoptic programmes at the National Solar Observatory (NSO) USA and USO-PRL is privileged to be a part of this important global partnership. A stellar panel of speakers from NSO included Dr. John Leibacher, Dr. Jack Harvey, Dr. Frank Hill, and Dr. Alexei Pevtsov. They spoke on the origin of the NSO-GONG partnership, the technical aspects of GONG, the transitions to the present, and the future of GONG, respectively. Dr. Anil Bhardwaj, Director PRL, welcomed the gathering, and the speakers were introduced by Prof. Nandita Srivastava. Prof. Shibu Mathew presented the vote of thanks and Dr. Rohan Louis coordinated the online programme. The event can be accessed at `https://www.youtube.com/watch?v=d7Z0RaABH-w`. A special word of appreciation to Mr. Jaya Krishna Meka, Dr. Bhushit Vaishnav, and Mr. Jigar Raval for setting up the online stream.

150^{th} Birth Anniversary of Mahatma Gandhi

150th Birth Anniversary of our Father of nation, Mahatma Gandhi's was celebrated amidst Covid-19 Pandemic restrictions in PRL. On this auspicious occasion, by following all COVID-19 prevention guidelines at workplace, the Director, PRL, Registrar PRL, Chair, PPEG, Heads of various Divisions and other staff members have offered their remembrance and paid floral tribute to Mahatma by offering prayers and a minute silence. Further, to commemorate his 150th birth anniversary, a specific area in the Auditorium foyer was dedicated to the Mahatma, where a photograph along with his autobiography in English/Hindi and Charaka were kept as a permanent display. Mahatma Gandhi's principles of truth, non-violence and love that paves the way for the welfare of the Society and world at large by bringing equality and harmony. In commemoration, an online Quiz Competition was organised, on the Monday 5th of October at 02.00 pm. Ms.Ankita Patel stood first and Mr.Yogesh the second and Mr.Chintan D Vasava the third in the event.

Celebration of Constitution Day at PRL

The Government of India has decided that "Constitution Day"" would be celebrated every year on 26 th November to commemorate the adoption of the Constitution of India and to honour, acknowledge the contribution of the Founding Fathers of the Constitution Accordingly, as per the directives received from Department, November 26 2020 Thursday was observed as "Constitution Day" at PRL, Ahmedabad.

On this occasion, all staff members were encouraged to read the “of the Constitution on 26 11 2020 (at 11 00 AM at their respective work place to inculcate the basic awareness and obligations as a Citizen. It was observed that the staff members participated enthusiastically in reading the “of the Constitution from their own work place and a feeling of Patriotism was felt by them. Besides this the “of the Constitution was displayed near entry Area of PRL Campus for attention of all Employees/Visitors. Due to Covid 19 the reading of “ of the Constitution in person was restricted up to the Senior Officers which was attended by our Director Dr Anil Bhardwaj, Registrar, Mr Chavali VRG Deekshitulu and the Dean, Prof D. Pallam Raju who all encouraged staff members to actively participate from their own work place in reading “PREAMBLE” of the Constitution and had enlightened the importance of event with their gracious presence Similarly, “ of the Constitution was also read by our staff members from their own work place at our Thaltej Campus, Udaipur Solar Observatory (USO) Udaipur and Infrared Observatory at Mt Abu Offices.

Vigilance Awareness Week 2020

The Vigilance Awareness Week 2020 was observed in Physical Research Laboratory, Ahmedabad from 27/10/2020 to 02/11/ 2020 and the Vigilance Awareness Pledge was undertaken by the staff members of PRL on 27/10/2020 through Online at one’s respective place. The banner and various pamphlets with regard to Vigilance Awareness were displayed at prime location of Physical Research Laboratory, Ahmedabad. An essay writing competition on this year’s theme “Satark Bharat, Samriddh Bharat (Vigilant India, Prosperous India)” as a part of vigilance awareness week was also organized on 29/10/2020. Besides, 87 Employees of PRL have registered for e Pledge in the CVC portal.

Republic Day Celebrations

The 72nd Republic Day was celebrated in all its solemnity and grandeur at PRL on 26th January 2021. Dr. Anil Bhardwaj, Director, PRL hoisted the national flag clock with a General Salute by the CISF personnel. He inspected the Guard of Honour presented by CISF personnel. After that, he briefed the audience about the activities, achievements, honours etc. acquired by PRL during the year. He also presented awards to CISF Personnel for their exceptional services and distributed the prizes to the winners of essay writing competition conducted during the Vigilance Awareness Week celebrations at PRL. At last, he extended his warm wishes to all staff members and their families on this auspicious occasion. Staff members attended the programme by strictly following the COVID-19 guidelines.

Republic Day Celebrations @ USO

The Republic Day was also celebrated at USO with Prof. Nandita Srivastava hoisting the National Flag. On this occasion prizes/trophies were awarded to the runners-up and winners from the Badminton Tournament, organized by the USO-SWC on 8th March 2020 by Prof. Shibu Mathew and Prof. Nandita Srivastava.

Pension Adalat held at PRL

As per the directives of Department of Pensions and Pensioners’ Welfare, New Delhi and Department of Space, Bangalore, a Pension Adalat was held on Tuesday, the 19th January 2021 at PRL, Ahmedabad through online mode for addressing various Pension related grievances. 7 Pensioners of PRL had attended the Pension Adalat. The Adalat was conducted by Shri Anand D Mehta, Head, P&GA, Shri Suresh Babu A, Head, Accounts & IFA and Shri Senthil Babu, Sr.AO (Establishment). The grievances/suggestions of Pensioners were heard and noted for early resolution. The pension Adalat was ended with vote of thanks by the Head, P&GA.

Swachhta Pakhwada 2021 @ PRL campuses

Swachhta Pakhwada 2021 was organized at PRL, Ahmedabad, with a focus on creating awareness on hygiene and sanitation. All the employees, faculty, scholars administered Swachhta pledge in Hindi as well as in English in a division-wise manner at PRL Navrangpura & Thaltej campuses, staff quarters by strictly adhering to all protocols and guidelines related to COVID-19. Apart from the sanitation of office premises, a special cleanliness drive was conducted at the staff quarters (Vikramnagar, Navrangpura) & guest house premises. PRL Doctors conducted a Medical camp for 70 staff working with the works contracts in a staggered manner. Face masks were distributed at “Jaspur” village.

As part of the Swachhta Pakhwada Celebrations-2021, a webinar on “Sanitation, Health and Solid Waste management” was delivered on 12th March 2020 by Shri Harshad Rai Solanki, Director, Solid Waste Management, Ahmedabad Municipal Corporation (AMC), through the online platform Webex. Through this webinar, the speaker had explained the importance of the sanitation practices, the hygiene practices amidst COVID-19 and necessity of segregation of dry and wet wastes at origin or source for their environment friendly disposal. Further, he explained about the PIRANA the waste dumping yard located in the city and the steps initiated to clear the garbage in eco-friendly manner. In order to dispose the waste generated, and for streamlining the disposal of dry and wet waste, colored dust bins (Blue and Green) are distributed for all the PRL campuses, staff quarters, Guest house areas, so that the waste can be segregated & disposed as per the AMC norms.

PRL has explored the ways to dispose the discarded electronic parts i.e., e-waste generated at the housing colonies. As a part of it, the collected e-waste was handed over to M/s ECS company (Authorized by AMC) which is taking care of safe and eco-friendly disposal. The M/s ECS company issued a “Certificate of Recycling” to PRL Ahmedabad which states that the supplied 3.30 Kg of e-waste has been processed according to the environment-friendly standards. During this Swachhta celebrations, an herbal garden development program was initiated at all the campuses of PRL including Mt. Abu & Udaipur campus.

Swachhta Pakhwada 2021 was organized at USO-PRL with a focus on creating awareness on hygiene and sanitation. The Swachhta Pakhwada began by taking the Pledge by staff and students on 22nd February at the office premises, strictly adhering to all protocols and guidelines related to COVID-19. Apart from sanitation of office premises & staff residential colony, a special cleanliness drive has been initiated at the Observatory Jetty area on the shore-side of Fatehsagar Lake. As part of Swachhta Pakhwada, USO staff members also participated in mass tree plantation in the office premises & office housing colony along with the adoption of plant saplings. A small herbal garden has also been developed at USO main campus during this fortnight. Face masks were distributed among housekeeping workers of USO during the cleanliness drive.

Swachhta Pakhwada was organized at PRL Mount Abu with strictly adhering to all protocols and guidelines related to COVID-19. PRL has received the Swachata Pakhwara Award of the Department of Space (DOS) for the year 2020 under the category of Best Maintained Autonomous Bodies.

Status of Scheduled Caste/ Scheduled Tribe Personnel as on 31/03/2021

Centre/ Unit	Total Strength of Employees 2020-21	Strength of SC Employees	Strength of ST Employees	Strength of OBC Employees
PRL	271	13	08	49

Status of Differently Abled persons as on 31/03/2021

Centre/ Unit	Total Strength of Employees	Strength of Differently Abled Persons	Classification of employees with Disabilities			
			Deaf and Dumb	Blind	Partially Blind	Orthopedically Handicapped
PRL	271	5	1	0	0	4

In addition to the events above, PRL regularly arranges mass pledge activity (in digital and physical modes) on the occasions of Swachhata Pakhwada (during the first fortnight of February), Anti-terrorism Day (May 19), Sadbhavna Diwas (August 18) and, Rashtriya Ekta Divas (October 31). The 'Preamble' of India's Constitution is read on November 26 to mark Constitution day. Celebrations of Independence Day and Republic Day are done in the presence of PRL staff, their family members and CISF personal with great joy and patriotic spirit. To spread awareness about the Fire Safety, a session is organized during Fire Service Week - April 10-15. An awareness talk and demonstration on precautions to be taken during fire events were conducted.

The said activities were conducted following COVID-19 protocols.

Measures undertaken by PRL to Contain the Spread of Covid-19

In order to contain the spread of Covid-19 and mitigate and manage its impact, PRL Dispensary undertook various measures. This includes the strict compliance of standard guidelines advocated by the central and state Governments and the innovative measures specific to PRL-Dispensary. All necessary measures were taken so those following standard guidelines by Central Government could be implemented.

A. Minimize Exposure

B. Social Distancing

C. Respiratory Etiquette

D. Frequent hand washing/hand sensitization

Innovative measures and good practices were adopted so that PRL Medical Services could face the important challenges arising from the Covid-19 situation and ensure that:

a) All CHSS beneficiaries get timely medical advice and treatment

b) All COVID 19 suspects get focused attention.

c) PRL Dispensary Complexes follow strict norms to prevent contamination and cross infections

d) Medical staff is thoroughly protected

A COVID-19 vaccination camp was also conducted; the details of which are given below. Due to such measures taken, PRL could manage to handle the pandemic in a reasonably successful manner and with minimum human lives loss of PRL staff and family.

COVID-19 Vaccination Camp

As per national directives for COVID 19 vaccination for frontline workers, Physical Research Laboratory in association with Ahmedabad Municipal Corporation (AMC) had organised COVID-19 vaccination Camps to facilitate the Covid-19 immunization for their employees, Scholars, PDFs and Contractual Workers under AMC – COVID-19 mass immunization drive. After extensive and exhaustive coordination by PRL team with AMC, it became possible to arrange camp at PRL on 31 March 2021. Utmost care had been taken to follow COVID-19 protocols while managing the beneficiaries at the camp site.

Capacity Building Programmes

RESPOND Programme

Physical Research Laboratory (PRL) administers the Indian Space Research Organization (ISRO) RESPOND to provide funding to academia in India for conducting research and development activities related to Space Science, particularly in the fields of Astronomy and Astrophysics, the Physics of Earth's atmosphere/ionosphere, Planetary Sciences, Solar Physics, Space Weather, Space Plasma Physics and Astrochemistry. The main aim of the RESPOND programme is to encourage quality research in areas of relevance to the Indian space programme. The main deliverables of the RESPOND programme at PRL have been publication of research papers in international and national refereed journals, developing trained scientists and PhD theses of associated Research Fellows. The proposers also seek funding for augmenting computational facilities; occasionally the RESPOND grant is also utilised to set up a new laboratory facility for research at the University or Institute.

The number of ongoing RESPOND projects is presently 18. In the year 2020-2021, PRL brought out a document on "Research Areas in Space" highlighting the major research programmes of PRL and also a "RESPOND BASKET" comprising of a good number of urgent and important research topics. The Research Areas in Space and Basket proposal documents were released on January 7, 2021 on ISRO Academia Day. In total 19 basket proposals were offered by PRL scientists for the proposers to select and prepare detailed proposals under RESPOND programme. In summary, the RESPOND programme of PRL has been very successful in training scientists in different parts of the country in various aspects and problems pertaining to Space Sciences, and developing research infrastructure across the country.

Online CSSTEAP Short Course on Space and Atmospheric Science

A short course on "Space and Atmospheric Science" was conducted during December 7-14, 2020 by Physical Research Laboratory (PRL), Ahmedabad under the auspices of Center for Space Science and Technology Education in Asia and the Pacific (CSSTEAP), affiliated to the United Nations. In view of the Covid-19 pandemic, the course was held online. The objective of the course was to create an understanding of the basics and current research trends in the field of space and atmospheric sciences with major focus on;

(1) Structure of the Sun, Solar Eruptions (flares, CMEs), Space Weather forecasting,

(2) Optical aeronomy, ionosphere, solar wind, magnetosphere,

(3) Space Instrumentation,

(4) Upper, Middle, Lower atmospheric dynamics and coupling,

(5) Atmospheric composition and chemistry,

(6) Aerosols and climate impacts.

The lectures were delivered by experts from the Space and Atmospheric Sciences Division and USO (Udaipur Solar Observatory) of PRL. Altogether 61 people from 11 countries (Bangladesh, Ethiopia, India, Lao PDR, Mongolia, Myanmar, Nepal, Sri Lanka, Thailand, Uzbekistan and Yemen) participated in this course. Feedback from the participants was very positive.

Induction Training 2020

Training refers to the learning & development activities carried out for the primary purpose of helping members of an organization to acquire and apply the knowledge, skills, abilities, and develop the right attitude, all of which are needed to execute various jobs. PRL Administration is committed to organizing such programme from time to time. In this regard, a Half-Day Orientation Training Programme was organized on 09/01/2020 in Nano SIMS Hall, PRL, Ahmedabad. The Orientation Training Programme was initiated by Shri Rathin Sengupta, the Head, P & GA and Shri Pradeep K. Sharma, Admin. Officer, with an intent of making the participants aware about the functioning rules and regulations of PRL/DOS and making them accustomed to the working environment of the Institute. The participants were newly recruited Assistant, Trainee Assistants and Office trainees, deployed in various Divisions/Areas of PRL. The Session began with Introduction of all the members. It covered subjects like Introduction to DOS & PRL, Machinery of the Government by Shri. Pradeep K Sharma, Session on Computer and introduction to COWAA/COINS by Shri. Girish D Padia and Team, Session on Communication Skills and Motivation by Shri Rathin Sengupta, Session on Purchase & Stores by Ms. Nandini R Rao and Mr. Sunil D Hansrajani, Session on Accounts by Shri Suresh Babu and a concluding session on Stress Management by Shri. Anand D Mehta. The Training was well applauded by all and significant interactions were held. It will help the new inductees to not only improve their efficiency and effectiveness at work but also will help in boosting their self-Confidence to assist others in an informed way.

Training of PRL Staff

As a part of the capacity building efforts PRL is sending its staff members (Scientific, Technical and Administrative) for various trainings/workshops from time to time. Following is a summary of PRL staff who attended various training/workshops during the Financial year 2020-2021.

Administrative Staff courses

1. Mr. Femics George, Online training programme on Public Procurement, AJNIFM, Faridabad, 06-08 July, 2020.
2. Ms. Shreya Pandey, Online training programme on Public Procurement, AJNIFM, Faridabad, 06-08 July, 2020.
3. Mr. Kanhav Mulasi, Online training programme on Public Procurement, AJNIFM, Faridabad, 06-08 July, 2020.
4. Ms. Jyoti Limbat, Online training programme on Public Procurement, AJNIFM, Faridabad, 06-08 July, 2020.
5. Mr. Shashikant, Online training programme on Public Procurement, AJNIFM, Faridabad, 06-08 July, 2020.
6. Mr. Deepak Kumar Prasad, Online training programme on Public Procurement, AJNIFM, Faridabad, 06-08 July, 2020.

Scientific and Technical Staff courses

7. Prof. R. D. Deshpande, Online Orientation Course on "Sexual harassment of women at workplace (Prevention, Prohibition and redressal) Act, 2013". Organized by National Institute of Public Cooperation and Child Development (NIPCCD), Regional Centre, Bengaluru, Ministry of Women and Child Development, Govt. of India. 10 December, 2020.
8. Prof. D. Pallamraju, Online Orientation Course on "Sexual harassment of women at workplace (Prevention, Prohibition and redressal) Act, 2013". Organized by National Institute of Public Cooperation and Child Development (NIPCCD), Regional Centre, Bengaluru, Ministry of Women and Child Development, Govt. of India. 10 December, 2020.
9. Prof. R. D. Deshpande, Orientation Workshop for Nodal Officers for Innovation Excellence Indicators of Public Funded R&D Institutions, organized by Confederation of Indian Industries (CII) and Centre for Technology Innovation and Economic Research, (CTIER), 20 August 2020.
10. Dr. Ravindra Pratap Singh, Training programme on "General Management Programme for Scientists", Administrative Staff College of India, Hyderabad, 18-29 Jan, 2021.
11. Dr. Neeraj Srivastava, Training programme on "General Management Programme for Scientists", Administrative Staff College of India, Hyderabad, 18-29 Jan, 2021.
12. Dr. Sachindranatha Naik, DST sponsored 2nd Science Administration and Research Management Programme through virtual platform using Learning Management System (LMS), Administrative Staff College of India, Hyderabad, 7-18 Dec, 2020.
13. Dr. J P Pabari, DST sponsored 2nd Science Administration and Research Management Programme through virtual platform using Learning Management System (LMS), Administrative Staff College of India, Hyderabad, 7-18 Dec, 2020.

Official Language promotion at PRL

Activities on the Promotion of Official Language

Owing to ongoing corona virus pandemic, the whole world has been exposed to a serious and sensitive situation. Everyone, in their own ways, is looking for ways for protection in this situation and, at the same time, many unique changes have been witnessed in the struggle to fight one's existence. While on one hand nature found back its lost lustre and on the other hand, we also witnessed many new changes in work areas. The whole world is now trying to strengthen its existence on the online platform, so that we can fight the pandemic and prevent its spread by following social distancing norms. In the scenario of online platform, our institute, the Physical Research Laboratory, also maintained its pride and enthusiasm by taking the initiatives on adopting the online medium, with full interest and zeal, in the promotion of Official Language activities. Some of the noteworthy points in this context are as follows:

1. Physical Research Laboratory (PRL) has received third prize for best implementation of Official Language Policy of Government of India during 2019-20 at Town Official Language Implementation level (TOLIC). In the meeting of the Town Official Language Implementation Committee, Dr. Anil Bhardwaj, Director, Physical Research Laboratory, was presented with a Trophy and a Citation by Shri Amit Jain, Chair, Town Official Language Committee, Ahmedabad.

   Smt. Rumkee Dutta, Hindi Officer, PRL was also presented with a Trophy and a Citation from Chair, Town Official Language Committee, Ahmedabad.

Dr. Anil Bhardwaj, Director, Physical Research Laboratory (PRL) receiving the Trophy and Citation from the hands of Shri Amit Jain, Chair, TOLIC.

2. The meeting of the Official Language Implementation Committee (OLIC) is held regularly in every quarter as per the Official Language Rules, which is chaired by the Director, PRL, Dr. Anil Bhardwaj. In these meetings, decisions on policy related to the Official language and its implementation are taken and the progress regarding the use of Hindi in PRL as a whole is reviewed. Due to Corona pandemic this year, all these meetings, were conducted through online mode.
3. The members of various Scientific Divisions and Administrative Sections of PRL campuses were involved in organizing Hindi Pakhwada for promotion of Rajbhasha in Physical Research Laboratory, Ahmedabad, Main Campus, Thaltej Campus, Mount Abu Infrared Observatory and Udaipur Solar Observatory. This year Hindi Pakhwada was celebrated during 14-28 September 2020 and was organized mostly online. Before the start of Hindi Pakhwada, the Director, PRL, requested all the staff members to undertake most of their, official work in Hindi by issuing an official order. The Hindi Pakhwada celebration Committee organized various programs and special care was taken, so that staff members from all language zone could participate in these Competitions. The Inaugural Program of Hindi Pakhwada celebrations was organised on September 14, 2020 through online mode. The DGP of Gujarat State, Dr. Vinod Kumar Mall was present as the Chief Guest. He delivered a lecture on the topic "Hindi and Indian Society". In the Inaugural Program, PRL Director, Registrar, Dean and Chairman of Pakhwada Committee also addressed the audience. The message of Home Minister, Shri Amit Shah was also read out to all by Shri Pradeep Kumar Sharma, Senior Administrative Officer, so that the staff members are encouraged to do more work in Hindi. The entire program was also telecast on YouTube.

   Programs conducted during Hindi Pakhwada are as below:

   - On Tuesday, 15th September, 2020, online Hindi typing competition was organized (for Hindi and non-Hindi speaking) in which 36 members participated.
   - Handwriting competition was organized on Thursday, 17th September, 2020 in which 06 support staff members participated.
   - Our Work Competition was organized on Monday, September 21, 2020. In this competition, various groups from scientific/technical/administrative divisions are formed and they participate in the competition as a team. In the competition, each division presents a description of the significant works done in their field. A total of 11 such groups were formed. This competition was telecast live on online medium.
   - On Wednesday, September 23, 2020, a very entertaining and first time initiative "Chitra Kya Bolta Hai" competition

was organized for people with Hindi and non-Hindi language speaking categories, wherein 25 members participated. In this contest, a picture was sent to the contestants by e-mail 10 minutes before. The picture was to be described by the participant in writing or in typed form.

- Short Speech Extempore Competition was organized on Friday, 25 September, 2020 in which the participants had to speak on the title chosen by them within specified time limit. 10 participants took part in this competition.
- Word Quiz Competition was also organized on 25th September. Every year, PRL Organizes, this word quiz competition which consists of various rounds in which the meaning and usage of Hindi words, synonyms and antonyms and topics like general knowledge, music etc. are included. 10 groups participated in this competition with a total of 30 participants.
- Poem/ Poetry Recitation competition was organized on Monday 28 September 2020. In this, opportunity is given to recite self-composed poems/ poetry and songs in Hindi. Nine members presented poems/songs and 62 viewers were connected online during this program.

Winner of Hindi Incentive Scheme for doing Original Work in Hindi are as follows:

(a) Smt. Nandini Rao, First prize

(b) Shri Abhishek, First prize

(c) Sushri Jayashree Balan Iyer, First prize

(d) Shri Kartik Patel, Second Prize

(e) Shri Bhagirath K. Kuntar, Second Prize

(f) Shri Keyur Panchasara, Second Prize

(g) Sushri Jyoti Limbat, Second Prize

(h) Smt. Richa Prashant Kumar, Third Prize

(i) Shri Sunil D. Hansrajani, Third Prize

(j) Smt. Sneha Nair, Third Prize

(k) Shri Rajendra Kumar Patel, Consolation prize

4. Apart from this, Hindi workshops were organized in every quarter. To boost the implementation of Hindi, in which members of different Sections are nominated by turn and with a view of training for official work in Hindi, workshops were organized in online mode during the quarters.
5. Smt. Rumkee Dutta, Hindi Officer presented in Workshops on 15 July 2020, 30 September 2020, and 25 February 2020. The topics were Official language Rules and day-to-day work, Incentive Schemes related to Hindi, Compilation of Hindi quarterly progress report. On 4 Dcember 2020, Smt. Neelu Seth, Senior Hindi Officer, SAC presented in Workshop on the subject of Imporatance of Hindi Training and different Incentive Schemes.
6. The Departmental Inspection related to progressive use of Hindi of all three campuses of PRL was conducted through online mode. On 7 December 2020, inspection of Mount Abu was conducted by the Controller, URSC. On 23 December 2020 PRL, Ahmedabad inspection was conducted by Director, OMPR, ISRO Headquarters and on 24 December 2020 Udaipur Solar Observatory was inspected by Deputy Secretary, Department of Space.
7. According to the instructions from the Department of Space, the wards of PRL Staff members, who have secured the highest marks in Hindi subject in CBSE/ICSE and State board in class XII and X board examinations in the year 2020, were given Merit Awards.
8. In the field of scientific writing, Meetings of the Original Book Writing in Hindi Committee was organized so that all the members of the Institute can be imparted guidance for writing original scientific book in Hindi.
9. The e-version of Hindi Patrika “Vikram” was released on 08 January 2021 in which the members of the Editorial Board joined online, thereafter the Editor, Dr. Som Kumar Sharma addressed about different topics covered in Patrika. December 2020 issue of Hindi Patrika Vikram was released by Director, Dr. Anil Bhardwaj. It was a moment of immense pride for PRL Family.
10. A Hindi Competition (Online) on “Biography of 20th Century Literary figure of Hindi” was organized by Physical Research Laboratory (PRL), Ahmedabad, on behalf of Town Official language Implementation Committee. Apart from this, an article writing on “Effects of Corona Pandemic” was also a part of this Competition. 35 nominations were received from the Central Government Offices of Ahmedabad. 28 members participated. The PRL members, Smt. Sneha Nair, Shri Mohit Kumar Soni and Shri Kapil Kumar Bhardwaj have received prizes in this competition.
11. In an Essay competition organized on 09 September 2020 by the Indian Oil Corporation, Ms. Jyoti Limbat - Assistant, Ms. Alka - Scientist/Engineer-S.C. And Shri Abhishek - Administrative Officer had participated. Shri Abhishek got the first prize in this competition. Hindi Cross Word competition was organized by Space Applications Centre, Ahmedabad on 16 March 2021 at Town Official language Implementation Committee level, in which 10 members of PRL participated.

Facilities and Services

Computer Centre

Computational Services Group

The Computational Services Group (CSG) is responsible for providing services/facilities like Networking (Internet, Local Area Network, Wifi, SPACENET), High performance Computing, E-mail, Web, DNS, Proxy, VPN, Centralized Printing, DHCP, Video Conference, EGPS, COWAA/COINS, software development and maintenance. Following services/facilities are provided during the year 2020-2021.

[A] ISRO Cyberspace Competition (ICC) 2020:

The Computational Services Group Members were team members of the ISRO/DOS wide team to develop a software to conduct ISRO Cyberspace Competition (ICC) 2020 quiz. The team has completely customize the open source software to cater the need of ICC-2020 quiz competition. The online live quiz was conducted on 29/August/2020 where total 2560 students had participated in online quiz. The event was successfully completed by the team. The sincere efforts, contribution of PRL CSG team members were acknowledged by Associate Director, CBPO, ISRO.

[B] National Science Day (NSD) 2021:

Due to COVID-19, there was a need to conduct the NSD-2020 examination completely in online mode. To cater the need, the Computational Services Group Members have fine tune and customize the open source software to conduct the NSD-2020 exam in completely online mode. Total 663 students from 163 schools had participated in the online examination. The examination went very well and without any technical glitch.

[C] Vulnerability Assessment & Penetration Testing:

Computational Services Group has actively participated & contributed in ISRO/DOS wide Vulnerability Assessment & Penetration Testing (VAPT) activities carried out during 2020-2021. Especially, the contribution of CSG team members was appreciated and acknowledged by Scientific Secretary, ISRO, Additional Chief Secretary to Government, Finance Department, Karnataka, for VAPT of Khajane-II, An Integrated Finance Management , Government of Karnataka.

[D] Cyber Security:

During the year 2020-2021, to protect PRL IT Infrastructure from cyber attacks/threats, the Computational Services Group members have taken suitable cyber security measures based on the advisory received from Computer Emergency Response Team (CERT-In) and ISRO.

[E] Data Networks and Services:

Computational Services Group has maintained and provided reliable communication access of LAN, WiFi during COVID-19 lockdown period and also for the entire year 2020-2021. Especially during COVID-19 lockdown, the CSG team has provided all the telephonic support to resolve the issues of PRL users. Occasionally during the lockdown period, the team member had attended the office to resolve few issue related to network license software, Internet link.

[F] Vikram 100 – High Performance Computing Cluster:

Vikram100 - 100TF High Performance Computing (HPC) facility is extensively used by PRL Scientific & Technical fraternity. During April 01, 2020 to March 31, 2021 period 35 Scientific Papers have been published in reputed Scientific Journals where Vikram100 facility has been acknowledged. In total, 108 Scientific Papers have been published since June 2015.

[G] Talk

A talk for Cyber Security Awareness on “Think B4U Click” at PRL – 07/January/2021.

Library & Information Services

Library and Information Services :

Library and Information Services plays an important role in catering to the information needs of the PRL researchers and staff members. These information services are being provided in all the campuses of PRL. A few important ones are - documents (books, journals, CDs) lending services, Online Access (intranet and through remote access) to Institutional Repository, E- journals, Theses, E-books, Archives, Technical Reports etc. Library also provides the facilities of Inter library loan, Plagiarism Check through Ithenticate tool, Reprographic tools. Library also facilitates Information display through Digital Notice Board and Book procurement for research scholars using their academic allowance. The updates and additions to the library during the year 2020-21 are mentioned below :

Statistics: In the year 2020-21, there has been an addition of 49 Scientific, 6 General and 18 Hindi books to the collections of three libraries in Main, Thaltej and USO campuses. 1440 visitors visited the library during the year. The reprographic service of the library is high in demand where the library facilitated 28879 photocopies in-house along with 2105 photocopies from outside agency. 553 e-books are available and 190 journals are subscribed out of which 141 are online.

Koha enabled New Web OPAC : Library now has a new Web OPAC by the Koha software for its users to enable them to browse the collection from their own work-desks. Library has also launched a mobile application which provides access to the OPAC on LAN from user's own mobile phones.

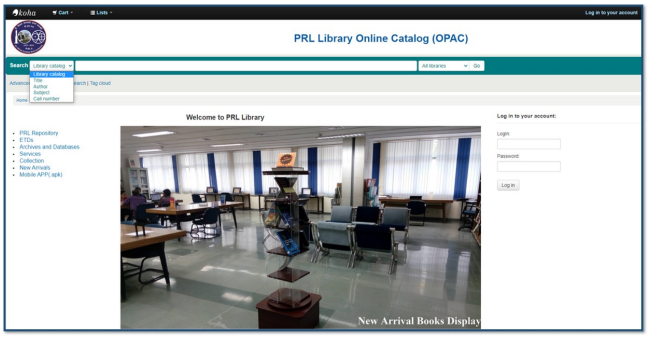

Figure No 1 : OPAC Screen powered by Koha

Library Online Resources : PRL Library continues to have access to full-text databases like AGU Digital Library, GSA Archive, PROLA, Science Archive, Library has the access to Nature.com and Springer ebooks in Engineering in addition to SPIE and IEEE Digital Library through Antakriksh Gyaan which is an ISRO Library Consortium. From 2020 all the ISRO libraries are able to access 603 Springer e-journals. The Library homepage gives access to this digital content.

New Library Website : This year Library as a part of new initiative, designed and developed a new website in-house to enable its users to have better access to the library resources. This website aims at providing seamless facility of online resources and information to the patrons of the library.

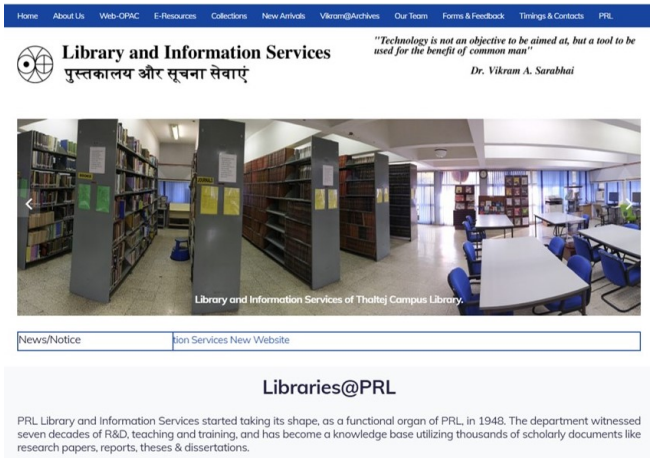

Figure No. 2: New Library Website

Plagiarism Check Facility : Library is responsible for carrying out the similarity check for students using the Ithenticate tool. They avail this facility before submitting the thesis; users also get their content checked for originality for the research papers they submit to various journals.

Digital Notice Board : It is maintained by the library to disseminate information about PRL activities like division seminars, colloquia, public talks, images of events like Republic Day celebration, Women's Day celebration, etc. In addition, list of recent publications of PRL scientists, new books added to the library collection are also displayed in 3 campuses simultaneously through the LAN. Mt. Abu campus will be linked soon.

Institutional Repository : The Institutional repository maintained by the Library consists of journal articles published by the PRL authors from 1990 to present and is also linked through the Library homepage. About 4300 articles by PRL authors are now part of this repository. All the PRL theses from 1952 onwards (439) are now available full text for PRL users. All the Technical Notes since 1977, published by PRL have been digitized (114) and are available full text for PRL users. Currently, Library is carrying out the digitization of the photographs archive. Giving the captions and metadata for each photograph for easy retrieval is in process using the digital library software – Greenstone Digital Library (GSDL).

Workshop

PRL's mechanical workshop has been actively working with various project groups in the PRL. The workshop is engaged in the design optimisation, fabrication and testing of various mechanical subsystems of several ongoing development works of the laboratory. The PRL workshop facilities in Navrangpura and Thaltej campuses are with several state-of-the-art machines for the manufacturing of mechanical parts, e.g. Vertical Machining Centre (VMC-850 & VMC 650), Wire-cut Electrical Discharge Machine (EDM), Turn Mill Center (TMC,nvu-200), CNC Turning Centre (DX 200) etc. In the academic year 2020-2021, the workshop has been deeply involved in the development of the new backend instrument for the upcoming PRL 2.5m telescope, namely PARAS-2 and NISP. Workshop has also worked closely with the members of Femtosecond laboratory to develop various experimental set-ups. The workshop has continued its support for various operational activities of various laboratories and facilities of PRL. These aspects are discussed below.

Development of PARAS-2 Mechanical Systems

The workshop has been fabricating several mechanical components of PARAS-2 (PRL Advance Radial-Velocity Abu-Sky Search -2) for the upcoming 2.5m PRL telescope.

PARAS-2 is a fiber-fed high-resolution spectrograph designed to detect the Exo-planets. PARAS-2 CASSEGRAIN Unit (figure-1) is an important part of the PARAS-2, which is to be attached to the side port of the PRL 2.5m telescope. It consists of the main Cassegrain unit and a calibration unit. Both are housed with different types of optical elements and motors. More than 170 parts of the PARAS-2 Cassegrain Unit were manufactured at PRL-workshop, main campus. Most of the parts were machined using VMC (vertical milling machine). XY stage with a positioning accuracy of better than 0.5 microns was developed to adjust the focal point in the Cassegrain unit by using linear guideways for smooth motion. The calibration unit was developed for the ball screw mechanism, which used for atomizing the selection of light source. Typical dimensional tolerances are achieved within the range of +/- 50 microns for all parts manufactured using a VMC machine.

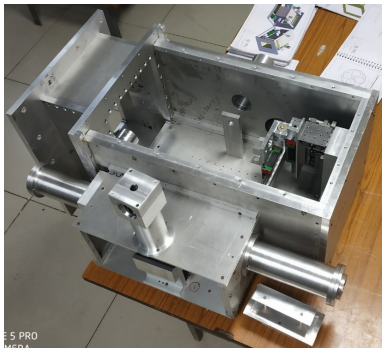

Figure No. 1 : PARAS-2 Cassegrain Unit

The integrating sphere assembly for the PARAS-2 instrumentation setup (figure-2) has also been developed using in-house CNC turning and VMC machines. Echelle grating is one of the most important optics of PARAS-2. Accurate measurement of blaze angle is crucial for the optical alignment of PARAS-2. Test setup for measuring blaze angle of echelle has been developed at the workshop (figure-3). Holders for the lens, optical posts, integrating sphere, holders for the optical fibers (figure-4), etc., have been fabricated at the workshop, which has been used during the testing and alignment of PARAS-2.

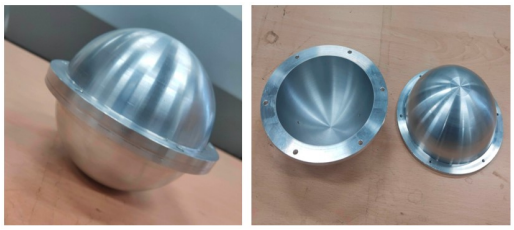

Figure No. 2 : Integrating Sphere Assembly for the PARAS-2

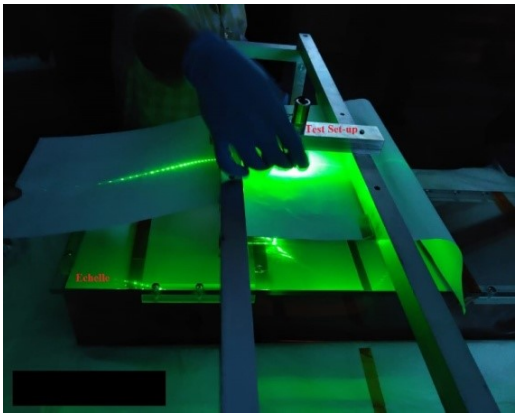

Figure No. 3 : Test Setup for Echelle Grating in PARAS-2

Figure No. 4 : Fiber Holders for PARAS-2

Development of NISP Test Dewar assembly

NISP instrument (for the upcoming PRL 2.5m telescope) is being designed and fabricated using in-house facilities. Precision components like detector assembly, cold plate, cold shield, and intermediate radiation shield were fabricated, and the integrated system is shown in Figure-5. Different parts of the assembly were machined from different materials like Aluminium, Copper, Ti6Al4V, and FR4 on VMC and EDM wire cut machine. A test Dewar was fabricated to test detector and filter wheel assemblies for 77K

temperature and 10-5 mbar pressure. The detector assembly was tested at cryogenic conditions, and it is being characterized.

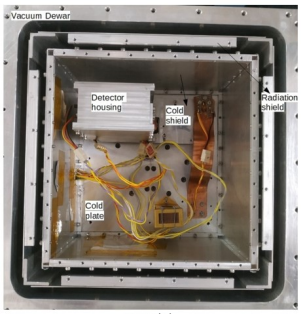

fig-1(a)

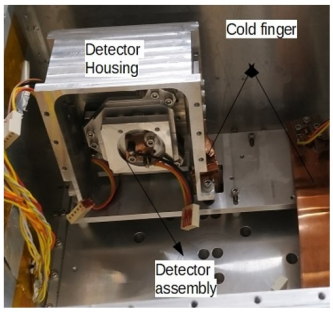

fig-1(b)

Figure No. 5 : NISP Test Dewar Assembly

Development of a new Grating mount unit for MFOSC-P instrument

Grating Motor is one of the motors used in the Mt. Abu Faint Object Spectrograph and Camera-Path finder (MFOSC-P) instrument on the 1.2 m telescope. The instrument has the ability to provide imaging and spectroscopy in a single focal reducer-based optical chain. There are three different plane-reflection gratings for spectroscopy and a fold mirror for imaging mode, which are mounted on the purpose-designed turret-like mechanism. This assembly is rotated by a stepper motor so that the desired grating or mirror can be placed at the pupil position. The hardware was developed in the PRL workshop (figure-6).

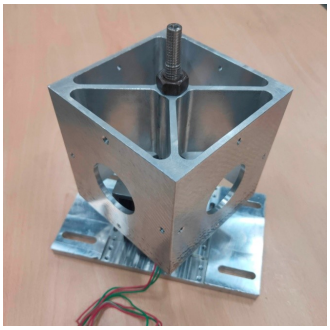

Figure No. 6 : Grating Mount Unit for MFOSC-P Instrument

The assembly comprises of 5 sub-systems viz. grating holder module, the base plate, mount for motor, bearing cover and the central shaft. There was a tight requirement in terms of surface smoothness and angle between adjacent surfaces of the grating holder module; otherwise, it would get reflected in the undesired shift in the spectrum. Provision for mounting the electronic limit sensors was also made. The assembly was satisfactorily built at the PRL workshop, and the mechanism was tested in the MFOSC-P optics laboratory. VMC and EDM wire cut machines were used for this development.

Graphite Pressing Unit for Atomic Mass Spectrometer

Sample targets in the Accelerator Mass Spectrometer have specific shape and sizes. These targets are made up of special Aluminum alloy. We have developed the pressing unit (figure-7) as per the dimensions required by the AMS machine. The parts of the graphite pressing unit are manufactured from Stainless Stee-304, Aluminum Alloy-6082, Brass, and oxygen-free Copper materials on the TMC-200 nvu (CNC) machine, and one assembly consist of a total 9 number of parts. A total of 50 number of these assemblies have been made and are proved to perform successfully. So far, 3200 nos. of Al. targets have been produced, and mass production of 3200 nos. of Pins from Oxygen Free Copper rods are in process on TMC m/c. Separate CNC Programs and Tools Settings were made for smooth machining of each of the parts.

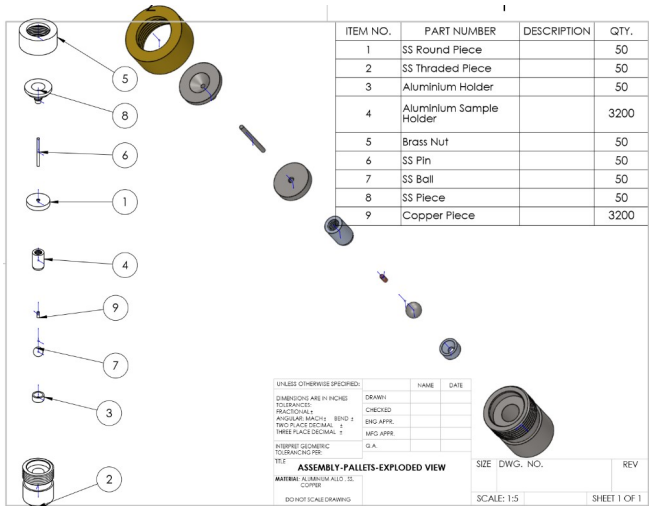

Figure No. 7 : Graphite Pressing Unit for Atomic Mass Spectrometer

Development of a Rain Water Sampler

The Automated Rain Water Sample Collector (figure-8) was designed to collect high-frequency precipitation for hydrology application, and it was tested during the last monsoon period successfully. Based on the Intensity and flow of Rain, this instrument can automatically calculate & sequentially store 90 numbers of empty vials each of 30 ml capacity. A copper funnel, a bracket for bearing, 5 Aluminium sheet covers (3 mm Thick), four brass couplers for solenoid valves, 2 Aluminium doors at the front of the instrument, 4 number caster wheels of 3-inch size was fabricated and assembled in the Rain Water Sampler for its actual operation. After the assembling of all these parts, the instrument has been tested to collect rainwater samples.

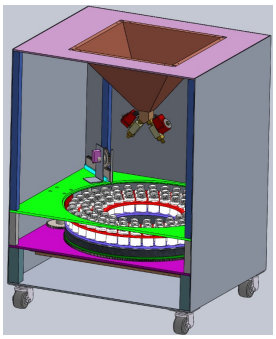

Figure No. 8 : Rain Water Sampler

CCD Based Multiwavelength Airglow Photometer (CMAP) - Flanged Version

A three-barrel arrangement enclosing optical lenses, brass housing with lock rings was designed and fabricated (figure-9) for placing lenses in CCD Based Multiwavelength Airglow Photometer (CMAP) Flanged Version. Total 20 different parts were assembled in CMAP Flanged Version, which consists of 2 number Aluminium barrels of size 200 mm x 75 mm, 4 number of Aluminium barrels of size 130 mm x 75 mm, 8 number of brass lens housing of size Dia. 75 mm x 50 mm and 6 number of lock rings of dia.60 mm x 3 mm thickness. The assembled instrument is known as CMAP and used to measure night glow emissions by focusing light onto a CCD which is fixed along the optical axis.

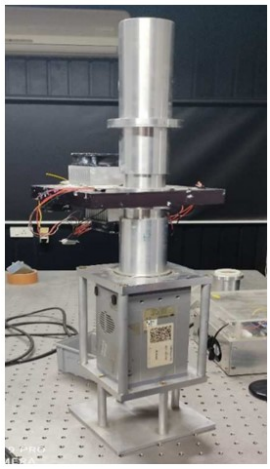

Figure No. 9 : CCD Based Multiwavelength Airglow Photometer (CMAP) Flanged Version

Spider Housing for X-ray Optics

In the recent progress towards the development of X-ray optics, the mechanical housing (figure-10) for a grazing incidence X-ray optic is designed and fabricated by the PRL X-ray optics laboratory along with the PRL workshop. This optics is designed for focusing a parallel X-ray beam of dimension 85mm X 85mm to a smaller size of 1mm X 1mm at its focal point. The groove sizes are 0.5mm wide and 5mm deep, with a 2-degree increment for each slot. Total 180 grooves are made for the housing. VMC and EDM wire cut machines are used for this purpose.

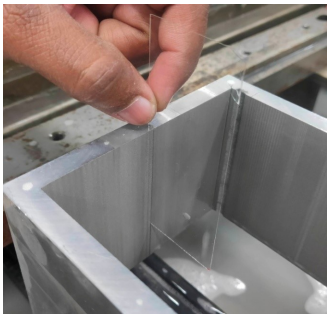

Figure No. 10 : Spider Housing for the X-ray Optics

Development activities for Femtosecond Laser Laboratory

PRL workshop has been working closely with the scientists and members of the Femtosecond laboratory to help and support the development of various experiments and subsystems. These are described below:

(A) Design and Fabrication of Various Components for Plasma Chemistry Setup

The Plasma chemistry setup was developed in a femtosecond laser lab at PRL to investigate the molecular species formation in the interaction of femtosecond laser-induced plasma plume with multiple gases. The aluminum frame and various components of this setup were designed and fabricated in PRL's workshop. The mounting of the fiber having an adjustable position as per requirement is manufactured based on the user requirements. We have also developed the various optical post, breadboards, and adapter plates for sample mounting. The plasma chemistry setup with an Al. the frame is shown in figure-11.

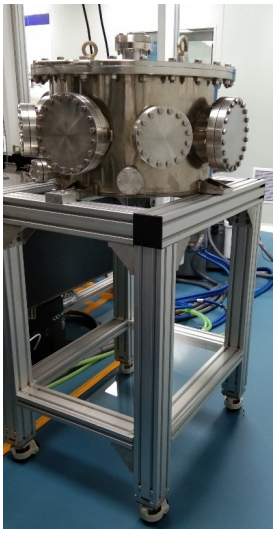

Figure No. 11 : Plasma Chemistry Setup, Femtosecond Laser Lab, AMOPH

(B) Fabrication of Gas-Cell and Laser Beam Shielding for High Harmonic Generation Setup

The Higher Harmonic Generation setup installation was going on in this year in Femtosecond laser laboratory. One of issues faced by the Femtosecond laser laboratory team is the background lights due to mirror finishing wall of the vacuum chamber. In the PRL workshop, various components were fabricated.

The gas-cell fabrication was performed in the PRL workshop. The gas cell is made of a stainless steel 0.25-inch pipe which is closed at one end, and open at the other end for introducing gas. The length and diameter of this pipe were chosen based on the pressure requirement in this gas cell. This gas cell should have two holes in lines having about 50 microns' hole. The laser beam should focus in the gas cell through about a 50-micron hole, and HHG generated XUV photons should pass along with the laser beam with another 50-micron hole on a pipe. Making sub-50-micron holes in SS pipe was difficult in the workshop, and thus we have used a femtosecond laser to create a 50-micron hole. After this work, multiple custom pipes

were fabricated to shield the background lights. Fabricated components are shown in figure-12.

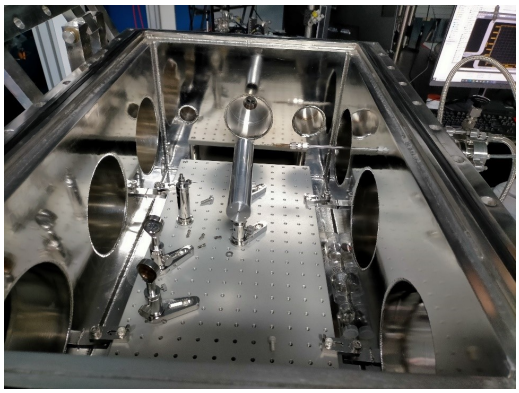

Figure No. 12 : High Harmonic Generation Setup, Femtosecond laser Lab, AMOPH

(C) Supersonic Molecular Beam Chamber: Fabrication of Al. Stand and Components

A new six-way cross vacuum chamber is installed in the femtosecond laser lab for generating the supersonic molecular beam. This vacuum chamber is connected to a High Harmonic Generation (XUV spectrometer) setup. Alignment of both vacuum chambers with respect to femtosecond laser beam was a challenging task. In the workshop, the design has been completed for finding out the center height of the vacuum chamber with reference to the floor. The C-clamps were fabricated and installed. In addition, the laser beam has to pass multiple times before focusing within the vacuum chamber. Thus, we developed a circular breadboard on which the fives mirror mounts were installed for guiding the laser beam. The drawings were made before fabricating the breadboard, Al. stand, mounts, and alignment c-clamps. The fabricated components are shown in figure-13.

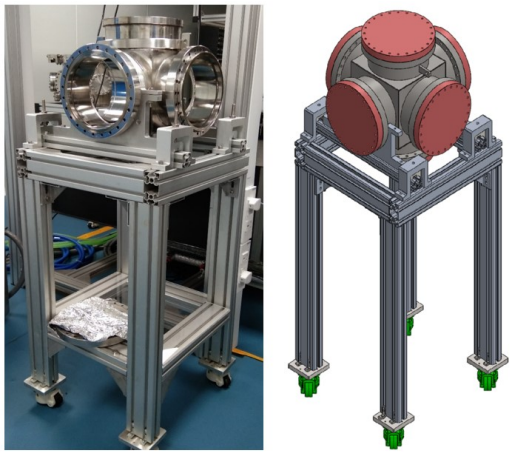

Figure No. 13 : Supersonic Molecular Beam Chamber of HHG Setup, Femtosecond Laser Lab, AMOPH

Other support activities

(A) Foot Operated Soap Dispenser During the COVID lockdown period in April-2020, the workshop has produced 20 numbers of Foot Operated Soap Dispenser Assemblies (figure-14), which were utilized in the PRL premises. These units were designed in-house to be used for the hand-free operation of sanitization. A total of 140 different parts were machined and fabricated. Overall dimensions of one assembly are 406 mm L x 406 mm W x 1050 mm H. The square base of the assembly was fabricated from MS flat bars of 8 mm thick for its strength and sturdiness. Automotive white paint and primer were sprayed on each part of all assemblies for prevention against corrosion.

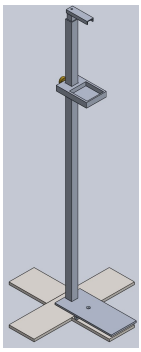

Figure No. 14 : Foot Operated Soap Dispenser

(B) Chopper Blade Unit and X-Y-Z Stage The workshop has developed components for the Quantum Science and Technology Laboratory, e.g. chopper blade unit, X-Y-Z stage for laboratory experiments. The X-Y-Z stage has been fabricated with precise components like Base, Upper Horizontal Slideways & Vertical Slideways, Instrument Mounting Pad, etc. (figures 15 and 16).

Figure No. 15 : Chopper Blade Unit

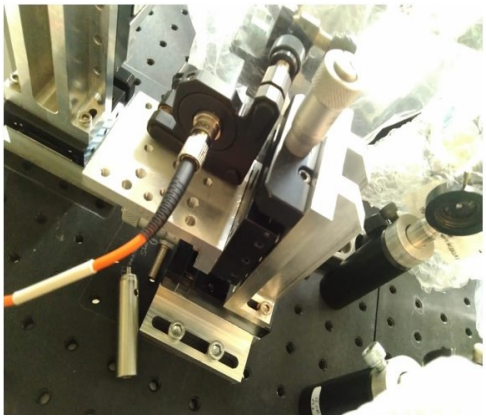

Figure No. 16 : X-Y-Z stage

(C) HV Connectors for ASPEX

High voltage (HV) connectors (figure-17), to be used within ASPEX payload of ADITYA-L1 mission, were fabricated from 6061T6 grade Al. material with a high grade of accuracy.

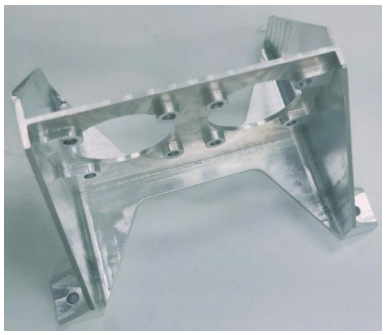

Figure No. 17 : HV Connectors for ASPEX

(D) Wheel Encoder System for PRL Telescope

The wheel encoder system is important for the synchronization of the PRL telescope with the dome. The wheel for the encoder has been fabricated in the workshop. The wheel driven by the rail of the dome forms a friction drive, as shown in figure-18.

Figure No. 18 : Wheel encoder sysetm for PRL telescope

Honorary Fellows & Faculty

Honorary Fellows

A. Hewish

J. E. Blamont - Deceased 13 April 2020

K. Kasturirangan

P. J. Crutzen - Deceased 28 January 2021

Honorary Faculty

A. K. Singhvi
FNA, FASc, FNASc, FTWAS
DST-SERB-Year of Science Chair Professor

A. S. Joshipura
FNA, FASc, FNASc
J.C. Bose & Raja Rammanna Fellow

J. N. Goswami
FNA, FASc, FNASc, FTWAS
INSA Sr. Scientist

S. A. Haider
FNA, FASc, FNASc
J. C. Bose Fellow

M. M. Sarin
FNA, FASc, FNASc
DST-SERB-Distinguished Fellowship.

R. Sridharan
FASc, FNASc,
NASI Honorary Senior Scientist

Shyam Lal
FNA, FASc, FNASc
INSA Sr. Scientist

S. D. Rindani
FNA, FNASc & INSA Sr. Scientist

D. P. K. Banerjee
CSIR Emiretus Scientist

PRL Staff

Sr. No.	Name	Designation	Specialization / Nature of Work	Division	Highest Degree Obtained
1	A B Shah	Sci./Engr.-SG	Automation, Robotics, Payload Development & FPGA	A&A	B.E. (1984)
2	A D Shukla	Asso. Professor	Geochemistry & Cosmochemistry	GSDN	Ph.D. (2012)
3	A K Sudheer	Sci./Engr.-SF	Chemistry of Atmospheric Aerosol & Biogeochemistry	GSDN	Ph.D. (2018)
4	A. Shivam	Sci./Engr.-SC	Electronics and Accelerator Mass Spectrometry	GSDN	M.Tech. (2018)
5	Aaditya Sarda	Sci./Engr.-SD	Design & Development of Space Based Instruments	SPASC	B.Tech. (2015)
6	Abhijit Chakraborty Chair, A & A	Professor	Astronomy, Exoplanets, Optical Instrumentation, Stellar High Resolution Spectroscopy	A&A	Ph.D. (1999)
7	Abhishek	Admn. Officer	General Administration	USO	PGDIP (2009)
8	Abhishek J. Verma	Sci./Engr.-SC	Mechanical design of payloads, Lab. reflectance spectroscopy, UHV Vacuum experimets	PSDN	B.E. (2016)
9	Abhishek Prasad	Assistant	Administration	ADMGN	B.Sc. (2013)
10	Adalja Hiteshkumar Lavjibhai	Sci./Engr.-SE	Mechanical and thermal design of space and ground based instruments	A&A	M.Tech. (2009)
11	Akash Ganguly	Sci./Engr.-SD	Machine Learning, Groundwater / Climate Change, Numerical Modelling and Instrumentation	GSDN	B.E. (2017)
12	Alka Singh	Sci./Engr.-SC	Hardware and Software Design and development, Embedded Systems	A&A	B.E. (2015)
13	Alok Shrivastava	Sci./Engr.-SD	Cyber Security, System Administration, Networking	COMSR	M.Sc. (1998)
14	Aman K Khatri	Sci./Engr.-SC	Civil Engineering	CMDV	B.E. (2017)
15	Amee K Patel	Sr. Proj. Assistant	Purchase and Accounts	ADMAC	MBA (2011)
16	Amit Basu Sarbadhikari	Asso. Professor	Planetary Geochemistry	PSDN	Ph.D. (2007)
17	Amitava Guharay	Asso. Professor	Atmospheric Waves, Middle Atmospheric Dynamics	SPASC	Ph.D. (2010)
18	Amogh Auknoor	Sci./Engr.-SC	Structural Design of Space-based Payloads, Vacuum Setup & Experimentation	PSDN	B.Tech. (2017)
19	Amzad Hussain Laskar	Asst. Professor	Paleoclimate, Isotope Hydrology, Non-Traditional Stable Isotope Geochemistry, Geochronology	GSDN	Ph.D. (2012)
20	Anand D Mehta	Head P & G A	Personnel and General Administration, Establishment	ADMGN	MBA (2012)
21	Angom Dilipkumar Singh	Sr. Professor	Atomic Structure and Properties, Discrete Symmetry Violations, and Ultracold Atoms	THEPH	Ph.D. (1998)
22	Anil Bhardwaj FNA, FASc, FNASc	Director	Planetary and Space Sciences, Solar System Exploration	ADMDIR	Ph.D. (1992)
23	Anilkumar L. Yadav	Sr. Sci. Assistant-A	Optical Instrumentation and GPS/GNSS/IRNSS For TEC Measurments	SPASC	M.Sc. (2014)
24	Anirban Ghosh	Sr. Sci. Assistant-A	Semiconductor Device, Photonics, Nonlinear Optics, Quantum Optics, Structured Optical Beams	AMOPH	M.Sc. (2016)
25	Anisha Kulhari	Sci. Assistant	Solar Observations	USO	M.Sc. (2016)
26	Ankala Raja Bayanna	Sci./Engr.-SF	Optical Instrumentation, Adaptive Optics, Solar Physics	USO	Ph.D. (2015)
27	Ankita Patel	Sci./Engr.-SC	Electronics and Instrumentation	A&A	B.E.. (2015)
28	Ankurkumar J Dabhi	Sr. Sci. Assistant-A	Graphitisation, Accelerator Mass Spectrometer, Radiocarbon Dating, Isotope-Ratio Mass Spectrometery	GSDN	M.Sc. (2016)
29	Arpit R Patel	Sci./Engr.-SE	FPGA based system, Hardware & Software for Space Missions	PSDN	M.E. (2010)
30	Arvind Singh	Asso. Professor	Ocean Biogeochemistry and Climate Change	GSDN	Ph.D. (2011)
31	Arvind Singh Rajpurohit	Asst. Professor	Atmosphere of Very Low Mass Stars and Brown Dwarfs	A&A	Ph.D. (2013)
32	Aseem Jaini	Sci./Engr.-SC	Civil Engineering	CMDV	B.Tech. (2016)
33	Ashirbad Nayak	Sci./Engr.-SC	Electronics	A&A	B.E.. (2017)
34	Ashish G Sawadkar	Sr. Assistant	Hindi and Administration	ADMGN	B.A. (1999)

Sr. No.	Name	Designation	Specialization / Nature of Work	Division	Highest Degree Obtained
35	Ashish Kumar	Sci./Engr.-SC	Civil Engineering	USO	B.Tech. (2016)
36	Atul A Manke	Sci./Engr.-SD	Software Development, Web-based application development	SPASC	M.Tech. (2013)
37	Avadh Kumar	Sci. Assistant	Noble Gase Mass spectrometery and Vacuum Setups	PSDN	M.Sc. (2018)
38	Aveek Sarkar	Asso. Professor	Magnetohydrodynamic Simulation	A&A	Ph.D. (2005)
39	Ayisha M Ashruf	Sci./Engr.-SC	Astronomy and Astrophysics	SPASC	M.Tech. (2019)
40	B G Thakor	Sr. Proj. Attendent	Purchase attendent	ADMPR	NINTH (1991)
41	B. Anne Matilda	Admn. Officer	General Administration and Accounts	ADMGN	M.Com. (1997)
42	Bankimchandra N Pandya	Technician-G	Scientific Glass Blowing	GSDN	I.T.I. (2003)
43	Bhalamurugan Sivaraman	Asso. Professor	Astrochemistry - Astrobiology	AMOPH	Ph.D. (2009)
44	Bhupendra J Panchal	Sr.Technician-A	Plumbing services	CMDV	M.A (2002)
45	Bhushit G Vaishnav	Sci./Engr.-SE	Atomic & Molecular Physics, Academic Administration	ADMDN	Ph.D. (2008)
46	Bhuwan Joshi	Asso. Professor	Solar Physics	USO	Ph.D. (2007)
47	Bijaya Kumar Sahoo	Professor	Probing Sub-Atomic Physics, Relativistic Atomic and Molecular Many-Body Methods, Computational Physics	AMOPH	Ph.D. (2006)
48	Binal P Umarwadia	Sr. Pharmacist-B	Pharmacy and PRL dispensary	DISSR	D.P. (1987)
49	Bireddy Ramya	Sci./Engr.-SD	Instrumentation, Programming and PCB Design	USO	M.Tech. (2019)
50	Brajesh Kumar	Asso. Professor	Solar Physics, Solar Oscillations, Solar Energetic Transients, Solar Adaptive Optics	USO	Ph.D. (2007)
51	Chandan Kumar	Sci./Engr.-SD	Payload Development, & Space Mission Data Anlaysis	PSDN	B.Tech. (2015)
52	Chavali VRG Deekshitulu	Registrar	Accounts and General Administration	ADMRO	PGDIP (1997)
53	Cherukuri Sree Vaishnava	Sci./Engr.-SC	High Energy Astrophysics and Instrumentation	A&A	M.Sc. (2019)
54	Chithra Raghavan	Sci./Engr.-SC	Space-Based Instrumentation and Simulations For Ionospheric Studies	SPASC	M.Tech. (2019)
55	D L Kalal	Project Cook	Project Cook	ADMGN	NINTH (1986)
56	D. Pallam Raju Dean & Chair, SPASC	Sr. Professor	Space Weather, Magnetoshpere - Ionosphere - Thermosphere Coupling Processes	SPASC	Ph.D. (1997)
57	Debabrata Banerjee	Professor	Planetary Science, Gamma Ray Spectroscopy and Luminescence Physics	PSDN	Ph.D. (1997)
58	Debi Prasad Pradhan	Admn. Officer	General and CHSS administration	ADMGN	MBA (2016)
59	Deekshya Roy Sarkar	Sci./Engr.-SD	Software and Ground Based Instrumentation	A&A	B.Tech. (2016)
60	Deepak Kumar Painkra	Sci./Engr.-SC	Electronics and Instrumentation	PSDN	B.Tech. (2018)
61	Deepak Kumar Prasad	Assistant	Accounts	ADMAC	B.Sc. (2014)
62	Dibyendu Chakrabarty	Professor	Space Weather, Ionosphere, Thermosphere, Magnetosphere, Solar Wind	SPASC	Ph.D. (2008)
63	Dinesh Mehta	Sci./Engr.-SD	Web Development, Database and System Administration, Cyber Security, IT Security	ADMDN	M.Tech. (2013)
64	Dinesh Yadav	Sci. Assistant	Observations	A&A	M.Sc. (2018)
65	Dipak J Panchal	Sr. Assistant	Accounts	ADMAC	S.S.C (1982)
66	Dipak Kumar Panda	Sci./Engr.-SF	Nuclear Instrumentation, Planetary Science, Meteorites, Geochemistry, Isotope Geochemistry	PSDN	Ph.D. (2019)
67	Dishendra	Sci. Assistant	Python, IoT, Blockhchains, Embedded Systems, Hardware Hacktivity	A&A	B.Sc. (2018)
68	Divyang G. Adyalkar	Sr. Nurse-B	PRL Dispensary	DISSR	D.N (2006)
69	Dwijesh Ray	Asso. Professor	Meteorites, Planetary Geology, Igneous Petrology, Geochemistry	PSDN	Ph.D. (2009)
70	Femics George	Assistant	Accounts	ADMAC	B.Com. (2015)
71	G S Rajpurohit	Sr. Tech. Asst.-C	Mt. Abu Telescope Operations	A&A	B.Sc. (1986)
72	Garima Arora	Sr. Sci. Assistant-A	Laboratory analysis of Meteorite samples	PSDN	M.Sc. (2015)
73	Girjesh R Gupta	Asst. Professor	Solar Physics	USO	Ph.D. (2011)
74	Goutam K Samanta	Asso. Professor	Quantum Optics, Photonics, Nonlinear Optics, Quantum Sensing, Quantum Communication	AMOPH	Ph.D. (2009)
75	H R Vaghela Head, Workshop	Sci./Engr.-SF	Workshop Management	WORSH	MBA (2003)

Sr. No.	Name	Designation	Specialization / Nature of Work	Division	Highest Degree Obtained
76	Harish S Gadhavi	Asso. Professor	Atmospheric Aerosols, Black Carbon, Remote Sensing, Climate Change	SPASC	Ph.D. (2006)
77	Harsh Chopra	Sr.Technician-A	PCB preparation and USO Maintenance	USO	I.T.I. (1990)
78	Harshaben Parmar	Sr. Proj. Assistant	General Administration	ADMGN	MBA (2011)
79	Hemal D. Shah	Head, Pur. & Stores	Stores and Purchase administration	ADMPR	MBA (2003)
80	Hiral D Modi	Sr. Assistant	Director's office administration	ADMDIR	B.Com. (2008)
81	Hiranmaya Mishra Chair, THEPH	Sr. Professor	Strong interaction under extreme conditions, Phase transitions, quark gluon plasma, relativistic hydrodynamics	THEPH	Ph.D. (1994)
82	Hitendra Dutta Mishra	Sci./Engr.-SD	System Management, Networks and IT Security	COMSR	MCA (2003)
83	Hitesh Chandulal Panchal	Accounts Officer	Accounts	ADMAC	M.Com. (2012)
84	Ishita P Shah	Accounts Officer	Accounting related services and Taxation	ADMAC	CA (2011)
85	J K Jain	Sr. Tech. Assistant-C	Scientific Observations	A&A	M.Sc (2009)
86	Jayesh P Pabari	Sci./Engr.-SF	Interplanetary Dust, Planetary Lightning, Space Instrumentation and Signal/Image Processing	PSDN	Ph.D. (2011)
87	Jaldhi T Mehta	Sr. Assistant	General Administration of Geosciences Division	GSDN	PGDBM (2012)
88	Janmejay Kumar	Sci./Engr.-SC	Mechanical Engineering, Payload Design	PSDN	B.Tech. (2015)
89	Jappji Mehar	Sci./Engr.-SC	Simulation of Instrument Performance	PSDN	M.Tech. (2019)
90	Jaya Krishna Meka	Sci./Engr.-SD	CAD Design, Instrumentation and FPGA Programming	AMOPH	B.Tech. (2015)
91	Jayashree Balan Iyer	Sr. Proj. Assistant	Administration, CHSS and Visitor Management	ADMGN	B.HSc. (1993)
92	Jigar A Raval Head, Computer Centre	Sci./Engr.-SF	Cyber Security, Linux System and Network Administration, High Performance Computing	COMSR	B.E. (1999)
93	Jitender Kumar	Sr. Sci. Assistant-A	Mass spectrometric instruments	GSDN	M.Sc. (2015)
94	Jitendra Kumar Panchal	Technician-G	Electrical Maintenance	CMDV	I.T.I. (2007)
95	Jyoti Limbat	Assistant	Registrar's office Administration	ADMRO	M.Sc. (2015)
96	Jyotiranjan S. Ray	Sr. Professor	Isotope Geochemistry	GSDN	Ph.D. (1998)
97	K J Bhavsar	Sci./Engr.-SE	Electrical Maintenance work	CMDV	B.E. (1995)
98	K R Nambiar	Sr. Pers. Secretary	Secretarial and Admn. Work	CMDV	P.U.C (1979)
99	K.K. Sasikumar	Sr. Admn. Officer	Administration, Transport, and Estate	ADMGN	MBA (2014)
100	Kaila Bipinkumar	Technician-F	Operating & Programing on CNC/VMC and EDM Machines, CAD Modeling and CAM Programming	WORSH	TC (2007)
101	Kanhav Mulasi	Assistant	General Administration	ADMGN	B.Sc. (2017)
102	Kapil Kumar	Sci./Engr.-SD	Astronomical, Mechanical Structural Design	A&A	B.Tech. (2015)
103	Karanam Durga Prasad	Sci./Engr.-SE	Lunar and Planetary Surface Science, Instrumentation	PSDN	Ph.D. (2018)
104	Kartik Patel	Admn. Officer	General Administration & Establishment	ADMGN	MBA (2011)
105	Kasarla Prashanth Kumar	Sci./Engr.-SC	Opto-Mechanical System Design and Instrumentation	A&A	B.E. (2017)
106	Ketan Patel	Asst. Professor	Theoretical High Energy Physics	THEPH	Ph.D. (2012)
107	Keyur D Panchasara	Sr. Proj. Assistant	Accounts work	ADMAC	B.Com. (2003)
108	Kinsuk Acharyya	Asso. Professor	Astrochemistry and Astrobiology	PSDN	Ph.D. (2008)
109	Kuljeet Kaur Marhas	Professor	Isotope Cosmochemistry, Planetary Science	PSDN	Ph.D. (2001)
110	Kuntar Bhagirathkumar K	Sr. Proj. Assistant	Admn. Work	ADMGN	MBA (2010)
111	Kushagra Upadhyay	Sci./Engr.-SC	Solar Radio Astronomy Instrumentation	USO	B.Tech. (2017)
112	Lad Kevikumar A	Sci./Engr.-SC	Instrumentation, CAD, Finite Element Analysis, Experimental and Computational Fluid Dynamics, Thin Film Coating Systems, Design and Optimization	A&A	B.E. (2017)
113	Lakhansinh G Chavda	Technician-G	Scientific Instruments, Soldering/Desoldering work	GSDN	I.T.I. (2006)
114	Lakum Yagnikkumar B.	Technician-F	Electronics and IT assistance	COMSR	I.T.I. (2010)
115	Lokesh K Dewangan	Asst. Professor	Star Formation	A&A	Ph.D. (2011)
116	Lokesh Kumar Sahu	Asso. Professor	Atmospheric Science, Trace Gases, Volatile Organic Compounds (VOCs)	SPASC	Ph.D. (2005)
117	Lovjeet Meena	Tech. Assistant	Civil work	USO	D.C.E (2013)
118	M G Yadava	Professor	Radiocarbon Dating and Paleoclimatology	GSDN	Ph.D. (2003)
119	Mahesh Gaddam	Sr. Sci. Assistant-A	Maintenance and Operation of Instruments	GSDN	M.Sc. (2013)
120	Mahesh A Raval	Sr. Lv Driver-B	Driver work	ADMGN	NINTH (1989)
121	Malaidevan P	Sci./Engr.-SC	Electronics simulation	SPASC	B.Tech. (2015)

Sr. No.	Name	Designation	Specialization / Nature of Work	Division	Highest Degree Obtained
122	Manan Shah	Sci./Engr.-SE	Development of Space and Ground Based Instruments	GSDN	M.Sc. (2016)
123	Manash Ranjan Samal	Asst. Professor	Star Formation, Star Clusters, Interstellar Medium, Young Stellar Objects	A&A	Ph.D. (2011)
124	Maniar Razaahmed M.	Sr. Assistant	Purchase administration	ADMPR	PGDIP (2018)
125	Manisha D Patel	Sr. Nurse-B	Nursing work	DISSR	B. Sc (2009)
126	Manisha Mishra	Sr. Proj. Assistant	Purchase and Procurement	ADMPR	M.Sc. (2011)
127	Mantu Meher	Assistant	Procurement and Purchase	ADMPR	B.Sc. (2015)
128	Md. Nurul Alam	Lib. Assistant-B	Lib. and Information Sciences	LIBSR	Ph.D. (2017)
129	Megha U Bhatt	Reader	Planetary Remote Sensing, Visible - Infrared Spectroscopy	PSDN	Ph.D. (2012)
130	Mitesh B Bhavsar	Technician-G	Supporting Space Science Instrumentation	SPASC	I.T.I. (1998)
131	Mithun Neelakandan Ps	Sci./Engr.-SD	High Energy Astrophysics and Instrumentation	A&A	B.Tech. (2014)
132	Mohit Kumar Soni	Sci./Engr.-SC	Avionics Instrumentation (Hardware and Software), Ground Based Insturmentation, Image Processing and Deep Learning	SPASC	B.Technician (2019)
133	Mudit Kumar Srivastava	Asso. Professor	Observational Astronomy, Development of Optical Imaging and Spectroscopy Instruments	A&A	Ph.D. (2012)
134	Mukesh M. Saradava	Sr.Technician-A	Mechanical components for solar instrument.	USO	I.T.I. (1998)
135	N Jain	Sci./Engr.-SD	Design, Development and Coordinate Maintenance of Electrical Systems at USO	USO	AMIE (2002)
136	N S Rajput	Sr.Technician-A	Assitance with Telescope operations	A&A	EIGHTH (1985)
137	Nafees Ahmad	Sci./Engr.-SC	Operations and Maintenance 1.2M Infrared Telescope	A&A	AMIE (2015)
138	Namit Mahajan	Professor	Theoretical High Energy Physics	THEPH	Ph.D. (2004)
139	Nandini Ravi Rao	Pur. & Stores Officer	Purchase administration	ADMPR	B.Sc. (1991)
140	Nandita Srivastava Dy. Head (Admin)	Sr. Professor	Solar Physics, Space Weather	USO	Ph.D. (1994)
141	Narendra Ojha	Reader	Atmospheric Chemistry, Earth System Modeling	SPASC	Ph.D. (2014)
142	Naveen Chauhan	Asst. Professor	Luminescence Dating, Luminescence Physics, Dosimetry	AMOPH	Ph.D. (2013)
143	Navinder Singh	Asso. Professor	Theoretical Condensed Matter Physics	THEPH	Ph.D. (2006)
144	Neelam J S S V Prasad	Sci./Engr.-SD	Development of Telescope Back-end Instruments and Control System, Antenna Design	A&A	B.Tech. (2015)
145	Neeraj Kumar Tiwari	Sci./Engr.-SD	Mechanical and Thermal Design of Space Instruments	A&A	B.Tech. (2015)
146	Neeraj Rastogi	Asso. Professor	Atmospheric Science: Aerosol Chemistry	GSDN	Ph.D. (2005)
147	Neeraj Srivastava	Asso. Professor	Planetary Remote Sensing, Laboratory Reflectance Spectroscopy	PSDN	Ph.D. (2015)
148	Nileshkumar N Dodiya	Sr.Technician-A	Carpentary Work	CMDV	S.S.C (2000)
149	Nimma Vinitha	Sci./Engr.-SC	Ultrafast Spectroscopy, Laser & Optical Instrumentation	AMOPH	M.Tech. (2019)
150	Nirbhay Upadhyay	Sci./Engr.-SE	System Engineering of Space Instrumentation	PSDN	M.Tech. (2008)
151	Nishant Singh	Sci./Engr.-SC	Design & Development of Space Based Instruments	PSDN	B.E. (2017)
152	Nishtha Anilkumar Head, Lib.	Lib. Officer-F	Lib. & Information Services	LIBSR	Ph.D. (2012)
153	P Narendra Babu	Sci./Engr.-SC	Electrical and Maintenance works	CMDV	B.Tech. (2013)
154	P S Patwal	Tech. Officer-C	Telescope Electrical Engineering	A&A	D.EL.E (1993)
155	P S Rajput	Sr.Technician-A	Assistance with Telescope operations	A&A	NINTH (1983)
156	Padia Girishkumar D	Sci./Engr.-SD	Database Administration, Web Application Security Auditing, Applicationvirtualization, Linux Server Administration, Shell Scripting	COMSR	M.Tech. (2013)
157	Pankaj K Kushwaha	Sci./Engr.-SC	Electronics for Space-Borne and Ground Based Instruments	SPASC	B.Tech. (2016)
158	Parmar Viral M.	Sci./Engr.-SE	Electrical Engineering and Maintenance works	CMDV	B.E. (2002)
159	Partha Konar	Asso. Professor	Theoretical Particle Physics, High Energy Collider, Deep Machine Learning	THEPH	Ph.D. (2005)
160	Patel Anil S.	Tech. Assistant	Electrical Maintenance	CMDV	B.E. (2015)
161	Peddireddy Kalyana Srinivasa R	Sci./Engr.-SC	Structural and Thermal Analysis of Payload Structures	PSDN	B.Tech. (2016)
162	Piyush Sharma	Sci./Engr.-SC	Electronics for Space Based Instruments	PSDN	M.Tech. (2017)

Sr. No.	Name	Designation	Specialization / Nature of Work	Division	Highest Degree Obtained
163	Pooja Chandravanshi	Sci./Engr.-SC	Quantum Communication, Data Acquisition and Automation	AMOPH	B.E. (2016)
164	Prabhaben T Chauhan	Sr. Assistant	Dispatch	ADMGN	B.A (1999)
165	Prachi V Prajapati	Sci./Engr.-SC	NIR-Optical Instrumentation and Observations	A&A	M.S. (2019)
166	Pradeep Kumar Sharma	Sr. Admn. Officer	General Administration, CISF Matters	ADMGN	M.A (2012)
167	Pradeep Singh Chauhan	Pur. & Stores Officer	Procurement, Contract Management	ADMPR	B.Sc. (2010)
168	Pradip S. Suryawanshi	Sr. Sci. Assistant-A	Ground and Space Based Optical Instrumentation	SPASC	M.Sc. (2016)
169	Pragya Pandey	Lib. Asst.-B	Information Services & Documentation	LIBSR	Ph.D. (2019)
170	Pranav R Adhyaru	Sci./Engr.-SF	Design & Development of Electronics for Scientific Instruments	GSDN	B.E. (1991)
171	Prashant Jangid	Sci./Engr.-SD	Web Application Development, Website Development	COMSR	B.Tech. (2015)
172	Prashant Kumar	Sci./Engr.-SE	Laser Plasma Physics, Energetic Particle Mass Spectroscopy Development	AMOPH	Ph.D. (2020)
173	Pratheeksha Nayak	Sci./Engr.-SC	Radiocarbon Dating Setups, Web Applications for Data Analysis	GSDN	B.Tech. (2017)
174	Priti K Poddar	Sr. Proj. Assistant	General Administration	ADMGN	PGDCA (1993)
175	R A Parmar	Sr. Proj. Attendent	Office attendant	ADMGN	NINTH (1988)
176	R D Deshpande Chair, GSDN	Professor	Isotope Hydrology, Hydrogeology	GSDN	Ph.D. (2007)
177	R H Kalal	Canteen Boy-C	Canteen work	ADMGN	EIGHTH (1987)
178	R K Jaroli	Sr. Proj. Assistant	Assistance with office work at USO	USO	B.Com. (1987)
179	R P Singh Chair, AMOPH	Sr. Professor	Laser Physics, Singular Optics, Quantum Optics and Quantum	AMOPH	Ph.D. (1994)
180	R R Mahajan	Sci./Engr.-SF	Meteorites, Noble Gas, Mass Spectrometry	PSDN	M.Tech. (1997)
181	R R Shah	Sci./Engr.- SG	Telescope Instrumentation & Control	A&A	MBA (1997)
182	Rahul Pathak	Sci./Engr.-SC	Design & Development of Electronics for Ground-Based and Space-Borne Instruments	SPASC	B.Tech. (2013)
183	Rahul Sharma	Sci./Engr.-SD	Database Administration (EGPS, COWAA), Networking	COMSR	M.Sc. (2013)
184	Rajendra Kumar Patel	Sr. Lv Driver-B	Driver work	ADMGN	EIGHTH (1984)
185	Rajesh A Patel	Technician-F	Refridgeration and Air Conditioning Maintenance	CMDV	I.T.I. (2014)
186	Rajesh Kumar Kushawaha	Asst. Professor	Femtosecond/Attosecond Spectroscopy, Collision Physics, Extreme Photonics	AMOPH	Ph.D. (2010)
187	Rajeshkumar G Kaila	Sr.Technician-A	Operating & Programing VMC/ TMC Machine Using Mastercam Software, Lathe/ Milling Machines	WORSH	I.T.I. (1998)
188	Rajiv Ranjan Bharti	Sci./Engr.-SD	Planetary Remote Sensing	PSDN	M.Sc. (2003)
189	Rakeshkumar G Mahar	Sr.Technician-A	Design and Fabrication Of User Specific Scientific Jobs	CMDV	I.T.I. (1998)
190	Ram Lakhan Agrawal	Sci./Engr.-SD	Conventional Lathe and Milling Machines	CMDV	B.Tech. (2013)
191	Ramitendranath Bhattacharyya	Professor	Solar Physics, Dynamics Of The Solar Corona, Magnetic Reconnection, Numerical Simulation.	USO	Ph.D. (2006)
192	Rashmi	Sci./Engr.-SC	Design & Development Of Space Based Instruments.	PSDN	B.Tech. (2019)
193	Rashmi Ranjan	Sr. Pur. & Stores Officer	Stores Administration, Dgs&D Contract	ADMST	M.A (2011)
194	Ravi Bhushan	Professor	Oceanography, Paleoclimate, Ocean Biogeochemistry, AMS Radiocarbon Dating	GSDN	Ph.D. (2009)
195	Ravindra Pratap Singh	Sci./Engr.-SF	MLT Dynamics, Airglow, Atmospheric Waves, Optical/IR Instrumentation	SPASC	Ph.D. (2018)
196	Richa Prashant Kumar	Catering Manager	Catering, Hospitality and Estate Management	ADMGN	B.Sc. (2009)
197	Rishikesh Sharma	Sr. Sci. Assistant-A	High-Resolution Spectroscopy & Photometric Data Analysis, Exoplanets, Astronomical Instrumentation	A&A	M.Sc. (2017)
198	Rishitosh Kumar Sinha	Sci./Engr.-SD	Planetary Remote Sensing of Mars and Moon	PSDN	M.Tech. (2011)
199	Rohan Eugene Louis	Asst. Professor	Solar Physics	USO	Ph.D. (2011)
200	Rohit Meena	Sci. Assistant	Aerosol Chemistry	GSDN	M.Sc. (2018)
201	Rumkee Dutta	Asst. Director, Official Language	Hindi Cell Administration	ADMGN	M.A (2004)
202	S Ramachandran	Sr. Professor	Aerosols, Radiation, and Chemistry-Climate Interactions	SPASC	Ph.D. (1996)
203	S Venkataramani	Sci./Engr.-SG	Atmospheric Science, Trace Gases	SPASC	M.Sc. (1986)
204	S Vijayan	Asst. Professor	Planetary Remote Sensing	PSDN	Ph.D. (2013)

Sr. No.	Name	Designation	Specialization / Nature of Work	Division	Highest Degree Obtained
205	Saba Abbasi	Assistant	Purchase services	ADMST	MBA (2015)
206	Sachindranatha Naik	Professor	High Energy Astronomy and Astrophysics	A&A	Ph.D. (2003)
207	Samir V Dani Head, Dispensary	Med. Officer-SF	Medical & CHSS Management	DISSR	MBBS (1993)
208	Sandeep B Manglani	Jr. Pers. Assistant	Stenography & Secretarial Work	ADMDIR	SHAND (2017)
209	Sandip H Doshi	Tech. Officer-D	Computer Maintenance	A&A	DIP (1982)
210	Sandipkumar S Galthara	Sr. Technician-A	Electrical Maintenance Work	CMDV	D.EL.E (2002)
211	Sangeeta Verma	Sr. Sci. Assistant-A	Geosciences, Stable Isotopes	GSDN	M.PHIL (2008)
212	Sanjay Kumar Mishra	Asst. Professor	Plasma Physics, Dusty Plasmas, Planetary Plasma Atmosphere	PSDN	Ph.D. (2009)
213	Sanjay S Wairagade Head, CMG	Sci./Engr.-SF	Construction and Maintenance	CMDV	B.E. (1993)
214	Sanjeev Kumar	Asso. Professor	Biogeochemistry, Stable Isotopes, Climate and Environmental Change	GSDN	Ph.D. (2006)
215	Sanjeev Kumar Mishra	Sci./Engr.-SD	Electronics Design & Development for Space-Based Applications	PSDN	B.Tech. (2016)
216	Sanket Patel	Sci. Assistant	Geosciences	GSDN	M.Sc. (2018)
217	Santosh V Vadawale	Professor	X-Ray Astronomy, Solar & Planetary X-Rays Astronomy & Instrumentation	A&A	Ph.D. (2003)
218	Satyajit Seth	Asst. Professor	Theoretical High Energy Physics	THEPH	Ph.D. (2014)
219	Senthil Babu T.J.	Sr. Admn. Officer	Establishment & General Administration	ADMGN	B.Sc. (1995)
220	Shaileshgiri I Goswami	Technician-F	Electrical Maintenance	CMDV	I.T.I. (2013)
221	Shanmugam M	Sci./Engr.-SF	Design & Development of Space Instruments	PSDN	Ph.D. (2017)
222	Shashank Urmalia	Sci./Engr.-SC	Mechanical Design for Ground Based and Space Instruments.	SPASC	B.E. (2014)
223	Shashi Kant	Assistant	CMG Office Assistance	CMDV	B.Sc. (2016)
224	Shashikiran Ganesh	Asso. Professor	Milky Way Galaxy, Comets, Astronomical Instrumentation, Polarimetry	A&A	Ph.D. (2010)
225	Shibu K Mathew Dy. Head (Tech)	Professor	Solar Physics, Solar Instrumentation	USO	Ph.D. (1999)
226	Shital Hitesh Patel	Med. Officer-SF	Medical Management of Communicable and Non-Communicable Diseases	DISSR	M.D (1999)
227	Shiv Kumar Goyal	Sci./Engr.-SE	Planetary and Space Instrumentation for Radiation Measurements (Charged Particles, X-Rays, Gamma-Rays) and Mass Spectrometer	PSDN	M.Tech. (2019)
228	Shreeya Natrajan	Sci./Engr.-SC	Organic Studies In Meteorites, Isotope Cosmochemistry, Spectroscopic Studies	PSDN	M.Tech. (2019)
229	Shreya Pandey	Assistant	Project Accounting & Coins Compilation	ADMAC	M.Com. (2019)
230	Sneha Nair	Sr. Assistant	Administration & Office Work	SPASC	M.Sc. (2012)
231	Som Kumar Sharma	Asso. Professor	Atmospheric Dynamics, Weather and Climate, Lidar Probing of Atmosphere	SPASC	Ph.D. (2010)
232	Somabhai N Koted	Sr. Proj. Attendent	Cleaner and assistance in Director's office	ADMDIR	FIFTH (1990)
233	Sonam Jitarwal	Sci./Engr.-SC	Design & Development of Space Based Instruments	PSDN	M.Tech. (2019)
234	Sourita Saha	Sci./Engr.-SC	Lower Atmosphere, Clouds, Boundary Layer, Ramanlidar, Ceilometer	SPASC	B.Tech. (2017)
235	Srirag Narayanan Nambiar	Sci./Engr.-SC	Planetary Science, Ablation Physics, Numerical Modelling, Space Instrumentation	PSDN	B.E. (2017)
236	Srishti Sharma	Sci./Engr.-SC	Web Application Development, Database Management	COMSR	B.Tech. (2012)
237	Srubabati Goswami FNA, FASc, FNASc, FTWAS	Sr. Professor	High Energy Physics	THEPH	Ph.D. (1998)
238	Sujata Krishna	Sr. Proj. Attendent	Office assistance	ADMGN	S.S.C (1982)
239	Sunil D Hansrajani	Sr. Proj. Assistant	Stores Administration	ADMST	B.Com. (1991)
240	Sunil Kumar Singh FNA, FNASc	Professor	Isotope and Elemental Geochemistry	GSDN	Ph.D. (1999)
241	Suraj Kumar	Assistant	General Administration	ADMGN	B.Com. (2015)
242	Surajit Mohanty	Sci./Engr.-SC	Astronomy & Astrophysics	A&A	B.Tech. (2018)

Sr. No.	Name	Designation	Specialization / Nature of Work	Division	Highest Degree Obtained
243	Suresh Babu A	Head, Accounts & IFA	Finance and Accounts	ADMAC	PGDIP (2005)
244	Sureshkumar K Patel	Accounts Officer	Accounts services	ADMAC	M.Com. (2014)
245	Sushil Kumar	Sci./Engr.-SC	Design & Development of Space Instruments	PSDN	B.Tech. (2014)
246	Suthar Pramodkumar	Technician-F	Workshop services	WORSH	D.M.E.. (2016)
247	Swetapuspa Soumyashree	Sci./Engr.-SD	LIBS, Femtosecond Physics, Payload related Simulations	AMOPH	B.E. (2017)
248	T A Rajesh	Sci./Engr.-SF	Atmospheric Aerosols, Black Carbon	SPASC	Ph.D. (2019)
249	T K Sunilkumar	Sr. Tech. Assistant-C	Maintenance of trace gas analyzers	SPASC	BPHARM (1991)
250	T. S. Neethu	Sr. Proj. Assistant	Stores Administration	ADMST	M.Com. (2007)
251	Tejas N Sarvaiya	Sci./Engr.-SE	Cyber Security, Server Virtualization, Linux/Unix Sysadmin, Network Administration, Shell Scripting, Website/Server Auditing	COMSR	M.E.. (2014)
252	Tinkal Ladiya	Tech. Officer-C	Electronics Design & Development for Space and Ground Based Instruments	PSDN	AMIE (2020)
253	V H Chavda	Technician-G	Masonary work	CMDV	NINTH (1980)
254	V R Patel	Sr. Technician-A	Workshop services	WORSH	TWELVE (1985)
255	Vaibhav Dixit	Sci./Engr.-SD	Optical Astronomical Instrumentation, Adaptive Optics, AI, Deep Learning	A&A	M.Tech. (2017)
256	Vaibhav Varish Singh Rathore	Sci./Engr.-SC	Cyber Security, Linux and Unix System Admin, Network Management, Virtulization, Sever/Website Audit	COMSR	B.Tech. (2017)
257	Varun Sheel Chair, PSDN	Professor	Modeling of Planetary Atmospheres	PSDN	Ph.D. (1996)
258	Veeresh Singh	Asst. Professor	Active Galactic Nuclei, Radio Astronomy	A&A	Ph.D. (2012)
259	Vijaysinh M Rathod	Sr.Technician-A	Electrical Repair and Maintance Work	CMDV	H.Sc. (1996)
260	Vikram Goyal	Sr. Sci. Assistant-A	Planetary Sciences, Isotope Cosmochemistry	PSDN	M.Sc. (2016)
261	Vimlesh Kumar	Sci./Engr.-SC	Mechanical, Photonics, Nonlinear Optics, Single Photons, Quantum Optics, Structured Optical Beams	AMOPH	B.Tech. (2016)
262	Vinayak Kumar	Sci./Engr.-SD	Astrophysics, Programming	AMOPH	B.Tech. (2013)
263	Vineet Goswami	Asst. Professor	Isotope Geochemistry, Geochronology, Chemical Oceanography	GSDN	Ph.D. (2012)
264	Virendra Kumar Padhya	Sci./Engr.-SD	Hydrology and IWIN Mass Spectrometery	GSDN	M.Tech. (2013)
265	Vishal Joshi	Asst. Professor	Astronomy & Astrophysics	A&A	Ph.D. (2014)
266	Vishal M Shah	Tech. Officer-E	Scientific and Space Electronic Instrumention	A&A	D.E.E (1982)
267	Vishnu Kumar Dhaker	Sr. Sci. Assistant-A	Atmospheric Aerosols	SPASC	M.Sc. (2016)
268	Vishnubhai R Patel	Sci./Engr.-SC	CAD, CAM Programming, workshop services	WORSH	B.E. (2018)
269	Vivek Kumar Mishra	Sci./Engr.-SC	Mechanical Design,Telescope Mirror Coating & Cleaning, Mechanical Maintainance Of Equipments	A&A	B.E. (2015)
270	Vudutala Naresh	Accounts Officer	Accounts services	ADMAC	CA (2012)
271	Yugal S Jain	Sr. Accounts Officer	Accounts work and Audit	ADMAC	CA (2014)

पी.आर.एल. में गतिविधियां
Events at PRL

Indian Planetary Science Conference(IPSC)-2021

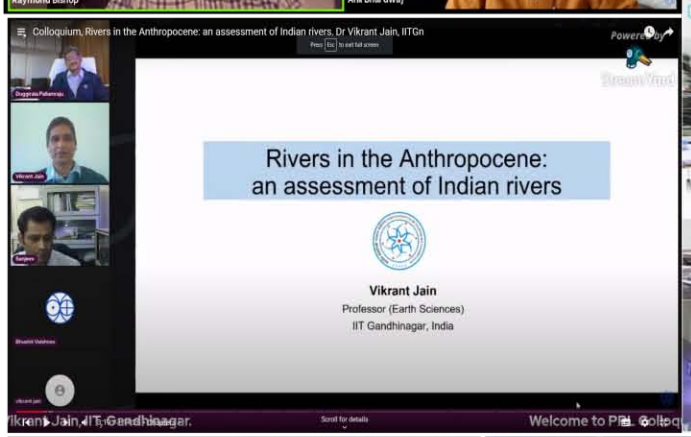

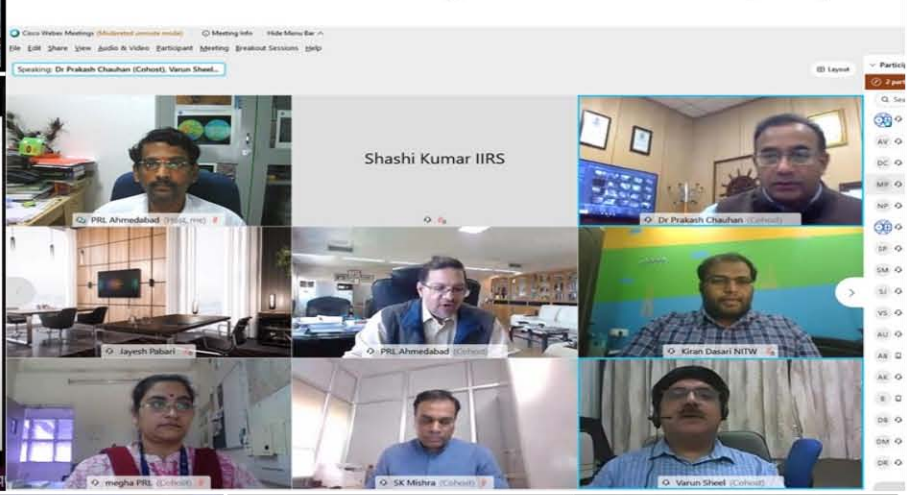

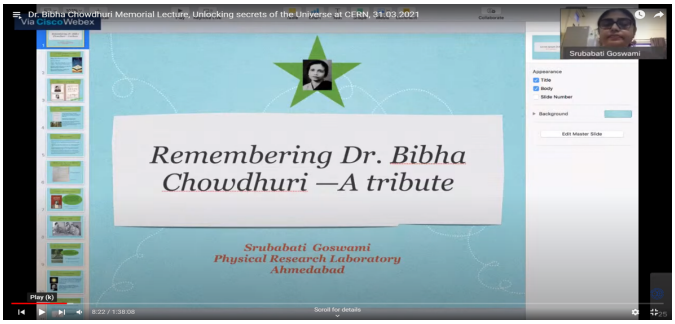

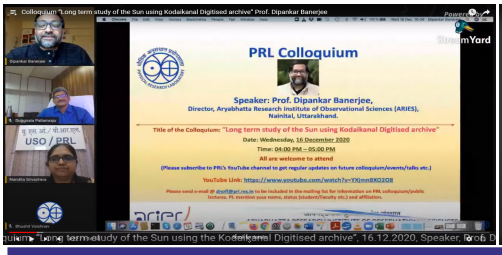

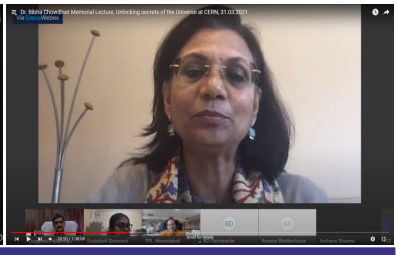

पी.आर.एल. में गतिविधियां
Events at PRL

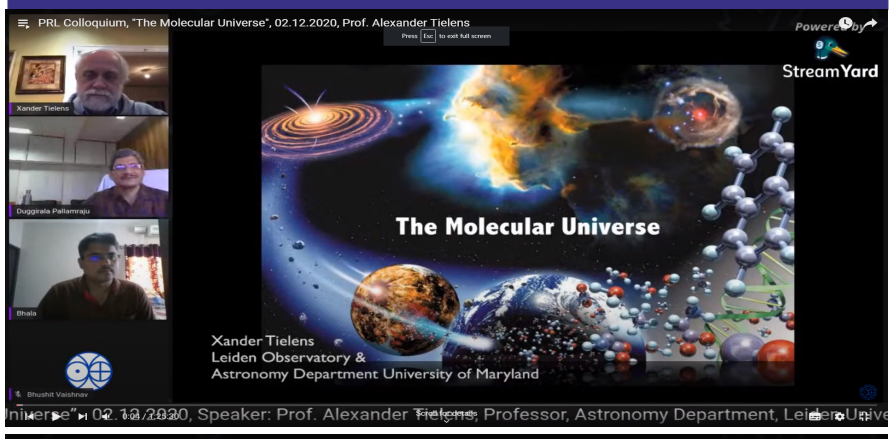

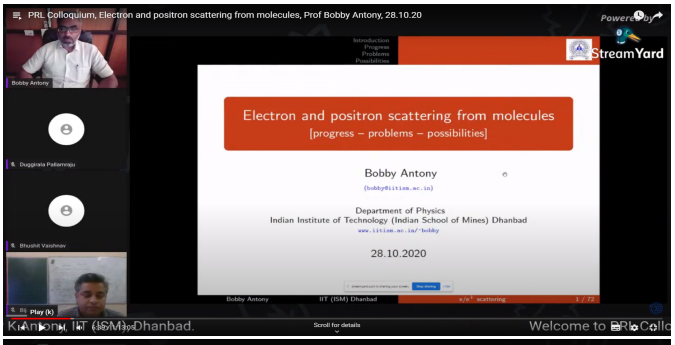

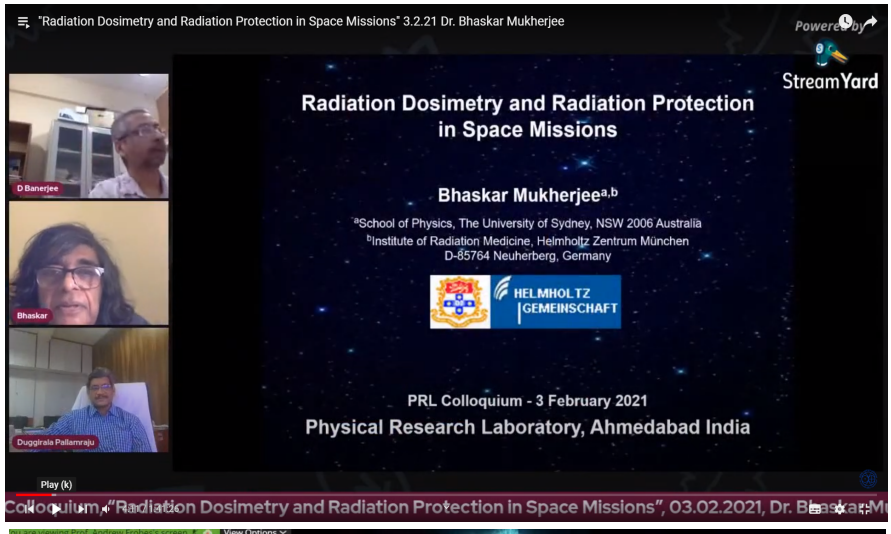

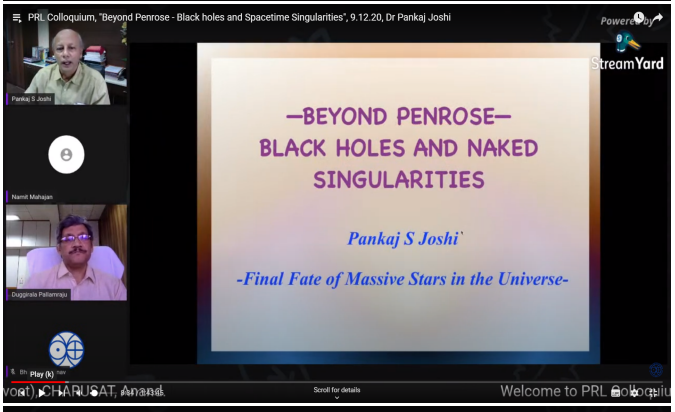

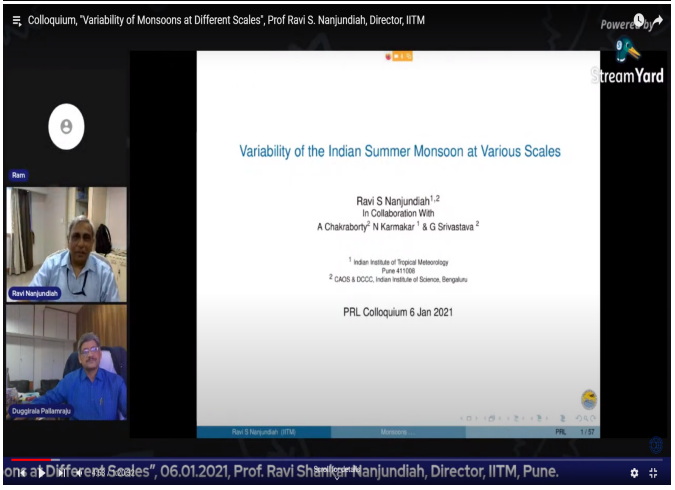

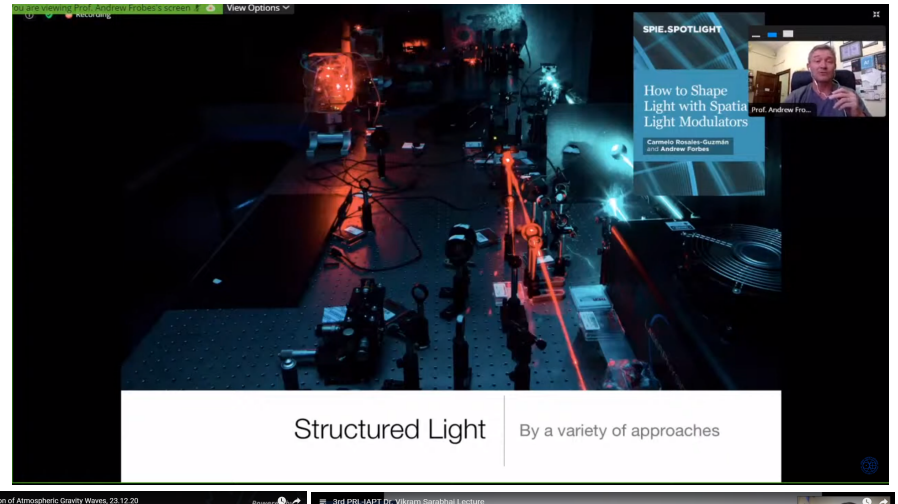

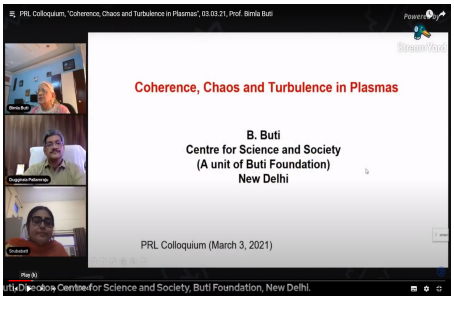

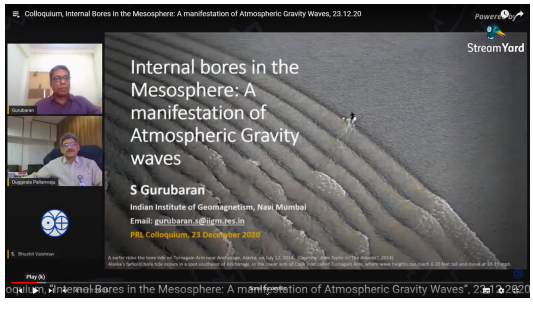

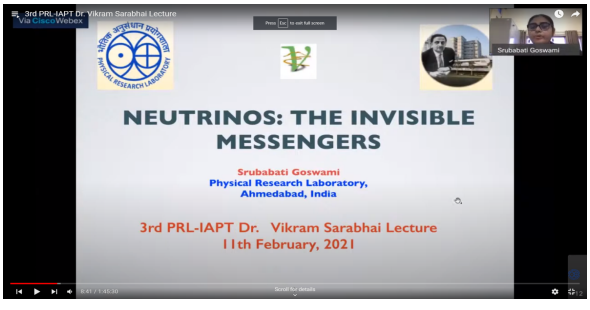

पी.आर.एल. में गतिविधियां
Events at PRL

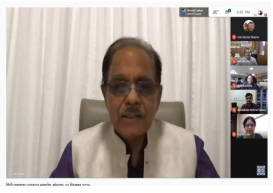

PRL International Women's Day Lecture - 2021-20210308

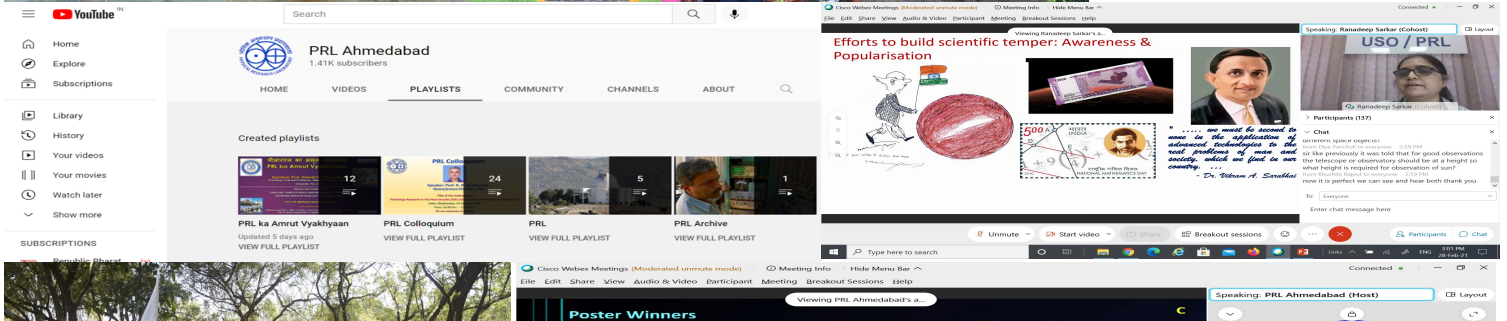

"समकालीन विश्व में अधिकांश कार्यों में ऐसे संगठनों की आवश्यकता है जिनमें सृजनात्मक सोच एवं नवप्रवर्तन, अस्तित्व एवं विकास के आवश्यक उपादान हों" -डॉ. विक्रम ए. साराभाई

"Most tasks encountered in the contemporary world call for organizations wherein creative thinking and innovation are essential ingredients of survival as well as growth" *-Dr. Vikram A. Sarabhai*